INVESTIGATING THE COMPLEXITY OF TIME-DEPENDENT DRUG-DRUG AND DRUG-FOOD INTERACTIONS INVOLVING CYP3A4 USING PHYSIOLOGICALLY BASED PHARMACOKINETIC MODELING

DISSERTATION

zur Erlangung des Grades des Doktors der Naturwissenschaften
der Naturwissenschaftlich-Technischen Fakultät
der Universität des Saarlandes

von
Laura Maria Fuhr
Diplom-Pharmazeutin/Apothekerin

Saarbrücken
2024

Die vorliegende Arbeit wurde von April 2019 bis Juni 2023 unter Anleitung von Herrn Professor Dr. Thorsten Lehr in der Fachrichtung Klinische Pharmazie der Naturwissenschaftlich-Technischen Fakultät der Universität des Saarlandes angefertigt.

TAG DES KOLLOQUIUMS:	22. August 2024
DEKAN:	Prof. Dr.-Ing. Michael Vielhaber
BERICHTERSTATTER:	Prof. Dr. Thorsten Lehr
	Prof. Dr. Markus Meyer
VORSITZ:	Prof. Dr. Andriy Luzhetskyy
AKAD. MITGLIED	Dr. Jessica Hoppstädter

PUBLICATIONS

PUBLICATIONS INCLUDED IN THIS THESIS

The following research articles [1–3] describing the work of Project I - III have been published in peer-reviewed journals and are included in this thesis:

I Fuhr, L.M.; Marok, F.Z.; Hanke, N.; Selzer, D.; Lehr, T. Pharmacokinetics of the CYP3A4 and CYP2B6 Inducer Carbamazepine and Its Drug-Drug Interaction Potential: A Physiologically Based Pharmacokinetic Modeling Approach. Pharmaceutics. 2021. 13(2): 270, doi: 10.3390/pharmaceutics13020270.

II Fuhr, L.M.; Marok, F.Z.; Mees, M.; Mahfoud, F.; Selzer, D.; Lehr, T. A Physiologically Based Pharmacokinetic and Pharmacodynamic Model of the CYP3A4 Substrate Felodipine for Drug-Drug Interaction Modeling. Pharmaceutics. 2022. 14(7): 1474, doi: 10.3390/pharmaceutics14071474.

III Fuhr, L.M.; Marok, F.Z.; Fuhr, U.; Selzer, D.; Lehr, T. Physiologically Based Pharmacokinetic Modeling of Bergamottin and 6,7-Dihydroxybergamottin to Describe CYP3A4 Mediated Grapefruit-Drug Interactions. Clinical Pharmacology & Therapeutics. 2023. 114(2): 470-482, doi: 10.1002/cpt.2968.

CONTRIBUTION REPORT

The author Laura Maria Fuhr would like to declare her contributions to the publications listed above, describing the work of Projects I - III, according to the contributor roles taxonomy (CRedIT) [4].

I Conceptualization, Investigation, Visualization, Writing–Original Draft, Writing–Review & Editing

II Conceptualization, Investigation, Visualization, Writing–Original Draft, Writing–Review & Editing

III Conceptualization, Formal Analysis, Investigation, Visualization, Writing–Original Draft, Writing–Review & Editing

ABSTRACT

Drug-drug interactions (DDIs) pose a high risk for adverse drug reactions. Therefore, safe drug therapy requires a thorough understanding of a drug's DDI potential. This is achieved by assessing enzyme metabolism, inhibition, and induction of a drug *in vitro* and in clinical trials. However, concentration- and time-dependent enzyme inactivation or induction, characterized by slow effect onset and prolonged duration, pose challenges in predicting DDI outcomes. In addition, the effect of food components on drug metabolism remains underinvestigated. Here, the wide natural variability complicates conducting reliable studies and understanding food-drug interactions (FDIs). DDIs and FDIs involving CYP3A4 are highly clinically relevant, as CYP3A4 metabolizes 50 – 60% of marketed drugs and its high intestinal expression can impact drug bioavailability.

In this thesis, whole-body physiologically based pharmacokinetic (PBPK) models of the CYP3A4 substrate felodipine, the inducer carbamazepine, and the mechanism-based inhibitor grapefruit were established. In a comprehensive interaction network, the models were applied to describe complex CYP3A4-mediated time-dependent DDIs and FDIs and the contribution of intestinal CYP3A4 modulation to the overall DDI outcome. The models can be applied to support investigations in drug development. The presented grapefruit PBPK model showcases the potential of PBPK modeling to describe FDIs and may serve as a blueprint for further FDI modeling approaches.

ZUSAMMENFASSUNG

Arzneimittelinteraktionen erhöhen das Risiko unerwünschter Arzneimittelwirkungen. Eine sichere Therapie erfordert daher ein tiefgreifendes Verständnis des Interaktionsrisikos eines Arzneistoffs, das in In-vitro-Experimenten und klinischen Studien untersucht wird. Hierbei stellen die Enzyminaktivierung und -induktion - gekennzeichnet durch einen langsam eintretenden, aber langanhaltenden Effekt - eine Herausforderung bei der Abschätzung des Interaktionspotenzials dar. Außerdem sind Nahrungsmittelinteraktionen nicht ausreichend erforscht. Die natürliche Variabilität der Nahrungsmittel erschwert die Planung von Studien und das Abschätzen des Effekts.
CYP3A4-vermittelte Interaktionen sind klinisch sehr relevant, da CYP3A4 50 – 60% der Arzneimittel metabolisiert und aufgrund der hohen intestinalen Expression ihre Bioverfügbarkeit beeinflussen kann.
In dieser Arbeit wurden Physiologie-basierte Pharmakokinetik (PBPK) Modelle für das CYP3A4-Substrat Felodipin, den Induktor Carbamazepin und den Mechanismus-basierten Inhibitor Grapefruit erstellt. In einem umfassenden Interaktionsnetzwerk wurden die Modelle verwendet, um CYP3A4-vermittelte zeitabhängige Arzneimittel- und Nahrungsmittelinteraktionen vorherzusagen und die Auswirkungen der intestinalen CYP3A4-Modulation zu beschreiben. Die Modelle können zukünftig in der Arzneimittelentwicklung eingesetzt werden. Das Grapefruit PBPK Modell kann als Grundlage für Modellierungsansätze zur Beschreibung von Nahrungsmittelinteraktionen dienen.

GRAPHICAL ABSTRACT

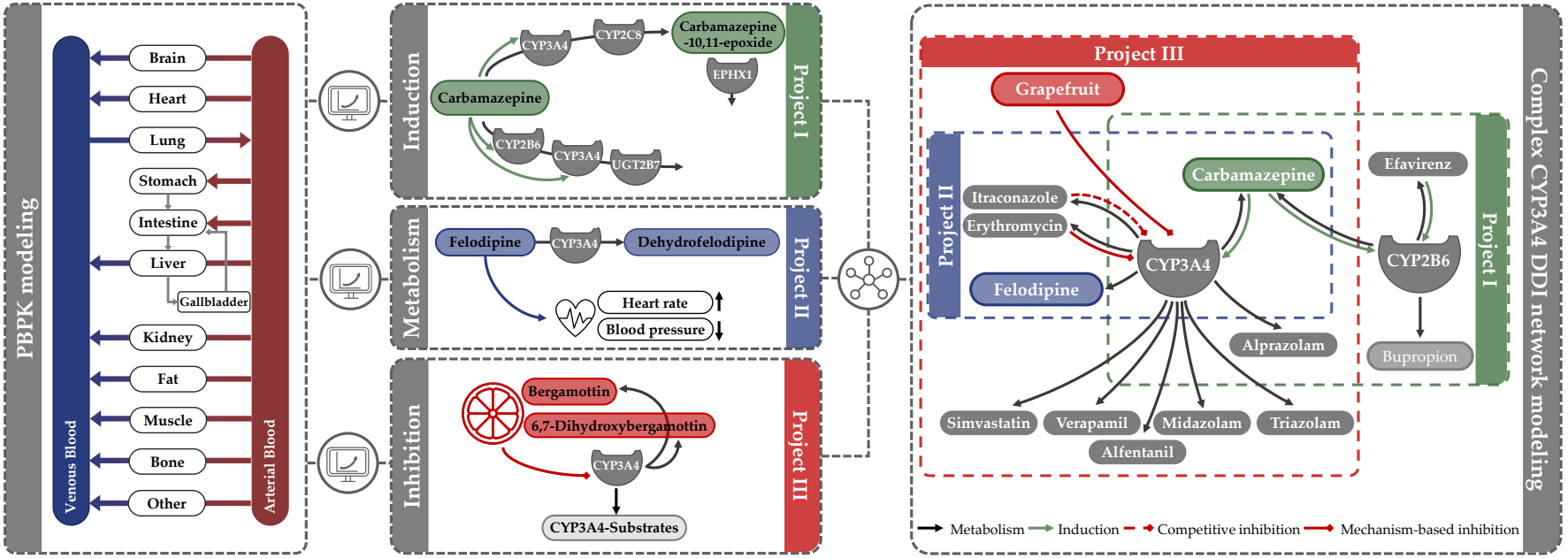

Graphical Abstract. CYP: cytochrome P450, DDI: drug-drug interaction, EPHX1: epoxide hydroxylase 1, PBPK: physiologically based pharmacokinetic, UGT: uridine 5′-diphospho-glucuronosyltransferase.

DANKSAGUNG

Auf diesem Weg möchte ich mich von ganzem Herzen bei allen bedanken, die mich in dieser herausfordernden Phase meines akademischen Werdegangs begleitet und während meiner Promotion unterstützt haben.

Allen voran gilt mein großer Dank meinem betreuenden Professor Thorsten Lehr, der während des Studiums mein Interesse für die Pharmakometrie geweckt hat und mir ermöglicht hat, in diesem spannenden Gebiet zu forschen und zu promovieren. Seine kreativen Ideen, Denkanstöße und Anmerkungen haben zum Gelingen dieser Arbeit essenziell beigetragen. Professor Markus R. Meyer danke ich herzlichst für die Übernahme des Zweitgutachtens dieser Arbeit und für seine wissenschaftliche Begleitung.

Teamwork makes the dream work! Daher gilt mein besonderer Dank der gesamten Arbeitsgruppe Klinische Pharmazie, für den wissenschaftlichen Austausch, aber auch für die vielfältigen Unternehmungen außerhalb des Arbeitsalltags. Insbesondere danke ich Dr. Nina Hanke dafür, dass sie ihr Wissen im Bereich PBPK an mich weitergegeben und sich stets Zeit für meine Fragen genommen hat. Eine große Bereicherung waren auch der regelmäßige Austausch sowie die hilfreichen Ideen und Ratschläge meiner Kolleginnen und Kollegen Fatima Marok, Dr. Denise Feick und Dr. Simeon Rüdesheim.

Nicht zuletzt danke ich von ganzem Herzen meinen Freundinnen und Freunden und meiner Familie. Ich danke meinem Freund Louis für sein liebevolles Verständnis und seine unermüdliche Geduld und Unterstützung. Mein unendlicher Dank gilt meiner Mutter Saskia und meinem Vater Markus, die mit grenzenloser Unterstützung alle meine Entscheidungen begleiten, mir stets zur Seite stehen und mir den Rücken stärken.

CONTENTS

LIST OF FIGURES

ACRONYMS

ADME	Absorption, distribution, metabolism, and excretion
ADR	Adverse drug reaction
AUC	Area under the (plasma) concentration-time curve
AUC_{last}	Area under the (plasma) concentration-time curve calculated from the time of drug administration to the time of the last concentration measurement
CAR	Constitutive androstane receptor
C_{max}	Maximum (plasma) concentration
CYP	Cytochrome P450
DNA	Deoxyribonucleic acid
DDI	Drug-drug interaction
EC_{50}	Concentration necessary to reach 50% of the maximal effect
EMA	European Medicines Agency
E_{max}	Maximum effect
FDA	U.S. Food and Drug Administration
FDI	Food-drug interaction
F_g	Fraction of the absorbed dose not metabolized by intestinal CYP3A4
GFJDI	Grapefruit juice-drug interaction
GMFE	Geometric mean fold error
k_{deg}	Enzyme degradation rate constant
K_I	Concentration necessary for half-maximal inactivation
k_{inact}	Maximum inactivation rate constant
K_m	Michaelis-Menten constant
k_{obs}	Observed inactivation rate constant
MID3	Model-informed drug discovery and development
MRD	Mean relative deviation
mRNA	Messenger ribonucleic acid

NDA	New drug application
OATP	Organic-anion-transporting polypeptides
PBPK	Physiologically based pharmacokinetic
P-gp	P-glycoprotein
PD	Pharmacodynamics
PK	Pharmacokinetics
PXR	Pregnane X receptor
R_{syn}	Enzyme snthesis rate
UGT	Uridine 5′-diphospho-glucuronosyltransferase

1 INTRODUCTION

1.1 MOTIVATION

The concomitant administration of multiple drugs poses a major challenge to pharmacotherapy as it increases the risk of drug-drug interactions (DDIs). Understanding and mitigating these interactions is important to ensure patient safety as DDIs are a major cause of adverse drug reactions (ADRs) [5]. For new drug applications (NDAs) it is therefore required to investigate their DDI potential, which usually involves *in vitro* tests and clinical trials with index substrates or perpetrators to investigate specific metabolic pathways [6, 7]. However, not only co-administered drugs but also foods, beverages, and dietary supplements can affect metabolic pathways, resulting in clinically relevant food-drug interactions (FDIs) [8] and an increased risk for ADRs. To understand FDIs, characterizing causative ingredients and underlying mechanisms of the interaction is crucial [9]. However, foods, beverages, and supplements are often complex mixtures of ingredients and vary in their ingredient composition and concentration. This can result in variable FDI effects [8] and complicates conducting robust FDI studies *in vivo* which adds complexity to understanding FDIs [9].

Pharmacokinetic drug interactions are commonly mediated by inhibition or induction of cytochrome P450 (CYP) enzymes [10]. CYP3A4 as the most prevalent CYP isoform contributes to the metabolism of approximately 50 – 60% of approved drugs [11]. Therefore, drug interactions involving CYP3A4 have high clinical importance. This is underlined by a recent analysis of submissions to the US Food and Drug Administration (FDA) revealing that a significant proportion of DDIs are linked to CYP3A4 [12]. The detailed mechanisms underlying drug interactions involving CYP3A4 can be highly complex. These include (1) the time-dependency associated with mechanism-based inhibition or induction of CYP3A4; (2) the presence of multiple DDI effects; (3) differential effects on intestinal and hepatic CYP3A4 as well as (4) FDIs, where the variability in ingredient composition and concentration adds further complexity.

In recent years, physiologically based pharmacokinetic (PBPK) modeling has become an established method in drug research and development to support the investigation of DDIs [13]. This powerful modeling technique allows for quantitative description and prediction of drug pharmacokinetics (PK), including DDIs, and can be used for *in vitro* to *in vivo* extrapolation as well as the prediction of untested DDIs, facilitating informed decision-making throughout drug development [6, 7, 14]. This thesis describes the application of PBPK modeling for the investigation of complex and time-dependent DDIs and FDIs involving CYP3A4 taking into account the distinct

characteristics of time-dependent interactions as well as differential DDI and FDI effects on intestinal and hepatic CYP3A4.

1.2 CYTOCHROME P450 3A4

Among the CYP enzyme superfamily, the CYP3A subfamily is responsible for the metabolism of approximately 50% – 60% of therapeutic drugs [11]. Respective substrates exhibit highly heterogenous characteristics and belong to various therapeutic classes, reflecting the broad substrate specificity of CYP3A [15]. In addition to its extensive involvement in the metabolism of exogenous compounds, the CYP3A subfamily also metabolizes endogenous substrates, such as steroid hormones or bile acids [16].
The CYP3A subfamily includes four major isoforms: (1) CYP3A4, the most abundant enzyme within the CYP superfamily in general; (2) CYP3A5, a highly polymorphic enzyme, with functional CYP3A5 being expressed in more than 70% of Africans but only 10 – 20% of Caucasians [16, 17]; (3) CYP3A7, the fetal isoform of the CYP3A family [16], which is rarely found in adults; and (4) CYP3A43, an isoform mainly expressed in the prostate and testes, which plays a minor role in adult drug metabolism [11]. The proportion of the different isoforms in the total amount of CYP3A protein is on average 85% for CYP3A4, 5% for CYP3A5, 3% for CYP3A7, and 6% for CYP3A43 [16, 18]. CYP3A is predominantly expressed in the liver and the intestine, where it accounts for approximately 40% and up to 80% of total organ CYP content, respectively (Figure 1.1) [19]. Both intestinal and hepatic metabolism are determinants of oral drug bioavailability (F), which can be expressed according to Equation 1.1:

$$F = F_a \cdot F_g \cdot F_h \tag{1.1}$$

with F_a = fraction of administered drug amount absorbed from the intestine, F_g = intestinal availability, describing the fraction of absorbed drug escaping intestinal metabolism, and F_h = hepatic availability, describing the fraction of administered drug escaping hepatic metabolism [20, 21].

Due to the high intestinal expression of CYP3A4, the intestinal metabolism can significantly contribute to the bioavailability of orally administered sensitive CYP3A4 substrates. Such drugs exhibit a low oral bioavailability as a result of sequential intestinal followed by hepatic first-pass metabolism mediated by CYP3A4 [20–22].
Overall, CYP3A4 shows high interindividual variability in protein expression and activity [18], which is impacted by physiological, genetic, and exogenous factors [25]. Physiological factors include biological sex, whereas women show higher CYP3A4 levels compared to men along with increased clearance of CYP3A4 substrates [26, 27], and inflammation, where different pro-inflammatory mediators lead to downregulation of CYP3A4 [28]. Furthermore, heritability is assumed to contribute to the observed interindi-

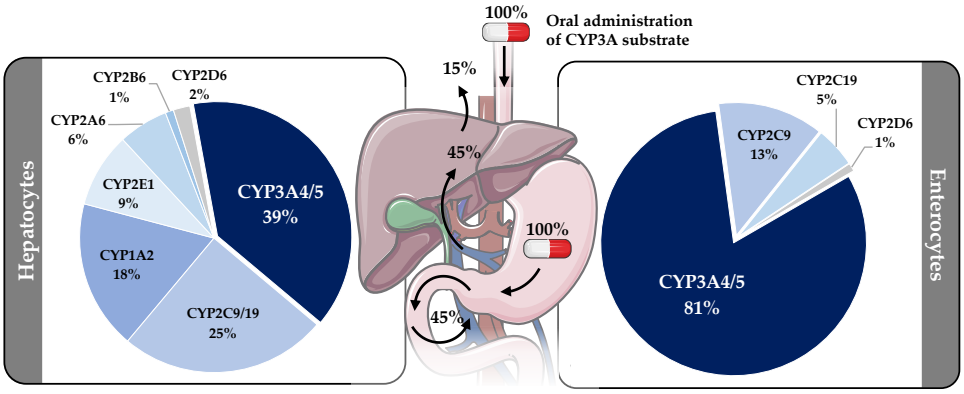

Figure 1.1: Hepatic and intestinal distribution of CYP enzymes and contribution of CYP3A4 to oral bioavailability of its substrates through sequential first-pass metabolism. After oral ingestion, the substrate is absorbed and undergoes intestinal metabolism. The non-metabolized drug moiety is transported to the liver via the portal vein where it undergoes hepatic metabolism. Illustration of sequential metabolism reproduced from [23]; Hepatic and intestinal distribution of CYP enzymes reproduced from [19]; Illustrations of capsules and organs were taken from Servier [24] CYP: cytochrome P450.

vidual differences. However, known polymorphisms in the *CYP3A4* gene can explain only a minor extent of interindividual variability due to low frequencies of respective polymorphisms in the general population or minor phenotypic impact [25]. In addition, CYP3A4 expression and activity can be modulated by exogenous compounds. Those include drugs but also food ingredients, that increase CYP3A4 expression or inhibit enzyme activity, posing a risk for DDIs or FDIs, respectively. The FDA lists examples of > 40 CYP3A4 inhibitors and >20 inducers of CYP3A4 [8]. Those examples not only include drugs but also St. John's wort, dietary supplements (curcumin and diosmin), tobacco, and grapefruit juice [8]. Given the important role of CYP3A4 in drug metabolism, it is important to assess the interaction potential of an NDA as a CYP3A4 victim or perpetrator.

1.2.1 *Case example: The CYP3A4 substrate felodipine*

The antihypertensive drug felodipine undergoes extensive metabolism by CYP3A4 to dehydrofelodipine [29] and is classified by the FDA as a sensitive CYP3A4 substrate [8]. Although it is nearly completely absorbed after oral administration, felodipine exhibits a low oral bioavailability of approximately 15% [21]. This can be attributed to sequential intestinal and hepatic first-pass metabolism of the drug [23], whereby more than 50% of the absorbed dose undergoes presystemic metabolism by intestinal CYP3A4, resulting in an F_g of 45% [21]. Here, felodipine exemplifies the impact of intestinal CYP3A4 on overall drug PK. As CYP3A4 significantly determines felodipine bioavailability and clearance, its PK are prone to DDIs with

CYP3A4 perpetrators like itraconazole, erythromycin, or carbamazepine [30–32]. In the 1990s, a coincidental observation revealed that intake of felodipine together with grapefruit juice increased its bioavailability, leading to a pronounced increase in felodipine plasma concentrations [33]. This finding marked the first instance of grapefruit-mediated FDIs via the inactivation of intestinal CYP3A4, as further described in Section 1.3.4. Upon this discovery, the effect of grapefruit was extensively studied with felodipine as a suitable probe substrate, exploring diverse scenarios and settings to gain a comprehensive understanding of the "grapefruit effect" [23].
As felodipine plasma concentrations directly correlate to its pharmacodynamic effect, DDIs affecting it PK also directly affect its pharmacodynamics (PD) [34, 35]. Felodipine blocks calcium channels in vascular smooth muscles. This leads to a decrease in vascular resistance and blood pressure. Additionally, a baroreflex-mediated increase in heart rate can be observed [36].

1.3 TIME-DEPENDENT CYP3A4-MEDIATED INTERACTIONS

The CYP enzyme system, particularly CYP3A4, plays a major role in drug metabolism, and the modulation of CYP3A4 by drugs or foods can result in clinically significant DDIs or FDIs. Here, CYP inducers enhance enzymatic activity primarily by increasing enzyme expression, whereas CYP inhibitors reduce enzymatic activity, mainly through direct interactions with the enzyme, either reversibly (e.g., competitive, noncompetitive, and mixed inhibition) or (quasi-)irreversibly [10].
The basic mechanisms of (quasi-)Irreversible inhibition and induction are illustrated in Figure 1.2 and will be described in more detail in the following. Both are concentration- and time-dependent processes [10, 37], exhibiting the following characteristics: (1) slow onset; (2) prolonged effect duration, persisting after the drug has been cleared from the body, as recovery requires either resynthesis of degraded CYP3A4 (mechanism-based inhibition) or degradation of overexpressed CYP3A4 (induction); as well as (3) cumulative but saturable effects [10]. Consequently, the magnitude of the effect depends on the administered dose of the perpetrator, the overall treatment duration and frequency as well as the time of intake in relation to the administration of the victim drug. In both cases, the interactions may not directly coincide with the intake of the perpetrator drug but can also occur if the victim drug is administered several hours after the perpetrator. Consequently, the outcome of time-dependent interactions is difficult to predict, which may complicate decision-making in chronic drug therapy. Therefore, mathematical models are helpful tools to improve the understanding of time-dependent DDIs and FDIs.

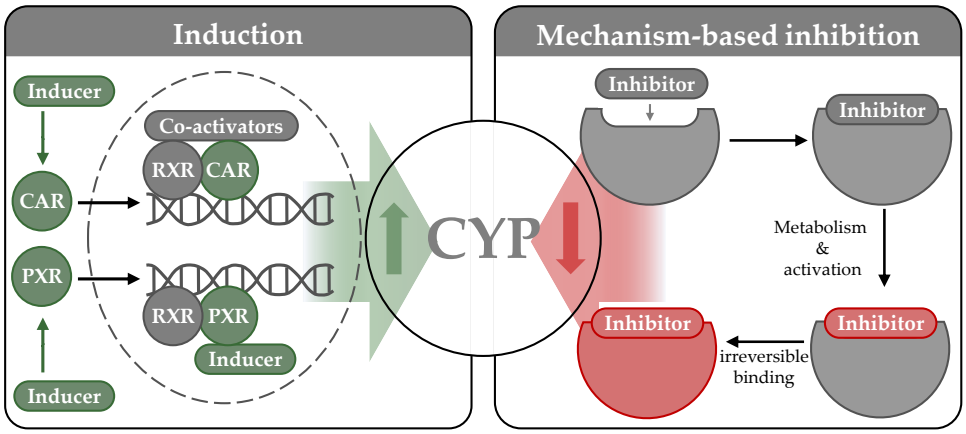

Figure 1.2: CYP induction [38] and mechanism-based inhibition. CAR: constitutive androstane receptor, CYP: cytochrome P450, PXR: human pregnane X receptor, RXR: retinoid X receptor.

1.3.1 *Induction*

Enzyme induction is mainly accomplished via activation of nuclear receptors inducing gene expression of the affected enzymes. This, in turn, increases the clearance of victim drugs which may potentially result in reduced drug efficacy or increased exposure to potentially toxic or pharmacologically active metabolites [39]. The baseline activity of the enzyme is not immediately regained after the inducer is eliminated from the body but requires degradation of the overexpressed enzyme. Consequently, enzyme induction is a time- and concentration-dependent process [10, 39]. The mechanism of CYP induction is illustrated in Figure 1.2. Here, the human pregnane X receptor (PXR) or the constitutive androstane receptor (CAR) are relevant nuclear receptors that mediate the transcription of CYP enzymes. These nuclear receptors interact with deoxyribonucleic acid (DNA) response elements and can thereby induce the transcription of *CYP* genes, among other proteins [39]. Hereby, a strong overlap in the target genes as well as the ligand spectrum has been observed. Both nuclear receptors can induce the transcription of *CYP2C*, *CYP2B* and *CYP3A* genes, and co-induction of multiple CYP enzymes can be observed [39]. To date, it is assumed that the induction of CYP3A4 for most known inducers, such as rifampicin, is mediated via activation of PXR [10]. However, CAR also binds to the CYP3A4 promotor region and activates the transcription of CYP3A4, although a more pronounced activation of CYP2B6 compared to CYP3A4 was observed for CAR-activating compounds [40]. Generally, compounds can activate different transcription pathways to varying degrees, resulting in unique patterns of CYP enzyme induction.

In vitro experiments studying the kinetics of CYP induction are usually performed with fresh or cryopreserved hepatocytes [10], incubated with different concentrations of the inducer. Different endpoints can be employed to evaluate the extent of CYP induction: measuring enzyme activity or

quantifying either enzyme content or messenger ribonucleic acid (mRNA) levels. Although measuring enzyme activity may be more clinically relevant [39], it may be confounded by concurrent enzyme inhibition [10]. Therefore, quantification of mRNA might provide a more intrinsic measurement of enzyme induction [10]. The relationship between CYP induction, measured by described endpoints, and the inducer concentration is illustrated in Figure 1.3 and can be described by a maximum effect (E_{max}) model according to Equation 1.2 [10, 41]. The parameters E_{max}, describing the maximum induction effect, and EC_{50}, describing the concentration necessary to reach 50% of maximal induction, can be determined from this relation and are used to support the interpretation of the inductive effects.

$$E = \frac{E_{max} \cdot [Ind]^{(h)}}{EC_{50}^{(h)} + [Ind]^{(h)}} \tag{1.2}$$

with E = induction effect, E_{max} = maximum induction effect, EC_{50} = concentration necessary to achieve half of E_{max} and $[Ind]$ = inducer concentration, h = Hill coefficient.

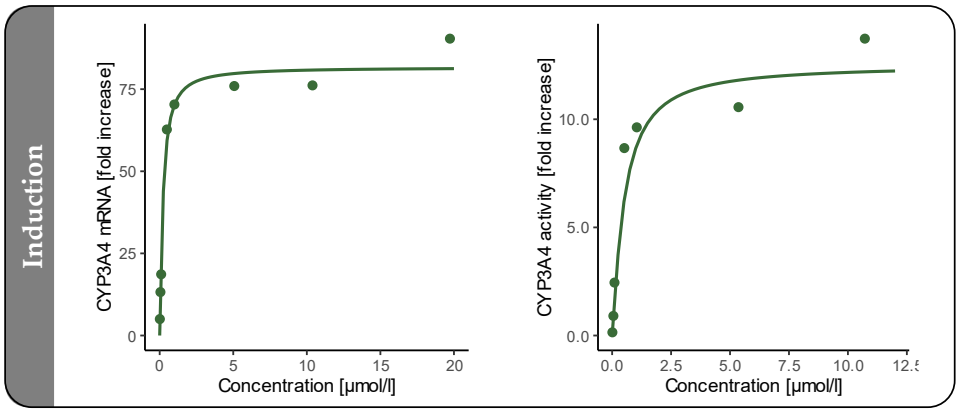

Figure 1.3: *In vitro* concentration-response relationship between inducer concentration (here: Rifampicin) and observed response, as measured by assessing CYP activity or quantifying mRNA expression. Adapted from [41]. CYP: cytochrome P 450, mRNA: messenger ribonucleic acid.

1.3.2 *Case example: Carbamazepine*

The anticonvulsive carbamazepine is indicated for the treatment of epilepsy and trigeminal neuralgia [42]. It undergoes extensive metabolism, with CYP3A4 as the major metabolizing enzyme. Additionally, CYP2C8, CYP2B6, and uridine 5'-diphosphate-glucuronosyltransferase (UGT) 2B7 contribute to the metabolism of carbamazepine [43–45]. At the same time, carbamazepine is an inducer of CYP3A4 and CYP2B6 [8, 46] and increases its own clearance during long-term treatment. It is assumed that this co-induction of respective enzymes is preferentially mediated via activation of CAR, as only minor effects on PXR could be observed [40]. The magnitude of CYP2B6 induction is greater compared to CYP3A4, which may be related to CAR activation [40]. Additionally, auto-induction has also been observed for other activators of CAR, for example, efavirenz, nevirapine, artemisinin, or cyclophosphamide [40].

DDIs with carbamazepine can be particularly complex as the drug (1) induces its own CYP3A4 and CYP2B6 mediated metabolism during long-term treatment, (2) induces the metabolism of CYP3A4 and CYP2B6 substrates during co-administration and at the same time (3) the metabolism of carbamazepine, mainly the major CYP3A4 pathway, can be affected by co-administered perpetrators. One illustrative example of such a complex DDI is the interaction of carbamazepine and efavirenz [47]. Both compounds are substrates of CYP3A4 and CYP2B6 [43, 44, 48]. Since each compound also induces the activity of respective enzymes [46, 49], they mutually induce not only their own but also each other's metabolism [1].

The effect of CYP3A4 inducers on victim drugs is regularly investigated in clinical DDI studies. Presently, rifampicin is frequently applied as an inducer in these studies. However, concerns have arisen due to potentially genotoxic N-nitrosamine impurities found in rifampicin products [51, 52]. As carbamazepine is listed as a strong CYP3A4 inducer by the FDA [50], it gained increasing interest as a substitute for rifampicin in clinical studies [51, 52].

1.3.3 *Mechanism-based inhibition*

Contrary to the time-dependent increase in CYP activity mediated by inducers, drugs can also mediate a time-dependent loss of enzyme activity [53]. Mechanism-based inhibition refers to a type of time-dependent inhibition where the inhibitor must undergo metabolic transformation into a reactive intermediate to interact with the enzyme [11, 53]. Therefore, mechanism-based inhibitors often exhibit reactive functional groups like furans, alkylamines, thiophenes, or methylenedioxy aromatic groups [37, 53]. The reactive intermediate interacts with nucleophile moieties of the CYP [53], for example, present at the apoprotein or the haem [37, 53]. Here, the intermediate can bind to the nucleophile irreversibly by forming covalent bonds or quasi-irreversibly, by forming an enzyme-inhibitor complex with very slow dissociation kinetics, resulting in the apparent inactivation of the enzyme (Figure 1.2) [54]. As the inhibition involves an activation step and restoration of enzyme activity requires *de novo* synthesis, mechanism-based inhibition is concentration- and time-dependent [10]. The concentration of the inhibitor and the inactivation rate show a hyperbolic relationship as the inactivation rate increases with increasing inhibitor concentration to a maximum [54].
Inhibition kinetics of MBIs *in vitro* are typically characterized by parameters K_I (concentration necessary for half-maximal inactivation) and k_{inact} (maximum inactivation rate constant). These parameters can be determined from two-step incubation experiments [54], usually performed with liver microsomes or recombinant CYP enzymes [53]. Here, the enzyme is incubated with multiple concentrations of the inactivator in the first step. In a second step, aliquots of this first mixture are incubated with a sensitive CYP substrate [53, 54] to assess the remaining CYP activity at different time points. For each investigated inhibitor concentration, the observed inactivation rate constant (k_{obs}) is calculated from the slope of the logarithm of the remaining CYP activity versus preincubation time as illustrated in Figure 1.4. K_I and k_{inact} are then determined from the hyperbolic plot of k_{obs} versus corresponding inhibitor concentration (Figure 1.4) according to Equation 1.3 [54].

$$k_{obs} = \frac{k_{inact} \cdot [Inh]}{K_I + [Inh]} \tag{1.3}$$

with k_{obs} = observed inactivation rate constant, k_{inact} = maximum inactivation rate constant, K_I = concentration required to achieve half-maximal inactivation, and $[Inh]$ = inhibitor concentration.

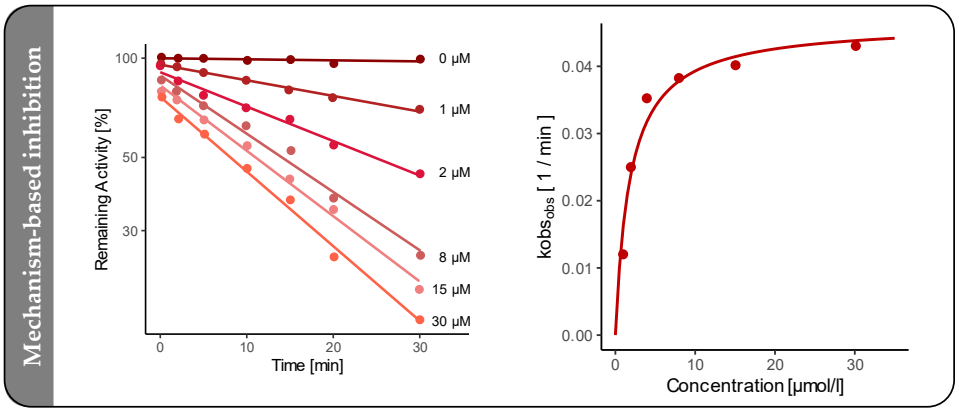

Figure 1.4: Relationship between mechanism-based inhibitor concentration and the observed effect on CYP activity *in vitro*. Left: Plot of remaining CYP activity versus time for all inhibitor concentrations tested with the two-step dilution method. Here, k_{obs} is determined from the log-linear phase of the decline. Right: Plot of k_{obs} versus inhibitor concentration. Non-linear regression can be applied to determine k_{inact} and K_I. Adapted from [10]. k_{obs}: observed inactivation rate constant

1.3.4 *Case example: Grapefruit*

Grapefruit juice-drug interactions (GFJDIs) are the most extensively examined and characterized FDIs [9]. Grapefruit (*Citrus* × *paradisi, Rutaceae*) – a hybrid of pomelo (*Citrus maxima*) and sweet orange (*Citrus sinensis*) [55] – is classified as an inhibitor of CYP3A4 by the FDA [8]. The fruit contains furanocoumarins such as bergamottin and 6,7-dihydroxybergamottin as causative agents [56]. As mechanism-based inhibitors, these compounds covalently bind to the CYP3A4 apoprotein [53]. Here, covalent binding is mediated via the furan moiety of both furanocoumarins [11, 53]. As shown in Figure 1.5, the compounds undergo enzymatic metabolism, converting the furan moiety into reactive intermediates that covalently interact with CYP3A4 [57].
As the inhibition is irreversible and requires *de novo* synthesis of CYP3A4, an interaction does not only occur if CYP3A4 substrates are taken concomitantly with grapefruit (juice) but also if the drug is consumed several hours after the fruit [58]. GFJDI studies involving felodipine, simvastatin, and midazolam reported that an effect of grapefruit could be observed more than 24 h after drinking grapefruit juice [58–60], and that CYP3A4 activity was fully restored approximately three days after juice consumption [59, 60]. Interestingly, the inhibition predominantly affects intestinal CYP3A4 after a single consumption of grapefruit (juice), while hepatic CYP3A4 is affected only after regular consumption [21, 61]. Consequently, grapefruit mainly impacts the bioavailability of drugs, which makes CYP3A4 substrates such as felodipine – characterized by low oral bioavailability and high intestinal first-pass metabolism – particularly susceptible to interactions with grapefruit.

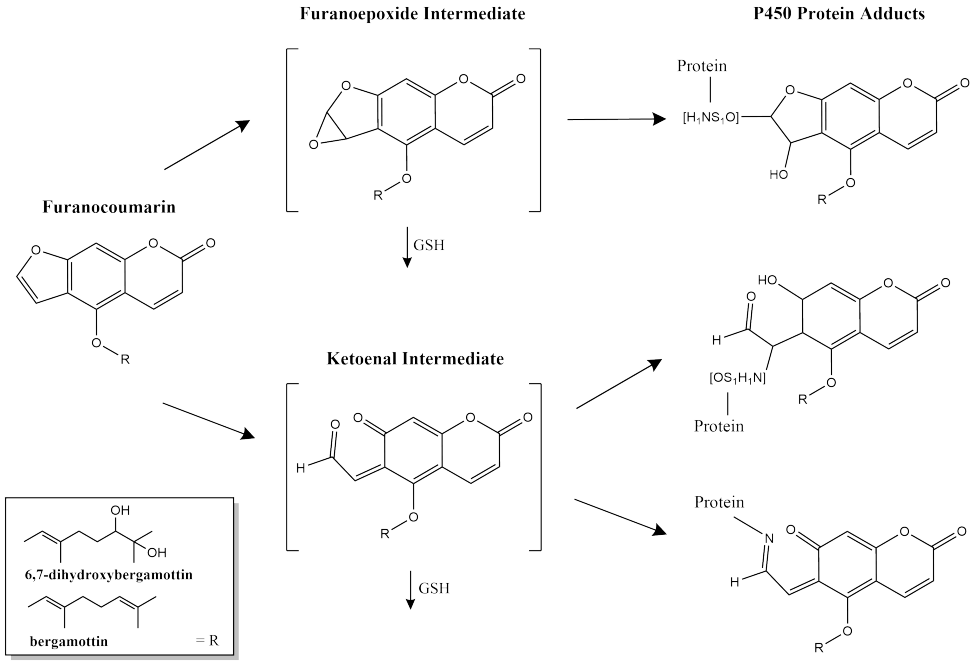

Figure 1.5: Bioactivation pathways of bergamottin and 6,7-dihydroxybergamottin to form protein adducts with CYP3A4. Adapted from [57].

1.4 PHYSIOLOGICALLY BASED PHARMACOKINETIC MODELING

1.4.1 *Concept*

According to the definition of the European Medicines Agency (EMA), PBPK modeling is a mathematical method aiming to mechanistically describe and predict drug concentrations in tissues and blood over time, taking into account the interplay between physiology and physico- and biochemical properties of the drug [62]. As a multi-compartmental modeling approach, whole-body PBPK modeling describes the human organism as a set of compartments, representing organs of the body, usually those relevant for the absorption, distribution, metabolism, and excretion (ADME) of drugs. In addition, each compartment can be further divided into subcompartments representing for instance blood plasma, red blood cells, intracellular and interstitial space. Compartments are interconnected by arterial and venous blood flow and ordinary differential equations are used to describe drug transfer between (sub-)compartments [63].
Thereby, this mechanistic modeling technique relies on an extensive number of parameters as it combines anatomical and physiological properties (system-dependent parameters) and characteristics of the drug (drug-dependent parameters). System-dependent parameters, usually provided in databases of available modeling software [64], characterize the physiological properties of the organism, for instance, tissue volume and blood flow. Drug-dependent parameters, usually derived from *in vitro* or *in vivo* measurements or *in silico* calculations, characterize physicochemical properties as well as

ADME-relevant processes, including metabolism or active transport. Additionally, measurements derived from clinical studies, such as drug plasma concentrations, are used to support model development and evaluation [65]. To establish virtual replicates of these clinical studies, information on study design, including dosing regimen and patient characteristics, is incorporated in the model simulations (study-dependent parameters).
Figure 1.6 illustrates the concept of PBPK modeling, relevant input parameters, model development, and model application.

1.4.2 *CYP-mediated drug-drug interaction modeling*

The main concept of CYP-mediated DDI modeling is illustrated in Figure 1.7. As relevant metabolic processes can be explicitly considered in a PBPK model, DDIs can be modeled by combining two or more PBPK models of verified perpetrator and victim drugs developed within the same modeling framework into one simulation and integrating all relevant inhibiting or inducing effects of the perpetrator drug on metabolizing enzymes [7]. This mechanistic implementation of DDIs in PBPK modeling relies on extensive knowledge of the mechanisms underlying the DDI and sufficient parametrization of the involved processes. Respective information and parameters are usually derived from *in vitro* experiments.
Mechanism-based inhibition and induction both affect enzyme abundances, and the recovery requires resynthesis of the inactivated enzyme or degradation of the overexpressed enzyme, respectively. In both cases, mechanistic modeling has to take enzyme turnover into account, which requires knowledge of the initial enzyme concentration as well as the enzyme half-life (for liver and intestine) [66]. These parameters can be derived from the literature or the protein expression databases of modeling software like PK-Sim® [66]. Respective parameters enable the calculation of enzyme turnover and changes in enzyme concentrations during the administration of a perpetrator as well as restoration of the "steady-state" concentration after the elimination of the perpetrator.
DDIs are dynamic processes *in vivo*, as plasma and tissue concentrations of the perpetrator vary over time [67]. For the time-dependent mechanism-based inhibition and induction, the variation in CYP concentration over time adds another layer of complexity. Due to their mechanistic nature, PBPK models are capable of quantitatively describing changes in perpetrator and victim concentrations over time in plasma and tissues expressing the enzyme. At the same time, PBPK modeling takes changes in CYP levels into account. Therefore, PBPK modeling emerges as a powerful technique to quantitatively predict the effect magnitude of pharmacokinetic interactions [7] and to predict the outcome of various DDI scenarios involving for instance different administration regimens of the perpetrator and the victim drug.
Therefore, mechanistic modeling facilitates (1) an enhanced understanding of DDIs by examining the contribution of each pathway to the overall effect;

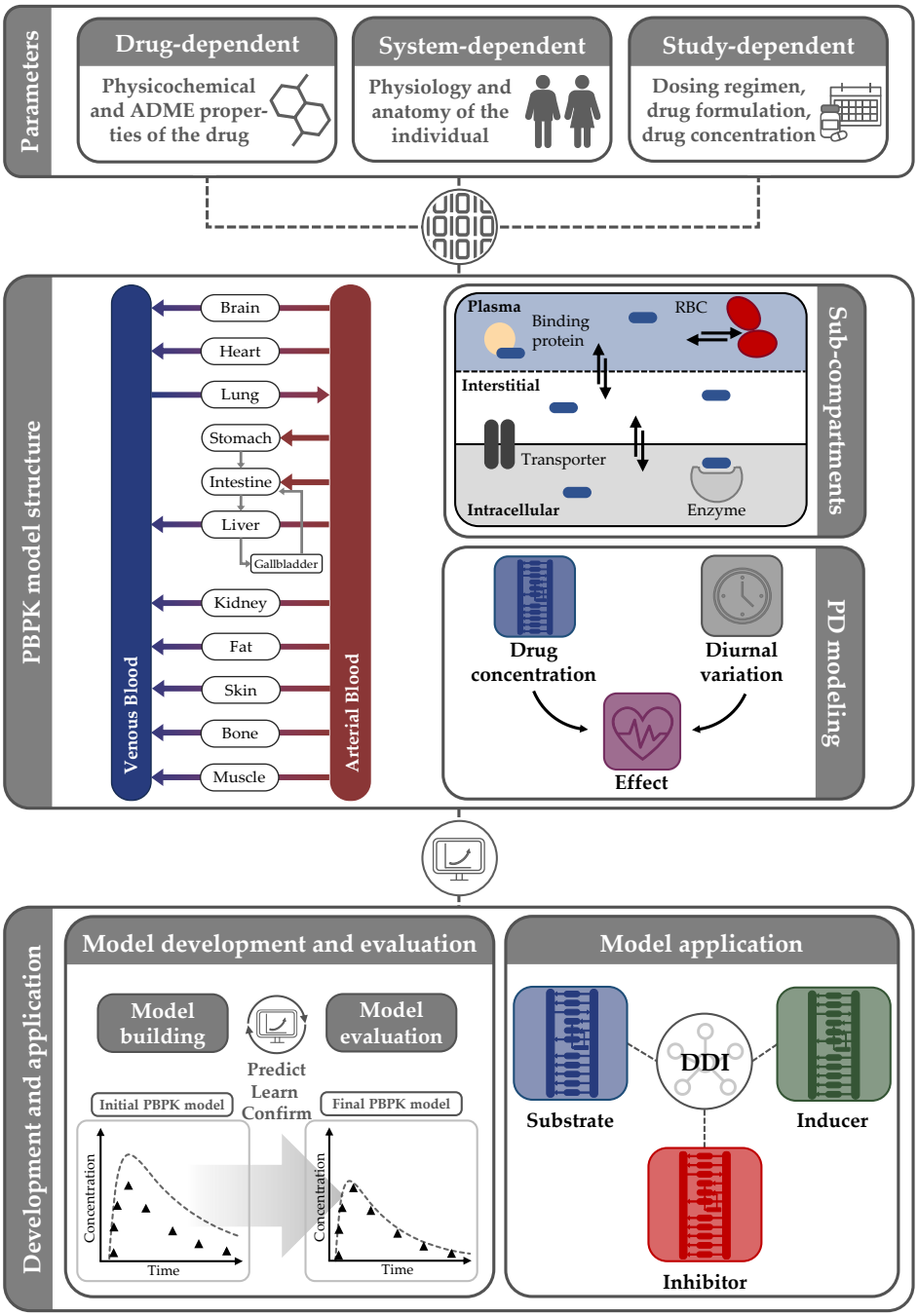

Figure 1.6: Concept of PBPK modeling. The model requires input of system-, drug- and clinical study-dependent parameters. In this multi-compartmental modeling approach, compartments represent organs of the body and are connected via arterial and venous blood flow. Each compartment is further divided into sub-compartments. The model is developed and evaluated in an iterative predict-learn-confirm cycle and upon successful evaluation it can be coupled with other PBPK models for DDI modeling.

(2) prediction of untested DDIs; and (3) hypothesis generation when the observed effect cannot be explained solely by the assumed mechanisms of

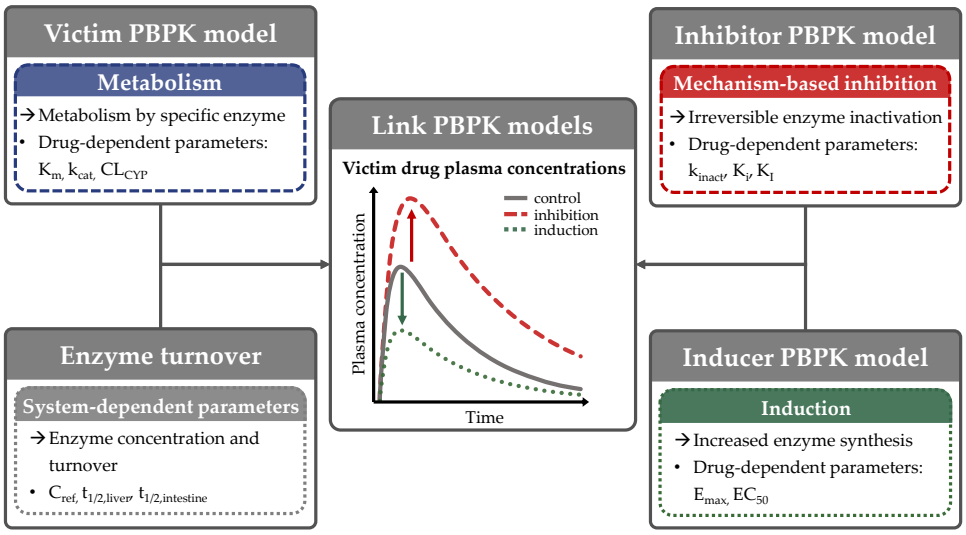

Figure 1.7: Concept of DDI modeling. Evaluated victim drug and perpetrator drug PBPK models are linked by implementing relevant parameters describing the mechanism-based inhibition or induction. CL_{CYP}: cytochrome P450 mediated enzymatic clearance, C_{ref}: enzyme reference concentration, EC_{50}: concentration necessary to reach 50% of the maximal induction, E_{max}: maximum induction effect, K_i: dissociation constant of the enzyme-inhibitor complex, k_{cat}: catalytic rate constant, K_I: concentration necessary for half-maximal inactivation, k_{inact}: maximum inactivation rate constant, K_m: Michaelis-Menten constant, $t_{1/2}$: enzyme half-life in liver and intestine.

interaction. This was for example accomplished within a PBPK DDI analysis of the CYP3A4 and P-glycoprotein (P-gp) perpetrator ketoconazole which led to the conclusion that the prolonged DDI effect is likely not only caused by ketoconazole but also by its metabolites [68]. DDI modeling is also an important means of model verification. The accurate prediction of DDIs from available clinical studies indicates that drug concentrations at the site(s) of interaction as well as the contribution of specific enzymes to overall drug metabolism and disposition are adequately described by the PBPK model [1].

1.4.3 *PBPK modeling in drug research and development*

Model-informed drug discovery and development (MID3) involves the application of computational models to support decision-making throughout drug development and regulatory review [69]. Over the last two decades, PBPK modeling has gained interest, which is underlined by the increasing number of available publications [64] as well as submissions to regulatory agencies [13, 70, 71], as illustrated in Figure 1.8. This increasing interest can be explained by the increasing computational power, necessary to compute these highly complex mathematical models, as well as the availability of user-friendly and open-source software tools such as PK-Sim® [64]. Moreover,

regulatory agencies have recognized and valued the potential of PBPK modeling and describe its potential application for MID3 in several guidelines [6, 7, 14, 62]. According to the corresponding guidelines, PBPK modeling can be applied to guide *in vitro* to *in vivo* extrapolation or predict DDIs that were previously not investigated in clinical studies. By incorporating information from various *in vitro* and *in vivo* experiments, the modeling technique can also be applied to predict complex DDIs involving multiple mechanisms [6]. Commonly, in regulatory decision-making, PBPK models are used to investigate and evaluate enzyme-mediated DDIs [13, 70, 71], with a significant focus on DDIs involving CYP3A4 [12]. Here, PBPK models support the planning of further clinical trials or are used to replace dedicated clinical trials to guide drug labeling [12, 72].

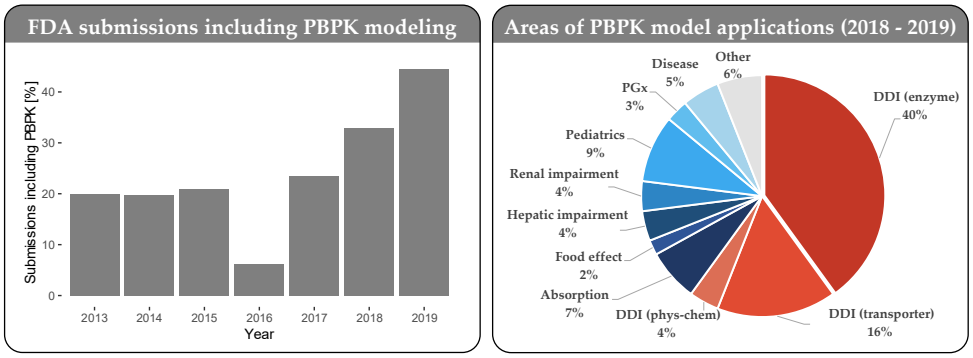

Figure 1.8: The role of PBPK modeling in FDA submissions. Number of submissions including PBPK modeling analyses (left) and areas of PBPK model applications (right). Adapted from [13]. DDI: drug-drug interaction, PBPK: physiologically based pharmacokinetic, PGx: pharmacogenetics, phys-chem: physico-chemical.

Overall, PBPK models hold great potential to support pharmaceutical research and to be applied in clinical practice. The modular and mechanistic quantitative modeling approach allows the investigation of a broad spectrum of scenarios in various research areas.

2

OBJECTIVES

The overall objective of the presented thesis was the application of PBPK modeling to comprehensively investigate complex and time-dependent DDIs and FDIs involving CYP3A4. This work was performed within the scope of the project OSMOSES (Open-Source MOdellierungs- und Simulationsplattform mit automatisierter Qualitätskontrolle für die Entwicklung komplexer Systemmodelle in den Lebenswissenschaften), funded by the Federal Ministry of Education and Research [73]. One major objective of this project was the development of whole-body PBPK models that serve as templates for the users of the PBPK modeling software PK-Sim®. The models were developed and evaluated to be applied for DDI and FDI modeling, for instance within the context of MID3. This was accomplished by a careful selection of compounds, guided by the FDA's table of substrates, inhibitors, and inducers [8, 50], including (I) carbamazepine as a clinical index inducer of CYP3A4 [50]; (II) felodipine as a sensitive CYP3A4 substrate [8] and (III) grapefruit (juice) as a moderate to strong mechanism-based CYP3A4 inhibitor [8]. Each compound possesses distinct properties that enable the investigation of unique DDI and FDI scenarios. PBPK modeling of respective compounds and investigation of DDI and FDI scenarios were realized within projects I-III:

2.1 PROJECT I - PHYSIOLOGICALLY BASED PHARMACOKINETIC MODELING OF CARBAMAZEPINE

Carbamazepine was selected for PBPK modeling as the FDA classifies the drug as a clinical index inducer of CYP3A4 [50]. In addition, carbamazepine is a substrate of CYP3A4 as well as a substrate and inducer of CYP2B6 [8, 43, 44]. This complexity makes it susceptible to DDIs as both perpetrator and victim drug across different enzymatic pathways. In Project I, a parent-metabolite PBPK model of carbamazepine and carbamazepine-10,11-epoxide as main metabolite was developed. The overall objectives of this PBPK modeling analysis were (i) to sufficiently describe carbamazepine autoinduction and (ii) to investigate the DDI potential of carbamazepine as CYP3A4 and CYP2B6 inducer and substrate within a PBPK DDI network.

2.2 PROJECT II - PHYSIOLOGICALLY BASED PHARMACOKINETIC AND PHARMACODYNAMIC MODELING OF FELODIPINE

Felodipine was selected for PBPK modeling as the FDA classifies the drug as a sensitive substrate of CYP3A4 [8] and it has been extensively applied as a victim drug for the investigation of GFJDIs [23]. In Project II, a parent-

metabolite PBPK/PD model of felodipine and dehydrofelodipine has been developed. The overall objectives of this PBPK modeling analysis were (i) to describe the PK of both compounds, taking into account the contribution of intestinal and hepatic CYP3A4, (ii) to describe the concentration-effect relationship of felodipine plasma concentration and diastolic blood pressure and heart rate and (iii) to sufficiently describe and predict DDIs with felodipine as CYP3A4 victim drug to subsequently apply the model to support the development of a GFJDI PBPK model in Project III.

2.3 PROJECT III - PHYSIOLOGICALLY BASED PHARMACOKINETIC MODELING OF GRAPEFRUIT JUICE AND ITS INTERACTION POTENTIAL

Grapefruit was selected for PBPK modeling as grapefruit juice is classified by the FDA as a moderate to strong inhibitor of CYP3A4 [8]. FDIs with grapefruit juice have been investigated in various GFJDI studies [9, 23]. However, the variable concentration of its ingredients and the time-dependent nature of its inhibition complicate the assessment of its impact on drug PK. In Project III, a GFJDI PBPK model has been established to investigate the potential of PBPK modeling to describe FDIs. The overall objectives of the PBPK modeling analysis were (i) to develop PBPK models of the causative ingredients bergamottin and 6,7-dihydroxybergamottin (ii) to describe and predict GFJDIs with various CYP3A4 substrates as well as (iii) to investigate different GFJDI scenarios.

3 METHODS

3.1 SOFTWARE

Concentration-time and effect-time profiles collected from the literature were digitalized using Engauge Digitizer Version 12.1 (M. Mitchell [74], 2020) or Get Data Graph Digitizer Version 2.26.0.20 (S. Fedorov, http://www.getdata-graphdigitizer.com). All models were developed using PK-Sim® and MoBi® (Open Systems Pharmacology, version 9.1 or higher, released under the GNU General Public License version 2 (GPLv2) by the Open Systems Pharmacology community, www.open-systems-pharmacology.org). Parameter optimizations (Monte Carlo and Levenberg-Marquardt algorithms) as well as sensitivity analyses were conducted within PK-Sim®. R (version 3.6.2 or higher, the R Foundation for Statistical Computing, Vienna, Austria) was used for performance evaluations, calculation of pharmacokinetic parameters, and generation of plots.

3.2 PHYSIOLOGICALLY BASED PHARMACOKINETIC MODELING

All PBPK models that were developed within Projects I - III were established as described in the following section.

3.2.1 *PBPK model development*

LITERATURE SEARCH: PBPK modeling starts by collecting information on the drug of interest covering its relevant drug-dependent parameters. Clinical studies, sourced from the literature, provide concentration-time profiles of the drug (and its metabolite) in plasma and other matrices, as well as data on drug excretion to urine and feces. Additionally, information on drug dosing regimens and the demographic characteristics of study participants were extracted from the respective studies (study-dependent parameters).
CLINICAL STUDY DATA: Data from clinical studies are digitized, analyzed, and assigned to a training and a test dataset for model building and evaluation, respectively. Here, the selection of the training dataset should be in accordance with the following criteria whenever possible: (1) intravenous and oral administration routes are considered, (2) studies cover a broad dosing range, (3) parent and metabolite data are available, and (4) studies were performed with healthy participants not taking any co-medication.
SIMULATIONS AND METABOLIC PROCESSES: Subsequently, simulations representing virtual replicates of each clinical study are set up. Here, a typical individual representing the study population is created based on

the mean or mode of reported demographics (e.g., age, height, weight, sex, ethnicity). System-dependent parameters are calculated based on the demographics according to the PK-Sim® population databases [66]. In addition, organ expressions of relevant metabolizing enzymes are defined according to the PK-Sim® expression database [75].
Metabolism by relevant enzymes is described according to current literature with first order (Equation 3.1) or Michaelis-Menten kinetics (Equation 3.2).

$$v = CL_{spec} \cdot [E] \cdot [S] \tag{3.1}$$

with v = reaction velocity, CL_{spec} = specific enzymatic clearance, [S] = substrate concentration and [E] = enzyme concentration.

$$v = \frac{v_{max} \cdot [S]}{K_m + [S]} = \frac{k_{cat} \cdot [E] \cdot [S]}{K_m + [S]} \tag{3.2}$$

with v = reaction velocity, v_{max} = maximum reaction velocity, K_m = Michaelis-Menten constant, [S] = substrate concentration, k_{cat} = catalytic rate constant and [E] = enzyme concentration.

PARAMETER OPTIMIZATION AND REFINEMENT: An initial model is established and parametrized based on the physicochemical information and clearance pathways identified in the literature. The parameter identification tool implemented in PK-Sim® is used to identify appropriate quantitative structure-activity relationship methods for the mathematical description of partition coefficients and cellular permeabilities as well as to estimate model input parameter values that cannot be informed from the literature. Here, the model is fitted to the observed data of the training dataset. Model predictions are subsequently compared to observed data from clinical studies, and in iterative predict-learn-confirm cycles, the model is further refined.

3.2.2 *Implementation of PD effects*

The concentration-effect relationship of felodipine plasma concentration and diastolic blood pressure and heart rate was described by an E_{max} model according to Equation 3.3.

$$E(t) = \frac{E_{max} \cdot C(t)^h}{EC_{50}^h + C(t)^h} \tag{3.3}$$

with E_{max} = maximum effect of felodipine on heart rate or diastolic blood pressure, EC_{50} = concentration necessary to achieve 50% of E_{max}, h = Hill coefficient, C = felodipine plasma concentration, t = time, E = felodipine-effect.

In addition, blood pressure and heart rate encompass natural diurnal variation, which was implemented using published models by Chae et al. [76] and

Lott et al. [77], respectively. Subsequently, changes in PD were described taking into account felodipine-mediated effects and diurnal variation according to Equation 3.4.

$$PD(t) = PD_{mean} \cdot (1 + circ_{PD}(t)) - E(t) \tag{3.4}$$

with PD = pharmacodynamic measurement (heart rate or diastolic blood pressure), PD_{mean} = mean heart rate or diastolic blood pressure over 24 h, t = time, $circ_{PD}$ = circadian rhythm of blood pressure at t and E(t) = felodipine-effect at t.

The implementation of PD effects is described in more detail by Fuhr et al. [2].

3.2.3 *Mathematical implementation of drug-drug and food-drug interactions*

As described in Section 1.4.2, DDIs can be modeled by coupling two distinct PBPK models and implementing all relevant enzyme inhibition or induction processes. The following sections describe the implementation of CYP induction by carbamazepine and mechanism-based CYP inhibition by grapefruit ingredients bergamottin and 6,7-dihydroxybergamottin.

3.2.3.1 *Induction by carbamazepine*

Due to interactions with transcription factors, carbamazepine increases the apparent enzyme synthesis rate ($R_{syn,\,app}$, Equation 3.5). Accordingly, the enzyme turnover during the administration of carbamazepine can be described by Equation 3.6, and the reaction velocity can be described by Equation 3.2 [66]:

$$R_{syn,app} = R_{syn} \cdot \left(1 + \frac{E_{max} \cdot [Ind]}{EC_{50} + [Ind]}\right) \tag{3.5}$$

$$\frac{dE(t)}{dt} = R_{syn,app} - k_{deg} \cdot E(t) \tag{3.6}$$

with $R_{syn,app}$ = enzyme synthesis rate in the presence of inducer, R_{syn} = enzyme synthesis rate, E_{max} = maximum induction effect, [Ind] = free inducer concentration, EC_{50} = concentration necessary to reach 50% of the maximal induction, E(t) = enzyme concentration and k_{deg} = enzyme degradation rate constant.

3.2.3.2 *Mechanism-based inactivation by grapefruit*

PBPK MODELING OF GRAPEFRUIT: To mechanistically implement GFJDIs, bergamottin and 6,7-dihydroxybergamottin were identified as the main causative ingredients based on their inhibitory activity assessed *in vitro* as

well as their concentration in grapefruit juice. Consequently, PBPK models of respective ingredients were established according to the methods described in Section 3.2.1, taking their physicochemical properties and ADME-relevant processes into account. The consumption of GFJ was then simulated as ingestion of bergamottin and 6,7-dihydroxybergamottin. Hereby, the ingested amount of bergamottin and 6,7-dihydroxybergamottin was calculated based on the ingested volume and the concentration of each compound in the juice. If concentrations were not determined in the simulated clinical study, mean concentrations had to be assumed. Therefore, concentration measurements were gathered from the literature, and mean concentrations of bergamottin and 6,7-dihydroxybergamottin were calculated stratified by juice preparation (canned juice or juice prepared from frozen concentrate) [3].

IMPLEMENTATION OF THE MECHANISM-BASED INACTIVATION: By irreversibly binding to CYP3A4, the grapefruit ingredients bergamottin and 6,7-dihydroxybergamottin increase the enzyme degradation rate constant (k_{deg}), which can be described according to Equation 3.7. Accordingly, the enzyme turnover during the administration of grapefruit juice can be described by Equation 3.8. Mechanism-based inhibitors also competitively inhibit the enzyme. This is reflected in the PBPK model by substituting the Michaelis-Menten constant (K_m) in Equation 3.2 by $K_{m,app}$ (Equation 3.9). [66].

$$k_{deg,app} = k_{deg} + \left(\frac{k_{inact} \cdot [Inh]}{K_I + [Inh]} \right) \tag{3.7}$$

$$\frac{dE(t)}{dt} = R_{syn} - k_{deg,app} \cdot E(t) \tag{3.8}$$

with $k_{deg,app}$ = enzyme degradation rate constant in the presence of the mechanism-based inactivator, k_{deg} = enzyme degradation rate constant, k_{inact} = maximum inactivation rate constant, [Inh] = free inhibitor concentration, K_I = concentration necessary for half-maximal inactivation, E(t) = enzyme concentration and R_{syn} = enzyme synthesis rate.

$$K_{m,app} = K_m \cdot (1 + \frac{[Inh]}{K_i}) \tag{3.9}$$

with $K_{m,app}$ = Michaelis-Menten constant in the presence of the mechanism-based inactivator, K_m = Michaelis-Menten constant, [Inh] = free inhibitor concentration, and K_i = dissociation constant of the enzyme-inhibitor complex.

3.2.4 *Model evaluation*

The performance of the PBPK models is evaluated graphically according to the following methods:

1. Simulated (plasma) concentration-time profiles are compared graphically to respective observed profiles.
2. Predicted concentration values are compared to corresponding observed measurements in goodness-of-fit plots.
3. Predicted and observed area under the (plasma) concentration-time curve calculated from the time of drug administration to the time of the last concentration measurement (AUC_{last}) and maximum (plasma) concentration (C_{max}) values are compared in goodness-of-fit plots.

Furthermore, the following quantitative measures are assessed to evaluate model performance:

1. Mean relative deviations (MRD) of predicted concentration values are calculated according to Equation 3.10.
2. Geometric mean fold error (GMFE) of predicted AUC_{last} and C_{max} values are calculated according to Equation 3.11.

$$MRD = 10^x, \text{ with } x = \sqrt{\frac{1}{m}\sum_{i=1}^{m}(\log_{10} c_{pred,i} - \log_{10} c_{obs,i})^2} \tag{3.10}$$

with $c_{pred,i}$ = predicted plasma concentration, $c_{obs,i}$ = corresponding observed plasma concentration, and m = number of observed values.

$$GMFE = 10^x, \text{ with } x = \frac{1}{n}\sum_{i=1}^{n}|\log_{10}(\frac{PK_{pred,i}}{PK_{obs,i}})| \tag{3.11}$$

with $PK_{pred,i}$ = predicted AUC_{last} or C_{max} value, $PK_{obs,i}$ = corresponding observed AUC_{last} or C_{max} value and n = number of studies.

3.2.4.1 *Drug-drug interaction model evaluation*

Modeled DDIs are evaluated by the following graphical and quantitative methods:

1. Predicted and observed plasma concentration-time profiles of the victim drug before and during perpetrator co-administration are compared graphically.
2. Predicted and observed DDI AUC_{last} and C_{max} ratios are calculated according to Equation 3.12 and compared in goodness-of-fit plots.
3. GMFE of the predicted DDI AUC_{last} and C_{max} ratios are calculated according to Equation 3.11

$$\text{DDI } PK_{param,victim} \text{ ratio} = \frac{PK_{param,victim} \text{ during DDI}}{PK_{param,victim} \text{ control}} \tag{3.12}$$

with $PK_{param,victim}$ = AUC_{last} or C_{max} value of the victim drug

4 RESULTS

4.1 PROJECT I - PHYSIOLOGICALLY BASED PHARMACOKINETIC MODELING OF CARBAMAZEPINE

PUBLICATION

Fuhr, L.M.; Marok, F.Z.; Hanke, N.; Selzer, D.; Lehr, T. Pharmacokinetics of the CYP3A4 and CYP2B6 Inducer Carbamazepine and Its Drug-Drug Interaction Potential: A Physiologically Based Pharmacokinetic Modeling Approach. Pharmaceutics. 2021. 13(2):270, doi: 10.3390/pharmaceutics13020270.

SUPPLEMENTARY MATERIALS

The supplementary materials to this publication are provided on the accompanying USB storage device and are available online via: https://www.mdpi.com/1999-4923/13/2/270/s1

COPYRIGHT

AUTHOR CONTRIBUTIONS

Laura Fuhr	Conceptualization, Investigation, Visualization, Writing–Original Draft, Writing–Review & Editing
Fatima Marok	Conceptualization, Investigation, Writing–Review & Editing
Nina Hanke	Conceptualization, Investigation, Writing–Review & Editing
Dominik Selzer	Conceptualization, Investigation, Writing–Review & Editing
Thorsten Lehr	Conceptualization, Funding Acquisition, Investigation, Writing–Review & Editing

pharmaceutics

MDPI

Article

Pharmacokinetics of the CYP3A4 and CYP2B6 Inducer Carbamazepine and Its Drug–Drug Interaction Potential: A Physiologically Based Pharmacokinetic Modeling Approach

Laura Maria Fuhr, Fatima Zahra Marok, Nina Hanke, Dominik Selzer and Thorsten Lehr *

Clinical Pharmacy, Saarland University, 66123 Saarbrücken, Germany; laura.fuhr@uni-saarland.de (L.M.F.); fatima.marok@uni-saarland.de (F.Z.M.); n.hanke@mx.uni-saarland.de (N.H.); dominik.selzer@uni-saarland.de (D.S.)

* Correspondence: thorsten.lehr@mx.uni-saarland.de; Tel.: +49-681-302-70255

Abstract: The anticonvulsant carbamazepine is frequently used in the long-term therapy of epilepsy and is a known substrate and inducer of cytochrome P450 (CYP) 3A4 and CYP2B6. Carbamazepine induces the metabolism of various drugs (including its own); on the other hand, its metabolism can be affected by various CYP inhibitors and inducers. The aim of this work was to develop a physiologically based pharmacokinetic (PBPK) parent−metabolite model of carbamazepine and its metabolite carbamazepine-10,11-epoxide, including carbamazepine autoinduction, to be applied for drug–drug interaction (DDI) prediction. The model was developed in PK-Sim, using a total of 92 plasma concentration−time profiles (dosing range 50–800 mg), as well as fractions excreted unchanged in urine measurements. The carbamazepine model applies metabolism by CYP3A4 and CYP2C8 to produce carbamazepine-10,11-epoxide, metabolism by CYP2B6 and UDP-glucuronosyltransferase (UGT) 2B7 and glomerular filtration. The carbamazepine-10,11-epoxide model applies metabolism by epoxide hydroxylase 1 (EPHX1) and glomerular filtration. Good DDI performance was demonstrated by the prediction of carbamazepine DDIs with alprazolam, bupropion, erythromycin, efavirenz and simvastatin, where 14/15 DDI AUC_{last} ratios and 11/15 DDI C_{max} ratios were within the prediction success limits proposed by Guest et al. The thoroughly evaluated model will be freely available in the Open Systems Pharmacology model repository.

Keywords: physiologically based pharmacokinetic (PBPK) modeling; carbamazepine; carbamazepine-10,11-epoxide; drug–drug interactions (DDIs); cytochrome P450 3A4 (CYP3A4); cytochrome P450 2B6 (CYP2B6); induction

Citation: Fuhr, L.M.; Marok, F.Z.; Hanke, N.; Selzer, D.; Lehr, T. Pharmacokinetics of the CYP3A4 and CYP2B6 Inducer Carbamazepine and Its Drug–Drug Interaction Potential: A Physiologically Based Pharmacokinetic Modeling Approach. *Pharmaceutics* **2021**, *13*, 270. https://doi.org/10.3390/pharmaceutics13020270

Academic Editor: Beom Soo Shin

Received: 22 December 2020
Accepted: 11 February 2021
Published: 17 February 2021

1. Introduction

The anticonvulsant drug carbamazepine is known to induce multiple metabolizing enzymes. It is classified by the U.S. Food and Drug Administration (FDA) as a strong inducer (area under the plasma concentration−time curve (AUC) decrease of victim drug $\geq$ 80%) of cytochromes P450 (CYP) 3A4 and CYP2B6 [1]. Furthermore, carbamazepine itself is also metabolized by the respective enzymes [2], with metabolism via CYP3A4 to the pharmacologically active metabolite carbamazepine-10,11-epoxide as one of the main routes of elimination [3]. As a result, carbamazepine induces its own—as well as other drugs'—metabolism during multiple dose administration. Additionally, carbamazepine plasma levels can also be affected by enzyme inhibitors and inducers. Therefore, the coadministration of carbamazepine with other drugs, i.e., sensitive CYP3A4 or CYP2B6 substrates or perpetrators, can result in complex interaction patterns. Elevated carbamazepine plasma concentrations, caused by CYP3A4 inhibition, as well as elevated carbamazepine-10,11-epoxide plasma concentrations, caused by CYP3A4 induction, are associated with carbamazepine-related adverse events, including nausea, vomiting, drowsiness or mental confusion [4–6]. Additionally, as a strong enzyme inducer, carbamazepine

significantly reduces plasma concentrations of coadministered victim drugs. For the CYP3A4 substrate simvastatin and the CYP2B6 substrate bupropion, AUC decreases of 82% and 90% were observed if coadministered with carbamazepine [7,8], risking loss of efficacy of those compounds.

As CYP3A4 is highly expressed in liver and intestine and metabolizes up to 50% of all marketed drugs independent of the drug class [9], interactions with a broad spectrum of substances are possible, for example with antiviral drugs (efavirenz) or antibiotics (erythromycin). The drug–drug interaction (DDI) with efavirenz illustrates the complexity of carbamazepine DDIs, as both compounds are CYP3A4 and CYP2B6 substrates as well as inducers and therefore, mutually induce each other's metabolism [10].

As carbamazepine plays a crucial role in the treatment of epilepsy (recommended as first line treatment option by Cochrane [11] and included in the World Health Organization (WHO) Model List of Essential Medicines [12]), surveillance and examination of its DDI potential is important to ensure a safe drug therapy. The FDA recommends the use of carbamazepine as CYP3A4 and CYP2B6 inducer in clinical drug–drug interaction studies and it was applied in recent clinical trials, for example, with etonorgestrel, basimglurant or bitopertin [13]. In this case, the physiologically based pharmacokinetic (PBPK) modeling technique can come in as a helpful tool. With PBPK modeling, the pharmacokinetics (PK) of carbamazepine can be quantitatively described and the model can be coupled with other PBPK models to dynamically describe and predict DDIs. This modeling technique is recognized and recommended by the regulatory agencies FDA and the European Medicines Agency (EMA) [14,15]. More than 60% of PBPK models submitted to the FDA investigate DDIs. Several published studies investigate the DDI potential of carbamazepine using a PBPK modeling approach [13,16–19]. While carbamazepine is typically used as an inducer to investigate the interaction with a substrate, our study aims to provide a comprehensive overview on the pharmacokinetics of carbamazepine and its DDIs, investigating carbamazepine not only as inducer but also as victim drug.

Hence, the aims of the current study were (1) to develop a parent−metabolite PBPK model of carbamazepine and its main metabolite carbamazepine-10,11-epoxide, with implementation of carbamazepine autoinduction and (2) to apply the developed model for DDI predictions with carbamazepine as a perpetrator and victim drug.

The thoroughly evaluated model will be publicly available in the Open Systems Pharmacology (OSP) repository and can be applied to investigate and predict CYP3A4 and CYP2B6 DDIs. The Supplementary Materials to this paper will serve as a reference manual with detailed documentation of the model development and performance.

2. Materials and Methods

2.1. Software

The PBPK model was developed with PK-Sim and MoBi (Open Systems Pharmacology Suite 9.1, released under the GNU General Public License version 2 (GPLv2) license by the Open Systems Pharmacology community, www.open-systems-pharmacology.org, 2020). Parameter optimization (Monte-Carlo and Levenberg-Marquardt algorithms) and sensitivity analysis were performed with PK-Sim. Clinical study data from literature were digitized with Engauge Digitizer Version 10.12 (M. Mitchell [20], 2019) according to guidelines by Wojtyniak et al. [21]. Pharmacokinetic parameters were calculated and plots were created with R 3.6.2 (The R Foundation for Statistical Computing, Vienna, Austria, 2019).

2.2. Clinical Data

Plasma and saliva concentration−time profiles and fraction excreted (fe) unchanged in urine measurements of carbamazepine and carbamazepine-10,11-epoxide were collected and digitized from published clinical studies. Studies were selected to cover the administration of carbamazepine (1) over a broad dosing range, (2) in single- and multiple-dosing regimens and (3) for different carbamazepine formulations. Clinical studies investigating

the oral administration of the metabolite carbamazepine-10,11-epoxide were also included. Studies were preferred if they were conducted with healthy participants without comedication and if frequent as well as late sampling data was provided.

The digitized clinical studies were split into a model building (training) dataset and a model evaluation (test) dataset. The studies for the training dataset were selected to inform the implemented pharmacokinetic processes by covering a broad dosing range, single- and multiple-dose studies, the application of different carbamazepine formulations, and information on saliva concentrations and urinary excretion of carbamazepine as well as plasma concentrations and urinary excretion of the metabolite carbamazepine-10,11-epoxide. An overview of all utilized clinical studies and their assignment to training or test dataset is documented in Table S1 of the Supplementary Materials.

2.3. Model Building

The modeling process was initiated with a literature search for physicochemical parameters and information on absorption, distribution, metabolism and excretion (ADME) processes. During model development, different reported parameter values and the impact of different ADME processes were tested. An overview of the ADME processes of carbamazepine is provided in the Supplementary Materials and corresponding literature parameters are listed in Table 1.

For simulations, virtual mean individuals were generated based on age, sex, ethnicity, body weight, and height as reported in the respective study protocols. If no information was provided, a 30-year-old, male, European individual with mean body weight and height characteristics from the PK-Sim population database was created. The PK-Sim expression database [22] was used to define the relative expression of relevant metabolizing enzymes in the different organs of the body. Model parameters that could not be described using information from literature were estimated by fitting the model to the observed data of the whole training dataset.

An overview of essential parameters needed to build a PBPK model, the whole-body PBPK model structure and implemented elimination processes are illustrated in Figure 1.

Elimination processes for carbamazepine include (1) metabolism by CYP3A4 and CYP2C8 to carbamazepine-10,11-epoxide, (2) metabolism by CYP3A4, CYP2B6 and UGT2B7 as well as hepatic clearance to cover further metabolic processes, (3) autoinduction of CYP3A4 and CYP2B6 and (4) passive glomerular filtration with tubular reabsorption [23]. The carbamazepine-10,11-epoxide metabolite model includes (1) metabolism by epoxide hydroxylase 1 (EPHX1) [24,25] and (2) renal elimination via passive glomerular filtration with tubular reabsorption.

Development of the parent−metabolite PBPK model was accomplished in a stepwise procedure. First, a model for the metabolite carbamazepine-10,11-epoxide was developed, based on three clinical studies that administered carbamazepine-10,11-epoxide. Metabolism by EPHX1 was implemented as a first-order clearance process according to Equation (1):

$$v = [E] * CL_{spec} * S \quad (1)$$

where [E] = enzyme concentration, CL_{spec} = specific enzymatic clearance and S = substrate amount.

Passive glomerular filtration with reabsorption was described using a glomerular filtration rate (GFR) fraction < 1. The metabolite carbamazepine-10,11-epoxide model was subsequently combined with the parent carbamazepine model and the implemented parameter values were refined during development of the parent−metabolite model using the whole training dataset.

Metabolic pathways of carbamazepine were implemented using Michaelis−Menten kinetics, according to Equation (2):

$$v = \frac{[E] * k_{cat} * [S]}{K_m + [S]} \quad (2)$$

where [E] = enzyme concentration, k_{cat} = catalytic rate constant, [S] = substrate concentration and K_m = Michaelis−Menten constant.

Induction of CYP3A4, CYP2B6 and EPHX1 was implemented using a maximum effect (E_{max}) model, as described in the Supplementary Materials Section 1.5. To inform the optimization of CYP3A4 induction, the carbamazepine-alprazolam DDI study was added to the training dataset. Renal clearance of carbamazepine, consisting of passive glomerular filtration with tubular reabsorption, was modeled using an estimated GFR fraction < 1.

Oral dosage forms of carbamazepine in the modeled clinical studies include solutions, suspensions, immediate release tablets and extended release tablets or capsules. To simulate solutions and suspensions, carbamazepine was modeled as a dissolved drug. The dissolution kinetics of the other formulations were described using Weibull functions. Different parameters were estimated for fasted or fed state, as Levy et al. and McLean et al. observed an increased carbamazepine absorption for ingestion of different carbamazepine formulations with food [26,27].

2.4. PBPK Model Evaluation

Model performance was evaluated (1) by comparing the predicted plasma concentration−time profiles to observed profiles and (2) by comparing predicted plasma concentration values to the corresponding observed values in goodness-of-fit plots, as well as (3) by comparing predicted with observed area under the plasma concentration−time curve (AUC) and maximum plasma concentration (C_{max}) values. AUC values were calculated from the time of drug administration to the time of the last concentration measurement (AUC_{last}). Predictions were considered successful if they did not deviate more than 2-fold from observed values.

For a quantitative description of the model performance, the mean relative deviation (MRD) of predicted plasma concentrations and the geometric mean fold error (GMFE) of predicted AUC_{last} and C_{max} values were calculated as described in the Supplementary Materials. We considered MRD and GMFE values ≤ 2 as adequate model performance metrics.

2.5. DDI Modeling

In addition to the previously described methods for PBPK model evaluation, the carbamazepine model was challenged by prediction of DDIs, with carbamazepine as CYP3A4 and CYP2B6 victim or perpetrator drug.

Clinical DDI studies with erythromycin, alprazolam, simvastatin, bupropion and efavirenz were available and used for DDI modeling. The previously developed PBPK models of erythromycin, alprazolam and efavirenz were downloaded from the OSP repository on GitHub (https://github.com/Open-Systems-Pharmacology [28–30]). The bupropion [31] and simvastatin [32] models were developed in our working group.

The parameters describing the induction of CYP3A4 and CYP2B6 by carbamazepine were already introduced during carbamazepine model building, as the compound induces its own metabolism. The mathematical implementation of the induction processes is described in Section 1.5 in the Supplementary Materials. The carbamazepine-alprazolam DDI study was used in the training dataset to inform the parametrization of the carbamazepine CYP3A4 induction. All other DDIs were purely predictive.

The DDI performance of all models except the efavirenz model (CYP2B6) was evaluated previously [28–32]. Therefore, all relevant interaction parameters were already implemented in the models and adopted in this project. The mathematical implementation of (1) the mechanism-based CYP3A4 inhibition by erythromycin, (2) the induction of CYP3A4 by efavirenz, (3) the induction of CYP2B6 by efavirenz and (4) the competitive inhibition of CYP3A4 by simvastatin are described in the Supplementary Materials. The drug-dependent parameters and interaction parameters of the previously developed models applied for carbamazepine DDI predictions are reproduced in Tables S6, S12, S15, S18 and S21 in the Supplementary Materials.

The performance of the efavirenz model as a CYP2B6 substrate and inducer was evaluated prior to DDI modeling with carbamazepine, using bupropion and rifampicin as CYP2B6 substrate and inducer, respectively. Based on this evaluation, the efavirenz model parameters were readjusted, which is further described in the Supplementary Materials.

2.6. DDI Model Evaluation

The DDI performance was assessed by comparison of predicted to observed victim drug plasma concentration−time profiles without and with coadministration of the perpetrator drug. Additionally, predicted DDI AUC_{last} ratios (Equation (3)) and DDI C_{max} ratios (Equation (4)) were compared to the respective observed ratios.

$$\text{DDI } AUC_{last} \text{ ratio} = \frac{AUC_{last \text{ victim drug during coadministration}}}{AUC_{last \text{ victim drug alone}}} \quad (3)$$

$$\text{DDI } C_{max} \text{ ratio} = \frac{C_{max \text{ victim drug during coadministration}}}{C_{max \text{ victim drug alone}}} \quad (4)$$

As stated by Guest et al. [33], allowing up to 2-fold deviation of predicted to observed DDI ratios is not appropriate to assess the success of DDI predictions. For observed DDI ratios of 1 (no interaction), the 2-fold deviation would allow predicted DDI ratios between 0.5 (induction) and 2 (weak to moderate inhibition), which could overstate the DDI performance for weak interactions. Therefore, the prediction success limits proposed by Guest et al. [33] were used to evaluate the DDI predictions, accepting 20% deviation for observed DDI ratios approaching 1.

For each DDI, GMFEs of the predicted DDI AUC_{last} ratios and DDI C_{max} ratios were calculated, as described in the Supplementary Materials.

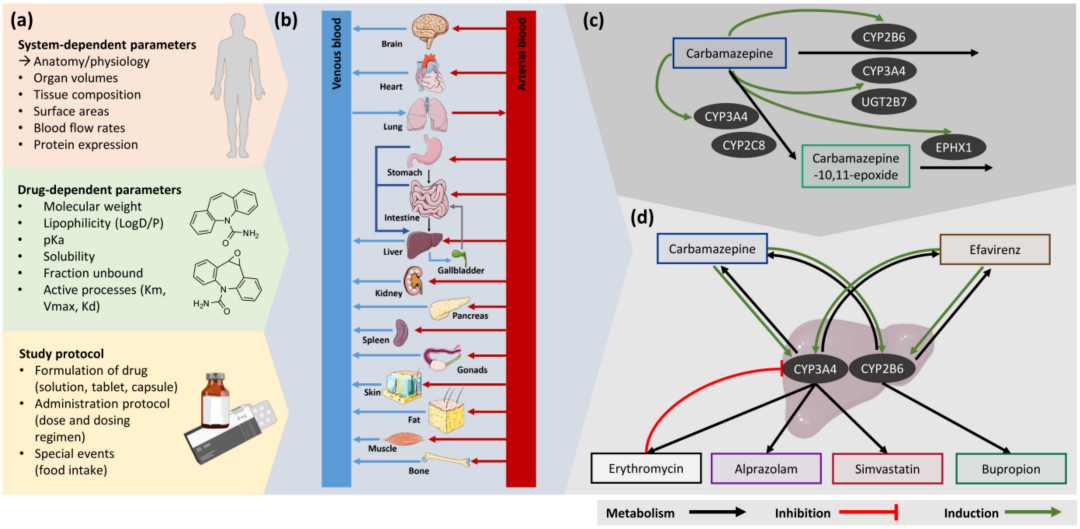

Figure 1. Schematic representation of the PBPK modeling workflow. (**a**) PBPK modeling requires system- and drug-dependent parameters, describing the anatomical and physiological characteristics of the individual and the properties of the simulated compound, respectively. Information on the study protocol of the described clinical study is relevant as well, e.g., formulation and administration of the simulated compound. (**b**) The PBPK model consists of multiple compartments, representing organs of the body, which are connected via the arterial and venous blood flows. (**c**) The final structure of the carbamazepine parent−metabolite PBPK model. (**d**) Overview of the modeled DDIs. Drawings by Servier, licensed under CC BY 3.0 [34]. CYP: cytochrome P450, EPHX1: epoxide hydroxylase 1, K_d: dissociation constant, K_m: Michaelis−Menten constant, pK_a: acid dissociation constant, UGT: UDP-glucuronosyltransferase, V_{max}: maximum velocity.

3. Results

3.1. PBPK Model Building

The parent−metabolite PBPK model of carbamazepine and carbamazepine-10,11-epoxide was built and evaluated using 40 clinical studies of oral administration, covering a broad dosing range (50–800 mg), different formulations as well as single- and multiple-dose regimens. In three of the included studies, the metabolite carbamazepine-10,11-epoxide was administered. In total, 58 and 34 plasma concentration−time profiles, and 4 and 5 fraction excreted unchanged in urine profiles, of carbamazepine and carbamazepine-10,11-epoxide were used, respectively. Additionally, 3 saliva concentration−time profiles were available for carbamazepine. All utilized clinical studies are listed in Table S1 of the Supplementary Materials.

Metabolism of carbamazepine by CYP2C8, CYP2B6 and UGT2B7 was described using K_m and k_{cat} values from literature. Two metabolic processes by CYP3A4 were implemented, as carbamazepine is metabolized by CYP3A4 to carbamazepine-10,11-epoxide as well as to hydroxylated metabolites [35]. For both reactions, K_m values were taken from literature, while k_{cat} values were optimized.

A half-maximal effective concentration EC_{50} = 20.0 µM (mean value calculated from literature values) was applied to describe the CYP3A4 induction. Although literature values for CYP2B6 EC_{50} were reported, the same EC_{50} = 20.0 µM was applied to describe the CYP2B6 induction, assuming that induction of both enzymes by carbamazepine is mediated via activation of the same nuclear receptor (constitutive androstane receptor [CAR]) [36]. The associated E_{max} values were optimized. Induction of EPHX1 was implemented as well, based on reports of an increase in carbamazepine-10,11-epoxide clearance during chronic carbamazepine treatment [37]. As no information on EC_{50} or E_{max} for EPHX1 was available, EC_{50} = 20.0 µM was used, assuming induction via activation of CAR as well, and E_{max} was optimized.

All implemented metabolic processes are summarized in Figure 1c. Drug-dependent parameters of carbamazepine and carbamazepine-10,11-epoxide are listed in Table 1, details on the distribution and localization of the implemented enzymes are provided in Table S45 of the Supplementary Materials.

Table 1. Drug-dependent parameters of carbamazepine and carbamazepine-10,11-epoxide.

Parameter	Unit	Model	Literature	Reference
Carbamazepine				
Molecular weight	g/mol	236.27 (Lit)	236.27	[38]
Lipophilicity	Log Units	2.00 (Fit)	1.45; 2.1; 2.45; 2.77	[38–40]
Solubility (FaHIF)	µg/mL	336 (Lit)	170; 283; 306; 336	[41–44]
Fraction unbound	%	25 (Lit)	21; 24; 25	[45–48]
K_m (CYP3A4) → CBZ-E	µM	248 (Lit)	119; 248; 442; 630	[2,49–51]
k_{cat} (CYP3A4) → CBZ-E	1/min	0.75 (Fit)	1.17; 1.7; 4.87; 5.3 [b]	[2,49–51]
K_m (CYP2C8) → CBZ-E	µM	757 (Lit)	757	[50]
k_{cat} (CYP2C8) → CBZ-E	1/min	0.67 (Lit)	0.67 [b]	[50]
K_m (CYP3A4)	µM	282 (Lit)	282	[35]
k_{cat} (CYP3A4)	1/min	0.20 (Fit)	0.16 [b]	[35]
K_m (CYP2B6)	µM	420 (Lit)	420	[35]
k_{cat} (CYP2B6)	1/min	0.43 (Lit)	0.43 [b]	[35]
K_m (UGT2B7)	µM	214 (Lit)	214	[52]
k_{cat} (UGT2B7)	1/min	9.53×10^{-3} (Lit)	9.53×10^{-3} [c]	[52]
CL_{hep}	1/min	0.02 (Fit)	-	-
GFR fraction	-	0.03 (Fit)	-	-
EC_{50} (CYP3A4)	µM	20.00 [a] (Lit)	4.3–137	[53–60]

Table 1. *Cont.*

Parameter	Unit	Model	Literature	Reference
Carbamazepine				
E_{max} (CYP3A4)	-	6.00 (Fit)	1.9–23	[53–60]
EC_{50} (CYP2B6)	µM	20.00 [a] (Asm)	22–145	[60–62]
E_{max} (CYP2B6)	-	17.00 (Fit)	3.1–21.5	[60–62]
EC_{50} (EPHX1)	µM	20.00 [a] (Asm)	-	-
E_{max} (EPHX1)	-	3.25 (Fit)	-	-
Intestinal permeability	cm/s	4.3×10^{-4} (Lit)	4.3×10^{-4}	[63]
Partition coefficients	-	Rodgers and Rowlands		[64,65]
Cellular permeabilities	cm/s	PK-Sim Standard		[66]
Carbamazepine-10,11-epoxide				
Molecular weight	g/mol	252.27 (Lit)	252.27	[67]
Lipophilicity	Log Units	1.00 (Fit)	1.58; 1.97	[67]
Solubility	µg/mL	1340 (Lit)	1340	[67]
Fraction unbound	%	51.8 (Lit)	46.8; 49.0; 47.0; 51.8; 50.0	[68]
CL_{spec} (EPHX1)	1/min	0.01 (Fit)	-	-
GFR fraction	-	0.21 (Fit)	-	-
Intestinal permeability	cm/s	5.0×10^{-3} (Fit)	-	-
Partition coefficients	-	Rodgers and Rowlands		[64,65]
Cellular permeabilities	cm/s	PK-Sim Standard		[66]

Asm: assumption, CBZ-E: carbamazepine-10,11-epoxide, CL_{hep}: hepatic clearance, CL_{spec}: specific clearance, CYP: cytochrome P450, GFR: glomerular filtration rate, EC_{50}: half maximal effective concentration, E_{max}: maximum effect, EPHX1: epoxide hydroxylase 1, FaHIF: fasted human intestinal fluid, Fit: fitted in parameter optimization, K_m: Michaelis–Menten constant, k_{cat}: catalytic rate constant, Lit: literature, UGT: UDP-glucuronosyltransferase, V_{max}: maximum reaction velocity. [a] mean of literature values of EC_{50} (CYP3A4), assumed for all EC_{50} values. [b] k_{cat} values calculated within PK-Sim from V_{max}/recombinant enzyme. [c] k_{cat} value calculated within PK-Sim from V_{max} = 0.79 pmol/min/microsomal protein, derived from in vitro assays in microsomes, assuming a microsomal UGT2B7 content of 82.9 pmol/mg microsomal protein [69]; k_{cat} = V_{max}/UGT2B7 content microsomes.

Figure 2 shows exemplary predictions of plasma concentration–time profiles compared to observed clinical data. Predicted compared to observed plasma concentration–time profiles of all studies are shown in the Supplementary Materials on a linear and semi-logarithmic scale.

Plasma concentration goodness-of-fit plots along with MRD values for all analyzed studies are provided in the Supplementary Materials. In total, 94% and 69% of all carbamazepine and carbamazepine-10,11-epoxide plasma concentrations lie within the 2-fold acceptance limits, with overall MRD values of 1.38 and 1.76, respectively. Figure 3 shows predicted compared to observed AUC_{last} and C_{max} values. Low overall GMFEs of 1.20 and 1.57 for carbamazepine and carbamazepine-10,11-epoxide AUC_{last} values, as well as 1.24 and 1.65 for carbamazepine and carbamazepine-10,11-epoxide C_{max} values, respectively, demonstrate a good model performance. Table S4 lists all AUC_{last} and C_{max} values with the corresponding GMFEs.

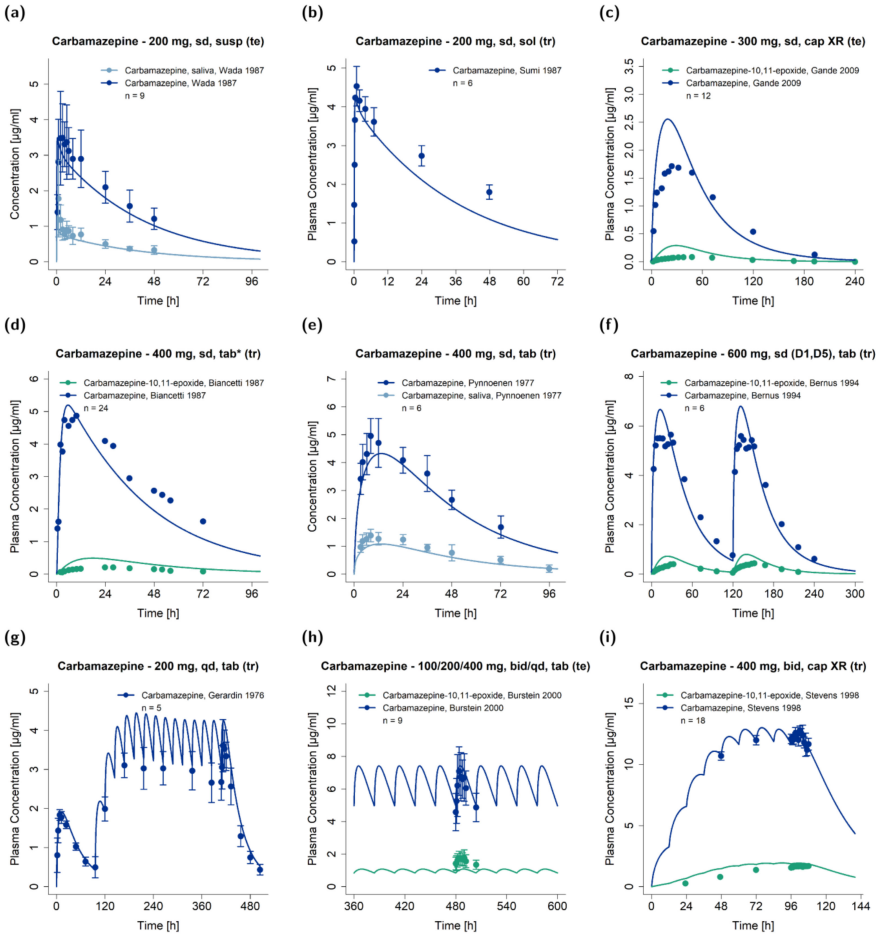

Figure 2. Model predictions of carbamazepine (dark blue: plasma, light blue: saliva) and carbamazepine-10,11-epoxide (green) concentration−time profiles of exemplary studies after (**a**–**e**) single- and (**f**–**i**) multiple-dose administration of different carbamazepine formulations [70–78] in comparison to observed data. Observed data are shown as dots ± SD (if available), simulations are shown as solid lines. Detailed information about the study protocols and model simulations of all clinical studies used to evaluate the carbamazepine model performance are provided in the Supplementary Materials. bid: twice daily, cap: capsule, D: day, n: number of subjects, qd: once daily, sd: single dose, sol: solution, susp: suspension, tab: tablet, tab*: tablet with concomitant food intake, te: test dataset, tr: training dataset, XR: extended release.

Sensitivity analysis of a simulation of 400 mg three times daily orally administered carbamazepine with a parameter perturbation of 1000% and a sensitivity threshold of 0.5 revealed that the carbamazepine AUC is mainly sensitive to the carbamazepine fraction unbound in plasma (literature), while the carbamazepine-10,11-epoxide AUC is sensitive to carbamazepine-10,11-epoxide fraction unbound in plasma (literature), EPHX1 clearance of carbamazepine-10,11-epoxide (optimized), K_m and k_{cat} of carbamazepine CYP3A4 metabolism to carbamazepine-10,11-epoxide (literature and optimized, respectively) and carbamazepine EPHX1 E_{max} (optimized). The full quantitative results of the sensitivity analysis of all tested parameters are documented in the Supplementary Materials.

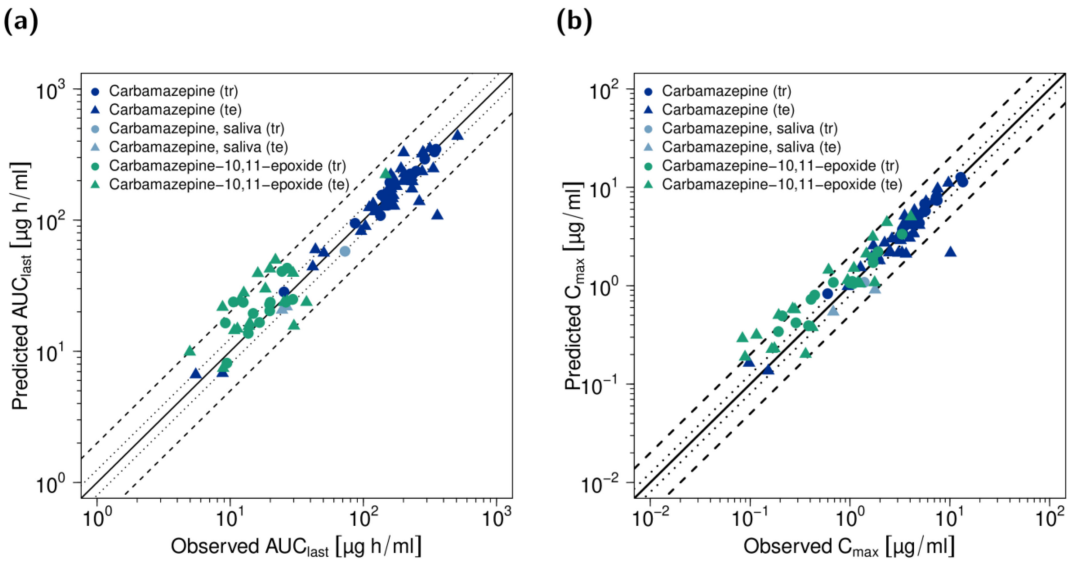

Figure 3. Performance of the carbamazepine parent−metabolite PBPK model. Predicted compared to observed (**a**) AUC_{last} values and (**b**) C_{max} values of carbamazepine and carbamazepine-10,11-epoxide of all analyzed studies. The line of identity is shown as solid line; 1.25-fold deviation is shown as dotted lines; 2-fold deviation is shown as dashed lines. AUC_{last}: area under the plasma concentration−time curve from dosing to the last concentration measurement, C_{max}: maximum plasma concentration, te: test dataset, tr: training dataset.

3.2. DDI Modeling

A total number of seven DDI studies, providing eight victim drug plasma concentration−time profiles and seven metabolite plasma concentration−time profiles, were used to evaluate the DDI performance of the carbamazepine parent−metabolite PBPK model. Those include studies with CYP3A4 victim drugs (alprazolam and simvastatin), a CYP3A4 inhibitor (erythromycin), a CYP2B6 victim drug (bupropion) as well as a CYP3A4 and CYP2B6 victim and perpetrator drug (efavirenz). The carbamazepine DDI network is illustrated in Figure 1d.

The DDI potential of carbamazepine as CYP3A4 substrate was assessed using three DDI studies with erythromycin as mechanism-based CYP3A4 inhibitor and substrate. In two studies a single dose of carbamazepine was applied after pretreatment with multiple doses of erythromycin [4,79]. In the third study, patients were pretreated with multiple doses of carbamazepine before coadministration of multiple doses of erythromycin [80], resulting in significant induction of CYP3A4 before the administration of the CYP3A4 inhibitor erythromycin.

The DDI potential of carbamazepine as CYP3A4 and CYP2B6 inducer was assessed using DDI studies with alprazolam and simvastatin as CYP3A4 and bupropion as CYP2B6 victim drugs. In those studies, pretreatment with multiple doses of carbamazepine was initiated to ensure significant enzyme induction before a single oral dose of the respective victim drugs was administered [7,8,81]. In the utilized efavirenz−carbamazepine DDI study, both compounds were administered in multiple oral dose regimens. The effect of drug coadministration was examined for each drug. Information on all utilized DDI studies along with detailed study protocols, demographics and references is provided in Tables S13, S16, S19, S22 and S24 in the Supplementary Materials.

The DDI performance of the carbamazepine model with carbamazepine as victim or perpetrator drug is shown in Figures 4 and 5, respectively. Plots show predicted victim drug plasma concentration−time profiles, with and without coadministration of the

perpetrator drug, compared to observed data. Predicted compared to observed plasma concentration−time profiles of all DDI studies are also depicted in the Supplementary Materials on a semi-logarithmic and linear scale.

Predicted compared to observed DDI AUC_{last} and DDI C_{max} ratios are visualized in Figure 6 and are listed along with the corresponding GMFE values in Section 5 of the Supplementary Materials. 14/15 DDI AUC_{last} ratios and 11/15 DDI C_{max} ratios were within the prediction success limits proposed by Guest et al., with low overall GMFEs of 1.26 and 1.30 for all predicted DDI AUC_{last} and C_{max} ratios, respectively.

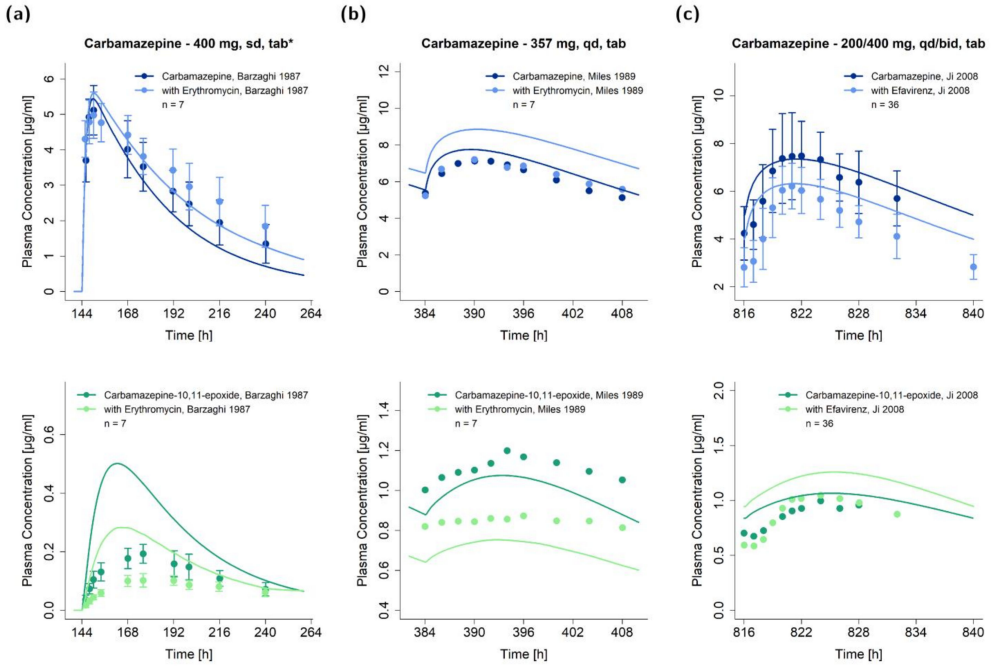

Figure 4. Victim drug plasma concentration−time profiles of the modeled drug–drug interactions with carbamazepine as victim drug (first row: carbamazepine, second row: metabolite carbamazepine-10,11-epoxide). Predictions of the victim drug plasma concentrations during the erythromycin−carbamazepine DDI (**a**) without and (**b**) with carbamazepine pretreatment [79,80] and (**c**) the efavirenz−carbamazepine DDI [8] are shown in comparison to observed data. Observed data are shown as dots ± SD (if available); predictions are shown as solid lines. Details on the study protocols and model simulations of all investigated DDI studies are provided in the Supplementary Materials. md: multiple dose, n: number of individuals, sd: single dose, tab: tablet, tab*: tablet with concomitant food intake.

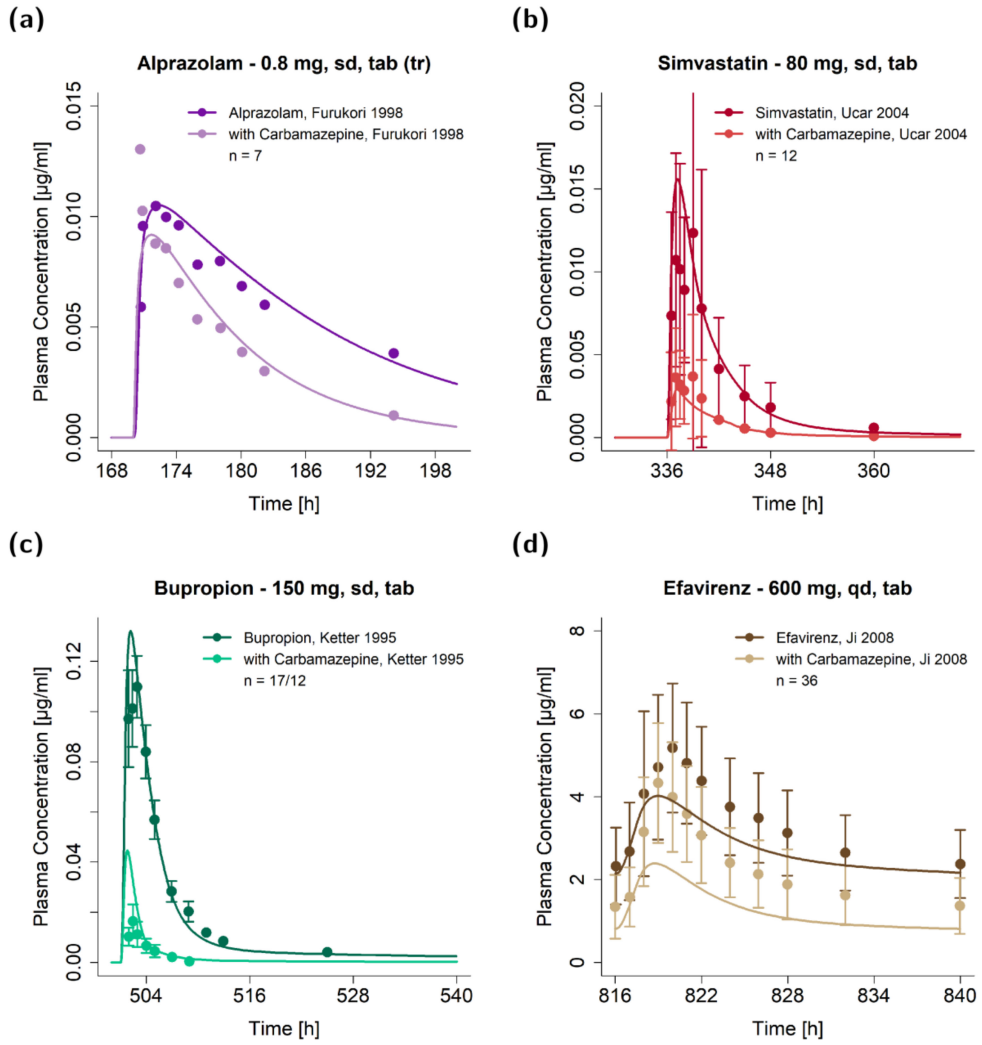

Figure 5. Victim drug plasma concentration−time profiles of the modeled drug–drug interactions with carbamazepine as perpetrator drug. Predictions of the victim drug plasma concentrations during the (**a**) carbamazepine−alprazolam DDI [81], **(b)** carbamazepine−simvastatin DDI [7] (**c**) carbamazepine−bupropion DDI [8] and (**d**) carbamazepine−efavirenz DDI [10] are shown in comparison to observed data. Observed data are shown as dots ± SD (if available); predictions are shown as solid lines. Details on the study protocols and model simulations of all investigated DDI studies are provided in the Supplementary Materials. md: multiple dose, n: number of individuals, sd: single dose, tab: tablet.

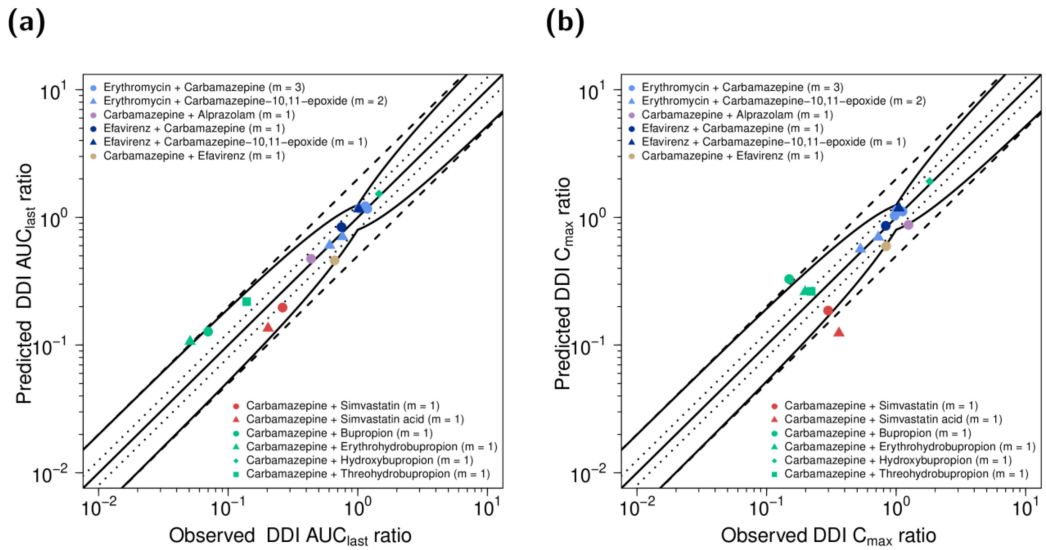

Figure 6. DDI performance of the carbamazepine parent−metabolite PBPK model. Predicted compared to observed (**a**) DDI AUC_{last} ratios and (**b**) DDI C_{max} ratios of all analyzed DDI studies. Dots represent the victim drug; triangles, diamonds and squares of the same color represent respective metabolites. The line of identity is shown as a straight solid line; the curved solid lines mark the prediction success limits proposed by Guest et al. [33]. A 1.25-fold deviation is shown as dotted lines; 2-fold deviation is shown as dashed lines. Details on the study protocols and all individual DDI AUC_{last} and DDI C_{max} ratios are provided in the Supplementary Materials. AUC_{last}: area under the plasma concentration−time curve from dosing to the last concentration measurement, C_{max}: maximum plasma concentration, DDI: drug–drug interaction, m: number of studies.

4. Discussion

In the presented study, a whole-body parent−metabolite PBPK model of carbamazepine and its main metabolite carbamazepine-10,11-epoxide was successfully established. The model adequately describes and predicts the plasma (and saliva) concentration−time profiles and the urinary excretion of carbamazepine and its main metabolite over a broad carbamazepine dosing range (50–800 mg) for oral administration of different formulations in single- and multiple-dose regimens, with and without concomitant food intake. The good model performance has been shown by a thorough evaluation of the PBPK model. Furthermore, the model was successfully applied for DDI simulations and predictions with erythromycin, alprazolam, simvastatin, bupropion and efavirenz.

The developed PBPK model includes a detailed description of carbamazepine metabolism via CYP3A4, CYP2C8, CYP2B6 and UGT2B7 and of carbamazepine-10,11-epoxide metabolism via EPHX1, including carbamazepine (auto-)induction of CYP3A4, CYP2B6 and EPHX1. Relevant ADME processes were predominantly parametrized using literature values. Only very few parameters were optimized, including lipophilicity, GFR fraction of parent and metabolite, CYP3A4 k_{cat} values, EPHX1 clearance as well as E_{max} values of the induction processes. The lipophilicity of a compound is used to calculate the organ permeabilities in PK-Sim. As logP is used as a surrogate input parameter for lipophilicity and might not fully describe the permeability properties of a compound, the lipophilicity value was optimized. GFR fraction was optimized to a value < 1, as passive reabsorption of carbamazepine along the renal tubule after glomerular filtration due to its high permeability is described in literature [23]. The CYP3A4 k_{cat} values were optimized, to correctly describe the plasma concentrations of the metabolite, while the EPHX1 clearance had to be optimized, as no information was available in the literature.

Predicted plasma concentration−time profiles of carbamazepine-10,11-epoxide showed discrepancies in comparison to observed data for some studies (Figure 2 and Figures S2–S5). The model tends to overpredict the data, while the observed plasma concentration−time profiles exhibit high variability of unknown origin. We reviewed the implemented formation, distribution and degradation processes of carbamazepine-10,11-epoxide, to understand the deviation between observations and model predictions. The formation of carbamazepine-10,11-epoxide is mediated by carbamazepine CYP3A4 and CYP2C8 metabolism, evaluated during DDI predictions. The good DDI performance of the parent−metabolite model indicates a reasonable implementation of the formation of carbamazepine-10,11-epoxide. As carbamazepine-10,11-epoxide is almost completely metabolized via EPHX1 [24,82], and high interindividual variability of EPHX1 activity was presumed [83], the variability observed in clinical study data might be caused by variability in EPHX1 metabolism. As no information on EPHX1 activity is provided in the reviewed studies, EPHX1 variability could not be reasonably reflected in the model. Furthermore, P-glycoprotein (P-gp) is discussed as carbamazepine-10,11-epoxide transporter [84]. Due to lack of conclusive evidence and studies parametrizing this transport, P-gp transport was not implemented. Overall, the carbamazepine-10,11-epoxide PBPK model was carefully developed, including studies of direct oral administration of carbamazepine-10,11-epoxide, and the model evaluation, including overall GMFE values of 1.57 and 1.65 for AUC_{last} and C_{max}, for carbamazepine-10,11-epoxide yet indicates an adequate model performance.

The observed concentrations of carbamazepine in saliva are also well captured, demonstrating the good description of carbamazepine distribution. Correct description of saliva concentrations can be useful for further model applications, as saliva is used as a surrogate for plasma sampling in clinical practice (ratio saliva:plasma = 1:4, reflecting the free fraction of carbamazepine [48]).

With regard to drug transporters, P-gp is also discussed as a carbamazepine transporter, but without conclusive evidence in the literature [84–88]. P-gp would impact the carbamazepine pharmacokinetics by limiting the absorption from the gastrointestinal tract, hindering the penetration into the central nervous system and increasing the urinary excretion [89]. How strong this impact would be, with a drug as lipophilic as carbamazepine (logP of 1.45–2.77 [38–40]), is not clear. As there is conflicting information, and in the absence of in vitro studies of carbamazepine transport by P-gp in the literature, transport via P-gp was not implemented into the model. However, the model successfully describes the absorption of low (50 mg) and high (800 mg) carbamazepine doses as well as the urinary excretion of the unchanged drug.

As carbamazepine induces its own metabolism by activation of nuclear receptors resulting in an increased CYP3A4 and CYP2B6 expression, the pharmacokinetics of carbamazepine are quite complex. CYP enzyme induction is highly variable, with reported EC_{50} and E_{max} values ranging between 4.3–108 μM and 1.9–24.7 for CYP3A4 and 22–145 μM and 3.1–29.1 for CYP2B6 induction, respectively. The mean EC_{50} = 20 μM of all included CYP3A4 induction studies was selected for all implemented induction processes, assuming that induction of those enzymes is the result of carbamazepine activation of the CAR receptor [36]. The incorporated CYP3A4 induction was evaluated by prediction of multiple dose carbamazepine studies from the test dataset, as well as by prediction of the carbamazepine−simvastatin DDI, showing a good DDI performance with a predicted DDI AUC_{last} ratio of 0.20 compared to the observed ratio of 0.26.

The implementation of CYP3A4 metabolism of carbamazepine was further evaluated via the prediction of three erythromycin−carbamazepine DDI studies. For single dose carbamazepine administration (negligible CYP3A4 induction) the effect on carbamazepine is very well described with predicted compared to observed DDI AUC_{last} ratios of 1.22 and 1.14, respectively (study by Barzaghi et al. [79]) and 1.17 and 1.18, respectively (study by Wong et al. [4]). For multiple dose carbamazepine administration (considerable CYP3A4 induction) the effect on carbamazepine is also well described, with predicted compared to observed DDI AUC_{last} ratios of 1.18 and 1.03, respectively (study by Miles et al. [80]). In all

cases, the effect of erythromycin on carbamazepine-10,11-epoxide plasma concentrations is well captured, with predicted compared to observed DDI AUC_{last} ratios of 0.60 and 0.61, respectively (study by Barzaghi et al. [79]) and 0.71 and 0.76, respectively (study by Miles et al. [80]). As carbamazepine-10,11-epoxide is mainly formed by CYP3A4 metabolism, it can be assumed that the fraction of carbamazepine metabolized via CYP3A4, and the effect of erythromycin on carbamazepine CYP3A4 metabolism, are accurately implemented in the applied models.

The E_{max} for CYP2B6 induction was identified during the carbamazepine model parameter identification and the description of CYP2B6 induction in the model was evaluated by prediction of the carbamazepine-bupropion and the efavirenz−carbamazepine DDIs. The simulated effect of carbamazepine on bupropion is underpredicted, showing predicted compared to observed DDI AUC_{last} ratios of 0.13 and 0.07, respectively. In this study, bupropion was administered to 12 patients with major affective disorders, who previously had chronic carbamazepine monotherapy and to 17 healthy individuals as control group. Carbamazepine doses for each patient as well as duration of their carbamazepine therapy were not provided in the study report. Furthermore, in the respective study, the pharmacokinetics of bupropion with and without carbamazepine coadministration were not investigated in a cross-over fashion, and therefore the results might be significantly influenced by the CYP2B6 genotypes of the two different study populations, because CYP2B6 polymorphism is a major determinant of bupropion pharmacokinetics.

The efavirenz−carbamazepine DDI was well described, with predicted compared to observed DDI AUC_{last} ratios of 0.84 and 0.75 for carbamazepine, and 1.16 and 1.06 for carbamazepine-10,11-epoxide, respectively, for the effect of efavirenz on carbamazepine. The interaction between efavirenz and carbamazepine is quite complex, as both compounds are substrates and well as inducers of CYP3A4 and CYP2B6, while CYP3A4 metabolism plays only a minor role for efavirenz [90]. Regarding the effect of carbamazepine on efavirenz, the effect is also well described with predicted compared to observed DDI AUC_{last} ratios of 0.46 and 0.66, respectively. The correct prediction of the impact of a perpetrator drug on the pharmacokinetics of a victim drug indicates that the perpetrator model adequately describes the drug concentrations at the sites of interaction and that the victim drug model simulates the right amount of drug eliminated via the affected pathway. The presented efavirenz−carbamazepine DDI example illustrates the value and power of PBPK DDI modeling, which allows us to dynamically compute the changes of perpetrator and victim drug plasma and tissue concentrations, as well as drug concentration-dependent induction of enzyme expression over time.

Several published studies investigate the pharmacokinetics of carbamazepine using PBPK modeling, (1) to predict the pharmacokinetics of carbamazepine in the pediatric population [91], (2) to describe gastrointestinal absorption of different carbamazepine formulations [92], (3) to investigate the DDI with levonorgestrel [93] and (4) to investigate the DDI performance of victim drug models with carbamazepine as enzyme inducer [15–18] using the default Simcyp parent−metabolite PBPK template model of carbamazepine and carbamazepine-10,11-epoxide [19].

In contrast to the previously published models, we used a large set of clinical data for model development (58 and 34 plasma profiles, as well as 4 and 5 fraction excreted in urine profiles, of carbamazepine and carbamazepine-10,11-epoxide, respectively). Additionally, our model provides an extensive overview on carbamazepine pharmacokinetics, including (1) the description of the metabolite carbamazepine-10,11-epoxide, (2) a detailed and mechanistic implementation of carbamazepine metabolism and autoinduction using in vitro literature parameter values, (3) the ability to describe different formulations applied in fasted or fed state and (4) thorough evaluation of metabolic and inductive processes in DDI simulations with CYP3A4 and CYP2B6 victim and perpetrator drugs. Carbamazepine is typically investigated as enzyme inducer. The presented study also investigated carbamazepine as a victim drug–a scenario which should not be neglected as illustrated

in the complex interaction with efavirenz, where both compounds mutually influence their pharmacokinetics.

The presented carbamazepine parent−metabolite PBPK model can be applied to investigate and predict DDI scenarios with carbamazepine as CYP3A4 and CYP2B6 inducer and substrate. Such predictions can be used to support the design of clinical DDI studies of new drugs. As carbamazepine is prescribed as a long-term treatment of epilepsy, at times it might be coadministered with interacting drugs in clinical practice. In this case, the presented model could be applied to guide dose recommendations. As carbamazepine is a known inducer of further enzymes and transporters, e.g., CYP2C9 [1] or P-gp [94], future applications of the model could include the implementation of those inductions, as soon as PBPK models of sensitive substrates and the corresponding clinical DDI studies become available.

5. Conclusions

A comprehensive whole-body parent−metabolite PBPK model of carbamazepine and its main metabolite carbamazepine-10,11-epoxide was successfully established. The model includes metabolism of carbamazepine by CYP3A4, CYP2C8, CYP2B6 and UGT2B7; all Michaelis−Menten constants and most of the metabolic rate constants for these reactions were implemented using published in vitro values. In addition, it incorporates the (auto-)induction of CYP3A4, CYP2B6 and the carbamazepine-10,11-epoxide hydroxylase EPHX1 by carbamazepine. The model can be applied to predict plasma concentration−time profiles of carbamazepine and carbamazepine-10,11-epoxide administered in single- and multiple-dose regimens or different formulations. Furthermore, the presented model was thoroughly challenged and evaluated by prediction of DDIs in an extensive DDI network with five perpetrator and victim drugs and different study protocols. Noteworthy is the good prediction of the complex efavirenz−carbamazepine DDI with its mutual induction of CYP3A4 and CYP2B6. The good DDI performance is fully documented in the Supplementary Materials and the model is considered qualified for CYP3A4 and CYP2B6 DDI prediction. The modeling files will be shared with the scientific community in the Open Systems Pharmacology model repository (www.open-systems-pharmacology.org).

Supplementary Materials: The following are available online at https://www.mdpi.com/1999-4923/13/2/270/s1: Comprehensive reference manual, providing documentation of the complete model performance assessment. Section 1: Physiologically based pharmacokinetic (PBPK) modeling. Section 2: Carbamazepine, Section 3: Efavirenz. Section 4: Efavirenz drug-gene interactions (DGI). Section 5: Carbamazepine drug-drug interactions (DDI). Section 6: Efavirenz drug-drug interactions (DDI). Section 7: System-dependent parameters.

Author Contributions: Conceptualization, L.M.F., F.Z.M., N.H., D.S. and T.L.; funding acquisition, T.L.; investigation, L.M.F., F.Z.M., N.H., D.S. and T.L.; visualization, L.M.F.; writing—original draft, L.M.F.; writing—review and editing, L.M.F., F.Z.M., N.H., D.S. and T.L. All authors have read and agreed to the published version of the manuscript.

Funding: This research was funded by the German Federal Ministry of Education and Research (BMBF), grant number 031L0161C ("OSMOSES"). We acknowledge support by the Deutsche Forschungsgemeinschaft (DFG, German Research Foundation) and Saarland University within the funding program Open Access Publishing.

Institutional Review Board Statement: Not applicable.

Informed Consent Statement: Not applicable.

Data Availability Statement: All modeling files including utilized clinical study data can be found here: https://github.com/Open-Systems-Pharmacology.

Conflicts of Interest: Thorsten Lehr has received research grants from the German Federal Ministry of Education and Research (grant 031L0161C). Laura Maria Fuhr, Fatima Zahra Marok, Nina Hanke and Dominik Selzer declare no conflict of interest. The funders had no role in the design of the

study; in the collection, analyses, or interpretation of data; in the writing of the manuscript, or in the decision to publish the results.

References

1. U.S. Food and Drug Administration. Drug Development and Drug Interactions. Available online: https://www.fda.gov/drugs/drug-interactions-labeling/drug-development-and-drug-interactions (accessed on 3 March 2020).
2. Kerr, B.M.; Thummel, K.E.; Wurden, C.J.; Klein, S.M.; Kroetz, D.L.; Gonzalez, F.J.; Levy, R.H. Human liver carbamazepine metabolism. Role of CYP3A4 and CYP2C8 in 10,11-epoxide formation. *Biochem. Pharmacol.* **1994**, *47*, 1969–1979. [CrossRef]
3. Pelkonen, O.; Myllynen, P.; Taavitsainen, P.; Boobis, A.R.; Watts, P.; Lake, B.G.; Price, R.J.; Renwick, A.B.; Gómez-Lechón, M.J.; Castell, J.V.; et al. Carbamazepine: A "blind" assessment of CYP-associated metabolism and interactions in human liver-derived in vitro systems. *Xenobiotica* **2001**, *31*, 321–343. [CrossRef]
4. Wong, Y.Y.; Ludden, T.M.; Bell, R.D. Effect of erythromycin on carbamazepine kinetics. *Clin. Pharmacol. Ther.* **1983**, *33*, 460–464. [CrossRef] [PubMed]
5. Shahzadi, A.; Javed, I.; Aslam, B.; Muhammad, F.; Asi, M.R.; Ashraf, M.Y.; Ur-Rahman, Z. Therapeutic effects of ciprofloxacin on the pharmacokinetics of carbamazepine in healthy adult male volunteers. *Pak. J. Pharm. Sci.* **2011**, *24*, 63–68.
6. Kim, K.A.; Sae, O.O.; Park, P.W.; Park, J.Y. Effect of probenecid on the pharmacokinetics of carbamazepine in healthy subjects. *Eur. J. Clin. Pharmacol.* **2005**, *61*, 275–280. [CrossRef]
7. Ucar, M.; Neuvonen, M.; Luurila, H.; Dahlqvist, R.; Neuvonen, P.J.; Mjörndal, T. Carbamazepine markedly reduces serum concentrations of simvastatin and simvastatin acid. *Eur. J. Clin. Pharmacol.* **2004**, *59*, 879–882. [CrossRef]
8. Ketter, T.A.; Jenkins, J.B.; Schroeder, D.H.; Pazzaglia, P.J.; Marangell, L.B.; George, M.S.; Callahan, A.M.; Hinton, M.L.; Chao, J.; Post, R.M. Carbamazepine but not valproate induces bupropion metabolism. *J. Clin. Psychopharmacol.* **1995**, *15*, 327–333. [CrossRef] [PubMed]
9. Tirona, R.; Kim, R. Introduction to clinical pharmacology. In *Clinical and Translational Science: Principles of Human Research*; Robertson, G., Williams, G., Eds.; Academic Press: Cambridge, MA, USA, 2017; pp. 365–388. ISBN 978-0-12802-101-9.
10. Ji, P.; Damle, B.; Xie, J.; Unger, S.E.; Grasela, D.M.; Kaul, S. Pharmacokinetic interaction between efavirenz and carbamazepine after multiple-dose administration in healthy subjects. *J. Clin. Pharmacol.* **2008**, *48*, 948–956. [CrossRef]
11. Chochrance. Antiepileptic Drug Monotherapy (Single Drug Treatment) for Epilepsy. Available online: https://www.cochrane.org/CD011412/EPILEPSY_antiepileptic-drug-monotherapy-single-drug-treatment-epilepsy (accessed on 25 November 2020).
12. World Health Organization. World Health Organization Model List of Essential Medicines; 21st List. Available online: https://www.who.int/publications/i/item/WHOMVPEMPIAU2019.06 (accessed on 25 November 2020).
13. Adiwidjaja, J.; Boddy, A.V.; McLachlan, A.J. Implementation of a physiologically based pharmacokinetic modeling approach to guide optimal dosing regimens for imatinib and potential drug interactions in paediatrics. *Front. Pharmacol.* **2020**, *10*, 1–18. [CrossRef]
14. *Guideline on the Reporting of Physiologically Based Pharmacokinetic (PBPK) Modelling and Simulation*; European Medicines Agency: Amsterdam, The Netherlands, 2018.
15. *Physiologically Based Pharmacokinetic Analyses—Format and Content*; U.S. Food and Drug Administration: Silver Spring, MD, USA, 2018.
16. Conner, T.M.; Nikolian, V.C.; Georgoff, P.E.; Pai, M.P.; Alam, H.B.; Sun, D.; Reed, R.C.; Zhang, T. Physiologically based pharmacokinetic modeling of disposition and drug-drug interactions for valproic acid and divalproex. *Eur. J. Pharm. Sci.* **2018**, *111*, 465–481. [CrossRef] [PubMed]
17. Johnson, T.N.; Zhou, D.; Bui, K.H. Development of physiologically based pharmacokinetic model to evaluate the relative systemic exposure to quetiapine after administration of IR and XR formulations to adults, children and adolescents. *Biopharm. Drug Dispos.* **2014**, *35*, 341–352. [CrossRef]
18. Schuck, E.; Ferry, J.; Gidal, B.; Hussein, Z. Changes in perampanel levels during de-induction: Simulations following carbamazepine discontinuation. *Acta Neurol. Scand.* **2020**, *142*, 131–138. [CrossRef]
19. Almond, L.M.; Mukadam, S.; Gardner, I.; Okialda, K.; Wong, S.; Hatley, O.; Tay, S.; Rowland-Yeo, K.; Jamei, M.; Rostami-Hodjegan, A.; et al. Prediction of drug-drug interactions arising from CYP3A induction using a physiologically based dynamic model. *Drug Metab. Dispos.* **2016**, *44*, 821–832. [CrossRef] [PubMed]
20. Mitchell, B.M.; Muftakhidinov, T.W.; Jędrzejewski-Szmek, Z. Engauge Digitizer Software. Available online: https://merkummitchell.github.io/engauge-digitizer (accessed on 15 February 2021).
21. Wojtyniak, J.G.; Britz, H.; Selzer, D.; Schwab, M.; Lehr, T. Data Digitizing: Accurate and Precise Data Extraction for Quantitative Systems Pharmacology and Physiologically-Based Pharmacokinetic Modeling. *CPT Pharmacomet. Syst. Pharmacol.* **2020**, *9*, 322–331. [CrossRef] [PubMed]
22. *Open Systems Pharmacology Suite Community PK-Sim®Ontogeny Database Documentation*, Version 7.3; Available online: Github.com/Open-Systems-Pharmacology/OSPSuite.Documentation/blob/master/PK-Sim%Ontogeny%20Database%20Version%207.3.pdf (accessed on 15 February 2021).
23. Vree, T.B.; Janssen, T.J.; Hekster, Y.A.; Termond, E.F.; van de Dries, A.C.; Wijnands, W.J. Clinical pharmacokinetics of carbamazepine and its epoxy and hydroxy metabolites in humans after an overdose. *Ther. Drug Monit.* **1986**, *8*, 297–304. [CrossRef] [PubMed]

24. Kerr, B.M.; Rettie, A.E.; Eddy, A.C.; Loiseau, P.; Guyot, M.; Wilensky, A.J.; Levy, R.H. Inhibition of human liver microsomal epoxide hydrolase by valproate and valpromide: In vitro/in vivo correlation. *Clin. Pharmacol. Ther.* **1989**, *46*, 82–93. [CrossRef]
25. Kitteringham, N.R.; Davis, C.; Howard, N.; Pirmohamed, M.; Park, B.K. Interindividual and interspecies variation in hepatic microsomal epoxide hydrolase activity: Studies with cis-stilbene oxide, carbamazepine 10,11- epoxide and naphthalene. *J. Pharmacol. Exp. Ther.* **1996**, *278*, 1018–1027. [PubMed]
26. Levy, R.H.; Pitlick, W.H.; Troupin, A.S.; Green, J.R.; Neal, J.M. Pharmacokinetics of carbamazepine in normal man. *Clin. Pharmacol. Ther.* **1975**, *17*, 657–668. [CrossRef]
27. McLean, A.; Browne, S.; Zhang, Y.; Slaughter, E.; Halstenson, C.; Couch, R. The influence of food on the bioavailability of a twice-daily controlled release carbamazepine formulation. *J. Clin. Pharmacol.* **2001**, *41*, 183–186. [CrossRef] [PubMed]
28. Frechen, S.; Wendel, T.; Solodenko, J. Building and Evaluation of a PBPK Model for Efavirenz in Healthy Adults. Available online: https://github.com/Open-Systems-Pharmacology/OSP-PBPK-Model-Library/blob/v9.1/Efavirenz/efavirenz_evaluation_report.pdf (accessed on 13 November 2020).
29. Frechen, S.; Dallmann, A. Building and Evaluation of a PBPK Model for Alprazolam in Healthy Adults. Available online: https://github.com/Open-Systems-Pharmacology/OSP-PBPK-Model-Library/blob/v9.1/Alprazolam/Alprazolam_evaluation_report.pdf (accessed on 13 November 2020).
30. Frechen, S.; Dallmann, A. Building and Evaluation of a PBPK Model for Erythromycin in Healthy Adults. Available online: https://github.com/Open-Systems-Pharmacology/OSP-PBPK-Model-Library/blob/v9.1/Erythromycin/Erythromycin_evaluation_report.pdf (accessed on 13 November 2020).
31. Marok, F.Z.; Fuhr, L.; Hanke, N.; Selzer, D.; Lehr, T. Physiologically Based Pharmacokinetic Modeling of Bupropion and its Metabolites in a CYP2B6 Drug-Drug-Gene Interaction Network. *Pharmaceutics* **2020**. submitted for publication.
32. Wojtyniak, J.; Selzer, D.; Schwab, M.; Lehr, T. Physiologically Based Precision Dosing Approach for Drug-Drug-Gene Interactions: A Simvastatin Network Analysis. *Clin. Pharmacol. Ther.* **2020**, *109*, 201–211. [CrossRef]
33. Guest, E.J.; Aarons, L.; Houston, J.B.; Rostami-Hodjegan, A.; Galetin, A. Critique of the Two-Fold Measure of Prediction Success for Ratios: Application for the Assessment of Drug-Drug Interactions. *Drug Metab. Dispos.* **2011**, *39*, 170–173. [CrossRef]
34. Les Laboratoires Servier. Servier Medical Art. Available online: https://smart.servier.com/ (accessed on 11 November 2020).
35. Pearce, R.E.; Vakkalagadda, G.R.; Steven Leeder, J. Pathways of carbamazepine bioactivation in vitro I. Characterization of human cytochromes P450 responsible for the formation of 2- and 3-hydroxylated metabolites. *Drug Metab. Dispos.* **2002**, *30*, 1170–1179. [CrossRef] [PubMed]
36. Faucette, S.R.; Zhang, T.C.; Moore, R.; Sueyoshi, T.; Omiecinski, C.J.; LeCluyse, E.L.; Negishi, M.; Wang, H. Relative activation of human pregnane X receptor versus constitutive androstane receptor defines distinct classes of CYP2B6 and CYP3A4 inducers. *J. Pharmacol. Exp. Ther.* **2007**, *320*, 72–80. [CrossRef] [PubMed]
37. Eichelbaum, M.; Tomson, T.; Tybring, G.; Bertilsson, L. Carbamazepine metabolism in man. Induction and pharmacogenetic aspects. *Clin. Pharmacokinet.* **1985**, *10*, 80–90. [CrossRef] [PubMed]
38. Drugbank. Carbamazepine. Available online: https://www.drugbank.ca/drugs/DB00564 (accessed on 9 February 2019).
39. Austin, R.P.; Barton, P.; Cockroft, S.L.; Wenlock, M.C.; Riley, R.J. The influence of nonspecific microsomal binding on apparent intrinsic clearance, and its prediction from physicochemical properties. *Drug Metab. Dispos.* **2002**, *30*, 1497–1503. [CrossRef]
40. Avdeef, A. *Absorption and Drug Development*; John Wiley & Sons, Inc.: Hoboken, NJ, USA, 2012; ISBN 978-1-11828-606-7.
41. Annaert, P.; Brouwers, J.; Bijnens, A.; Lammert, F.; Tack, J.; Augustijns, P. Ex vivo permeability experiments in excised rat intestinal tissue and in vitro solubility measurements in aspirated human intestinal fluids support age-dependent oral drug absorption. *Eur. J. Pharm. Sci.* **2010**, *39*, 15–22. [CrossRef] [PubMed]
42. Clarysse, S.; Brouwers, J.; Tack, J.; Annaert, P.; Augustijns, P. Intestinal drug solubility estimation based on simulated intestinal fluids: Comparison with solubility in human intestinal fluids. *Eur. J. Pharm. Sci.* **2011**, *43*, 260–269. [CrossRef]
43. Heikkilä, T.; Karjalainen, M.; Ojala, K.; Partola, K.; Lammert, F.; Augustijns, P.; Urtti, A.; Yliperttula, M.; Peltonen, L.; Hirvonen, J. Equilibrium drug solubility measurements in 96-well plates reveal similar drug solubilities in phosphate buffer pH 6.8 and human intestinal fluid. *Int. J. Pharm.* **2011**, *405*, 132–136. [CrossRef]
44. Söderlind, E.; Karlsson, E.; Carlsson, A.; Kong, R.; Lenz, A.; Lindborg, S.; Sheng, J.J. Simulating fasted human intestinal fluids: Understanding the roles of lecithin and bile acids. *Mol. Pharm.* **2010**, *7*, 1498–1507. [CrossRef] [PubMed]
45. Heumann Pharma GmbH & Co. Generica KG Fachinformation—Carbamazepin 200/400 Heumann. Available online: https://www.fachinfo.de/suche/fi/006667 (accessed on 30 November 2020).
46. Novartis. Tegretol®Label. Available online: https://www.accessdata.fda.gov/drugsatfda_docs/label/2009/016608s101,018281s048lbl.pdf (accessed on 30 November 2020).
47. Bertilsson, L. Clinical pharmacokinetics of carbamazepine. *Clin. Pharmacokinet.* **1978**, *3*, 128–1473. [CrossRef]
48. Pynnönen, S. The Pharmacokinetics of Carbamazepine in Plasma and Saliva of Man. *Acta Pharmacol. Toxicol. (Copenh.)* **1977**, *41*, 465–471.
49. Henshall, J.; Galetin, A.; Harrison, A.; Houston, J.B. Comparative analysis of CYP3A heteroactivation by steroid hormones and flavonoids in different in vitro systems and potential in vivo implications. *Drug Metab. Dispos.* **2008**, *36*, 1332–1340. [CrossRef] [PubMed]
50. Cazali, N.; Tran, A.; Treluyer, J.M.; Rey, E.; Athis, P.; Vincent, J.; Pons, G. Inhibitory effect of stiripentol on carbamazepine and saquinavir metabolism in human. *Br. J. Clin. Pharmacol.* **2003**, *56*, 526. [CrossRef]

51. Huang, W.; Lin, Y.S.; McConn, D.J.; Calamia, J.C.; Totah, R.A.; Isoherranen, N.; Glodowski, M.; Thummel, K.E. Evidence of significant contribution from CYP3A5 to hepatic drug metabolism. *Drug Metab. Dispos.* **2004**, *32*, 1434–1445. [CrossRef] [PubMed]
52. Staines, A.G.; Coughtrie, M.W.H.; Burchell, B. N-glucuronidation of carbamazepine in human tissues is mediated by UGT2B7. *J. Pharmacol. Exp. Ther.* **2004**, *311*, 1131–1137. [CrossRef]
53. Shou, M.; Hayashi, M.; Pan, Y.; Xu, Y.; Morrissey, K.; Xu, L.; Skiles, G.L. Modeling, prediction, and in vitro in vivo correlation of CYP3A4 induction. *Drug Metab. Dispos.* **2008**, *36*, 2355–2370. [CrossRef] [PubMed]
54. McGinnity, D.F.; Zhang, G.; Kenny, J.R.; Hamilton, G.A.; Otmani, S.; Stams, K.R.; Haney, S.; Brassil, P.; Stresser, D.M.; Riley, R.J. Evaluation of multiple in vitro systems for assessment of CYP3A4 induction in drug discovery: Human hepatocytes, pregnane X receptor reporter gene, and Fa2N-4 and HepaRG cells. *Drug Metab. Dispos.* **2009**, *37*, 1259–1268. [CrossRef]
55. Fahmi, O.A.; Raucy, J.L.; Ponce, E.; Hassanali, S.; Lasker, J.M. Utility of DPX2 cells for predicting CYP3A induction-mediated drug-drug interactions and associated structure-activity relationships. *Drug Metab. Dispos.* **2012**, *40*, 2204–2211. [CrossRef]
56. Zhang, J.G.; Ho, T.; Callendrello, A.L.; Clark, R.J.; Santone, E.A.; Kinsman, S.; Xiao, D.; Fox, L.G.; Einolf, H.J.; Stresser, D.M. Evaluation of calibration curve-based approaches to predict clinical inducers and noninducers of CYP3A4 with plated human hepatocytes. *Drug Metab. Dispos.* **2014**, *42*, 1379–1391. [CrossRef]
57. Moore, A.; Chothe, P.P.; Tsao, H.; Hariparsad, N. Evaluation of the interplay between uptake transport and CYP3A4 induction in micropatterned cocultured hepatocytes. *Drug Metab. Dispos.* **2016**, *44*, 1910–1919. [CrossRef]
58. Fahmi, O.A.; Kish, M.; Boldt, S.; Scott Obach, R. Cytochrome P450 3A4 mRNA is a more reliable marker than CYP3A4 activity for detecting pregnane X receptor-activated induction of drug-metabolizing enzymes. *Drug Metab. Dispos.* **2010**, *38*, 1605–1611. [CrossRef] [PubMed]
59. Zuo, R.; Li, F.; Parikh, S.; Cao, L.; Cooper, K.L.; Hong, Y.; Liu, J.; Faris, R.A.; Li, D.; Wang, H. Evaluation of a novel renewable hepatic cell model for prediction of clinical CYP3A4 induction using a correlation-based relative induction score approach. *Drug Metab. Dispos.* **2017**, *45*, 198–207. [CrossRef] [PubMed]
60. Zhang, J.G.; Patel, R.; Clark, R.J.; Ho, T.; Trisdale, S.K.; Fang, Y.; Stresser, D.M. Effect of Fifteen CYP3A4 in vitro Inducers on the Induction of Hepatocytes: A Trend Analysis. In Proceedings of the 20th North American ISSX Meeting, Orlando, FL, USA, 18–22 October 2015.
61. Fahmi, O.A.; Shebley, M.; Palamanda, J.; Sinz, M.W.; Ramsden, D.; Einolf, H.J.; Chen, L.; Wang, H. Evaluation of CYP2B6 induction and prediction of clinical drug-drug interactions: Considerations from the iq consortium induction working group—An industry perspective. *Drug Metab. Dispos.* **2016**, *44*, 1720–1730. [CrossRef] [PubMed]
62. Dickmann, L.J.; Isoherranen, N. Quantitative prediction of CYP2B6 induction by estradiol during pregnancy: Potential explanation for increased methadone clearance during pregnancy. *Drug Metab. Dispos.* **2013**, *41*, 270–274. [CrossRef] [PubMed]
63. Lennernäs, H. Intestinal permeability and its relevance for absorption and elimination. *Xenobiotica* **2007**, *37*, 1015–1051. [CrossRef]
64. Rodgers, T.; Leahy, D.; Rowland, M. Physiologically based pharmacokinetic modeling 1: Predicting the tissue distribution of moderate-to strong bases. *J. Pharm. Sci.* **2005**, *94*, 1259–1276. [CrossRef]
65. Taylor, M.J.; Tanna, S.; Sahota, T. In vivo study of a polymeric glucose-sensitive insulin delivery system using a rat model. *J. Pharm. Sci.* **2010**, *99*, 4215–4227. [CrossRef]
66. Kawai, R.; Lemaire, M.; Steimer, J.L.; Bruelisauer, A.; Niederberger, W.; Rowland, M. Physiologically based pharmacokinetic study on a cyclosporin derivative, SDZ IMM 125. *J. Pharmacokinet. Biopharm.* **1994**, *22*, 327–365. [CrossRef]
67. Drugbank. Metabolite 10,11-Epoxycarbamazepine. Available online: https://www.drugbank.ca/metabolites/DBMET00291 (accessed on 16 December 2020).
68. Morselli, P.L.; Gerna, M.; de Maio, D.; Zanda, G.; Viani, F.; Garattini, S. Pharmacokinetic studies on carbamazepine in volunteers and in epileptic patients. In *Clinical Pharmacology of Anti-Epileptic Drugs*; Schneider, H., Janz, D., Gardner-Thorpe, C., Meinardi, H., Sherwin, A.L., Eds.; Springer: Berlin, Germany, 1975; pp. 166–180. ISBN 978-3-64285-923-6.
69. Achour, B.; Russell, M.R.; Barber, J.; Rostami-Hodjegan, A. Simultaneous quantification of the abundance of several cytochrome P450 and uridine 5′-diphospho-glucuronosyltransferase enzymes in human liver microsomes using multiplexed targeted proteomics. *Drug Metab. Dispos.* **2014**, *42*, 500–510. [CrossRef]
70. Wada, J.A.; Troupin, A.S.; Friel, P.; Remick, R.; Leal, K.; Pearmain, J. Pharmacokinetic comparison of tablet and suspension dosage forms of carbamazepine. *Epilepsia* **1978**, *19*, 251–255. [CrossRef] [PubMed]
71. Sumi, M.; Watari, N.; Umezawa, O.; Kaneniwa, N. Pharmacokinetic study of carbamazepine and its epoxide metabolite in humans. *J. Pharmacobiodyn.* **1987**, *10*, 652–661. [CrossRef] [PubMed]
72. Bianchetti, G.; Padovani, P.; Thénot, J.P.; Thiercelin, J.F.; Morselli, P.L. Pharmacokinetic interactions of progabide with other antiepileptic drugs. *Epilepsia* **1987**, *28*, 68–73. [CrossRef] [PubMed]
73. Pynnönen, S. Pharmacokinetics of Carbamazepine in man: A review. *Ther. Drug Monit.* **1979**, *1*, 409–431. [CrossRef] [PubMed]
74. Bernus, I.; Dickinson, R.G.; Hooper, W.D.; Eadie, M.J. Early stage autoinduction of carbamazepine metabolism in humans. *Eur. J. Clin. Pharmacol.* **1994**, *47*, 355–360. [CrossRef]
75. Gérardin, A.P.; Abadie, F.V.; Campestrini, J.A.; Theobald, W. Pharmacokinetics of carbamazepine in normal humans after single and repeated oral doses. *J. Pharmacokinet. Biopharm.* **1976**, *4*, 521–535. [CrossRef]
76. Møller, S.E.; Larsen, F.; Khan, A.Z.; Rolan, P.E. Lack of effect of citalopram on the steady-state pharmacokinetics of carbamazepine in healthy male subjects. *J. Clin. Psychopharmacol.* **2001**, *21*, 493–499. [CrossRef]

77. Stevens, R.E.; Limsakun, T.; Evans, G.; Mason, D.H. Controlled, multidose, pharmacokinetic evaluation of two extended-release carbamazepine formulations (Carbatrol and Tegretol-XR). *J. Pharm. Sci.* **1998**, *87*, 1531–1534. [CrossRef]
78. Gande, M.; Gondalia, R.; Kothapalli, M.; Velishala, N.M.; Koppuri, V. Carbamazepine Extended Release Dosage Form. US Patent US 2009/01696.19A1, 2 July 2009.
79. Barzaghi, N.; Gatti, G.; Crema, F.; Monteleone, M.; Amione, C.; Leone, L.; Perucca, E. Inhibition by erythromycin of the conversion of carbamazepine to its active 10,11-epoxide metabolite. *Br. J. Clin. Pharmacol.* **1987**, *24*, 836–838. [CrossRef]
80. Miles, M.V.; Tennison, M.B. Erythromycin Effects on Multiple-Dose Carbamazepine Kinetics. *Ther. Drug Monit.* **1989**, *11*, 47–52. [CrossRef]
81. Furukori, H. Effect of Carbamazepine on the Single Oral Dose Pharmacokinetics of Alprazolam. *Neuropsychopharmacology* **1998**, *18*, 364–369. [CrossRef]
82. Tomson, T.; Tybring, G.; Bertilsson, L. Single-dose kinetics and metabolism of carbamazepine-10,11-epoxide. *Clin. Pharmacol. Ther.* **1983**, *33*, 58–65. [CrossRef]
83. Václavíková, R.; Hughes, D.J.; Souček, P. Microsomal epoxide hydrolase 1 (EPHX1): Gene, structure, function, and role in human disease. *Gene* **2015**, *571*, 1–8. [CrossRef] [PubMed]
84. Zhang, C.; Kwan, P.; Zuo, Z.; Baum, L. The transport of antiepileptic drugs by P-glycoprotein. *Adv. Drug Deliv. Rev.* **2012**, *64*, 930–942. [CrossRef]
85. Zhang, C.; Zuo, Z.; Kwan, P.; Baum, L. In vitro transport profile of carbamazepine, oxcarbazepine, eslicarbazepine acetate, and their active metabolites by human P-glycoprotein. *Epilepsia* **2011**, *52*, 1894–1904. [CrossRef]
86. Luna-Tortós, C.; Fedrowitz, M.; Löscher, W. Several major antiepileptic drugs are substrates for human P-glycoprotein. *Neuropharmacology* **2008**, *55*, 1364–1375. [CrossRef]
87. Owen, A.; Pirmohamed, M.; Tettey, J.N.; Morgan, P.; Chadwick, D.; Kevin Park, B. Carbamazepine is not a substrate for P-glycoprotein. *Br. J. Clin. Pharmacol.* **2001**, *51*, 345–349. [CrossRef] [PubMed]
88. Shen, X.M.; Cheng, J. Effects of MDR1 (C3435T) Polymorphism on Resistance, Uptake, and Efflux to Antiepileptic Drugs. *DNA Cell. Biol.* **2019**, *38*, 250–255. [CrossRef]
89. Shirasaka, Y.; Sakane, T.; Yamashita, S. Effect of P-glycoprotein expression levels on the concentration-dependent permeability of drugs to the cell membrane. *J. Pharm. Sci.* **2008**, *97*, 553–565. [CrossRef]
90. Ward, B.A.; Gorski, J.C.; Jones, D.R.; Hall, S.D.; Flockhart, D.A.; Desta, Z. The cytochrome P450 2B6 (CYP2B6) is the main catalyst of efavirenz primary and secondary metabolism: Implication for HIV/AIDS therapy and utility of efavirenz as a substrate marker of CYP2B6 catalytic activity. *J. Pharmacol. Exp. Ther.* **2003**, *306*, 287–300. [CrossRef] [PubMed]
91. Kohlmann, P.; Stillhart, C.; Kuentz, M.; Parrott, N. Investigating Oral Absorption of Carbamazepine in Pediatric Populations. *AAPS J.* **2017**, *19*, 1864–1877. [CrossRef] [PubMed]
92. Zhang, X.; Lionberger, R.A.; Davit, B.M.; Yu, L.X. Utility of physiologically based absorption modeling in implementing quality by design in drug development. *AAPS J.* **2011**, *13*, 59–71. [CrossRef] [PubMed]
93. Cicali, B.; Lingineni, K.; Cristofoletti, R.; Wendl, T.; Hoechel, J.; Wiesinger, H.; Chaturvedula, A.; Vozmediano, V.; Schmidt, S. Quantitative Assessment of Levonorgestrel Binding Partner Interplay and Drug-Drug Interactions Using Physiologically Based Pharmacokinetic Modeling. *CPT Pharmacomet. Syst. Pharmacol.* **2021**, *10*(1), 48–58. [CrossRef] [PubMed]
94. Yamada, S.; Yasui-Furukori, N.; Akamine, Y.; Kaneko, S.; Uno, T. Effects of the P-glycoprotein inducer carbamazepine on fexofenadine pharmacokinetics. *Ther. Drug Monit.* **2009**, *31*, 764–768. [CrossRef]

4.2 PROJECT II - PHYSIOLOGICALLY BASED PHARMACOKINETIC AND PHARMACODYNAMIC MODELING OF FELODIPINE

PUBLICATION

Fuhr, L.M.; Marok, F.Z.; Mees, M.; Mahfoud, F.; Selzer, D.; Lehr, T. A Physiologically Based Pharmacokinetic and Pharmacodynamic Model of the CYP3A4 Substrate Felodipine for Drug-Drug Interaction Modeling. Pharmaceutics. 2022. 14(7):1474, doi: 10.3390/pharmaceutics14071474.

SUPPLEMENTARY MATERIALS

The supplementary materials to this publication are provided on the accompanying USB storage device and are available online via: https://www.mdpi.com/article/10.3390/pharmaceutics14071474/s1

COPYRIGHT

AUTHOR CONTRIBUTIONS

Laura Fuhr	Conceptualization, Investigation, Visualization, Writing–Original Draft, Writing–Review & Editing
Fatima Marok	Conceptualization, Investigation, Writing–Review & Editing
Maximilian Mees	Conceptualization, Investigation, Writing–Review & Editing
Felix Mahfoud	Conceptualization, Writing–Review & Editing
Dominik Selzer	Conceptualization, Writing–Review & Editing
Thorsten Lehr	Conceptualization, Funding Acquisition, Investigation, Writing–Review & Editing

pharmaceutics

MDPI

Article

A Physiologically Based Pharmacokinetic and Pharmacodynamic Model of the CYP3A4 Substrate Felodipine for Drug–Drug Interaction Modeling

Laura Maria Fuhr [1], Fatima Zahra Marok [1], Maximilian Mees [1], Felix Mahfoud [2,3], Dominik Selzer [1] and Thorsten Lehr [1,*]

[1] Department of Clinical Pharmacy, Saarland University, 66123 Saarbrücken, Germany; laura.fuhr@uni-saarland.de (L.M.F.); fatima.marok@uni-saarland.de (F.Z.M.); max.mees@prepair.de (M.M.); dominik.selzer@uni-saarland.de (D.S.)

[2] Department of Internal Medicine III (Cardiology, Angiology, Intensive Care Medicine), Saarland University Medical Center and Saarland University Faculty of Medicine, 66421 Homburg, Germany; felix.mahfoud@uks.eu

[3] Institute for Medical Engineering and Science, Massachusetts Institute of Technology, Cambridge, MA 02139, USA

* Correspondence: thorsten.lehr@mx.uni-saarland.de; Tel.: +49-681-302-70255

Abstract: The antihypertensive felodipine is a calcium channel blocker of the dihydropyridine type, and its pharmacodynamic effect directly correlates with its plasma concentration. As a sensitive substrate of cytochrome P450 (CYP) 3A4 with high first-pass metabolism, felodipine shows low oral bioavailability and is susceptible to drug–drug interactions (DDIs) with CYP3A4 perpetrators. This study aimed to develop a physiologically based pharmacokinetic/pharmacodynamic (PBPK/PD) parent–metabolite model of felodipine and its metabolite dehydrofelodipine for DDI predictions. The model was developed in PK-Sim® and MoBi® using 49 clinical studies (94 plasma concentration–time profiles in total) that investigated different doses (1–40 mg) of the intravenous and oral administration of felodipine. The final model describes the metabolism of felodipine to dehydrofelodipine by CYP3A4, sufficiently capturing the first-pass metabolism and the subsequent metabolism of dehydrofelodipine by CYP3A4. Diastolic blood pressure and heart rate PD models were included, using an E_{max} function to describe the felodipine concentration–effect relationship. The model was tested in DDI predictions with itraconazole, erythromycin, carbamazepine, and phenytoin as CYP3A4 perpetrators, with all predicted DDI AUC_{last} and C_{max} ratios within two-fold of the observed values. The model will be freely available in the Open Systems Pharmacology model repository and can be applied in DDI predictions as a CYP3A4 victim drug.

Keywords: physiologically based pharmacokinetic (PBPK) modeling; pharmacodynamics; felodipine; drug–drug interactions (DDIs); cytochrome P450 3A4 (CYP3A4)

Citation: Fuhr, L.M.; Marok, F.Z.; Mees, M.; Mahfoud, F.; Selzer, D.; Lehr, T. A Physiologically Based Pharmacokinetic and Pharmacodynamic Model of the CYP3A4 Substrate Felodipine for Drug–Drug Interaction Modeling. *Pharmaceutics* **2022**, *14*, 1474. https://doi.org/10.3390/pharmaceutics14071474

Academic Editor: Neal M. Davies

Received: 14 June 2022
Accepted: 13 July 2022
Published: 15 July 2022

1. Introduction

The dihydropyridine felodipine is used for the treatment of hypertension [1–3]. By blocking calcium channels, mainly in vascular smooth muscles, felodipine causes a reduction in vascular resistance, which subsequently results in blood pressure lowering. This effect has been demonstrated to be dose-dependent and directly correlated with felodipine plasma concentrations [4,5]. Moreover, an increase in the heart rate was observed directly after felodipine administration, which is likely caused by baroreflex-activated sympathetic mechanisms [5].

Felodipine is a BCS class II compound of high lipophilicity and low solubility [6]. Despite a nearly complete absorption of the drug, the oral bioavailability is only 15–20% due to the high first-pass metabolism [1,7]. Felodipine is listed by the FDA as a sensitive

CYP3A4 substrate [8], and it is primarily metabolized by cytochrome P450 (CYP) 3A4 [9], with dehydrofelodipine as its main but pharmacologically inactive metabolite. As CYP3A4 is one of the major enzymes expressed in the gastrointestinal tract, intestinal metabolism after drug absorption strongly contributes to presystemic drug elimination, as observed for many other sensitive CYP3A4 substrates [10]. For felodipine, it is reported that more than 50% of the absorbed dose is metabolized in the gut wall [11]. Hence, the bioavailability and clearance of felodipine can be strongly affected by CYP3A4 perpetrators, resulting in significant changes in plasma concentrations and leading to an increased risk of adverse drug reactions, such as flush, headache, hypotension, tachycardia, or peripheral edema [1,12]. For example, a six-fold or two-fold increase in the felodipine area under the plasma concentration–time curve (AUC) could be observed after co-administration with the CYP3A4 inhibitors itraconazole or erythromycin [13,14]. Furthermore, the oral intake of felodipine with grapefruit juice, which acts as an intestinal CYP3A4 inactivator, increases its bioavailability from 15% to about 25%, resulting in a mean increase in the felodipine AUC of 72% [11]. In contrast, a 15-fold decrease in the AUC could be observed if felodipine was administered to patients treated with carbamazepine and phenytoin, inducers of CYP3A4, resulting in felodipine plasma concentrations below the therapeutic range [15]. Thus, the impact of CYP3A4-mediated drug–drug interactions (DDIs) on the pharmacokinetics and pharmacodynamics (PD) of felodipine should be throrougly investigated. For this purpose, physiologically based pharmacokinetic (PBPK) modeling is recognized as a valuable tool by the regulatory agencies FDA and EMA [16–19].

Therefore, this study aimed to develop a parent–metabolite PBPK/PD model of felodipine and its metabolite dehydrofelodipine that comprehensively describes (1) the pharmacokinetics of felodipine and its metabolite and (2) the effect of felodipine on the diastolic blood pressure and heart rate, and (3) to apply the model in DDI simulations with felodipine as a CYP3A4 victim drug and erythromycin, itraconazole, carbamazepine, and phenytoin as CYP3A4 perpetrators. The thoroughly evaluated model is publicly available in the Open Systems Pharmacology (OSP) repository on GitHub and can be applied to investigate and predict the effect of CYP3A4 perpetrators.

2. Materials and Methods

2.1. Software

Concentration–time profiles from published clinical studies were digitized with Engauge Digitizer Version 12.1 (M. Mitchell [20], 2020) according to the best practices proposed by Wojtyniak et al. [21]. The PBPK/PD model was developed with PK-Sim® and MoBi® (Open Systems Pharmacology Suite 9.1, released under the GNU General Public License version 2 (GPLv2) by the Open Systems Pharmacology community, www.open-systems-pharmacology.org, 2020). Parameter optimization (via Monte Carlo and Levenberg–Marquardt algorithms) and sensitivity analyses were performed within PK-Sim®. R 3.6.3 (The R Foundation for Statistical Computing, Vienna, Austria, 2019) was used for performance evaluations, non-compartmental analyses, and generation of plots.

2.2. Clinical Data

Plasma concentration−time profiles of felodipine and dehydrofelodipine as well as effect–time profiles of diastolic blood pressure and heart rate were gathered and digitized from published clinical studies. The collected studies provided plasma concentration–time and effect–time profiles (1) after intravenous and oral administration of felodipine in (2) single- and multiple-dosing regimens (3) over a broad dose range. Studies were split into a training dataset for model building and a test dataset for model evaluation. Concentration–time profiles for the training dataset were selected according to the following criteria: (1) coverage of intravenous and oral administration routes, (2) broad dosing range, (3) availability of both felodipine and dehydrofelodipine data, and (4) measurements in healthy participants without co-medication. Effect–time profiles for the PD model training dataset were selected from studies (1) covering a broad dosing range and (2) providing

diastolic blood pressure and heart rate placebo measurements to analyze diurnal variations in baseline blood pressure and heart rate.

2.3. PBPK Model Building

To perform mathematical simulations of the collected clinical studies, virtual individuals were generated based on the mean and mode demographics reported in the respective study protocols. If no information was provided, a 30-year-old, male, European individual with body weight and height calculated based on the PK-Sim® population database was used [22–25]. The relative expression of CYP3A4 in the different organs of the body was defined using the PK-Sim® expression database [26]. Information on the selected expression profile and CYP3A4 reference concentration is provided in Table S18 of the Supplementary Materials.

Information on physicochemical parameters and absorption, distribution, metabolism, and excretion (ADME) processes were collected from the literature. Model input parameter values that could not be informed from the literature were estimated by mathematical optimization.

The felodipine parent–metabolite PBPK model was built in a stepwise procedure. First, an initial parent felodipine PBPK model was developed. Second, the initial model was complemented by the dehydrofelodipine metabolite model. Parameter values optimized for the initial parent PBPK model were then refined together with the parameter values of the metabolite PBPK model. As it can be assumed that small molecules like felodipine and its metabolite undergo passive glomerular filtration in the kidney, a glomerular filtration rate (GFR) fraction of 1 was used in the model. This parameter describes the fraction of drug that is passively filtered into the urine. Saturable metabolic processes were implemented via Michaelis–Menten kinetics. Otherwise, first-order clearance processes were used. The contribution of intestinal CYP3A4 metabolism after oral felodipine administration was predicted by calculating the intestinal fraction metabolized ($f_{m,int}$) as the amount of felodipine metabolized in all intestinal compartments expressing CYP3A4 relative to the total amount of felodipine. The dissolution of tablet formulations with different felodipine release kinetics was described using Weibull dissolution functions implemented in PK-Sim®. The mathematical implementation of the Weibull dissolution is described in more detail in Section 1.1 of the Supplementary Materials. To evaluate the implemented dissolution parameters for the description of the extended-release formulation, the model was applied to predict in vivo dissolution profiles measured by Weitschies et al. [27] as an external model evaluation step.

2.4. PD Model Building

The PBPK model of felodipine was extended by a diastolic blood pressure and a heart rate PD model. As blood pressure and heart rate undergo fluctuations throughout the day, diurnal variation in the baseline diastolic blood pressure and heart rate was included based on models developed by Chae et al. [28] and Lott et al. [29]. The effect of felodipine on diastolic blood pressure and heart rate was described using a direct-effect E_{max} model without lag time according to Equation (1).

$$E = \frac{E_{max} \times C^h}{EC_{50}^h + C^h} \quad (1)$$

where E_{max} is the maximum effect of felodipine on diastolic blood pressure or heart rate, EC_{50} is the concentration necessary to achieve half of E_{max}, h is the hill coefficient, and C is the felodipine plasma concentration.

E_{max} and EC_{50} values were optimized using the diastolic blood pressure and heart rate training dataset. A detailed description of the PD model building is provided in the Supplementary Materials Section 1.6.

2.5. Model Evaluation

The performance of the felodipine model was evaluated graphically by comparing (1) simulated plasma concentration−time profiles, as well as diastolic blood pressure and heart rate profiles, to the respective observed measurements; (2) all predicted plasma concentration, diastolic blood pressure, and heart rate values to their corresponding observed values in goodness-of-fit plots; and (3) predicted and observed AUC (calculated from the time of drug administration to the time of the last concentration measurement (AUC_{last})) and maximum plasma concentration (C_{max}) values in goodness-of-fit plots. Additionally, the mean relative deviation (MRD) of predicted plasma concentrations, diastolic blood pressure, and heart rate values, as well as the geometric mean fold error (GMFE) of predicted AUC_{last} and C_{max} values, were calculated as quantitative measures, as described in Equations (S3) and (S4) in the Supplementary Materials.

2.6. DDI Modeling

The felodipine PBPK model was applied as a CYP3A4 victim drug model to predict DDIs with the CYP3A4 inhibitors erythromycin and itraconazole and the CYP3A4 inducers carbamazepine and phenytoin. For erythromycin [30], itraconazole [31], carbamazepine [32], and phenytoin (unpublished, in-house), we used available PBPK models that have been previously evaluated for DDI predictions as CYP3A4 perpetrator models.

To establish DDI simulations, virtual individuals were generated and administration protocols of felodipine and the perpetrator drugs were established according to the information provided in the study protocols, which is summarized in Tables S10, S13 and S16 of the Supplementary Materials. In the itraconazole–felodipine study, an extended-release formulation of felodipine was administered that was not reflected in the felodipine PBPK model. To describe the dissolution kinetics of this formulation, the Weibull parameters were optimized based on felodipine control plasma concentration–time profiles. In the carbamazepine–phenytoin–felodipine DDI study, felodipine was administered to healthy individuals as a control and to epileptic patients receiving carbamazepine or phenytoin as a long-term anticonvulsant treatment. Based on information provided in the study protocol and dosing recommendations from the drug labels, a typical administration protocol was established to simulate carbamazepine and phenytoin administration. In the DDI simulation, felodipine administration began after reaching carbamazepine and phenytoin steady-state levels. The pharmacokinetics of the perpetrators were implemented using the published drug-dependent parameters of the PBPK models without any further adjustments.

The PBPK perpetrator models were coupled with the felodipine model using the CYP3A4 interaction parameters that were implemented and evaluated in these models. The mathematical implementation of (1) the mechanism-based CYP3A4 inhibition by erythromycin, (2) the competitive inhibition of CYP3A4 by itraconazole and its metabolites, and (3) CYP3A4 induction by carbamazepine and phenytoin is described in the Supplementary Materials Section 4. Furthermore, drug-dependent parameters of the perpetrator models are provided in the Supplementary Materials in the respective section.

The DDI performance of felodipine as a CYP3A4 victim drug was assessed by comparing predicted versus observed (1) felodipine and dehydrofelodipine plasma concentration–time profiles, as well as diastolic blood pressure and heart-rate effect–time profiles, with and without co-administration of the perpetrators and (2) DDI AUC_{last} ratios and DDI C_{max} ratios of felodipine and dehydrofelodipine in goodness-of-fit plots. Here, the limits proposed by Guest et al. [33] were used to evaluate the prediction success. Additionally, GMFEs of the predicted DDI AUC_{last} and C_{max} ratios were calculated.

3. Results

3.1. Pharmacokinetic Model

The parent−metabolite PBPK model of felodipine and dehydrofelodipine was built and evaluated using 49 clinical studies. Overall, these clinical studies provided 82 concentration–time profiles of felodipine for intravenous and oral administration, as summarized in

Table 1. Additionally, 12 concentration–time profiles of the metabolite dehydrofelodipine were reported. A detailed overview of all clinical studies involved, including administration protocols, the demographics of the participants, and the assignment to the test or training dataset is provided in the Supplementary Materials Table S1.

Table 1. Clinical studies used for the development of the felodipine PBPK/PD model.

Route	Dose (mg)	n (PK)	n (DBP)	n (HR)	Reference
Healthy Individuals					
iv	1–3	9	1	1	[5,11,34–38]
sol, sd	5–40	15	8	8	[5,7,34–36,39–44]
sol, md	10	1	0	0	[45]
tab, sd	5–10	4	1	2	[7,46–50]
tab, md	5–10	4	0	0	[45,51,52]
tabER, sd	5–40	24	7	6	[7,11,13,14,53–69]
tabER, md	5–10	6	1	1	[45,57,68,70]
Profiles (healthy)		**63**	**18**	**18**	
Hypertensive Individuals					
iv	1–2.25	2	1	1	[71,72]
sol, sd	0.83–10	3	2	0	[34,72]
tab, sd	10	2	2	0	[73]
tab, md	5–10	5	5	1	[51,73–75]
tabER, sd	20	3	1	1	[71,76]
tabER, md	20	4	1	1	[71,75,76]
Profiles (hypertensive)		**19**	**12**	**4**	
Profiles (total)		**82**	**30**	**22**	

DBP: diastolic blood pressure, HR: heart rate, iv: intravenous, md: multiple dose, n: number of profiles, PK: pharmacokinetics, sd: single dose, sol: solution, tab: tablet, tabER: extended-release tablet.

The compartmental structure of a whole-body PBPK model and the implemented metabolic pathways for felodipine and dehydrofelodipine are illustrated in Figure 1a,b, respectively. The final felodipine model accounts for (1) CYP3A4 metabolism to dehydrofelodipine and (2) passive glomerular filtration, and the dehydrofelodipine model accounts for (3) CYP3A4-mediated clearance, (4) unspecific hepatic clearance, and (5) passive glomerular filtration. To describe the biotransformation of felodipine to dehydrofelodipine via CYP3A4, the Michaelis–Menten constant (K_m) was acquired from the literature, while the catalytic rate constant (k_{cat}) was estimated. To adequately describe the plasma concentrations after the administration of the extended-release formulation, the formulation-specific felodipine solubility was estimated in addition to the Weibull parameters, which was approximately eight-fold lower compared to the felodipine solubility gathered from the literature and used in the model otherwise. Only sparse information on the metabolism of dehydrofelodipine was found in the literature; therefore, the implemented clearance processes had to be estimated. The final drug-dependent input parameters in comparison to the parameters available in the literature are listed in Table 2.

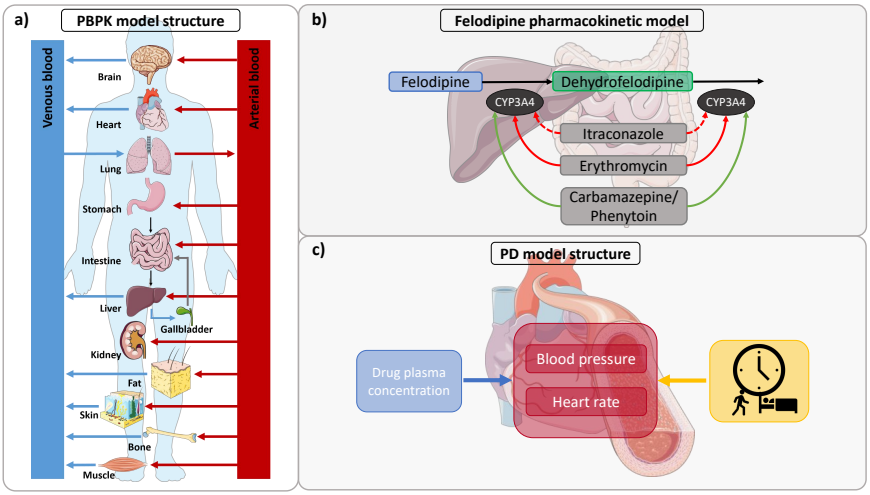

Figure 1. (**a**) Structure of a whole-body PBPK model. In this multi-compartmental modeling approach, compartments represent ADME-relevant organs of the body. The compartments are interconnected with arterial (red arrows) and venous (blue arrows) blood flows. (**b**) Metabolic pathways of felodipine and dehydrofelodipine and DDI network. Felodipine is metabolized by CYP3A4 to dehydrofelodipine, which is also metabolized by CYP3A4 (black arrows). Itraconazole and erythromycin are competitive (dotted red arrow) and mechanism-based (red arrow) inhibitors of CYP3A4, respectively, and inhibit the metabolism of felodipine and its metabolite, while carbamazepine and phenytoin induce CYP3A4. (**c**) Structure of the PBPK/PD model extension. Blood pressure and heart rate undergo diurnal variations (yellow). Alterations in diastolic blood pressure and heart rate are directly correlated to felodipine plasma concentrations (blue). Drawings by Servier, licensed under CC BY 3.0 [77]. CYP: cytochrome P450, DDI: drug–drug interaction, PBPK: physiologically based pharmacokinetic, PD: pharmacodynamics.

Table 2. Drug-dependent parameters of the felodipine PBPK model.

Parameter	Unit	Model	Literature	Reference	Description
			Felodipine		
MW	g/mol	384.25	384.25	[78]	Molecular weight
fu, plasma	%	0.36	0.36	[79]	fraction unbound in plasma
Solubility (pH)	mg/L	7.15 (6.5)	1.2 (7) 7.15 (6.5) 14.3 (7.1) 19.7 (7)	[80–82]	Solubility at reference pH
Solubility-tabER (pH)	mg/L	0.89 (7)	-	-	Solubility at reference pH used for extended-release tablets
logP	-	4.36	3.44 3.80 4.36 4.46 4.64	[78,81–83]	Lipophilicity
Intestinal permeability	cm/min	2.76×10^{-4}	4.42×10^{-4} 3.06×10^{-4} 2.64×10^{-4}	[81,84]	Transcellular intestinal permeability

Table 2. *Cont.*

Parameter	Unit	Model	Literature	Reference	Description
			Felodipine		
GFR fraction	-	1	-	-	Fraction of filtered drug in the urine
K_m-CYP3A4	µmol/L	2.81	0.94 2.81 26.4	[9,81,85]	CYP3A4 Michaelis–Menten constant
k_{cat}-CYP3A4	1/min	250.44	-	-	CYP3A4 catalytic rate constant
Weibull time-tab	min	54.86	-	-	Tablet dissolution profile shape
Weibull shape-tab	-	1.32	-	-	Tablet dissolution time (50% dissolved)
Weibull time-tabER	min	173.04	-	-	Extended-release tablet dissolution profile shape
Weibull shape-tabER	-	1.30	-	-	Extended-release tablet dissolution time (50% dissolved)
Partition coefficient	-	Diverse	RR		Cell to plasma partition coefficients
Cellular permeability	cm/min	0.42	PK-Sim		Permeability into the cellular space
			Dehydrofelodipine		
MW	g/mol	382.24	382.24	[86]	Molecular weight
pKa (base)	-	4.06	4.06	[86]	Acid dissociation constant
fu, plasma	%	0.68	-	-	fraction unbound in plasma
Solubility (pH)	mg/L	2.93	2.93	[86]	Solubility at reference pH
logP	-	3.32	4.24	[86]	Lipophilicity
Intestinal permeability	cm/min	1.38×10^{-4}	estimated via PK-Sim®		Transcellular intestinal permeability
GFR fraction	-	1	-	-	Fraction of filtered drug in the urine
CL-CYP3A4	1/min	35.74	-	-	CYP3A4-mediated clearance
CL-hepatic	1/min	2.76	-	-	Unspecific hepatic clearance
Partition coefficient	-	Diverse	S		Cell to plasma partition coefficients
Cellular permeability	cm/min	0.04	CDS		Permeability into the cellular space

CYP3A4: cytochrome P450 3A4, GFR: glomerular filtration rate, PK-Sim: PK-Sim standard, RR: Rodgers and Rowland, S: Schmitt, CDS: charge-dependent Schmitt, tab: tablet, tabER: extended-release tablet.

The predicted in vivo dissolution–time profiles after the administration of an extended-release felodipine tablet are displayed in Figure S4 of the Supplementary Materials. Here, the dissolution was well-predicted by the model, with a mean MRD of 1.51 for all dissolution measurements.

Furthermore, the model predicted the $f_{m,int}$ as ~53% and an oral bioavailability of 13–18% after oral felodipine administration, implying a high extent of intestinal metabolism as well as a high first-pass metabolism.

When the model was applied to predict the pharmacokinetics in hypertensive individuals, the plasma concentrations were underpredicted. The adjustment of the CYP3A4 k_{cat} for each study could improve the model predictions considerably. Hence, the k_{cat}

values were reduced on average by 32% (range: 20–43%), resulting in an overall lower felodipine clearance.

Figure 2 shows selected plasma concentration−time profiles predicted by the model in comparison to observed clinical data, and Figure 3 shows goodness-of-fit plots comparing predicted versus observed AUC_{last} and C_{max} values of felodipine and dehydrofelodipine for all studies. A comprehensive evaluation of the felodipine parent–metabolite PBPK model is provided in the Supplementary Materials, including linear and semi-logarithmic plasma concentration–time profiles of all simulated studies (Figures S2 and S3); goodness-of-fit plots of predicted versus observed (1) AUC_{last}, (2) C_{max}, and (3) plasma concentration values (Figures S5 and S6); and the GMFE and MRD values of all studies (Tables S3 and S4). Overall, 89% and 82% of all felodipine and dehydrofelodipine predicted plasma concentrations, respectively, deviated less than two-fold from the observed values. The overall mean MRD of 1.67 and GMFE values for the AUC_{laxt} and C_{max} of 1.26 and 1.28, respectively, indicated a good model performance.

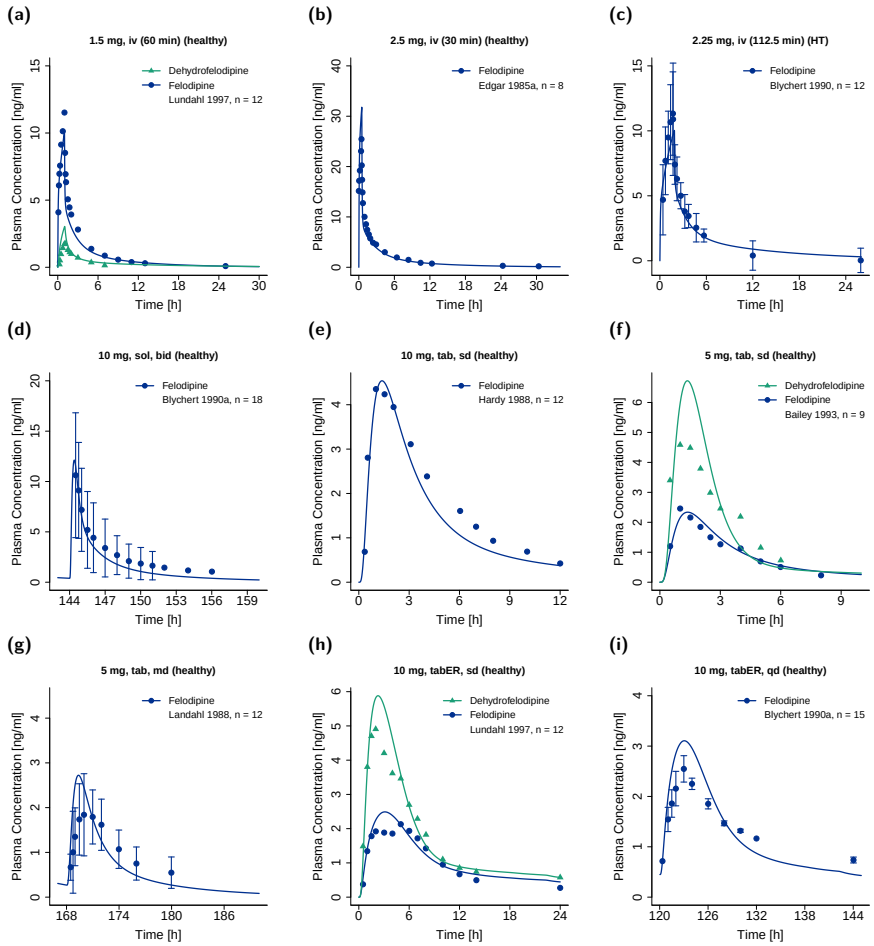

Figure 2. Predicted plasma concentration–time profiles of felodipine after administration as (**a**–**c**) intravenous infusion, (**d**) oral solution, (**e**–**g**) conventional tablet, or (**h**,**i**) extended-release tablet in comparison to observed data [11,35,45,47,48,51,71]. Observed data are shown as dots (felodipine) and triangles (dehydrofelodipine) ± standard deviation (if available); model predictions are shown as lines (blue: felodipine, green: dehydrofelodipine). bid: twice daily, HT: hypertensive, iv: intravenous, n: number of individuals, sd: single dose, sol: solution, tab: tablet, tabER: extended-release tablet.

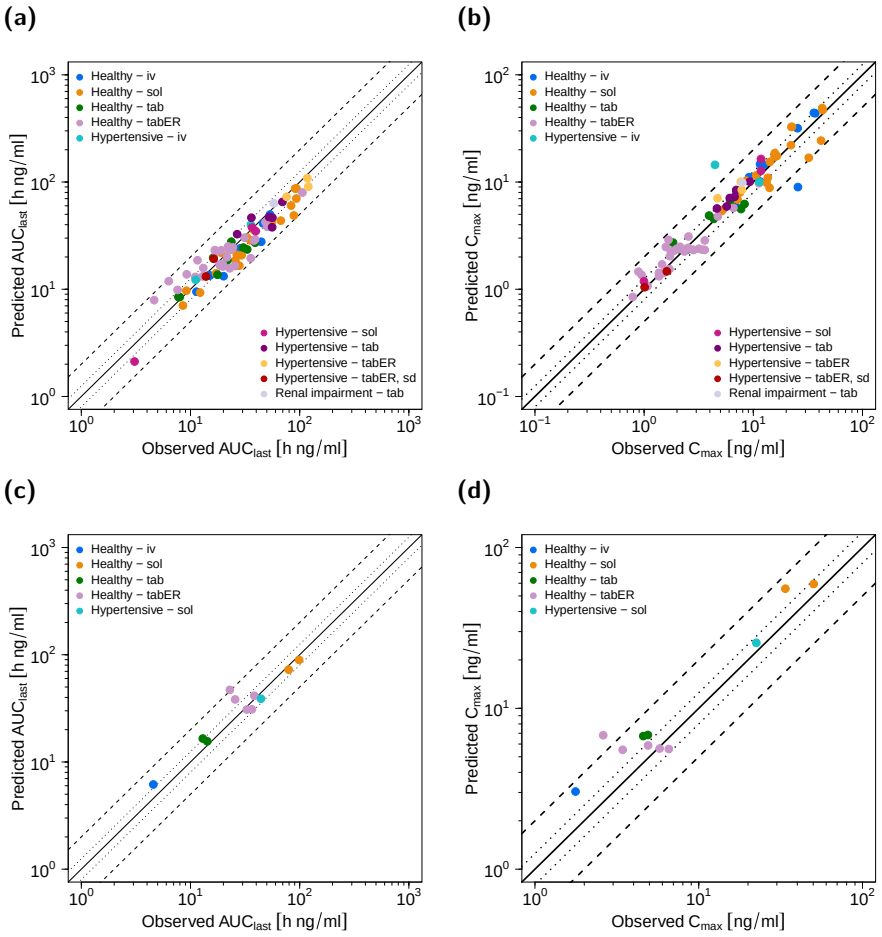

Figure 3. Performance of the felodipine PBPK model. Predicted compared to observed AUC_{last} and C_{max} values of (**a**,**b**) felodipine and (**c**,**d**) dehydrofelodipine stratified by route of administration and health status of the study participants. The line of identity is shown as a solid line; 1.25-fold deviation is shown as dotted lines; 2-fold deviation is shown as dashed lines. Study references are listed in Table 1. AUC_{last}: area under the plasma concentration−time curve from the time of dosing to the time of last concentration measurement, C_{max}: maximum plasma concentration, iv: intravenous, sol: solution, tab: tablet, tabER: extended-release tablet, sd: single dose.

3.2. Pharmacodynamic Model

The felodipine parent–metabolite PBPK model was extended by a PD model, describing the effect of felodipine on the diastolic blood pressure and heart rate. Overall, 30 blood pressure–time profiles and 22 heart rate–time profiles from a total of 17 clinical studies were used to establish the PD model. The measurements were derived from healthy as well as hypertensive individuals.

Some parameters of the circadian models [28,29] were adjusted for each study individually, as described in detail in the Supplementary Materials Section 1.6. In summary, values for the circadian amplitudes (*amp*) were used as provided by the model authors, while the circadian phase and the mean diastolic blood pressure and heart rate (BP_{mean}, HR_{mean}) were optimized. After individually optimizing the diurnal model parameters for the studies of the training dataset using placebo blood pressure and heart rate profiles, parameter values

of the E_{max} model were estimated. The parameters used in the final PBPK/PD model are listed in Table 3.

Table 3. Parameters used for the diastolic blood pressure and heart rate PD model.

Parameter	Unit	Model	Literature	Reference	Description
Diastolic Blood Pressure Model					
E_{max}	mmHg	56.18	-	-	Maximum effect on diastolic blood pressure
EC_{50}	µmol/L	0.04	-	-	Concentration for half-maximal effect
amp_{24}	%	2.14	2.14	[28]	Amplitude for 24 h period
amp_{12}	%	5.93	5.93	[28]	Amplitude for 12 h period
$phase_{24}$	h	5.28 (2.10) [a]	-	-	Phase for 24 h period
$phase_{12}$	h	0.16 (2.10) [a]	-	-	Phase for 12 h period
BP_{mean}	mmHg	70.4 (6.76) [a]; 91.9 (6.60) [a,b]	69.5	[28]	Mean diastolic blood pressure over 24 h
Heart Rate Model					
E_{max}	bpm	39.71	-	-	Maximum effect on heart rate
EC_{50}	µmol/L	0.05	-	-	Concentration for half-maximal effect
h	-	1.40	-	-	Hill coefficient
amp	%	6.3	6.3	[29]	Amplitude
phase	h	11.8 (5.13) [a]	9.2	[29]	Phase
HR_{mean}	bpm	62.2 (4.21) [a]; 66.4 (3.32) [a,b]	66.2	[29]	Mean heart rate over 24 h

[a] mean (standard deviation), individually optimized values for individual simulations in Supplementary Materials Table S5. [b] mean diastolic blood pressure and heart rate values used for hypertensive individuals.

Selected effect–time profiles of diastolic blood pressure and heart rate predicted by the model in comparison to observed measurements are shown in Figure 4, along with corresponding felodipine plasma concentration–time profiles. Overall, the mean MRD values of 1.06 for both predicted diastolic blood pressure and heart rate measurements during felodipine administration indicated a good model performance. Predicted compared to observed effect–time profiles of diastolic blood pressure and heart rate for all studies are shown in Figures S9 and S10 in the Supplementary Materials. Goodness-of-fit plots of all predicted compared to observed diastolic blood pressure and heart rate measurements, as well as corresponding calculated MRD values, are shown in Figure S11 and Tables S7 and S8 in the Supplementary Materials.

3.3. DDI Modeling

The performance of the model for felodipine as a CYP3A4 victim drug in DDI simulations was assessed using one DDI study with erythromycin as the mechanism-based CYP3A4 inhibitor and one study with itraconazole (and its metabolites) as the competitive CYP3A4 inhibitor. Furthermore, one DDI study with carbamazepine and phenytoin as CYP3A4 inducers was used. In all studies, participants were pretreated with multiple doses of the perpetrator before felodipine was administered.

The setup of all DDI simulations is described in the Supplementary Materials Section 4.

The DDI performance of the felodipine model is presented in Figure 5, showing (1) predicted compared to observed victim drug plasma concentration−time profiles, with and without the co-administration of the perpetrator drug; (2) predicted compared to observed diastolic blood pressure and heart rate effect–time profiles, with and without

the co-administration of itraconazole; and (3) goodness-of-fit plots of predicted compared to observed DDI AUC_{last} and DDI C_{max} ratios. All predicted DDI AUC_{last} and DDI C_{max} ratios were within the limits proposed by Guest et al. [33], with mean GMFE values of 1.31 and 1.23, respectively.

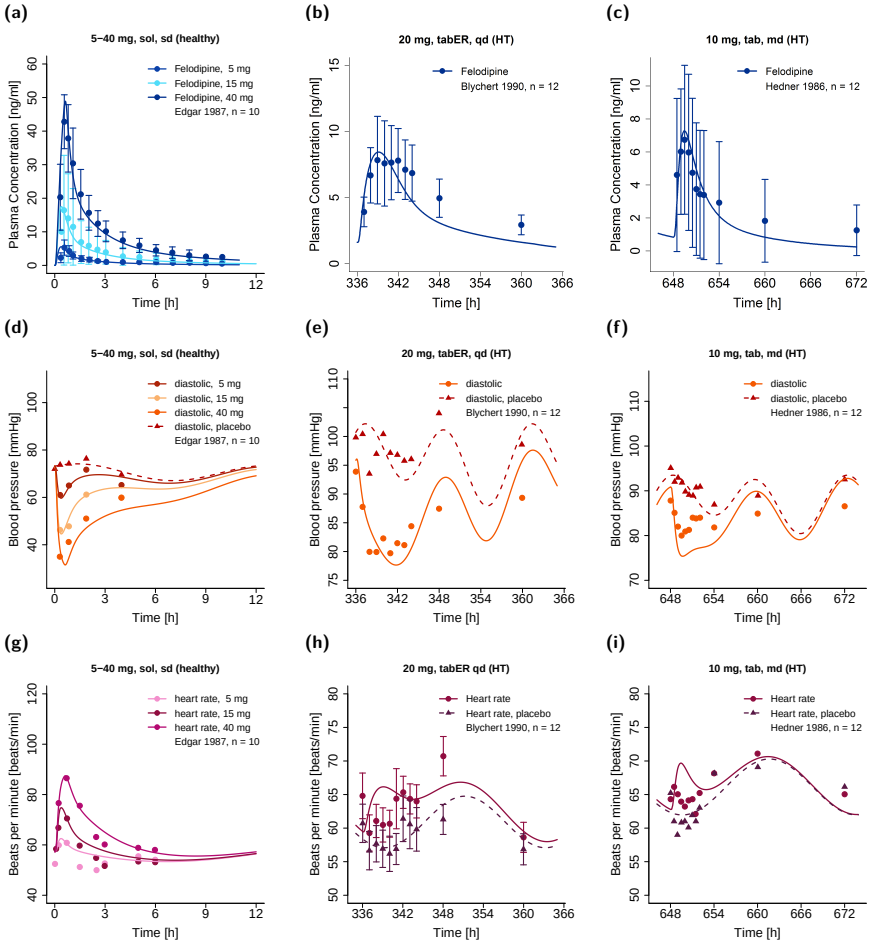

Figure 4. Predicted (**a**–**c**) plasma concentration–time profiles of felodipine with corresponding predicted (**d**–**f**) diastolic blood pressure (**g**–**i**) and heart rate effect–time profiles in healthy individuals (left panel) and hypertensive patients (center and right panels) in comparison to observed data [36,71,74]. Observed data are shown as dots and triangles ± standard deviation (if available); model predictions are shown as lines. HT: hypertensive, md: multiple dose, n: number of individuals, qd: once daily, sd: single dose, sol: solution, tab: tablet, tabER: extended-release tablet.

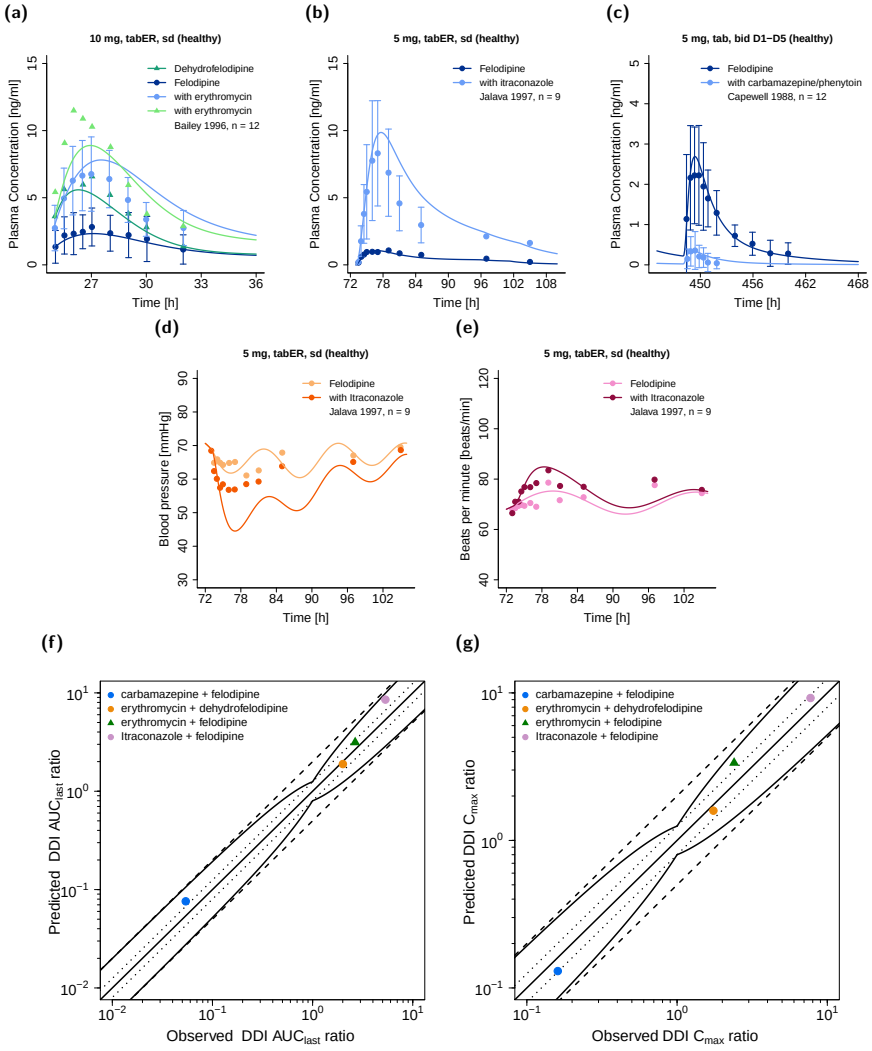

Figure 5. Upper row: predicted felodipine plasma concentration–time profiles with and without co-administration of the perpetrators (**a**) erythromycin, (**b**) itraconazole, and (**c**) carbamazepine and phenytoin in comparison to observed data [13–15]. Center row: predicted (**d**) diastolic blood pressure and (**e**) heart rate–time profiles with and without co-administration of itraconazole in comparison to observe data. Lower row: goodness-of-fit plots of predicted versus observed (**f**) DDI AUC_{last} ratios and (**g**) DDI C_{max} ratios. AUC_{last}: area under the plasma concentration−time curve from the time of dosing to the time of last concentration measurement, bid: twice daily, C_{max}: maximum plasma concentration, D: day, DDI: drug–drug interaction, n: number of individuals, sd: single dose, tab: tablet, tabER: extended-release tablet.

4. Discussion

A whole-body parent−metabolite PBPK/PD model of felodipine and its main metabolite dehydrofelodipine was successfully established. The model was able to describe and predict plasma concentration−time profiles of felodipine and dehydrofelodipine as well as alterations in the diastolic blood pressure and heart rate after the intravenous administration (1–3 mg) of felodipine and oral administration (5–40 mg) as a solution, tablet, or

extended-release tablet. The performance of the parent–metabolite PBPK/PD model was thoroughly evaluated, and the model was applied to predict DDI scenarios with felodipine as a CYP3A4 victim drug.

PBPK modeling of felodipine has previously been applied to investigate specific scenarios, such as the study of intestinal availability and metabolism [81,87,88] or the comparison of the pharmacokinetics after the administration of extended-release formulations from different manufacturing sites [89]. In contrast to prior work investigating the felodipine concentration–effect relationship [4,73,90], the presented model is the first parent–metabolite PBPK/PD model of felodipine. Moreover, the model is capable of investigating the effect of DDIs on both felodipine pharmacokinetics and pharmacodynamics. The model was developed by considering a broad range of clinical studies (n = 49, Table 1), with model development and evaluation being comprehensively documented and the model files freely available in the Open Systems Pharmacology repository (https://github.com/Open-Systems-Pharmacology, accessed on 12 July 2022).

Felodipine is extensively metabolized by CYP3A4, and the implementation of CYP3A4 as the sole route of felodipine metabolism was sufficient to describe its pharmacokinetics. It undergoes extensive metabolic degradation, and no unchanged felodipine is found in the urine, which is in line with the simulations obtained by the presented model, as only a very low fraction (<0.5%) of felodipine was predicted to be excreted unchanged in the urine. The dissolution of solid oral formulations was described by Weibull functions. For the extended-release formulation, the Lint80 dissolution model was tested as well, assuming the linear release of felodipine from the formulation until 80% of the administered dose was dissolved. Although a linear dissolution pattern was described in the literature [27], felodipine plasma concentration–time profiles could be more accurately described using a Weibull dissolution model with an estimated dissolution time (50% dissolved) of 173 min, which is in accordance with dissolution measurements from the literature [27]. However, to predict the plasma concentration–time profiles for extended-release tablets, a separate, formulation-specific felodipine solubility had to be estimated, as the application of the literature-derived felodipine solubility (7.15 mg/L) resulted in an overprediction of felodipine plasma concentrations after ~5–6 h hours. It was assumed that this overprediction resulted from an overestimation of the felodipine absorption after the transition of the tablet to distal intestinal compartments (e.g., caecum and colon ascendens). Here, the solubility was optimized as a surrogate to reduce felodipine absorption from these compartments. This resulted in an eight-fold lower solubility (compared to the literature value), which markedly improved the prediction of felodipine plasma concentrations. However, the fraction dissolved and fraction absorbed were not affected by the reduced solubility, and the model successfully described the dissolution–time profile of the extended-release tablet (Figure S4) [27].

Independent of the formulations, the model predicted the near-complete oral absorption of felodipine (fraction absorbed >95%), which was in accordance with the literature [1]. Moreover, the fraction of the administered dose metabolized by CYP3A4 in the intestines was predicted as approximately 53%, confirming the high extent of intestinal felodipine metabolism reported by Lundahl and coworkers [11]. The model also successfully described the observed low oral bioavailability of felodipine (13–18%) resulting from the extensive presystemic CYP3A4 metabolism [36]. In conclusion, intestinal absorption, metabolism, and bioavailability were well described, allowing the application of DDI simulations to investigate the influence of CYP3A4 perpetrators on felodipine pharmacokinetics. The overall good model performance could be quantified by the calculated mean GMFE values for the AUC_{last} and C_{max} of 1.26 and 1.28, respectively.

The felodipine parent–metabolite PBPK model was developed using plasma concentration–time profiles from healthy individuals and was subsequently applied to predict felodipine pharmacokinetics in hypertensive individuals, which resulted in an underprediction of the observed plasma concentration–time profiles. Higher felodipine exposure in hypertensive patients was also observed in the literature, along with a decrease in felodipine

clearance by approximately two-fold, while absorption and distribution were similar compared to healthy individuals [51]. It was assumed that the observed differences in pharmacokinetics were mainly related to the older age of the hypertensive patients compared with healthy individuals and not to hypertension itself [51,91]. However, as the age of the individuals was considered during the establishment of the virtual simulations and was sufficient to describe the pharmacokinetics of felodipine in healthy middle-aged and elderly individuals (Figures S2 and S3(av,be,by)), an additional impact of hypertension-related factors may not fully be excluded. No information on the potential effects of hypertension on felodipine pharmacokinetics could be found in the literature. However, hypertension is a common risk factor for cardiovascular and renal disease [92], and inflammatory processes are involved in the genesis of hypertension and the progression of organ damage [92,93]. The downregulation of CYP enzymes, including CYP3A4, by inflammation has previously been described [94] and has also been observed in patients with, e.g., chronic kidney disease [95]. Hence, an immune-mediated downregulation of CYP3A4 in hypertensive individuals appears plausible. Therefore, CYP3A4 k_{cat} was separately optimized for healthy and hypertensive populations, yielding a mean reduction in CYP3A4 k_{cat} of 32% for hypertensive individuals and thus improving predictions in comparison to an unstratified CYP3A4 k_{cat} approach. However, clinical studies are needed to further investigate this hypothesis.

The PD model focused on the effect of felodipine on diastolic blood pressure and heart rate but not systolic blood pressure, due to a lack of data. Pronounced decreases in systolic blood pressure have been observed in hypertensives [71] but not in healthy individuals, even after high doses of up to 40 mg [5,54]. Thus, more systolic blood pressure measurements from healthy individuals would have been necessary to accurately describe the differences in PD effect magnitudes.

To describe the effect of felodipine on diastolic blood pressure and heart rate, the concentration–effect relationship was described using a direct-effect E_{max} model without lag time, similar to other PD models of felodipine [4,73,90]. The concentration–effect relationship was established using felodipine plasma concentrations instead of heart concentrations, as felodipine shows a higher pharmacodynamic potency in vascular muscles compared to the myocardium [96]. An EC_{50} value of 40 nmol/L and an E_{max} value of 56.18 mmHg were estimated for the diastolic blood pressure PD model. In contrast, other studies reported lower EC_{50} (~8 nmol/L) and E_{max} (~29 mmHg) values to describe the plasma concentration–effect relationship [4,73]. However, our PBPK/PD analysis included blood pressure effect–time profiles for broader felodipine dosing, plasma concentration, and PD effect ranges, which unsurprisingly resulted in a higher estimated E_{max} and related EC_{50} values.

Overall, the pharmacodynamic effect of felodipine was sufficiently described for healthy as well as hypertensive individuals, regardless of potential antihypertensive comedication or initial baseline blood pressure. As only three studies provided heart rate data after multiple doses of felodipine, it was impossible to include the tolerance effects described in the literature [1] in the current model.

The PBPK/PD model was finally applied in DDI simulations, and the impact of CYP3A4 perpetrators on felodipine plasma concentrations was overall well described. For the DDI prediction with the CYP3A4 inhibitors erythromycin or itraconazole, C_{max} and t_{max} were slightly overpredicted. Nonetheless, the magnitude of the interaction was sufficiently explained by the model, illustrated by predicted versus observed DDI AUC_{last} and C_{max} ratios of 1.17 and 1.39 for the erythromycin–felodipine DDI and 1.60 and 1.19 for the itraconazole–felodipine DDI. The erythromycin–felodipine DDI study revealed the possible CYP3A4 metabolism of dehydrofelodipine [14]. Therefore, a CYP3A4-mediated clearance of dehydrofelodipine was implemented in addition to an unspecific hepatic clearance process. As no further information on dehydrofelodipine metabolism was available from the literature, the erythromycin–felodipine DDI was used in the training dataset to guide the estimation of the clearance parameters. Furthermore, the effect of the CYP3A4

inducers carbamazepine and phenytoin on felodipine pharmacokinetics was well described, although the carbamazepine–phenytoin-felodipine DDI study was conducted in patients undergoing long-term anticonvulsant treatment and did not provide detailed information on their treatment regimen. A decrease in felodipine bioavailability from 15% to around 1% was reported if felodipine was administered to patients on anticonvulsant therapy, while the model predicted a decrease in bioavailability from around 13% to 2% [15]. Here, DDI AUC_{last} and C_{max} ratios of 1.40 and 0.81 were calculated. Overall, the DDI AUC_{last} and DDI C_{max} effect ratios were within the limits proposed by Guest et al. [33], with mean GMFE values of 1.31 and 1.23, respectively.

The itraconazole–felodipine DDI study additionally provided pharmacodynamic measurements of diastolic blood pressure and heart rate. The model was capable of describing the observed increase in heart rate if felodipine was co-administered with itraconazole; however, the observed decrease in blood pressure was slightly overpredicted. Previous studies showed that itraconazole may increase blood pressure by inhibiting 11β-hydroxysteroid dehydrogenase type 2 [97], and various case reports in the literature have described elevated blood pressure during itraconazole treatment. However, increased blood pressure was mainly associated with high itraconazole doses (>400 mg/day) [98], and controlled studies investigating the potential effects of itraconazole on blood pressure are lacking. Based on the available data, the potential effects of itraconazole on blood pressure could not be determined for the itraconazole–felodipine DDI study, where itraconazole was administered in low doses (200 mg/day) over a short time period (4 days).

Overall, the presented analysis demonstrated that felodipine is susceptible to CYP3A4-mediated DDIs. Case reports describing the occurrence of major side effects, such as edema or tachycardia, if itraconazole or erythromycin was administered to felodipine-treated patients emphasize the clinical relevance of these interactions [12,99]. The parent–metabolite PBPK model of felodipine can be applied in DDI simulations to predict the effect of CYP3A4 perpetrators on bioavailability and plasma concentrations, which may help to support the design of dedicated clinical DDI studies. As the model also describes the effects on heart rate and diastolic blood pressure, it may also be applied to guide treatment decisions or optimizations.

5. Conclusions

A felodipine parent–metabolite PBPK/PD model was successfully developed to describe the pharmacokinetics of felodipine after intravenous and oral administrations over a broad dosing range, along with the effect of felodipine on diastolic blood pressure and heart rate. The pharmacokinetics of felodipine, especially its metabolism via CYP3A4, were sufficiently described, as shown by the adequate description of the oral felodipine bioavailability and the successful prediction of DDIs with CYP3A4 inhibitors and inducers. The felodipine PBPK model can be applied in DDI predictions as a CYP3A4 victim drug to evaluate the effects of CYP3A4 perpetrators, e.g., as a probe model to investigate grapefruit–drug interactions. Thereby, the PBPK model can be used to estimate the contribution of intestinal metabolism to overall bioavailability.

Supplementary Materials: The following are available online at https://www.mdpi.com/article/10.3390/pharmaceutics14071474/s1: Comprehensive reference manual, providing documentation of the complete model performance assessment.

Author Contributions: Conceptualization, L.M.F., F.Z.M., M.M., F.M., D.S. and T.L.; funding acquisition, T.L.; investigation, L.M.F., F.Z.M., M.M. and T.L.; visualization, L.M.F.; writing—original draft, L.M.F.; writing—review and editing, L.M.F., F.Z.M., M.M., F.M., D.S. and T.L. All authors have read and agreed to the published version of the manuscript.

Funding: This research was funded by the German Federal Ministry of Education and Research (BMBF), grant number 031L0161C ("OSMOSES").

Data Availability Statement: All modeling files, including utilized clinical study data, can be found at: https://github.com/Open-Systems-Pharmacology.

Conflicts of Interest: Thorsten Lehr has received research grants from the German Federal Ministry of Education and Research (grant 031L0161C). Felix Mahfoud is supported by Deutsche Gesellschaft für Kardiologie (DGK), Deutsche Forschungsgemeinschaft (SFB TRR219), and Deutsche Herzstiftung. He has received scientific support from Medronic and ReCor Medical and speaker honoraria from Astra-Zeneca, Bayer, Boehringer Ingelheim, Inari, Medtronic, Merck, and ReCor Medical. Laura Maria Fuhr, Fatima Zahra Marok, Maximilian Mees, and Dominik Selzer declare no conflict of interest. The funders had no role in the design of the study; in the collection, analyses, or interpretation of data; in the writing of the manuscript; or in the decision to publish the results.

References

1. AstraZeneca LP. Plendil (Felodipine). Extended-Release Tablets. Available online: https://www.accessdata.fda.gov/drugsatfda_docs/label/2012/019834s025lbl.pdf (accessed on 26 October 2021).
2. Heumann Pharma. Felodipin Retard Heumann. Available online: https://www.heumann.de/fileadmin/user_upload/produkte/infos/Fachinformation-Felodipin-retard-Heumann.pdf (accessed on 26 October 2021).
3. Williams, B.; Mancia, G.; Spiering, W.; Agabiti Rosei, E.; Azizi, M.; Burnier, M.; Clement, D.L.; Coca, A.; de Simone, G.; Dominiczak, A.; et al. 2018 ESC/ESH Guidelines for the management of arterial hypertension. *Eur. Heart J.* **2018**, *39*, 3021–3104. [CrossRef] [PubMed]
4. Blychert, E.; Edgar, B.; Elmfeldt, D.; Hedner, T. Plasma concentration—Effect relationships for felodipine: A meta analysis. *Clin. Pharmacol. Ther.* **1992**, *52*, 80–89. [CrossRef] [PubMed]
5. Bengtsson-Hasselgren, B.; Edgar, B.; Rönn, O. Dose-dependent effects of felodipine on diuresis and natriuresis in healthy subjects. *J. Cardiovasc. Pharmacol.* **1988**, *12*, 134–139. [CrossRef] [PubMed]
6. Benet, L.Z.; Broccatelli, F.; Oprea, T.I. BDDCS applied to over 900 drugs. *AAPS J.* **2011**, *13*, 519–547. [CrossRef]
7. Edgar, B.; Lundborg, P.; Regårdh, C.G. Clinical pharmacokinetics of felodipine. A summary. *Drugs* **1987**, *34*, 16–27. [CrossRef]
8. U.S. Food and Drug Administration. Drug Development and Drug Interactions. Table of Substrates, Inhibitors and Inducers. Available online: https://www.fda.gov/drugs/drug-interactions-labeling/drug-development-and-drug-interactions-table-substrates-inhibitors-and-inducers (accessed on 31 March 2022).
9. Walsky, R.L.; Obach, R.S. Validated assays for human cytochrome P450 activities. *Drug Metab. Dispos.* **2004**, *32*, 647–660. [CrossRef] [PubMed]
10. Fritz, A.; Busch, D.; Lapczuk, J.; Ostrowski, M.; Drozdzik, M.; Oswald, S. Expression of clinically relevant drug-metabolizing enzymes along the human intestine and their correlation to drug transporters and nuclear receptors: An intra-subject analysis. *Basic Clin. Pharmacol. Toxicol.* **2019**, *124*, 245–255. [CrossRef] [PubMed]
11. Lundahl, J.; Regårdh, C.G.; Edgar, B.; Johnsson, G. Effects of grapefruit juice ingestion-pharmacokinetics and haemodynamics of intravenously and orally administered felodipine in healthy men. *Eur. J. Clin. Pharmacol.* **1997**, *52*, 139–145. [CrossRef]
12. Neuvonen, P.J.; Suhonen, R. Itraconazole interacts with felodipine. *J. Am. Acad. Dermatol.* **1995**, *33*, 134–135. [CrossRef]
13. Jalava, K.M.; Olkkola, K.T.; Neuvonen, P.J. Itraconazole greatly increases plasma concentrations and effects of felodipine. *Clin. Pharmacol. Ther.* **1997**, *61*, 410–415. [CrossRef]
14. Bailey, D.G.; Bend, J.R.; Arnold, J.M.; Tran, L.T.; Spence, J.D. Erythromycin-felodipine interaction: Magnitude, mechanism, and comparison with grapefruit juice. *Clin. Pharmacol. Ther.* **1996**, *60*, 25–33. [CrossRef]
15. Capewell, S.; Freestone, S.; Critchley, J.A.J.H.; Pottage, A.; Prescott, L.F. Reduced felodipine bioavailability in patients taking anticonvulsants. *Lancet* **1988**, *2*, 480–482. [CrossRef]
16. European Medicines Agency. Guideline on the Investigation of Drug Interactions. Available online: https://www.ema.europa.eu/en/documents/scientific-guideline/guideline-investigation-drug-interactions-revision-1_en.pdf (accessed on 12 July 2022).
17. European Medicines Agency. Guideline on the Reporting of Physiologically Based Pharmacokinetic (PBPK) Modelling and Simulation. Available online: https://www.ema.europa.eu/en/documents/scientific-guideline/guideline-reporting-physiologically-based-pharmacokinetic-pbpk-modelling-simulation_en.pdf (accessed on 12 July 2022).
18. Zhang, X.; Yang, Y.; Grimstein, M.; Fan, J.; Grillo, J.A.; Huang, S.-M.; Zhu, H.; Wang, Y. Application of PBPK Modeling and Simulation for Regulatory Decision Making and Its Impact on US Prescribing Information: An Update on the 2018–2019 Submissions to the US FDA's Office of Clinical Pharmacology. *J. Clin. Pharmacol.* **2020**, *60* (Suppl. 1), S160–S178. [CrossRef] [PubMed]
19. U.S. Food and Drug Administration. Physiologically Based Pharmacokinetic Analyses—Format and Content. Available online: https://www.fda.gov/media/101469/download (accessed on 12 July 2022).
20. Mitchell, M.; Muftakhidinov, B.; Winchen, T. Engauge Digitizer Software. Available online: http://markummitchell.github.io/engauge-digitizer (accessed on 22 March 2022).
21. Wojtyniak, J.; Britz, H.; Selzer, D.; Schwab, M.; Lehr, T. Data Digitizing: Accurate and Precise Data Extraction for Quantitative Systems Pharmacology and Physiologically-Based Pharmacokinetic Modeling. *CPT Pharmacomet. Syst. Pharmacol.* **2020**, *9*, 322–331. [CrossRef] [PubMed]
22. National Center for Health Statistics Hyattsville MD 20782. Third National Health and Nutrition Examination Survey, (NHANES III). Available online: http://www.cdc.gov/nchs/nhanes.htm (accessed on 12 July 2022).

23. Valentin, J. Basic anatomical and physiological data for use in radiological protection: Reference values. A report of age- and gender-related differences in the anatomical and physiological characteristics of reference individuals. ICRP Publication 89. *Ann. ICRP* **2002**, *32*, 5–265. [CrossRef]
24. Tanaka, G.; Kawamura, H. *Anatomical and Physiological Characteristics for Asian Reference Man: Male and Female of Different Ages: Tanaka Model*; Division of Radioecology; Report Number: NIRS-M-115; National Institute of Radiological Sciences: Hitachinaka, Japan, 1996.
25. Schlender, J.F.; Meyer, M.; Thelen, K.; Krauss, M.; Willmann, S.; Eissing, T.; Jaehde, U. Development of a Whole-Body Physiologically Based Pharmacokinetic Approach to Assess the Pharmacokinetics of Drugs in Elderly Individuals. *Clin. Pharm.* **2016**, *55*, 1573–1589. [CrossRef]
26. Open Systems Pharmacology Suite Community PK-Sim®Ontogeny Database Documentation, Version 7.3. Available online: https://github.com/Open-Systems-Pharmacology/OSPSuite.Documentation/blob/master/PK-SimOntogenyDatabaseVersion7.3.pdf (accessed on 12 July 2022).
27. Weitschies, W.; Wedemeyer, R.-S.; Kosch, O.; Fach, K.; Nagel, S.; Söderlind, E.; Trahms, L.; Abrahamsson, B.; Mönnikes, H. Impact of the intragastric location of extended release tablets on food interactions. *J. Control. Release* **2005**, *108*, 375–385. [CrossRef]
28. Chae, D.; Kim, Y.; Park, K. Characterization of circadian blood pressure patterns using non-linear mixed effects modeling. *Transl Clin. Pharmacol.* **2019**, *27*, 24–32. [CrossRef]
29. Lott, D.; Lehr, T.; Dingemanse, J.; Krause, A. Modeling Tolerance Development for the Effect on Heart Rate of the Selective S1P1 Receptor Modulator Ponesimod. *Clin. Pharmacol. Ther.* **2018**, *103*, 1083–1092. [CrossRef]
30. Frechen, S.; Dallmann, A.; Solodenko, J. Building and Evaluation of a PBPK Model for Erythromycin in Healthy Adults. Available online: https://github.com/Open-Systems-Pharmacology/OSP-PBPK-Model-Library/blob/master/Erythromycin/Erythromycin_evaluation_report.md (accessed on 14 March 2022).
31. Hanke, N.; Frechen, S.; Moj, D.; Britz, H.; Eissing, T.; Wendl, T.; Lehr, T. PBPK Models for CYP3A4 and P-gp DDI prediction: A modeling network of rifampicin, itraconazole, clarithromycin, midazolam, alfentanil, and digoxin. *CPT Pharmacomet. Syst. Pharmacol.* **2018**, *7*, 647–659. [CrossRef]
32. Fuhr, L.M.; Marok, F.Z.; Hanke, N.; Selzer, D.; Lehr, T. Pharmacokinetics of the CYP3A4 and CYP2B6 Inducer Carbamazepine and Its Drug-Drug Interaction Potential: A Physiologically Based Pharmacokinetic Modeling Approach. *Pharmaceutics* **2021**, *13*, 270. [CrossRef] [PubMed]
33. Guest, E.J.; Aarons, L.; Houston, J.B.; Rostami-Hodjegan, A.; Galetin, A. Critique of the two-fold measure of prediction success for ratios: Application for the assessment of drug-drug interactions. *Drug Metab. Dispos.* **2011**, *39*, 170–173. [CrossRef] [PubMed]
34. Edgar, B.; Bengtsson, B.; Elmfeldt, D.; Lundborg, P.; Nyberg, G.; Raner, S.; Rönn, O. Acute diuretic/natriuretic properties of felodipine in man. *Drugs* **1985**, *29*, 176–184. [CrossRef] [PubMed]
35. Edgar, B.; Regårdh, C.G.; Johnsson, G.; Johansson, L.; Lundborg, P.; Löfberg, I.; Rönn, O. Felodipine kinetics in healthy men. *Clin. Pharmacol. Ther.* **1985**, *38*, 205–211. [CrossRef]
36. Edgar, B.; Regårdh, C.G.; Lundborg, P.; Romare, S.; Nyberg, G.; Rönn, O. Pharmacokinetic and pharmacodynamic studies of felodipine in healthy subjects after various single, oral and intravenous doses. *Biopharm. Drug Dispos.* **1987**, *8*, 235–248. [CrossRef]
37. Sluiter, H.E.; Huysmans, F.T.; Thien, T.A.; Koene, R.A.P. Haemodynamic effects of intravenous felodipine in normotensive and hypertensive subjects. *Drugs* **1985**, *29*, 144–153. [CrossRef]
38. Sutfin, T.A.; Lind, T.; Gabrielsson, M.; Regårdh, C.G. Biliary secretion of felodipine metabolites in man after intravenous [14C]felodipine. *Eur. J. Clin. Pharmacol.* **1990**, *38*, 421–424. [CrossRef]
39. Soons, P.A.; Mulders, T.M.T.; Uchida, E.; Schoemaker, H.C.; Cohen, A.F.; Breimer, D.D. Stereoselective pharmacokinetics of oral felodipine and nitrendipine in healthy subjects: Correlation with nifedipine pharmacokinetics. *Eur. J. Clin. Pharmacol.* **1993**, *44*, 163–169. [CrossRef]
40. Abrahamsson, B.; Johansson, D.; Torstensson, A.; Wingstrand, K. Evaluation of solubilizers in the drug release testing of hydrophilic matrix extended-release tablets of felodipine. *Pharm. Res.* **1994**, *11*, 1093–1097. [CrossRef]
41. Bengtsson-Hasselgren, B.; Rönn, O.; Blychert, L.O.; Edgar, B.; Raner, S. Acute effects of felodipine and nifedipine on hepatic and forearm blood flow in healthy men. *Eur. J. Clin. Pharmacol.* **1990**, *38*, 529–533. [CrossRef]
42. Johnsson, G.; Murray, G.; Tweddel, A.; Hutton, I. Haemodynamic effects of a new vasodilator drug, felodipine, in healthy subjects. *Eur. J. Clin. Pharmacol.* **1983**, *24*, 49–53. [CrossRef] [PubMed]
43. Wingstrand, K.; Abrahamsson, B.; Edgar, B. Bioavailability from felodipine extended-release tablets with different dissolution properties. *Int. J. Pharm.* **1990**, *60*, 151–156. [CrossRef]
44. Soons, P.A.; Roosemalen, M.C.M.; Breimer, D.D. Enantioselective determination of felodipine and other chiral dihydropyridine calcium entry blockers in human plasma. *J. Chromatogr.* **1990**, *528*, 343–356. [CrossRef]
45. Blychert, E.; Wingstrand, K.; Edgar, B.; Lidman, K. Plasma concentration profiles and antihypertensive effect of conventional and extended-release felodipine tablets. *Br. J. Clin. Pharmacol* **1990**, *29*, 39–45. [CrossRef]
46. Guo, L.-Q.; Chen, Q.-Y.; Wang, X.; Liu, Y.-X.; Chu, X.-M.; Cao, X.-M.; Li, J.-H.; Yamazoe, Y. Different roles of pummelo furanocoumarin and cytochrome P450 3A5*3 polymorphism in the fate and action of felodipine. *Curr. Drug Metab.* **2007**, *8*, 623–630. [CrossRef]
47. Hardy, B.G.; Bartle, W.R.; Myers, M.; Bailey, D.G.; Edgar, B. Effect of indomethacin on the pharmacokinetics and pharmacodynamics of felodipine. *Br. J. Clin. Pharmacol.* **1988**, *26*, 557–562. [CrossRef] [PubMed]

48. Bailey, D.G.; Arnold, J.M.; Munoz, C.; Spence, J.D. Grapefruit juice-felodipine interaction: Mechanism, predictability, and effect of naringin. *Clin. Pharmacol. Ther.* **1993**, *53*, 637–642. [CrossRef]
49. Edgar, B.; Bailey, D.; Bergstrand, R.; Johnsson, G.; Regårdh, C.G. Acute effects of drinking grapefruit juice on the pharmacokinetics and dynamics of felodipine-and its potential clinical relevance. *Eur. J. Clin. Pharmacol.* **1992**, *42*, 313–317. [CrossRef]
50. Sakamoto, T.; Ohtake, Y.; Itoh, M.; Tabata, S.; Kuriki, T.; Uno, K. Determination of felodipine enantiomers using chiral stationary phase liquid chromatography and gas chromatography/mass spectrometry, and the study of their pharmacokinetic profiles in human and dog. *Biomed. Chromatogr.* **1993**, *7*, 99–103. [CrossRef]
51. Landahl, S.; Edgar, B.; Gabrielsson, M.; Larsson, M.; Lernfelt, B.; Lundborg, P.; Regårdh, C.G. Pharmacokinetics and blood pressure effects of felodipine in elderly hypertensive patients. A comparison with young healthy subjects. *Clin. Pharm.* **1988**, *14*, 374–383. [CrossRef]
52. Smith, S.R.; Wilkins, M.R.; Jack, D.B.; Kendall, M.J.; Laugher, S. Pharmacokinetic interactions between felodipine and metoprolol. *Eur. J. Clin. Pharmacol.* **1987**, *31*, 575–578. [CrossRef] [PubMed]
53. Goosen, T.C.; Cillié, D.; Bailey, D.G.; Yu, C.; He, K.; Hollenberg, P.F.; Woster, P.M.; Cohen, L.; Williams, J.A.; Rheeders, M.; et al. Bergamottin contribution to the grapefruit juice-felodipine interaction and disposition in humans. *Clin. Pharmacol. Ther.* **2004**, *76*, 607–617. [CrossRef] [PubMed]
54. Hasselgren, B.; Rönn, O.; Edgar, B.; Johansson, P.; Wall, B. Pharmacokinetics and hemodynamic and diuretic/natriuretic effects of felodipine administered as an extended-release tablet. *Cardiovasc. Drugs Ther.* **1990**, *4*, 1495–1500. [CrossRef]
55. Lown, K.S.; Bailey, D.G.; Fontana, R.J.; Janardan, S.K.; Adair, C.H.; Fortlage, L.A.; Brown, M.B.; Guo, W.; Watkins, P.B. Grapefruit juice increases felodipine oral availability in humans by decreasing intestinal CYP3A protein expression. *J. Clin. Investig.* **1997**, *99*, 2545–2553. [CrossRef]
56. Lundahl, J.; Regårdh, C.G.; Edgar, B.; Johnsson, G. Relationship between time of intake of grapefruit juice and its effect on pharmacokinetics and pharmacodynamics of felodipine in healthy subjects. *Eur. J. Clin. Pharmacol.* **1995**, *49*, 61–67. [CrossRef] [PubMed]
57. Lundahl, J.U.E.; Regårdh, C.G.; Edgar, B.; Johnsson, G. The interaction effect of grapefruit juice is maximal after the first glass. *Eur. J. Clin. Pharmacol.* **1998**, *54*, 75–81. [CrossRef]
58. Patel Devang, S.; Shanker, N.; Shah Sweety, K.; Thakkar Vaishali, K.; Mehta Nirali, N.; Srivstava Ambrish, K.; Singh, S.; Patel Chitrang, G. Bioequivalence study of two oral extended release formulations of felodipine 10 mg tablets in healthy volunteers under fed condition. *Pharma Sci. Monit. Int. J. Pharm. Sci.* **2011**, *2*, 9–20.
59. Pop, A.; Vlase, L. Leucuta Pharmacokinetic study of felodipine after single oral dose of slow release formulations in healthy volunteers. *Farmacia* **2008**, *56*, 474–482.
60. Xiang, Q.; Li, C.; Zhao, X.; Cui, Y.M. The influence of CYP3A5*3 and BCRPC421A genetic polymorphisms on the pharmacokinetics of felodipine in healthy Chinese volunteers. *J. Clin. Pharm. Ther.* **2017**, *42*, 345–349. [CrossRef]
61. Bailey, D.G.; Kreeft, J.H.; Munoz, C.; Freeman, D.J.; Bend, J.R. Grapefruit juice-felodipine interaction: Effect of naringin and 6′,7′-dihydroxybergamottin in humans. *Clin. Pharmacol. Ther.* **1998**, *64*, 248–256. [CrossRef]
62. Gelal, A.; Balkan, D.; Ozzeybek, D.; Kaplan, Y.C.; Gurler, S.; Guven, H.; Benowitz, N.L. Effect of menthol on the pharmacokinetics and pharmacodynamics of felodipine in healthy subjects. *Eur. J. Clin. Pharmacol.* **2005**, *60*, 785–790. [CrossRef] [PubMed]
63. Madsen, J.K.; Jensen, J.D.; Jensen, L.W.; Pedersen, E.B. Pharmacokinetic interaction between cyclosporine and the dihydropyridine calcium antagonist felodipine. *Eur. J. Clin. Pharmacol.* **1996**, *50*, 203–208. [CrossRef] [PubMed]
64. Aguilar-Carrasco, J.C.; Carrasco-Portugal, M.d.C.; Flores-Murrieta, F.J.; Canizales-Quinteros, S. Oral pharmacokinetics of felodipine in mexican healthy volunteers: Evidence for interethnic differences. *Int. J. Pharmacol.* **2015**, *11*, 382–386. [CrossRef]
65. Bailey, D.G.; Arnold, J.M.; Bend, J.R.; Tran, L.T.; Spence, J.D. Grapefruit juice-felodipine interaction: Reproducibility and characterization with the extended release drug formulation. *Br. J. Clin. Pharmacol.* **1995**, *40*, 135–140.
66. Bailey, D.G.; Dresser, G.K.; Kreeft, J.H.; Munoz, C.; Freeman, D.J.; Bend, J.R. Grapefruit-felodipine interaction: Effect of unprocessed fruit and probable active ingredients. *Clin. Pharmacol. Ther.* **2000**, *68*, 468–477. [CrossRef]
67. Bailey, D.G.; Dresser, G.K.; Bend, J.R. Bergamottin, lime juice, and red wine as inhibitors of cytochrome P450 3A4 activity: Comparison with grapefruit juice. *Clin. Pharmacol. Ther.* **2003**, *73*, 529–537. [CrossRef]
68. Dresser, G.K.; Bailey, D.G.; Carruthers, S.G. Grapefruit juice-felodipine interaction in the elderly. *Clin. Pharmacol. Ther.* **2000**, *68*, 28–34. [CrossRef]
69. Dresser, G.K.; Urquhart, B.L.; Proniuk, J.; Tieu, A.; Freeman, D.J.; Arnold, J.M.; Bailey, D.G. Coffee inhibition of CYP3A4 in vitro was not translated to a grapefruit-like pharmacokinetic interaction clinically. *Pharmacol. Res. Perspect.* **2017**, *5*, e00346. [CrossRef]
70. A Comparative Study on the Relative Bioavailability of 2.5 and 5mg ER Tablets of Felodipine. 19834. Available online: https://www.accessdata.fda.gov/drugsatfda_docs/nda/pre96/19834-S002_PLENDILTABLETS_BIOEQR.PDF (accessed on 22 April 2022).
71. Blychert, E.; Hedner, T.; Dahlöf, C.; Elmfeldt, D. Plasma concentration-effect relationships of intravenous and extended-release oral felodipine in hypertensive patients. *J. Cardiovasc. Pharmacol.* **1990**, *15*, 428–435. [CrossRef]
72. Edgar, B.; Regårdh, C.G.; Attman, P.O.; Aurell, M.; Herlitz, H.; Johnsson, G. Pharmacokinetics of felodipine in patients with impaired renal function. *Br. J. Clin. Pharmacol.* **1989**, *27*, 67–74. [CrossRef]

73. Larsson, R.; Karlberg, B.E.; Gelin, A.; Aberg, J.; Regårdh, C.-G. Acute and steady-state pharmacokinetics and antihypertensive effects of felodipine in patients with normal and impaired renal function. *J. Clin. Pharmacol.* **1990**, *30*, 1020–1030. [CrossRef] [PubMed]
74. Hedner, T.; Samuelsson, O.; Sjögren, E.; Elmfeldt, D. Treatment of essential hypertension with felodipine in combination with a diuretic. *Eur. J. Clin. Pharmacol.* **1986**, *30*, 133–139. [CrossRef] [PubMed]
75. Hedner, T.; Elmfeldt, D.; Dahlöf, C.; Sjögren, E. Comparison of antihypertensive effect and pharmacokinetics of conventional and extended release felodipine tablets in patients with arterial hypertension. *Drugs* **1987**, *34*, 125–131. [CrossRef] [PubMed]
76. Leenen, F.H.H.; Coletta, E. Pharmacokinetic and antihypertensive profile of amlodipine and felodipine-ER in younger versus older patients with hypertension. *J. Cardiovasc. Pharmacol.* **2010**, *56*, 669–675. [CrossRef]
77. Les Laboratoires Servier. Servier Medical Art. Available online: https://smart.servier.com/ (accessed on 14 June 2022).
78. Human Metabolome Database. Metabocard for Felodipine (HMDB0015158). Available online: https://hmdb.ca/metabolites/HMDB0015158 (accessed on 28 March 2022).
79. Regårdh, C.G.; Edgar, B.; Olsson, R.; Kendall, M.; Collste, P.; Shansky, C. Pharmacokinetics of felodipine in patients with liver disease. *Eur. J. Clin. Pharmacol.* **1989**, *36*, 473–479. [CrossRef]
80. Felle, K.; Persson, B.; Vessman, J. Dissolution test for felodipine tablets using chemical oxidation in situ to maintain 'sink conditions'. *J. Pharm Biomed. Anal.* **1984**, *2*, 527–536. [CrossRef]
81. Takano, J.; Maeda, K.; Bolger, M.B.; Sugiyama, Y. The Prediction of the Relative Importance of CYP3A/P-glycoprotein to the Nonlinear Intestinal Absorption of Drugs by Advanced Compartmental Absorption and Transit Model. *Drug Metab. Dispos.* **2016**, *44*, 1808–1818. [CrossRef]
82. DRUGBANK Online-Felodipine. Available online: https://go.drugbank.com/drugs/DB01023 (accessed on 28 March 2022).
83. Van der Lee, R.; Pfaffendorf, M.; Koopmans, R.P.; van Lieshout, J.J.; van Montfrans, G.A.; van Zwieten, P.A. Comparison of the time courses and potencies of the vasodilator effects of nifedipine and felodipine in the human forearm. *Blood Press* **2001**, *10*, 217–222. [CrossRef]
84. Berben, P.; Brouwers, J.; Augustijns, P. Assessment of Passive Intestinal Permeability Using an Artificial Membrane Insert System. *J. Pharm. Sci.* **2018**, *107*, 250–256. [CrossRef]
85. Galetin, A.; Clarke, S.E.; Houston, J.B. Quinidine and haloperidol as modifiers of CYP3A4 activity: Multisite kinetic model approach. *Drug Metab. Dispos.* **2002**, *30*, 1512–1522. [CrossRef]
86. Chemaxon. Chemicalize-Dehydrofelodipine. Available online: https://chemicalize.com (accessed on 28 March 2022).
87. Gertz, M.; Houston, J.B.; Galetin, A. Physiologically based pharmacokinetic modeling of intestinal first-pass metabolism of CYP3A substrates with high intestinal extraction. *Drug Metab. Dispos.* **2011**, *39*, 1633–1642. [CrossRef] [PubMed]
88. Heikkinen, A.T.; Baneyx, G.; Caruso, A.; Parrott, N. Application of PBPK modeling to predict human intestinal metabolism of CYP3A substrates-An evaluation and case study using GastroPlus^{TM}. *Eur. J. Pharm. Sci.* **2012**, *47*, 375–386. [CrossRef] [PubMed]
89. Jamei, M.; Abrahamsson, B.; Brown, J.; Bevernage, J.; Bolger, M.B.; Heimbach, T.; Karlsson, E.; Kotzagiorgis, E.; Lindahl, A.; McAllister, M.; et al. Current status and future opportunities for incorporation of dissolution data in PBPK modeling for pharmaceutical development and regulatory applications: OrBiTo consortium commentary. *Eur. J. Pharm. Biopharm.* **2020**, *155*, 55–68. [CrossRef] [PubMed]
90. Wade, J.R.; Sambol, N.C. Felodipine population dose-response and concentration-response relationships in patients with essential hypertension. *Clin. Pharmacol. Ther.* **1995**, *57*, 569–581. [CrossRef]
91. Blychert, E.; Edgar, B.; Elmfeldt, D.; Hedner, T. A population study of the pharmacokinetics of felodipine. *Br. J. Clin. Pharmacol.* **1991**, *31*, 15–24. [CrossRef] [PubMed]
92. Oparil, S.; Acelajado, M.C.; Bakris, G.L.; Berlowitz, D.R.; Cífková, R.; Dominiczak, A.F.; Grassi, G.; Jordan, J.; Poulter, N.R.; Rodgers, A.; et al. Hypertension. *Nat. Rev. Dis. Prim.* **2018**, *4*, 18014. [CrossRef]
93. Muller, D.N.; Kvakan, H.; Luft, F.C. Immune-related effects in hypertension and target-organ damage. *Curr. Opin. Nephrol. Hypertens.* **2011**, *20*, 113–117. [CrossRef]
94. De Jong, L.M.; Jiskoot, W.; Swen, J.J.; Manson, M.L. Distinct Effects of Inflammation on Cytochrome P450 Regulation and Drug Metabolism: Lessons from Experimental Models and a Potential Role for Pharmacogenetics. *Genes* **2020**, *11*, 1509. [CrossRef]
95. Zhao, P.; Vieira, M.D.L.T.; Grillo, J.A.; Song, P.; Wu, T.-C.; Zheng, J.H.; Arya, V.; Berglund, E.G.; Atkinson, A.J.; Sugiyama, Y.; et al. Evaluation of Exposure Change of Nonrenally Eliminated Drugs in Patients With Chronic Kidney Disease Using Physiologically Based Pharmacokinetic Modeling and Simulation. *J. Clin. Pharmacol* **2012**, *52*, 91–108. [CrossRef]
96. Elmfeldt, D.; Hedner, T. Antihypertensive effects of felodipine compared with placebo. *Drugs* **1985**, *29*, 109–116. [CrossRef]
97. Beck, K.R.; Thompson, G.R.; Odermatt, A. Drug-induced endocrine blood pressure elevation. *Pharmacol Res.* **2020**, *154*, 104311. [CrossRef] [PubMed]
98. Hoffmann, W.J.; McHardy, I.; Thompson, G.R. Itraconazole induced hypertension and hypokalemia: Mechanistic evaluation. *Mycoses* **2018**, *61*, 337–339. [CrossRef] [PubMed]
99. Liedholm, H.; Nordin, G. Erythromycin-Felodipine Interaction. *DICP* **1991**, *25*, 1007–1008. [CrossRef] [PubMed]

4.3 PROJECT III - PHYSIOLOGICALLY BASED PHARMACOKINETIC MODELING OF GRAPEFRUIT JUICE AND ITS INTERACTION POTENTIAL

PUBLICATION

Fuhr, L.M.; Marok, F.Z.; Fuhr, U.; Selzer, D.; Lehr, T. Physiologically Based Pharmacokinetic Modeling of Bergamottin and 6,7-Dihydroxybergamottin to Describe CYP3A4 Mediated Grapefruit-Drug Interactions. Clinical Pharmacology & Therapeutics. 2023. 114(2):470-482, doi: 10.1002/cpt.2968.

SUPPLEMENTARY MATERIALS

The supplementary materials to this publication are provided on the accompanying USB storage device and are available online via: https://ascpt.onlinelibrary.wiley.com/action/downloadSupplement?doi=10.1002%2Fcpt.2968&file=cpt2968-sup-0001-SupinfoS1.pdf

COPYRIGHT

AUTHOR CONTRIBUTIONS

Laura Fuhr	Conceptualization, Formal Analysis, Investigation, Visualization, Writing–Original Draft, Writing–Review & Editing
Fatima Marok	Conceptualization, Formal Analysis, Writing–Review & Editing
Uwe Fuhr	Writing–Review & Editing
Thorsten Lehr	Conceptualization, Funding Acquisition,
Dominik Selzer	Formal Analysis, Writing–Review & Editing
	Writing–Review & Editing

ARTICLE

Physiologically Based Pharmacokinetic Modeling of Bergamottin and 6,7-Dihydroxybergamottin to Describe CYP3A4 Mediated Grapefruit-Drug Interactions

Laura Maria Fuhr[1], Fatima Zahra Marok[1], Uwe Fuhr[2], Dominik Selzer[1] and Thorsten Lehr[1,*]

Grapefruit is a moderate to strong inactivator of CYP3A4, which metabolizes up to 50% of marketed drugs. The inhibitory effect is mainly attributed to furanocoumarins present in the fruit, irreversibly inhibiting preferably intestinal CYP3A4 as suicide inhibitors. Effects on CYP3A4 victim drugs can still be measured up to 24 hours after grapefruit juice (GFJ) consumption. The current study aimed to establish a physiologically-based pharmacokinetic (PBPK) grapefruit-drug interaction model by modeling the relevant CYP3A4 inhibiting ingredients of the fruit to simulate and predict the effect of GFJ consumption on plasma concentration-time profiles of various CYP3A4 victim drugs. The grapefruit model was developed in PK-Sim and coupled with previously developed PBPK models of CYP3A4 substrates that were publicly available and already evaluated for CYP3A4-mediated drug–drug interactions. Overall, 43 clinical studies were used for model development. Models of bergamottin (BGT) and 6,7-dihydroxybergamottin (DHB) as relevant active ingredients in GFJ were established. Both models include: (i) CYP3A4 inactivation informed by *in vitro* parameters, (ii) a CYP3A4 mediated clearance estimated during model development, as well as (iii) passive glomerular filtration. The final model successfully describes interactions of GFJ ingredients with 10 different CYP3A4 victim drugs, simulating the effect of the CYP3A4 inactivation on the victims' pharmacokinetics as well as their main metabolites. Furthermore, the model sufficiently captures the time-dependent effect of CYP3A4 inactivation as well as the effect of grapefruit ingestion on intestinal and hepatic CYP3A4 concentrations.

Study Highlights

WHAT IS THE CURRENT KNOWLEDGE ON THE TOPIC?

☑ Grapefruit ingredients are irreversible inactivators of CYP3A4. Furanocoumarins present in the juice are mainly responsible for this effect.

WHAT QUESTION DID THIS STUDY ADDRESS?

☑ The current study aimed to establish a physiologically-based pharmacokinetic (PBPK) model of grapefruit juice (GFJ) ingestion by identifying and explicitly modeling relevant CYP3A4-inhibiting ingredients.

WHAT DOES THIS STUDY ADD TO OUR KNOWLEDGE?

☑ PBPK models of the furanocoumarins bergamottin (BGT) and 6,7-dihydroxybergamottin (DHB) as relevant CYP3A4 inhibitors in grapefruit were successfully developed and coupled to existing PBPK models of CYP3A4 substrates to predict the "grapefruit effect" as well as the effect of furanocoumarin-containing juices from limes and Seville oranges.

HOW MIGHT THIS CHANGE CLINICAL PHARMACOLOGY OR TRANSLATIONAL SCIENCE?

☑ The models support the exploration of "what-if" scenarios, such as: (i) the application of GFJ as "booster" to increase the oral availability of CYP3A4 substrates; (ii) the consideration of GFJ as CYP3A4 inhibitor in clinical studies; (iii) the adjustment of drug doses in patients consuming GFJ; and (iv) the use of the models as a foundation to study drug interactions with furanocoumarin-rich foods.

Grapefruit (*Citrux × paradisi*, *Rutaceae*), a citrus fruit with a characteristic bitter-sweet taste, is a hybrid between sweet orange (*Citrus sinensis*) and pomelo (*Citrus maxima*).[1] In the United States, the consumption of pink grapefruit is more popular than white grapefruit.[2] Independent of the variety, 57% of fruits are further processed with grapefruit juice (GFJ) or juice derivatives being a popular product category.[2] However, since the 1970s, the United States consumption of grapefruits

[1]Clinical Pharmacy, Saarland University, Saarbrücken, Germany; [2]Department of Pharmacology, Center for Pharmacology, Faculty of Medicine and University Hospital Cologne, University of Cologne, Cologne, Germany. *Correspondence: Thorsten Lehr (thorsten.lehr@mx.uni-saarland.de)

Received February 7, 2023; accepted May 17, 2023. doi:10.1002/cpt.2968

decreased by about 80% to a per capita consumption of ~0.7 kg in 2018.[2]

The US Food and Drug Administration (FDA) classifies GFJ as a moderate to strong inhibitor of cytochrome P450 (CYP) 3A4,[3] which metabolizes about 50% of marketed drugs.[4] Potential interactions with over 85 different drugs are mentioned in the current literature.[4] Although the FDA classification only considers the juice, the effect is independent of the preparation (whole fruit or juice) or the grapefruit variety. But variety, storage, and differences in juice manufacturing may influence ingredient concentrations.[1] Grapefruit contains a variety of flavonoids and furanocoumarins with the flavonoid naringin being the most abundant ingredient. Flavonoids are assumed to have only a minor contribution to the inhibitory effect after grapefruit consumption, in contrast to furanocoumarins that irreversibly inhibit CYP3A4 as suicide inhibitors.[5,6] Here, the furanocoumarins bergamottin (BGT) and 6,7-dihydroxybergamottin (DHB) are among the most important CYP3A4 inactivators present in grapefruit.[7] The "grapefruit effect" is characterized by a time-dependent CYP3A4 inhibition, lasting more than 24 hours,[8] and by the more pronounced effect on intestinal rather than hepatic CYP3A4.[9,10] Hence, especially drugs with a low oral bioavailability related to CYP3A4 metabolism bear a high risk of interaction.[4] Thereby, one glass of juice (200—250 mL $\triangleq$ 1 fruit) might already cause a clinically relevant effect.[4] For example, pronounced increases in felodipine (up to 3.3-fold[9,11]) and simvastatin (up to 18-fold[12]) area under the plasma concentration-time curve (AUC) were observed after GFJ ingestion, which could result in pronounced pharmacodynamic effects or increased risk of adverse effects.[9,12] The consumption of furanocoumarin-containing citrus fruits (e.g., Seville oranges and limes), was also shown to affect drug pharmacokinetics.[13,14]

Clinically relevant interactions with GFJ are listed on drug labels but these listings are often based on the metabolic characteristics of the drug instead of clinical trials.[15] Here, dose-effect models of grapefruit juice-drug interactions (GFJDIs), derived by, for example, physiologically-based pharmacokinetic (PBPK) modeling as a mechanistic modeling technique, could be viable to predict and quantify the effect of grapefruit consumption on the pharmacokinetics and pharmacodynamics of administered drugs and subsequently guide drug labeling. PBPK modeling is accepted by the regulatory agencies, the FDA, and the EMA, with the investigation of drug interactions to support drug clinical study design as a prominent use case.[16] Hence, the presented project aimed to establish a mechanistic PBPK model of grapefruit juice, by modeling its naturally occurring active ingredients BGT and DHB to predict the effect of GFJ ingestion on the pharmacokinetics of CYP3A4 substrates. The GFJDI PBPK model files as well as all the implementation of GFJDIs will be publicly shared with the scientific community on GitHub (http://models.clinicalpharmacy.me).

METHODS

Software

Concentration-time profiles extracted from published clinical studies were digitized with Engauge Digitizer version 12.1 (M. Mitchell,[17] 2020). The PBPK model was developed with PK-Sim and MoBi (Open Systems Pharmacology Suite 9.1, released under the GNU General Public License version 2 (GPLv2) license by the Open Systems Pharmacology community, www.open-systems-pharmacology.org, 2020). Parameter optimization (Monte-Carlo and Levenberg–Marquardt algorithms) and sensitivity analyses were performed with PK-Sim. Pharmacokinetic and statistical analyses as well as plot generation were performed with R version 4.1.3 (The R Foundation for Statistical Computing, Vienna, Austria, 2019).

Literature research and clinical data

Information on the absorption, distribution, metabolism, and elimination (ADME) properties of BGT and DHB as well as information on their inhibition kinetics were derived from literature. Additionally, concentration measurements of these ingredients in GFJ were collected from the literature to analyze typical concentrations as well as the variability of concentrations in the juice. Furthermore, plasma concentration-time profiles of BGT and DHB after GFJ consumption were collected.

Clinical studies investigating the effect of grapefruit consumption on the pharmacokinetics of CYP3A4 victim drugs were collected from the literature. Here, studies were included in the analysis if PBPK models of the victim drugs were available in the Open Systems Pharmacology repository (https://github.com/Open-Systems-Pharmacology/OSP-PBPK-Model-Library) and previously evaluated as CYP3A4 victim drugs in drug–drug interaction predictions. Plasma concentration-time profiles of victim drugs (and their metabolites) with and without administration of GFJ were extracted and digitized from available clinical GFJDI studies. The gathered studies were split into a training dataset for model building and a test dataset for model evaluation. The training dataset was selected to include plasma concentration-time profiles of BGT and DHB and of felodipine with co-administration of isolated BGT and DHB (instead of whole GFJ) to separate the inhibiting effects of both substances. Moreover, the dataset included plasma concentration-time profiles of felodipine and midazolam administered with or after one or multiple glasses of GFJ.

PBPK modeling of grapefruit juice

To establish PBPK models of BGT and DHB, parameter values that could not be informed from the literature were identified by mathematical optimization. Overall, the development of the GFJDI PBPK model was accomplished in a stepwise procedure. First, a set of preliminary drug-dependent parameters of the ingredient models was identified using available plasma concentration-time profiles of the compounds. Subsequently, the preliminary models were coupled to PBPK models of the CYP3A4 victim drugs felodipine[18] and midazolam[19] to simulate the GFJDI studies of the training dataset. The implemented mechanism-based inhibition of CYP3A4 by the ingredients is further described in the **Supplementary Material**, Section 1.2. Based on the simulation results, the preliminary drug-dependent parameter values of the ingredients were further refined and different literature values were tested to parametrize the mechanism-based inhibition of CYP3A4, using the whole training dataset for parameter estimation. Subsequently, the grapefruit interaction PBPK model was used to predict GFJDIs of felodipine and midazolam assigned to the test dataset and GFJDIs with further CYP3A4 victim drugs, namely alfentanil,[19] carbamazepine,[20] itraconazole,[19] verapamil,[21] simvastatin,[22] alprazolam, erythromycin, and triazolam (https://github.com/Open-Systems-Pharmacology/OSP-PBPK-Model-Library). Prior to predicting the GFJDI, the control simulations (without GFJ ingestion) were conducted. Based on the simulation results of the victim drug control, the CYP3A4 k_{cat} of the victim drugs was refined, fitting the simulation to the observed data of the control. The optimized k_{cat} was then used in the GFJDI simulation to predict the interaction.

Grapefruit-drug interaction model evaluation

The performance of the grapefruit PBPK model to predict the effect of GFJDIs was evaluated graphically by comparing (i) predicted victim drug plasma concentration-time profiles without and with GFJ consumption

to those observed in the clinical studies and (ii) predicted GFJDI area under the plasma concentration-time curve from the time of drug administration to the time of the last plasma concentration measurement (AUC_{last}) ratios and GFJDI maximum plasma concentration (C_{max}) ratios to corresponding observed data ratios in goodness-of-fit plots. Geometric mean fold errors (GMFEs) of all GFJDI AUC_{last} and C_{max} ratios were calculated as quantitative performance metrics. The model evaluation is described in more detail in the **Supplementary Material**, Section 1.1.

RESULTS

In total, 43 clinical studies were used for the development of the grapefruit PBPK model, providing 118 mean and 3 median plasma concentration-time profiles of the victim drugs felodipine, midazolam, alprazolam, triazolam, carbamazepine, alfentanil, erythromycin, itraconazole, simvastatin, and verapamil (50 control profiles, 71 GFJDI profiles) as well as 42 plasma concentration-time profiles of their metabolites (18 control profiles, 24 GFJDI profiles). Overall, a broad spectrum of GFJDI scenarios was investigated. Victim drugs were applied: (i) orally or intravenously, (ii) once or repeatedly, and (iii) together with GFJ or 0–144 hours after juice consumption. GFJ was administered (iv) as single- or double-strength preparation (1:3 or 1:1 dilution of juice concentrate with water) or grapefruit segments or ethanolic extract from segment-free parts, (v) in volumes of 200–300 mL, and (vi) in single or multiple doses before victim drug administration. Additionally, 2 studies investigated (vii) the effect of different doses of BGT or (viii) DHB on felodipine plasma concentration-time profiles. Last, two studies investigated (ix) the effect of Seville orange juice and (x) lime juice on felodipine pharmacokinetics. A detailed description of all clinical studies is provided in the **Supplementary Material**, Section 3. An overview of the modeling workflow and the developed GFJDI network is provided in **Figure 1**.

PBPK models of BGT and DHB were established and consumption of GFJ was simulated as oral administration of the respective compounds. To determine the ingested doses of these compounds, information on the administered juice volume and the concentration of ingredients in GFJ is required. As concentrations of BGT and DHB contained in the GFJ were only measured for 13 of 71 and 11 of 71 investigated scenarios, additional concentration measurements were gathered from the literature and all available concentration measurements were analyzed. Overall, reported doses were highly variable, ranging from 0.50 to 94.56 µmol/L (mean [± SD]: 18.49 [± 14.04]) for BGT and from 0.80 to 132.57 µmol/L (mean [± SD]: 28.9 [± 33.23]) for DHB and differed among the available juice preparations, as illustrated in **Figure 2a,b**, respectively. Mean DHB concentrations measured in juice prepared from frozen concentrate (mean [± SD]: 25.1 µmol/L [± 20.48], $n = 20$) were significantly higher (t-test; $P = 0.00637$) than those measured in canned juice (mean [± SD]: 9.92 µmol/L [± 10.58], $n = 20$). For BGT concentrations, differences in frozen concentrate (mean [± SD]: 18.7 [± 6.66], $n = 20$) and canned juice (mean [± SD]: 16.63 [± 20.4], $n = 19$) were not statistically significant (t-test; $P = 0.677$). The complete analysis of reported ingredient concentrations is described in the **Supplementary Material**, Section 2.1. Mean concentrations of BGT and DHB for each juice preparation obtained from the available measurements were used to calculate administered doses in the administered GFJ if the clinical study did not provide concentration measurements.

BGT and DHB exhibit similar ADME properties. Both furanocoumarins are of moderate lipophilicity and presumably well absorbed from the intestines.[5] It is assumed that both compounds undergo extensive metabolic elimination and that enzyme inactivation is mediated by reactive metabolites.[23] Hence, the BGT and DHB PBPK models include: (i) a CYP3A4-mediated clearance process, (ii) mechanism-based inhibition of CYP3A4, and (iii) free glomerular filtration. The mechanism-based inactivation of CYP3A4 was parametrized using literature values. The CYP3A4-mediated clearance was described using Michaelis–Menten kinetics. As no measurements of the CYP3A4 metabolism were available in the literature, the inhibition constant (K_I) was used as a surrogate for the Michaelis–Menten constant and the catalytic rate constant was estimated. Other drug-dependent parameters were either taken from the literature (e.g., molecular weight, pK_a, solubility, and fraction unbound), calculated within PK-Sim (e.g., cellular permeabilities) or optimized (e.g., specific intestinal permeability and lipophilicity). All drug-dependent parameters used in the final models are listed in **Table 1**. Predicted vs. observed plasma concentration-time profiles of both ingredients are illustrated in **Figure 2c,d**, thereby the plasma concentration-time profiles for BGT and DHB are sufficiently described, with average GMFE values of 1.53 and 1.02 for AUC_{last}, and 1.10 and 1.08 for C_{max} of DHB and BGT, respectively. The corresponding AUC_{last} and C_{max} values can be found in **Table S5**, whereas goodness-of-fit plots of predicted vs. observed: (i) AUC_{last}, (ii) C_{max}, and (iii) plasma concentration values are depicted in **Figure S5**.

Overall, the ingredient models successfully described the effect of grapefruit intake on various CYP3A4 victim drugs. **Figure 3** displays predicted vs. observed plasma concentration-time profiles of different victim drugs and their metabolites (if metabolite models were available) of exemplary studies with and without the consumption of GFJ.

Figure 4 illustrates predicted compared with observed plasma concentration-time profiles of the victim drug felodipine and illustrates the versatility of the ingredient models to describe different scenarios. Felodipine is the drug in which the "grapefruit effect" was observed first and which subsequently was used extensively as a probe drug to further assess the GFJDI in clinical studies. The models describe the GFJDI with felodipine: (i) after intravenous or after oral administration of felodipine with GFJ (ii) ingested once or repeatedly, (iii) ingested with or up 24 hours before felodipine, and administered as (iv) single- or double-strength preparation. Furthermore, the model predicts the effect of (v) individual grapefruit ingredients or (vi) Seville orange or (vii) lime juice on felodipine plasma concentrations. Compared with the effect of one glass of single-strength GFJ on oral felodipine, the model successfully predicts the lack of effect on intravenously applied felodipine (**Figure 4a**), a 55% (observed: 46%) higher felodipine AUC_{last} if GFJ was ingested over several days before felodipine administration (**Figure 4c**) as well

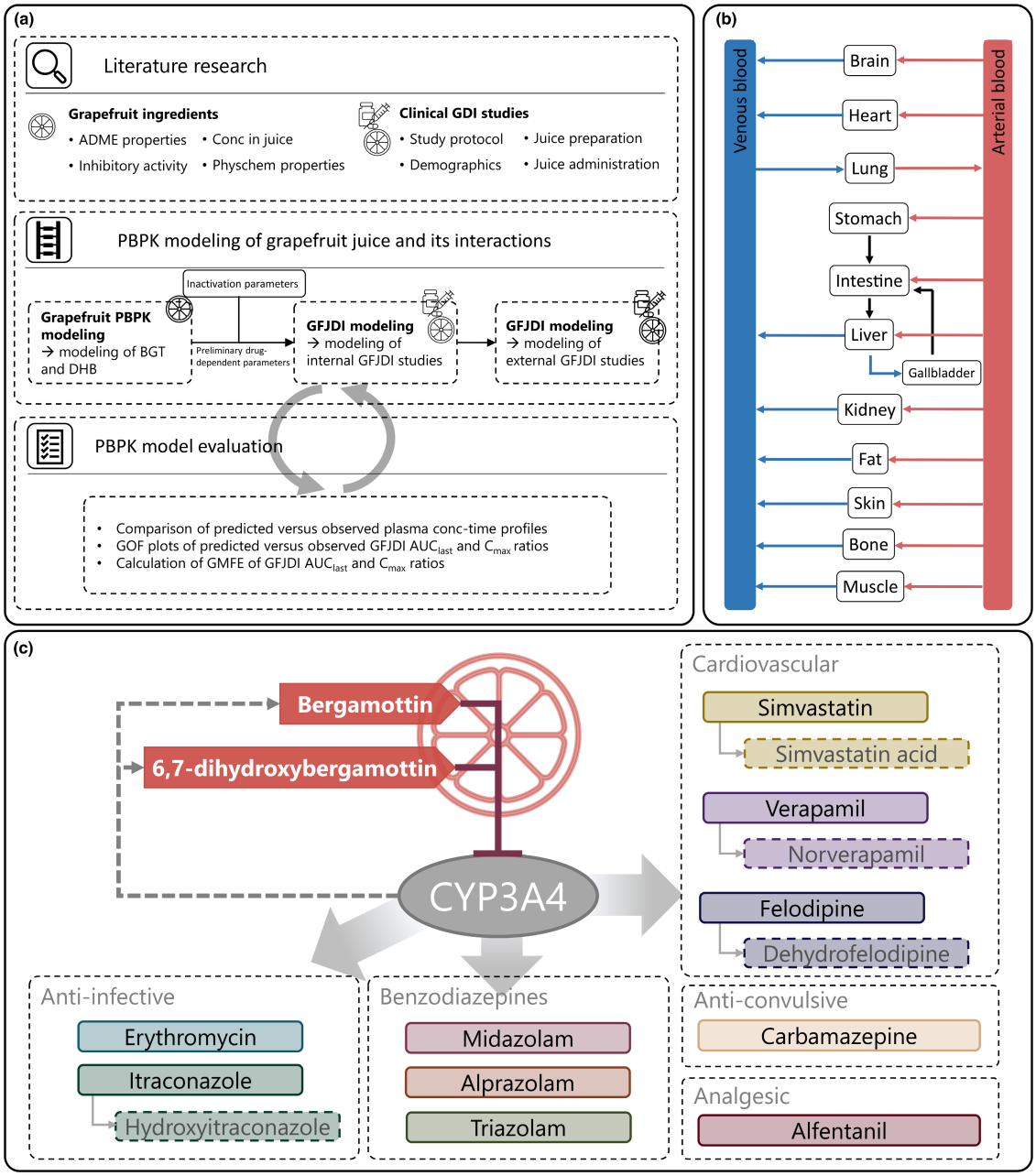

Figure 1 Modeling workflow and model overview. (**a**) The modeling process can be divided into literature research on GFJ and its active ingredients, model development of GFJ ingredients and its interactions and model evaluation. (**b**) Overview of the PBPK model structure. Different compartments represent ADME-relevant organs of the body. Connections between compartments represent arterial and venous blood flow. (**c**) The final GFJDI model describes mechanism-based inhibition of CYP3A4 by BGT and DHB to cover the effect of GFJ and includes a broad range of CYP3A4 victim drugs along with their metabolites. ADME, absorption, distribution, metabolism, and excretion; AUC, area under the plasma concentration-time curve; BGT, bergamottin; C_{max}, maximum plasma concentration; conc, concentration; CYP3A4, cytochrome P450 3A4; DHB, 6,7-dihydroxybergamottin; GFJDI, grapefruit juice-drug interaction; GMFE, geometric mean fold error; GOF, goodness-of-fit; PBPK, physiologically-based pharmacokinetic.

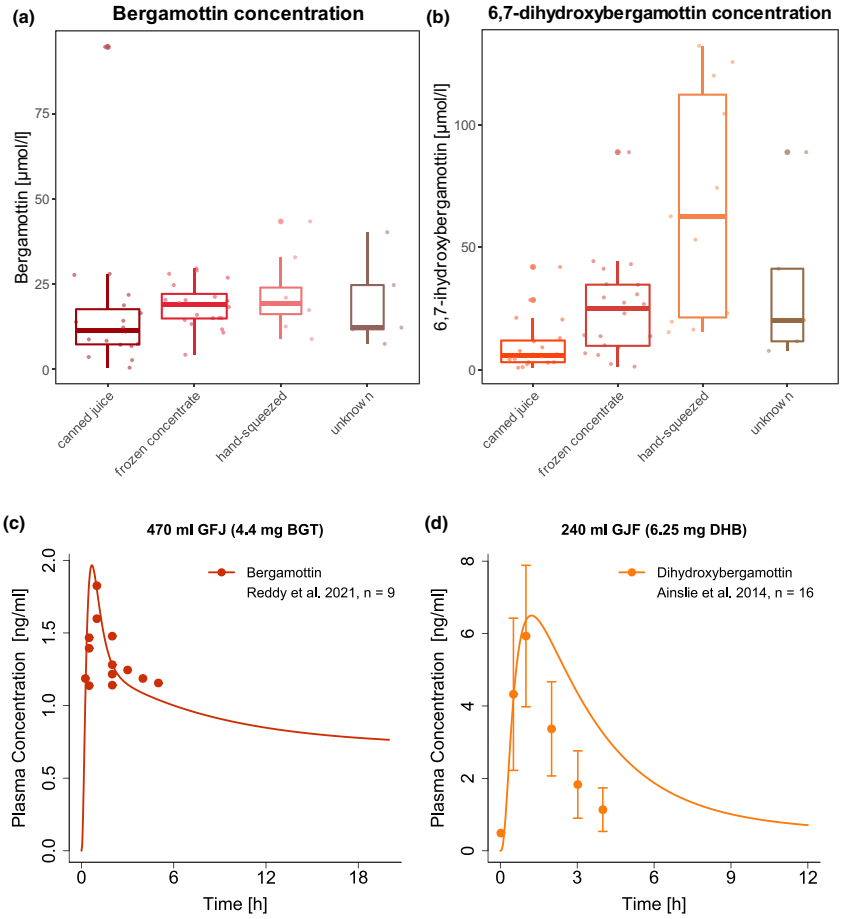

Figure 2 Concentration measurements of (**a**) BGT and (**b**) DHB in different GFJ preparations. Boxplots show the following descriptive statistics: The median value, the IQR, and the 1.5-fold IQR, as well as individual measurements (small dots) and potential outliers (big dot; at least 1.5 IQR greater than the third quartile); as well as predicted vs. observed plasma concentration-time profiles of (**c**) BGT and (**d**) DHB. Solid lines represent model predictions while the different shapes represent observed data. BGT, bergamottin; DHB, 6,7-dihydroxybergamottin; GFJ, grapefruit juice; IQR, interquartile range; K_i, concentration for half-maximal inactivation; *n*: number of participants.

as a 10% (observed: 19%) higher felodipine AUC_{last} if double-strength GFJ was administered (**Figure 4f**). Furthermore, the performance of the BGT and DHB model was investigated by simulating the inhibiting effect of single ingredients and by simulating the effect of juices of limes (**Figure 4j**) and Seville oranges (**Figure 4k**). In the corresponding clinical studies, BGT and DHB concentrations of 5 and 36 µmol/L were determined in Seville oranges, whereas concentrations in GFJ were 16 and 23 µmol/L, respectively.[13] Pure lime juice contained 100 µmol/L BGT and no DHB and was diluted to ¼ strength, whereas the administered GFJ contained 25 µmol/L BGT (DHB concentrations not indicated).[14] Solely the effect of grapefruit segments (**Figure 4i**; blended segments without flavedo, albedo, and vascular elements) and extract (segment-free parts extracted with ethanol) could not be sufficiently described.

The impact of different juice types, and consequently ingredient concentrations, was examined for alprazolam. In this case, the effects of canned juice (BGT: 1.13 mg, DHB: 0.74 mg) and juice from frozen concentrate (BGT: 1.27, DHB: 1.87 mg) were analyzed to investigate if the grapefruit effect may be more potent when using a frozen concentrate preparation. A moderate increase in the effect on alprazolam AUC (up to 25%) was observed if frozen concentrate was used compared with canned juice.

Plasma concentration-time profiles of all clinical studies included in the PBPK modeling analysis are depicted in the **Supplementary Material**, Section 3. The overall model performance is illustrated in **Figure 5a,b** in goodness-of-fit plots of predicted compared with observed GFJDI AUC_{last} and C_{max} ratios of victim drugs and their metabolites of all included clinical studies. Overall, mean (range) GMFE values of 1.30 (1.00–3.66) and 1.31 (1.00–3.08) were calculated for GFJDI AUC_{last} and C_{max} ratios, respectively, with 93% of predicted GFJDI AUC_{last} and C_{max} ratios deviating less than 2-fold from the corresponding observed values.

ARTICLE

Table 1 Drug-dependent parameters of bergamottin and 6,7-dihydroxybergamottin

		Bergamottin			6,7-dihydroxybergamottin		
Parameter	Unit	Model	Literature	Ref	Model	Literature	Ref
MW	g/mol	338.4 (lit)	338.4	46	372.417 (lit)	372.417	47
log*P*		4.95 (opt)	4.81, 5.3	46	3.72 (opt)	2.67, 3.4	47
pK_a		—	—	—	13.84 (lit)	13.84	47
$f_{u,plasma}$	%	2.73 (calc)	2.73	48	7.70 (calc)	7.70	48
Solubility	mg/L	10 (7) (lit)	10 (7)	46	44 (7) (lit)	44 (7)	47
K_m (CYP3A4)	µmol/L	1.9 (asm)	—	—	1.10 (asm)	—	—
k_{cat} (CYP3A4)	1/minute	0.05 (opt)	—	—	2.10 (opt)	—	—
GFR fraction		1 (asm)	—	—	1 (asm)	—	—
K_I (CYP3A4)	µmol/L	1.9 (lit)	1.9–40	6,29,49	1.10 (lit)	1.1–59	6,49,50
k_{inact} (CYP3A4)	1/minute	0.70 (lit)	0.08–0.70	6,29,49	0.41 (lit)	0.06–0.52	6,49,50
K_i (CYP3A4)	µmol/L	6.10 (lit)	0.5–13.3	6	0.50 (lit)	0.4–0.9	6
Intestinal permeability	cm/minute	1.60 E-3 (opt)	—	—	6.41 E-5 (opt)	—	—

asm, assumed; calc, calculated; GFR, glomerular filtration rate; k_{cat}, catalytic rate constant; K_I, concentration for half-maximal inhibition; K_I, concentration for half-maximal inhibition k_{inact} maximum inactivation rate constant; K_m, Michaelis–Menten constant; lit, literature; log*P*, lipophilicity; MW, molecular weight; opt, optimized; pK_a, acid dissociation constant.

The effect of GFJ on CYP3A4 exhibits two key characteristics. First, BGT and DHB are irreversible inhibitors of CYP3A4, resulting a time-dependent CYP3A4 inhibition, lasting more than 24 hours. Consequently, the effects of GFJ on victim drug pharmacokinetics can be observed even if the victim drug is taken 24 hours after grapefruit consumption, which is sufficiently covered by the model as shown in **Figure 4d,e**. Second, the CYP3A4 inhibition is more pronounced in the intestine, whereas hepatic CYP3A4 is only affected after frequent juice consumption over several days. Overall, the model successfully described the effect of GFJ ingestion on oral drug bioavailability and successfully simulated the decreased intestinal CYP3A4 metabolism, as illustrated in **Figure 5c** comparing predicted to observed GFJDI bioavailability and intestinal availability (F_G) ratios. The effect of intestinal and hepatic CYP3A4 inhibition by GFJ simulated with the model is exemplarily shown for midazolam as a victim drug. **Figure 6a** depicts predicted compared with observed plasma concentration-time profiles of midazolam with or without the ingestion of one glass of GFJ (single- or double-strength), whereas **Figure 6b** shows plasma concentration-time profiles of midazolam without or after consumption of a total of 6 glasses of GFJ for 2 days prior to midazolam administration. The model sufficiently described the effect of GFJ ingestion on midazolam plasma concentration-time profiles in all 3 cases and predicted a 276% (observed: 276%) higher midazolam AUC for the consumption of 6 glasses compared with one glass of GFJ. Furthermore, marked increases in midazolam terminal half-life ($t_{1/2}$) could be observed if the drug was administered after multiple doses of GFJ but not for co-administration with a single glass of GFJ. As illustrated in **Figure 5d**, comparing predicted to observed GFJDI $t_{1/2}$ ratios, the model was able to describe the effect of single and multiple doses of GFJ on midazolam, felodipine, and triazolam $t_{1/2}$.

To further investigate the difference in the effect magnitude of GFJ on duodenal vs. hepatic CYP3A4, the model was applied to predict CYP3A4, BGT, and DHB concentrations in the duodenum and liver during administration of one glass of juice (**Figure 6**, left column) or multiple glasses of juice (**Figure 6**, right column). For the ingestion of one glass of juice, the model predicts maximum hepatic ingredient concentrations below K_I, whereas concentrations close to or above K_I are predicted for frequent GFJ ingestion. Ingredient concentrations in the duodenum exceed K_I by several fold for single and frequent juice ingestion. Subsequently, the model predicts a strong decrease in intestinal CYP3A4, independent of frequency of juice consumption, as well as a frequency-dependent decrease in hepatic CYP3A4.

DISCUSSION

In the presented analysis, a GFJDI PBPK model was successfully established and evaluated. The model describes the consumption of GFJ as oral administration of the furanocoumarins BGT and DHB and successfully describes and predicts CYP3A4-mediated GFJDIs for a broad spectrum of victim drugs and scenarios.

Models of BGT and DHB were established as important CYP3A4 inactivators in grapefruit, regarding: (i) their abundance in the juice as well as (ii) their inactivation activity.[7] *In vivo* studies could show that a naringin solution[24] or furanocoumarin-free GFJ[25] did not markedly impact felodipine pharmacokinetics, implying that furanocoumarins are the main CYP3A4 inactivators in GFJ. However, the inhibitory effects of BGT and DHB observed *in vivo* were slightly smaller compared with the effect of whole GFJ.[26,27] Hence, the effect cannot be attributed to one of these ingredients alone. Overall, CYP3A4 inactivation by grapefruit is complex and may result from a combination of ingredients present in the juice.[7] This may explain why the current grapefruit model covering solely BGT and DHB could not sufficiently describe the administration of GFJ ethanol extract and homogenized segments. This may be related to altered ingredient concentrations in respective preparations, and thus an altered

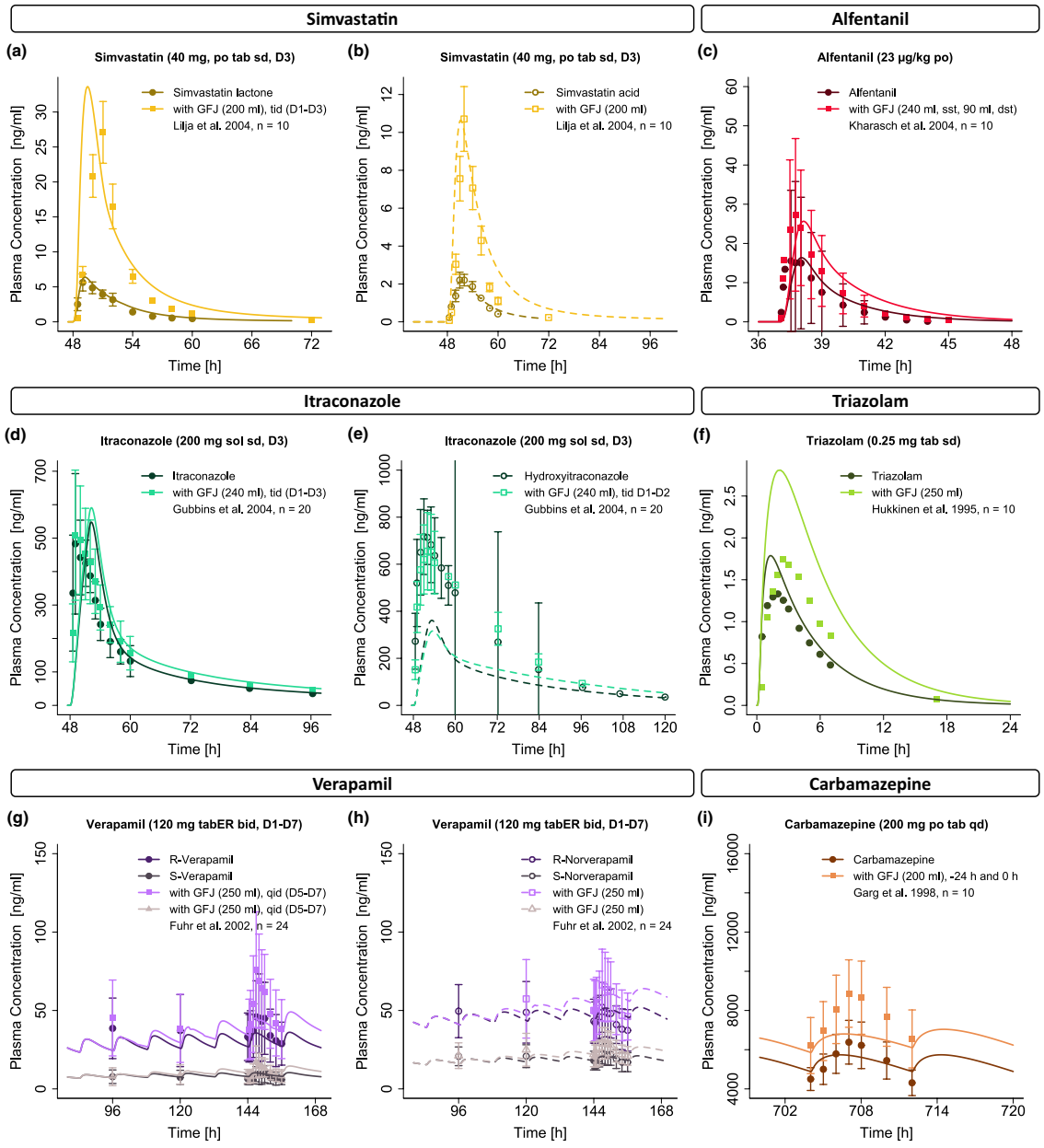

Figure 3 Comparison of predicted and observed victim drug plasma concentration-time profiles with and without the administration of GFJ of (**a**) simvastatin and (**b**) its metabolite simvastatin acid,[12] (**c**) alfentanil,[39] (**d**) itraconazole, and (**e**) its metabolite hydroxyitraconazole,[40] (**f**) triazolam,[41] (**g**) R- and S-verapamil, and (**h**) their metabolites R- and S-norverapamil,[42] (**i**) carbamazepine.[43] Lines represent model predictions while the different shapes represent observed data (± SD, if available). D, day; d, double strength; GFJ, grapefruit juice; iv, intravenous; *n*, number of participants; po, oral, qd, once daily; s, single strength; sd, single dose; sol, solution; tab, tablet; tabER, extended-release tablet; tid, three times daily.

contribution of the ingredients to the grapefruit effect. For example, naringin concentrations in the ethanol extracts were ninefold higher compared with GFJ. Even though naringin and/or its metabolite naringenin does not strongly contribute to the CYP3A4 inhibition at concentrations measured in GFJ, it is conceivable that especially naringenin may additionally impact victim drug concentrations at such high concentrations.[5] The characterization of the pharmacokinetics of BGT and DHB has been challenging

ARTICLE

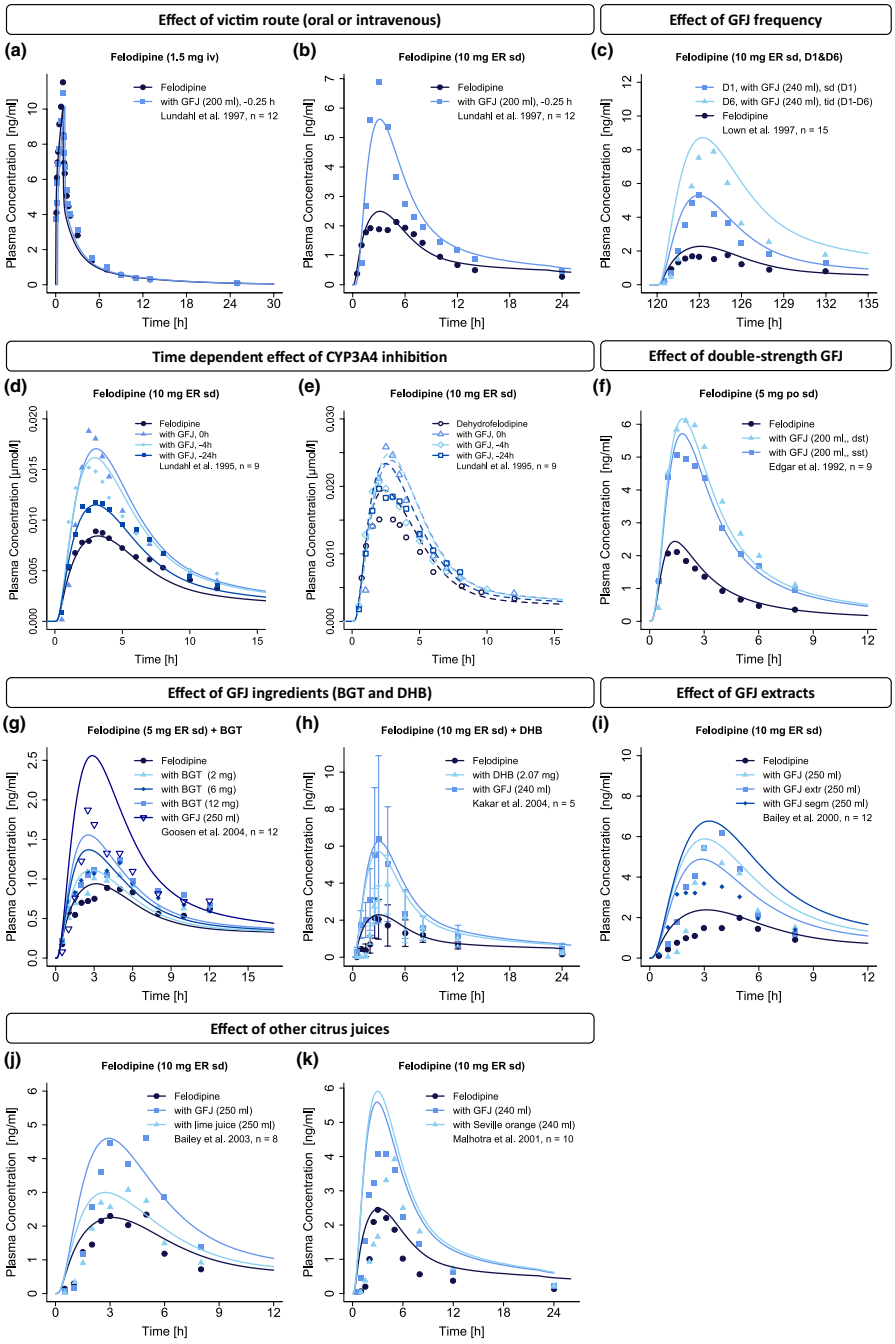

due to the limited information on their metabolism and concentration measures in the human body. Within the scope of the presented analysis, the models were developed to describe GFJDIs with CYP3A4 victim drugs. As more comprehensive information becomes available, these models can be easily refined.

Overall, CYP3A4-mediated GFJDIs are highly variable. First, this can be related to the high interindividual variability of intestinal CYP3A4, where up to an 8-fold difference in intestinal concentrations was reported.[28] Second, it should be considered that grapefruit is a natural product and the concentration of ingredients

Figure 4 Comparison of predicted and observed felodipine drug plasma concentration-time profiles with and without administration of GFJ (**a**) after intravenous administration or (**b**) oral administration of felodipine,[9] (**c**) with and without the administration of GFJ (frequently administered or a single glass), (**d**) with and without grapefruit ingestion concomitantly, 4 hours or 24 hours before felodipine administration along with corresponding (**e**) dehydrofelodipine plasma concentration-time profiles (**f**) with and without the administration of double- or single-strength GFJ[11] (**g**) with and without the administration of different doses of BGT (2–12 mg) compared with GFJ,[26] (**h**) with and without the administration of juice "serum" (aqueous supernatant of frozen concentrate suspended in water, containing primarily DHB) compared with GFJ,[27] as well as (**i**) blended segments (segments) and ethanol extract from segment free parts (extract)[44] and (**j**) with and without the administration of lime juice[14] or (**k**) Seville orange[13] in comparison to GFJ. Lines represent model predictions, whereas the different shapes represent observed data (± SD, if available). BGT, bergamottin; D, day; d, double strength; DHB, 6,7-dihydroxybergamottin; ER, extended-release formulation; extr, extract; GFJ, grapefruit juice; iv, intravenous; *n*, number of participants; po, oral; s, single strength; sd, single dose; segm, segments; sol, solution; tab, tablet; tid, three times daily.

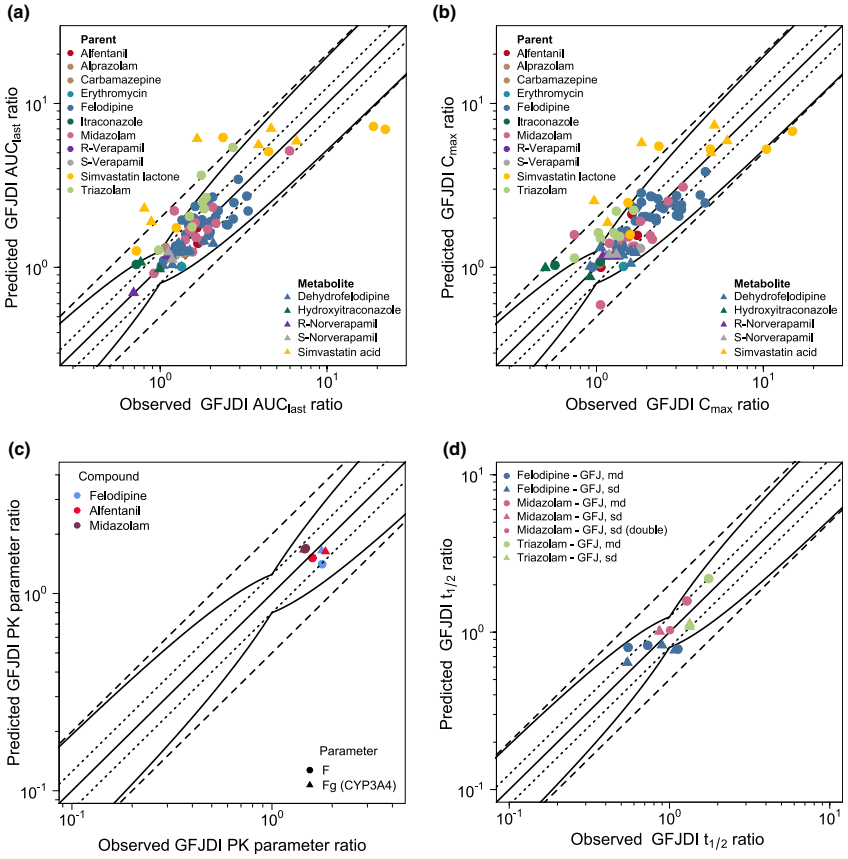

Figure 5 Performance of the GFJDI model. The performance of the model to predict the effect on the included victim drugs is illustrated in goodness-of-fit plots, comparing predicted versus observed (**a**) GFJDI AUC_{last} ratios and (**b**) GFJDI C_{max} ratios of all GFJDI studies as well as (**c**) GFJDI bioavailability and F_g ratios and (**d**) GFJDI $t_{1/2}$ ratios of selected studies. The line of identity is shown as a straight solid line; the curved solid lines mark the prediction success limits proposed by Guest et al.[45] A 1.25-fold deviation is shown as dotted lines; a 2-fold deviation is shown as dashed lines. Details on the GFJDI studies and all references are provided in the **Supplementary Material**, Section 3. AUC_{last}, area under the plasma concentration–time curve from dosing to the last concentration measurement; C_{max}, maximum plasma concentration; F, oral bioavailability; F_g, intestinal availability; GFJ, grapefruit juice; GFJDI, grapefruit–drug interaction; PK, pharmacokinetic; $t_{½}$, terminal half-life.

may vary[7] depending, for example, on external growing conditions and the fruit variety. Storage and processing of the fruit can also influence the concentrations.[1] A high variability of BGT and DHB concentrations in GFJ with differences of more than 100-fold could be observed during the analysis of ingredient concentrations reported in the literature. For ~ 80% of the simulated scenarios, the ingredient concentrations were not indicated in the clinical study but had to be assumed based on the administered juice preparation to estimate the ingested dose. Even though in most cases the true concentration of BGT and DHB was unknown, the model sufficiently described and predicted GFJDIs for different victim drugs assuming mean ingredient concentrations which is supported by

ARTICLE

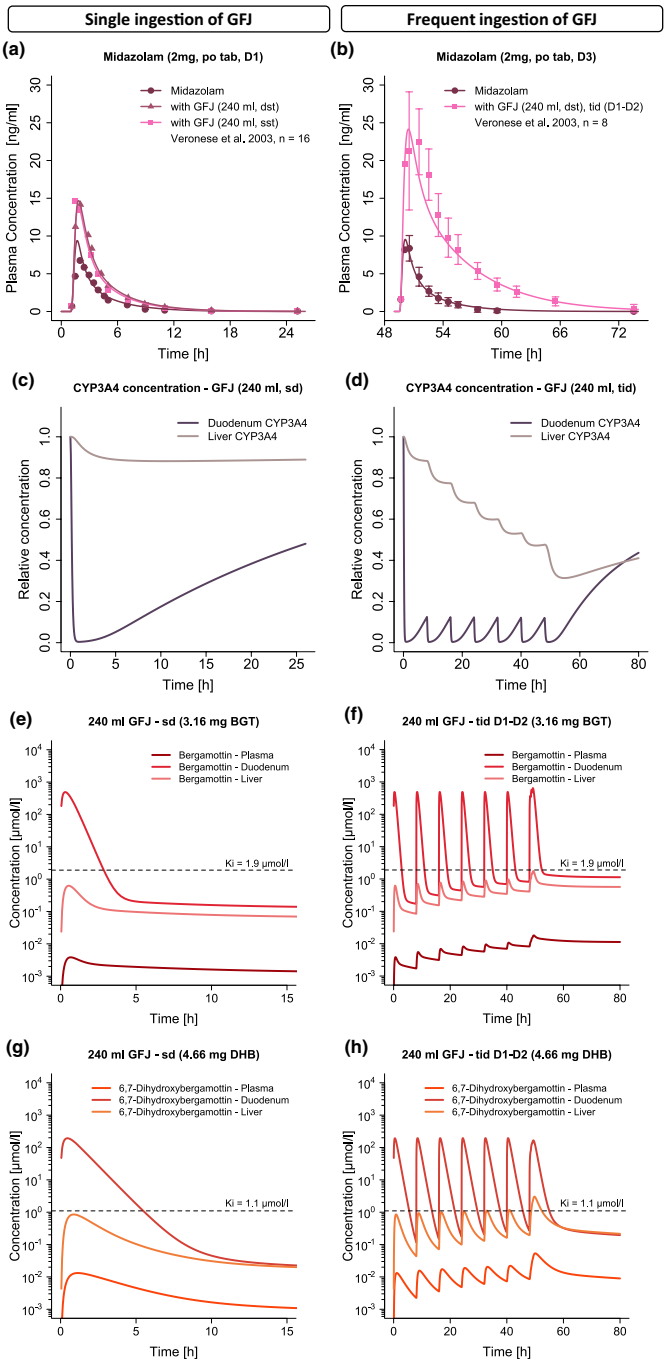

Figure 6 Effect of grapefruit on intestinal and hepatic CYP3A4. Comparison of predicted and observed (**a, b**) midazolam plasma concentration-time profiles, (**c, d**) predicted duodenum and liver CYP3A4 concentrations and predicted (**e, f**) BGT and (**g, h**) DHB concentrations in plasma, duodenum and liver after oral administration of midazolam with and without concomitant consumption of one glass of single- or double-strength GFJ (left column) or after consumption of GFJ over 2 days before midazolam administration (right column).[10] BGT, bergamottin; CYP3A4, cytochrome P450; d, double-strength; DHB, 6,7-dihydroxybergamottin; GFJ, grapefruit juice; GFJDI, grapefruit-drug interaction; D, day; po, oral; tab, tablet; *n*, number of participants; s, single-strength; sd, single dose; tid, three times daily.

mean calculated GMFEs of 1.30 and 1.31 for GFJDI AUC_{last} and C_{max} ratios. This may be due to the fact that the effect is almost completely established after the consumption of 200 mL of juice, and doubling the dose of perpetrator moieties (e.g., by administering double-strength juice), does not considerably impact the effect.[10,11] However, regarding the pronounced variability, specifying ingredient concentrations in future studies would enhance comparability between studies and improve comprehension of the grapefruit effect. Although GFJDIs with triazolam are generally well-described (GMFE GFJDI AUC_{last} ratio = 1.49; GFJDI GMFE C_{max} ratio = 1.40), the model tends to overpredict the effect of GFJ, which cannot be solely attributed to high variability in CYP3A4 and juice ingredients. Given that GFJDIs with the structurally related CYP3A4 substrate midazolam are sufficiently described (GMFE GFJDI AUC_{last} ratio = 1.17; GMFE GFJDI C_{max} ratio = 1.24), it is plausible to assume that the overprediction of the effect could also result from an inadequate description of intestinal CYP3A4 metabolism of triazolam.

The current model only reflects the inhibition of CYP3A4. However, inhibition of further metabolic and transport proteins besides CYP3A4 is reported.[29] For verapamil, transport via P-glycoprotein (P-gp) may be considered, however, clinical studies with digoxin as sensitive P-gp victim drug showed that grapefruit ingestion did not impact P-gp-mediated transport.[30] For simvastatin and erythromycin, transport via OATP may also be impacted by GFJ. Plasma concentrations of simvastatin lactone and its metabolite simvastatin acid were adequately predicted for co-administration with single-strength GFJ. However, when co-administrated with double-strength juice, the predicted grapefruit effect deviated from the observed effect. In this case, it cannot be ruled out that concentrations of other ingredients, such as naringin, might be high enough to markedly impact the transport of simvastatin. For example, it has been demonstrated that the flavonoid naringin can impair OATP-mediated transport of pravastatin and pitavastatin.[31] Carbamazepine is additionally metabolized via CYP2C8 and CYP2B6.[20] Even though grapefruit has been shown to inhibit CYP2B6 as well,[23] the current simulation, only considering CYP3A4 inhibition, adequately describes the grapefruit-carbamazepine interaction. This is demonstrated by GMFEs of GFJDI AUC_{last} and C_{max} ratios of 1.16 and 1.17, respectively. Hereby, the model describes the complex interaction with carbamazepine as a victim and autoinducer of CYP3A4, whereby CYP3A4 is mutually induced and inhibited.

The two key characteristics of the "grapefruit effect"—the time-dependent CYP3A4 inhibition, lasting more than 24 hours, and the predominant intestinal inhibition—were well-captured by the model. The time-dependent CYP3A4 inhibition could be described using inhibition parameters from the literature, demonstrated by the sufficient prediction of felodipine and dehydrofelodipine plasma concentration-time profiles, if felodipine was administered simultaneously, or up to 24 hours after GFJ.[8] The CYP3A4 inhibition is primarily limited to intestinal CYP3A4, whereas only frequent juice consumption causes hepatic CYP3A4 inhibition.[10] The model reasonably described this characteristic by predicting: (i) the lack of effect of one glass of juice on intravenous victim drugs, (ii) the effect on oral bioavailability and F_g, and (iii) the effect on drug $t_{1/2}$. Based on model predictions of BGT, DHB, and CYP3A4 concentrations in the duodenum and liver, concentrations of the ingredients in the liver after the consumption of one glass of juice are well below K_I and, thus, insufficient to inactivate CYP3A4. In contrast, predicted duodenal ingredient concentrations are severalfold above K_I and a strong decrease in intestinal CYP3A4 concentrations is predicted, independently of the frequency of GFJ ingestion.

Additional PBPK modeling approaches to describe the "grapefruit effect" are available in the literature. These approaches aimed to describe the "grapefruit effect "either mechanistically by modeling BGT[32] or DHB as active ingredients,[33,34] or non-mechanistically by adjusting intestinal CYP3A4 concentrations, gastric emptying time,[35] or $V_{max.}$[36,37] The herein presented analysis included a particularly large set of clinical studies ($n = 43$), investigating 10 different CYP3A4 victim drugs as well as their metabolites. Thereby, the model was thoroughly challenged and used to extensively investigate the unique features of the "grapefruit effect." The GFJDI model sufficiently describes: (i) the effect on intravenously and orally applied victim drugs, (ii) the effect on oral bioavailability and F_G, (iii) the impact on drug $t_{1/2}$ for single vs. repeated grapefruit consumption, (iv) the effect on victim drug metabolite plasma concentration-time profiles, and (v) the time-dependent effect of the CYP3A4 inhibition. In addition, no other modeling approach aimed to predict the effect of GFJ by modeling both active ingredients—BGT and DHB—although the effect cannot be attributed to one of these ingredients alone. Furthermore, the models of BGT and DHB could be successfully applied to predict the effects of Seville orange and lime juice consumption on the pharmacokinetics of felodipine. Both furanocoumarins are found in several commonly consumed fruits and their respective juices, herbs, and vegetables (e.g., parsley, different citrus fruits but also celeriac and parsnip).[38] Here, the developed PBPK models could provide the basis to investigate the effects of additional furanocoumarin-containing foods on CYP3A4 substrates.

In summary, a grapefruit PBPK model was successfully developed and the effect of GFJ on various victim drugs could be described by modeling ingestion of GFJ as oral administration of the active ingredients BGT and DHB. The selection of modeled GFJDIs was based on the availability of victim drug PBPK models within the Open Systems Pharmacology Suite as well as clinical studies providing plasma concentration-time profiles in the literature. However, the GFJDI model can be easily adapted to predict GFJDIs with additional CYP3A4 substrates, such as buspirone, lovastatin, or tacrolimus,[3] which may also provide further insights into the performance of the presented grapefruit model. Moreover, the model could also be utilized to investigate dosing adjustments and provide a building block to investigate potential effects of furanocoumarins in foods. Additionally, the model can also be used for educational purposes to illustrate the pronounced effect that the consumption of GFJ might have on a patient's medication.

ARTICLE

SUPPORTING INFORMATION
Supplementary information accompanies this paper on the *Clinical Pharmacology & Therapeutics* website (www.cpt-journal.com).

FUNDING
This research was funded by the German Federal Ministry of Education and Research (BMBF), grant number 031L0161C ("OSMOSES").

ACKNOWLEDGMENT
Open Access funding enabled and organized by Projekt DEAL.

CONFLICT OF INTEREST
T.L. has received research grants from the German Federal Ministry of Education and Research (grant 031L0161C). All other authors declared no competing interests for this work. The funders had no role in the design of the study; in the collection, analyses, or interpretation of data; in the writing of the manuscript, or in the decision to publish the results.

AUTHOR CONTRIBUTIONS
L.M.F., F.Z.M., U.F., D.S., and T.L. wrote the manuscript. L.M.F., F.Z.M., and T.L. designed the research. L.M.F. performed the research. L.M.F., F.Z.M., and D.S. analyzed the data.

1. Hung, W.L., Suh, J.H. & Wang, Y. Chemistry and health effects of furanocoumarins in grapefruit. *J. Food Drug Anal.* **25**, 71–83 (2017).
2. Chen, L.A. & House, L. An overview of the grapefruit market in the U.S. *EDIS* **2021**, 1–7 (2021).
3. U.S. Food and Drug Administration. Drug development and drug interactions. Table of substrates, inhibitors and inducers. <https://www.fda.gov/drugs/drug-interactions-labeling/drug-development-and-drug-interactions-table-substrates-inhibitors-and-inducers>. Accessed March 31, 2023.
4. Bailey, D.G., Dresser, G. & Arnold, J.M.O. Grapefruit-medication interactions: forbidden fruit or avoidable consequences? *CMAJ* **185**, 309–316 (2013).
5. Fuhr, U. Drug interactions with grapefruit juice. Extent, probable mechanism and clinical relevance. *Drug Saf.* **18**, 251–272 (1998).
6. Paine, M.F., Criss, A.B. & Watkins, P.B. Two major grapefruit juice components differ in intestinal CYP3A4 inhibition kinetic and binding properties. *Drug Metab. Dispos.* **32**, 1146–1153 (2004).
7. Guo, L.Q., Fukuda, K., Ohta, T. & Yamazoe, Y. Role of furanocoumarin derivatives on grapefruit juice-mediated inhibition of human CYP3A activity. *Drug Metab. Dispos.* **28**, 766–771 (2000).
8. Lundahl, J., Regårdh, C.G., Edgar, B. & Johnsson, G. Relationship between time of intake of grapefruit juice and its effect on pharmacokinetics and pharmacodynamics of felodipine in healthy subjects. *Eur. J. Clin. Pharmacol.* **49**, 61–67 (1995).
9. Lundahl, J., Regårdh, C.G., Edgar, B. & Johnsson, G. Effects of grapefruit juice ingestion-pharmacokinetics and haemodynamics of intravenously and orally administered felodipine in healthy men. *Eur. J. Clin. Pharmacol.* **52**, 139–145 (1997).
10. Veronese, M.L. *et al*. Exposure-dependent inhibition of intestinal and hepatic CYP3A4 in vivo by grapefruit juice. *J. Clin. Pharmacol.* **43**, 831–839 (2003).
11. Edgar, B., Bailey, D., Bergstrand, R., Johnsson, G. & Regårdh, C.G. Acute effects of drinking grapefruit juice on the pharmacokinetics and dynamics of felodipine—and its potential clinical relevance. *Eur. J. Clin. Pharmacol.* **42**, 313–317 (1992).
12. Lilja, J.J., Neuvonen, M. & Neuvonen, P.J. Effects of regular consumption of grapefruit juice on the pharmacokinetics of simvastatin. *Br. J. Clin. Pharmacol.* **58**, 56–60 (2004).
13. Malhotra, S., Bailey, D.G., Paine, M.F. & Watkins, P.B. Seville orange juice-felodipine interaction: comparison with dilute grapefruit juice and involvement of furocoumarins. *Clin. Pharmacol. Ther.* **69**, 14–23 (2001).
14. Bailey, D.G., Dresser, G.K. & Bend, J.R. Bergamottin, lime juice, and red wine as inhibitors of cytochrome P450 3A4 activity: comparison with grapefruit juice. *Clin. Pharmacol. Ther.* **73**, 529–537 (2003).
15. Huang, S.M. *et al*. Drug interactions with herbal products and grapefruit juice: a conference report. *Clin. Pharmacol. Ther.* **75**, 1–12 (2004).
16. European Medicines Agency. Guideline on the investigation of drug interactions. <https://www.ema.europa.eu/en/documents/scientific-guideline/guideline-investigation-drug-interactions-revision-1_en.pdf> (2015). Accessed April 4, 2023.
17. Mitchell, M., Muftakhidinov, B. & Winchen, T. Engauge Digitizer Software. <http://markummitchell.github.io/engauge-digitizer> Accessed March 22, 2023.
18. Fuhr, L.M., Marok, F.Z., Mees, M., Mahfoud, F., Selzer, D. & Lehr, T. A physiologically based pharmacokinetic and Pharmacodynamic model of the CYP3A4 substrate Felodipine for drug–drug interaction modeling. *Pharmaceutics* **14**, 1474 (2022).
19. Hanke, N. *et al*. PBPK models for CYP3A4 and P-gp DDI prediction: a modeling network of rifampicin, itraconazole, clarithromycin, midazolam, alfentanil, and digoxin. *CPT Pharmacometr. Syst. Pharmacol.* **7**, 647–659 (2018).
20. Fuhr, L.M., Marok, F.Z., Hanke, N., Selzer, D. & Lehr, T. Pharmacokinetics of the CYP3A4 and CYP2B6 inducer carbamazepine and its drug-drug interaction potential: a physiologically based pharmacokinetic modeling approach. *Pharmaceutics* **13**, 1–21 (2021).
21. Hanke, N. *et al*. A mechanistic, enantioselective, physiologically based pharmacokinetic model of verapamil and Norverapamil, built and evaluated for drug-drug interaction studies. *Pharmaceutics* **12**, 556 (2020).
22. Wojtyniak, J., Selzer, D., Schwab, M. & Lehr, T. Physiologically based precision dosing approach for drug-drug-gene interactions: a simvastatin network analysis. *Clin. Pharmacol. Ther.* **109**, 201–211 (2021).
23. Kent, U.M., Lin, H.L., Noon, K.R., Harris, D.L. & Hollenberg, P.F. Metabolism of bergamottin by cytochromes P450 2B6 and 3A5. *J. Pharmacol. Exp. Ther.* **318**, 992–1005 (2006).
24. Bailey, D.G., Arnold, J.M., Munoz, C. & Spence, J.D. Grapefruit juice--felodipine interaction: mechanism, predictability, and effect of naringin. *Clin. Pharmacol. Ther.* **53**, 637–642 (1993).
25. Paine, M.F. *et al*. A furanocoumarin-free grapefruit juice establishes furanocoumarins as the mediators of the grapefruit juice-felodipine interaction. *Am. J. Clin. Nutr.* **83**, 1097–1105 (2006).
26. Goosen, T.C. *et al*. Bergamottin contribution to the grapefruit juice-felodipine interaction and disposition in humans. *Clin. Pharmacol. Ther.* **76**, 607–617 (2004).
27. Kakar, S.M., Paine, M.F., Stewart, P.W. & Watkins, P.B. 6′7′-Dihydroxybergamottin contributes to the grapefruit juice effect. *Clin. Pharmacol. Ther.* **75**, 569–579 (2004).
28. Sica, D.A. Interaction of grapefruit juice and calcium channel blockers. *Am. J. Hypertens.* **19**, 768–773 (2006).
29. He, K., Iyer, K.R., Hayes, R.N., Sinz, M.W., Woolf, T.F. & Hollenberg, P.F. Inactivation of cytochrome P450 3A4 by bergamottin, a component of grapefruit juice. *Chem. Res. Toxicol.* **11**, 252–259 (1998).
30. Parker, R.B., Yates, C.R., Soberman, J.E. & Laizure, S.C. Effects of grapefruit juice on intestinal P-glycoprotein: evaluation using digoxin in humans. *Pharmacotherapy* **23**, 979–987 (2003).
31. Shirasaka, Y., Suzuki, K., Nakanishi, T. & Tamai, I. Differential effect of grapefruit juice on intestinal absorption of statins due to inhibition of organic anion transporting polypeptide and/or P-glycoprotein. *J. Pharm. Sci.* **100**, 3843–3853 (2011).
32. Pilla Reddy, V., Jo, H. & Neuhoff, S. Food constituent– and herb–drug interactions in oncology: influence of quantitative modelling on drug labelling. *Br. J. Clin. Pharmacol.* **87**, 3988–4000 (2021).

33. Fenneteau, F., Poulin, P. & Nekka, F. Physiologically based predictions of the impact of inhibition of intestinal and hepatic metabolism on human pharmacokinetics of CYP3A substrates. *J. Pharm. Sci.* **99**, 486–514 (2010).
34. Ainslie, G. R. A translational approach to assess the risk of dietary substance-drug interactions [doctoral dissertation, University of North Carolina]. Carolina Digital Repository. (2014). https://doi.org/10.17615/9ynp-bg55
35. Wagner, C., Thelen, K., Willmann, S., Selen, A. & Dressman, J.B. Utilizing In vitro and PBPK tools to link ADME characteristics to plasma profiles: case example Nifedipine immediate release formulation. *J. Pharm. Sci.* **102**, 3205–3219 (2013).
36. Pepin, X.J.H. *et al*. Bridging in vitro dissolution and in vivo exposure for acalabrutinib. Part II. A mechanistic PBPK model for IR formulation comparison, proton pump inhibitor drug interactions, and administration with acidic juices. *Eur. J. Pharm. Biopharm.* **142**, 435–448 (2019).
37. Marsousi, N. *et al*. Coadministration of ticagrelor and ritonavir: toward prospective dose adjustment to maintain an optimal platelet inhibition using the PBPK approach. *Clin. Pharmacol. Ther.* **100**, 295–304 (2016).
38. Melough, M.M. *et al*. Identification and quantitation of Furocoumarins in popularly consumed foods in the U.S. using QuEChERS extraction coupled with UPLC-MS/MS analysis. *J. Agric. Food Chem.* **65**, 5049–5055 (2017).
39. Kharasch, E.D., Walker, A., Hoffer, C. & Sheffels, P. Intravenous and oral alfentanil as in vivo probes for hepatic and first-pass cytochrome P450 3A activity: noninvasive assessment by use of pupillary miosis. *Clin. Pharmacol. Ther.* **76**, 452–466 (2004).
40. Gubbins, P.O. *et al*. Influence of grapefruit juice on the systemic availability of itraconazole oral solution in healthy adult volunteers. *Pharmacotherapy* **24**, 460–467 (2004).
41. Hukkinen, S.K., Varhe, A., Olkkola, K.T. & Neuvonen, P.J. Plasma concentrations of triazolam are increased by concomitant ingestion of grapefruit juice. *Clin. Pharmacol. Ther.* **58**, 127–131 (1995).
42. Fuhr, U. *et al*. Effects of grapefruit juice and smoking on verapamil concentrations in steady state. *Eur. J. Clin. Pharmacol.* **58**, 45–53 (2002).
43. Garg, S.K., Kumar, N., Bhargava, V.K. & Prabhakar, S.K. Effect of grapefruit juice on carbamazepine bioavailability in patients with epilepsy. *Clin. Pharmacol. Ther.* **64**, 286–288 (1998).
44. Bailey, D.G., Dresser, G.K., Kreeft, J.H., Munoz, C., Freeman, D.J. & Bend, J.R. Grapefruit-felodipine interaction: effect of unprocessed fruit and probable active ingredients. *Clin. Pharmacol. Ther.* **68**, 468–477 (2000).
45. Guest, E.J., Aarons, L., Houston, J.B., Rostami-Hodjegan, A. & Galetin, A. Critique of the two-fold measure of prediction success for ratios: application for the assessment of drug-drug interactions. *Drug Metab. Dispos.* **39**, 170–173 (2011).
46. Human Metabolome Database. Metabocard for bergamottin (HMDB0033782). <https://hmdb.ca/metabolites/HMDB0033782> (2022). Accessed January 31, 2023.
47. Human Metabolome Database. Metabocard for 6,7-dihydroxybergamottin (HMDB0039066). <https://hmdb.ca/metabolites/HMDB0039066> (2022). Accessed January 31, 2023.
48. Watanabe, R. *et al*. Predicting fraction unbound in human plasma from chemical structure: improved accuracy in the low value ranges. *Mol. Pharm.* **15**, 5302–5311 (2018).
49. Tassaneeyakul, W., Guo, L.Q., Fukuda, K., Ohta, T. & Yamazoe, Y. Inhibition selectivity of grapefruit juice components on human cytochromes P450. *Arch. Biochem. Biophys.* **378**, 356–363 (2000).
50. Schmiedlin-Ren, P. *et al*. Mechanisms of enhanced oral availability of CYP3A4 substrates by grapefruit constituents: decreased enterocyte CYP3A4 concentration and mechanism-based inactivation by furanocoumarins. *Drug Metab. Dispos.* **25**, 1228–1233 (1997).

5 DISCUSSION AND FUTURE DIRECTIONS

This thesis explores the capability of PBPK modeling to describe complex and time-dependent DDIs and FDIs involving CYP3A4. Within this work, new whole-body PBPK models of various CYP3A4 substrates and perpetrators were developed, namely carbamazepine (Project I, inducer), felodipine (Project II, substrate), and grapefruit juice (Project III, mechanism-based inhibitor). A CYP3A4 interaction network was established, including the aforementioned compounds as well as previously developed PBPK models of further substrates and perpetrators, mainly focusing on CYP3A4 but also including CYP2B6-mediated DDIs. The final network encompasses a total of thirteen compounds, illustrating the modularity of the PBPK modeling approach that allows the coupling of various models to predict DDIs.

5.1 PBPK MODELING OF COMPLEX CYP3A4-MEDIATED DDIS

5.1.1 *Implementation of time-dependent drug interactions in PBPK modeling*

Synthesis and degradation of CYP3A4 have to be taken into account to mechanistically describe time-dependent DDIs. Therefore, PBPK modeling relies on an extensive number of parameters. System-dependent parameters, including information on CYP3A4 organ expression, initial enzyme concentration, and half-life in liver and intestine are implemented in the modeling software PK-Sim® [66]. The effect of a mechanism-based inhibitor or inducer on enzyme degradation or synthesis, respectively, is then usually described using parameters derived from *in vitro* experiments as outlined in Section 1.3.

However, parametrization of the inductive effect of carbamazepine in Project I was challenging as EC_{50} and E_{max} values from published *in vitro* analyses were highly variable (EC_{50}: 4.3 – 137 μmol/l; E_{max}: 1.90 – 23) [1]. Here, variations in experimental conditions or the selected endpoint may have contributed to respective differences in obtained EC_{50} and E_{max} [39]. Additionally, high inter-donor variability in CYP activity was observed in *in vitro* hepatocyte systems [78].

In the final carbamazepine PBPK model, the CYP3A4 induction process was parametrized using a mean EC_{50} = 20 μmol/l calculated from available literature values while E_{max} = 6 was estimated during a parameter identification. The estimated value used in the model was within the range of reported literature values and sufficiently described carbamazepine autoinduction as well as DDIs with carbamazepine as CYP3A4 inducer, with GMFE values of 1.21 for DDI AUC_{last} ratios and 1.61 for DDI C_{max} ratios.

Inhibition parameters for bergamottin and 6,7-dihydroxybergamottin were

also highly variable between different published *in vitro* experiments. These differences may be attributed to the experimental design or the use of microsomes versus recombinant CYP3A4 [53, 54]. Microsomes are widely used as the gold standard to assess MBI [79]. Experiments with recombinant CYPs frequently reveal a higher MBI potential of the investigated drug, which might result in an overestimation of the effect *in vivo* [54]. This may be related to a more efficient generation of the reactive intermediate necessary for the MBI with recombinant CYPs, facilitated by higher oxidoreductase levels [54, 79] as well as the absence of further CYP enzymes [79]. Furthermore, comparably high protein concentrations can be observed in microsomal preparations [79]. High protein concentrations can lead to sequestration of the investigated drug as it may bind nonspecifically to proteins or partition into membranes, reducing the concentration of free drug available for CYP3A4 inactivation [80]. Here, not taking the unbound fraction of the drug into account may underestimate its inhibitory activity [56, 80]. Paine et al. compared inactivation parameters of 6,7-dihydroxybergamottin and bergamottin obtained utilizing microsomes or recombinant CYP3A4, concluding that high degrees of sequestration led to an underestimation of the inhibitory activity in microsomal preparations [56].
The mechanism-based inhibition of CYP3A4 by bergamottin and 6,7-dihydroxybergamottin in the GFJDI PBPK model was therefore parametrized using K_I and k_{inact} values derived from recombinant CYP enzymes reported by Paine et al. [56]. Overall, the presented GFJDI PBPK model sufficiently described GFJDIs with a broad range of CYP3A4 substrates for different scenarios with overall GMFEs of 1.30 for GFJDI AUC_{last} ratios and 1.31 for GFJDI C_{max} ratios.

5.1.2 *The application of PBPK modeling to investigate complex DDIs involving CYP3A4*

Initial clinical studies evaluate the inhibitory or inductive potential of an NDA on specific enzymes using index substrates or test an NDA's susceptibility to DDIs using clinical index perpetrators targeting a specific pathway [6]. While outcomes of these studies provide insights into involved CYP-mediated processes, the findings of the investigated DDI scenario with one particular perpetrator cannot be directly extrapolated to other DDI scenarios as the intricate mechanisms underlying a DDI can be very complex. In addition, the controlled setting of clinical DDI studies may not reflect clinical reality. DDIs often occur in polymedicated patients, taking five or more medications in different regimens [81]. FDIs resulting from individual dietary habits further add to the complexity of drug interactions. Overall, (1) time-dependent effects of mechanism-based inhibitors or inducers (2) the presence of multiple DDI effects, including different enzymatic pathways, autoinduction, or co-administration of more than two DDI partners; (3) differential effects on intestinal and hepatic CYP3A4 as well as (4) interactions involving common foods, such as grapefruit contribute to the unique

outcome of a particular DDI.
PBPK modeling is a powerful technique to investigate the outcome of complex DDIs. For instance, it could be applied to extrapolate the results of clinical DDI studies to investigate untested real-world DDI scenarios involving complex DDI mechanisms. As changes in drug and CYP concentrations over time can be quantitatively predicted, the mechanistic modeling approach could improve the understanding of the DDI while at the same time potentially reducing the need for additional clinical trials. The capability of whole-body PBPK modeling to capture complex and time-dependent DDIs and FDIs involving CYP3A4 was thoroughly investigated within Projects I - III.

5.1.2.1 *Differentiating intestinal and hepatic CYP3A4 DDI effects*

CYP3A4 is not only highly expressed in the liver, but also in the intestines, where it is the predominant CYP isoform [19] and contributes to a drug's first-pass metabolism and total bioavailability. Drugs undergoing significant intestinal CYP3A4 metabolism are particularly susceptible to DDIs, as CYP3A4 perpetrators can have a significant impact on their bioavailability [20–22]. Therefore, understanding the contribution of intestinal and hepatic metabolism to the PK of a CYP3A4 substrate is important to comprehend and predict DDIs. For instance, Heinig et al. extensively investigated finerenone CYP3A4 metabolism through *in vitro* and *in vivo* DDI studies [82]. The results were used to inform a finerenone PBPK model to predict untested DDIs and subsequently guide drug labeling [83].
In Project II, the contribution of intestinal CYP3A4 metabolism to the overall PK of the substrate felodipine was sufficiently described by PBPK modeling. Here, the PBPK model of felodipine predicted that 53% of the administered dose is metabolized by CYP3A4 in the intestines (observed F_g = 45% [21]) and an overall oral bioavailability of 13 - 18% (observed F = 14.2% [21]). Furthermore, the model captured the impact of carbamazepine treatment on felodipine bioavailability. Here, the model predicted a decrease from 15% to 1%, closely correlating with observed decreases from approximately 13% to 2% [32]. The thorough evaluation of the felodipine model – adequately covering felodipine intestinal metabolism, bioavailability, and CYP3A4-mediated DDIs – within Project II enabled the establishment of the grapefruit DDI PBPK model in Project III. Within this project, the capability of whole-body PBPK modeling to describe differential DDI effects on intestinal and hepatic CYP3A4 was extensively investigated. Notably, grapefruit primarily inhibits intestinal CYP3A4, with effects on hepatic CYP3A4 only emerging after consuming the fruit or its juice frequently or in high amounts [61]. Consequently, a single glass of grapefruit juice does not affect the PK of intravenously administered CYP3A4 substrates, as sufficiently described by the PBPK model for GFJDIs with intravenously applied felodipine, midazolam, and alfentanil [21, 84]. For orally administered compounds, a single glass of grapefruit affects drug bioavailability but not half-life. Here, the grapefruit PBPK model comprehensively described GFJDIs with orally administered

drugs, including effects on AUC and C_{max} and bioavailability. For the victim drugs felodipine and midazolam, the model also adequately predicted more pronounced effects associated with frequent grapefruit juice consumption, extending to effects on drug half-life.
The explicit representation of different tissues in the PBPK model enabled the prediction of bergamottin and 6,7-dihydroxybergamottin concentration in the duodenum and liver after the consumption of one or multiple glasses of grapefruit juice. This led to the hypothesis that hepatic ingredient concentrations may be insufficient to inhibit CYP3A4 in the liver after ingesting a single glass of grapefruit juice.

5.1.2.2 *Time-dependence of CYP3A4-mediated DDIs*

Grapefruit as a mechanism-based inhibitor and carbamazepine as a CYP3A4 inducer both mediate concentration- and time-dependent DDIs. These types of DDIs exhibit characteristics of slow onset, prolonged duration, and a cumulative but saturable effect [10], as outlined in Section 1.3. The capability of PBPK modeling to describe respective characteristics could be thoroughly investigated within Project III: The presented GFJDI PBPK model sufficiently captured the prolonged effect of grapefruit on victim drugs, including felodipine, midazolam, simvastatin, and triazolam, administered up to 144 hours after grapefruit consumption. Furthermore, the cumulative and saturable kinetics were also covered by the PBPK model, demonstrated through the adequate description of (1) GFJDIs for single- versus double-strength grapefruit juice, reflecting a 2-fold difference in bergamottin and 6,7-dihydroxybergamottin concentrations, and (2) GFJDIs following frequent administration of grapefruit juice. This comprehensive PBPK analysis illustrates the power of PBPK modeling to dynamically compute changes in active CYP3A4 in the presence of two mechanism-based inhibitors of CYP3A4 – bergamottin and 6,7-dihydroxybergamottin – by taking into account the kinetics of the inhibition processes as well as CYP3A4 turnover. This enabled an accurate description of the time-dependent grapefruit-mediated FDIs, depending on the balance of CYP degradation and synthesis.

The complex PK of carbamazepine involve extensive metabolism by CYP3A4, CYP2B6, CYP2C8, and UGT2B7 [43–45], as well as autoinduction, increasing its own CYP3A4- and CYP2B6-mediated clearance [8]. This time- and dose-dependent process results in nonlinear kinetics and an increased clearance during initiation of a long-term treatment [85, 86], with the full effect established after up to 3 – 5 weeks of treatment [42]. In Project I the intricate metabolism of carbamazepine was thoroughly investigated, implementing relevant metabolic and inductive processes. Considering a diverse set of clinical studies covering single- and multiple-dose studies administering carbamazepine over a broad range of doses (50 – 800 mg), aimed to ensure that the concentration- and time-dependent characteristics of the CYP autoinduction were adequately implemented in the model. To further verify the adequate description of CYP metabolism and induction, the model

was applied in DDI predictions and sufficiently predicted interactions with simvastatin and alprazolam as CYP3A4 substrates, bupropion as CYP2B6 substrate as well as erythromycin as a CYP3A4 inhibitor. In the following Projects II and III, the carbamazepine PBPK model was also successfully applied to predict a DDI with the CYP3A4 substrate felodipine or a GFJDI with grapefruit, respectively.

5.1.2.3 *Involvement of multiple DDI effects*

The overall outcome of a DDI can be the result of the confluence of multiple distinct mechanisms, making it challenging to predict. This complexity becomes evident in scenarios where the perpetrator impacts several relevant CYP pathways at the same time or where co-administered drugs impact each other's metabolic pathways mutually. The administration of more than two drugs simultaneously increases the number of potentially affected pathways. The impact of multiple DDI effects on the overall DDI outcome is examined within two illustrative examples in the following.
As a dual substrate and inducer of CYP3A4 and CYP2B6 [43, 44, 46], carbamazepine acts as both a perpetrator and victim at the same time. An intricate example is the interaction between carbamazepine and efavirenz [47]. Both compounds induce CYP3A4 and CYP2B6 but are also substrates of respective enzymes. Here, CYP3A4 is the major enzyme in the metabolism of carbamazepine [43], while CYP2B6 is the main metabolizing enzyme of efavirenz [48]. The adequate prediction of the mutual effects of efavirenz and carbamazepine on each other's metabolism indicates that the PBPK models sufficiently describe (1) the contribution of each affected pathway to overall drug metabolism as well as (2) the drug concentrations at the sites of the interaction. The prediction of the efavirenz-carbamazepine DDI within Project I exemplifies the power of PBPK DDI modeling, to describe the dynamic changes in drug concentrations and the time- and concentration-dependency of CYP induction [1].
By activating nuclear receptors, inducers typically increase the expression of multiple proteins simultaneously, as outlined in Section 1.3.1. In future applications, the carbamazepine PBPK model can be readily expanded to include further processes, for instance, induction of CYP2C9 [8] or P-gp.

The capability of PBPK modeling to predict DDIs with three interacting drugs was illustrated in Project II, predicting the felodipine-carbamazepine-phenytoin DDI. On the enzymatic level, the interaction between these compounds is particularly complex. It is assumed that felodipine does not affect the PK of the co-administered drugs and therefore acts as a victim drug in this interaction. However, phenytoin and carbamazepine both induce the CYP3A4-mediated metabolism of felodipine. Additionally, both antiepileptic drugs mutually affect each other's metabolism. Phenytoin induces the CYP3A4-mediated carbamazepine metabolism, while carbamazepine induces CYP2C9- and CYP2C19-mediated phenytoin metabolism. All interaction processes were considered in the PBPK model and the inter-

action could be sufficiently described. In the clinical study that was used to evaluate the DDI prediction [32], participants received carbamazepine and phenytoin as part of their long-term epilepsy medication, highlighting the challenges associated with initiating treatments for patients taking strong CYP3A4 inducers. Overall, this example underscores that real-world DDIs are often far more complex than the isolated DDIs investigated with index compounds in clinical DDI studies. Especially fragile and multimorbid populations receiving polymedication face a high risk for DDIs. However, investigating all possible DDI scenarios in clinical studies is unfeasible due to the combinatorial explosion and could bear a high risk for participants. PBPK modeling may overcome those challenges by extrapolating results derived from clinical DDI studies to investigate untested real-world settings and emerges as a valuable tool to enhance understanding of these complex DDIs and inform treatment decisions.

5.2 CYP3A4-MEDIATED FOOD-DRUG INTERACTIONS

5.2.1 *PBPK modeling of CYP-mediated food-drug interactions*

In Project III, the grapefruit effect was mathematically described within a whole-body PBPK modeling framework by explicitly modeling two ingredients of the fruit, bergamottin and 6,7-dihydroxybergamottin. The model adequately described the observed effects of grapefruit on ten different victim drugs, although the grapefruit effect cannot be attributed to one specific causative ingredient. Moreover, ingredient concentrations of the fruit are highly variable and were not indicated in approximately 80% of available clinical studies. Successful application of the bergamottin and 6,7-dihydroxybergamottin PBPK models to predict FDIs with lime and Seville orange illustrates the potential of respective ingredient PBPK models in predicting FDIs with further foods containing respective ingredients aside from grapefruit. The effect of grapefruit juice extends beyond the inhibition of CYP3A4 to further CYP enzymes and drug transporters such as organic-anion-transporting polypeptides (OATP) [87]. As the inhibition of transport proteins is assumed to be mediated by flavonoids, a potential extension of the presented grapefruit PBPK model could involve the incorporation of flavonoids.

Further foods have also been shown to affect metabolizing enzymes and transporters, bearing a potential risk for DDIs. For instance, apple and orange juice have been found in clinical trials to inhibit OATP2B1 [88]. Furthermore, CYP3A4 inactivation by tomato juice has been shown *in vitro* [89] and in the rat [90]. However, relevant effects have not yet been observed in humans [90]. In general, FDIs are complex as the overall effect is often the result of a food's unique ingredient composition, and their clinical relevance depends on consumed amounts, the timing of the consumption, and the characteristics of the victim drug [88]. Here, the grapefruit modeling

approach can serve as a blueprint for further FDI modeling analyses, to gain mechanistic insights and assess the clinical relevance of FDIs. However, a comprehensive understanding of FDIs with PBPK modeling would require a detailed characterization of the causative ingredients of the investigated food.

By increasing the exposure of CYP3A4 victim drugs, grapefruit increases the risk for ADRs. Severe ADRs associated with grapefruit consumption include torsade de points (amiodarone) [91], rhabdomyolysis (atorvastatin) [92], or nephrotoxicity (tacrolimus) [23, 93]. As grapefruit irreversibly inhibits CYP3A4, the interaction cannot be avoided by a staggered intake of grapefruit and the drug, wherefore drug labels of respective drugs advise against the consumption of grapefruit [94–96]. However, recommendations in drug labels, for instance for mifepristone [97], are not always based on clinical trials but on metabolic characteristics of the drug [98]. This may also lead to inconsistencies in drug labels and patient information leaflets as observed by Van et al. [99]. Additionally, the awareness of the grapefruit effect on medication in the general public is low [100]. For instance, interactions of grapefruit or Seville orange with anti-cancer medication were reported as the most frequent FDI [101, 102]. Koni et al. reported that approximately 30% of included cancer patients were regularly consuming grapefruit juice [102], while Prely et al. identified GFJDIs for approximately 10% of patients [101].

However, for cancer treatments that are often associated with severe ADRs, clinical trials bear a high risk for patients, especially if the drug is markedly affected by grapefruit juice. Here, PBPK modeling could be a valuable alternative to assess potential interactions and guide labeling recommendations if clinical trials are not feasible. After a thorough evaluation of the grapefruit PBPK model in a DDI network with ten different CYP3A4 victim drugs within Project III, the presented grapefruit PBPK model was applied in a recent PBPK analysis to predict the untested grapefruit-dasatinib FDI [103]. The models predict an increase in dasatinib AUC of up to 1.4-fold after daily consumption of grapefruit, supporting the package insert recommendation to avoid concomitant intake of dasatinib with grapefruit juice. This example illustrates potential future applications of the GFJDI PBPK model to guide drug labeling.

5.2.2 *Potential applications of grapefruit*

Besides the increased risk for ADRs associated with grapefruit, its potential to increase the bioavailability of substrates by inhibiting intestinal CYP3A4 could provide the opportunity to apply grapefruit as a bioavailability enhancer. In clinical practice, bioavailability enhancement is regularly achieved by low-dose administration of the antiretroviral drug ritonavir to boost the availability of further antiretroviral drugs like lopinavir [104] or of the COVID-19 treatment nirmatrelvir [105]. However, ritonavir treatment is asso-

ciated with adverse events including increased triglycerides or gastrointestinal disturbances [105]. Additionally, the effect of ritonavir on victim drugs is challenging to predict as it acts as a mutual inducer and inhibitor [106]. Here, grapefruit juice may emerge as a potentially favorable alternative. The potential of grapefruit juice to enhance the availability of the antiretroviral drug saquinavir was hypothesized as early as 1998 [107] and has been investigated in recent case reports [108]. However, given the high variability of furanocoumarin concentration in juice preparations, it would be preferable to apply purified bergamottin and/or 6,7-dihydroxybergamottin in fixed doses. First advances in drug therapy were made by Paolini et al. in 2017 [109] by intravenous co-administration of 6,7-dihydroxybergamottin-containing micelles with the cancer treatment docetaxel to decrease its hepatic first-pass metabolism in mice. The developed PBPK models of bergamottin and 6,7-dihydroxybergamottin could be used to (1) predict the effect of different doses of (6,7-dihydroxy)bergamottin on various victim drugs, (2) assess the impact of different dosing regimens on intestinal versus hepatic CYP3A4 as well as (3) determine the time to achieve maximum CYP inhibition. Here, the modeling approach not only provides a more mechanistic understanding of the interaction but could also guide the design of clinical studies to explore the potential of grapefruit components as bioavailability enhancers.
As a moderate to strong inhibitor of CYP3A4 [8], grapefruit may also present as an alternative to the pharmaceutically active index CYP3A4 inhibitors itraconazole (strong inhibitor) or verapamil (moderate inhibitor), recommended by the FDA for use in clinical DDI studies [6, 50]. Through virtual PBPK DDI studies, the effect of grapefruit juice on a CYP3A4 victim drug could be compared to the effect of itraconazole or verapamil, using previously developed itraconazole and verapamil PBPK models [110, 111]. Hereby, the potential application of grapefruit ingredients in clinical DDI studies could be further explored.

5.3 PBPK MODELING OF DDIS IN MID3

PBPK modeling is gaining increasing recognition in the field of MID3. This is evident in NDA submissions, including PBPK approaches, to the FDA, which have strongly increased over the last decade [70]. While in 2013 approximately 20% of all submitted NDAs included PBPK analyses, the percentage increased to 45% in 2019 [13]. Here, the primary purpose of PBPK modeling is the investigation of enzyme-mediated DDIs [13]. An analysis of NDAs approved by the FDA in 2017 revealed CYP3A as the main DDI target. CYP3A was involved in the metabolism of two-thirds of approved NDAs (n = 35). Among 16 drugs identified as inhibitors, one drug was classified as a strong and mechanism-based inhibitor *in vivo*. Furthermore, two drugs exhibited CYP3A4 induction *in vivo* [12]. Here, PBPK modeling was applied to explore untested DDIs for five of the NDAs classified as CYP3A4 substrates. For the NDA identified as a mechanism-based inhibitor,

PBPK modeling was utilized to investigate its inhibitory effect at different doses [12]. In all cases, PBPK modeling analyses guided drug labeling and reduced the need for further dedicated clinical studies.
This emphasizes the importance and current relevance of the presented thesis, aiming to enhance understanding of complex time-dependent DDIs and FDIs involving CYP3A4 using PBPK modeling. Within the scope of the project OSMOSES, PBPK models for the CYP3A4 inducer carbamazepine, the substrate felodipine, and the mechanism-based inhibitor grapefruit were thoroughly evaluated within extensive DDI networks and subsequently shared with the Open Systems Pharmacology community to be used for future applications. Within the context of MID3 the models may be applied to investigate complex and time-dependent interactions evolving around CYP3A4. This includes the investigation of untested interaction scenarios.
The Open Systems Pharmacology follows an open-source approach to improve the exchange of scientific knowledge and facilitate the sharing of PBPK modeling files. Therefore, the files of the presented PBPK models are publicly available on GitHub. The PBPK models developed within Projects I - III were embedded into a comprehensive CYP3A4 and CYP2B6 DDI network featuring previously developed substrates and inhibitors to evaluate their DDI performance. This network approach not only highlights the modularity of PBPK modeling, allowing to couple models developed within the same framework but also the benefits of the open-source concept of the Open Systems Pharmacology platform. The use of PBPK models available on the Open Systems Pharmacology GitHub page (github.com/Open-Systems-Pharmacology) enabled the establishment of a comprehensive GFJDI network. By predicting GFJDIs with various substrates with different pharmacokinetic characteristics, the grapefruit PBPK model could be thoroughly evaluated.
Before applying a publicly available PBPK model for future research, its adequate predictive performance and suitability for the intended research objectives have to be evaluated. This evaluation is facilitated through a transparent and comprehensive description of model development and evaluation. Therefore, all models developed and published within Projects I – III are accompanied by detailed supplementary information, describing all utilized data, incorporated processes, and final model parameters, as well as a comprehensive performance evaluation of the models and implemented DDIs. This comprehensive approach empowers prospective users to apply and extend the developed models for future research.

6

CONCLUSION AND OUTLOOK

CYP3A4 is the most abundant metabolizing CYP enzyme in the human body. Its high abundance in the liver and intestine determines not only the clearance of its substrates but also their oral bioavailability. As CYP3A4 is involved in the metabolism of >50% of available drugs, investigation of potential DDIs is crucial during pharmaceutical drug development. Recent literature illustrates the importance of PBPK modeling to support those investigations. However, CYP3A4 cannot only be impacted by drugs but also by common foods, as illustrated by the example of grapefruit. PBPK models of carbamazepine, felodipine, and grapefruit were developed within this thesis, and within an extensive PBPK CYP3A4 DDI network, the complexity of time-dependent DDIs and FDIs involving CYP3A4 was thoroughly investigated. The thesis illustrates the capability of mechanistic whole-body PBPK models in predicting the outcome of respective complex interactions. It was shown that the PBPK models can quantitatively describe and predict the time-dependent effect magnitude as well as the resulting changes in drug plasma concentration-time profiles. The PBPK models developed within this work were made publicly available and can be applied to support time-dependent CYP3A4-mediated DDI investigations within the context of MID3. In addition, the grapefruit PBPK model may be applied to investigate potential applications of grapefruit ingredients. Furthermore, the GFJDI modeling approach may serve as a blueprint for the application of PBPK modeling to investigate FDIs.

BIBLIOGRAPHY

1. Fuhr, L. M., Marok, F. Z., Hanke, N., Selzer, D. & Lehr, T. Pharmacokinetics of the CYP3A4 and CYP2B6 Inducer Carbamazepine and Its Drug-Drug Interaction Potential: A Physiologically Based Pharmacokinetic Modeling Approach. *Pharmaceutics.* 2021**. 13**(2): 270. doi:10.3390/pharmaceutics13020270.
2. Fuhr, L. M. et al. A Physiologically Based Pharmacokinetic and Pharmacodynamic Model of the CYP3A4 Substrate Felodipine for Drug–Drug Interaction Modeling. *Pharmaceutics.* 2022**. 14**(7): 1474. doi:10.3390/pharmaceutics14071474.
3. Fuhr, L. M., Marok, F. Z., Fuhr, U., Selzer, D. & Lehr, T. Physiologically Based Pharmacokinetic Modeling of Bergamottin and 6,7-Dihydroxybergamottin to Describe CYP3A4 Mediated Grapefruit-Drug Interactions. *Clinical Pharmacology and Therapeutics.* 2023**. 114**(2): 470–482. doi:10.1002/cpt.2968.
4. Brand, A., Allen, L., Altman, M., Hlava, M. & Scott, J. Beyond authorship: attribution, contribution, collaboration, and credit. *Learned Publishing.* 2015**. 28**(2): 151–155. doi:10.1087/20150211.
5. Franceschi, M. et al. Prevalence, clinical features and avoidability of adverse drug reactions as cause of admission to a geriatric unit: a prospective study of 1756 patients. *Drug Safety.* 2008**. 31**(6): 545–56. doi:10.2165/00002018-200831060-00009.
6. U.S. Food and Drug Administration. Clinical Drug Interaction Studies - Cytochrome P450 Enzyme- and Drug Interactions. Guidance for Industry. 2020. Available from: https://www.fda.gov/media/134581/download (accessed: 2023-02-24).
7. U.S. Food and Drug Administration. In Vitro Drug Interaction Studies – Cytochrome P450 Enzyme- and Transporter-Mediated Drug Interactions. Guidance for Industry. 2020. Available from: https://www.fda.gov/media/134582/download (accessed: 2024-02-08).
8. U.S. Food and Drug Administration. For Healthcare Professionals | FDA's Examples of Drugs that Interact with CYP Enzymes and Transporter Systems. 2023. Available from: https://www.fda.gov/drugs/drug-interactions-labeling/healthcare-professionals-fdas-examples-drugs-interact-cyp-enzymes-and-transporter-systems (accessed: 2024-03-01).
9. Won, C. S., Oberlies, N. H. & Paine, M. F. Mechanisms underlying food-drug interactions: inhibition of intestinal metabolism and transport. *Pharmacology & Therapeutics.* 2012**. 136**(2): 186–201. doi:10.1016/j.pharmthera.2012.08.001.

10. Riley, R. J. & Wilson, C. E. Cytochrome P450 time-dependent inhibition and induction: Advances in assays, risk analysis and modelling. *Expert Opinion on Drug Metabolism and Toxicology.* 2015**. 11**(4): 557–572. doi:10.1517/17425255.2015.1013095.

11. Zhou, S. et al. Mechanism-based inhibition of cytochrome P450 3A4 by therapeutic drugs. *Clinical Pharmacokinetics.* 2005**. 44**(3): 279–304. doi:10.2165/00003088-200544030-00005.

12. Yu, J., Petrie, I. D., Levy, R. H. & Ragueneau-Majlessi, I. Mechanisms and clinical significance of pharmacokinetic-based drug-drug interactions with drugs approved by the U.S. Food and drug administration in 2017. *Drug Metabolism and Disposition.* 2019**. 47**(2): 135–144. doi:10.1124/dmd.118.084905.

13. Zhang, X. et al. Application of PBPK Modeling and Simulation for Regulatory Decision Making and Its Impact on US Prescribing Information: An Update on the 2018-2019 Submissions to the US FDA's Office of Clinical Pharmacology. *Journal of Clinical Pharmacology.* 2020**. 60**(S1): S160–S178. doi:10.1002/jcph.1767.

14. U.S. Food and Drug Administration. Physiologically Based Pharmacokinetic Analyses — Format and Content. 2018. Available from: https://www.fda.gov/media/101469/download (accessed: 2024-03-01).

15. Thummel, K. E. & Wilkinson, G. R. In vitro and in vivo drug interactions involving human CYP3A. *Annual review of pharmacology and toxicology.* 1998**. 38** 389–430. doi:10.1146/annurev.pharmtox.38.1.389.

16. Klyushova, L. S., Perepechaeva, M. L. & Grishanova, A. Y. The Role of CYP3A in Health and Disease. *Biomedicines.* 2022**. 10**(11): 2686. doi:10.3390/biomedicines10112686.

17. Türk, D. et al. Novel models for the prediction of drug–gene interactions. *Expert Opinion on Drug Metabolism & Toxicology.* 2021**. 17**(11): 1293–1310. doi:10.1080/17425255.2021.1998455.

18. Ohtsuki, S. et al. Simultaneous absolute protein quantification of transporters, cytochromes P450, and UDP-glucuronosyltransferases as a novel approach for the characterization of individual human liver: comparison with mRNA levels and activities. *Drug Metabolism and Disposition.* 2012**. 40**(1): 83–92. doi:10.1124/dmd.111.042259.

19. Gundert-Remy, U. et al. Extrahepatic metabolism at the body's internal-external interfaces. *Drug Metabolism Reviews.* 2014**. 46**(3): 291–324. doi:10.3109/03602532.2014.900565.

20. Kato, M. Intestinal first-pass metabolism of CYP3A4 substrates. *Drug Metabolism and Pharmacokinetics.* 2008**. 23**(2): 87–94. doi:10.2133/dmpk.23.87.

21. Lundahl, J., Regårdh, C. G., Edgar, B. & Johnsson, G. Effects of grapefruit juice ingestion – pharmacokinetics and haemodynamics of intravenously and orally administered felodipine in healthy men. *European Journal of Clinical Pharmacology.* 1997**. 52**(2): 139–145. doi:10.1007/s002280050263.

22. Kato, M. et al. The Intestinal First-pass Metabolism of Substrates of CYP3A4 and P-glycoprotei—Quantitative Analysis Based on Information from the Literature. *Drug Metabolism and Pharmacokinetics.* 2003**. 18**(6): 365–372. doi:10.2133/dmpk.18.365.

23. Bailey, D. G., Dresser, G. & Arnold, J. M. O. Grapefruit-medication interactions: forbidden fruit or avoidable consequences? *Canadian Medical Association Journal.* 2013**. 185**(4): 309–316. doi:10.1503/cmaj.120951.

24. Les Laboratoires Servier. Servier Medicat Art (SMART). Available from: https://smart.servier.com/ (accessed: 2024-02-08).

25. Klein, K. & Zanger, U. M. Pharmacogenomics of Cytochrome P450 3A4: Recent Progress Toward the "Missing Heritability" Problem. *Frontiers in Genetics.* 2013**. 4**(FEB): 12. doi:10.3389/fgene.2013.00012.

26. Waxman, D. J. & Holloway, M. G. Sex differences in the expression of hepatic drug metabolizing enzymes. *Molecular Pharmacology.* 2009**. 76**(2): 215–228. doi:10.1124/mol.109.056705.

27. Wolbold, R. et al. Sex is a major determinant of CYP3A4 expression in human liver. *Hepatology.* 2003**. 38**(4): 978–988. doi:10.1053/jhep.2003.50393.

28. De Jong, L. M., Jiskoot, W., Swen, J. J. & Manson, M. L. Distinct Effects of Inflammation on Cytochrome P450 Regulation and Drug Metabolism: Lessons from Experimental Models and a Potential Role for Pharmacogenetics. *Genes.* 2020**. 11**(12): 1509. doi:10.3390/genes11121509.

29. Guengerich, F. P. et al. Oxidation of dihydropyridine calcium channel blockers and analogues by human liver cytochrome P-450 IIIA4. *Journal of Medicinal Chemistry.* 1991**. 34**(6): 1838–1844. doi:10.1021/jm00110a012.

30. Jalava, K. M., Olkkola, K. T. & Neuvonen, P. J. Itraconazole greatly increases plasma concentrations and effects of felodipine. *Clinical Pharmacology and Therapeutics.* 1997**. 61**(4): 410–415. doi:10.1016/S0009-9236(97)90191-0.

31. Bailey, D. G., Bend, J. R., Arnold, J. M., Tran, L. T. & Spence, J. D. Erythromycin-felodipine interaction: magnitude, mechanism, and comparison with grapefruit juice. *Clinical Pharmacology and Therapeutics.* 1996**. 60**(1): 25–33. doi:10.1016/S0009-9236(96)90163-0.

32. Capewell, S., Freestone, S., Critchley, J. A., Pottage, A. & Prescott, L. F. Reduced felodipine bioavailability in patients taking anticonvulsants. *Lancet (London, England).* 1988**.** **332**(8609): 480–482. doi:10.1016/s0140-6736(88)90124-9.

33. Bailey, D. G., Malcolm, J., Arnold, O. & David Spence, J. Grapefruit juice–drug interactions. *British Journal of Clinical Pharmacology.* 1998**.** **46**(2): 101–110. doi:10.1046/j.1365-2125.1998.00764.x.

34. Bengtsson-Hasselgren, B, Edgar, B & Rönn, O. Dose-dependent effects of felodipine on diuresis and natriuresis in healthy subjects. *Journal of Cardiovascular Pharmacology.* 1988**.** **12**(2): 134–139. doi:10.1097/00005344-198808000-00002.

35. Blychert, E., Edgar, B., Elmfeldt, D. & Hedner, T. Plasma concentration-effect relationships for felodipine: a meta analysis. *Clinical Pharmacology and Therapeutics.* 1992**.** **52**(1): 80–89. doi:10.1038/clpt.1992.105.

36. Nakajima, Y. et al. In Vitro-in Vivo Correlation of Pharmacodynamics of Felodipine in Essential Hypertensive Patients Based on an Ion-Channel Binding Model. *Biological and Pharmaceutical Bulletin.* 1996**.** **19**(8): 1097–1099. doi:10.1248/bpb.19.1097.

37. Venkatakrishnan, K., Obach, R. S. & Rostami-Hodjegan, A. Mechanism-based inactivation of human cytochrome P450 enzymes: Strategies for diagnosis and drug-drug interaction risk assessment. *Xenobiotica.* 2007**.** **37**(10-11): 1225–1256. doi:10.1080/00498250701670945.

38. Brodie, M. J. et al. Enzyme induction with antiepileptic drugs: Cause for concern? *Epilepsia.* 2013**.** **54**(1): 11–27. doi:10.1111/j.1528-1167.2012.03671.x.

39. Lin, J. H. CYP induction-mediated drug interactions: in vitro assessment and clinical implications. *Pharmaceutical Research.* 2006**.** **23**(6): 1089–1116. doi:10.1007/s11095-006-0277-7.

40. Faucette, S. R. et al. Relative activation of human pregnane X receptor versus constitutive androstane receptor defines distinct classes of CYP2B6 and CYP3A4 inducers. *Journal of Pharmacology and Experimental Therapeutics.* 2007**.** **320**(1): 72–80. doi:10.1124/jpet.106.112136.

41. Shou, M. et al. Modeling, prediction, and in vitro in vivo correlation of CYP3A4 induction. *Drug Metabolism and Disposition.* 2008**.** **36**(11): 2355–2370. doi:10.1124/dmd.108.020602.

42. Novartis. Tegretol ® (Carbamazepine) - Prescribing information. 2009. Available from: https://www.accessdata.fda.gov/drugsatfda_docs/label/2009/016608s101,018281s048lbl.pdf (accessed: 2024-02-08).

43. Kerr, B. M. et al. Human liver carbamazepine metabolism. Role of CYP3A4 and CYP2C8 in 10,11-epoxide formation. *Biochemical Pharmacology.* 1994**.** **47**(11): 1969–1979. doi:10.1016/0006-2952(94)90071-x.

44. Pearce, R. E., Vakkalagadda, G. R. & Steven Leeder, J. Pathways of carbamazepine bioactivation in vitro I. Characterization of human cytochromes P450 responsible for the formation of 2- and 3-hydroxylated metabolites. *Drug Metabolism and Disposition.* 2002**.** **30**(11): 1170–1179. doi:10.1124/dmd.30.11.1170.

45. Staines, A. G., Coughtrie, M. W. & Burchell, B. N-glucuronidation of carbamazepine in human tissues is mediated by UGT2B7. *Journal of Pharmacology and Experimental Therapeutics.* 2004**.** **311**(3): 1131–1137. doi:10.1124/jpet.104.073114.

46. Zhang, J. G. et al. Effect of Fifteen CYP3A4 in vitro Inducers on the Induction of Hepatocytes: A Trend Analysis. In proceedings of the 20th North American ISSX Meeting; 18-22 Oct; Orlando Florida. 2015.

47. Ji, P. et al. Pharmacokinetic interaction between efavirenz and carbamazepine after multiple-dose administration in healthy subjects. *Journal of Clinical Pharmacology.* 2008**.** **48**(8): 948–956. doi:10.1177/0091270008319792.

48. Ward, B. A. et al. The Cytochrome P450 2B6 (CYP2B6) Is the Main Catalyst of Efavirenz Primary and Secondary Metabolism: Implication for HIV/AIDS Therapy and Utility of Efavirenz as a Substrate Marker of CYP2B6 Catalytic Activity. *Journal of Pharmacology and Experimental Therapeutics.* 2003**.** **306**(1): 287–300. doi:10.1124/jpet.103.049601.

49. Ke, A., Barter, Z., Rowland-Yeo, K & Almond, L. Towards a Best Practice Approach in PBPK Modeling: Case Example of Developing a Unified Efavirenz Model Accounting for Induction of CYPs 3A4 and 2B6. *CPT: Pharmacometrics & Systems Pharmacology.* 2016**.** **5**(7): 367–376. doi:10.1002/psp4.12088.

50. U.S. Food and Drug Administration. Drug development and drug interactions. Table of substrates, inhibitors and inducers. 2023. Available from: https://www.fda.gov/drugs/drug-interactions-labeling/drug-development-and-drug-interactions-table-substrates-inhibitors-and-inducers (accessed: 2024-03-01).

51. Bolleddula, J., Gopalakrishnan, S., Hu, P., Dong, J. & Venkatakrishnan, K. Alternatives to rifampicin: A review and perspectives on the choice of strong CYP3A inducers for clinical drug–drug interaction studies. *Clinical and Translational Science.* 2022**.** **15**(9): 2075–2095. doi:10.1111/cts.13357.

52. Chen, K. F. & Jones, H. M. PBPK perspective on alternative CYP3A4 inducers for rifampin. *CPT: Pharmacometrics & Systems Pharmacology.* 2022**.** **11**(12): 1543–1546. doi:10.1002/psp4.12864.

53. Yadav, J., Paragas, E., Korzekwa, K. & Nagar, S. Time-dependent enzyme inactivation: Numerical analyses of in vitro data and prediction of drug-drug interactions. *Pharmacology and Therapeutics.* 2020**.** **206** 107449. doi:10.1016/J.PHARMTHERA.2019.107449.

54. Polasek, T. M. & Miners, J. O. In vitro approaches to investigate mechanism-based inactivation of CYP enzymes. *Expert Opinion on Drug Metabolism and Toxicology.* 2007. **3**(3): 321–329. doi:10.1517/17425255.3.3.321.

55. Hung, W. L., Suh, J. H. & Wang, Y. Chemistry and health effects of furanocoumarins in grapefruit. *Journal of Food and Drug Analysis.* 2017. **25**(1): 71–83. doi:10.1016/j.jfda.2016.11.008.

56. Paine, M. F., Criss, A. B. & Watkins, P. B. Two major grapefruit juice components differ in intestinal CYP3A4 inhibition kinetic and binding properties. *Drug Metabolism and Disposition.* 2004. **32**(10): 1146–1153. doi:10.1124/dmd.104.000547.

57. Lin, H.-l., Kent, U. M. & Hollenberg, P. F. The grapefruit juice effect is not limited to cytochrome P450 (P450) 3A4: evidence for bergamottin-dependent inactivation, heme destruction, and covalent binding to protein in P450s 2B6 and 3A5. *The Journal of Pharmacology and Experimental Therapeutics.* 2005. **313**(1): 154–164. doi:10.1124/jpet.104.079608.

58. Lundahl, J, Regårdh, C. G., Edgar, B & Johnsson, G. Relationship between time of intake of grapefruit juice and its effect on pharmacokinetics and pharmacodynamics of felodipine in healthy subjects. *European Journal of Clinical Pharmacology.* 1995. **49**(1-2): 61–67. doi:10.1007/BF00192360.

59. Lilja, J. J., Kivistö, K. T. & Neuvonen, P. J. Duration of effect of grapefruit juice on the pharmacokinetics of the CYP3A4 substrate simvastatin. *Clinical Pharmacology and Therapeutics.* 2000. **68**(4): 384–390. doi:10.1067/mcp.2000.110216.

60. Greenblatt, D. J. et al. Time course of recovery of cytochrome p450 3A function after single doses of grapefruit juice. *Clinical Pharmacology and Therapeutics.* 2003. **74**(2): 121–129. doi:10.1016/S0009-9236(03)00118-8.

61. Veronese, M. L. et al. Exposure-dependent inhibition of intestinal and hepatic CYP3A4 in vivo by grapefruit juice. *Journal of Clinical Pharmacology.* 2003. **43**(8): 831–839. doi:10.1177/0091270003256059.

62. European Medicines Agency. Guideline on the reporting of physiologically based pharmacokinetic (PBPK) modelling and simulation. 2018. Available from: https://www.ema.europa.eu/en/documents/scientific-guideline/guideline-reporting-physiologically-based-pharmacokinetic-pbpk-modelling-simulation_en.pdf (accessed: 2024-02-16).

63. Peters, S. A. *Physiologically-Based Pharmacokinetic (PBPK) Modeling and Simulations* ISBN: 9780470484067 (John Wiley & Sons, Inc., Hoboken, NJ, USA, 2012).

64. El-Khateeb, E. et al. Physiological-based pharmacokinetic modeling trends in pharmaceutical drug development over the last 20-years; in-depth analysis of applications, organizations, and platforms. *Biopharmaceutics & Drug Disposition.* 2021. **42**(4): 107–117. doi:10.1002/bdd.2257.

65. Frechen, S. & Rostami-Hodjegan, A. Quality Assurance of PBPK Modeling Platforms and Guidance on Building, Evaluating, Verifying and Applying PBPK Models Prudently under the Umbrella of Qualification: Why, When, What, How and By Whom? *Pharmaceutical Research.* 2022. **39**(8): 1733–1748. doi:10.1007/s11095-022-03250-w.

66. Open Systems Pharmacology Suite Community. Open Systems Pharmacology Suite Manual. 2024. Available from: https://docs.open-systems-pharmacology.org/ (accessed: 2024-02-08).

67. Peng, Y., Cheng, Z. & Xie, F. Evaluation of Pharmacokinetic Drug-Drug Interactions: A Review of the Mechanisms, In Vitro and In Silico Approaches. *Metabolites.* 2021. **11**(2): 75. doi:10.3390/metabo11020075.

68. Marok, F. Z. et al. A Physiologically Based Pharmacokinetic Model of Ketoconazole and Its Metabolites as Drug–Drug Interaction Perpetrators. *Pharmaceutics.* 2023. **15**(2): 679. doi:10.3390/pharmaceutics15020679.

69. Wang, Y. et al. Model-Informed Drug Development: Current US Regulatory Practice and Future Considerations. *Clinical Pharmacology and Therapeutics.* 2019. **105**(4): 899–911. doi:10.1002/cpt.1363.

70. Grimstein, M. et al. Physiologically Based Pharmacokinetic Modeling in Regulatory Science: An Update From the U.S. Food and Drug Administration's Office of Clinical Pharmacology. *Journal of Pharmaceutical Sciences.* 2019. **108**(1): 21–25. doi:10.1016/j.xphs.2018.10.033.

71. Luzon, E et al. Physiologically based pharmacokinetic modeling in regulatory decision-making at the European Medicines Agency. *Clinical Pharmacology & Therapeutics.* 2017. **102**(1): 98–105. doi:10.1002/cpt.539.

72. Samineni, D. et al. Physiologically Based Pharmacokinetic Model-Informed Drug Development for Polatuzumab Vedotin: Label for Drug-Drug Interactions Without Dedicated Clinical Trials. *Journal of Clinical Pharmacology.* 2020. **60**(S1): S120–S131. doi:10.1002/jcph.1718.

73. Bundesministerium für Bildung und Forschung. OSMOSES-Open-Source MOdellierungs- und Simulationsplattform mit automatisierter Qualitätskontrolle für die Entwicklung komplexer Systemmodelle in den Lebenswissenschaften. 2019. Available from: https://www.gesundheitsforschung-bmbf.de/de/osmoses-open-source-modellierungs-und-simulationsplattform-mit-automatisierter-9163.php (accessed: 2024-03-01).

74. Mitchell, M., Muftakhidinov, B., Winchen, T., Wilms, A. & van Schaik, B. Engauge Digitizer Software. Available from: http://markummitchell.github.io/engauge-digitizer (accessed: 2024-03-01).

75. Open Systems Pharmacology Suite Community. PK-Sim® Ontogeny Database Documentation, Version 7.3. 2018. Available from: https://github.com/Open-Systems-Pharmacology/OSPSuite.Documentation/blob/master/PK-SimOntogenyDatabaseVersion7.3.pdf (accessed: 2024-03-01).

76. Chae, D., Kim, Y. & Park, K. Characterization of circadian blood pressure patterns using non-linear mixed effects modeling. *Translational and Clinical Pharmacology.* 2019. **27**(1): 24–32. doi:10.12793/tcp.2019.27.1.24.

77. Lott, D., Lehr, T., Dingemanse, J. & Krause, A. Modeling Tolerance Development for the Effect on Heart Rate of the Selective S1P1 Receptor Modulator Ponesimod. *Clinical Pharmacology and Therapeutics.* 2018. **103**(6): 1083–1092. doi:10.1002/cpt.877.

78. Gómez-Lechón, M. J., Castell, J. V. & Donato, M. T. Hepatocytes–the choice to investigate drug metabolism and toxicity in man: in vitro variability as a reflection of in vivo. *Chemico-biological interactions.* 2007. **168**(1): 30–50. doi:10.1016/j.cbi.2006.10.013.

79. Fowler, S. & Zhang, H. In vitro evaluation of reversible and irreversible cytochrome P450 inhibition: current status on methodologies and their utility for predicting drug-drug interactions. *The AAPS journal.* 2008. **10**(2): 410–24. doi:10.1208/s12248-008-9042-7.

80. Nagar, S. & Korzekwa, K. Commentary: nonspecific protein binding versus membrane partitioning: it is not just semantics. *Drug Metabolism and Disposition.* 2012. **40**(9): 1649–1652. doi:10.1124/dmd.112.046599.

81. Alhumaidi, R. M. et al. Risk of Polypharmacy and Its Outcome in Terms of Drug Interaction in an Elderly Population: A Retrospective Cross-Sectional Study. *Journal of Clinical Medicine.* 2023. **12**(12): 3960. doi:10.3390/jcm12123960.

82. Heinig, R., Gerisch, M., Engelen, A., Nagelschmitz, J. & Loewen, S. Pharmacokinetics of the Novel, Selective, Non-steroidal Mineralocorticoid Receptor Antagonist Finerenone in Healthy Volunteers: Results from an Absolute Bioavailability Study and Drug-Drug Interaction Studies In Vitro and In Vivo. *European Journal of Drug Metabolism and Pharmacokinetics.* 2018. **43**(6): 715–727. doi:10.1007/s13318-018-0483-9.

83. Wendl, T., Frechen, S., Gerisch, M., Heinig, R. & Eissing, T. Physiologically-based pharmacokinetic modeling to predict CYP3A4-mediated drug-drug interactions of finerenone. *CPT: Pharmacometrics & Systems Pharmacology.* 2022. **11**(2): 199–211. doi:10.1002/psp4.12746.

84. Kharasch, E. D., Walker, A., Hoffer, C. & Sheffels, P. Intravenous and oral alfentanil as in vivo probes for hepatic and first-pass cytochrome P450 3A activity: noninvasive assessment by use of pupillary miosis. *Clinical Pharmacology and Therapeutics.* 2004. **76**(5): 452–466. doi:10.1016/j.clpt.2004.07.006.

85. Eichelbaum, M., Ekbom, K., Bertilsson, L., Ringberger, V. A. & Rane, A. Plasma kinetics of carbamazepine and its epoxide metabolite in man after single and multiple doses. *European Journal of Clinical Pharmacology.* 1975. **8**(5): 337–341. doi:10.1007/BF00562659.

86. Kudriakova, T. B., Sirota, L. A., Rozova, G. I. & Gorkov, V. A. Autoinduction and steady-state pharmacokinetics of carbamazepine and its major metabolites. *British Journal of Clinical Pharmacology.* 1992. **33**(6): 611–615. doi:10.1111/j.1365-2125.1992.tb04089.x.

87. Shirasaka, Y., Suzuki, K., Nakanishi, T. & Tamai, I. Differential effect of grapefruit juice on intestinal absorption of statins due to inhibition of organic anion transporting polypeptide and/or P-glycoprotein. *Journal of Pharmaceutical Sciences.* 2011. **100**(9): 3843–3853. doi:10.1002/jps.22586.

88. Chen, M., Zhou, S.-Y., Fabriaga, E., Zhang, P.-H. & Zhou, Q. Food-drug interactions precipitated by fruit juices other than grapefruit juice: An update review. *Journal of Food and Drug Analysis.* 2018. **26**(2S): S61–S71. doi:10.1016/j.jfda.2018.01.009.

89. Sunaga, K. et al. Mechanism-based inhibition of recombinant human cytochrome P450 3A4 by tomato juice extract. *Biological and Pharmaceutical Bulletin.* 2012. **35**(3): 329–334. doi:10.1248/bpb.35.329.

90. Ohkubo, A., Chida, T., Kikuchi, H., Tsuda, T. & Sunaga, K. Effects of tomato juice on the pharmacokinetics of CYP3A4-substrate drugs. *Asian Journal of Pharmaceutical Sciences.* 2017. **12**(5): 464–469. doi:10.1016/j.ajps.2017.05.004.

91. Agosti, S. et al. A dangerous fruit juice. *The American Journal of Emergency Medicine.* 2012. **30**(1): 248.e5–248.e8. doi:10.1016/j.ajem.2010.08.031.

92. Mazokopakis, E. E. Unusual causes of rhabdomyolysis. *Internal Medicine Journal.* 2008. **38**(5): 364–367. doi:10.1111/j.1445-5994.2007.01550.x.

93. Peynaud, D., Charpiat, B., Vial, T., Gallavardin, M. & Ducerf, C. Tacrolimus severe overdosage after intake of masked grapefruit in orange marmalade. *European Journal of Clinical Pharmacology.* 2007. **63**(7): 721–722. doi:10.1007/s00228-007-0323-3.

94. Pfizer. Cordarone® (Amiodarone) - Prescribing information (Ref. ID: 4336449). 2018. Available from: https://www.accessdata.fda.gov/drugsatfda_docs/label/2018/018972s054lbl.pdf (accessed: 2024-03-01).

95. Astellas Pharma US, Inc. Prograf® (Tacrolimus) - Prescribing information (Ref. ID : 3083402). 2012. Available from: https://www.accessdata.fda.gov/drugsatfda_docs/label/2012/050709s031lbl.pdf (accessed: 2024-03-01).

96. Pfizer. Lipitor® (atorvastatin calcium) - Prescribing information. 2009. Available from: https://www.accessdata.fda.gov/drugsatfda_docs/label/2009/020702s056lbl.pdf (accessed: 2024-03-01).

97. Danco Laboratories. Mifeprex® (mifepristone) - Predcribing information (Ref. ID: 3909592). 2016. Available from: https://www.accessdata.fda.gov/drugsatfda_docs/label/2016/020687s020lbl.pdf (accessed: 2024-03-01).

98. Huang, S. M. et al. Drug interactions with herbal products and grapefruit juice: A conference report. *Clinical Pharmacology and Therapeutics.* 2004. **75**(1): 1–12. doi:10.1016/J.CLPT.2003.07.002.

99. Van, L. B., Huynh, D. D., Breen, J. K. & Ratto, N. J. Consumer Medication Information: A Reliable Source of Information on Grapefruit Juice Interactions? 2014. Available from: https://www.fdbhealth.com/-/media/documents/form-not-required/us/posters/poster---consistency-of-drug-food-interactions.ashx (accessed: 2024-02-16).

100. Kim, H., House, L. A. & Salois, M. Consumer response to media information: the case of grapefruit-medicine interaction. *Health Economics Review.* 2015. **5**(1): 33. doi:10.1186/s13561-015-0069-z.

101. Prely, H. et al. Real-life drug-drug and herb-drug interactions in outpatients taking oral anticancer drugs: comparison with databases. *Journal of Cancer Research and Clinical Oncology.* 2022. **148**(3): 707–718. doi:10.1007/s00432-021-03645-z.

102. Koni, A. A. et al. A comprehensive evaluation of potentially significant drug-drug, drug-herb, and drug-food interactions among cancer patients receiving anticancer drugs. *BMC cancer.* 2022. **22**(1): 547. doi:10.1186/s12885-022-09649-3.

103. Kovar, C. et al. A Physiologically-Based Pharmacokinetic Precision Dosing Approach to Manage Dasatinib Drug-Drug Interactions. *CPT: Pharmacometrics & Systems Pharmacology (submitted for publication).*

104. Hull, M. W. & Montaner, J. S. G. Ritonavir-boosted protease inhibitors in HIV therapy. *Annals of Medicine.* 2011. **43**(5): 375–388. doi:10.3109/07853890.2011.572905.

105. Martins, V. et al. A commentary on the use of pharmacoenhancers in the pharmaceutical industry and the implication for DMPK drug discovery strategies. *Xenobiotica; the fate of foreign compounds in biological systems.* 2022. **52**(8): 786–796. doi:10.1080/00498254.2022.2130838.

106. Arya, V., Robertson, S. M., Struble, K. A. & Murray, J. S. Scientific considerations for pharmacoenhancers in antiretroviral therapy. *Journal of Clinical Pharmacology.* 2012. **52**(8): 1128–1133. doi:10.1177/0091270011410569.

107. Kupferschmidt, H. H., Fattinger, K. E., Ha, H. R., Follath, F. & Krähenbühl, S. Grapefruit juice enhances the bioavailability of the HIV protease inhibitor saquinavir in man. *British Journal of Clinical Pharmacology.* 1998. **45**(4): 355–359. doi:10.1046/j.1365-2125.1998.t01-1-00687.x.

108. Long, Z. et al. The successful combination of grapefruit juice and venetoclax in an unfit acute myeloid leukemia patient with adverse risk: A case report. *Frontiers in Oncology.* 2022. **12**(September): 1–6. doi:10.3389/fonc.2022.912696.

109. Paolini, M. et al. A new opportunity for nanomedicines: Micellar cytochrome P450 inhibitors to improve drug efficacy in a cancer therapy model. *Nanomedicine: Nanotechnology, Biology, and Medicine.* 2017. **13**(5): 1715–1723. doi:10.1016/j.nano.2017.03.006.

110. Hanke, N. et al. PBPK Models for CYP3A4 and P-gp DDI prediction: a modeling network of rifampicin, itraconazole, clarithromycin, midazolam, alfentanil, and digoxin. *CPT: Pharmacometrics & Systems Pharmacology.* 2018. **7**(10): 647–659. doi:10.1002/psp4.12343.

111. Hanke, N. et al. A Mechanistic, Enantioselective, Physiologically Based Pharmacokinetic Model of Verapamil and Norverapamil, Built and Evaluated for Drug-Drug Interaction Studies. *Pharmaceutics.* 2020. **12**(6): 556. doi:10.3390/pharmaceutics12060556.

A

SUPPLEMENTARY INFORMATION

A.1 SUPPLEMENTARY INFORMATION - PROJECT I - PHYSIOLOGICALLY BASED PHARMACOKINETIC MODELING OF CARBAMAZEPINE

pharmaceutics

Pharmacokinetics of the CYP3A4 and CYP2B6 inducer carbamazepine and its drug-drug interaction potential: a physiologically based pharmacokinetic modeling approach

Supplementary Materials

Laura Maria Fuhr[1], Fatima Zahra Marok[1], Nina Hanke[1], Dominik Selzer[1], Thorsten Lehr[1]

[1]Clinical Pharmacy, Saarland University, Saarbrücken, Germany

Funding
This research was funded by the German Federal Ministry of Education and Research (BMBF), grant number 031L0161C ("OSMOSES"). We acknowledge support by the Deutsche Forschungsgemeinschaft (DFG, German Research Foundation) and Saarland University within the funding program Open Access Publishing.

Conflict of Interest
Thorsten Lehr has received research grants from the German Federal Ministry of Education and Research (grant 031L0161C). Laura Maria Fuhr, Fatima Zahra Marok, Nina Hanke and Dominik Selzer declare no conflict of interest.

Corresponding Author
Thorsten Lehr, PhD
Clinical Pharmacy, Saarland University
Campus C2 2
66123 Saarbrücken, Germany
ORCID: 0000 0002 8372 1465
Phone: +49 681 302 70255
Email: thorsten.lehr@mx.uni-saarland.de

Contents

1 Physiologically based pharmacokinetic (PBPK) modeling

1.1 PBPK model building

PBPK model building was initiated with a literature search to collect physicochemical parameters, information on absorption, distribution, metabolism and excretion (ADME) processes and clinical studies of intravenous and oral administration in single- and multiple-dose regimens. In addition to drug plasma concentration-time profiles, fraction excreted unchanged in urine or feces measurements and tissue or saliva concentrations should be integrated if available. The clinical study data were digitized and divided into a model building (training) dataset and a model evaluation (test) dataset. The studies for the training dataset were selected to include studies covering the whole published dosing range, single- and multiple-dose studies and information on tissue or saliva concentrations and urinary or fecal excretion, if available. Model input parameter values that could not be informed from literature were optimized by fitting the model to observed data of the whole training dataset.

1.2 Virtual individuals

Virtual mean individuals were generated for each study according to the reported age, weight, height, sex and ethnicity. If no information was provided, a default individual was created (30 years of age, male, European, mean weight and height characteristics from the PK-Sim population database). Enzymes, transporters and binding partners were incorporated according to current literature. The PK-Sim expression database [1] was used to define their relative expression in the different organs of the body. Details and references for the implementation of relevant metabolizing enzymes, transport proteins and protein binding partners are provided in Section 7.

1.3 PBPK model evaluation

Model performance was evaluated (1) by comparing the predicted plasma concentration-time profiles to observed profiles and (2) by comparing predicted plasma concentration values to the corresponding observed values in goodness-of- fit plots, as well as (3) by comparing predicted with observed area under the plasma concentration-time curve (AUC) and maximum plasma concentration (C_{max}) values. AUC values (predicted as well as observed) were calculated from the time of drug administration to the time of the last concentration measurement (AUC_{last}). For a quantitative description of the model performance, the mean relative deviation (MRD) of predicted plasma concentrations and the geometric mean fold error ($GMFE$) of predicted AUC_{last} and C_{max} values were calculated according to Equations S1 and S2. We considered MRD and GMFE values < 2 as an adequate model performance metrics.

$$MRD = 10^x, \text{ with } x = \sqrt{\frac{1}{m}\sum_{i=1}^{m}(\log_{10} c_{pred,i} - \log_{10} c_{obs,i})^2} \tag{S1}$$

where $c_{pred,i}$ = predicted plasma concentration, $c_{obs,i}$ = corresponding observed plasma concentration and m = number of observed values.

$$GMFE = 10^x, \text{ with } x = \frac{1}{n}\sum_{i=1}^{n}|\log_{10}(\frac{PK_{pred,i}}{PK_{obs,i}})| \tag{S2}$$

where $PK_{pred,i}$ = predicted AUC_{last} or C_{max} value, $PK_{obs,i}$ = corresponding observed AUC_{last} or C_{max} value and n = the number of studies.

1.4 Sensitivity analysis

Sensitivity of the final models to single parameter values (local sensitivity analysis) was measured as relative change of the AUC. Sensitivity analysis was carried out using a relative perturbation of 1000% (variation range 10.0, maximum number of 9 steps). Parameters were included into the analysis if they were optimized, if they are associated with optimized parameters or if they might have a strong impact due to calculation methods used in the model.

The sensitivity to a parameter value was calculated as the ratio of the relative change of the simulated AUC to the relative variation of the parameter around its value used in the final model according to Equation S3.

$$S = \frac{\Delta AUC}{AUC} \cdot \frac{p}{\Delta p} \tag{S3}$$

where S = sensitivity of the AUC to the examined model parameter, ΔAUC = change of the simulated AUC, AUC = simulated AUC with the original parameter value, Δp = change of the examined parameter value, p = original parameter value. A sensitivity of +1.0 signifies that a 10% increase of the examined parameter value causes a 10% increase of the simulated AUC.

1.5 Mathematical implementation of drug-drug interactions (DDIs)

Competitive inhibition

Competitive inhibitors compete with the substrate for binding to the active site of an enzyme or transporter. As binding of the inhibitor is reversible, the inhibition can be overcome by high substrate concentrations (concentration-dependency); The maximum reaction velocity (v_{max}) remains unaffected, while the Michaelis-Menten constant (K_m) is increased ($K_{m,app}$, Equation S4). The reaction velocity (v) during co-administration of substrate and competitive inhibitor is described by Equation S5 [2]:

$$K_{m,app} = K_m \cdot \left(1 + \frac{[I]}{K_i}\right) \tag{S4}$$

$$v = \frac{v_{max} \cdot [S]}{K_{m,app} + [S]} \tag{S5}$$

where $K_{m,app}$ = Michaelis-Menten constant in the presence of inhibitor, K_m = Michaelis-Menten constant, $[I]$ = free inhibitor concentration, K_i = dissociation constant of the inhibitor-enzyme or inhibitor-transporter complex, v = reaction velocity, v_{max} = maximum reaction velocity, $[S]$ = free substrate concentration.

Mechanism-based inactivation

Mechanism-based inactivation is an irreversible inhibition. The baseline activity of the protein is regained after clearance of the inactivator and de novo synthesis of the inactivated protein (time-dependency). The degradation rate constant (k_{deg}) of respective protein is increased ($k_{deg,app}$, Equation S6), while the synthesis rate (R_{syn}) remains unaffected. The enzyme or transporter turnover during administration of a mechanism-based inactivator is described by Equation S7. Mechanism-based inactivators are also competitive inhibitors. Therefore, the reaction velocity is calculated accodring to Equation S8, substituting K_m by $K_{m,app}$ [2]:

$$k_{deg,app} = k_{deg} + \left(\frac{k_{inact} \cdot [I]}{K_I + [I]}\right) \tag{S6}$$

$$\frac{dE(t)}{dt} = R_{syn} - k_{deg,app} \cdot E(t) \tag{S7}$$

$$v = \frac{v_{max} \cdot [S]}{K_{m,app} + [S]} = \frac{k_{cat} \cdot E(t) \cdot [S]}{K_{m,app} + [S]} \tag{S8}$$

where $k_{deg,app}$ = enzyme or transporter degradation rate constant in the presence of mechanism-based inactivator, k_{deg} = enzyme or transporter degradation rate constant, k_{inact} = maximum inactivation rate constant, $[I]$ = free inactivator concentration, K_I = concentration for half-maximal inactivation, $E(t)$ = enzyme or transporter concentration, R_{syn} = enzyme or transporter synthesis rate, v = reaction velocity, v_{max} = maximum reaction velocity, $[S]$ = free substrate concentration, $K_{m,app}$ = Michaelis-Menten constant in the presence of inactivator, k_{cat} = catalytic rate constant.

Induction

Induction of enzymes and transporters is mediated by the activation of nuclear receptors (constitutive androstane receptor (CAR) or pregnane X receptor (PXR)), increasing gene expression. The baseline activity of the protein is regained after clearance of the inducer and degradation of the induced protein (time-dependency). The enzyme or transporter synthesis rate (R_{syn}) is increased ($R_{syn,app}$, Equation S9), while its degradation rate constant (k_{deg}) remains unaffected. The enzyme or transporter turnover during administration of an inducer is described by S10 [2], the reaction velocity is described by Equation S11:

$$R_{syn,app} = R_{syn} \cdot \left(1 + \frac{E_{max} \cdot [Ind]}{EC_{50} + [Ind]}\right) \tag{S9}$$

$$\frac{dE(t)}{dt} = R_{syn,app} - k_{deg} \cdot E(t) \tag{S10}$$

$$v = \frac{v_{max} \cdot [S]}{K_m + [S]} = \frac{k_{cat} \cdot E(t) \cdot [S]}{K_m + [S]} \tag{S11}$$

where $R_{syn,app}$ = enzyme or transporter synthesis rate in the presence of inducer, R_{syn} = enzyme or transporter synthesis rate, E_{max} = maximal induction effect in vivo, $[Ind]$ = free inducer concentration, EC_{50} = concentration for half-maximal induction in vivo, $E(t)$ = enzyme or transporter concentration, k_{deg} = enzyme or transporter degradation rate constant, v = reaction velocity, v_{max} = maximum reaction velocity, $[S]$ = free substrate concentration, K_m = Michaelis-Menten constant, k_{cat} = catalytic rate constant.

2 Carbamazepine

2.1 PBPK model building

The anticonvulsive carbamazepine is used for the treatment of epilepsy and trigeminal neuralgia [3]. It is a BCS Class II drug of low solubility and high permeability. The drug is mainly cleared from the body by enzymatic degradation. About 20-40% of the administered carbamazepine is metabolized to carbamazepine-10,11-epoxide [4, 5]. Cytochrome P450 (CYP) 3A4 and CYP2C8 are the major enzymes catalyzing this conversion, while the contribution of CYP2C8 is between 20-40% [6]. 10% of the dose are metabolized to hydroxylated metabolites, mainly by CYP3A4 and CYP2B6 [7]. Less than 3% are excreted unchanged in the urine [8] and less than 1% are excreted unchanged in the bile [9]. Carbamazepine is a strong inducer (AUC decrease of a victim drug ≥ 80%) of CYP3A4 and CYP2B6 [10]. As a result, carbamazepine induces its own - as well as other drugs' - metabolism during multiple-dose administration. Carbamazepine-10,11-epoxide is almost completely converted to its trans-diol form via epoxide hydroxylase 1 (EPHX1) [5, 11] and it is assumed that carbamazepine also induces EPHX1 clearance after multiple-dose administration [4].

The parent-metabolite PBPK model of carbamazepine and carbamazepine-10,11-epoxide was established using 40 clinical studies of oral administration, covering a broad range of doses (50–800 mg) in single- and multiple-dose administration of different formulations. In three of the included studies, the metabolite carbamazepine-10,11-epoxide itself was orally administered. In total, the clinical studies provided 58 plasma concentration-time profiles, 3 saliva concentration-time profiles and 4 fraction excreted unchanged in urine measurements of carbamazepine, as well as 34 plasma concentration-time profiles (24 as metabolite, 10 as administered drug) and 5 fraction excreted unchanged in urine measurements of carbamazepine-10,11-epoxide. All clinical studies are listed in Table S1.

As elimination processes in the carbamazepine model (1) metabolism by CYP3A4 and CYP2C8 to carbamazepine-10,11-epoxide, (2) metabolism by CYP3A4, CYP2B6 and UDP-glucuronosyltransferase (UGT) 2B7 as well as a hepatic clearance to cover further metabolic processes, (3) auto-induction of CYP3A4 and CYP2B6 and (4) passive glomerular filtration with tubular reabsorption [12] were implemented. The carbamazepine-10,11-epoxide metabolite model includes (1) metabolism by EPHX1 [11, 13] and (2) renal elimination via passive glomerular filtration. The metabolic processes implemented in the parent-metabolite PBPK model are summarized in Figure S1. The drug-dependent parameters of carbamazepine and carbamazepine-10,11-epoxide are listed in Table S2, details on the distribution and localization of the implemented enzymes are provided in Table S45.

The carbamazepine-10,11-epoxide PBPK model was developed first, based on the three clinical studies (10 plasma concentration-time profiles) that administered carbamazepine-10,11-epoxide. Metabolism by EPHX1 was implemented as a first-order clearance process, and passive glomerular filtration was described using a GFR fraction < 1. The metabolite carbamazepine-10,11-epoxide model was subsequently combined with the parent carbamazepine model and the parameter values were used as starting values for the establishment of the parent-metabolite model. Metabolic pathways of carbamazepine were implemented using Michaelis-Menten kinetics. All K_m and k_{cat} values were taken from literature, except for the two implemented CYP3A4 processes where k_{cat} was optimized. As CYP induction by carbamazepine is mediated via activation of the CAR [14], the same EC_{50} = 20.0 µmol/l was applied to describe the CYP3A4, CYP2B6 as well as the EPHX1 induction by carbamazepine. The associated E_{max} values were optimized. To inform the optimization of the CYP3A4 E_{max}, the carbamazepine-alprazolam DDI study was added to the training dataset. Renal elimination was described using an estimated GFR fraction < 1. Oral dosage forms of carbamazepine in the analyzed clinical studies include

solutions, suspensions, immediate release tablets and extended release tablets or capsules. To simulate solutions and suspensions, carbamazepine was modeled as dissolved drug. The dissolution kinetics of the other formulations were described using Weibull functions. Different Weibull functions were optimized for fasted or fed state, as an increased carbamazepine absorption was observed for ingestion with food [15, 16].

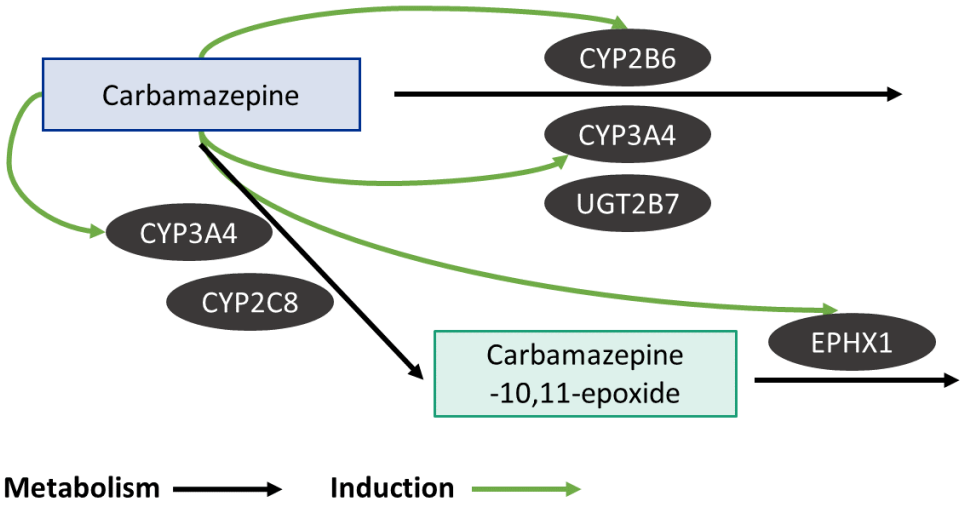

Figure S1: Metabolic pathways of carbamazepine. Carbamazepine is metabolized by CYP3A4 and CYP2C8 to its main metabolite carbamazepine-10,11-epoxide, which is then further metabolized via EPHX1. Other metabolic pathways of carbamazepine clearance are metabolism by CYP2B6 and CYP3A4 to 3-hydroxycarbamazepine and by UGT2B7 to glucuronide metabolites. Carbamazepine is an inducer of CYP3A4, CYP2B6 and EPHX1

Figures S2 and S3 show the good performance of the carbamazepine-10,11-epoxide model after oral application of carbamazepine-10,11-epoxide in linear and semi-logarithmic plots of predicted compared to observed plasma concentration-time profiles. Goodness-of-fit plots comparing all predicted to the corresponding observed plasma concentration values are presented in Figure S7 and correlation of predicted and observed AUC_{last} and C_{max} values is presented in Figure S10.

The precise performance of the carbamazepine parent-metabolite model is demonstrated in linear and semi-logarithmic plots of predicted compared to observed plasma and saliva concentration-time profiles in Figures S4 and S5. Predicted fraction excreted unchanged in urine profiles in comparison to observed values are presented in Figure S6. Goodness-of-fit plots for plasma concentrations and fractions excreted to urine values are presented in Figures S8 and S9, respectively. The correlation of predicted and observed AUC_{last} and C_{max} values is presented in Figure S11. MRD values of plasma concentration predictions for all studies are given in Table S3 . Predicted and observed AUC_{last} and C_{max} values and overall GMFE values of all studies are listed in Table S4.

2.2 Carbamazepine and Carbamazepine-10,11-epoxide clinical studies

Table S1: Clinical studies used for the development of the carbamazepine parent-metabolite PBPK model

Dose [mg]	Route	Dataset	n	Healthy [%]	Females [%]	Age[a] [years]	Weight[a] [kg]	Height[a] [cm]	CBZE measured	Reference
Carbamazepine-10,11-epoxide										
50	po (susp), sd	training	1	100	0	31	65	-	NA	Tomson 1983 [5]
50	po (susp), sd	test	1	100	0	27	63	-	NA	Tomson 1983 [5]
100	po (susp), sd	training	1	100	0	34	69	-	NA	Tomson 1983 [5]
100	po (susp), sd	test	1	100	100	50	53	-	NA	Tomson 1983 [5]
100	po (susp), sd	test	1	100	0	31	65	-	NA	Tomson 1983 [5]
150	po (sol), sd	test	6	-	33	25.7 (23-32)	56.2 (44-59)	-	NA	Sumi 1987 [17]
200	po (susp), sd	training	1	100	0	34	69	-	NA	Tomson 1983 [5]
200	po (susp), sd	test	1	100	100	50	53	-	NA	Tomson 1983 [5]
100	po (tab), sd	training	6	100	33	(20-43)	(55-75)	-	NA	Pisani 1990 [18]
100	po (tab), sd	test	6	100	33	(20-50)	(50-74)	-	NA	Pisani 1992 [19]
Carbamazepine										
100/10	po (susp), sd; iv (2 h)	test	1	100	0	43	76	-	no	Gerardin 1990 [20]
100/10	po (susp), sd; iv (2 h)	test	1	100	0	49	89	-	no	Gerardin 1990 [20]
50	po (sol), sd	training	1	100	0	29	-	-	no	Rawlins 1975 [21]
100	po (sol), sd	test	1	100	0	29	-	-	no	Rawlins 1975 [21]
200	po (susp), sd	test	1	100	100	29	62	-	no	Eichelbaum 1985 [4]
200	po (sol), sd	test	1	100	0	29	-	-	no	Rawlins 1975 [21]
200	po (sol), sd	training	6	-	33	25.7 (23-32)	56.2 (44-59)	-	no	Sumi 1987 [17]
200	po (susp), sd	test	1	100	100	50	53	-	no	Tomson 1983 [5]
200	po (susp), sd	test	9	100	0	-	69.1 (53-104)	-	no	Wada 1978 [22]
100	po (tab), sd	test	6	100	0	-	-	-	no	Gerardin 1976 [23]
200	po (tab), sd	test	12	100	0	29.15 (25-30)	67.5 (55-81)	-	yes	Bedada 2015 [24]
200	po (tab), sd	test	12	100	0	(28-32)	(58-76)	-	yes	Bedada 2016 [25]
200	po (tab), sd	test	1	0	0	57	80	-	yes	Eichelbaum 1975 [26]
200	po (tab), sd	test	1	0	0	50	80	-	yes	Eichelbaum 1975 [26]

-: not given, bid: twice daily, cap: capsule, D: day, iv: intravenous, NA: not applicable, po: oral, qd: once daily, sd: single dose, sol: solution, susp: suspension, tab: tablet, tid: three times daily, XR: extended release

[a] mean (range)

[b] 6 mg/kg

Table S1: Clinical studies used for the development of the carbamazepine parent-metabolite PBPK model *(continued)*

Dose [mg]	Route	Dataset	n	Healthy [%]	Females [%]	Age[a] [years]	Weight[a] [kg]	Height[a] [cm]	CBZE measured	Reference
200	po (tab), sd	test	6	100	0	-	-	-	no	Gerardin 1976 [23]
200	po (tab), sd	test	10	100	0	(22-35)	(62-75)	-	yes	Kim 2005 [27]
200	po (tab), sd	test	24	100	0	(21-35)	(61-93)	-	no	Meyer 1992 [28]
200	po (tab), sd	test	20	100	20	(22-36)	(50-98)	-	no	Meyer 1998 [29]
200	po (tab), sd	test	8	100	0	23 (20-25)	70 (65-75)	-	yes	Shahzadi 2011 [30]
200	po (tab), sd	test	12	100	0	(18-32)	-	-	no	SaintSalvi 1987 [31]
200	po (tab), sd	test	9	100	0	-	69.1 (53-104)	-	no	Wada 1978 [22]
400	po (-, fed), sd	test	7	-	-	(21-27)	(70-90)	-	yes	Barzaghi 1987 [32]
400	po (-, fed), sd	training	24	100	-	(20-40)	-	-	yes	Bianchetti 1987 [33]
400	po (-), sd	training	1	100	0	37	78	-	yes	Faigle 1975 [8]
400	po (-), sd	test	1	100	0	34	83	-	yes	Faigle 1975 [8]
400	po (tab), sd	test	24	100	-	31.8 (20-52)	69.8 (50-96)	-	no	Kovacevic 2009 [34]
400	po (tab), sd	test	5	100	0	25.4	72 8	-	no	Morselli 1975 [35]
400	po (tab), sd	training	6	100	0	(21-22)	(62-77)	-	no	Pynnoenen 1977 [36]
400	po (-), sd	test	12	100	50	(20-31)	-	-	no	Strandjord [37]
400	po (-), sd	test	8	100	0	(24-36)	(72-96)	-	no	Wong 1983 [38]
415.8[b]	po (tab), sd	training	6	100	50	25.8	69.3	-	no	Levy 1975 [15]
415.8[b]	po (tab, fed), sd	training	6	100	50	25.8	69.3	-	no	Levy 1975 [15]
600	po (tab), sd	test	8	100	0	(24-35)	83.4	-	yes	Dalton 1985 [39]
600	po (tab), sd	test	8	100	0	(23-26)	81	-	yes	Dalton 1985a [40]
600	po (tab), sd	test	6	100	0	29	-	-	no	Gerardin 1976 [23]
800	po (tab, fed), sd	test	6	100	50	(21-32)	-	-	no	Cotter 1977 [41]
100/	D1-D3: po (tab), bid	test	9	100	37.5	31 (24-43)	-	-	yes	Burstein 2000 [42]
200/	D4-D6: po (tab), bid									
400	D7-D35: po (tab), qd									
100/	D1-D3: po (tab), bid	training	16	100	0	-	-	-	yes	Moller 2001 [43]
200/	D4-D6: po (tab), bid									
400	D7-D35: po (tab), qd									

-: not given, bid: twice daily, cap: capsule, D: day, iv: intravenous, NA: not applicable, po: oral, qd: once daily, sd: single dose, sol: solution, susp: suspension, tab: tablet, tid: three times daily, XR: extended release

[a] mean (range)

[b] 6 mg/kg

Table S1: Clinical studies used for the development of the carbamazepine parent-metabolite PBPK model *(continued)*

Dose [mg]	Route	Dataset	n	Healthy [%]	Females [%]	Age[a] [years]	Weight[a] [kg]	Height[a] [cm]	CBZE measured	Reference
200	D1: po (tab), bid D2-D21: po (tab), tid	test	1	0	0	57	80	-	yes	Eichelbaum 1975 [26]
200	D1: po (tab), bid D2-D21: po (tab), tid	test	1	0	0	50	80	-	yes	Eichelbaum 1975 [26]
200	po (tab), qd	training	5	100	0	-	77 (69-84)	-	no	Gerardin 1976 [23]
200	po (tab), qd	test	1	100	0	-	84	-	no	Gerardin 1976 [23]
200	po (tab), qd	test	1	100	0	-	80	-	no	Gerardin 1976 [23]
200	po (tab), qd	test	1	100	0	-	73	-	no	Gerardin 1976 [23]
200	po (tab), qd	test	1	100	0	-	69	-	no	Gerardin 1976 [23]
200	po (tab), qd	test	1	100	0	-	79	-	no	Gerardin 1976 [23]
200/ 400	D1-D3: po (tab), qd D4-D6: po (tab), bid D7-D21: po (tab), qd	training	36	100	31	30 (20-45)	75.5 (54-92)	-	yes	Ji 2008 [44]
357	po (tab), qd	test	7	100	0	25.4	78.8	-	yes	Miles 1989 [45]
600	D1,D5: po (tab), sd	training	6	100	0	23.3 (22-26)	67.5 (62-67)	-	yes	Bernus 1994 [46]
400	po (tab XR), sd	test	-	-	-	-	-	-	no	Graf 1990 [47]
400	po (tab XR), sd	test	36	100	0	(20-55)	-	-	yes	Licht 2005 [48]
400	po (tab XR), sd	test	18	100	-	33 (29-37)	72 (70-81)	-	no	Kovacevic 2009 [34]
400	po (tab XR, fed), sd	test	14	100	0	(18-45)	-	-	no	Kshirsagar 2014 [49]
600	po (tab XR), sd	training	19	100	0	24 (19-27)	75	-	no	Licht 2005 [48]
400	po (tab XR), bid	training	18	100	33	27.5	71.4	171.5	yes	Stevens 1998 [50]
300	po (cap XR), sd	test	12	100	33	-	-	-	yes	Gande 2009 [51]
400	po (cap XR), sd	training	12	100	0	33.8 (21-48)	81.3	176.8	yes	McLean 2001 [16]
400	po (cap XR, fed), sd	training	12	100	0	33.8 (21-48)	81.3	176.8	yes	McLean 2001 [16]
400	po (cap XR), bid	training	18	100	33	27.5	71.4	171.5	yes	Stevens 1998 [50]

-: not given, bid: twice daily, cap: capsule, D: day, iv: intravenous, NA: not applicable, po: oral, qd: once daily, sd: single dose, sol: solution, susp: suspension, tab: tablet, tid: three times daily, XR: extended release

[a] mean (range)

[b] 6 mg/kg

2.3 Carbamazepine and Carbamazepine-10,11-epoxide drug-dependent parameters

Table S2: Drug-dependent parameters of the carbamazepine and carbamazepine-10,11-epoxide PBPK model

Parameter	Unit	Model	Literature	Reference	Description
Carbamazepine					
MW	g/mol	236.27 (Lit)	236.27	[54]	Molecular weight
logP	Log Units	2.00 (Fit)	1.45, 2.10, 2.45, 2.77	[54–56]	Lipophilicity
Solubility (pH)	mg/ml	0.336 (6.2) (Lit)	0.170 (6.2), 0.283 (7.0), 0.306 (6.9), 0.336 (6.2)	[57–60]	Solubility FaHIF
fu	%	25.0 (Lit)	21.0, 24.0, 25.0	[3, 36, 61, 62]	Fraction unbound in plasma
K_m (CYP3A4) CBZE	µmol/l	248.0 (Lit)	119.0, 248.0, 442.0, 630.0	[6, 63–65]	CYP3A4 Michaelis-Menten constant
k_{cat} (CYP3A4) CBZE	1/min	0.75 (Fit)	1.17, 1.70, 4.87, 5.30[b]	[6, 63–65]	CYP3A4 catalytic rate constant
K_m (CYP2C8)	µmol/l	757.0 (Lit)	757.0	[64]	CYP2C8 Michaelis-Menten constant
k_{cat} (CYP2C8)	1/min	0.67 (Lit)	0.67[b]	[64]	CYP2C8 catalytic rate constant
K_m (CYP2B6)	µmol/l	420.0 (Lit)	420.0	[7]	CYP2B6 Michaelis-Menten constant
k_{cat} (CYP2B6)	1/min	0.43 (Lit)	0.43[b]	[7]	CYP2B6 catalytic rate constant
K_m (CYP3A4)	µmol/l	282.0 (Lit)	282.0	[7]	CYP3A4 Michaelis-Menten constant
k_{cat} (CYP3A4)	1/min	0.20 (Fit)	0.16[b]	[7]	CYP3A4 catalytic rate constant
K_m (UGT2B7)	µmol/l	214.0 (Lit)	214.0	[52]	UGT2B7 Michaelis-Menten constant
k_{cat} (UGT2B7)	1/min	9.53E-3 (Lit)	9.53E-3[c]	[52]	UGT2B7 catalytic rate constant
CL_{hep}	1/min	0.02 (Fit)	-	-	Unspecified hepatic clearance
GFR fraction	-	0.03 (Fit)	-	-	Fraction of filtered drug in the urine
EC_{50} (CYP3A4)	µmol/l	20.00[a] (Lit)	4.3 - 137	[66–73]	Concentration for half-maximal induction
E_{max} (CYP3A4)	-	6.00 (Fit)	1.90 - 23.0	[66–73]	CYP3A4 maximum induction effect
EC_{50} (CYP2B6)	µmol/l	20.0[a] (Asm)	22 - 145	[73–75]	Concentration for half-maximal induction
E_{max} (CYP2B6)	-	17.0 (Fit)	3.10 - 21.50	[73–75]	CYP2B6 maximum induction effect
EC_{50} (EPHX1)	µmol/l	20.0[a] (Asm)	-	-	Concentration for half-maximal induction
E_{max} (EPHX1)	-	3.25 (Fit)	-	-	EPHX1 maximum induction effect
Intestinal permeability	cm/min	2.58E-2 (Lit)	2.58E-2	[76]	Transcellular intestinal permeability
Partition coefficients	-	Diverse	Rodgers and Rowlands	[77, 78]	Cell to plasma partition coefficients

asm: assumption, calc: calculated, CBZE: carbamazepine-10,11-epoxide, CL_{hep}: hepatic clearance, CL_{spec}: specific clearance, CYP: cytochrome P450, EPHX1: epoxide hydroxylase 1, FaHIF: fasted human intestinal fluid, IR: immediate release, fit: optimized during parameter optimization, lit: literature, UGT: UDP-glucuronosyltransferase, XR: extended release

[a] mean of literature values for EC_{50} (CYP3A4), assumed for all EC_{50} values

[b] k_{cat} values calculated within PK-Sim from V_{max}/recombinant enzyme

[c] k_{cat} value calculated within PK-Sim from V_{max} = 0.79 pmol/min/microsomal protein [52], assuming a microsomal UGT2B7 content of 82.9 pmol/mg microsomal protein [53], kcat = Vmax/ UGT2B7 content microsomes

Table S2: Drug-dependent parameters of the carbamazepine and carbamazepine-10,11-epoxide PBPK model *(continued)*

Parameter	Unit	Model	Literature	Reference	Description
Cellular permeability	cm/min	0.02 (Calc)	PK-Sim Standard	[79]	Permeability into the cellular space
IR tablet (fasted) Weibull time	min	200.0	-	-	Dissolution time (50% dissolved)
IR tablet (fasted) Weibull shape	-	0.74	-	-	Dissolution profile shape
IR tablet (fed) Weibull time	min	100.0	-	-	Dissolution time (50% dissolved)
IR tablet (fed) Weibull shape	-	1.20	-	-	Dissolution profile shape
XR tablet (fasted) Weibull time	min	767.2	-	-	Dissolution time (50% dissolved)
XR tablet (fasted) Weibull shape	-	0.76	-	-	Dissolution profile shape
XR tablet (fed) Weibull time	min	436.5	-	-	Dissolution time (50% dissolved)
XR tablet (fed) Weibull shape	-	1.16	-	-	Dissolution profile shape
XR capsule (fed) Weibull time	min	361.4	-	-	Dissolution time (50% dissolved)
XR capsule (fed) Weibull shape	-	2.13	-	-	Dissolution profile shape
XR capsule (fasted) Weibull time	min	439.5	-	-	Dissolution time (50% dissolved)
XR capsule (fasted) Weibull shape	-	0.7	-	-	Dissolution profile shape
Carbamazepine-10,11-epoxide					
logP	Log Units	1.00 (Fit)	1.58, 1.97	[80]	Lipophilicity
Solubility	mg/ml	1.34 (Lit)	1.34	[80]	Solubility
fu	%	51.8 (Lit)	46.8-51.8	[35]	Fraction unbound in plasma
CL_{spec} (EPHX1)	1/min	0.01 (Fit)	0.05	-	EPHX1 first-order clearance
GFR fraction	-	0.21 (Fit)	-	-	Fraction of filtered drug in the urine
Intestinal permeability	cm/min	0.3 (Fit)	-	-	Transcellular intestinal permeability
Partition coefficients	-	Diverse	Rodgers and Rowlands	[77, 78]	Cell to plasma partition coefficients
Cellular permeability	cm/min	1.61E-3 (Calc)	PK-Sim Standard	[79]	Permeability into the cellular space
Tablet Weibull time	min	200.0	-	-	Dissolution time (50% dissolved)
Tablet Weibull shape	-	0.75	-	-	Dissolution profile shape

asm: assumption, calc: calculated, CBZE: carbamazepine-10,11-epoxide, CL_{hep}: hepatic clearance, CL_{spec}: specific clearance, CYP: cytochrome P450, EPHX1: epoxide hydroxylase 1, FaHIF: fasted human intestinal fluid, IR: immediate release, fit: optimized during parameter optimization, lit: literature, UGT: UDP-glucuronosyltransferase, XR: extended release

[a] mean of literature values for EC_{50} (CYP3A4), assumed for all EC_{50} values

[b] k_{cat} values calculated within PK-Sim from V_{max}/recombinant enzyme

[c] k_{cat} value calculated within PK-Sim from V_{max} = 0.79 pmol/min/microsomal protein [52], assuming a microsomal UGT2B7 content of 82.9 pmol/mg microsomal protein [53], kcat = Vmax/ UGT2B7 content microsomes

2.4 Profiles

2.4.1 Carbamazepine-10,11-epoxide model

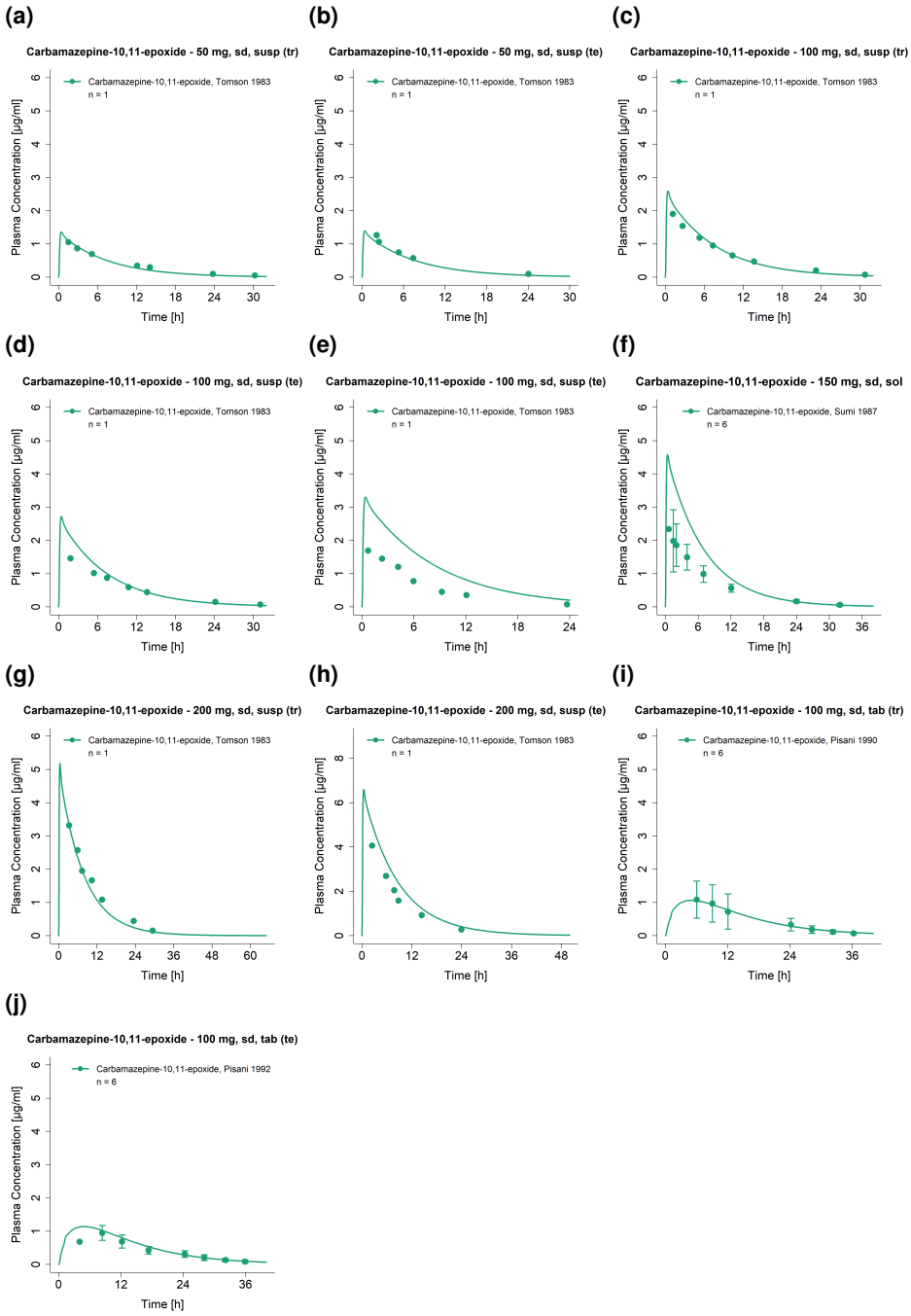

Figure S2: Predicted compared to observed carbamazepine-10,11-epoxide plasma concentration-time profiles (linear) after oral administration of carbamazepine-10,11-epoxide. Observed data are shown as dots ± standard deviation; model predictions are shown as solid lines. Details on dosing regimens, study populations and literature references are listed in Table S1. sd: single dose, sol: solution, susp: suspension, tab: tablet

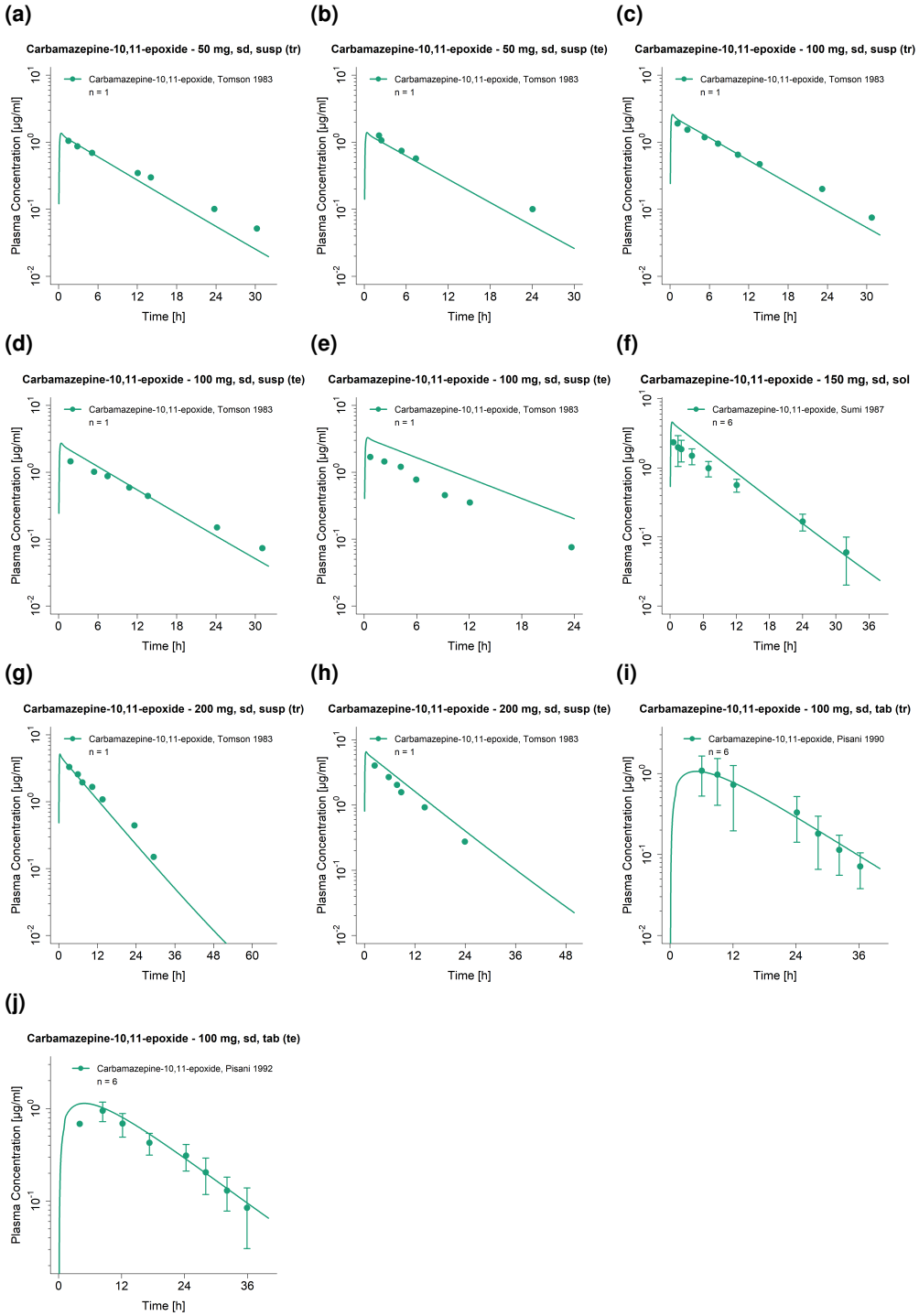

Figure S3: Predicted compared to observed carbamazepine-10,11-epoxide plasma concentration-time profiles (semi-logarithmic) after oral administration of carbamazepine-10,11-epoxide. Observed data are shown as dots ± standard deviation; model predictions are shown as solid lines. Details on dosing regimens, study populations and literature references are listed in Table S1. sd: single dose, sol: solution, susp: suspension, tab: tablet

2.4.2 Carbamazepine parent-metabolite model

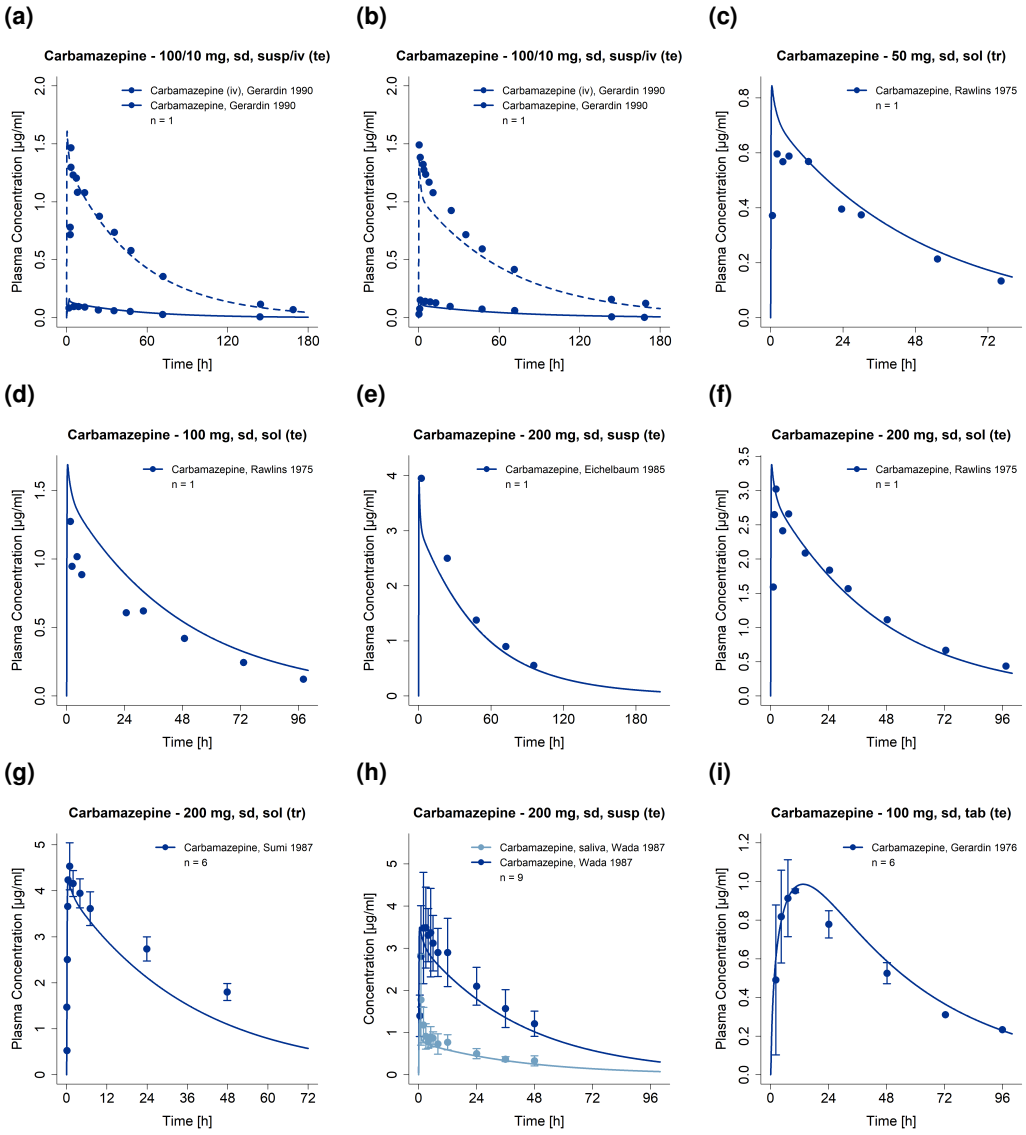

Figure S4: Predicted compared to observed carbamazepine and carbamazepine-10,11-epoxide plasma (and saliva) concentration-time profiles (linear) after intravenous and oral administration of carbamazepine. Observed data are shown as dots ± standard deviation; model predictions are shown as solid lines. Details on dosing regimens, study populations and literature references are listed in Table S1. bid: twice daily, cap: capsule, D: day, iv: intravenous, qd: once daily, sd: single dose, sol: solution, susp: suspension, tab: tablet, tab*: tablet with concomitant food intake, tid: three times daily, XR: extended release

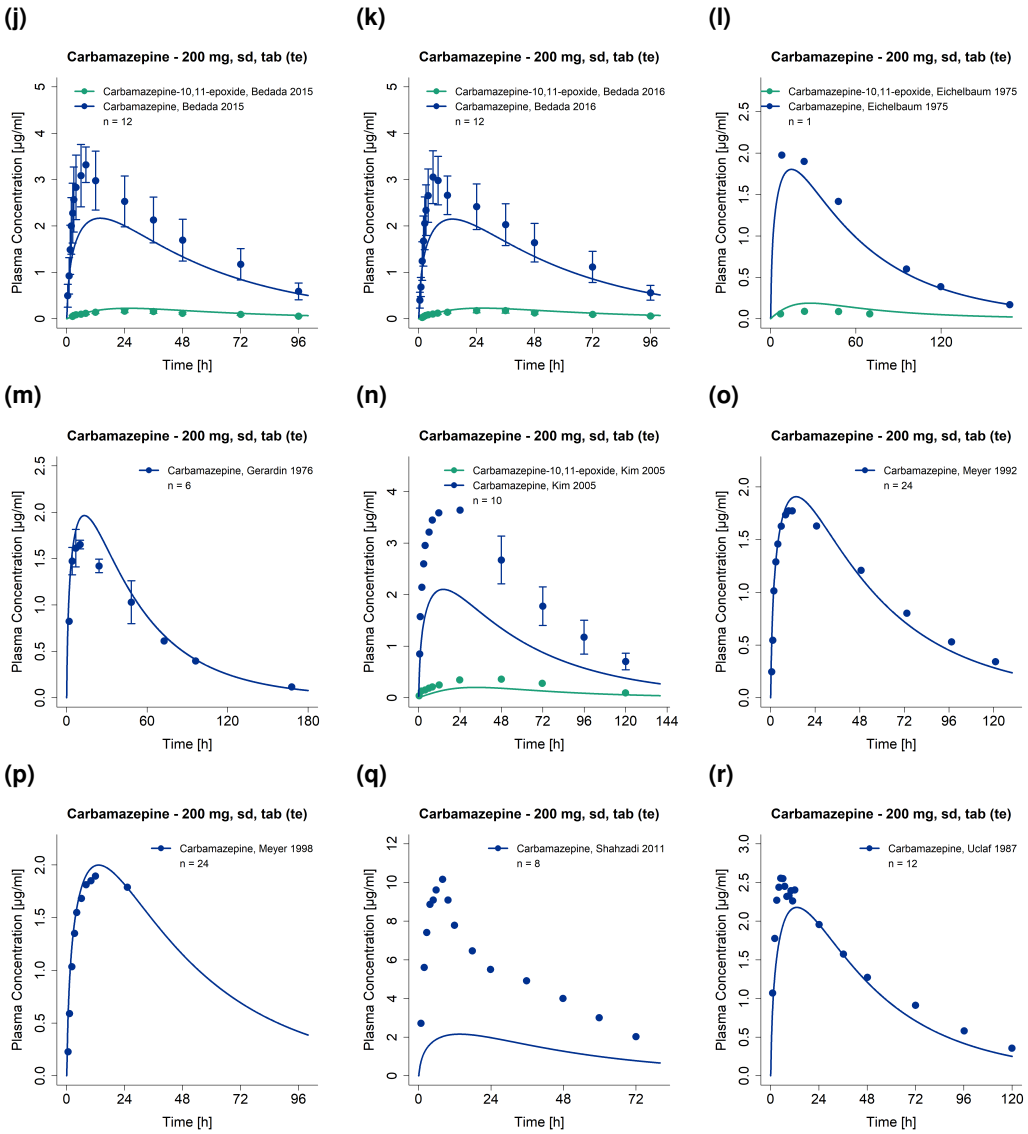

Figure S4: Predicted compared to observed carbamazepine and carbamazepine-10,11-epoxide plasma (and saliva) concentration-time profiles (linear) after intravenous and oral administration of carbamazepine. Observed data are shown as dots ± standard deviation; model predictions are shown as solid lines. Details on dosing regimens, study populations and literature references are listed in Table S1. bid: twice daily, cap: capsule, D: day, iv: intravenous, qd: once daily, sd: single dose, sol: solution, susp: suspension, tab: tablet, tab*: tablet with concomitant food intake, tid: three times daily, XR: extended release *(continued)*

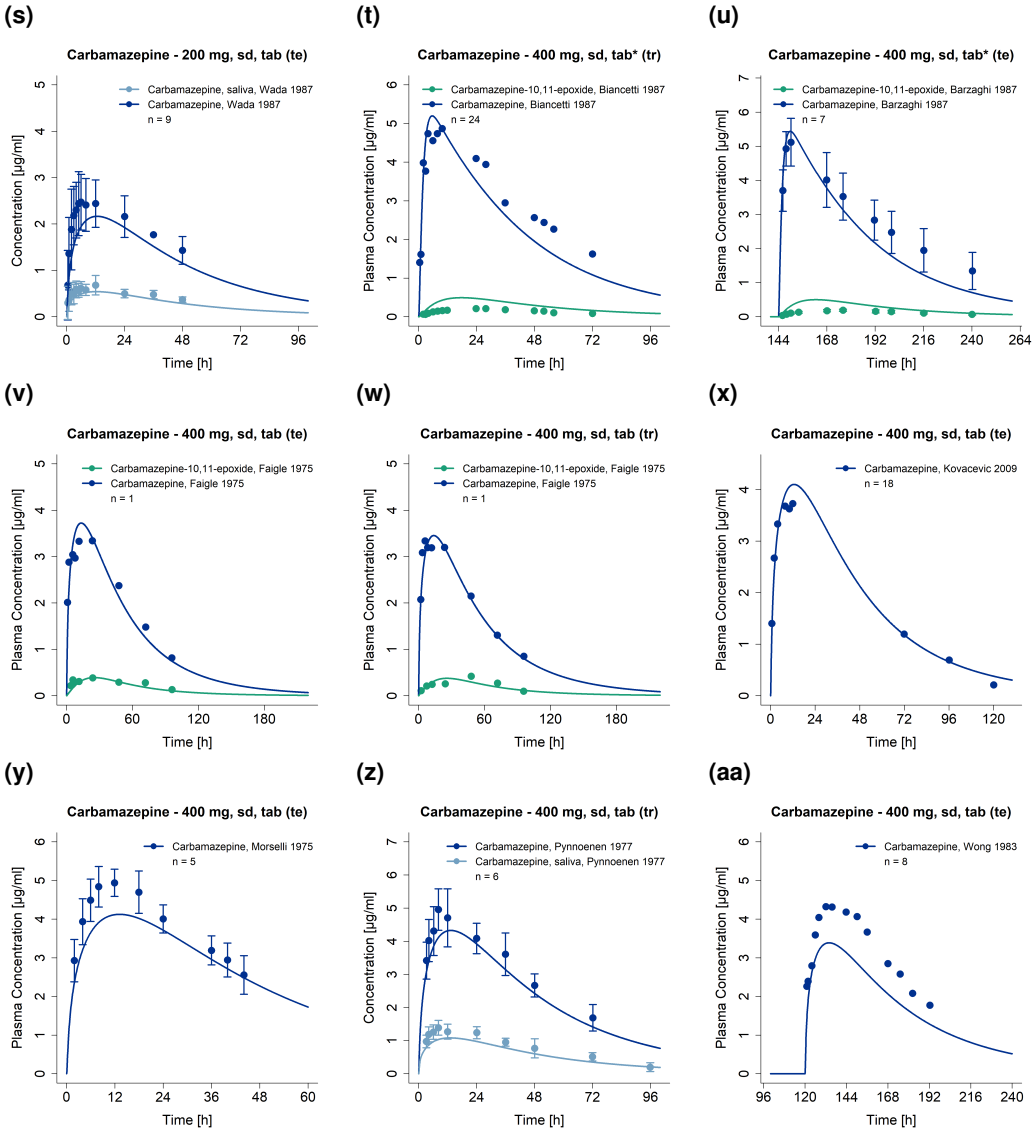

Figure S4: Predicted compared to observed carbamazepine and carbamazepine-10,11-epoxide plasma (and saliva) concentration-time profiles (linear) after intravenous and oral administration of carbamazepine. Observed data are shown as dots ± standard deviation; model predictions are shown as solid lines. Details on dosing regimens, study populations and literature references are listed in Table S1. bid: twice daily, cap: capsule, D: day, iv: intravenous, qd: once daily, sd: single dose, sol: solution, susp: suspension, tab: tablet, tab*: tablet with concomitant food intake, tid: three times daily, XR: extended release *(continued)*

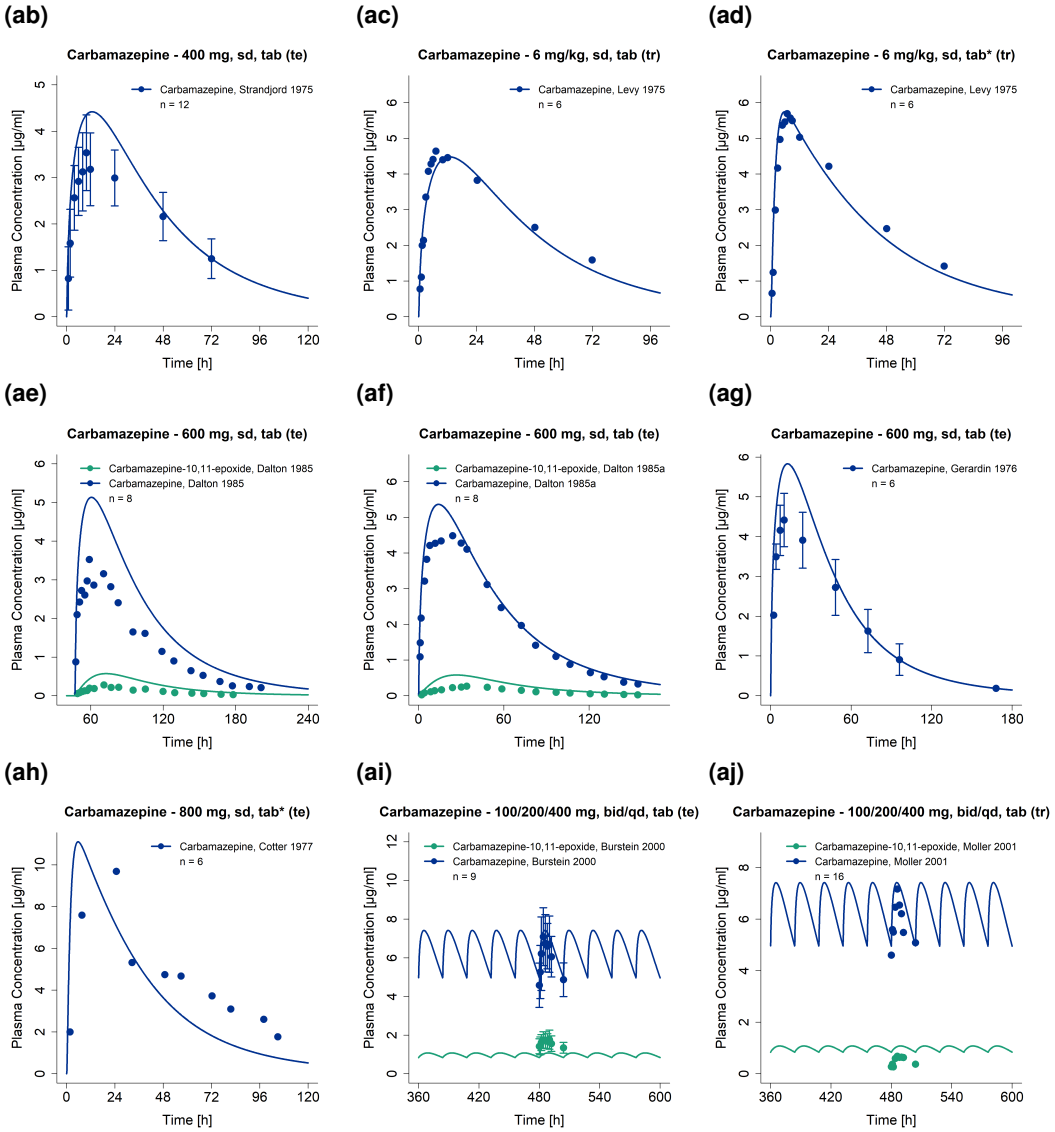

Figure S4: Predicted compared to observed carbamazepine and carbamazepine-10,11-epoxide plasma (and saliva) concentration-time profiles (linear) after intravenous and oral administration of carbamazepine. Observed data are shown as dots ± standard deviation; model predictions are shown as solid lines. Details on dosing regimens, study populations and literature references are listed in Table S1. bid: twice daily, cap: capsule, D: day, iv: intravenous, qd: once daily, sd: single dose, sol: solution, susp: suspension, tab: tablet, tab*: tablet with concomitant food intake, tid: three times daily, XR: extended release *(continued)*

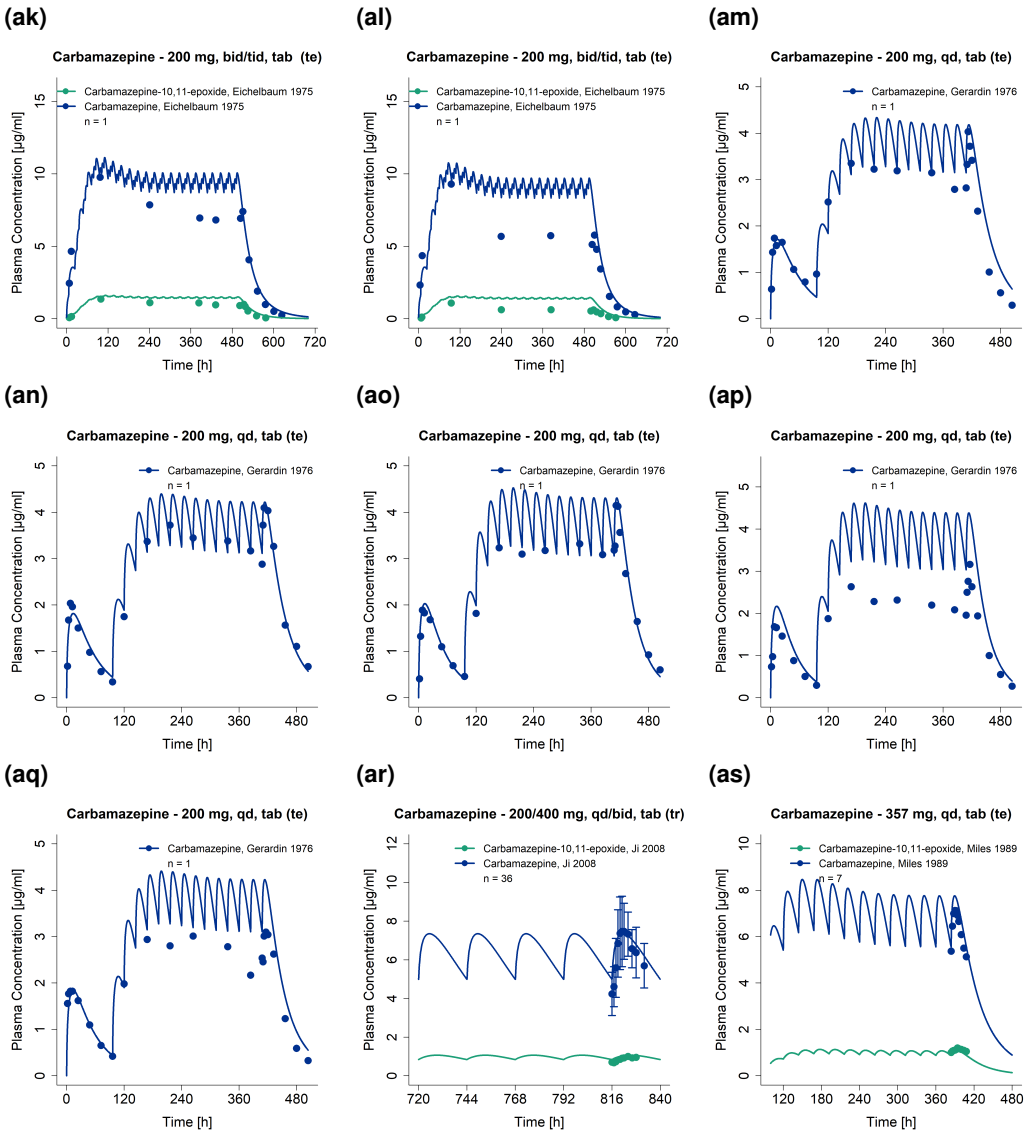

Figure S4: Predicted compared to observed carbamazepine and carbamazepine-10,11-epoxide plasma (and saliva) concentration-time profiles (linear) after intravenous and oral administration of carbamazepine. Observed data are shown as dots ± standard deviation; model predictions are shown as solid lines. Details on dosing regimens, study populations and literature references are listed in Table S1. bid: twice daily, cap: capsule, D: day, iv: intravenous, qd: once daily, sd: single dose, sol: solution, susp: suspension, tab: tablet, tab*: tablet with concomitant food intake, tid: three times daily, XR: extended release *(continued)*

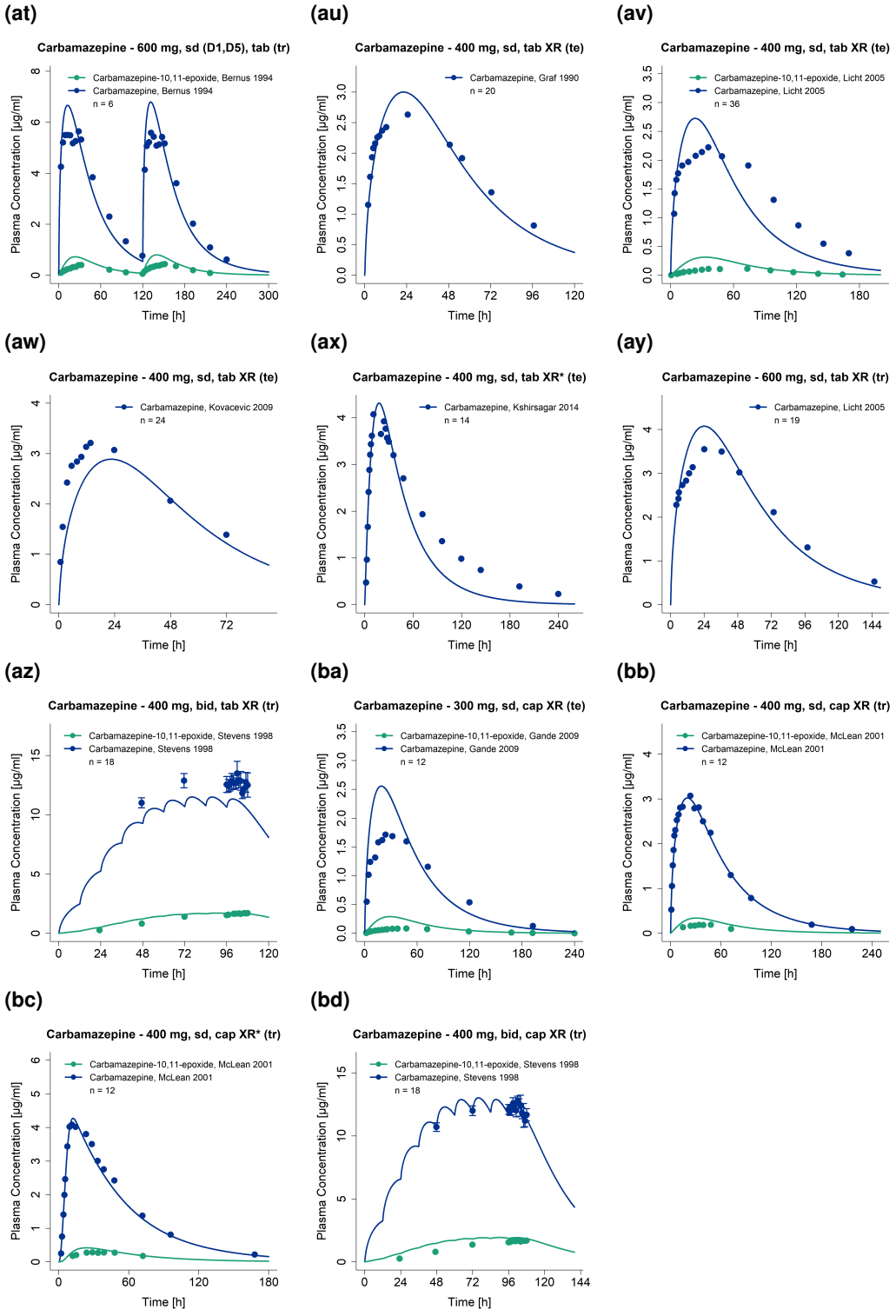

Figure S4: Predicted compared to observed carbamazepine and carbamazepine-10,11-epoxide plasma (and saliva) concentration-time profiles (linear) after intravenous and oral administration of carbamazepine. Observed data are shown as dots ± standard deviation; model predictions are shown as solid lines. Details on dosing regimens, study populations and literature references are listed in Table S1. bid: twice daily, cap: capsule, D: day, iv: intravenous, qd: once daily, sd: single dose, sol: solution, susp: suspension, tab: tablet, tab*: tablet with concomitant food intake, tid: three times daily, XR: extended release *(continued)*

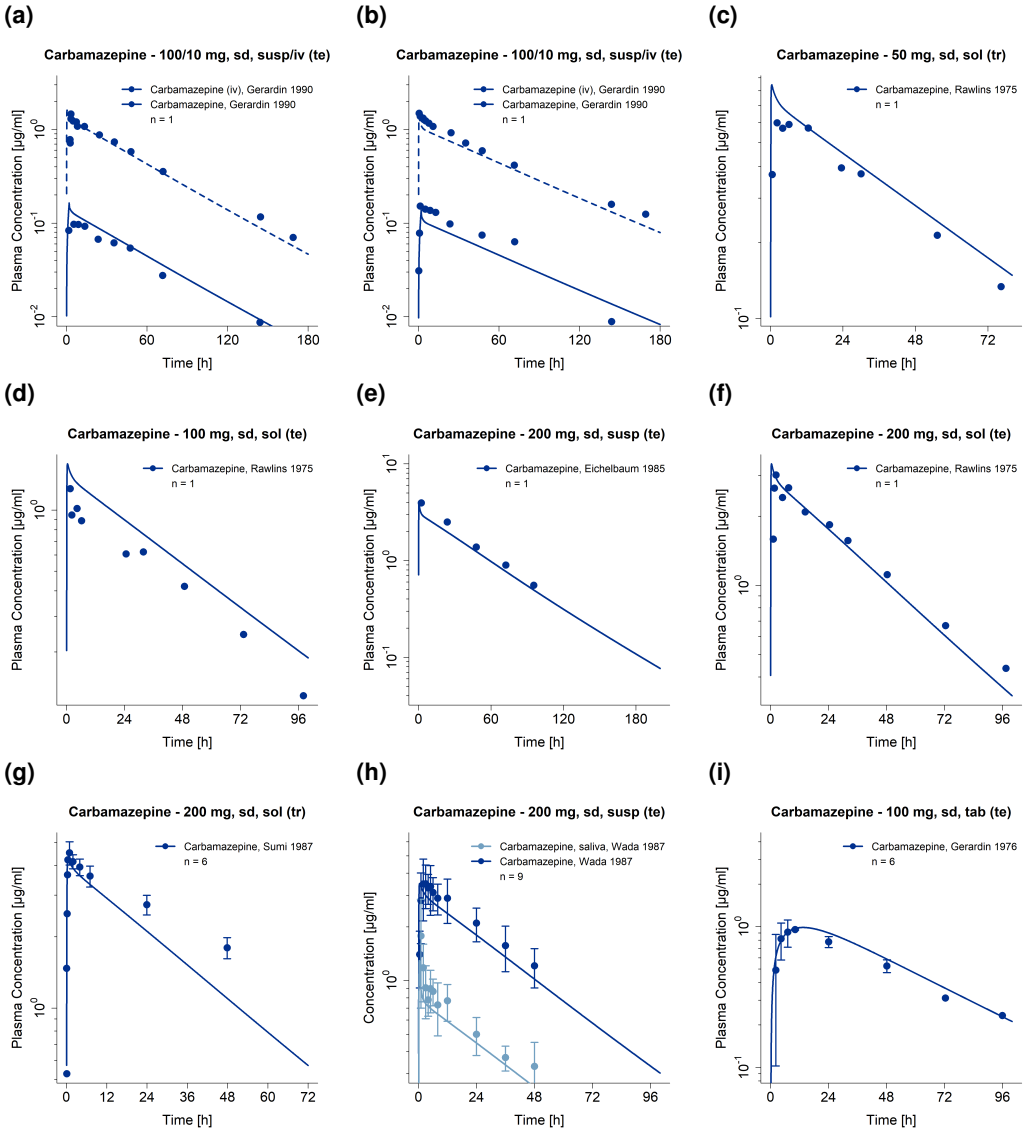

Figure S5: Predicted compared to observed carbamazepine and carbamazepine-10,11-epoxide plasma (and saliva) concentration-time profiles (semi-logarithmic) after intravenous and oral administration of carbamazepine. Observed data are shown as dots ± standard deviation; model predictions are shown as solid lines. Details on dosing regimens, study populations and literature references are listed in Table S1. bid: twice daily, cap: capsule, D: day, iv: intravenous, qd: once daily, sd: single dose, sol: solution, susp: suspension, tab: tablet, tab*: tablet with concomitant food intake, tid: three times daily, XR: extended release

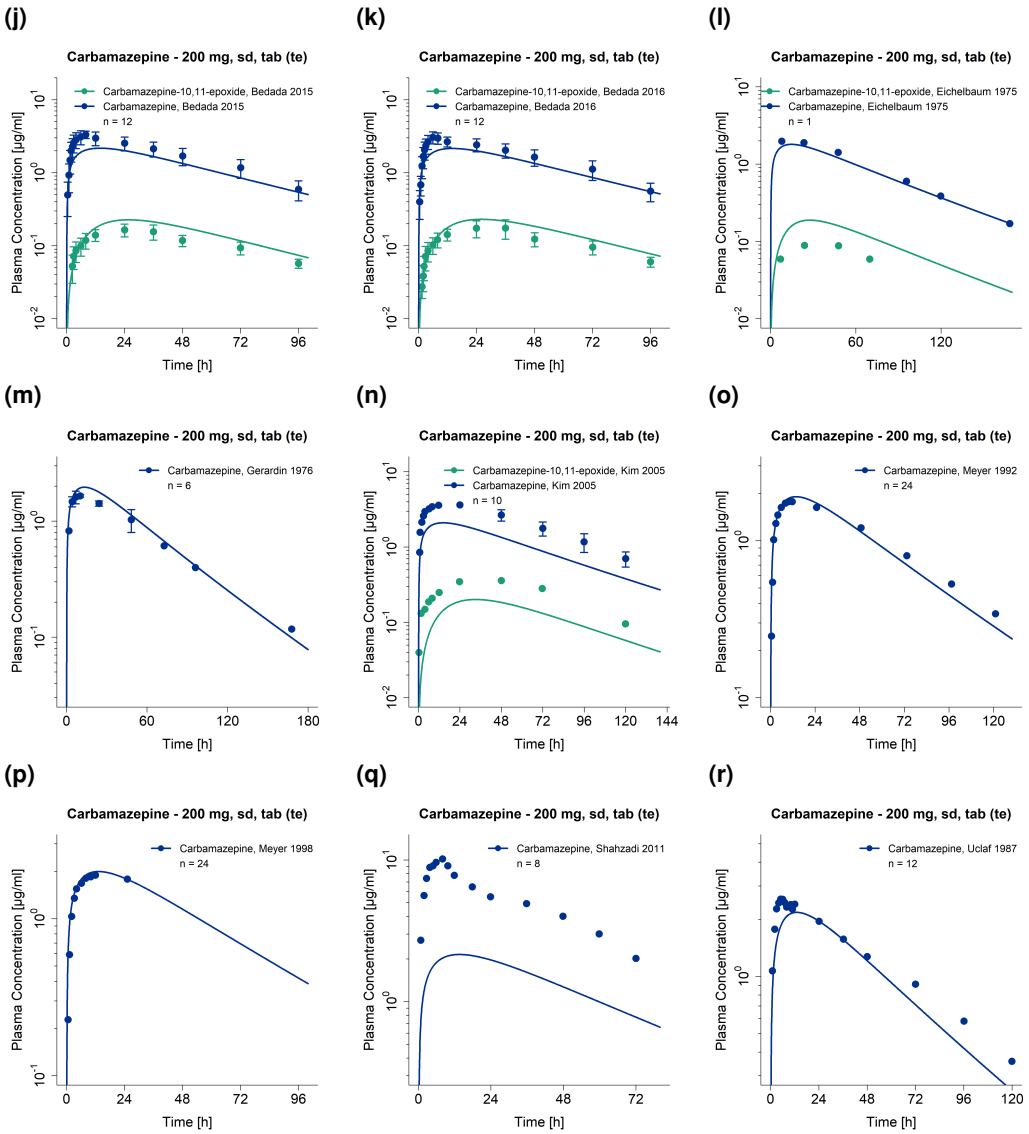

Figure S5: Predicted compared to observed carbamazepine and carbamazepine-10,11-epoxide plasma (and saliva) concentration-time profiles (semi-logarithmic) after intravenous and oral administration of carbamazepine. Observed data are shown as dots ± standard deviation; model predictions are shown as solid lines. Details on dosing regimens, study populations and literature references are listed in Table S1. bid: twice daily, cap: capsule, D: day, iv: intravenous, qd: once daily, sd: single dose, sol: solution, susp: suspension, tab: tablet, tab*: tablet with concomitant food intake, tid: three times daily, XR: extended release *(continued)*

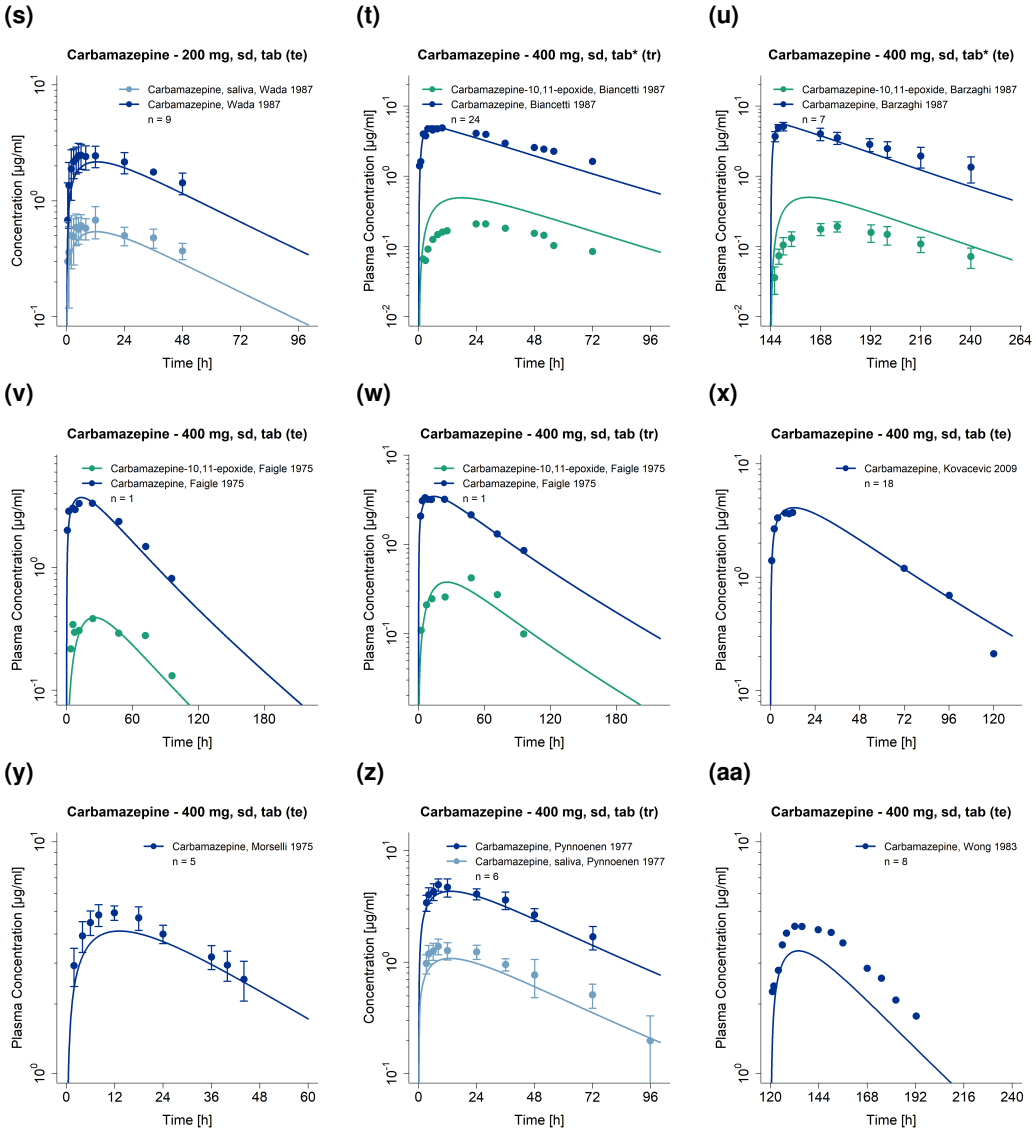

Figure S5: Predicted compared to observed carbamazepine and carbamazepine-10,11-epoxide plasma (and saliva) concentration-time profiles (semi-logarithmic) after intravenous and oral administration of carbamazepine. Observed data are shown as dots ± standard deviation; model predictions are shown as solid lines. Details on dosing regimens, study populations and literature references are listed in Table S1. bid: twice daily, cap: capsule, D: day, iv: intravenous, qd: once daily, sd: single dose, sol: solution, susp: suspension, tab: tablet, tab*: tablet with concomitant food intake, tid: three times daily, XR: extended release *(continued)*

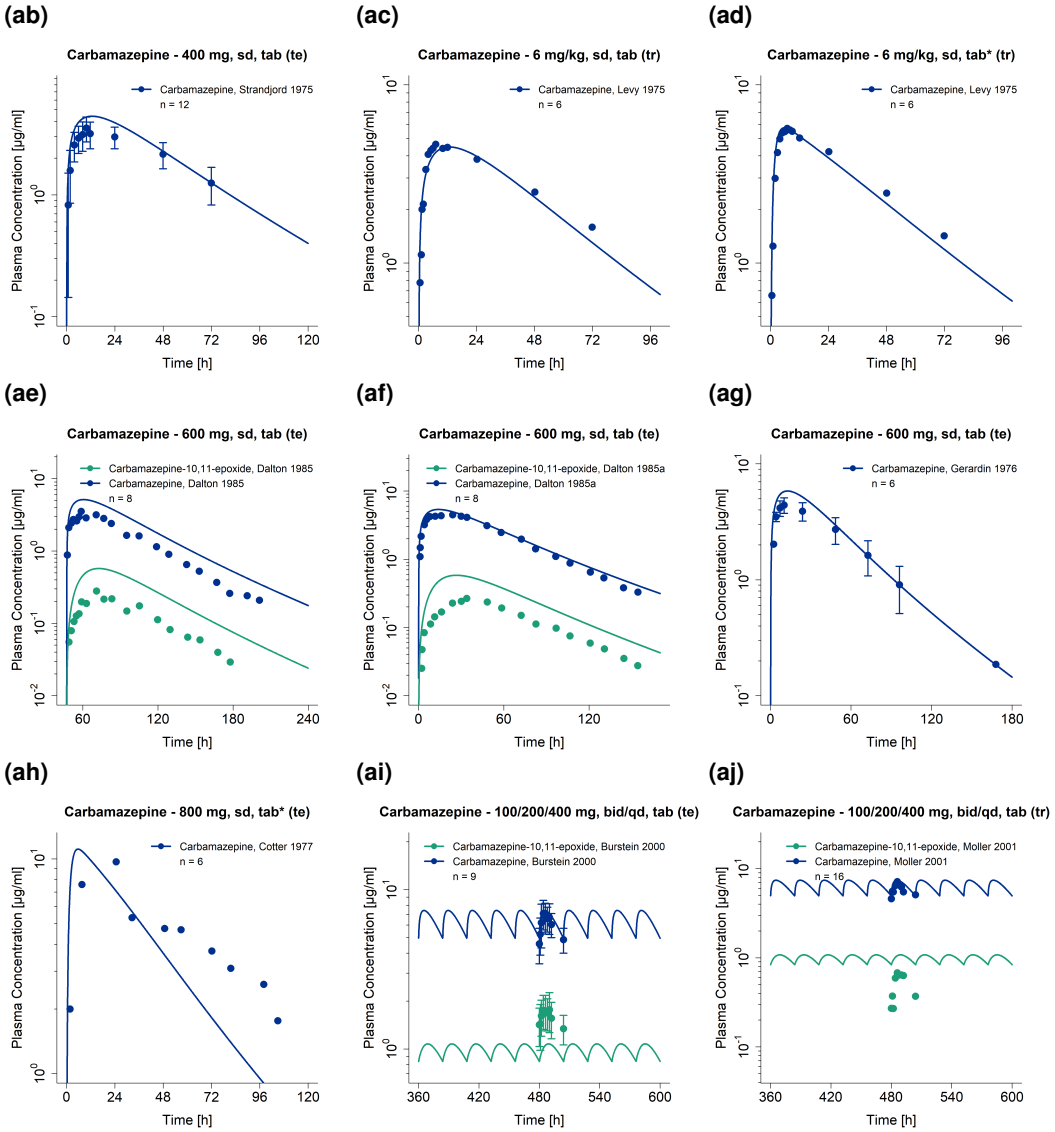

Figure S5: Predicted compared to observed carbamazepine and carbamazepine-10,11-epoxide plasma (and saliva) concentration-time profiles (semi-logarithmic) after intravenous and oral administration of carbamazepine. Observed data are shown as dots ± standard deviation; model predictions are shown as solid lines. Details on dosing regimens, study populations and literature references are listed in Table S1. bid: twice daily, cap: capsule, D: day, iv: intravenous, qd: once daily, sd: single dose, sol: solution, susp: suspension, tab: tablet, tab*: tablet with concomitant food intake, tid: three times daily, XR: extended release *(continued)*

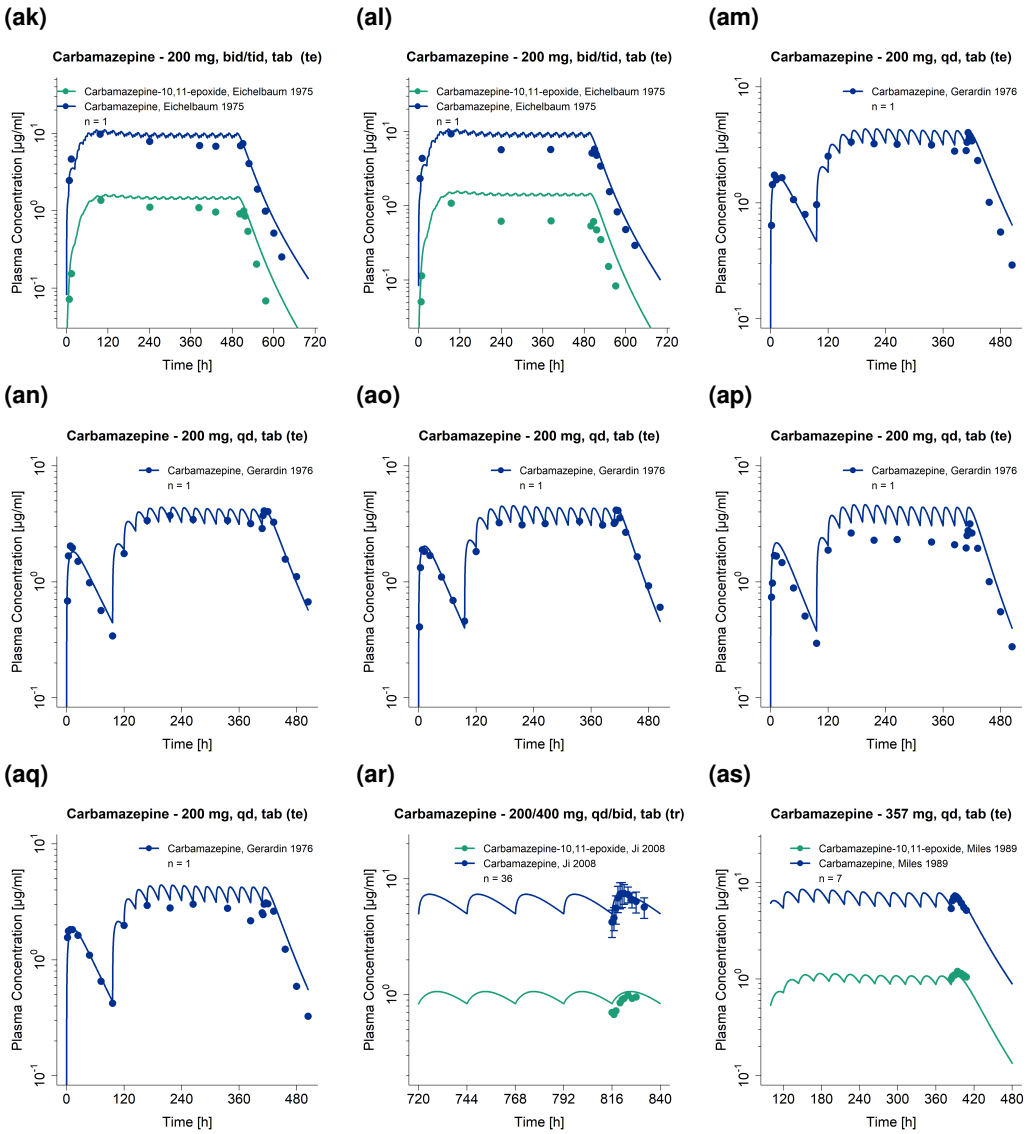

Figure S5: Predicted compared to observed carbamazepine and carbamazepine-10,11-epoxide plasma (and saliva) concentration-time profiles (semi-logarithmic) after intravenous and oral administration of carbamazepine. Observed data are shown as dots ± standard deviation; model predictions are shown as solid lines. Details on dosing regimens, study populations and literature references are listed in Table S1. bid: twice daily, cap: capsule, D: day, iv: intravenous, qd: once daily, sd: single dose, sol: solution, susp: suspension, tab: tablet, tab*: tablet with concomitant food intake, tid: three times daily, XR: extended release *(continued)*

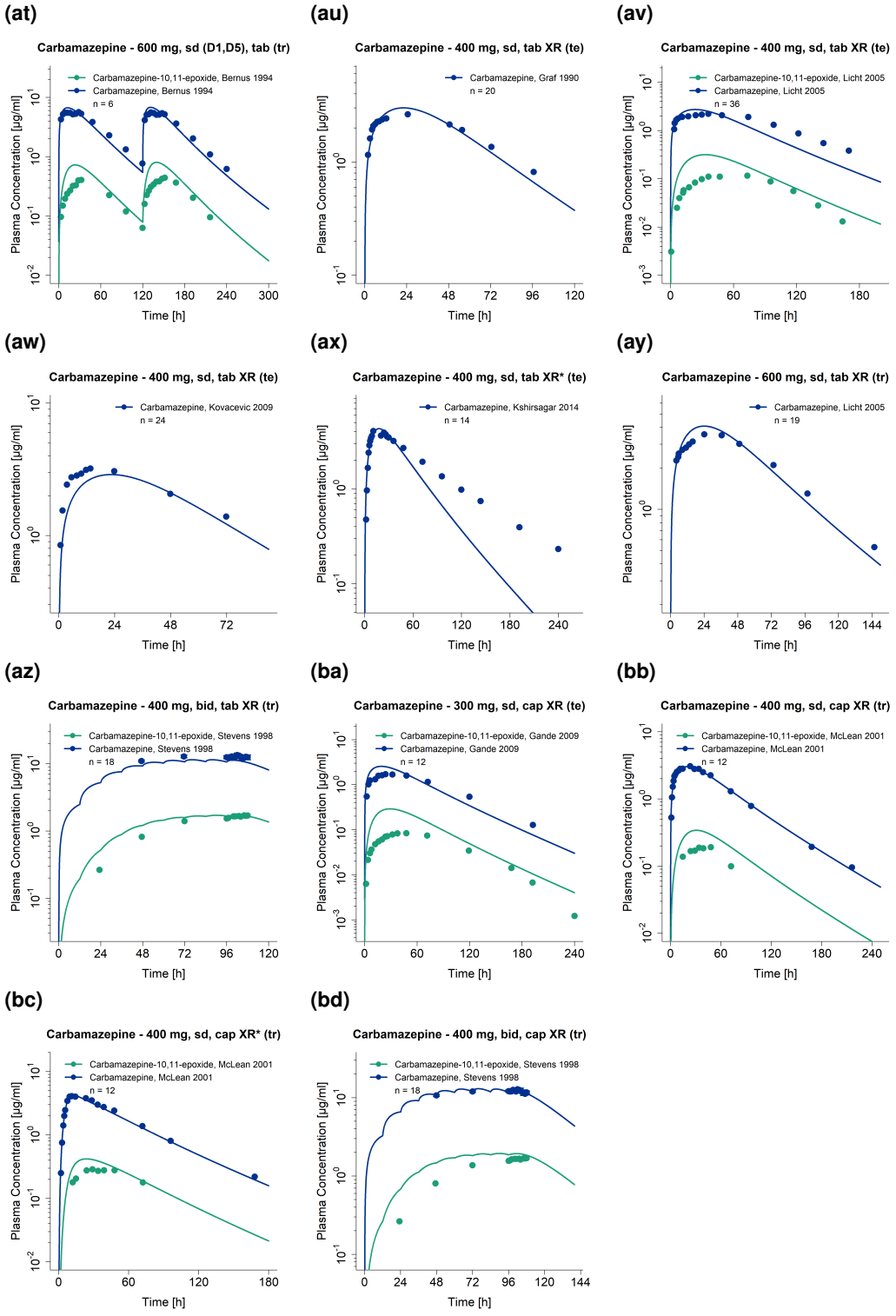

Figure S5: Predicted compared to observed carbamazepine and carbamazepine-10,11-epoxide plasma (and saliva) concentration-time profiles (semi-logarithmic) after intravenous and oral administration of carbamazepine. Observed data are shown as dots ± standard deviation; model predictions are shown as solid lines. Details on dosing regimens, study populations and literature references are listed in Table S1. bid: twice daily, cap: capsule, D: day, iv: intravenous, qd: once daily, sd: single dose, sol: solution, susp: suspension, tab: tablet, tab*: tablet with concomitant food intake, tid: three times daily, XR: extended release *(continued)*

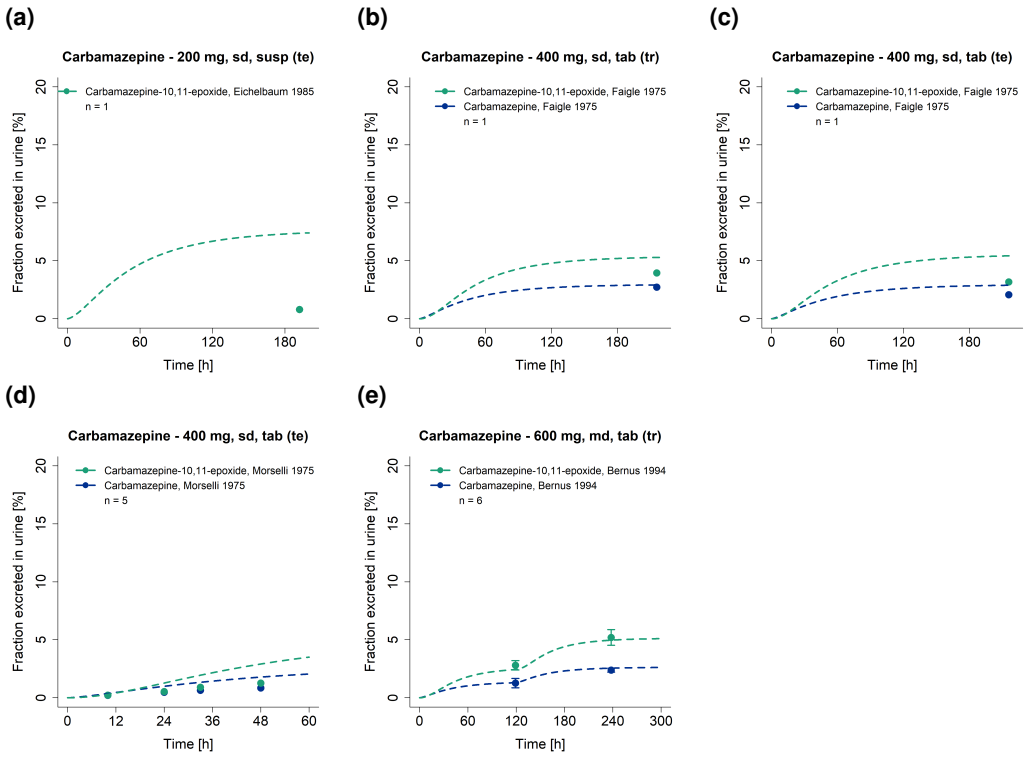

Figure S6: Predicted compared to observed carbamazepine and carbamazepine-10,11-epoxide fractions excreted unchanged in urine profiles (linear). Observed data are shown as dots ± standard deviation; model predictions are shown as solid lines. Details on dosing regimens, study populations and literature references are listed in Table S1. md: multiple dose, susp: suspension, sd: single dose, tab: tablet

2.5 Model evaluation

2.5.1 Plasma concentration goodness-of-fit plots

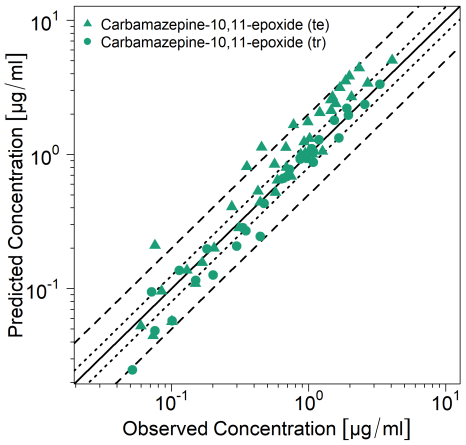

Figure S7: Predicted compared to observed carbamazepine-10,11-epoxide plasma concentrations after oral administration of carbamazepine-10,11-epoxide, predicted with the carbamazepine-10,11-epoxide PBPK model. The solid line marks the line of identity. Dotted lines indicate 1.25-fold, dashed lines indicate 2-fold deviation.

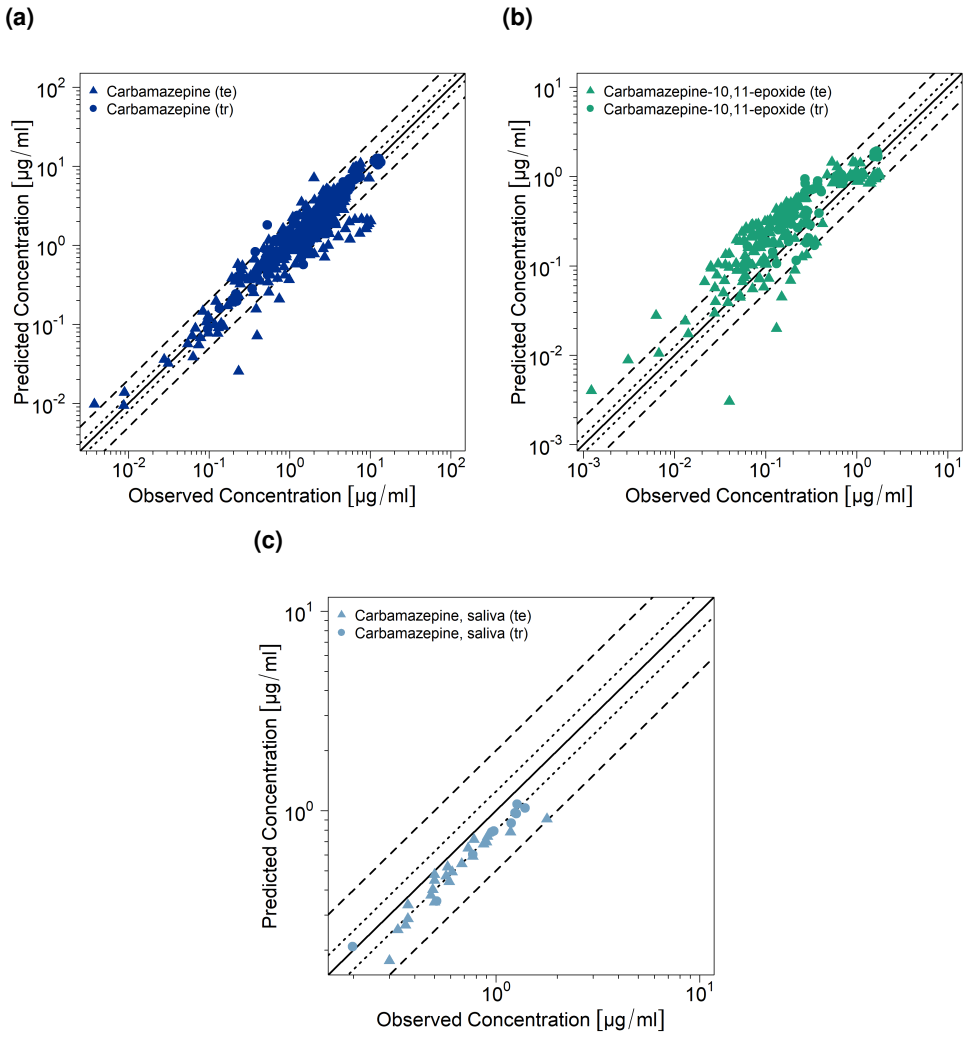

Figure S8: Predicted compared to observed (a) carbamazepine plasma concentrations (b) carbamazepine-10,11-epoxide plasma concentrations and (c) carbamazepine saliva concentrations after intravenous and oral administration of carbamazepine. The solid line marks the line of identity. Dotted lines indicate 1.25-fold, dashed lines indicate 2-fold deviation.

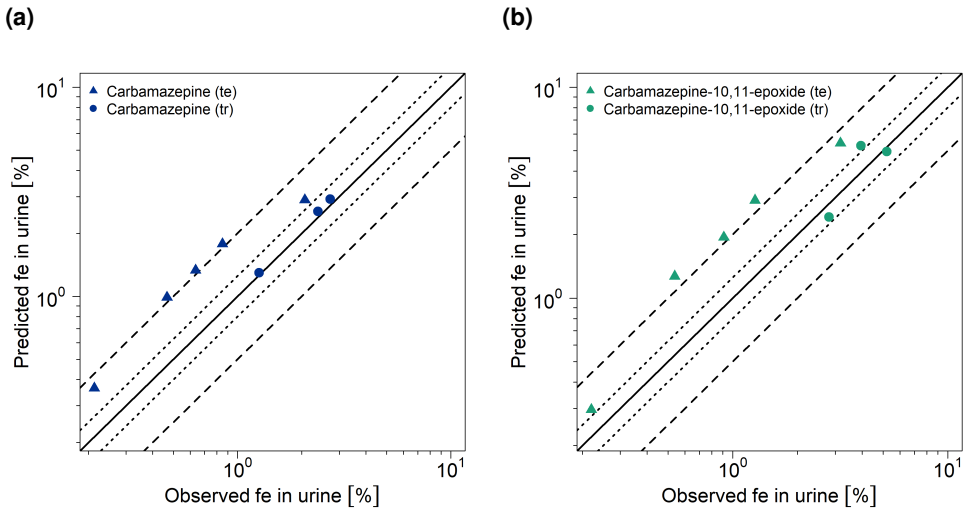

Figure S9: Predicted compared to observed fractions excreted unchanged in urine of (a) carbamazepine and (b) carbamazepine-10,11-epoxide after oral administration of carbamazepine. The solid line marks the line of identity. Dotted lines indicate 1.25-fold, dashed lines indicate 2-fold deviation

2.5.2 Mean relative deviation of predicted plasma concentrations

Table S3: Mean relative deviation values of predicted carbamazepine and carbamazepine-10,11-epoxide plasma and saliva concentrations

Dose [mg]	Route	CBZ MRD	CBZE MRD	CBZ (saliva) MRD	Reference
Carbamazepine-10,11-epoxide administration					
50	po (sol), sd	-	1.41	-	Tomson 1983 [5]
50	po (sol), sd	-	1.25	-	Tomson 1983 [5]
100	po (sol), sd	-	1.27	-	Tomson 1983 [5]
100	po (sol), sd	-	2.21	-	Tomson 1983 [5]
100	po (sol), sd	-	1.35	-	Tomson 1983 [5]
150	po (sol), sd	-	1.67	-	Sumi 1987 [17]
200	po (sol), sd	-	1.25	-	Tomson 1983 [5]
200	po (sol), sd	-	1.46	-	Tomson 1983 [5]
100	po (tab), sd	-	1.16	-	Pisani 1990 [18]
100	po (tab), sd	-	1.23	-	Pisani 1992 [19]
mean MRD (range)		**-**	**1.42 (1.16-2.21)**	**-**	
		-	**9/10 with MRD $\leq$ 2**	**-**	
Carbamazepine administration					
100/10	po (susp), sd; iv (2 h)	1.30	-	-	Gerardin 1990 [81]
100/10	po (susp), sd; iv (2 h)	1.55	-	-	Gerardin 1990 [81]
50	po (sol), sd	1.35	-	-	Rawlins 1975 [21]
100	po (sol), sd	1.39	-	-	Rawlins 1975 [21]
200	po (susp), sd	1.20	-	-	Eichelbaum 1985 [4]
200	po (sol), sd	1.26	-	-	Rawlins 1975 [21]
200	po (sol), sd	1.68	-	-	Sumi 1987 [17]
200	po (susp), sd	1.60	-	-	Tomson 1983 [5]
200	po (susp), sd	1.35	-	1.35	Wada 1978 [22]
100	po (tab), sd	1.12	-	-	Gerardin 1976 [23]
200	po (tab), sd	1.44	1.28	-	Bedada 2015 [24]
200	po (tab), sd	1.36	1.24	-	Bedada 2016 [25]
200	po (tab), sd	1.12	1.86	-	Eichelbaum 1975 [26]
200	po (tab), sd	1.17	-	-	Gerardin 1976 [23]
200	po (tab), sd	1.83	3.47	-	Kim 2005 [27]

bid: twice daily, cap: capsule, CBZ: carbamazepine, CBZE: carbamazepine-10,11-epoxide, D: day, iv: intravenous, MRD: mean relative deviation, po: oral, qd: once daily, sd: single dose, sol: solution, susp: suspension, tab: tablet, tid: three times daily, XR: extended release

Table S3: Mean relative deviation values of predicted carbamazepine and carbamazepine-10,11-epoxide plasma and saliva concentrations *(continued)*

Dose [mg]	Route	CBZ MRD	CBZE MRD	CBZ (saliva) MRD	Reference
200	po (tab), sd	1.27	-	-	Meyer 1992 [28]
200	po (tab), sd	1.39	-	-	Meyer 1998 [29]
200	po (tab), sd	3.98	-	-	Shahzadi 2011 [30]
200	po (tab), sd	1.27	-	-	Saint-Salvi 1987 [31]
200	po (tab), sd	1.32	-	1.31	Wada 1978 [22]
400	po (tab, fed), sd	1.35	2.41	-	Barzaghi 1987 [32]
400	po (tab, fed), sd	1.31	2.28	-	Bianchetti 1987 [33]
400	po (tab), sd	1.22	1.48	-	Faigle 1975 [8]
400	po (tab), sd	1.08	1.35	-	Faigle 1975 [8]
400	po (tab), sd	1.24	-	-	Kovacevic 2009 [34]
400	po (tab), sd	1.17	-	-	Morselli 1975 [35]
400	po (tab), sd	1.14	-	1.28	Pynnoenen 1977 [36]
400	po (tab), sd	1.40	-	-	Strandjord 1975 [37]
400	po (tab), sd	1.35	-	-	Wong 1983 [38]
420	po (tab), sd	1.26	-	-	Levy 1975 [15]
420	po (tab, fed), sd	1.30	-	-	Levy 1975 [15]
600	po (tab), sd	1.66	2.41	-	Dalton 1985 [39]
600	po (tab), sd	1.28	2.27	-	Dalton 1985a [40]
600	po (tab), sd	1.32	-	-	Gerardin 1976 [23]
800	po (tab, fed), sd	2.05	-	-	Cotter 1977 [41]
100/200/400	po (tab), bid/qd	1.11	1.63	-	Burstein 2000 [42]
100/200/400	po (tab), bid/qd	1.15	2.19	-	Moller 2001 [43]
200	po (tab), bid/tid	1.41	1.75	-	Eichelbaum 1975 [26]
200	po (tab), bid/tid	1.31	2.37	-	Eichelbaum 1975 [26]
200	po (tab), qd	1.15	-	-	Gerardin 1976 [23]
200/400	po (tab), bid/qd	1.15	1.2	-	Ji 2008 [44]
357	po (tab), qd	1.09	1.12	-	Miles 1989 [45]
600	po (tab), sd (D1,D5)	1.19	2.00	-	Bernus 1994 [46]
400	po (tab XR), sd	1.11	-	-	Graf 1990 [47]
400	po (tab XR), sd	1.55	2.72	-	Licht 2005 [48]
400	po (tab XR), sd	1.38	-	-	Kovacevic 2009 [34]
400	po (tab XR, fed), sd	2.08	-	-	Kshirsagar 2014 [49]

bid: twice daily, cap: capsule, CBZ: carbamazepine, CBZE: carbamazepine-10,11-epoxide, D: day, iv: intravenous, MRD: mean relative deviation, po: oral, qd: once daily, sd: single dose, sol: solution, susp: suspension, tab: tablet, tid: three times daily, XR: extended release

Table S3: Mean relative deviation values of predicted carbamazepine and carbamazepine-10,11-epoxide plasma and saliva concentrations *(continued)*

Dose [mg]	Route	CBZ MRD	CBZE MRD	CBZ (saliva) MRD	Reference
600	po (tab XR), sd	1.15	-	-	Licht 2005 [48]
400	po (tab XR), bid	1.15	1.04	-	Stevens 1998 [50]
300	po (cap XR), sd	1.57	3.24	-	Gande 2009 [51]
400	po (cap XR), sd	1.10	1.83	-	McLean 2001 [16]
400	po (cap XR, fed), sd	1.13	1.45	-	McLean 2001 [16]
400	po (cap XR), bid	1.03	1.16	-	Stevens 1998 [50]
mean MRD (range)		**1.38 (1.03-3.98)**	**1.90 (1.04-3.47)**	**1.31 (1.28-1.35)**	
		52/55 with MRD ≤ 2	**14/23 with MRD ≤ 2**	**3/3 with MRD ≤ 2**	

bid: twice daily, cap: capsule, CBZ: carbamazepine, CBZE: carbamazepine-10,11-epoxide, D: day, iv: intravenous, MRD: mean relative deviation, po: oral, qd: once daily, sd: single dose, sol: solution, susp: suspension, tab: tablet, tid: three times daily, XR: extended release

2.5.3 AUC_{last} and C_{max} goodness-of-fit plots

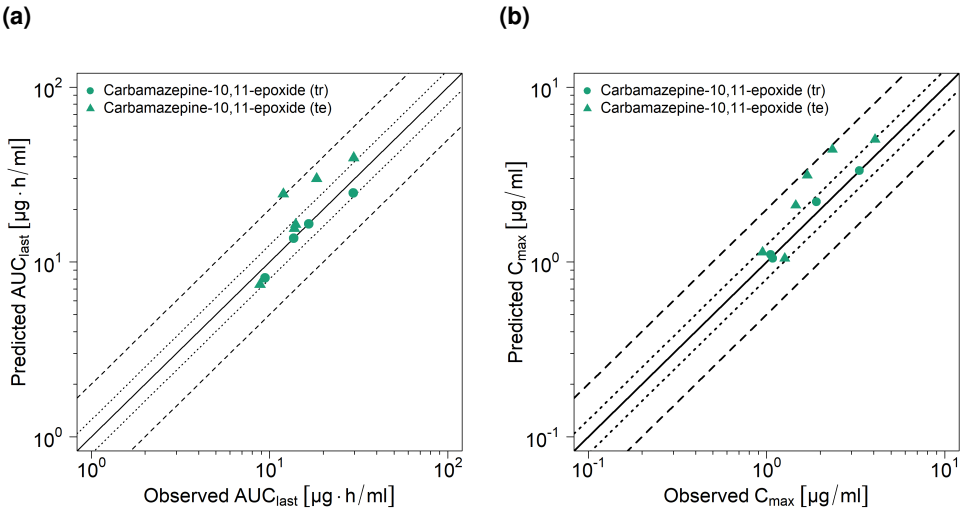

Figure S10: Predicted compared to observed carbamazepine-10,11-epoxide (a) AUC_{last} and (b) C_{max} values after oral administration of carbamazepine-10,11-epoxide. The solid line marks the line of identity. Dotted lines indicate 1.25-fold, dashed lines indicate 2-fold deviation. AUC_{last}: area under the plasma concentration-time curve from the time of drug administration to the last concentration measurement, C_{max}: maximum plasma concentration

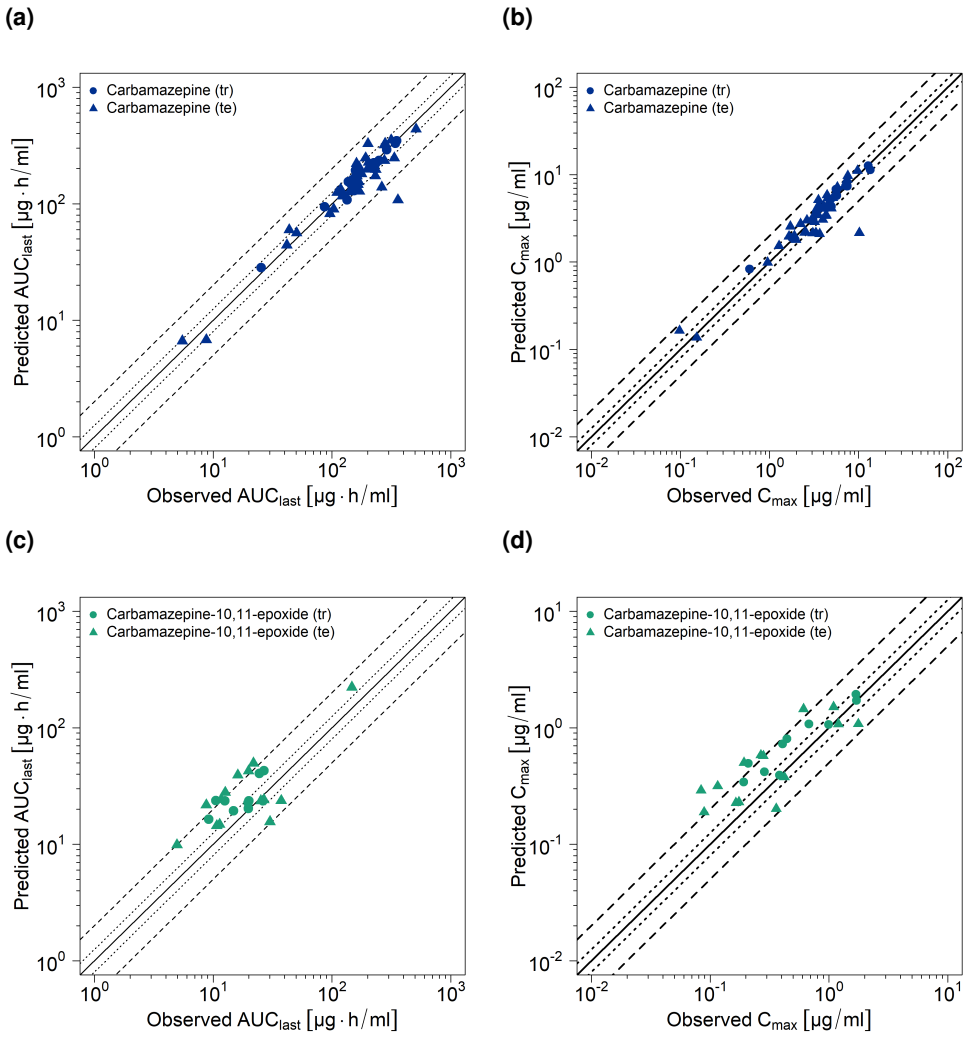

Figure S11: Predicted compared to observed (a,c) AUC_{last} and (b,d) C_{max} values of carbamazepine and carbamazepine-10,11-epoxide after intravenous and oral administration of carbamazepine. The solid line marks the line of identity. Dotted lines indicate 1.25-fold, dashed lines indicate 2-fold deviation. AUC_{last}: area under the plasma concentration-time curve from the time of drug administration to the last concentration measurement, C_{max}: maximum plasma concentration

2.5.4 Geometric mean fold error of predicted AUC_{last} and C_{max} values

Table S4: Predicted and observed AUC_{last} and C_{max} values with geometric mean fold errors of carbamazepine and carbamazepine-10,11-epoxide

		AUC_{last} [µg*h/ml]			C_{max} [µg/ml]			
Dose [mg]	**Route**	**Pred**	**Obs**	**Pred/Obs**	**Pred**	**Obs**	**Pred/Obs**	**Reference**
Carbamazepine-10,11-epoxide administration								
50	po (susp), sd	8.78	9.43	0.93	1.22	1.05	1.16	Tomson 1983 [5]
50	po (susp), sd	8.03	8.84	0.91	1.13	1.26	0.90	Tomson 1983 [5]
100	po (susp), sd	17.91	16.57	1.08	2.51	1.90	1.32	Tomson 1983 [5]
100	po (susp), sd	25.98	11.94	2.18	3.24	1.69	1.92	Tomson 1983 [5]
100	po (susp), sd	16.79	13.79	1.22	2.29	1.46	1.57	Tomson 1983 [5]
150	po (sol), sd	29.94	18.36	1.63	4.40	2.34	1.88	Sumi 1987 [17]
200	po (susp), sd	26.83	29.47	0.91	3.59	3.32	1.08	Tomson 1983 [5]
200	po (susp), sd	42.20	29.66	1.42	5.37	4.06	1.32	Tomson 1983 [5]
100	po (tab), sd	13.70	13.65	1.00	1.05	1.08	0.97	Pisani 1990 [18]
100	po (tab), sd	16.40	14.01	1.17	1.14	0.95	1.20	Pisani 1992 [19]
mean GMFE (range)				**1.29 (1.00-2.18)**			**1.35 (1.03-1.92)**	
				9/10 with GMFE ≤ 2			**10/10 with GMFE ≤ 2**	
Carbamazepine administration								
Carbamazepine								
10	iv (2 h), sd	6.64	5.51	1.21	0.16	0.10	1.68	Gerardin 1990 [81]
10	iv (2 h), sd	6.81	8.75	0.78	0.14	0.15	0.90	Gerardin 1990 [81]
50	po (sol), sd	28.32	25.33	1.12	0.83	0.60	1.39	Rawlins 1975 [21]
100	po (susp), sd	64.36	68.95	0.93	1.33	1.47	0.91	Gerardin 1990 [81]
100	po (susp), sd	66.14	78.08	0.85	1.38	1.49	0.93	Gerardin 1990 [81]
100	po (sol), sd	59.64	43.65	1.37	1.53	1.27	1.20	Rawlins 1975 [21]
200	po (susp), sd	128.67	157.26	0.82	3.06	3.95	0.77	Eichelbaum 1985 [4]
200	po (sol), sd	116.19	121.69	0.95	3.15	3.02	1.04	Rawlins 1975 [21]
200	po (sol), sd	108.22	134.16	0.81	4.22	4.53	0.93	Sumi 1987 [17]
200	po (susp), sd	133.02	118.44	1.12	3.47	4.32	0.80	Tomson 1983 [5]
200	po (susp), sd	89.8	103.48	0.87	3.49	3.49	1.00	Wada 1978 [22]
100	po (tab), sd	56.18	50.42	1.11	0.99	0.95	1.04	Gerardin 1976 [23]
200	po (tab), sd	128.13	170.03	0.75	2.17	3.32	0.65	Bedada 2015 [24]

bid: twice daily, cap: capsule, D: day,. GMFE: geometric mean fold error, iv: intravenous, po: oral, qd: once daily, sd: single dose, sol: solution, susp: suspension, tab: tablet, tid: three times daily, XR: extended release

Table S4: Predicted and observed AUC_{last} and C_{max} values with geometric mean fold errors of carbamazepine and carbamazepine-10,11-epoxide *(continued)*

		AUC_{last} [µg*h/ml]			C_{max} [µg/ml]			
Dose [mg]	**Route**	**Pred**	**Obs**	**Pred/Obs**	**Pred**	**Obs**	**Pred/Obs**	**Reference**
200	po (tab), sd	128.11	160.04	0.80	2.15	3.05	0.70	Bedada 2016 [25]
200	po (tab), sd	126.04	140.33	0.90	1.80	1.98	0.91	Eichelbaum 1975 [26]
200	po (tab), sd	124.99	110.69	1.13	1.96	1.65	1.19	Gerardin 1976 [23]
200	po (tab), sd	138.97	262.77	0.53	2.10	3.64	0.58	Kim 2005 [27]
200	po (tab), sd	119.95	122.94	0.98	1.91	1.77	1.08	Meyer 1992 [28]
200	po (tab), sd	44.2	41.66	1.06	2.00	1.89	1.05	Meyer 1998 [29]
200	po (tab), sd	107.98	359.4	0.30	2.15	10.16	0.21	Shahzadi 2011 [30]
200	po (tab), sd	126.94	143.96	0.88	2.18	2.56	0.85	Saint-Salvi 1987 [31]
200	po (tab), sd	82.24	96.00	0.86	2.17	2.47	0.88	Wada 1978 [22]
400	po (tab, fed), sd	234.54	276.37	0.85	5.44	5.12	1.06	Barzaghi 1987 [32]
400	po (tab, fed), sd	200.37	228.97	0.88	5.20	4.87	1.07	Bianchetti 1987 [33]
400	po (tab), sd	206.67	212.95	0.97	3.72	3.34	1.11	Faigle 1975 [8]
400	po (tab), sd	198.00	198.57	1.00	3.45	3.34	1.04	Faigle 1975 [8]
400	po (tab), sd	226.83	202.93	1.12	4.10	3.73	1.10	Kovacevic 2009 [34]
400	po (tab), sd	146.33	165.79	0.88	4.12	4.94	0.83	Morselli 1975 [35]
400	po (tab), sd	205.58	227.06	0.91	4.33	4.96	0.87	Pynnoenen 1977 [36]
400	po (tab), sd	207.00	168.63	1.23	4.42	3.54	1.25	Strandjord 1975 [37]
400	po (tab), sd	173.19	231.79	0.75	3.39	4.32	0.78	Wong 1983 [38]
420	po (tab), sd	211.66	216.88	0.98	4.48	4.64	0.97	Levy 1975 [15]
420	po (tab, fed), sd	221.80	233.35	0.95	5.74	5.69	1.01	Levy 1975 [15]
600	po (tab), sd	327.24	200.72	1.63	5.13	3.53	1.46	Dalton 1985 [39]
600	po (tab), sd	351.54	315.78	1.11	5.36	4.49	1.20	Dalton 1985a [40]
600	po (tab), sd	329.88	280.14	1.18	5.83	4.42	1.32	Gerardin 1976 [23]
800	po (tab, fed), sd	436.96	510.2	0.86	11.10	9.69	1.15	Cotter 1977 [41]
100/200/400	po (tab), bid/qd	155.41	142.38	1.09	7.42	7.09	1.05	Burstein 2000 [42]
100/200/400	po (tab), bid/qd	155.17	137.49	1.13	7.42	7.17	1.04	Moller 2001 [43]
200	po (tab), bid/tid	320.59	276.79	1.16	8.74	7.40	1.18	Eichelbaum 1975 [26]
200	po (tab), bid/tid	247.34	191.72	1.29	7.17	5.77	1.24	Eichelbaum 1975 [26]
200	po (tab), qd	94.53	86.57	1.09	1.90	1.83	1.04	Gerardin 1976 [23]
200	po (tab), qd	193.6	157.84	1.23	4.25	3.61	1.18	Gerardin 1976 [23]

bid: twice daily, cap: capsule, D: day,. GMFE: geometric mean fold error, iv: intravenous, po: oral, qd: once daily, sd: single dose, sol: solution, susp: suspension, tab: tablet, tid: three times daily, XR: extended release

Table S4: Predicted and observed AUC_{last} and C_{max} values with geometric mean fold errors of carbamazepine and carbamazepine-10,11-epoxide *(continued)*

		AUC_{last} [µg*h/ml]			C_{max} [µg/ml]			
Dose [mg]	**Route**	**Pred**	**Obs**	**Pred/Obs**	**Pred**	**Obs**	**Pred/Obs**	**Reference**
200/400	po (tab), bid/qd	154.51	142.44	1.08	7.35	7.47	0.98	Ji 2008 [44]
357	po (tab), qd	165.9	150.75	1.10	7.76	7.13	1.09	Miles 1989 [45]
600	po (tab), sd (D1)	330.92	341.99	0.97	6.66	5.64	1.18	Bernus 1994 [46]
600	po (tab), sd (D5)	346.93	350.82	0.99	6.79	5.59	1.22	Bernus 1994 [46]
400	po (tab XR), sd	181.03	177.3	1.02	3.00	2.63	1.14	Graf 1990 [47]
400	po (tab XR), sd	196.87	233.60	0.84	2.73	2.22	1.23	Licht 2005 [48]
400	po (tab XR), sd	154.75	167.70	0.92	2.89	3.21	0.90	Kovacevic 2009 [34]
400	po (tab XR, fed), sd	246.84	335.01	0.74	4.31	4.07	1.06	Kshirsagar 2014 [49]
600	po (tab XR), sd	291.55	288.8	1.01	4.07	3.55	1.15	Licht 2005 [48]
400	po (tab XR), bid	132.14	151.81	0.87	11.33	13.49	0.84	Stevens 1998 [50]
300	po (cap XR), sd	173.88	161.97	1.07	2.56	1.71	1.49	Gande 2009 [51]
400	po (cap XR), sd	225.08	225.12	1.00	3.02	3.07	0.98	McLean 2001 [16]
400	po (cap XR, fed), sd	236.09	249.01	0.95	4.27	4.09	1.05	McLean 2001 [16]
400	po (cap XR), bid	146.45	145.39	1.01	12.63	12.82	0.98	Stevens 1998 [50]
mean GMFE (range)				**1.20 (1.00-3.33)**			**1.24 (1.00-4.72)**	
				58/59 with GMFE ≤ 2			**58/59 with GMFE ≤ 2**	
Carbamazepine-10,11-epoxide								
200	po (tab), sd	14.43	10.72	1.35	0.23	0.16	1.37	Bedada 2015 [24]
200	po (tab), sd	14.83	11.32	1.31	0.23	0.17	1.31	Bedada 2016 [25]
200	po (tab), sd	9.89	4.97	1.99	0.19	0.09	2.12	Eichelbaum 1975 [26]
200	po (tab), sd	15.61	30.07	0.52	0.20	0.36	0.56	Kim 2005 [27]
600	po (tab), sd	39.26	16.11	2.44	0.57	0.28	2.05	Dalton 1985 [39]
600	po (tab), sd	42.57	19.85	2.14	0.58	0.27	2.18	Dalton 1985a [40]
400	po (tab, fed), sd	27.88	12.63	2.21	0.50	0.19	2.60	Barzaghi 1987 [32]
400	po (tab, fed), sd	23.76	10.54	2.25	0.49	0.21	2.35	Bianchetti 1987 [33]
400	po (tab), sd	23.67	26.17	0.90	0.39	0.38	1.02	Faigle 1975 [8]
400	po (tab), sd	23.63	25.20	0.94	0.38	0.42	0.89	Faigle 1975 [8]
100/200/400	po (tab), bid/qd	23.67	37.37	0.63	1.08	1.77	0.61	Burstein 2000 [42]
100/200/400	po (tab), bid/qd	23.62	12.51	1.89	1.08	0.68	1.59	Moller 2001 [43]
200	po (tab), bid/tid	222.76	147.11	1.51	1.51	1.09	1.38	Eichelbaum 1975 [26]

bid: twice daily, cap: capsule, D: day,. GMFE: geometric mean fold error, iv: intravenous, po: oral, qd: once daily, sd: single dose, sol: solution, susp: suspension, tab: tablet, tid: three times daily, XR: extended release

Table S4: Predicted and observed AUC_{last} and C_{max} values with geometric mean fold errors of carbamazepine and carbamazepine-10,11-epoxide *(continued)*

		AUC_{last} [µg*h/ml]			C_{max} [µg/ml]			
Dose [mg]	**Route**	**Pred**	**Obs**	**Pred/Obs**	**Pred**	**Obs**	**Pred/Obs**	**Reference**
200	po (tab), bid/tid	49.65	21.85	2.27	1.45	0.61	2.37	Eichelbaum 1975 [26]
200/ 400	po (tab), bid/qd	23.63	19.96	1.18	1.07	1.00	1.07	Ji 2008 [44]
357	po (tab), md	24.12	26.72	0.90	1.08	1.20	0.90	Miles 1989 [45]
600	po (tab), sd (D1)	40.6	24.41	1.66	0.73	0.41	1.79	Bernus 1994 [46]
600	po (tab), sd (D5)	43.02	26.72	1.61	0.80	0.44	1.81	Bernus 1994 [46]
400	po (tab XR), sd	24.15	11.68	2.07	0.32	0.12	2.73	Licht 2005 [48]
400	po (tab XR), bid	20.33	19.77	1.03	1.72	1.71	1.01	Stevens 1998 [50]
300	po (cap XR), sd	21.71	8.75	2.48	0.29	0.08	3.47	Gande 2009 [51]
400	po (cap XR), sd	16.44	9.18	1.79	0.34	0.19	1.78	McLean 2001 [16]
400	po (cap XR, fed), sd	19.43	14.85	1.31	0.42	0.29	1.46	McLean 2001 [16]
400	po (cap XR), bid	22.76	19.71	1.15	1.93	1.69	1.14	Stevens 1998 [50]
mean GMFE (range)				**1.68 (1.03-2.48)**			**1.76 (1.01-3.47)**	
				17/24 with GMFE ≤ 2			**16/24 with GMFE ≤ 2**	

bid: twice daily, cap: capsule, D: day,. GMFE: geometric mean fold error, iv: intravenous, po: oral, qd: once daily, sd: single dose, sol: solution, susp: suspension, tab: tablet, tid: three times daily, XR: extended release

2.5.5 Sensitivity analysis

Sensitivity of the final carbamazepine-10,11-epoxide PBPK model to single parameters (local sensitivity analysis) was calculated as the relative change of the predicted carbamazepine-10,11-epoxide $AUC_{0\text{-}24}$ following a single dose of 100 mg carbamazepine-10,11-epoxide as tablet. Sensitivity analysis was carried out using a relative parameter perturbation of 1000% (variation range 10.0, maximum number of 9 steps). Parameters were included into the analysis if they were optimized (lipophilicity, EPHX1 clearance, GFR fraction, intestinal permeability, dissolution shape, dissolution time) or if they might have a strong impact due to calculation methods used in the model (solubility, fraction unbound in plasma). Results of the sensitivity analysis are illustrated in Figure S12. The carbamazepine-10,11-epoxide model is mainly sensitive to the value fraction unbound in plasma (literature), and to the EPHX1 clearance (optimized).

Sensitivity of the carbamazepine parent-metabolite PBPK model to single parameters (local sensitivity analysis) was calculated as the relative change of the predicted carbamazepine and carbamazepine-10,11-epoxide AUC at steady-state (AUC_{ss}) of 400 mg carbamazepine three times daily as immediate release tablet. Sensitivity analysis was carried out using a relative parameter perturbation of 1000% (variation range 10.0, maximum number of 9 steps). Parameters were included into the analysis if they were optimized (lipophilicity, CYP3A4 k_{cat} values, carbamazepine hepatic clearance, EPHX1 clearance, GFR fraction, CYP3A4, CYP2B6 and EPHX1 E_{max} values, intestinal permeability (carbamazepine-10,11-epoxide), dissolution shape, dissolution time), if they are associated with optimized parameters (CYP3A4, CYP2C8, CYP2B6 and UGT2B7 K_m values, CYP2C8, CYP2B6 and UGT2B7 k_{cat} values, CYP3A4, CYP2B6 and EPHX1 EC_{50} values) or if they might have a strong impact due to calculation methods used in the model (solubility, fraction unbound in plasma, intestinal permeability (carbamazepine)). Results of the sensitivity analysis are illustrated in Figure S13. Sensitivity analysis of the carbamazepine parent-metabolite model revealed that the carbamazepine AUC_{ss} is mainly sensitive to the carbamazepine fraction unbound in plasma (literature), while the carbamazepine-10,11-epoxide AUC_{ss} is sensitive to carbamazepine-10,11-epoxide fraction unbound in plasma (literature), EPHX1 clearance of carbamazepine-10,11-epoxide (optimized), K_m and k_{cat} of carbamazepine CYP3A4 metabolism to carbamazepine-10,11-epoxide (literature and optimized, respectively) and carbamazepine EPHX1 E_{max} (optimized).

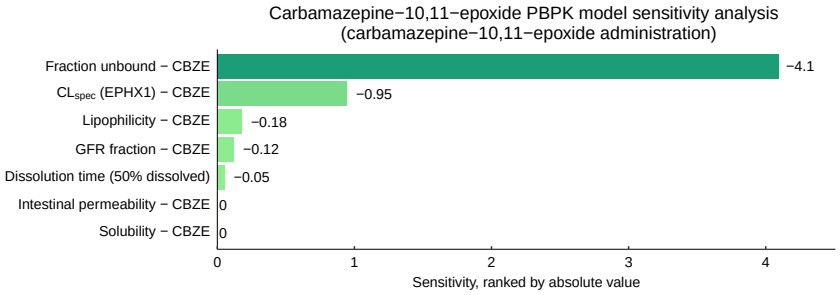

Figure S12: Carbamazepine-10,11-epoxide PBPK model sensitivity analysis. Sensitivity of the carbamazepine-10,11-epoxide model to single parameters, calculated as change of the simulated carbamazepine-10,11-epoxide $AUC_{0\text{-}24}$ following a single dose of 100 mg carbamazepine-10,11-epoxide as tablet. CBZE: carbamazepine-10,11-epoxide, CL_{spec}: specific clearance, EPHX1: epoxide hydroxylase 1, GFR: glomerular filtration rate

(a)

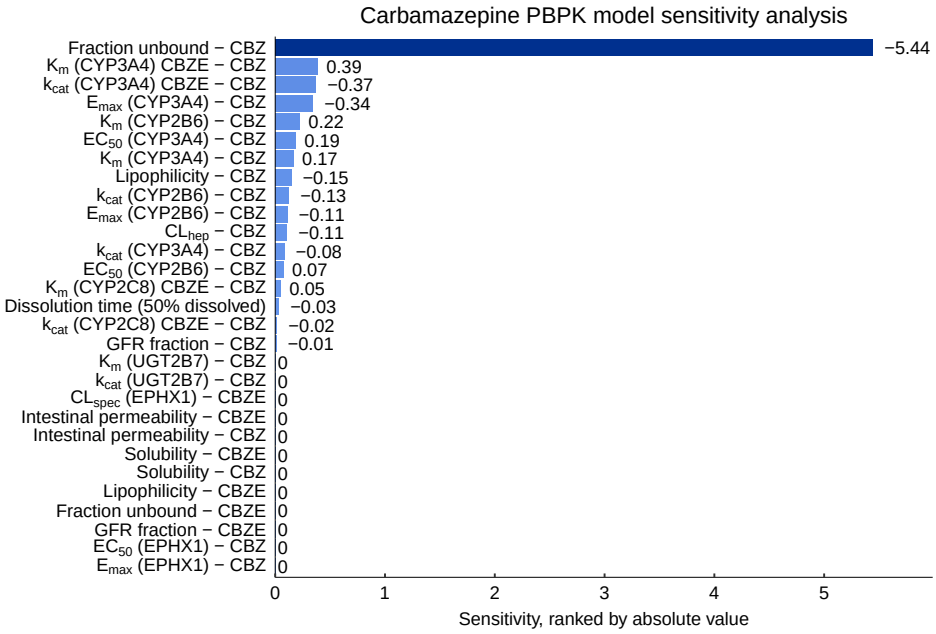

(b)

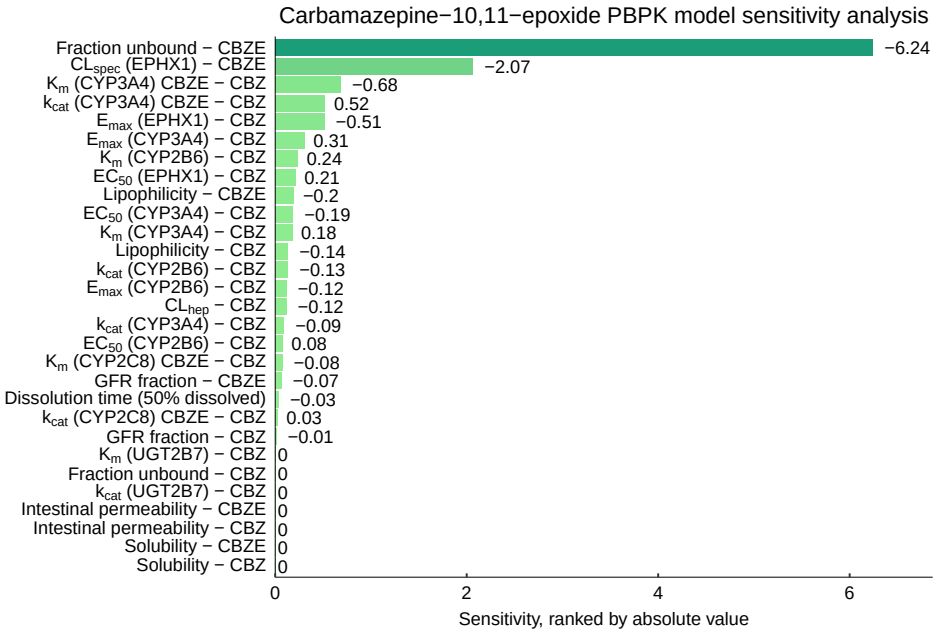

Figure S13: Carbamazepine parent-metabolite PBPK model sensitivity analysis. Sensitivity of the carbamazepine parent-metabolite PBPK model to single parameters, calculated as change of the simulated (a) carbamazepine AUC_{ss} and (b) carbamazepine-10,11-epoxide AUC_{ss} of 400 mg carbamazepine three times daily as immediate release tablet. CBZ: carbamazepine, CBZE: carbamazepine-10,11-epoxide, CL_{hep}: hepatic clearance, CL_{spec}: specific clearance, CYP: cytochrome P450, EC_{50}: half-maximal effective concentration, E_{max}: maximum effect, EPHX1: epoxide hydroxylase 1, GFR: glomerular filtration rate, k_{cat}: catalytic rate constant, K_m: Michaelis-Menten constant, UGT: UDP-glucuronosyltransferase

3 Efavirenz

3.1 PBPK model building

The antiretroviral drug efavirenz is a non-nucleoside reverse transcriptase inhibitor and used for the treatment of human immunodeficiency virus infections [82]. Its major metabolizing enzyme is CYP2B6, but CYP3A4, CYP3A5, CYP1A2 and CYP2A6 are also involved in efavienz metabolism [83, 84]. By activation of nuclear receptors (PXR and CAR), efavirenz increases the expression of CYP2B6 and CYP3A4. As a consequence, efavirenz induces its own metabolism and the metabolism of other drugs after multiple-dose administration [66, 85, 86]. The drug is classified by the FDA as moderate inducer (50-80% AUC decrease of the victim drug) of CYP2B6 and CYP3A4, and as moderately sensitive substrate of CYP2B6 [10].

CYP2B6 polymorphisms are a major determinant of clinical efavirenz disposition. CYP2B6 is highly polymorphic with more than 30 known alleles. The most frequent decreased function allele is CYP2B6*6. Heterozygosity (CYP2B6*1|*6, intermediate metabolizer (IM)) and homozygosity (CYP2B6*6|*6, poor metabolizer (PM)) for this allele are associated with elevated efavirenz plasma levels caused by decreased efavirenz metabolism. Little to no auto-induction was observed for CYP2B6*6|*6 [86].

The efavirenz PBPK model was downloaded from the Open Systems Pharmacology (OSP) GitHub model repository (https://github.com/Open-Systems-Pharmacology/Efavirenz-Model). This model includes (1) metabolism by CYP2B6 (2) metabolism via CYP1A2, CYP2A6, CYP3A4 and CYP3A5 and (3) glomerular filtration [87]. All metabolic processes are illustrated in Figure S14.

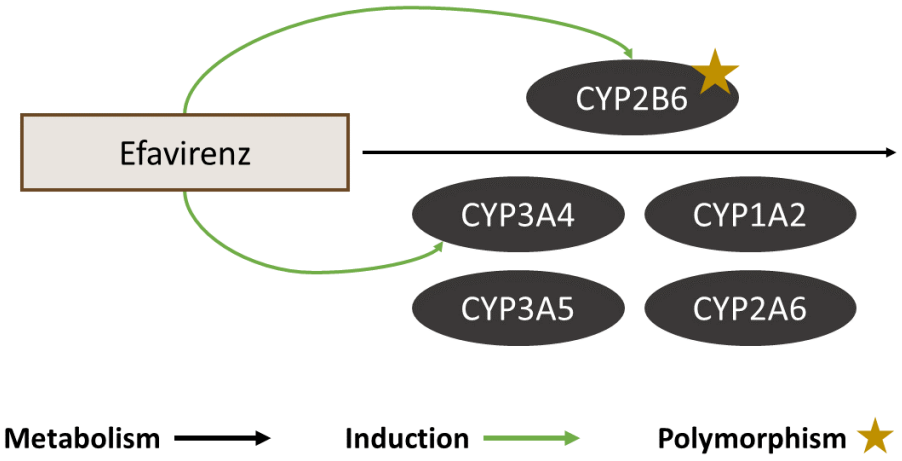

Figure S14: Metabolic pathways of efavirenz. Efavirenz is metabolized by CYP1A2, CYP2A6, CYP3A4, CYP3A5 and CYP2B6 (black arrow), while the latter is the main enzyme catalyzing efavirenz metabolism. Therefore, polymorphisms of CYP2B6 are a major determinant of efavirenz pharmacokinetics. Furthermore, efavirenz induces its own metabolism by induction of CYP2B6 and CYP3A4 (green arrows)

Prior to predicting the carbamazepine-efavirenz interaction, the DDI potential of efavirenz as a CYP2B6 substrate and inducer was evauated, using data of clinical DDI studies of efavirenz with rifampin, voriconazole (perpetrators) and bupropion (victim) as interaction partners. Based on this evaluation, the efavirenz model was updated using plasma concentration-time profiles of 13 publications, covering a dosing range of 50-600 mg administered in single- or multiple-dose regimens. All studies used are listed in Table S5.

All metabolic and inductive processes were retained, but literature values for Michaelis-Menten constants - used to describe enzymatic metabolism - and EC_{50} values - used to describe enzyme induction - were corrected for unspecific binding of efavirenz in microsomal preparations ($fu_{incubation}$). If no $fu_{incubation}$ was reported for the in vitro assay, it was calculated according to Equation S12 [55], using logP and microsomal protein concentration (C_{mic}). If no microsomal protein concentration was reported for the in vitro assay, a low protein concentration of 0.25 mg/ml was assumed.

$$fu_{incubation} = \frac{1}{C_{mic} * 10^{0.56 * logP - 1.41} + 1} \tag{S12}$$

where C_{mic} = microsomal protein concentration [mg/ml] and $logP$ = lipophilicity of the molecule.

Furthermore, a competitive inhibition of CYP2B6 and CYP3A4 was implemented in the model, according to literature [74, 88], using in vitro values that were also corrected for $fu_{incubation}$. Drug-dependent parameters of efavirenz used in the model, compared to literature values and the values used in the original model, are listed in Table S6.

The good descriptive and predictive performance of the updated efavirenz model is demonstrated in linear (Figure S15) as well as semi-logarithmic plots (Figure S16) of predicted compared to observed plasma concentration-time profiles of all clinical studies. Goodness-of-fit plots comparing all predicted to their corresponding observed plasma concentrations are presented in Figure S17 and corresponding MRD values for each study are given in Table S7. Furthermore, the correlation of predicted to observed AUC_{last} and C_{max} values is shown in Figure S18 and Table S8 lists the corresponding predicted and observed AUC_{last} and C_{max} values of all clinical studies including calculated GMFE values.

3.2 Efavirenz clinical studies

Table S5: Clinical studies used for the update of the efavirenz PBPK model

Dose [mg]	Route	Dataset	n	Healthy [%]	Females [%]	Age[a] [years]	Weight[a] [kg]	Height[a] [cm]	CYP2B6 genotype	Reference
50	po (tab), sd	training	16	100	0	23.8 (20-35)	23.5 (20.6-27.5)[b]	-	56% IM[c]	Derungs 2015 [89]
200	po (-), qd	training	8	100	4	29.9 (19-49) ± 8.7	-	-	-	Mouly 2002 [90]
400	po (cap), qd	test	34	100	0	(20-49)	(59-95)	-	-	Liu 2008 [91]
400	po (-), qd	training	8	100	4	29.9 (19-49) ± 8.7	-	-	-	Mouly 2002 [90]
600	po (-), sd	test	20	100	50	27.5 (19-44)	72.9 (57-88)	-	40% EM[c] 45% IM[c] 15% PM[c]	Cho 2016 [92]
600	po (-), sd	test	5	100	-	-	-	-	-	Ogburn 2010 [84]
600	po (-), sd	training	8	100	50	-	-	-	EM[c]	Xu 2013 [93]
600	po (-), sd	test	9	100	50	-	-	-	IM[c]	Xu 2013 [93]
600	po (-), sd	test	3	100	50	-	-	-	PM[c]	Xu 2013 [93]
600	po (-), qd	training	18	100	8	44[e] (19-62)	82.9[e] (57-119)	-	EM[d]	Dooley 2012 [94]
600	po (-), qd	training	12	100	8	44[e] (19-62)	82.9[e] (57-119)	-	IM[d]	Dooley 2012 [94]
600	po (-), qd	training	3	100	8	44[e] (19-62)	82.9[e] (57-119)	-	PM[d]	Dooley 2012 [94]
600	po (-), qd	test	16	100	0	29.6 (20-42)	24.3 (19-30)[b]	-	-	Damle 2008 [95]
600	po (tab), qd	training	21	100	4	24.5[e] (20-52)	26.3[e] (20.4-31.5)[b]	-	-	Garg 2013 [96]
600	po (-), qd	test	12	100	17	36 (24–53)	79.5 (64.7–92.5)	176 (165–192)	-	Huang 2012 [97]
600	po (-), qd	test	36	100	31	(20-45)	(54-92)	-	-	Ji 2008 [44]
600	po (-), qd	test	12	100	50	22 (18-29)	71 (57-96)	-	-	Kharasch 2012 [98]
600	po (-), qd	test	11	100	55	42.6 ± 7.4	76.9 ± 18.9	-	18% EM 55% IM 27% PM	Kwara 2011 [99]
600	po (tab), qd	test	18	100	29	43 (19-57)	-	-	-	Malvestutto 2014 [100]

-: not given, cap: capsule CYP2B6: cytochrome P450 2B6, EM: extensive metabolizer, IM: intermediate metabolizer, PM: poor metabolizer, po: oral, qd: once daily, sd: single dose, tab: tablet

[a] mean (range) ± standard deviation

[b] body mass index [kg/m^2]

[c] subjects were tested for the diminished-function allele CYP2B6*6

[d] subjects were tested for the diminished-function alleles CYP2B6*6 and CYP2B6*18

[e] median values

Table S5: Clinical studies used for the revision of the efavirenz PBPK model *(continued)*

Dose [mg]	Route	Dataset	n	Healthy [%]	Females [%]	Age[a] [years]	Weight[a] [kg]	Height[a] [cm]	CYP2B6 genotype	Reference
600	po (-), qd	test	12	100	41	(24-49)	(50-83)	-	-	Soon 2010 [101]

-: not given, cap: capsule CYP2B6: cytochrome P450 2B6, EM: extensive metabolizer, IM: intermediate metabolizer, PM: poor metabolizer, po: oral, qd: once daily, sd: single dose, tab: tablet

[a] mean (range) ± standard deviation

[b] body mass index [kg/m^2]

[c] subjects were tested for the diminished-function allele CYP2B6*6

[d] subjects were tested for the diminished-function alleles CYP2B6*6 and CYP2B6*18

[e] median values

3.3 Efavirenz drug-dependent parameters

Table S6: Drug-dependent parameters of the efavirenz PBPK model

Parameter	Unit	Updated model	Original model[a]	Literature[a]	Reference	Description
MW	g/mol	315.68 (Lit)	315.68 (Lit)	315.68	[102]	Molecular weight
logP	log Units	3.87 (Fit)	3.44 (Fit)	2.07, 4.6 (logP)	[102, 103]	Lipophilicity
				5.1 (logD)	[104]	
Solubility	mg/ml	0.10 (pH 7.0) (Fit)	0.039 (pH 0) (Fit)	0.011 (6.4), 0.06 (FaSSIF)	[105, 106]	Solubility
fu	%	0.60 (Lit)	0.60 (Lit)	0.60 (0.4-1.5)	[103]	Fraction unbound in plasma
pKa	-	10.1 (Lit)	10.1 (Lit)	10.1	[107]	Acid dissociation constant
K_m (CYP2B6)	μM	1.54[b] (Lit)	6.4 (Lit)	6.4	[83]	CYP2B6 Michaelis-Menten constant
k_{cat} (CYP2B6*1|*1)	1/min	2.84 (Fit)	1.60 (Fit)	-	-	CYP2B6 catalytic rate constant for *1|*1 (EM) genotype
k_{cat} (CYP2B6*1|*6)	1/min	2.27 (Fit)	2.27 (Fit)	-	-	CYP2B6 catalytic rate constant for *1|*6 (IM) genotype
k_{cat} (CYP2B6*6|*6)	1/min	1.45 (Fit)	1.45 (Fit)	-	-	CYP2B6 catalytic rate constant for *6|*6 (PM) genotype
K_m (CYP1A2)	μM	1.99[b] (Lit)	8.3 (Lit)	8.3	[83]	CYP1A2 Michaelis-Menten constant
k_{cat} (CYP1A2)	1/min	0.24 (Fit)	0.191 (Fit)	-	-	CYP1A2 catalytic rate constant
K_m (CYP2A6)	μM	7.70 (Lit)	7.70 (Lit)	7.70	[83]	CYP2A6 Michaelis-Menten constant
k_{cat} (CYP2A6)	1/min	0.28 (Fit)	0.318 (Fit)	-	-	CYP2A6 catalytic rate constant
K_m (CYP3A4)	μM	5.64[b] (Lit)	23.5 (Lit)	23.5	[83]	CYP3A4 Michaelis-Menten constant
k_{cat} (CYP3A4)	1/min	0.03 (Fit)	0.05 (Fit)	-	-	CYP3A4 catalytic rate constant
K_m (CYP3A5)	μM	4.58[b] (Lit)	19.1 (Lit)	19.1	[83]	CYP3A5 Michaelis-Menten constant
k_{cat} (CYP3A5)	1/min	0.11 (Fit)	0.19 (Fit)	-	-	CYP3A5 catalytic rate constant
GFR fraction	-	1	1	-	-	Fraction of filtered drug in the urine
EC_{50} (CYP2B6)	μM	0.23[c] (Lit)	0.01 (Fit)	1.62, 1.20	[74, 85]	Concentration for half-maximal induction
E_{max} (CYP2B6)	-	8.13 (Fit)	5.20 (Fit)	6.20, 10.8	[74, 85]	Maximum induction effect
EC_{50} (CYP3A4)	μM	0.23[c] (Asm)	0.07 (Fit)	4.59, 3.80, 2.18, 12.5	[66, 74, 85]	Concentration for half-maximal induction
E_{max} (CYP3A4)	-	12.00 (Fit)	5.21 (Fit)	7.27, 3.15, 19.6	[66, 74, 85]	Maximum induction effect
K_i (CYP2B6)	µmol/l	0.40[b] (Lit)	-	2.7, 2.96, 0.39, 1.38	[74, 93]	Concentration for half-maximal inhibition
K_i (CYP3A4)	µmol/l	9.67[b] (Lit)	-	40.33	[74, 93]	Concentration for half-maximal inhibition

-: not given, asm: assumption, calc: calculated, CYP: cytochrome P450, EM: extensive metabolizer (wildtype), FaSSIF: fasted state simulated intestinal fluid, fit: optimized during parameter identification, GFR: glomerular filtration rate, IM: intermediate metabolizer, lit: literature, PM: poor metabolizer

[a] adopted from [87]

[b] $fu_{incubation}$ = 0.24 was applied to literature value [83], calculated according to [55]

[c] $fu_{incubation}$ = 0.14 was applied to literature value [74], calculated according to [55]

Table S6: Drug-dependent parameters of efavirenz *(continued)*

Parameter	Unit	Updated Model	Original Model[a]	Literature[a]	Reference	Description
Intestinal permeability	cm/min	4.46E-05 (Fit)	2.972E-5 (Fit)	-	-	Transcellular intestinal permeability
Partition coefficients	-	Diverse	Diverse	Schmitt	[108]	Cell to plasma partition coefficients
Cellular permeability	cm/min	1.04	0.39	PK-Sim Standard	[79]	Permeability into the cellular space
Tablet Weibull time	min	44.15 (Fit)	60 (Fit)	-	-	Dissolution time (50% dissolved)
Tablet Weibull shape	-	0.31 (Fit)	0.272 (Fit)	-	-	Dissolution profile shape

-: not given, asm: assumption, calc: calculated, CYP: cytochrome P450, EM: extensive metabolizer (wildtype), FaSSIF: fasted state simulated intestinal fluid, fit: optimized during parameter identification, GFR: glomerular filtration rate, IM: intermediate metabolizer, lit: literature, PM: poor metabolizer

[a] adopted from [87]

[b] $fu_{incubation}$ = 0.24 was applied to literature value [83], calculated according to [55]

[c] $fu_{incubation}$ = 0.14 was applied to literature value [74], calculated according to [55]

3.4 Profiles

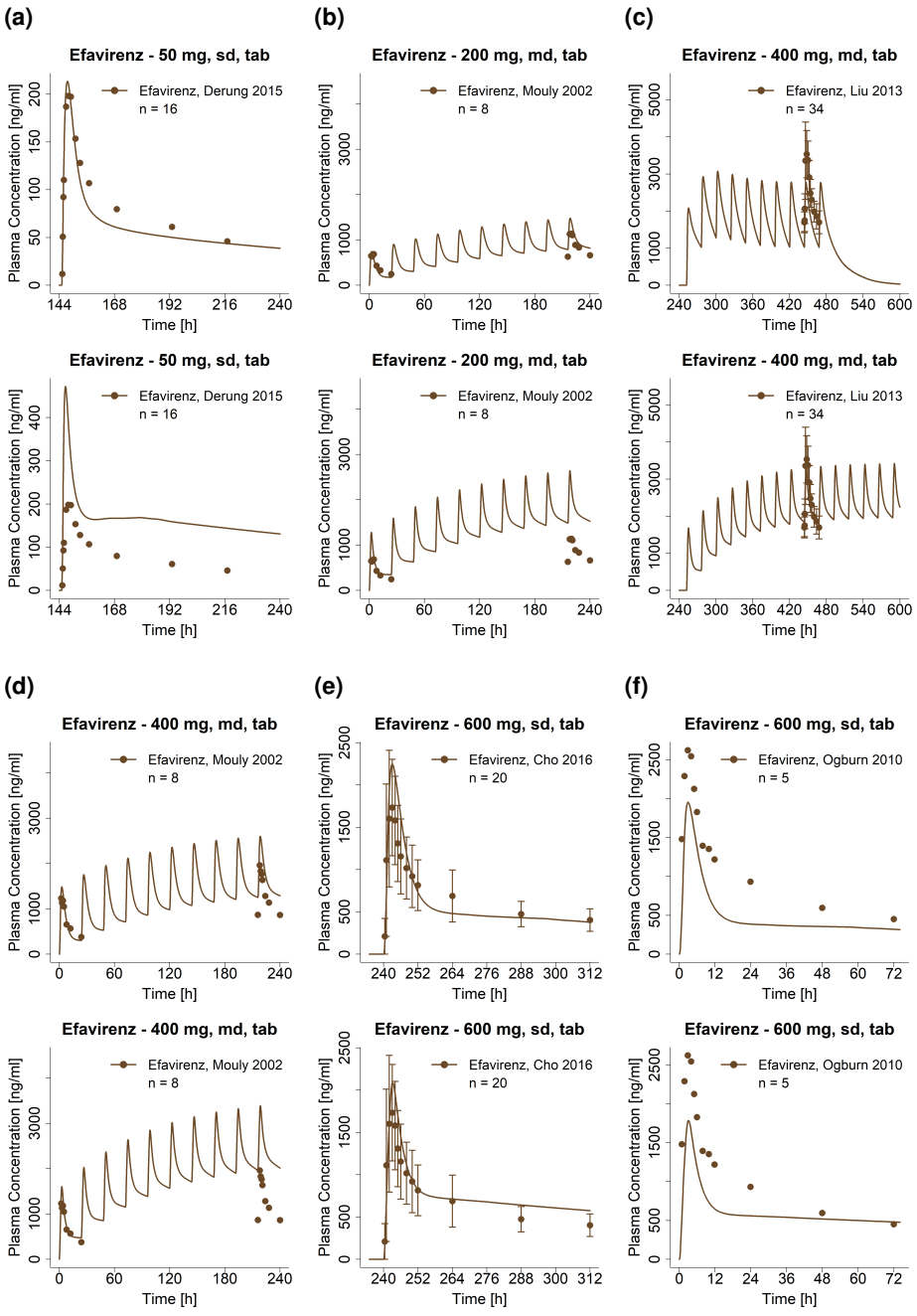

Figure S15: Predicted compared to observed efavirenz plasma concentration-time profiles (linear) predicted with the updated model (upper rows) or the original model (lower rows). Observed data are shown as dots ± standard deviation; model predictions are shown as solid lines. Details on dosing regimens, study populations and literature references are listed in Table S5.EM: extensive metabolizer, IM: intermediate metabolizer, md: multiple-dose, PM: poor metabolizer, tab: tablet, sd: single dose

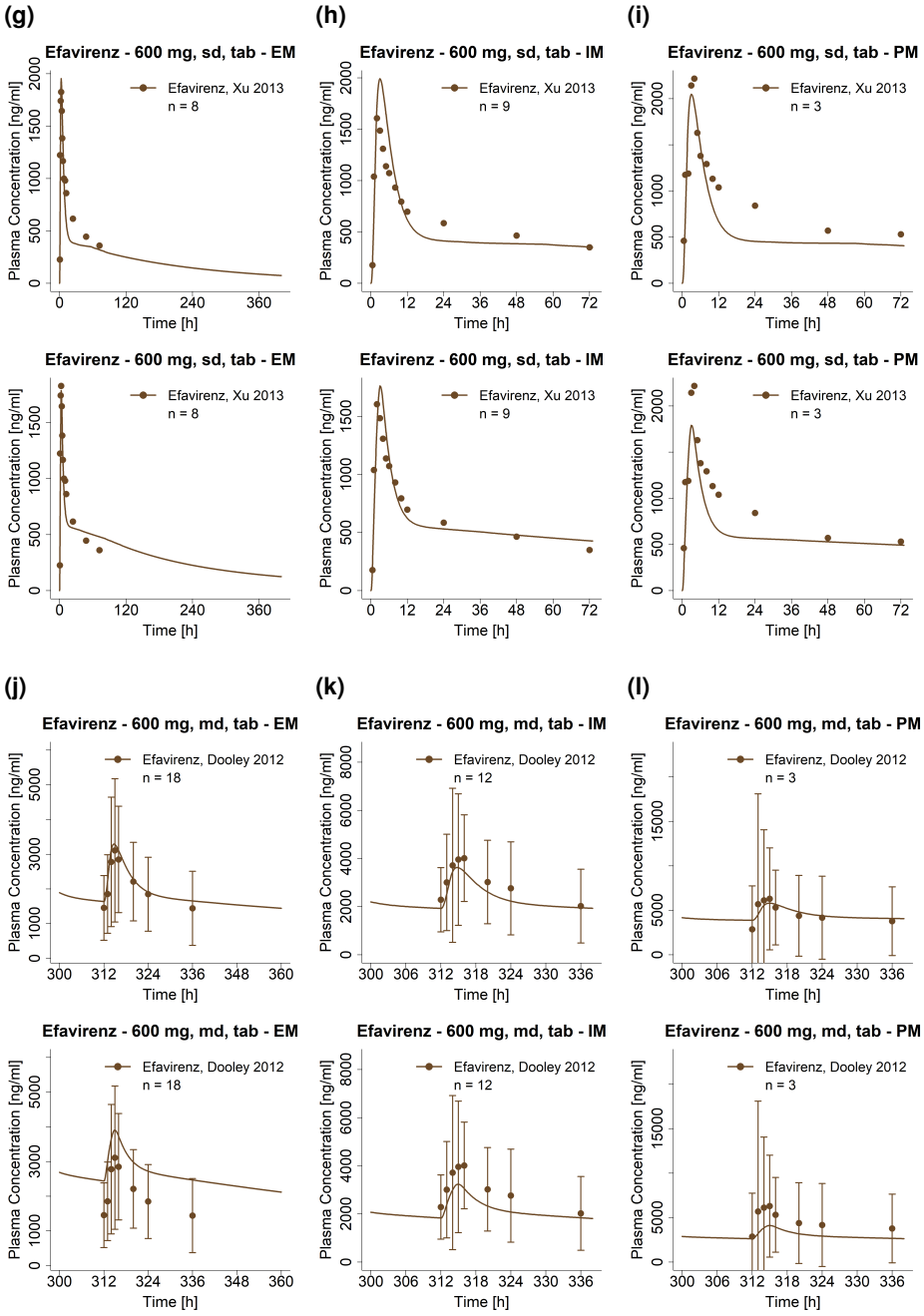

Figure S15: Predicted compared to observed efavirenz plasma concentration-time profiles (linear) predicted with the updated model (upper rows) or the original model (lower rows). Observed data are shown as dots ± standard deviation; model predictions are shown as solid lines. Details on dosing regimens, study populations and literature references are listed in Table S5. EM: extensive metabolizer, IM: intermediate metabolizer, md: multiple-dose, PM: poor metabolizer, tab: tablet, sd: single dose *(continued)*

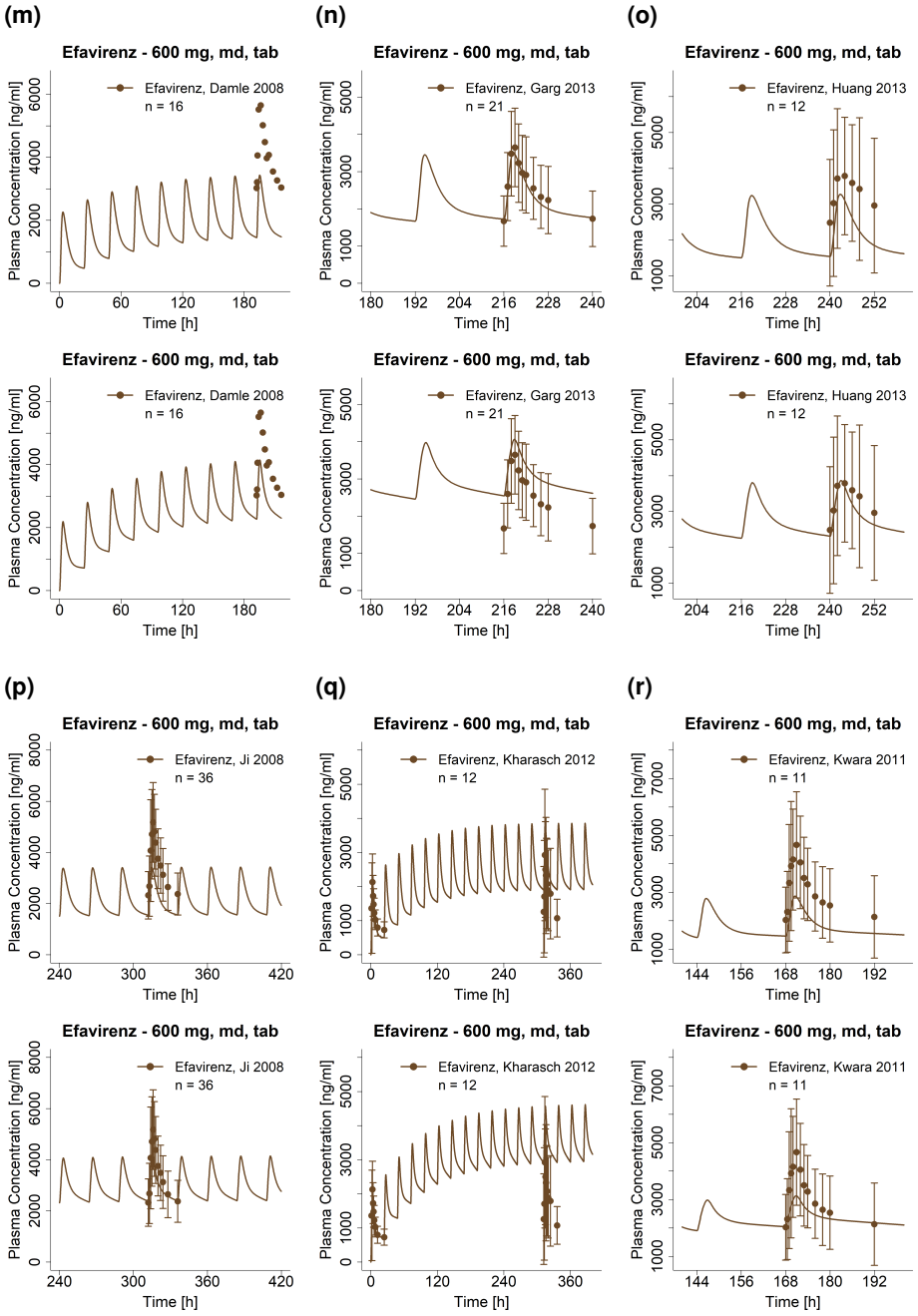

Figure S15: Predicted compared to observed efavirenz plasma concentration-time profiles (linear) predicted with the updated model (upper rows) or the original model (lower rows). Observed data are shown as dots ± standard deviation; model predictions are shown as solid lines. Details on dosing regimens, study populations and literature references are listed in Table S5. EM: extensive metabolizer, IM: intermediate metabolizer, md: multiple-dose, PM: poor metabolizer, tab: tablet, sd: single dose *(continued)*

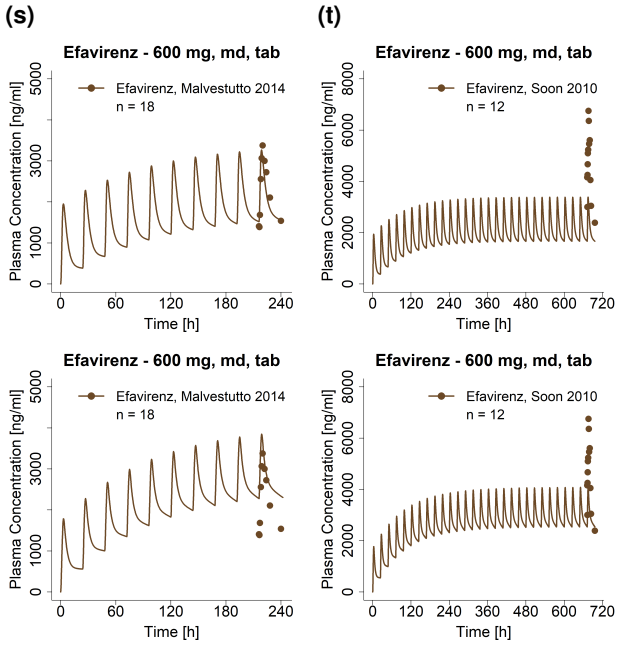

Figure S15: Predicted compared to observed efavirenz plasma concentration-time profiles (linear) predicted with the updated model (upper rows) or the original model (lower rows). Observed data are shown as dots ± standard deviation; model predictions are shown as solid lines. Details on dosing regimens, study populations and literature references are listed in Table S5. EM: extensive metabolizer, IM: intermediate metabolizer, md: multiple-dose, PM: poor metabolizer, tab: tablet, sd: single dose *(continued)*

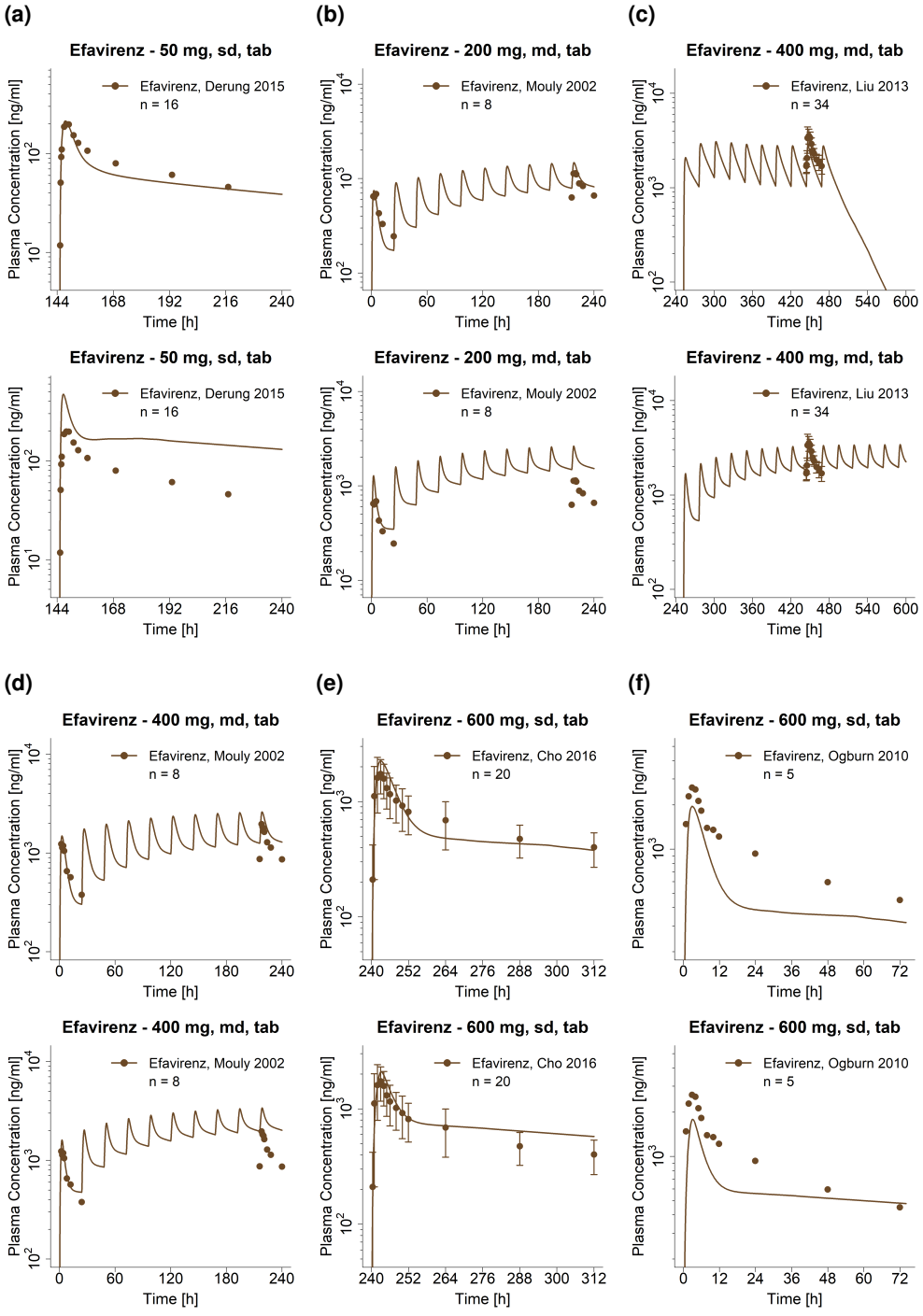

Figure S16: Predicted compared to observed efavirenz plasma concentration-time profiles (semi-logarithmic) predicted with the updated model (upper rows) or the original model (lower rows). Observed data are shown as dots ± standard deviation; model predictions are shown as solid lines. Details on dosing regimens, study populations and literature references are listed in Table S5. EM: extensive metabolizer, IM: intermediate metabolizer, md: multiple-dose, PM: poor metabolizer, tab: tablet, sd: single dose

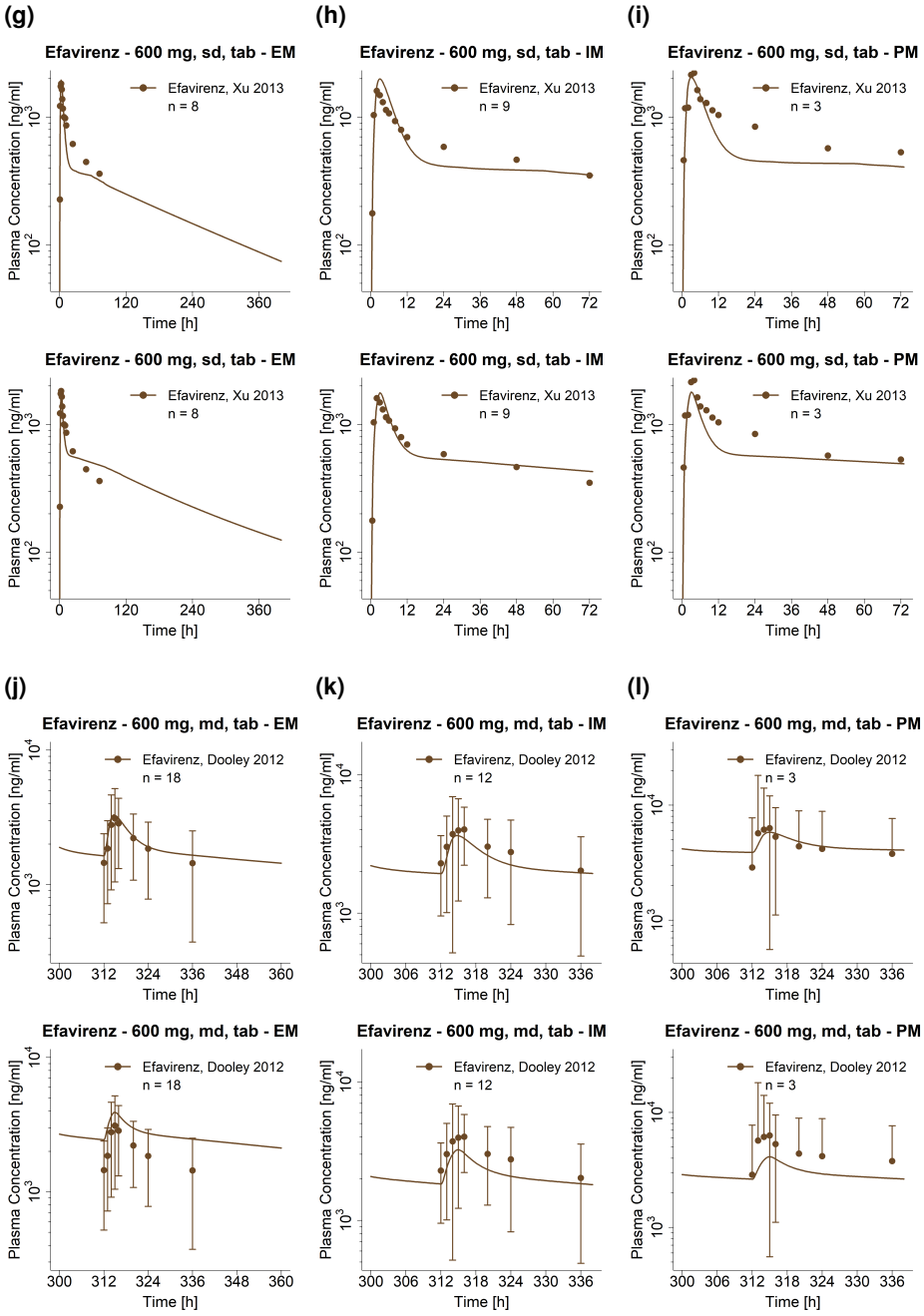

Figure S16: Predicted compared to observed efavirenz plasma concentration-time profiles (semi-logarithmic) predicted with the updated model (upper rows) or the original model (lower rows). Observed data are shown as dots ± standard deviation; model predictions are shown as solid lines. Details on dosing regimens, study populations and literature references are listed in Table S5. EM: extensive metabolizer, IM: intermediate metabolizer, md: multiple-dose, PM: poor metabolizer, tab: tablet, sd: single dose *(continued)*

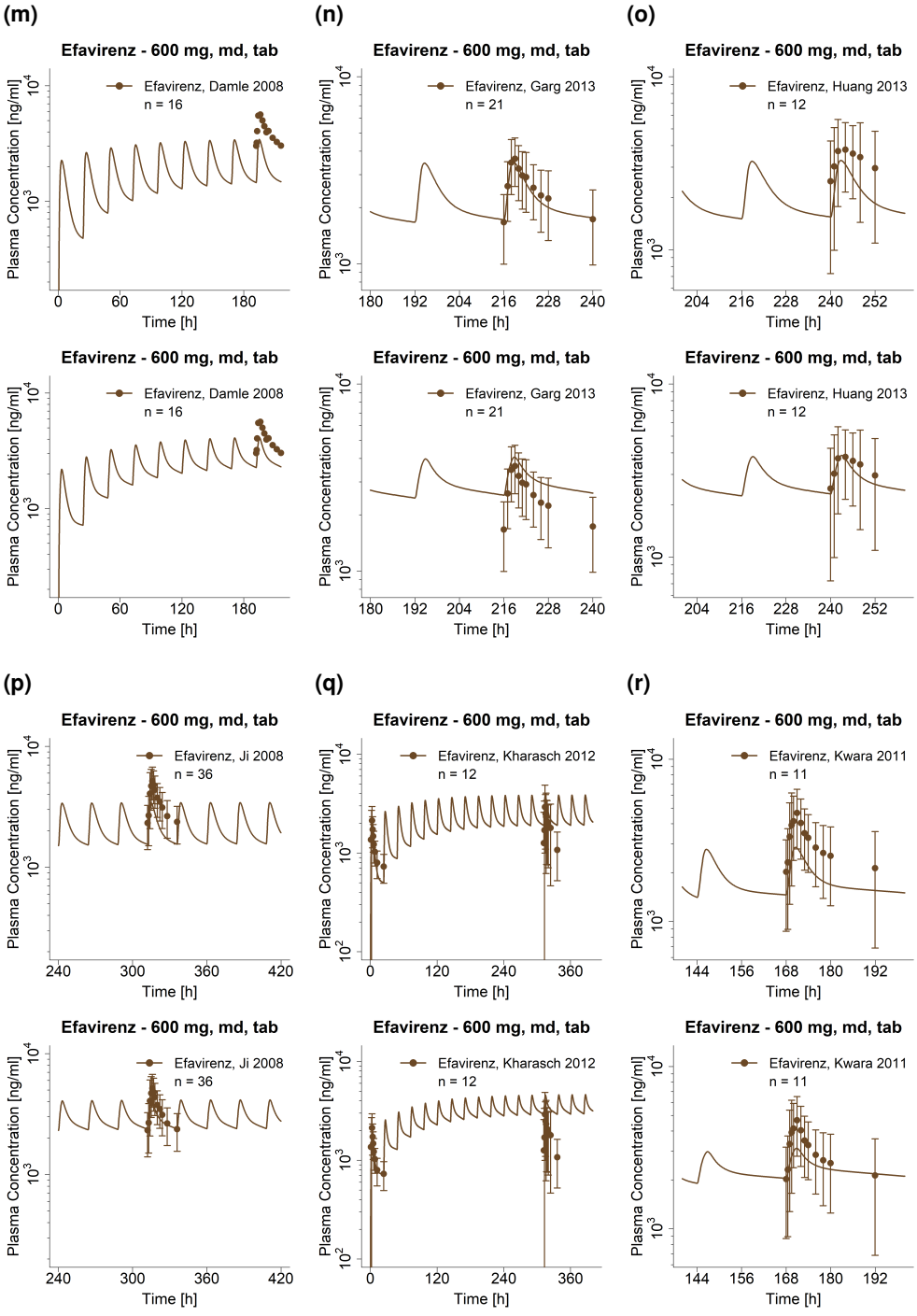

Figure S16: Predicted compared to observed efavirenz plasma concentration-time profiles (semi-logarithmic) predicted with the updated model (upper rows) or the original model (lower rows). Observed data are shown as dots ± standard deviation; model predictions are shown as solid lines. Details on dosing regimens, study populations and literature references are listed in Table S5. EM: extensive metabolizer, IM: intermediate metabolizer, md: multiple-dose, PM: poor metabolizer, tab: tablet, sd: single dose *(continued)*

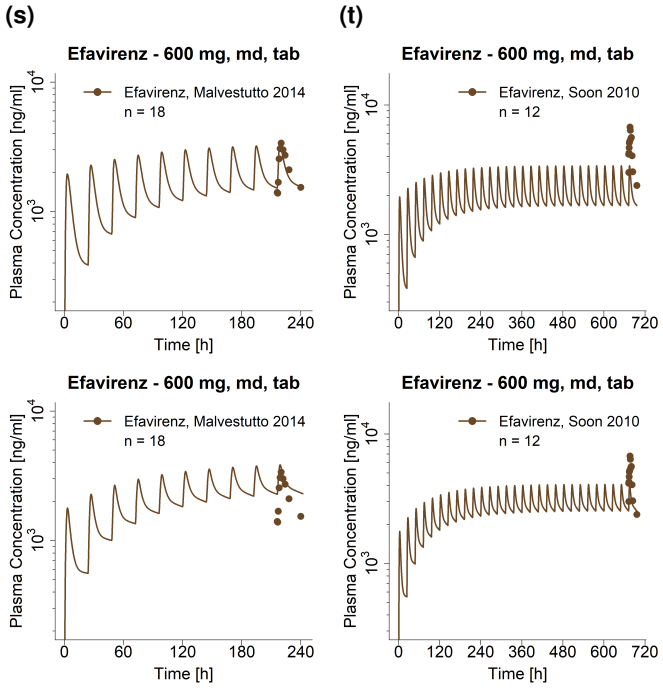

Figure S16: Predicted compared to observed efavirenz plasma concentration-time profiles (semi-logarithmic) predicted with the updated model (upper rows) or the original model (lower rows). Observed data are shown as dots ± standard deviation; model predictions are shown as solid lines. Details on dosing regimens, study populations and literature references are listed in Table S5. EM: extensive metabolizer, IM: intermediate metabolizer, md: multiple-dose, PM: poor metabolizer, tab: tablet, sd: single dose *(continued)*

3.5 Model evaluation

3.5.1 Plasma concentration goodness-of-fit plots

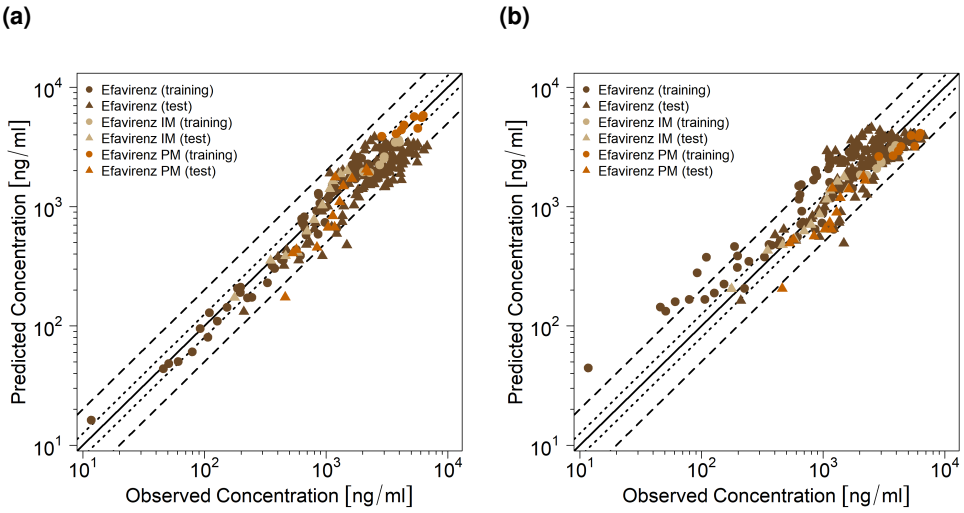

Figure S17: Predicted compared to observed efavirenz plasma concentrations of the training (triangles) and test (circles) datasets. (a) shows the updated model, (b) shows the original efavirenz model goodness-of-fit plot. The solid line marks the line of identity. Dotted lines indicate 1.25-fold, dashed lines indicate 2-fold deviation. IM: intermediate metabolizers (CYP2B6*1|*6), PM: poor metabolizers (CYP2B6*6|*6)

3.5.2 Mean relative deviation of predicted plasma concentrations

Table S7: Mean relative deviation values of predicted efavirenz plasma concentrations of the updated model in comparison to the original model

Route	Dose [mg]	MRD updated	MRD original	Reference
po, sd	50	1.19	2.42	Derungs 2015 [89]
po, qd (D1)	200	1.25	1.47	Mouly 2002 [90]
po, qd (D10)	200	1.23	2.14	Mouly 2002 [90]
po, qd	400	1.39	1.13	Liu 2013 [91]
po, qd (D1)	400	1.20	1.19	Mouly 2002 [90]
po, qd (D10)	400	1.39	1.94	Mouly 2002 [90]
po, sd	600	1.33	1.27	Cho 2016 [92]
po, sd	600	1.78	1.72	Ogburn 2010 [84]
po, sd	600	1.33	1.27	Xu 2013 (EM) [93]
po, sd	600	1.28	1.21	Xu 2013 (IM) [93]
po, sd	600	1.52	1.47	Xu 2013 (PM) [93]
po, qd	600	1.11	1.48	Dooley 2012 (EM) [94]
po, qd	600	1.15	1.26	Dooley 2012 (IM) [94]
po, qd	600	1.16	1.47	Dooley 2012 (PM) [94]
po, qd	600	1.96	1.40	Damle 2008 [95]
po, qd	600	1.06	1.28	Garg 2013 [96]
po, qd	600	1.44	1.09	Huang 2012 [97]
po, qd	600	1.51	1.18	Ji 2008 [44]
po, qd (D1)	600	1.30	1.22	Kharasch 2012 [98]
po, qd (D14)	600	1.48	1.99	Kharasch 2012 [98]
po, qd	600	1.51	1.26	Kwara 2011 [99]
po, qd	600	1.16	1.42	Malvestutto 2014 [100]
po, qd	600	1.89	1.46	Soon 2010 [101]
mean MRD (range)		**1.38 (1.06-1.96)**	**1.47 (1.09-2.42)**	
		23/23 with MRD $\leq$ 2	**21/23 with MRD $\leq$ 2**	

D: day, EM: extensive metabolizer, IM: intermediate metabolizer, MRD: mean relative deviation, po: oral, PM: poor metabolizer, qd: once daily, sd: single dose

3.5.3 AUC_{last} and C_{max} goodness-of-fit plots

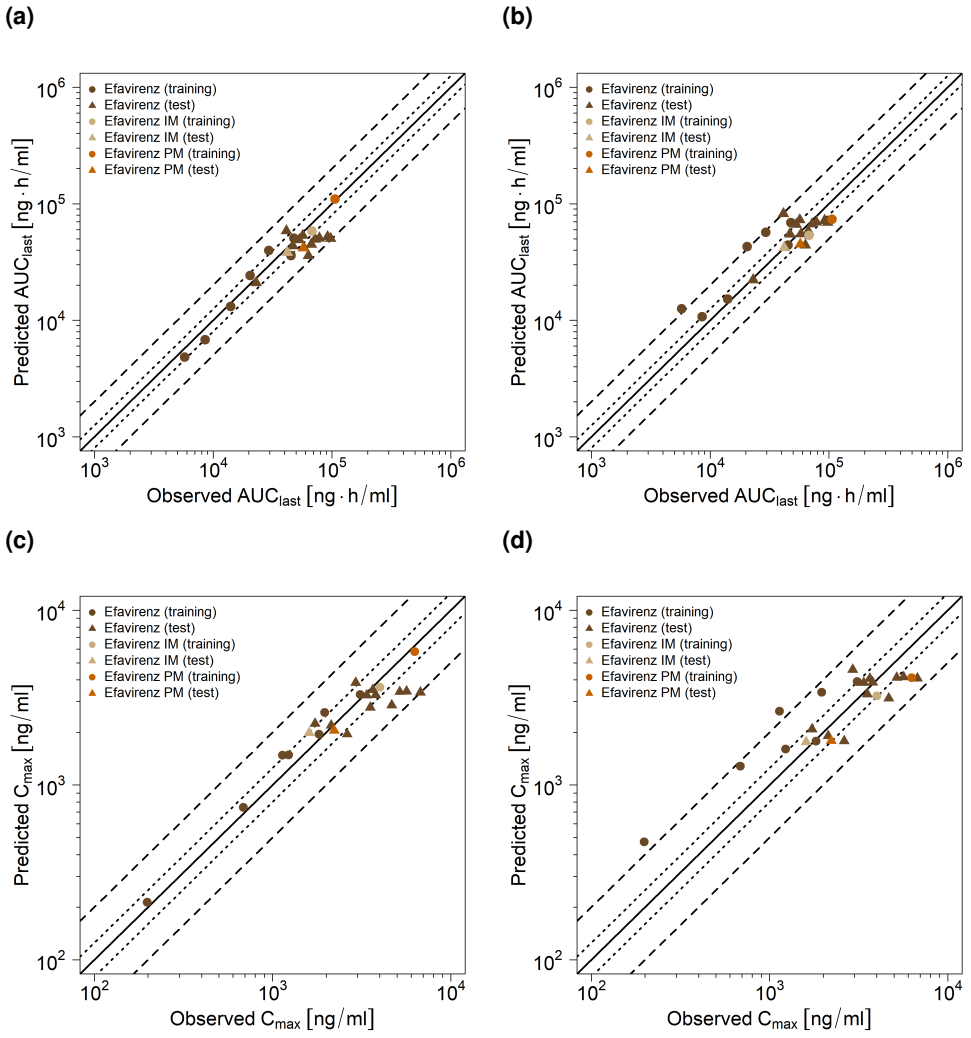

Figure S18: Predicted compared to observed (a,b) efavirenz AUC_{last} and (c,d) C_{max} values of the training (triangles) and test (circles) datasets. (a,c) show the updated efavirenz model, (b,d) show the original model. The solid line marks the line of identity. Dotted lines indicate 1.25-fold, dashed lines indicate 2-fold deviation. AUC_{last}: area under the plasma concentration-time curve from the time of drug administration to the last concentration measurement, C_{max}: maximum plasma concentration, IM: intermediate metabolizers (CYP2B6*1|*6), PM: poor metabolizers (CYP2B6*6|*6)

3.5.4 Geometric mean fold error of predicted AUC_{last} and C_{max} values

Table S8: Predicted and observed efavirenz AUC_{last} and C_{max} values with geometric mean fold errors of the updated model in comparison to the original model

		AUC_{last} [ng*h/ml]					C_{max} [ng/ml]					
			updated		original			updated		original		
Route	**Dose [mg]**	**Obs**	**Pred**	**Pred/Obs**	**Pred**	**Pred/Obs**	**Obs**	**Pred**	**Pred/Obs**	**Pred**	**Pred/Obs**	**Reference**
po, sd	50	5754.87	4838.42	0.84	12595.07	2.19	198.20	213.44	1.08	471.99	2.38	Derungs 2015 [89]
po, qd (D1)	200	8549.99	6814.78	0.80	10762.34	1.26	686.44	744.67	1.08	1279.23	1.86	Mouly 2002 [90]
po, qd (D10)	200	20499.16	24229.34	1.18	42920.81	2.09	1137.10	1478.74	1.30	2641.49	2.32	Mouly 2002 [90]
po, qd	400	58122.94	41716.36	0.72	55023.35	0.95	3534.24	2774.52	0.79	3308.00	0.94	Liu 2013 [91]
po, qd (D1)	400	14010.97	13152.89	0.94	15204.11	1.09	1232.47	148.96	1.21	1606.67	1.30	Mouly 2002 [90]
po, qd (D10)	400	29345.59	39868.54	1.36	57080.77	1.95	1960.69	2601.95	1.33	3388.03	1.73	Mouly 2002 [90]
po, sd	600	46884.25	43472.37	0.93	54901.73	1.17	1732.67	2245.91	1.30	2086.42	1.20	Cho 2016 [92]
po, qd	600	63363.54	35800.32	0.56	44097.59	0.70	2621.60	1952.53	0.74	1784.62	0.68	Ogburn 2010 [84]
po, sd	600	42014.64	38187.36	0.91	41888.82	1.00	1605.82	1991.59	1.24	1763.64	1.10	Xu 2013 (IM) [93]
po, sd	600	57284.66	41735.85	0.73	44946.79	0.78	2216.72	2048.71	0.92	1789.51	0.81	Xu 2013 (PM) [93]
po, sd	600	45168.30	35992.96	0.80	44340.57	0.98	1825.76	1952.54	1.07	1784.66	0.98	Xu 2013 (EM) [93]
po, qd	600	47653.02	50815.19	1.07	69063.36	1.45	3110.08	3291.76	1.06	3906.06	1.26	Dooley 2012 (EM) [94]
po, qd	600	67827.78	58427.85	0.86	53655.34	0.79	4013.47	3628.21	0.90	3237.77	0.81	Dooley 2012 (IM) [94]
po, qd	600	106157.40	109939.29	1.04	73853.54	0.70	6287.26	5800.13	0.92	4110.63	0.65	Dooley 2012 (PM) [94]
po, qd	600	97456.28	50278.98	0.52	69013.33	0.71	5651.38	3435.26	0.61	4146.26	0.73	Damle 2008 [95]
po, qd	600	56807.83	53486.71	0.94	72666.54	1.28	3650.55	3503.60	0.96	4064.81	1.11	Garg 2013 [96]
po, qd	600	72191.85	49600.72	0.69	67066.50	0.93	3790.09	3278.26	0.86	3863.82	1.02	Huang 2012 [97]
po, qd	600	78208.11	50642.86	0.65	69413.52	0.89	5176.12	3415.81	0.66	4121.84	0.80	Ji 2008 [44]
po, qd (D1)	600	22997.58	21008.78	0.91	22235.47	0.97	2130.00	2193.17	1.03	1912.06	0.90	Kharasch 2012 [98]
po, qd (D14)	600	41374.61	58497.10	1.41	82034.77	1.98	2926.26	3846.35	1.31	4574.00	1.56	Kharasch 2012 [98]
po, qd	600	66987.63	44762.00	0.67	58089.72	0.87	4665.93	2862.26	0.61	3130.82	0.67	Kwara 2011 [99]
po, qd	600	53003.19	49042.46	0.93	66377.21	1.25	3378.21	3262.64	0.97	3845.35	1.14	Malvestutto 2014 [100]
po, qd	600	92045.45	52013.69	0.57	71848.96	0.78	6751.46	3383.10	0.50	4077.99	0.60	Soon 2010 [101]
mean GMFE (range)				**1.31 (1.04-1.94)**		**1.36 (1.00-2.19)**			**1.26 (1.03-1.99)**		**1.41 (1.02-2.38)**	
				23/23 with GMFE ≤ 2		**21/23 with GMFE ≤ 2**			**23/23 with GMFE ≤ 2**		**21/23 with GMFE ≤ 2**	

AUC_{last}: area under the plasma concentration-time curve from the time of drug administration to the last concentration measurement, C_{max}: maximum plasma concentration, D: day, EM: extensive metabolizer, GMFE: geometric mean fold error, IM: intermediate metabolizer, obs: observed, po: oral, PM: poor metabolizer, pred: predicted, qd: once daily, sd: single dose

3.5.5 Sensitivity analysis

Sensitivity of the updated and original efavirenz PBPK models to single parameters (local sensitivity analysis) was calculated as the relative change of the predicted efavirenz AUC_{ss} at steady-state of an oral administration of 600 mg efavirenz once daily as tablet. Sensitivity analysis was carried out using a relative parameter perturbation of 1000% (variation range 10.0, maximum number of 9 steps). Parameters were included into the analysis if they were optimized (lipophilicity, solubility, CYP2B6, CYP1A2, CYP2A6, CYP3A4, CYP3A5 k_{cat} values, CYP3A4, CYP2B6 E_{max} values, intestinal permeability, Weibull tablet dissolution shape and time), if they are associated with optimized parameters (CYP2B6, CYP1A2, CYP2A6, CYP3A4, CYP3A5 K_m values, CYP3A4 and CYP2B6 EC_{50} values) or if they might have a strong impact due to calculation methods used in the model (fraction unbound in plasma, pKa, GFR fraction).

(a)

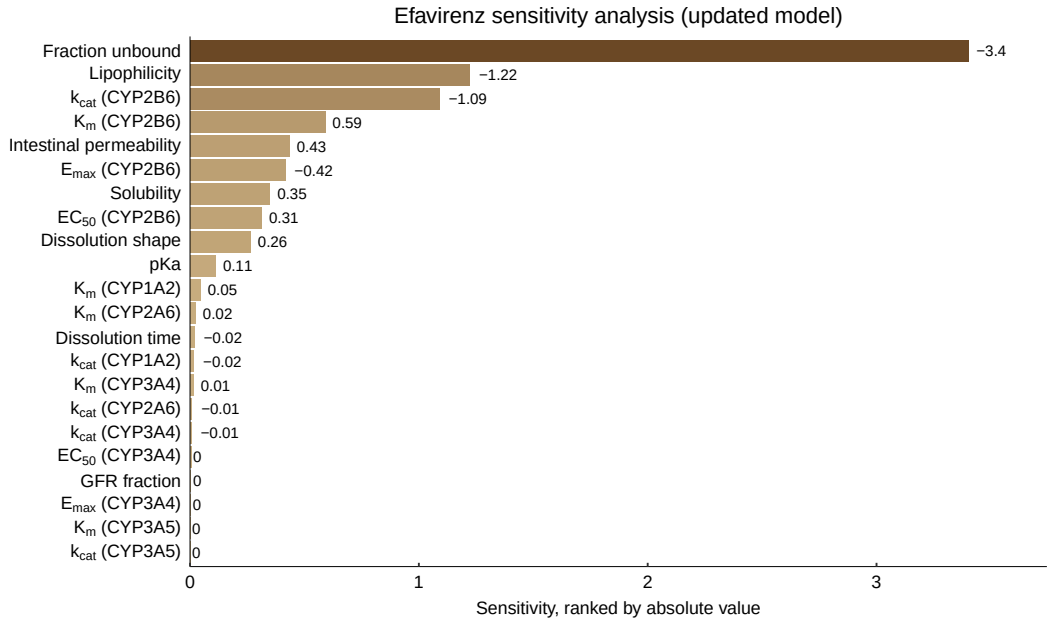

Figure S19: Efavirenz PBPK model sensitivity analysis. Sensitivity of the updated model to single parameters, calculated as change of the simulated efavirenz AUC_{ss} at steady-state of an oral administration of 600 mg efavirenz once daily as tablet. CYP: cytochrome P450, EC_{50}: half-maximal effective concentration, E_{max}: maximum effect, GFR: glomerular filtration rate, k_{cat}: catalytic rate constant, K_m: Michaelis-Menten constant

(a)

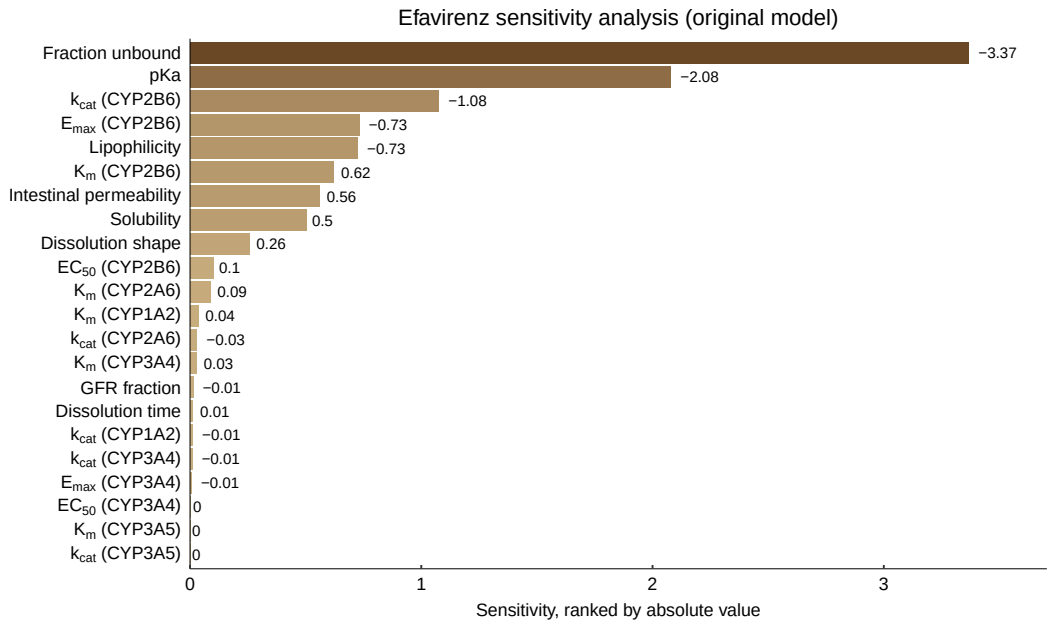

Figure S20: Efavirenz PBPK model sensitivity analysis. Sensitivity of the original model to single parameters, calculated as change of the simulated efavirenz AUC_{ss} at steady-state of an oral administration of 600 mg efavirenz once daily as tablet. CYP: cytochrome P450, EC_{50}: half-maximal effective concentration, E_{max}: maximum effect, GFR: glomerular filtration rate, k_{cat}: catalytic rate constant, K_m: Michaelis-Menten constant

4 Efavirenz drug-gene interactions (DGI)

4.1 DGI modeling - general

As CYP2B6 polymorphisms are a major determinant of efavirenz metabolism, the CYP2B6*6 polymorphism was integrated in the efavirenz PBPK model. Carriers of the CYP2B6*6 allele (either heterozygous or homozygous) show higher plasma concentrations of efavirenz than CYP2B6*1|*1 (wild type) carriers, due to decreased drug metabolism by CYP2B6 [86]. Parametrization of CYP2B6 metabolism in the efavirenz PBPK model describes efavirenz pharmacokinetics for the wild type. Intermediate metabolizers (CYP2B6*1|*6) and poor metabolizers (CYP2B6*6|*6) were described in the model by adjusting k_{cat}, assuming the same literature value vor K_m. Additionally, for CYP2B6 poor metabolizers no CYP2B6 auto-induction was assumed, as described in literature [86]. K_m and k_{cat} values used for DGI modeling are included in Table S6. Details on the modeled clinical studies investigating the efavirenz-CYP2B6*6 DGI are given in Table S9. Predicted efavirenz plasma concentration-time profiles for different CYP2B6 genotypes in comparison to their respective observed data are presented in Figures S21 (linear) and S22 (semi-logarithmic). The correlation of predicted to observed DGI AUC_{last} and C_{max} ratios is shown in Figure S23. Tables S10 and S11 list the corresponding predicted and observed DGI AUC_{last} ratios, DGI C_{max} ratios as well as model GMFE values of the updated model and the original model, respectively.

4.2 Efavirenz clinical DGI studies

Table S9: Clinical studies used for the establishment of the efavirenz DGI parameters

Dose [mg]	Route	Dataset	n	Healthy [%]	Females [%]	Age[a] [years]	Weight[a] [kg]	Height[a] [cm]	CYP2B6 genotype	Reference
600	po (-), sd	training	8	100	50	-	-	-	EM[b]	Xu 2013 [93]
600	po (-), sd	test	9	100	50	-	-	-	IM[b]	Xu 2013 [93]
600	po (-), sd	test	3	100	50	-	-	-	PM[b]	Xu 2013 [93]
600	po (-), qd	training	18	100	8	44[d] (19-62)	82.9[d] (57-119)	-	EM[c]	Dooley 2012 [94]
600	po (-), qd	training	12	100	8	44[d] (19-62)	82.9[d] (57-119)	-	IM[c]	Dooley 2012 [94]
600	po (-), qd	training	3	100	8	44[d] (19-62)	82.9[d] (57-119)	-	PM[c]	Dooley 2012 [94]

-: not given, CYP2B6: cytochrome P450 2B6, EM: extensive metabolizer, IM: intermediate metabolizer, PM: poor metabolizer, qd: once daily, sd: single dose

[a] mean (range)

[b] subjects were tested for the diminished-function allele CYP2B6*6

[c] subjects were tested for the diminished-function alleles CYP2B6*6 and CYP2B6*18

[d] median values

4.3 Profiles

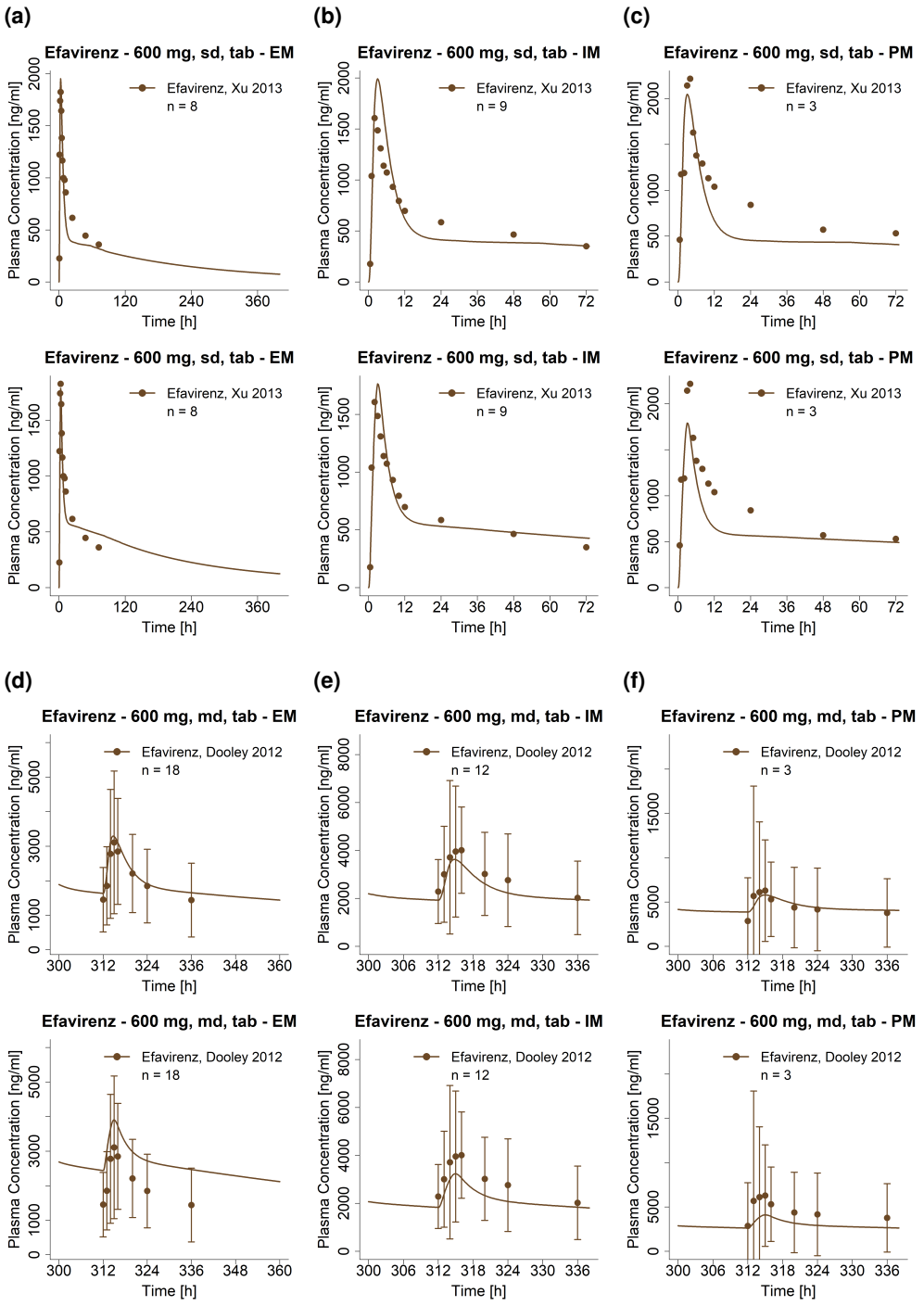

Figure S21: Predicted compared to observed efavirenz plasma concentration-time profiles (linear) of different CYP2B6 genotypes predicted with the updated model (upper rows) or the original model (lower rows). Observed data are shown as dots ± standard deviation; model predictions are shown as solid lines. Details on dosing regimens, study populations and literature references are listed in Table S5. md: multiple-dose, tab: tablet, sd: single dose

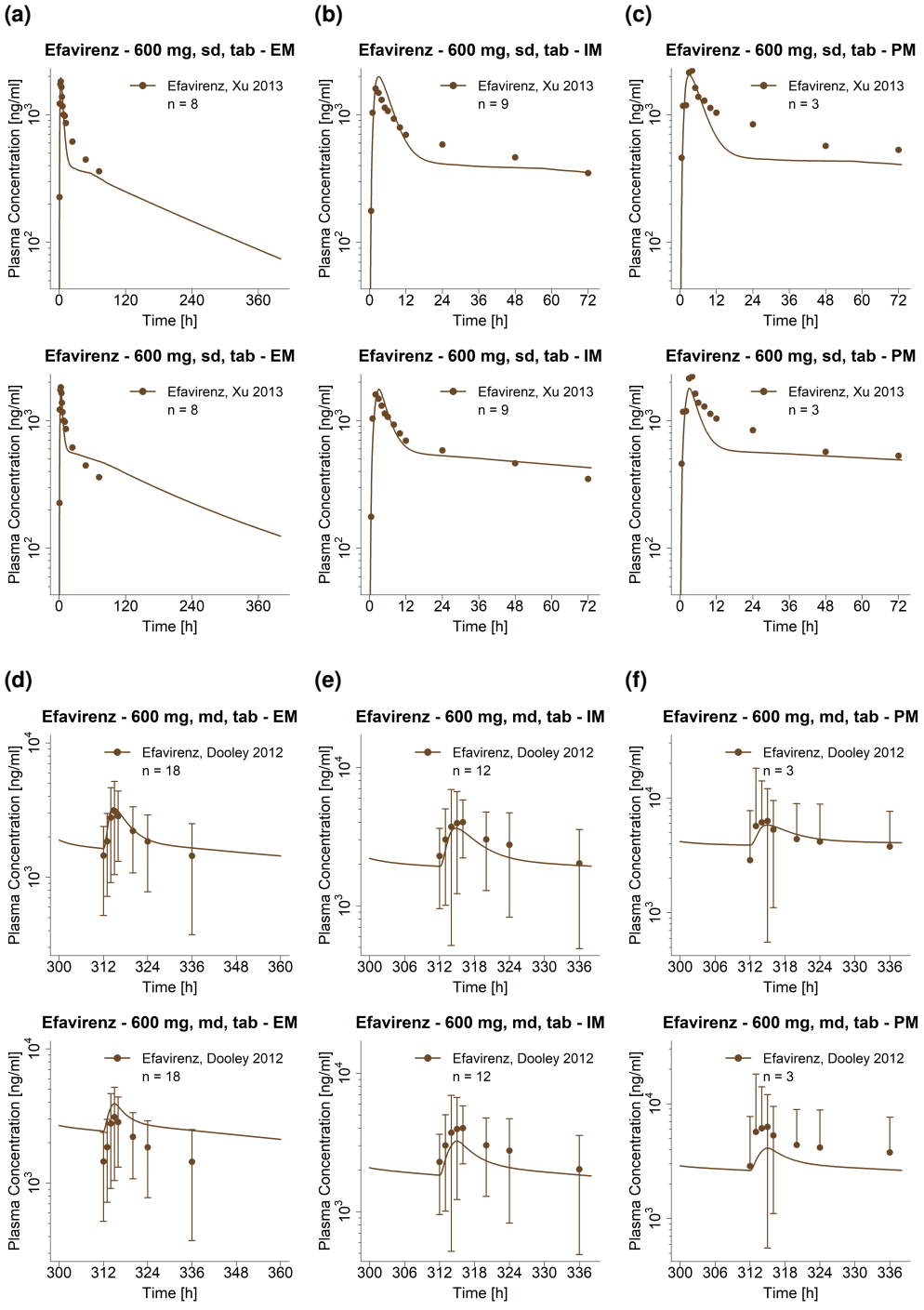

Figure S22: Predicted compared to observed efavirenz plasma concentration-time profiles (semi-logarithmic) of different CYP2B6 genotypes predicted with the updated model (upper rows) or the original model (lower rows). Observed data are shown as dots ± standard deviation; model predictions are shown as solid lines. Details on dosing regimens, study populations and literature references are listed in Table S5. md: multiple-dose, tab: tablet, sd: single dose

4.4 DGI AUC_{last} and C_{max} ratio goodness-of-fit plots

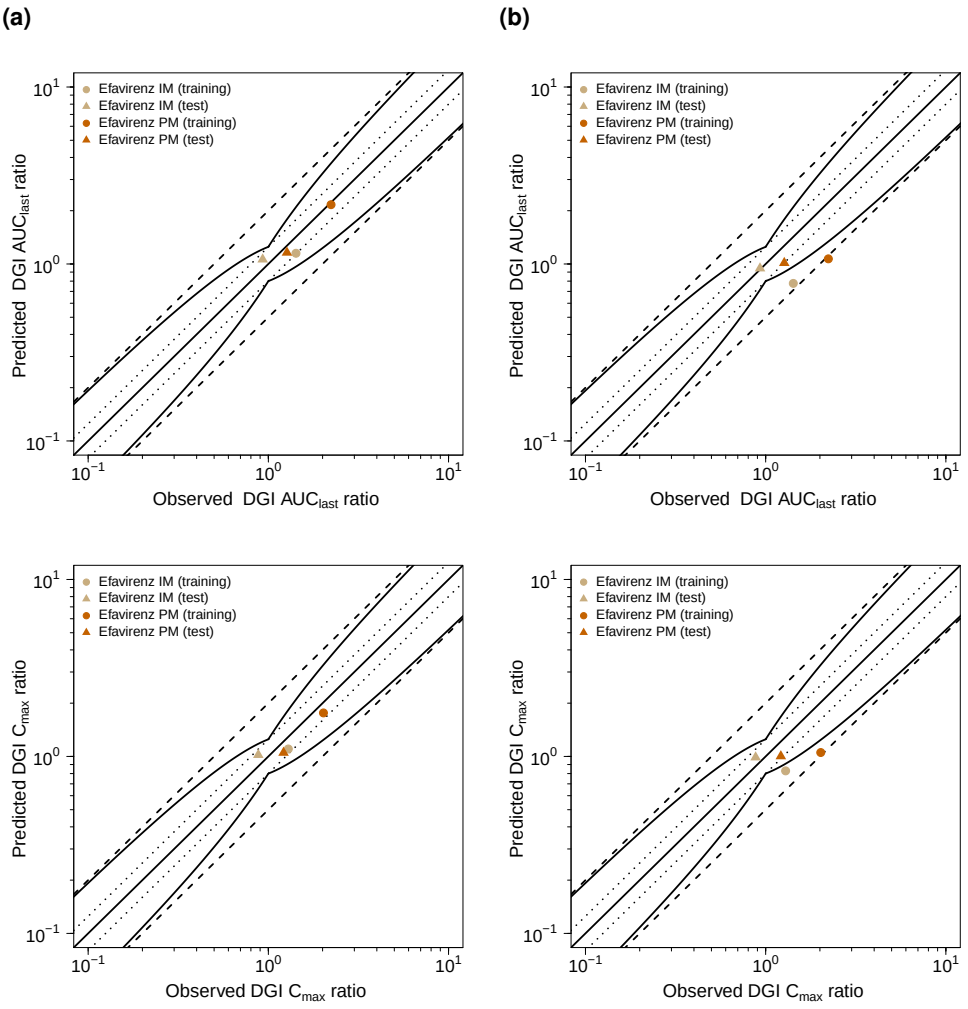

Figure S23: Predicted compared to observed efavirenz (a,b) DGI AUC_{last} and (c,d) DGI C_{max} ratios predicted with the updated efavirenz PBPK model (left) or the original PBPK model (right). The straight solid line marks the line of identity, the curved solid lines show the prediction success limits proposed by Guest et al. allowing for 1.25-fold variability of the DGI ratio [109]. Dotted lines indicate 1.25-fold, dashed lines indicate 2-fold deviation. AUC_{last}: area under the plasma concentration-time curve from the time of drug administration to the last concentration measurement, C_{max} : maximum plasma concentration, DGI: drug-gene interaction, IM: intermediate metabolizers (CYP2B6*1|*6), PM: poor metabolizers (CYP2B6*6|*6)

4.5 Geometric mean fold error of predicted DGI AUC_{last} and C_{max} ratios

Table S10: Predicted and observed DGI AUC_{last} and C_{max} ratios with geometric mean fold errors of the updated model

		DGI AUC_{last} ratio			DGI C_{max} ratio			
Administration	**Genotype**	**Pred**	**Obs**	**Pred/Obs**	**Pred**	**Obs**	**Pred/Obs**	**Reference**
600 mg, po, sd	CYP2B6*1|*6	1.06	0.93	1.14	1.02	0.88	1.16	Xu 2013 [93]
600 mg, po, sd	CYP2B6*6|*6	1.16	1.27	0.91	1.05	1.21	0.86	Xu 2013 [93]
600 mg, po, qd	CYP2B6*1|*6	1.14	1.42	0.81	1.10	1.29	0.85	Dooley 2012 [94]
600 mg, po, qd	CYP2B6*6|*6	2.16	2.23	0.97	1.76	2.02	0.87	Dooley 2012 [94]
mean GMFE (range)				**1.12 (1.03-1.24)**			**1.16 (1.14-1.17)**	
				4/4 with GMFE ≤ 2			**4/4 with GMFE ≤ 2**	

AUC_{last}: area under the plasma concentration-time curve from the time of drug administration to the last concentration measurement, C_{max}: maximum plasma concentration, CYP2B6: cytochrome P450 2B6, DGI: drug-gene interaction, GMFE: geometric mean fold error, obs: observed, po: oral, pred: predicted, qd: once daily, sd: single dose

Table S11: Predicted and observed DGI AUC_{last} and C_{max} ratios with geometric mean fold errors of the original model

		DGI AUC_{last} ratio			DGI C_{max} ratio			
Administration	**Genotype**	**Pred**	**Obs**	**Pred/Obs**	**Pred**	**Obs**	**Pred/Obs**	**Reference**
600 mg, po, sd	CYP2B6*1|*6	0.94	0.93	1.02	0.99	0.88	1.12	Xu 2013 [93]
600 mg, po, sd	CYP2B6*6|*6	1.01	1.27	0.80	1.00	1.21	0.83	Xu 2013 [93]
600 mg, po, qd	CYP2B6*1|*6	0.78	1.42	0.55	0.83	1.29	0.64	Dooley 2012 [94]
600 mg, po, qd	CYP2B6*6|*6	1.07	2.23	0.48	1.05	2.02	0.52	Dooley 2012 [94]
mean GMFE (range)				**1.54 (1.01-2.08)**			**1.45 (1.12-1.92)**	
				3/4 with GMFE ≤ 2			**4/4 with GMFE ≤ 2**	

AUC_{last}: area under the plasma concentration-time curve from the time of drug administration to the last concentration measurement, C_{max}: maximum plasma concentration, CYP2B6: cytochrome P450 2B6, DGI: drug-gene interaction, GMFE: geometric mean fold error, obs: observed, po: oral, pred: predicted, qd: once daily, sd: single dose

5 Carbamazepine drug-drug interactions (DDI)

5.1 DDI modeling - general

The accurate prediction of DDIs indicates that the perpetrator model adequately describes the drug concentrations at the site(s) of interaction and that the victim drug model sufficiently describes the amount of drug eliminated via the affected pathway. Therefore, DDI predictions are considered as additional evaluation of both models.

A total number of 7 DDI studies, providing 8 victim drug plasma concentration-time profiles and 7 metabolite plasma concentration-time profiles, was utilized to evaluate the DDI performance of the carbamazepine parent-metabolite PBPK model, including studies with a CYP3A4 inhibitor (erythromycin), CYP3A4 victim drugs (alprazolam and simvastatin), a CYP2B6 victim drug (bupropion) as well as a CYP3A4 and CYP2B6 victim and perpetrator drug (efavirenz). The carbamazepine DDI network is illustrated in Figure S24.

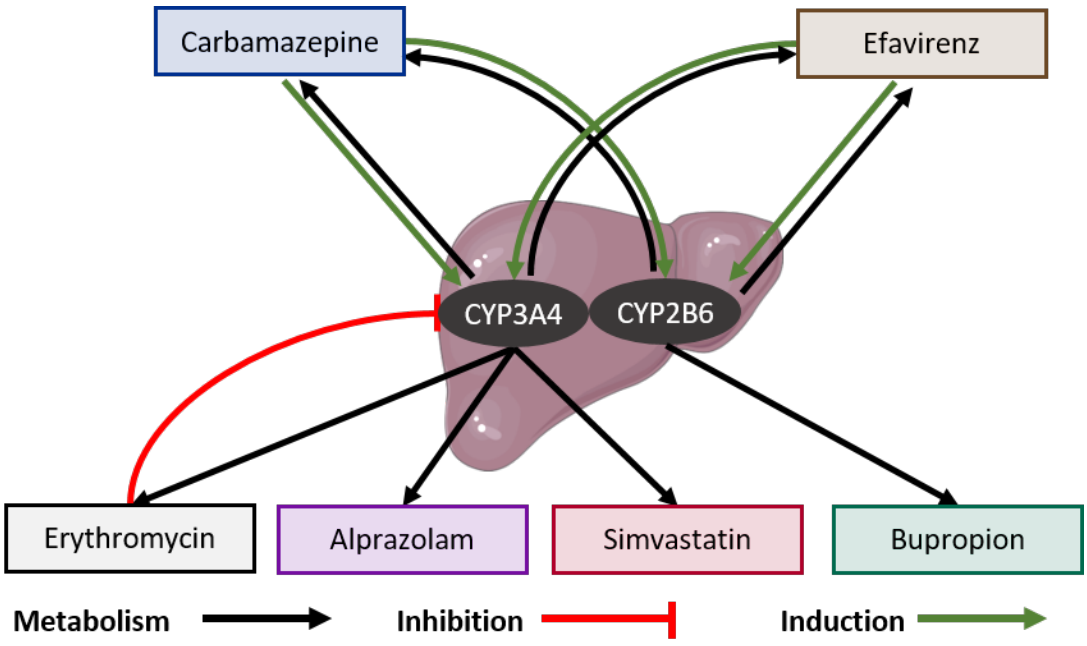

Figure S24: Carbamazepine drug-drug interaction network. Black arrows represent metabolism of the compounds, red and green arrows represent inhibition or induction of the CYP enzymes, respectively

The parameters describing the induction of CYP3A4 and CYP2B6 by carbamazepine were already introduced during carbamazepine model building, as the compound induces its own metabolism. While the carbamazepine-alprazolam DDI study was used in the training dataset to inform the parametrization of the carbamazepine CYP3A4 induction, all other DDIs were purely predicted. The implementation of these DDIs is described in more detail in the following sections.

5.2 Erythromycin-carbamazepine DDI

The erythromycin-carbamazepine DDI was modeled using a previously developed whole-body PBPK model of erythromycin, available in the OSP GitHub model repository (https://github.com/Open-Systems-Pharmacology/Erythromycin-Model). Erythromycin is a substrate and mechanism-based inhibitor of CYP3A4. The drug-dependent parameters of the erythromycin model are reproduced in Table S12.

The erythromycin-carbamazepine DDI was modeled as mechanism-based inhibition of carbamazepine CYP3A4 metabolism by erythromycin. K_i and K_{inact} values, describing the mechanism-based CYP3A4 inhibition by erythromycin, were qualified previously in different DDI preditions [110, 111]. Induction of erythromycin CYP3A4 metabolism by carbamazepine was also implemented, as significant CYP3A4 induction can be assumed after multiple-dose administration of carbamazepine, although the effect of carbamazepine on erythromycin metabolism has not been investigated in clinical studies, yet. CYP3A4 induction by carbamazepine was described using EC_{50} = 20.0 µmol/l from literature, the carbamazepine-alprazolam DDI study was used in the training dataset to inform the parametrization of the E_{max} = 6.0.

Details on the modeled clinical DDI studies are given in Table S13. Model predictions of carbamazepine and carbamazepine-10,11-epoxide plasma concentration-time profiles before and during erythromycin co-administration, compared to observed data, are shown in Figures S25 (linear) and S26 (semi-logarithmic). The correlation of predicted to observed DDI AUC_{last} and C_{max} ratios is shown in Figure S27. Table S14 lists the corresponding predicted and observed DDI AUC_{last} ratios, DDI C_{max} ratios, as well as GMFE values.

5.2.1 Erythromycin drug-dependent parameters

Table S12: Drug-dependent parameters of the erythromycin PBPK model (adopted from [110])

Parameter	Unit	Model	Literature	Reference	Description
MW	g/mol	733.9 (Lit)	733.9	[112]	Molecular weight
logP	Log Units	2.82 (Lit)	2.82 (2.48-3.06)[a]	[113–115]	Lipophilicity
Solubility (pH)	mg/ml	200.0 (7.0) (lactobionate) (Lit), 0.028 (7.0) (stearate) (Fit), 0.50 (7.0) (base pellets) (Fit), 0.0084 (7.0) (base tablet) (Fit)	200.0 (7.0) (lactobionate), 0.182 (7.0) (stearate), 2.10 (7.0) (base)	[116] [117] [118]	Solubility
fu	%	30.5 (Lit)	27.0, 28.0, 30.5, 32.6	[119–122]	Fraction unbound in plasma
pKa (base)	-	8.88 (Lit)	8.88	[115]	Acid dissociation constant
K_m (CYP3A4)	µmol/l	70.0 (Lit)	70 (44.0-88.0)[a]	[123, 124]	CYP3A4 Michaelis-Menten constant
k_{cat} (CYP3A4)	1/min	8.50 (Fit)	-	-	CYP3A4 catalytic rate constant
K_m (OATP1B1)	µmol/l	0.74 (Fit)	13.2	[125]	OATP1B1 Michaelis-Menten constant
k_{cat} (OATP1B1)	1/min	2.02 (Fit)	-	-	OATP1B1 transport rate constant
CL_{hep}	1/min	4.15 (Fit)	-	-	Hepatic plasma clearance
GFR fraction	-	1.16 (Fit)	-	-	Fraction of filtered drug in the urine
K_i (CYP3A4)	µmol/l	7.60 (Fit)	18.4 (0.76-109.0)[b]	[122, 126–136]	Concentration for half-maximal inactivation
k_{inact} (CYP3A4)	1/min	0.03 (Fit)	0.06 (0.01-0.30)[b]	[122, 126–136]	Maximum inactivation rate constant
Intestinal permeability	cm/min	3.87E-04 (Fit)	-	-	Transcellular intestinal permeability
Partition coefficients	-	Diverse	Rogers and Rowland	[77, 78]	Cell to plasma partition coefficients
Cellular permeability	cm/min	1.22E-4 (Calc)	Charge-dependent Schmitt	[2]	Permeability into the cellular space
Coated pellets Weibull time	min	1.75 (Fit)	-	-	Dissolution time (50% dissolved)
Coated pellets Weibull lag time	min	54.35 (Fit)	-	-	Dissolution lag time
Coated pellets Weibull shape	-	1.06 (Fit)	-	-	Dissolution profile shape
Coated tablet Weibull time	min	79.63 (Fit)	-	-	Dissolution time (50% dissolved)
Coated tablet Weibull lag time	min	78.79 (Fit)	-	-	Dissolution lag time
Coated tablet Weibull shape	-	1.08 (Fit)	-	-	Dissolution profile shape
Film tablet Weibull time	min	1.70 (Fit)	-	-	Dissolution time (50% dissolved)
Film tablet Weibull shape	-	1.10 (Fit)	-	-	Dissolution profile shape

-: not given, calc: calculated, CYP3A4: cytochrome P450 3A4, fit: optimized during parameter identification, GFR: glomerular filtration rate, lit: literature, OATP1B1: organic anion transporting polypeptide 1B1

[a] mean (range)

5.2.2 Erythromycin-carbamazepine clinical DDI studies

Table S13: Clinical studies investigating the erythromycin-carbamazepine DDI

Erythromycin administration		Carbamazepine administration		n	Healthy [%]	Females [%]	Age[a] [years]	Weight[a] [kg]	Height [cm]	Reference
Dose [mg]	**Route**	**Dose [mg]**	**Route**							
250	po (cap), qid (D15-D17)	357[b]	po (tab), qd (D1-D17)	7	100	0	25.4 (22-27)	78.8 (70.8-90.9)	-	Miles 1989 [45]
500	po (-), tid (D1-D10)	400	po (tab*), sd (D7)	7	-	-	(21-27)	(70-90)	-	Barzaghi 1987 [32]
250	po (-), qid (D1-D8)	400	po (tab), sd (D6)	8	100	0	(24-36)	(72.3-96.4)	-	Wong 1983 [38]

-: not given, cap: capsule, D: day, po: oral, qd: once daily, qid: four times daily, sd: single dose, tab: tablet, tab*: tablet with concomitant food intake, tid: three times daily

[a] mean (range)

[b] mean administered dose (range: 300-400 mg)

5.2.3 Profiles

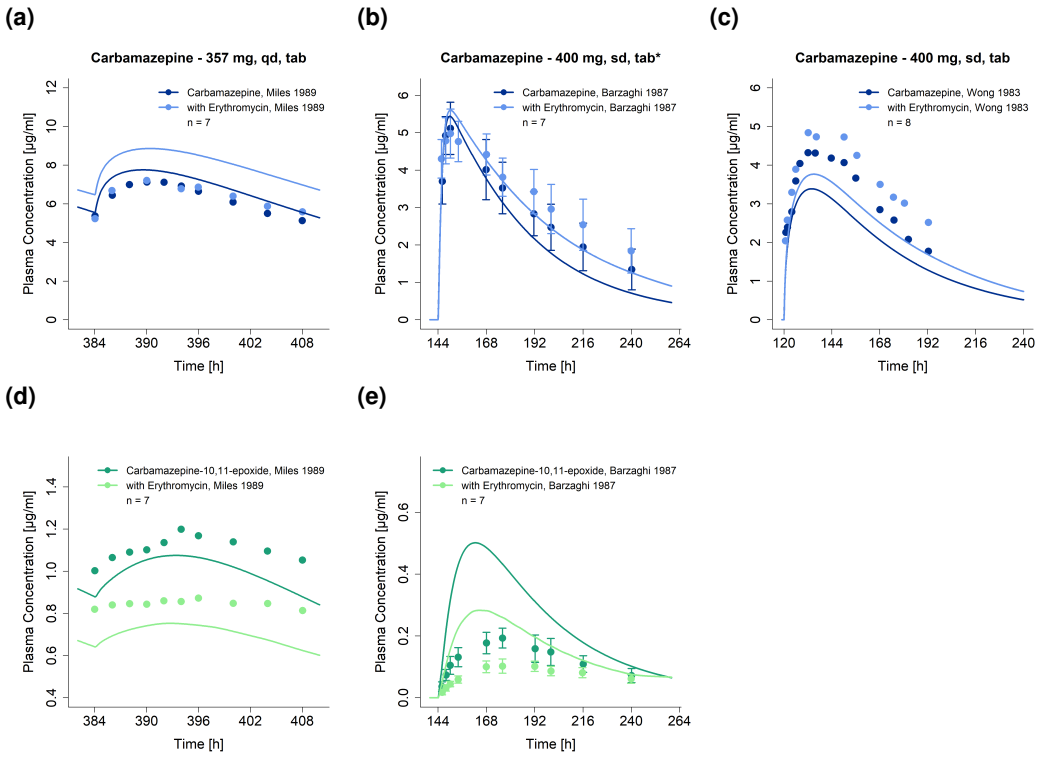

Figure S25: Predicted compared to observed carbamazepine (upper row) and carbamazepine-10,11-epoxide (lower row) plasma concentration-time profiles (linear) before and during erythromycin co-administration. Observed data are shown as dots ± standard deviation; model predictions are shown as solid lines. Details on dosing regimens, study populations and literature references are listed in Table S13. qd: once daily, sd: single dose, tab: tablet, tab*: tablet with concomitant food intake

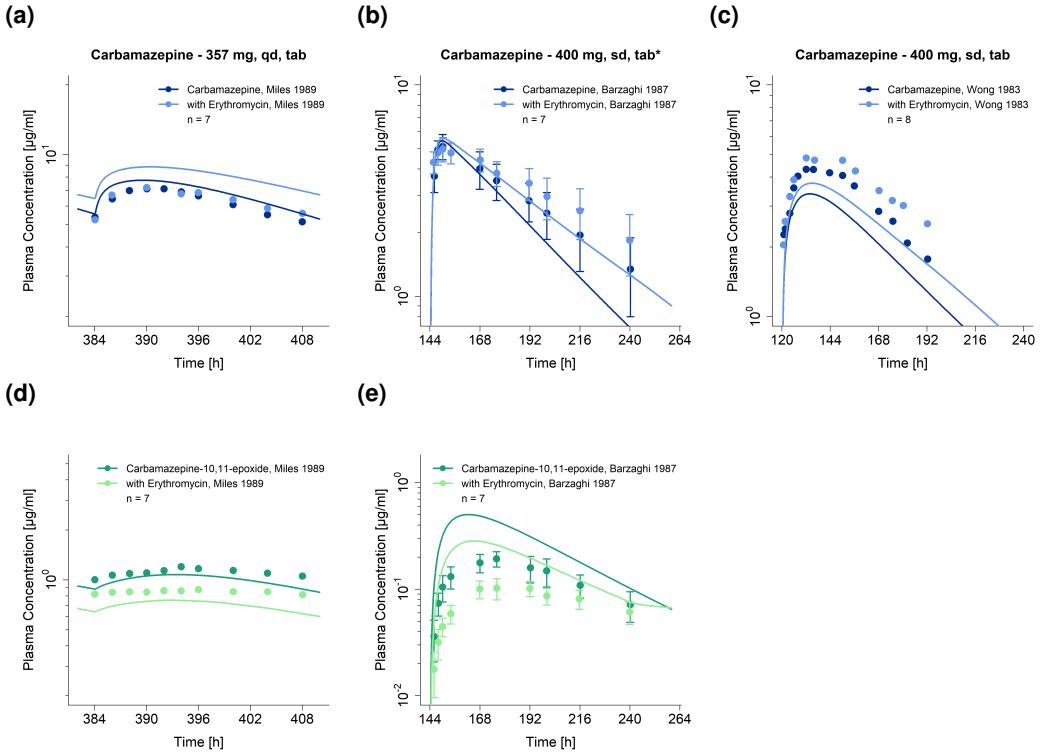

Figure S26: Predicted compared to observed carbamazepine (upper row) and carbamazepine-10,11-epoxide (lower row) plasma concentration-time profiles (semi-logarithmic) before and during erythromycin co-administration. Observed data are shown as dots ± standard deviation; model predictions are shown as solid lines. Details on dosing regimens, study populations and literature references are listed in Table S13. qd: once daily, sd: single dose, tab: tablet, tab*: tablet with concomitant food intake

5.2.4 DDI AUC_{last} and C_{max} ratio goodness-of-fit plots

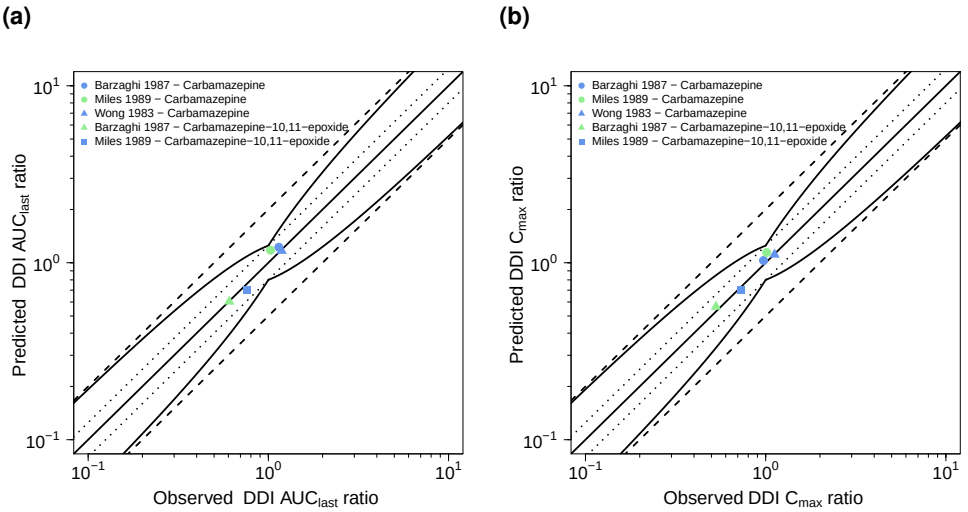

Figure S27: Predicted compared to observed erythromycin-carbamazepine (a) DDI AUC_{last} and (b) DDI C_{max} ratios. The straight solid line marks the line of identity, the curved solid lines show the prediction success limits proposed by Guest et al. allowing for 1.25-fold variability of the DDI ratio [109]. Dotted lines indicate 1.25-fold, dashed lines indicate 2-fold deviation. AUC_{last}: area under the plasma concentration-time curve from the time of drug administration to the last concentration measurement, C_{max}: maximum plasma concentration, DDI: drug-drug interaction

5.2.5 Geometric mean fold error of predicted DDI AUC_{last} and C_{max} ratios

Table S14: Predicted and observed erythromycin-carbamazepine DDI AUC_{last} and C_{max} ratios with geometric mean fold errors

Perpetrator	**Victim**				**DDI AUC_{last} ratio**			**DDI C_{max} ratio**			
Erythromycin	Carbamazepine	**Compound**	**Dose gap [h]**	**n**	**Pred**	**Obs**	**Pred/Obs**	**Pred**	**Obs**	**Pred/Obs**	**Reference**
250 mg, po, qid	357 mg[a], po, qd	Carbamazepine	-	7	1.18	1.03	1.14	1.14	1.01	1.13	Miles 1989 [45]
250 mg, po, qid	357 mg[a], po, qd	Carbamazepine-10,11-epoxide	-	7	0.71	0.76	0.93	0.70	0.73	0.96	Miles 1989 [45]
500 mg, po, tid	400 mg, po, sd	Carbamazepine	-	7	1.22	1.14	1.05	1.03	0.97	1.06	Barzaghi 1987 [32]
500 mg, po, tid	400 mg, po, sd	Carbamazepine-10,11-epoxide	-	7	0.60	0.61	1.00	0.56	0.53	1.06	Barzaghi 1987 [32]
250 mg, po, qid	400 mg, po, sd	Carbamazepine	-	8	1.17	1.18	0.99	1.11	1.12	0.99	Wong 1983 [38]
mean GMFE (range) (Carbamazepine)							**1.08 (1.01-1.14)**			**1.06 (1.01-1.13)**	
							3/3 with GMFE ≤ 2			**3/3 with GMFE ≤ 2**	
mean GMFE (range) (Carbamazepine-10,11-epoxide)							**1.04 (1.00-1.08)**			**1.05 (1.04-1.06)**	
							2/2 with GMFE ≤ 2			**2/2 with GMFE ≤ 2**	

-: not given, AUC_{last}: area under the plasma concentration-time curve from the time of drug administration to the last concentration measurement, C_{max}: maximum plasma concentration, DDI: drug-drug interaction, GMFE: geometric mean fold error, obs: observed, po: oral, pred: predicted, qd: once daily, qid: four times daily, sd: single dose, tid: three times daily

[a] Mean administered carbamazepine dose

5.3 Carbamazepine-alprazolam DDI

The carbamazepine-alprazolam DDI was modeled using a previously developed whole-body PBPK model of alprazolam, available in the OSP GitHub model repository (https://github.com/Open-Systems-Pharmacology/Alprazolam-Model). The metabolism of the CYP3A4 substrate alprazolam is described using Michaelis-Menten kinetics [137]. The drug-dependent parameters of the alprazolam model are reproduced in Table S15.

The carbamazepine-alprazolam DDI was modeled as induction of alprazolam CYP3A4 metabolism by carbamazepine. CYP3A4 induction by carbamazepine was described using EC_{50} = 20.0 µmol/l from literature, the carbamazepine-alprazolam DDI study was used in the training dataset to inform the parametrization of the E_{max} = 6.0.

Details on the modeled clinical DDI study are given in Table S16. Model predictions of alprazolam plasma concentration-time profiles before and during carbamazepine co-administration, compared to observed data, are shown in Figures S28 (linear) and S29 (semi-logarithmic). The correlation of predicted to observed DDI AUC_{last} and C_{max} ratios is shown in Figure S30. Table S17 lists the corresponding predicted and observed DDI AUC_{last} ratios, DDI C_{max} ratios, as well as GMFE values.

5.3.1 Alprazolam drug-dependent parameters

Table S15: Drug-dependent parameters of the alprazolam PBPK model (adopted from [137])

Parameter	Unit	Model	Literature	Reference	Description
MW	g/mol	308.77 (Lit)	308.77	[138]	Molecular weight
logP	Log Units	2.05 (Fit)	1.26 (logD)	[139]	Lipophilicity
			2.19 (logP)	[140]	
Solubility (pH)	mg/ml	0.04 (7.0) (Lit)	0.012 (1.2),	[138]	Solubility
			0.04 (7.0),	[138]	
			0.08 (7.0)	[141]	
fu	%	23.3 (Lit)	20.0, 23.3, 31.1	[142–144]	Fraction unbound in plasma
pKa (base)	-	2.40 (Lit)	2.40, 2.48	[145–147]	Acid dissociation constant
K_m (CYP3A4) α-hydroxy	µmol/l	269.0 (Lit)	269.0	[148]	CYP3A4 Michaelis-Menten constant for α-hydroxy-alprazolam formation
k_{cat} (CYP3A4) α-hydroxy	1/min	0.73 (Fit)	-	-	CYP3A4 catalytic rate constant for α-hydroxy-alprazolam formation
K_m (CYP3A4) 4-hydroxy	µmol/l	704.0 (Lit)	704.0	[148]	CYP3A4 Michaelis-Menten constant for 4-hydroxy-alprazolam formation
k_{cat} (CYP3A4) 4-hydroxy	1/min	12.44 (Fit)	-	-	CYP3A4 catalytic rate constant for 4-hydroxy-alprazolam formation
GFR fraction	-	0.52 (Fit)	-	-	Fraction of filtered drug in the urine
Intestinal permeability	cm/min	0.65 (Fit)	-	-	Transcellular intestinal permeability
Partition coefficients	-	Diverse	Rogers and Rowland	[77, 78]	Cell to plasma partition coefficients
Cellular permeability	cm/min	5.74E-3 (Calc)	PK-Sim Standard	[79]	Permeability into the cellular space
Tablet (Solanax®) Weibull time	min	35.72 (Fit)	-	-	Dissolution time (50% dissolved)
Tablet (Solanax®) Weibull shape	-	0.72 (Fit)	-	-	Dissolution profile shape

-: not given, calc: calculated, CYP: cytochrome P450, fit: optimized during parameter identification, GFR: glomerular filtration rate, lit: literature

5.3.2 Carbamazepine-alprazolam clinical DDI studies

Table S16: Clinical studies investigating the carbamazepine-alprazolam DDI

Carbamazepine administration		Alprazolam administration		n	Healthy [%]	Females [%]	Age[a] [years]	Weight[a] [kg]	Height [cm]	Reference
Dose [mg]	**Route**	**Dose [mg]**	**Route**							
100	po (tab), tid (D1-D10)	0.8	po (tab), sd (D8)	7	100	0	32.7	60.9	-	Furukori 1998 [149]

-: not given, D: day, po: oral, sd: single dose, tab: tablet, tid: three times daily

[a] Mean values

5.3.3 Profiles

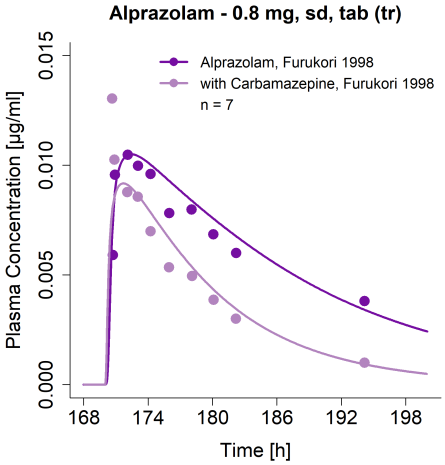

Figure S28: Predicted compared to observed alprazolam plasma concentration-time profiles (linear) before and during carbamazepine co-administration. Observed data are shown as dots; model predictions are shown as solid lines. Details on dosing regimens, study population and literature reference are listed in Table S16. sd: single dose, tab: tablet

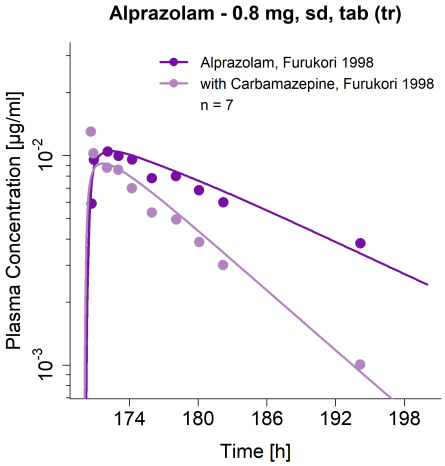

Figure S29: Predicted compared to observed alprazolam plasma concentration-time profiles (semi-logarithmic) before and during carbamazepine co-administration. Observed data are shown as dots; model predictions are shown as solid lines. Details on dosing regimens, study population and literature reference are listed in Table S16. sd: single dose, tab: tablet

5.3.4 DDI AUC_{last} and C_{max} ratio goodness-of-fit plots

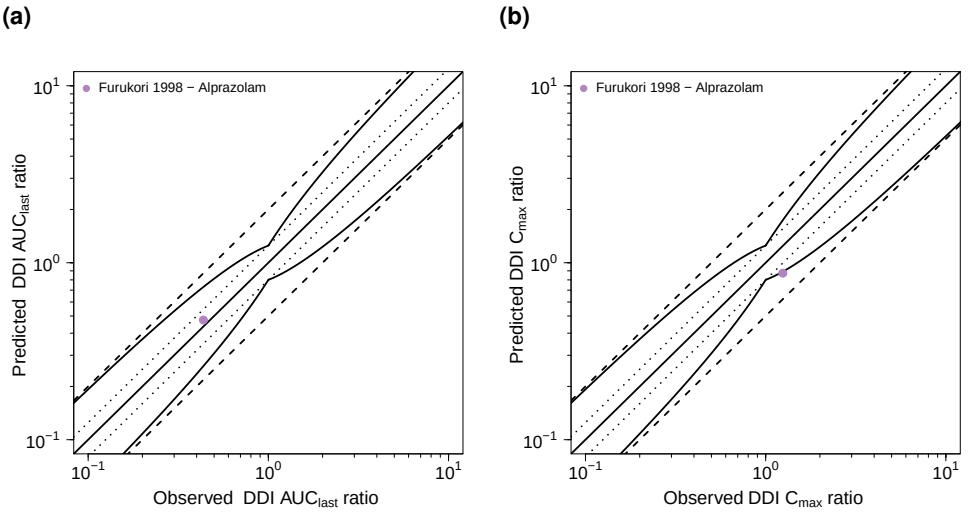

Figure S30: Predicted compared to observed carbamazepine-alprazolam (a) DDI AUC_{last} and (b) DDI C_{max} ratios. The straight solid line marks the line of identity, the curved solid lines show the prediction success limits proposed by Guest et al. allowing for 1.25-fold variability of the DDI ratio [109]. Dotted lines indicate 1.25-fold, dashed lines indicate 2-fold deviation. AUC_{last}: area under the plasma concentration-time curve from the time of drug administration to the last concentration measurement, C_{max}: maximum plasma concentration, DDI: drug-drug interaction

5.3.5 Geometric mean fold error of predicted DDI AUC_{last} and C_{max} ratios

Table S17: Predicted and observed carbamazepine-alprazolam DDI AUC_{last} and C_{max} ratios with geometric mean fold errors

Perpetrator	**Victim**			**DDI AUC_{last} ratio**			**DDI C_{max} ratio**			
Carbamazepine	Alprazolam	**Dose gap [h]**	**n**	**Pred**	**Obs**	**Pred/Obs**	**Pred**	**Obs**	**Pred/Obs**	**Reference**
100 mg, po, tid	0.8 mg, po, sd	2	7	0.47	0.44	1.09	0.87	1.24	0.70	Furukori 1998 [149]
mean GMFE						**1.09**			**1.43**	
						1/1 with GMFE ≤ 2			**1/1 with GMFE ≤ 2**	

AUC_{last}: area under the plasma concentration-time curve from the time of drug administration to the last concentration measurement, C_{max}: maximum plasma concentration, DDI: drug-drug interaction, GMFE: geometric mean fold error, obs: observed, po: oral, pred: predicted, sd: single dose, tid: three times daily

5.4 Carbamazepine-simvastatin DDI

The carbamazepine-simvastatin DDI was modeled using a previously established whole-body parent-metabolite PBPK model of simvastatin [150]. Simvastatin is metabolized by CYP3A4, with simvastatin acid as the main metabolite. Simvastatin acid is also a substrate of CYP3A4. Metabolism of simvastatin and simvastatin acid by CYP3A4 is described in the model using Michaelis-Menten kinetics. Both compounds are also competitive inhibitors of CYP3A4 as well as CYP2C8. The drug-dependent parameters of the simvastatin model are reproduced in Table S18.

The carbamazepine-simvastatin DDI was modeled as induction of simvastatin and simvastatin acid CYP3A4 metabolism by carbamazepine. CYP3A4 induction by carbamazepine was described using EC_{50} = 20.0 µmol/l from literature, E_{max} = 6.0 was identified during the carbamazepine parameter identification. Competitive inhibition of carbamazepine CYP3A4 and CYP2C8 metabolism by simvastatin and simvastatin acid was also implemented, although the effect of simvastatin and simvastatin acid on carbamazepine metabolism has not been investigated in clinical studies, yet. K_i values, describing the competitive CYP3A4 and CYP2C8 inhibition by simvastatin and simvastatin acid, were qualified previously in different DDI preditions [150].

Details on the modeled clinical DDI study are given in Table S19. Model predictions of simvastatin and simvastatin acid plasma concentration-time profiles before and during carbamazepine co-administration, compared to observed data, are shown in Figures S31 (linear) and S32 (semi-logarithmic). The correlation of predicted to observed DDI AUC_{last} and C_{max} ratios is shown in Figure S33. Table S20 lists the corresponding predicted and observed DDI AUC_{last} ratios, DDI C_{max} ratios, as well as GMFE values.

5.4.1 Simvastatin drug-dependent parameters

Table S18: Drug-dependent parameters of the simvastatin PBPK model (adopted from [150])

Parameter	Unit	Model	Literature[a]	Reference	Description
Simvastatin					
MW	g/mol	418.57 (Lit)	418.57	[151]	Molecular weight
logP	Log Units	4.68 (Lit)	4.60 (2.06-5.19)	[152, 153]	Lipophilicity
Solubility (pH)	mg/ml	0.016 (5.0) (Lit)	0.016 (1.40E-3-0.061) (5.0)	[151, 152, 154–157]	Solubility
fu	%	1.34 (Lit)	2.37 (1.09-6.00)	[152, 158, 159]	Fraction unbound in plasma
K_m (CYP3A4)	µmol/l	21.0 (Lit)	2.55 (0.46-30.0)	[160–162]	CYP3A4 Michaelis-Menten constant
k_{cat} (CYP3A4)	1/min	5194.04 (Fit)	-	-	CYP3A4 catalytic rate constant
K_m (CYP3A5)	µmol/l	39.1 (Fit)	88.0 (62.0-91.0)	[160]	CYP3A5 Michaelis-Menten constant
k_{cat} (CYP3A5)	1/min	162281.57 (Fit)	-	-	CYP3A5 catalytic rate constant
K_m (PON3)	µmol/l	840.0 (Lit)	840.0	[163]	PON3 Michaelis-Menten constant
k_{cat} (PON3)	1/min	4952.08 (Fit)	-	-	PON3 catalytic rate constant
Chemical hydrolysis rate	l/µmol/min	9.80E-4 (Lit)	8.21E-4 (1.67E-06-1.96E-2)	[151, 164, 165]	Chemical hydrolysis rate (ubiquitous)
Plasma hydrolysis rate	l/µmol/min	6.03E-2 (Lit)	6.03E-2	[166]	Plasma hydrolysis rate
K_m (BCRP)	µmol/l	5.00[b] (Asm)	(1.20-10.8)	[167–172]	BCRP Michaelis-Menten constant
k_{cat} (BCRP)	1/min	32.61 (Fit)	-	-	BCRP catalytic rate constant
GFR fraction	-	1 (Asm)	-	-	Fraction of filtered drug in the urine
K_i (CYP2C8)	µmol/l	1.10 (Lit)	5.7 (1.10-12.3)	[173]	Concentration for half-maximal inhibition
K_i (CYP3A4)	µmol/l	0.16 (Lit)	2.1 (0.16-35.0)	[160, 174–177]	Concentration for half-maximal inhibition
K_i (OATP1B1)	µmol/l	5.00 (Lit)	7.85 (5.00-12.5)	[178, 179]	Concentration for half-maximal inhibition
K_i (Pgp)	µmol/l	4.60 (Lit)	37.7 (4.60-209.0)	[180, 180–186]	Concentration for half-maximal inhibition
Intestinal permeability	cm/min	1.08E-3 (Fit)	0.258	[151]	Transcellular intestinal permeability
Partition coefficients	-	Diverse	Berezhkovskiy	[187]	Cell to plasma partition coefficients
Cellular permeability	cm/min	0.26 (Calc)	PK-Sim Standard	[79]	Permeability into the cellular space
Tablet Weibull time	min	86.38 (Fit)	-	-	Dissolution time (50% dissolved)
Tablet Weibull shape	-	1.30 (Fit)	-	-	Dissolution profile shape

-: not given, asm: assumption, BCRP: breast cancer resistance protein, calc: calculated, CYP: cytochrome P450, fit: optimized during parameter identification, GFR: glomerular filtration rate, lit: literature, OATP: organic anion transporting polypeptide, Pgp: P-glycoprotein, PON3: paraoxonase 3, UGT: UDP-glucuronosyltransferase

[a] median (range)

[b] assumed from other statins

[c] calculated from V_{max}

[d] calculated from liver S9

Table S18: Drug-dependent parameters of the simvastatin PBPK model (adopted from [150]) *(continued)*

Parameter	Unit	Model	Literature[a]	Reference	Description
Simvastatin acid					
MW	g/mol	436.58 (Lit)	436.58	[188]	Molecular weight
logP	Log Units	1.45 (Lit)	3.82 (1.45-4.70)	[151, 152, 154, 188, 189]	Lipophilicity
Solubility (pH)	mg/ml	13.09 (6.8) (Lit)	45.1 (0.13-51.5) (6.8)	[154, 157, 188]	Solubility
fu	%	5.68 (Lit)	6.26 (5.48-9.61)	[159]	Fraction unbound in plasma
pKa (acidic)	-	4.21 (Lit)	4.20 (4.18-5.5)	[152, 188–190]	Acid dissociation constant
K_m (CYP3A4)	µmol/l	26.0 (Lit)	26.0 (21.0-29.0)	[191]	CYP3A4 Michaelis-Menten constant
k_{cat} (CYP3A4)	1/min	31.0[c] (Lit)	-	-	CYP3A4 catalytic rate constant
K_m (CYP2C8)	µmol/l	38.6 (Lit)	38.6 (16.0-88.0)	[191, 192]	CYP2C8 Michaelis-Menten constant
k_{cat} (CYP2C8)	1/min	52.3[c] (Lit)	-	-	CYP2C8 catalytic rate constant
K_m (UGT1A1)	µmol/l	349.0 (Lit)	349.0	[193]	UGT1A1 Michaelis-Menten constant
k_{cat} (UGT1A1)	1/min	6.5[c] (Lit)	-	-	UGT1A1 catalytic rate constant
K_m (UGT1A3)	µmol/l	349.0 (Lit)	349.0	[193]	UGT1A3 Michaelis-Menten constant
k_{cat} (UGT1A3)	1/min	6.5[c] (Lit)	-	-	UGT1A3 catalytic rate constant
Liver lactonization rate	l/µmol/min	2.43E-3 (Lit)	2.43E-3[d]	[151]	Liver lactonization rate
K_m (Pgp)	µmol/l	10.0 (Asm)	-	-	Pgp Michaelis-Menten constant
k_{cat} (Pgp)	1/min	50.0 (Fit)	-	-	Pgp transport rate constant
K_m (OATP1B1)	µmol/l	2.00 (Lit)	1.99 (1.17-2.53)	[194]	OATP1B1 Michaelis-Menten constant
k_{cat} (OATP1B1)	1/min	10.25 (Fit)	-	-	OATP1B1 transport rate constant
K_m (OATP1B3)	µmol/l	2.0 (Asm)	-	-	OATP1B3 Michaelis-Menten constant
k_{cat} (OATP1B3)	1/min	2.15 (Fit)	-	-	OATP1B3 transport rate constant
GFR fraction	-	1 (Asm)	-	-	Fraction of filtered drug in the urine
K_i (CYP2C8)	µmol/l	41.1 (Lit)	41.1	[192]	Concentration for half-maximal inhibition
K_i (CYP3A4)	µmol/l	69.6 (Lit)	56.1 (42.6-69.6)	[176, 195]	Concentration for half-maximal inhibition
K_i (BCRP)	µmol/l	18 (Lit)	18	[169]	Concentration for half-maximal inhibition
K_i (OATP1B1)	µmol/l	3.6 (Lit)	3.6	[179]	Concentration for half-maximal inhibition
Intestinal permeability	cm/min	5.92E-07 (Calc)	-	-	Transcellular intestinal permeability
Partition coefficients	-	Diverse	Schmitt	[108]	Cell to plasma partition coefficients

-: not given, asm: assumption, BCRP: breast cancer resistance protein, calc: calculated, CYP: cytochrome P450, fit: optimized during parameter identification, GFR: glomerular filtration rate, lit: literature, OATP: organic anion transporting polypeptide, Pgp: P-glycoprotein, PON3: paraoxonase 3, UGT: UDP-glucuronosyltransferase

[a] median (range)

[b] assumed from other statins

[c] calculated from V_{max}

[d] calculated from liver S9

Table S18: Drug-dependent parameters of the simvastatin PBPK model (adopted from [150]) *(continued)*

Parameter	Unit	Model	Literature[a]	Reference	Description
Cellular permeability	cm/min	1.17E-4 (Calc)	Charge-dependent Schmitt normalized to PK-Sim	[2]	Permeability into the cellular space

-: not given, asm: assumption, BCRP: breast cancer resistance protein, calc: calculated, CYP: cytochrome P450, fit: optimized during parameter identification, GFR: glomerular filtration rate, lit: literature, OATP: organic anion transporting polypeptide, Pgp: P-glycoprotein, PON3: paraoxonase 3, UGT: UDP-glucuronosyltransferase

[a] median (range)

[b] assumed from other statins

[c] calculated from V_{max}

[d] calculated from liver S9

5.4.2 Carbamazepine-simvastatin clinical DDI studies

Table S19: Clinical studies investigating the carbamazepine-simvastatin DDI

Carbamazepine administration		Simvastatin administration		n	Healthy [%]	Females [%]	Age[a] [years]	Weight[a] [kg]	Height [cm]	Reference
Dose [mg]	**Route**	**Dose [mg]**	**Route**							
200/300	po (tab), 200 mg bid (D1-D2), 300 mg tid (D3-D14)	80	po (tab), sd (D15)	12	100	0	22-31	66-93	-	Ucar 2004 [196]

-: not given, bid: twice daily, D: day, po: oral, sd: single dose, tab: tablet, tid: three times daily

[a] range

5.4.3 Profiles

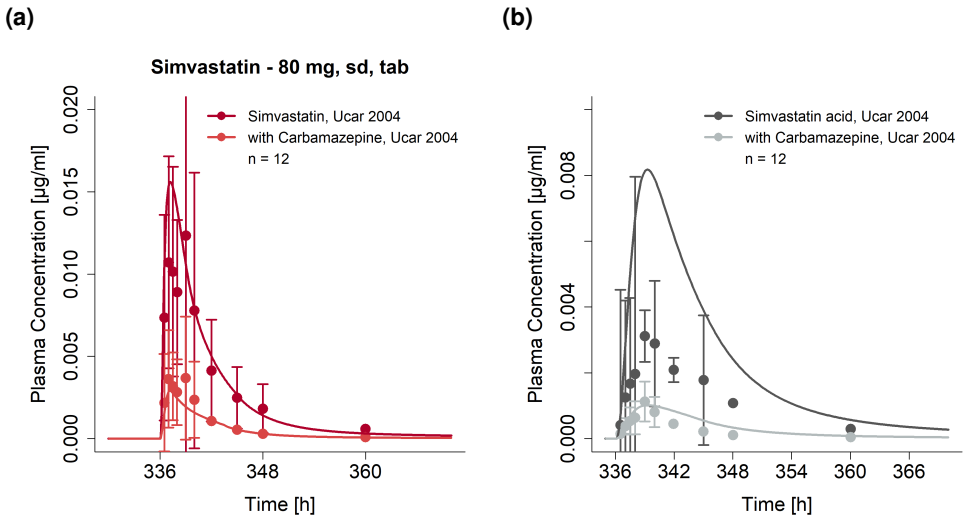

Figure S31: Predicted compared to observed (a) simvastatin and (b) simvastatin acid plasma concentration-time profiles (linear) before and during carbamazepine co-administration. Observed data are shown as dots ± standard deviation; model predictions are shown as solid lines. Details on dosing regimens, study population and literature reference are listed in Table S19. sd: single dose, tab: tablet

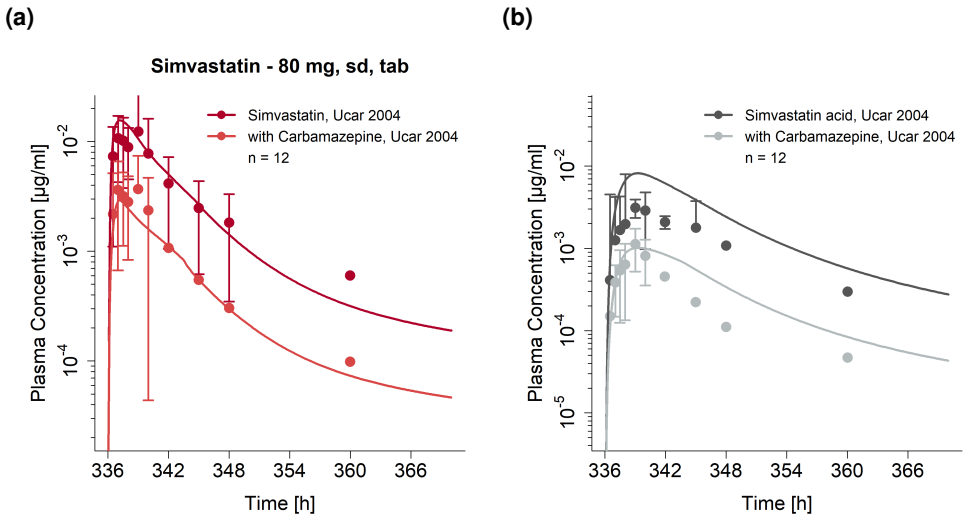

Figure S32: Predicted compared to observed (a) simvastatin and (b) simvastatin acid plasma concentration-time profiles (semi-logarithmic) before and during carbamazepine co-administration. Observed data are shown as dots ± standard deviation; model predictions are shown as solid lines. Details on dosing regimens, study population and literature reference are listed in Table S19. sd: single dose, tab: tablet

5.4.4 DDI AUC_{last} and C_{max} ratio goodness-of-fit plots

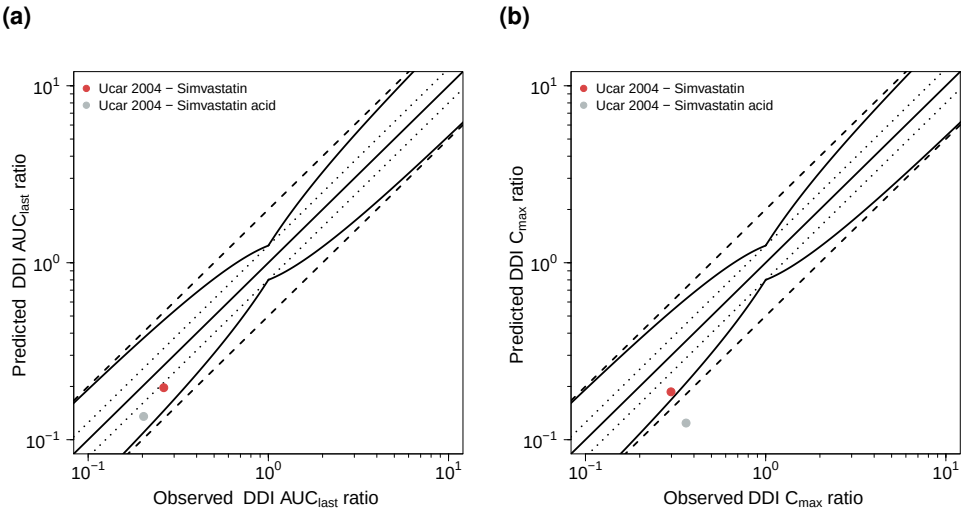

Figure S33: Predicted compared to observed carbamazepine-simvastatin (a) DDI AUC_{last} and (b) DDI C_{max} ratios. The straight solid line marks the line of identity, the curved solid lines show the prediction success limits proposed by Guest et al. allowing for 1.25-fold variability of the DDI ratio [109]. Dotted lines indicate 1.25-fold, dashed lines indicate 2-fold deviation. AUC_{last}: area under the plasma concentration-time curve from the time of drug administration to the last concentration measurement, C_{max}: maximum plasma concentration, DDI: drug-drug interaction

5.4.5 Geometric mean fold error of predicted DDI AUC_{last} and C_{max} ratios

Table S20: Predicted and observed carbamazepine-simvastatin DDI AUC_{last} and C_{max} ratios with geometric mean fold errors

Perpetrator	**Victim**				**DDI AUC_{last} ratio**			**DDI C_{max} ratio**			
Carbamazepine	Simvastatin	**Compound**	**Dose gap [h]**	**n**	**Pred**	**Obs**	**Pred/Obs**	**Pred**	**Obs**	**Pred/Obs**	**Reference**
200/300 mg, po, bid/tid	80 mg, po, sd	Simvastatin	12	12	0.20	0.26	0.75	0.19	0.30	0.63	Ucar 2004 [196]
200/300 mg, po, bid/tid	80 mg, po, sd	Simvastatin acid	12	12	0.14	0.20	0.67	0.12	0.36	0.34	Ucar 2004 [196]
mean GMFE (Simvastatin)							**1.34**			**1.60**	
							1/1 with GMFE ≤ 2			**1/1 with GMFE ≤ 2**	
mean GMFE (Simvastatin acid)							**1.50**			**2.91**	
							1/1 with GMFE ≤ 2			**0/1 with GMFE ≤ 2**	

AUC_{last}: area under the plasma concentration-time curve from the time of drug administration to the last concentration measurement, bid: twice daily, C_{max}: maximum plasma concentration, DDI: drug-drug interaction, GMFE: geometric mean fold error, obs: observed, po: oral, pred: predicted, sd: single dose, tid: three times daily

5.5 Carbamazepine-bupropion DDI

The carbamazepine-bupropion interaction was modeled using a previously established whole-body parent-metabolite PBPK model of bupropion [197]. Bupropion is a sensitive CYP2B6 substrate, with hydroxybupropion as the main metabolite. CYP2B6 metabolism is described in the model using Michaelis-Menten kinetics. The drug-dependent parameters of the bupropion model are reproduced in Table S21. The k_{cat} for bupropion CYP2B6 metabolism was slightly adjusted (k_{cat} = 40.0 1/min), assuming variability of the CYP2B6 expression in the relatively small DDI study population, to better match the plasma concentration-time profile. The adjusted k_{cat} was then applied for the control and the DDI simulations of this study.

The carbamazepine-bupropion DDI was modeled as induction of bupropion CYP2B6 metabolism by carbamazepine. Induction of CYP2B6 by carbamazepine was described using EC_{50} = 20.0 µmol/l from literature and E_{max} = 17.0 identified during the carbamazepine parameter identification.

Details on the modeled clinical DDI study are given in Table S22. Model predictions of bupropion, hydroxybupropion, erythrohydrobupropion and threohydrobupropion plasma concentration-time profiles before and during carbamazepine co-administration, compared to observed data, are shown in Figures S34 (linear) and S35 (semi-logarithmic). The correlation of predicted to observed DDI AUC_{last} and C_{max} ratios is shown in Figure S36. Table S23 lists the corresponding predicted and observed DDI AUC_{last} ratios, DDI C_{max} ratios, as well as GMFE values.

5.5.1 Bupropion drug-dependent parameters

Table S21: Drug-dependent parameters of the bupropion PBPK model (adopted from [197])

Parameter	Unit	Model	Literature	Reference	Description
Bupropion					
MW	g/mol	239.74 (Lit)	239.74	[154]	Molecular weight
logP	-	2.70 (Fit)	3.27	[154]	Lipophilicity
Solubility (pH)	mg/ml	364.56 (7.4) (Lit)	364.56 (7.4)	[198]	Solubility
fu	%	16.0 (Lit)	16.0	[199]	Fraction unbound in plasma
pKa (base)	-	8.75 (Lit)	8.75	[200]	Acid dissociation constant
K_m (CYP2B6)	µmol/l	25.80 (Lit)	25.80[a]	[88]	CYP2B6 Michaelis-Menten constant
k_{cat} (CYP2B6)	1/min	21.74 (Fit)	-	-	CYP2B6 catalytic rate constant for wildtype
K_m (CYP2C19)	µmol/l	8.30 (Lit)	8.30	[201]	CYP2C19 Michaelis-Menten constant
k_{cat} (CYP2C19)	1/min	2.59 (Fit)	-	-	CYP2C19 catalytic rate constant
K_m (11β-HSD1) EBUP	µmol/l	39.1 (Lit)	39.1	[202]	11β-HSD Michaelis-Menten constant for EBUP formation
k_{cat} (11β-HSD1) EBUP	1/min	2.15 (Fit)	-	-	11β-HSD catalytic rate constant for EBUP formation
K_m (11β-HSD1) TBUP	µmol/l	39.1 (Lit)	39.1	[202]	11β-HSD Michaelis-Menten constant for TBUP formation
k_{cat} (11β-HSD1) TBUP	1/min	8.18 (Fit)	-	-	11β-HSD catalytic rate constant for TBUP formation
K_D (NAT1)	µmol/l	0.44 (Lit)	0.44	[203]	NAT1 dissociation constant
k_{off} (NAT1)	1/min	0.05 (Fit)	-	-	NAT1 dissociation rate constant
GFR fraction	-	1 (Asm)	-	-	Fraction of filtered drug in the urine
Intestinal permeability	cm/min	3.30E-05 (Fit)	-	-	Transcellular intestinal permeability
Partition coefficients	-	Diverse	PK-Sim Standard	[79]	Cell to plasma partition coefficients
Cellular permeability	cm/min	0.14 (Calc)	Charge-dependent Schmitt	[2]	Permeability into the cellular space
IR tablet Weibull time	min	3.12 (Fit)	-	-	Dissolution time (50% dissolved)
IR tablet Weibull shape	-	0.75 (Fit)	-	-	Dissolution profile shape
Hydroxybupropion					
MW	g/mol	255.74 (Lit)	255.74	[154]	Molecular weight
logP	-	1.90 (Fit)	2.20	[204]	Lipophilicity

-: not given, 11β-HSD1: 11β-hydroxysteroid dehydrogenase 1, asm: assumption, calc: calculated, CYP: cytochrome P450, EBUP: erythrohydrobupropion, fit: optimized during parameter identification, IR: immediate release tablet formulation, GFR: glomerular filtration rate, lit: literature, NAT1: norepinephrine transporter 1, TBUP: threohydrobupropion, UGT: UDP-glucuronosyltransferase

[a] $fu_{incubation}$ was applied to in vitro literature value

Table S21: Drug-dependent parameters of the bupropion PBPK model (adopted from [197]) *(continued)*

Parameter	Unit	Model	Literature	Reference	Description
Solubility (pH)	mg/ml	0.91 (7.4) (Lit)	0.91 (7.4)	[154]	Solubility
fu	%	23.0 (Lit)	23.0	[199]	Fraction unbound in plasma
pKa (base)	-	7.65 (Lit)	7.65	[154]	Acid dissociation constant
K_m (UGT2B7)	µmol/l	14.64 (Lit)	14.64[a]	[205]	UGT2B7 Michaelis-Menten constant
k_{cat} (UGT2B7)	1/min	1.38 (Fit)	-	[205]	UGT2B7 catalytic rate constant
GFR fraction	-	1 (Asm)	-	-	Fraction of filtered drug in the urine
Partition coefficients	-	Diverse	Berezhkovskiy	[187]	Cell to plasma partition coefficients
Cellular permeability	cm/min	0.01 (Calc)	Charge-dependent Schmitt	[2]	Permeability into the cellular space
Erythrohydrobupropion					
MW	g/mol	241.76 (Lit)	241.76	[154]	Molecular weight
logP	-	1.76 (Fit)	2.88	[206]	Lipophilicity
Solubility (pH)	mg/ml	82.98 (7.4) (Lit)	82.98 (7.4)	[154]	Solubility
fu	%	58.0 (Lit)	58.0	[199]	Fraction unbound in plasma
pKa (base)	-	9.71 (Lit)	9.71	[154]	Acid dissociation constant
K_m (UGT2B7)	µmol/l	9.33 (Lit)	9.33[a]	[205]	UGT2B7 Michaelis-Menten constant
k_{cat} (UGT2B7)	1/min	0.38 (Fit)	-	-	UGT2B7 catalytic rate constant
GFR fraction	-	1 (Asm)	-	-	Fraction of filtered drug in the urine
Partition coefficients	-	Diverse	Berezhkovskiy	[187]	Cell to plasma partition coefficients
Cellular permeability	cm/min	0.01 (Calc)	Charge-dependent Schmitt	[2]	Permeability into the cellular space
Threohydrobupropion					
MW	g/mol	241.76 (Lit)	241.76	[154]	Molecular weight
logP	-	1.76 (Fit)	2.88	[206]	Lipophilicity
Solubility (pH)	mg/ml	82.98 (7.4) (Lit)	82.98 (7.4)	[154]	Solubility
fu	%	58.0 (Lit)	58.0	[199]	Fraction unbound in plasma
pKa (base)	-	9.71 (Lit)	9.71	[154]	Acid dissociation constant
K_m (UGT2B7)	µmol/l	6.22 (Lit)	6.22[a]	[205]	UGT2B7 Michaelis-Menten constant
k_{cat} (UGT2B7)	1/min	0.10 (Fit)	-	-	UGT2B7 catalytic rate constant

-: not given, 11β-HSD1: 11β-hydroxysteroid dehydrogenase 1, asm: assumption, calc: calculated, CYP: cytochrome P450, EBUP: erythrohydrobupropion, fit: optimized during parameter identification, IR: immediate release tablet formulation, GFR: glomerular filtration rate, lit: literature, NAT1: norepinephrine transporter 1, TBUP: threohydrobupropion, UGT: UDP-glucuronosyltransferase

[a] $fu_{incubation}$ was applied to in vitro literature value

Table S21: Drug-dependent parameters of the bupropion PBPK model (adopted from [197]) *(continued)*

Parameter	Unit	Model	Literature	Reference	Description
GFR fraction	-	1 (Asm)	-	-	Fraction of filtered drug in the urine
Partition coefficients	-	Diverse	Berezhkovskiy	[187]	Cell to plasma partition coefficients
Cellular permeability	cm/min	0.01 (Calc)	Charge-dependent Schmitt	[2]	Permeability into the cellular space

-: not given, 11β-HSD1: 11β-hydroxysteroid dehydrogenase 1, asm: assumption, calc: calculated, CYP: cytochrome P450, EBUP: erythrohydrobupropion, fit: optimized during parameter identification, IR: immediate release tablet formulation, GFR: glomerular filtration rate, lit: literature, NAT1: norepinephrine transporter 1, TBUP: threohydrobupropion, UGT: UDP-glucuronosyltransferase

[a] $fu_{incubation}$ was applied to in vitro literature value

5.5.2 Carbamazepine-bupropion clinical DDI studies

Table S22: Clinical studies investigating the carbamazepine-bupropion DDI

Carbamazepine administration		Bupropion administration		n	Healthy [%]	Females [%]	Age[a] [years]	Weight [kg]	Height [cm]	Reference
Dose [mg]	Route	Dose [mg]	Route							
-	-	150	po (tab), sd	17	100	53	38.5	-	-	Ketter 1995[d] [207]
314[b]	po (-), tid[b]	150	po (tab), sd	12	0[c]	40	35.4	-	-	Ketter 1995[e] [207]

-: not given, po: oral, sd: single dose, tab: tablet, tid: three times daily, qid: four times daily

[a] mean

[b] patients received a mean dose of 942 mg per day, in three to four doses

[c] patients with major affective disorders on chronic carbamazepine treatment for at least 3 weeks before bupropion intake

[d] control arm of the study

[e] DDI arm of the study

5.5.3 Profiles

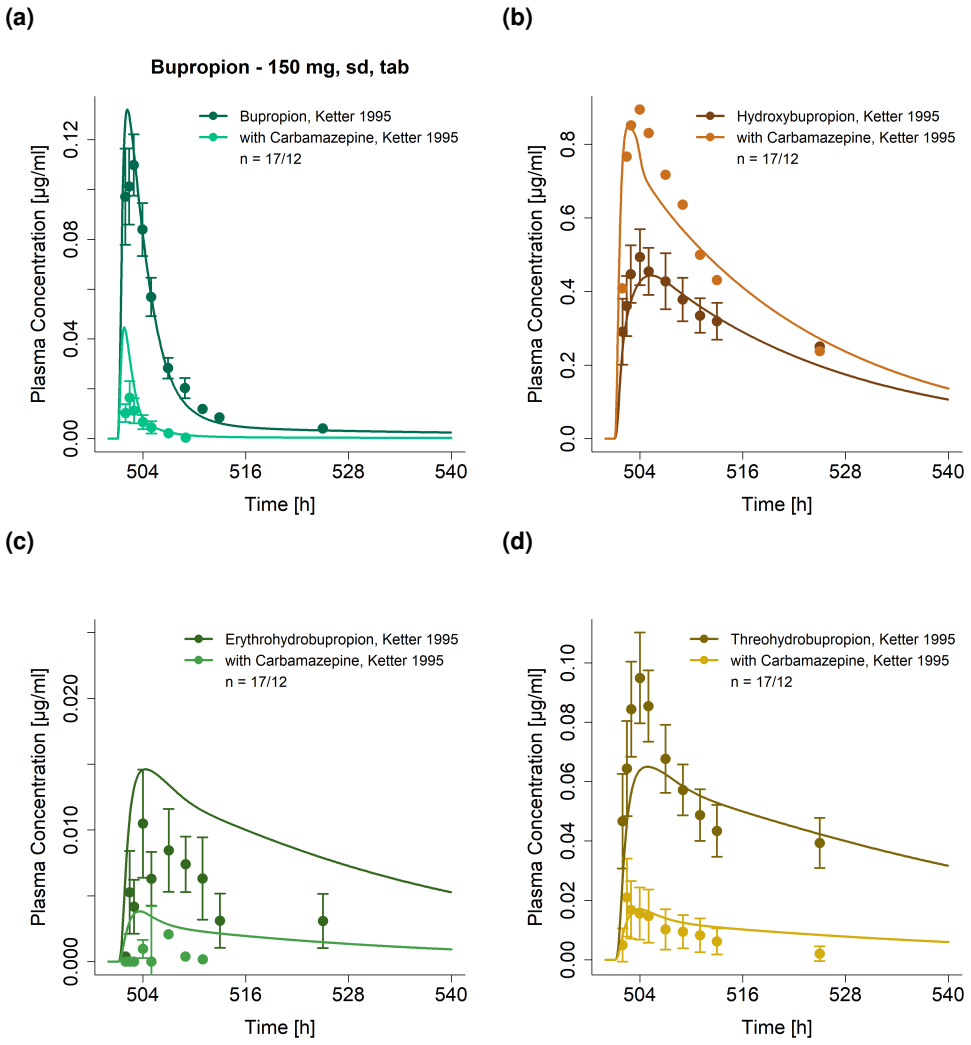

Figure S34: Predicted compared to observed (a) bupropion, (b) hydroxybupropion, (c) erythrohydrobupropion and (d) threohydrobupropion plasma concentration-time profiles (linear) before and during carbamazepine co-administration. Observed data are shown as dots ± standard deviation; model predictions are shown as solid lines. Details on dosing regimens, study populations and literature reference are listed in Table S22. sd: single dose, tab: tablet

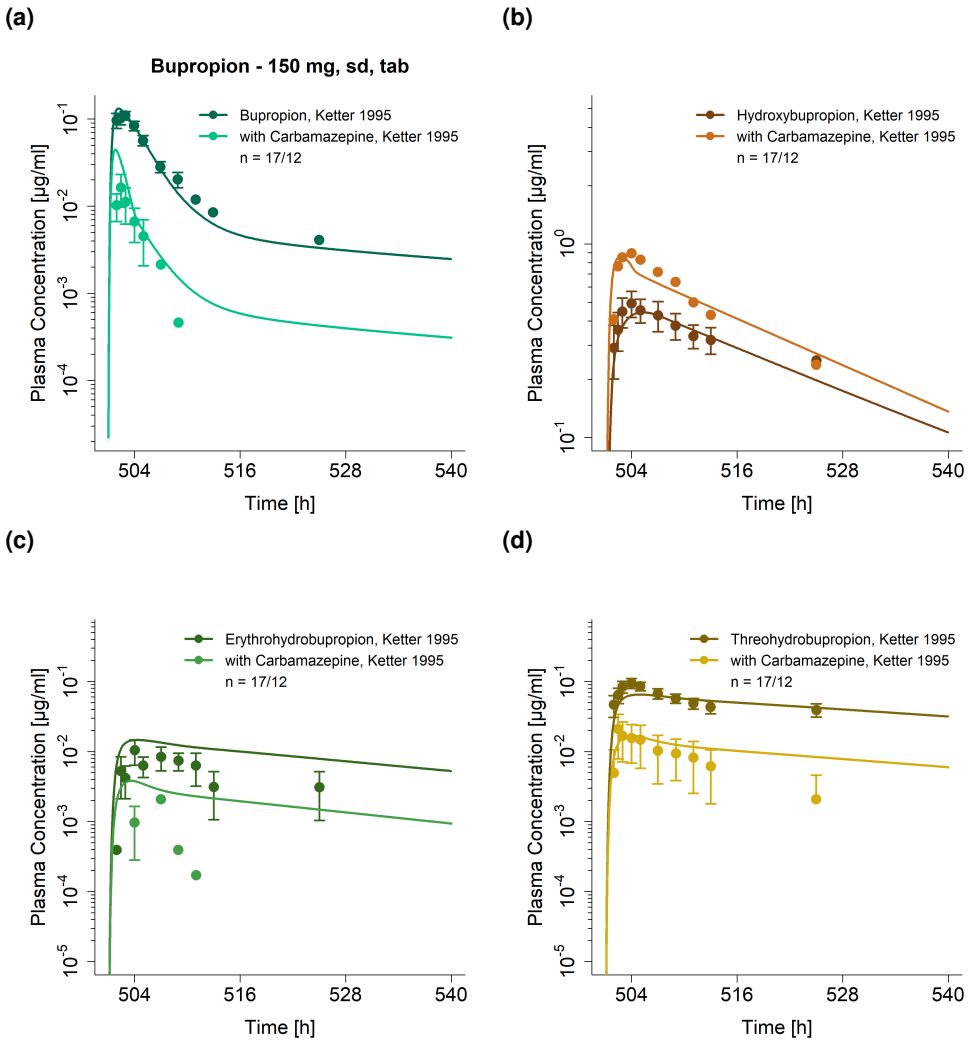

Figure S35: Predicted compared to observed (a) bupropion, (b) hydroxybupropion, (c) erythrohydrobupropion (d) and threohydrobupropion plasma concentration-time profiles (semi-logarithmic) before and during carbamazepine co-administration. Observed data are shown as dots ± standard deviation; model predictions are shown as solid lines. Details on dosing regimens, study populations and literature reference are listed in Table S22. sd: single dose, tab: tablet

5.5.4 DDI AUC_{last} and C_{max} ratio goodness-of-fit plots

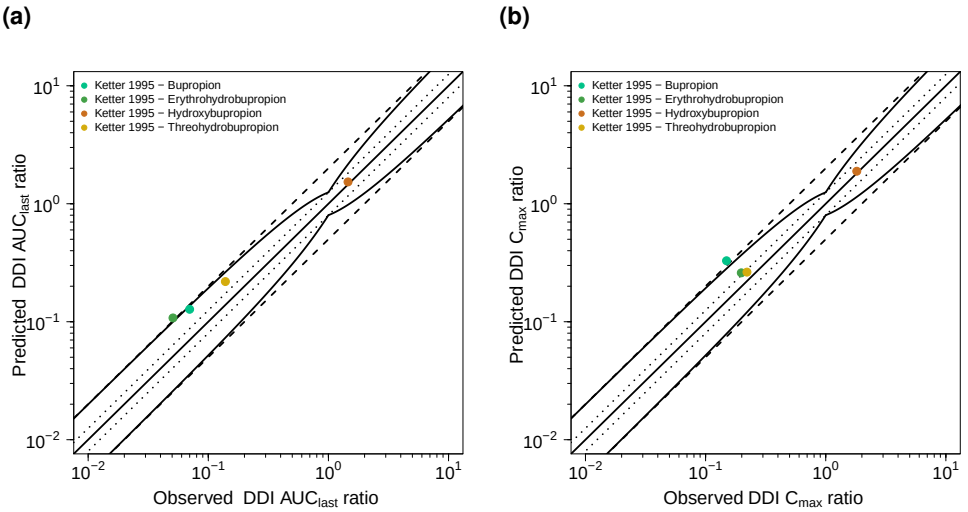

Figure S36: Predicted compared to observed carbamazepine-bupropion (a) DDI AUC_{last} and (b) DDI C_{max} ratios. The straight solid line marks the line of identity, the curved solid lines show the prediction success limits proposed by Guest et al. allowing for 1.25-fold variability of the DDI ratio [109]. Dotted lines indicate 1.25-fold, dashed lines indicate 2-fold deviation. AUC_{last}: area under the plasma concentration-time curve from the time of drug administration to the last concentration measurement, C_{max}: maximum plasma concentration, DDI: drug-drug interaction

5.5.5 Geometric mean fold error of predicted DDI AUC_{last} and C_{max} ratios

Table S23: Predicted and observed carbamazepine-bupropion DDI AUC_{last} and C_{max} ratios with geometric mean fold errors

Perpetrator	**Victim**				**DDI AUC_{last} ratio**			**DDI C_{max} ratio**			
Carbamazepine	Bupropion	**Compound**	**Dose gap [h]**	**n**	**Pred**	**Obs**	**Pred/Obs**	**Pred**	**Obs**	**Pred/Obs**	**Reference**
314 mg, po, tid	150 mg, po, sd	Bupropion	3	17/12	0.13	0.07	1.82	0.33	0.15	2.20	Ketter 1995 [207]
314 mg, po, tid	150 mg, po, sd	Hydroxybupropion	3	17/12	1.53	1.46	1.05	1.89	1.81	1.04	Ketter 1995 [207]
314 mg, po, tid	150 mg, po, sd	Erythrohydrobupropion	3	17/12	0.11	0.05	2.12	0.26	0.20	1.31	Ketter 1995 [207]
314 mg, po, tid	150 mg, po, sd	Threohydrobupropion	3	17/12	0.22	0.14	1.58	0.26	0.22	1.19	Ketter 1995 [207]
mean GMFE (Bupropion)							**1.82**			**2.20**	
							1/1 with GMFE ≤ 2			**0/1 with GMFE ≤ 2**	
mean GMFE (Hydroxybupropion)							**1.05**			**1.04**	
							1/1 with GMFE ≤ 2			**1/1 with GMFE ≤ 2**	
mean GMFE (Erythrohydrobupropion)							**2.12**			**1.31**	
							0/1 with GMFE ≤ 2			**1/1 with GMFE ≤ 2**	
mean GMFE (Threohydrobupropion)							**1.58**			**1.19**	
							1/1 with GMFE ≤ 2			**1/1 with GMFE ≤ 2**	

AUC_{last}: area under the plasma concentration-time curve from the time of drug administration to the last concentration measurement, C_{max}: maximum plasma concentration, DDI: drug-drug interaction, GMFE: geometric mean fold error, obs: observed, po: oral, pred: predicted, sd: single dose, tid: three times daily

5.6 Efavirenz-carbamazepine DDI

The efavirenz-carbamazepine DDI was modeled using a previously developed whole-body PBPK model of efavirenz, available in the OSP GitHub model repository (https://github.com/Open-Systems-Pharmacology/Efavirenz-Model), which was updated prior to DDI modeling with carbamazepine as described in Sections 3 and 6. Efavirenz is substrate and inducer of CYP3A4 and CYP2B6. The drug-dependent parameters of the updated efavirenz model are shown in Table S6.

The efavirenz-carbamazepine DDI was modeled as induction and simultaneous competitive inhibition of carbamazepine CYP3A4 and CYP2B6 metabolism by efavirenz and as induction of efavirenz CYP3A4 and CYP2B6 metabolism by carbamazepine. K_i = 9.67 µmol/l and K_i = 0.40 µmol/l, describing the competitive CYP3A4 and CYP2B6 inhibition by efavirenz, respectively, were taken from literature and corrected for binding in the in vitro assay, as described in Section 3. EC_{50} = 0.23 µmol/l to describe the CYP3A4 and CYP2B6 induction by efavirenz was taken from literature and corrected for binding in the in vitro assay, E_{max} = 12.0 (CYP3A4) and E_{max} = 8.13 (CYP2B6), were identified during parameter identification. EC_{50} = 20.0 µmol/l describing CYP3A4 and CYP2B6 induction by carbamazepine was taken from literature. E_{max} = 6.0 (CYP3A4) and E_{max} = 17.0 (CYP2B6), were optimized during parameter identification.

Details on the modeled clinical DDI study are given in Table S24. Model predictions of carbamazepine, carbamazepine-10-11-epoxide and efavirenz plasma concentration-time profiles before and during co-administration, compared to observed data, are shown in Figures S37 (linear) and S38 (semi-logarithmic). The correlation of predicted to observed DDI AUC_{last} and C_{max} ratios is shown in Figure S39. Table S25 lists the corresponding predicted and observed DDI AUC_{last} ratios, DDI C_{max} ratios, as well as GMFE values.

5.6.1 Efavirenz-carbamazepine clinical DDI studies

Table S24: Clinical studies investigating the efavirenz-carbamazepine DDI

Efavirenz administration		Carbamazepine administration		n	Healthy [%]	Females [%]	Age[a] [years]	Weight[a] [kg]	Height [cm]	Reference
Dose [mg]	**Route**	**Dose [mg]**	**Route**							
600	po (tab), qd (D22-D35)	200/400	po (tab), 200 mg, qd (D1-D3), mg, bid (D4-D6), 400 mg, qd (D7-D35)	36	100	31	20-45	54-92	-	Ji 2008[b] [44]
600	po (tab), qd (D1-D35)	200/400	po (tab), 200 mg, qd (D15-D17), mg, bid (D18-D20), 400 mg, qd (D21-D35)	36	100	31	20-45	54-92	-	Ji 2008[c] [44]

-: not given, bid: twice daily, D: day, po: oral, qd: once daily, tab: tablet

[a] range

[b] Carbamazepine as victim drug

[c] Efavirenz as victim drug

5.6.2 Profiles

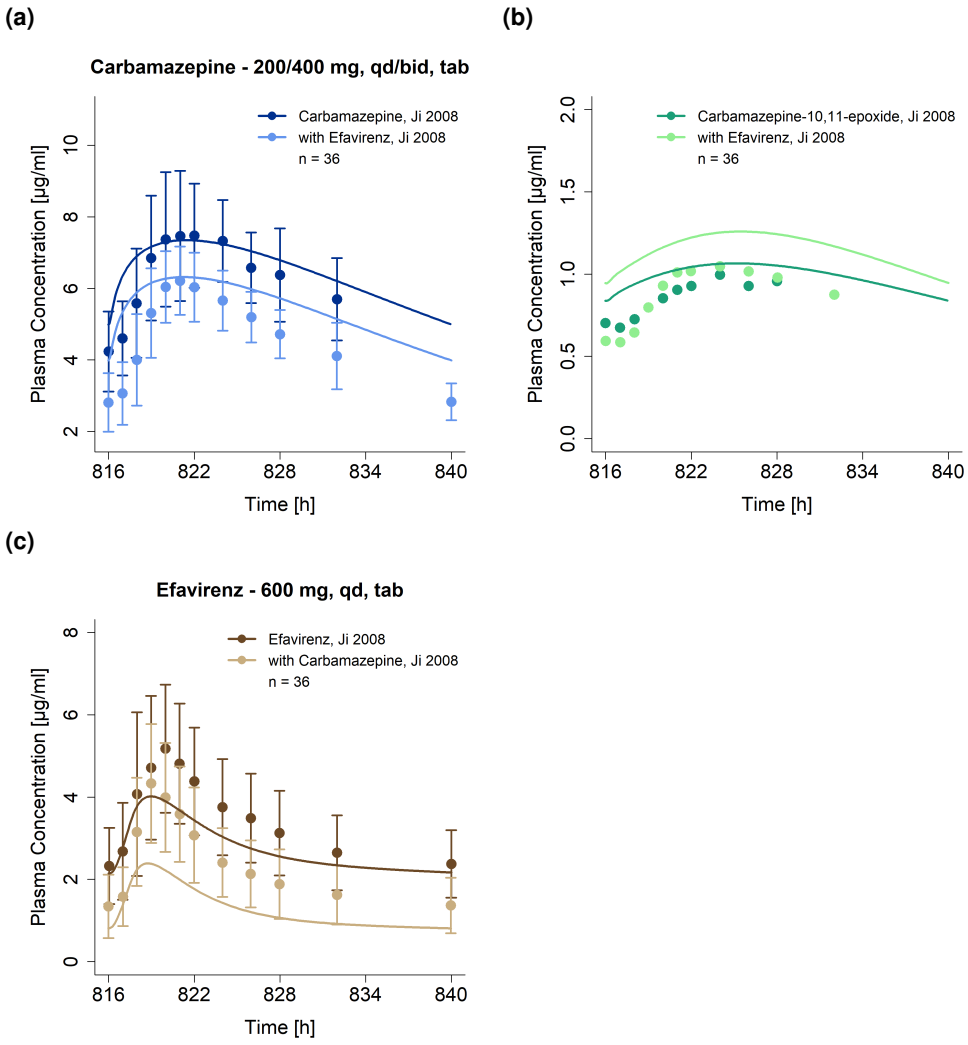

Figure S37: Predicted compared to observed (a) carbamazepine, (b) carbamazepine-10-11-epoxide and (c) efavirenz plasma concentration-time profiles (linear) before and during co-administration. Observed data are shown as dots ± standard deviation; model predictions are shown as solid lines. Details on dosing regimens, study population and literature reference are listed in Table S24. bid: twice daily, qd: once daily, tab: tablet

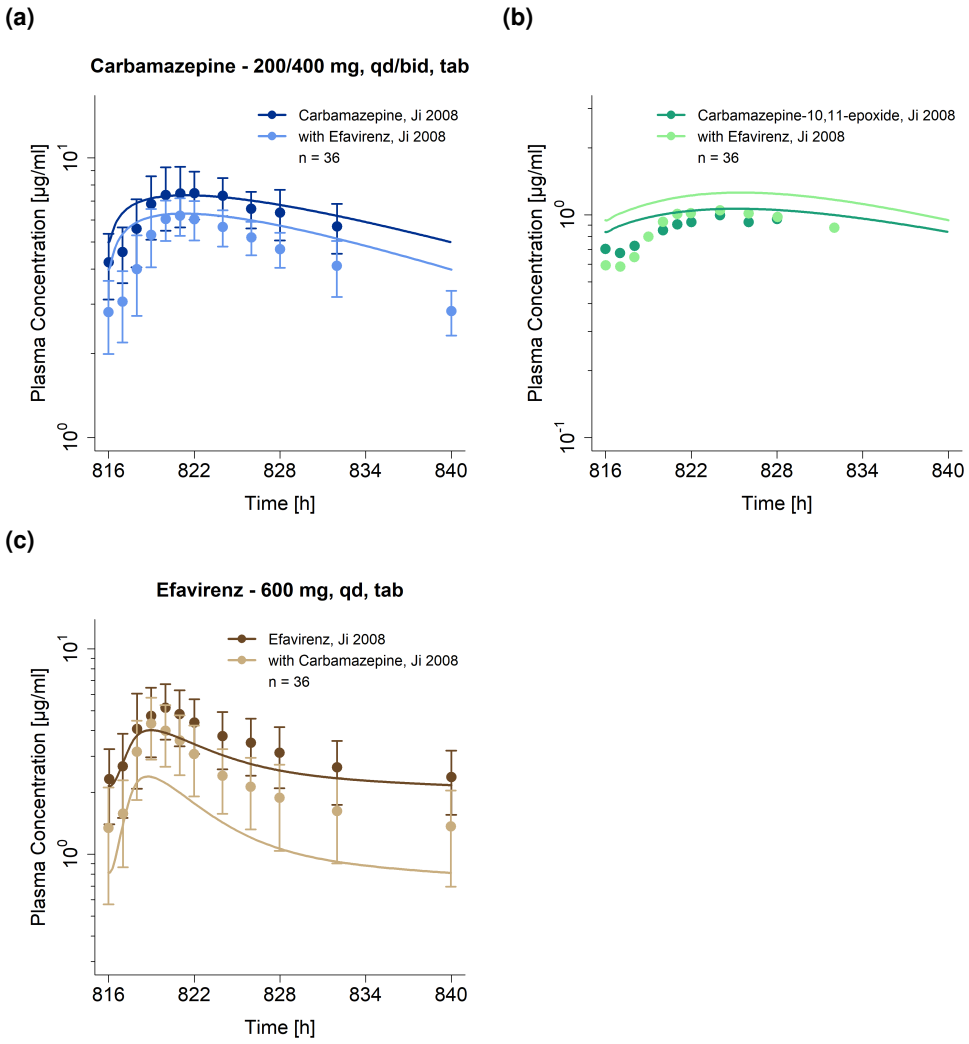

Figure S38: Predicted compared to observed (a) carbamazepine, (b) carbamazepine-10-11-epoxide and (c) efavirenz plasma concentration-time profiles (semi-logarithmic) before and during co-administration. Observed data are shown as dots ± standard deviation; model predictions are shown as solid lines. Details on dosing regimens, study population and literature reference are listed in Table S24. bid: twice daily, qd: once daily, tab: tablet

5.6.3 DDI AUC_{last} and C_{max} ratio goodness-of-fit plots

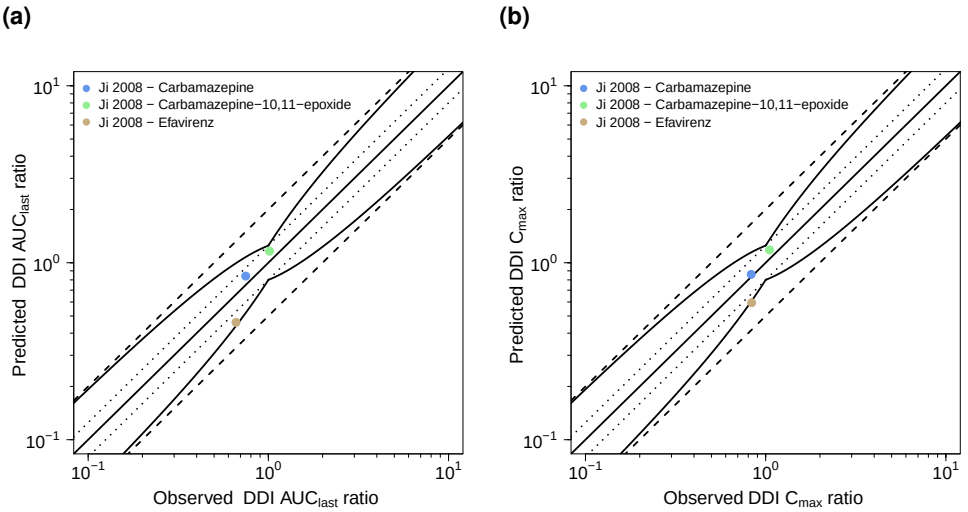

Figure S39: Predicted compared to observed efavirenz-carbamazepine (a) DDI AUC_{last} and (b) DDI C_{max} ratios. The straight solid line marks the line of identity, the curved solid lines show the prediction success limits proposed by Guest et al. allowing for 1.25-fold variability of the DDI ratio [109]. Dotted lines indicate 1.25-fold, dashed lines indicate 2-fold deviation. AUC_{last}: area under the plasma concentration-time curve from the time of drug administration to the last concentration measurement, C_{max}: maximum plasma concentration, DDI: drug-drug interaction

5.6.4 Geometric mean fold error of predicted DDI AUC_{last} and C_{max} ratios

Table S25: Predicted and observed efavirenz-carbamazepine DDI AUC_{last} and C_{max} ratios with geometric mean fold errors

					DDI AUC_{last} ratio			DDI C_{max} ratio			
Perpetrator	**Victim**	**Compound**	**Dose gap [h]**	**n**	**Pred**	**Obs**	**Pred/Obs**	**Pred**	**Obs**	**Pred/Obs**	**Reference**
Efavirenz	*Carbamazepine*										
600 mg, po, qd	200/400 mg, po, bid/qd	Carbamazepine	0	36	0.84	0.75	1.12	0.86	0.83	1.03	Ji 2008 [44]
600 mg, po, qd	200/400 mg, po, bid/qd	Carbamazepine-10,11-epoxide	0	36	1.16	1.02	1.14	1.18	1.05	1.12	Ji 2008 [44]
Carbamazepine	*Efavirenz*										
200/400 mg, po, bid/qd	600 mg, po, qd	Efavirenz	0	36	0.46	0.66	0.70	0.59	0.84	0.71	Ji 2008 [44]
mean GMFE (Carbamazepine)							**1.12**			**1.03**	
							1/1 with GMFE ≤ 2			**1/1 with GMFE ≤ 2**	
mean GMFE (Carbamazepine-10,11-epoxide)							**1.14**			**1.12**	
							1/1 with GMFE ≤ 2			**1/1 with GMFE ≤ 2**	
mean GMFE (Efavirenz)							**1.44**			**1.41**	
							1/1 with GMFE ≤ 2			**1/1 with GMFE ≤ 2**	

AUC_{last}: area under the plasma concentration-time curve from the time of drug administration to the last concentration measurement, bid: twice daily, C_{max}: maximum plasma concentration, DDI: drug-drug interaction, GMFE: geometric mean fold error, md: multiple-dose, obs: observed, po: oral, pred: predicted, qd: once daily

6 Efavirenz drug-drug interactions (DDI)

6.1 DDI modeling - general

A total number of 9 different clinical DDI studies was utilized to evaluate the DDI performance of the efavirenz PBPK model, including studies with CYP3A4 victim drugs (midazolam and alfentanil), a CYP2B6 victim drug (bupropion), a CYP3A4 and CYP2B6 perpetrator (rifampin) and a simultaneous CYP3A4 substrate and inhibitor and CYP2B6 inhibitor (voriconazole). The efavirenz DDI network is illustrated in Figure S40. The implementation of the DDIs is described in more detail in the following sections.

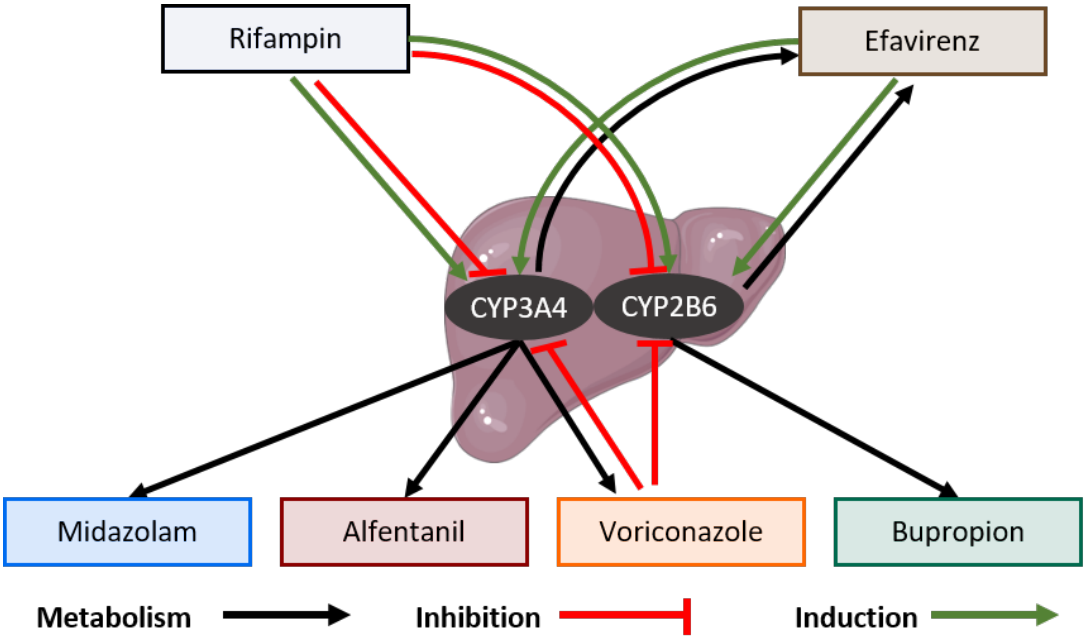

Figure S40: Efavirenz drug-drug interaction network. Black arrows represent metabolism of the compounds, red and green arrows represent inhibition or induction of the CYP enzymes, respectively

The parameters describing the induction of CYP3A4 and CYP2B6 by efavirenz were already introduced during efavirenz model building, as the compound induces its own metabolism. While the efavirenz-midazolam DDI study by Mikus et al. 2017 [208] was used in the training dataset to inform the parametrization of the efavirenz CYP3A4 induction, all other DDIs were purely predictive.

6.2 Efavirenz-midazolam DDI

The ability of the efavirenz model to predict the available clinical efavirenz-midazolam DDI data was already evaluated with the original efavirenz PBPK model [87], using a previously developed whole-body PBPK model of midazolam, available in the OSP GitHub model repository (https://github.com/Open-Systems-Pharmacology/Midazolam-Model). The metabolism of the sensitive CYP3A4 substrate midazolam is described using Michaelis-Menten kinetics [209]. The drug-dependent parameters of the midazolam model are reproduced in Table S26.

The efavirenz-midazolam DDI was modeled as induction with simultaneous competitive inhibition of midazolam CYP3A4 metabolism by efavirenz. The inhibition was described using K_i = 9.67 µmol/l from literature, corrected for binding in the in vitro assay, as described in Section 3. The induction was described using EC_{50} = 0.23 µmol/l (taken from literature and corrected for $fu_{incubation}$). The efavirenz-midazolam DDI study by Mikus et al. [208] was used in the training dataset to inform the parametrization of CYP3A4 E_{max} = 12.0.

Details on the modeled clinical DDI studies are given in Table S27. Model predictions of midazolam plasma concentration-time profiles before and during efavirenz co-administration, compared to observed data, are shown in Figures S41 (linear) and S42 (semi-logarithmic). The correlation of predicted to observed DDI AUC_{last} and C_{max} ratios is shown in Figure S43. Tables S28 and S29 list the corresponding predicted and observed DDI AUC_{last} ratios, DDI C_{max} ratios, as well as GMFE values for the updated and the original efavirenz PBPK model, respectively.

6.2.1 Midazolam drug-dependent parameters

Table S26: Drug-dependent parameters of the midazolam PBPK model (adopted from [209] and [210])

Parameter	Unit	Model	Literature	Reference	Description
MW	g/mol	325.77 (Lit)	325.77	[211]	Molecular weight
logP	log Units	2.89 (Fit)	3.00, 3.10, 3.37, 3.53	[212–215]	Lipophilicity
Solubility (pH)	mg/ml	0.05 (6.5) (Lit)	0.09 (5.0), 0.13 (5.0), 0.05 (6.5),	[216]	Solubility
fu	%	3.10 (Lit)	2.20, 3.10, 3.10	[158, 217–219]	Fraction unbound in plasma
pKa (base)	-	6.20 (Lit)	6.20	[212]	Acid dissociation constant
pKa (acid)	-	10.95 (Lit)	10.95	[212]	Acid dissociation constant
K_m (CYP3A4)	µmol/l	4.00 (Lit)	2.16, 2.69, 3.80, 3.90, 4.00	[212, 214, 220–222]	CYP3A4 Michaelis-Menten constant
k_{cat} (CYP3A4)	1/min	8.76 (Fit)	-	-	CYP3A4 catalytic rate constant
K_m (UGT1A4)	µmol/l	37.8 (Lit)	37.8	[223]	UGT1A4 Michaelis-Menten constant
k_{cat} (UGT1A4)	1/min	3.59 (Fit)	-	-	UGT1A4 catalytic rate constant
K_D (GABRG2)	nmol/l	1.80 (Lit)	1.8	[224]	GABRG2 dissociation constant
GFR fraction	-	0.64 (Fit)	-	-	Fraction of filtered drug in the urine
k_{off} (GABRG2)	1/min	1 (Asm)	-	-	GABRG2 dissociation rate constant
Intestinal permeability	cm/min	1.55E-04 (Fit)	-	-	Transcellular intestinal permeability
Partition coefficients	-	diverse	Rodgers and Rowland	[77, 78]	Cell to plasma partition coefficients
Cellular permeability	cm/min	0.04 (Calc)	PK-Sim Standard	[2]	Permeability into the cellular space
Tablet Weibull time	min	0.01 (Fit)	-	-	Dissolution time (50% dissolved)
Tablet Weibull shape	-	4.38 (Fit)	-	-	Dissolution profile shape

-: not given, asm: assumption, calc: calculated, CYP: cytochrome P450, UGT: UDP-glucuronosyltransferase, fit: optimized during parameter optimization, GABRG2: gamma-aminobutyric acid receptor subunit gamma 2, GFR: glomerular filtration rate, lit: literature

6.2.2 Efavirenz-midazolam clinical DDI studies

Table S27: Clinical studies investigating the efavirenz-midazolam DDI

Efavirenz administration		Midazolam administration		n	Healthy [%]	Females [%]	Age [years]	Weight [kg]	Height [cm]	Reference
Dose [mg]	Route	Dose [mg]	Route							
400	po (tab), qd (D1-D14)	3	po (sol), (D13)	12	-	-	-	-	-	Katzenmaier 2010 [225]
400	po (tab), sd (D1)	4	po (sol), sd (D2)	12	100	50	21-34	-	-	Mikus 2017 [208]
		2	iv, sd (D2, 6 h after po)							

-: not given, D: day, iv: intravenous, po: oral, qd: once daily, sd: single dose, sol: solution, tab: tablet

6.2.3 Profiles

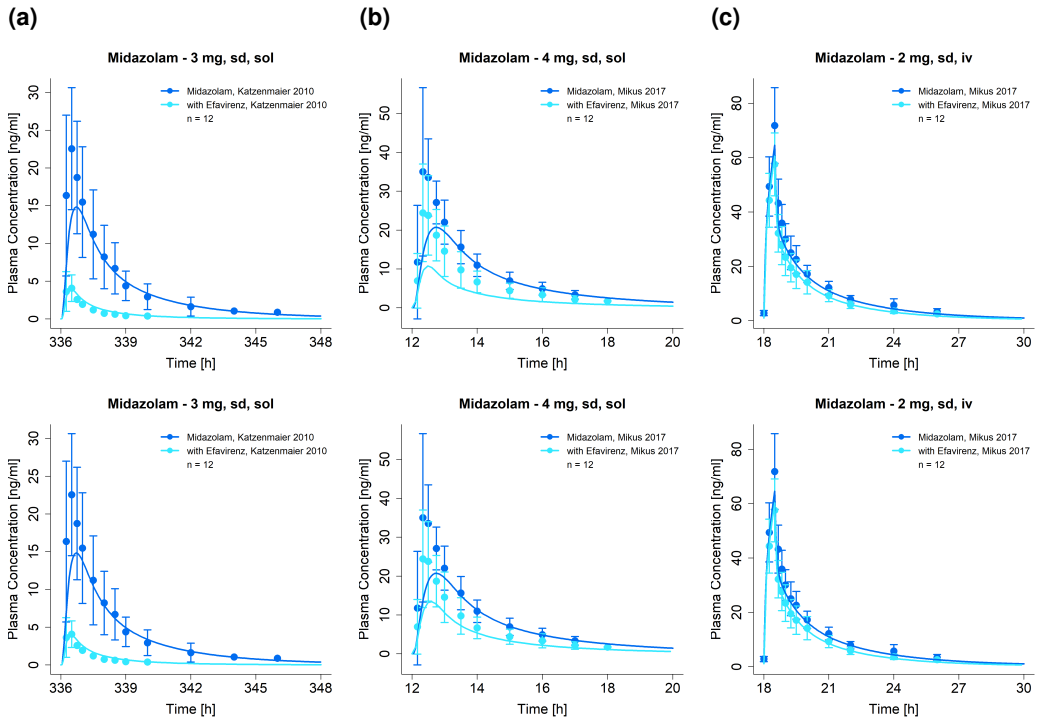

Figure S41: Predicted compared to observed midazolam plasma concentration-time profiles (linear) before and during efavirenz co-administration, predicted with the updated efavirenz model (upper row) or the original efavirenz model (lower row). Observed data are shown as dots ± standard deviation; model predictions are shown as solid lines. Details on dosing regimens, study populations and literature references are listed in Table S27. iv: intravenous, sd: single dose, sol: solution

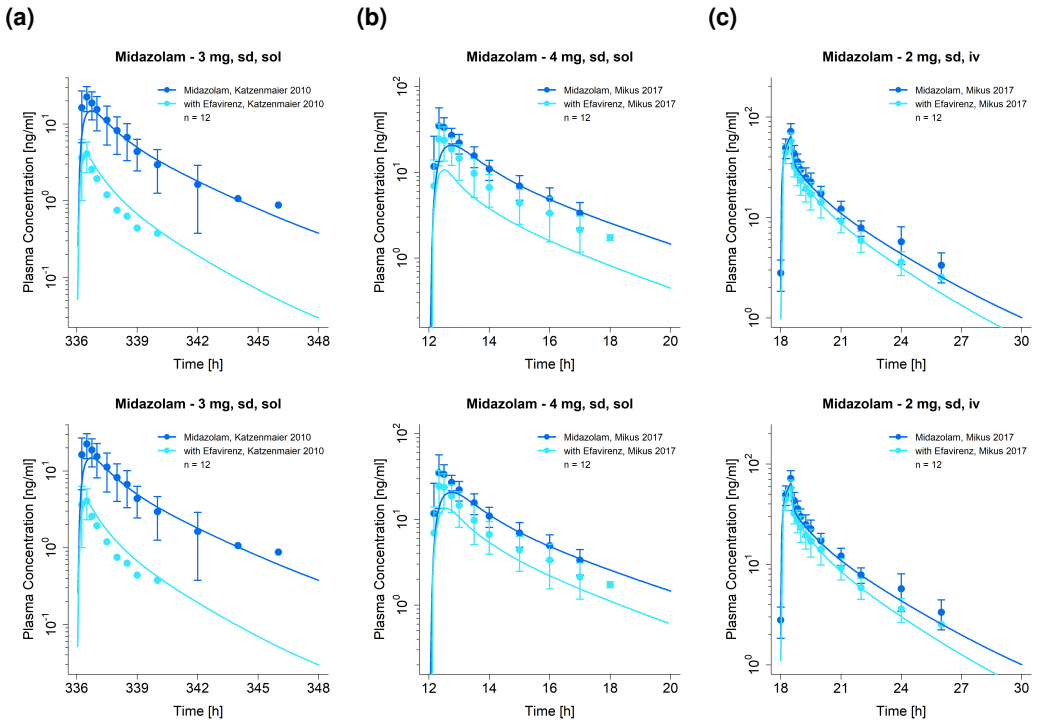

Figure S42: Predicted compared to observed midazolam plasma concentration-time profiles (semi-logarithmic) before and during efavirenz co-administration, predicted with the updated efavirenz model (upper row) or the original efavirenz model (lower row). Observed data are shown as dots ± standard deviation; model predictions are shown as solid lines. Details on dosing regimens, study populations and literature references are listed in Table S27. iv: intravenous, sd: single dose, sol: solution

6.2.4 DDI AUC_{last} and C_{max} ratio goodness-of-fit plots

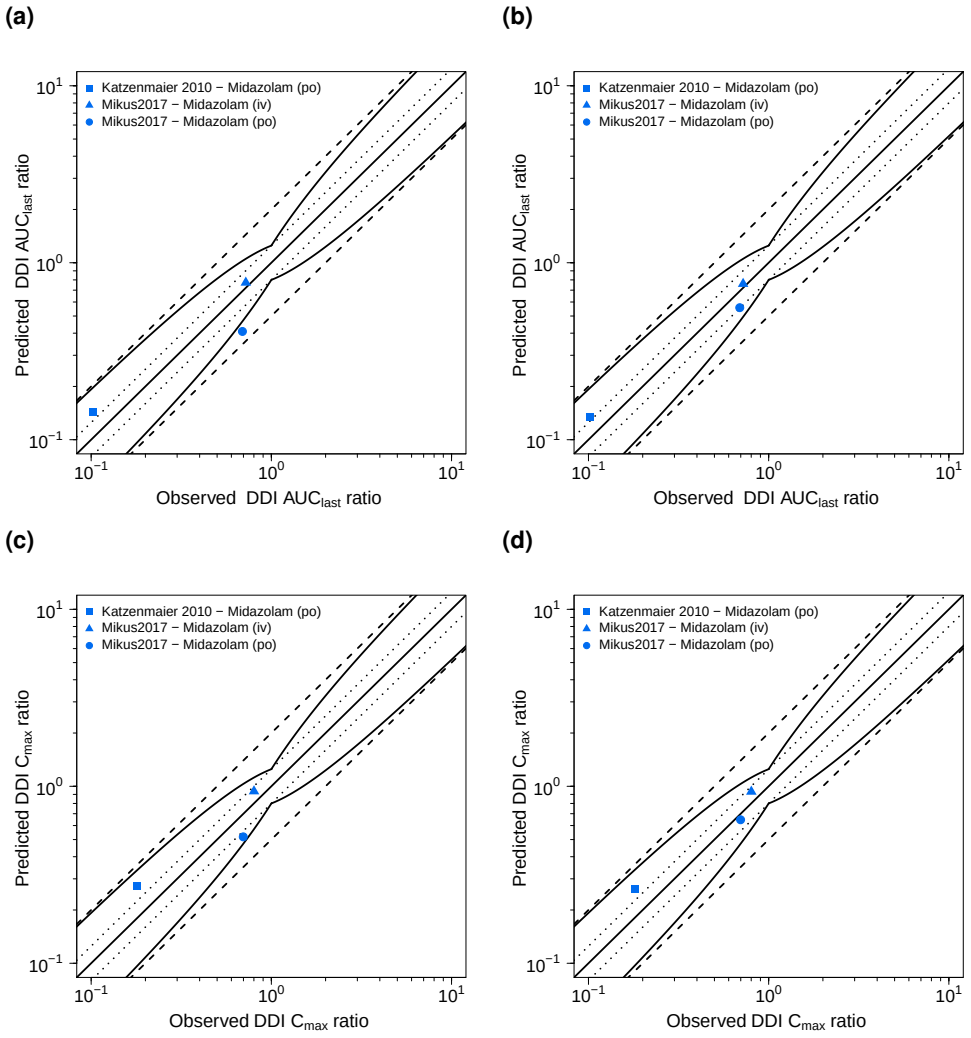

Figure S43: Predicted compared to observed efavirenz-midazolam (a,b) DDI AUC_{last} and (c,d) DDI C_{max} ratios, predicted with the updated efavirenz PBPK model (left) or the original PBPK model (right). The straight solid line marks the line of identity, the curved solid lines show the prediction success limits proposed by Guest et al. allowing for 1.25-fold variability of the DDI ratio [109]. Dotted lines indicate 1.25-fold, dashed lines indicate 2-fold deviation. AUC_{last}: area under the plasma concentration-time curve from the time of drug administration to the last concentration measurement, C_{max}: maximum plasma concentration, DDI: drug-drug interaction, iv: intravenous, po: oral

6.2.5 Geometric mean fold error of predicted DDI AUC_{last} and C_{max} ratios

Table S28: Predicted and observed efavirenz-midazolam DDI AUC_{last} and C_{max} ratios with geometric mean fold errors of the updated model

Perpetrator	**Victim**			**DDI AUC_{last} ratio**			**DDI C_{max} ratio**			
Efavirenz	Midazolam	**Dose gap [h]**	**n**	**Pred**	**Obs**	**Pred/Obs**	**Pred**	**Obs**	**Pred/Obs**	**Reference**
400 mg, po, qd	3 mg, po, sd	-	12	0.15	0.10	1.46	0.28	0.18	1.57	Katzenmaier 2010 [225]
400 mg, po, sd	4 mg, po, sd	12	12	0.42	0.69	0.61	0.53	0.70	0.75	Mikus 2017 [208]
400 mg, po, sd	2 mg, iv, sd	18	12	0.78	0.72	1.08	0.94	0.80	1.17	Mikus 2017 [208]
mean GMFE (range)						**1.40 (1.08-1.65)**			**1.36 (1.17-1.57)**	
						3/3 with GMFE ≤ 2			**3/3 with GMFE ≤ 2**	

-: not given, AUC_{last}: area under the plasma concentration-time curve from the time of drug administration to the last concentration measurement, C_{max}: maximum plasma concentration, DDI: drug-drug interaction, GMFE: geometric mean fold error, iv: intravenous, obs: observed, po: oral, pred: predicted, qd: once daily, sd: single dose

Table S29: Predicted and observed efavirenz-midazolam DDI AUC_{last} and C_{max} ratios with geometric mean fold errors of the original model

Perpetrator	**Victim**			**DDI AUC_{last} ratio**			**DDI C_{max} ratio**			
Efavirenz	Midazolam	**Dose gap [h]**	**n**	**Pred**	**Obs**	**Pred/Obs**	**Pred**	**Obs**	**Pred/Obs**	**Reference**
400 mg, po, qd	3 mg, po, sd	-	12	0.13	0.10	1.31	0.26	0.18	1.46	Katzenmaier 2010 et al. [225]
400 mg, po, sd	4 mg, po, sd	12	12	0.56	0.69	0.81	0.65	0.70	0.93	Mikus 2017 et al. [208]
400 mg, po, sd	2 mg, iv, sd	18	12	0.76	0.72	1.05	0.93	0.80	1.16	Mikus 2017 et al. [208]
mean GMFE (range)						**1.20 (1.05-1.31)**			**1.23 (1.08-1.46)**	
						3/3 with GMFE ≤ 2			**3/3 with GMFE ≤ 2**	

-: not given, AUC_{last}: area under the plasma concentration-time curve from the time of drug administration to the last concentration measurement, C_{max}: maximum plasma concentration, DDI: drug-drug interaction, GMFE: geometric mean fold error, iv: intravenous, obs: observed, po: oral, pred: predicted, qd: once daily, sd: single dose

6.3 Efavirenz-alfentanil DDI

The ability of the efavirenz model to predict the available clinical efavirenz-alfentanil DDI data was already evaluated with the original efavirenz PBPK model [87], using a previously developed whole-body PBPK model of alfentanil [210, 226] available in the OSP GitHub model repository (https://github.com/Open-Systems-Pharmacology/Alfentanil-Model). The metabolism of the sensitive CYP3A4 substrate is described in the model by a specific first-order CYP3A4 clearance (CL_{spec}). The drug-dependent parameters of the alfentanil model are reproduced in Table S30.

The efavirenz-alfentanil DDI was modeled as induction with simultaneous competitive inhibition of alfentanil CYP3A4 metabolism by efavirenz. The inhibition was described using K_i = 9.67 µmol/l from literature, corrected for binding in the in vitro assay, as described in Section 3. The induction was described using EC_{50} = 0.23 µmol/l (taken from literature and corrected for $fu_{incubation}$).

Details on the modeled clinical DDI studies are given in Table S31. Model predictions of alfentanil plasma concentration-time profiles before and during efavirenz co-administration, compared to observed data, are shown in Figures S44 (linear) and S45 (semi-logarithmic). The correlation of predicted to observed DDI AUC_{last} and C_{max} ratios is shown in Figure S52. Tables S32 and S33 list the corresponding predicted and observed DDI AUC_{last} ratios, DDI C_{max} ratios, as well as GMFE values for the updated and the original efavirenz PBPK model, respectively.

6.3.1 Alfentanil drug-dependent parameters

Table S30: Drug-dependent parameters of alfentanil (adopted from [226] and [210])

Parameter	Unit	Model	Literature	Reference	Description
MW	g/mol	416.52 (Lit)	416.52	[227]	Molecular weight
logP	Log Units	1.85 (Fit)	2.10, 2.20 (logD)	[228, 229]	Lipophilicity
Solubility (pH)	mg/ml	0.992 (6.5) (Lit)	0.992 (6.5)	[228]	Solubility
fu	%	10.0 (Lit)	8.6, 10.0, 12.0	[158, 230, 231]	Fraction unbound in plasma
pKa (base)	-	6.50 (Lit)	6.50	[229]	Acid dissociation constant
CL_{spec} (CYP3A4)	l/min	0.527 (Fit)	-	-	CYP3A4 clearance
GFR fraction	-	0.06 (Fit)	-	-	Fraction of filtered drug in the urine
Basolateral mucosa permeability	cm/min	5.42E-4 (Fit)	-	-	Basolateral mucosa permeability P(interstitial → intracellular), P(intracellular → interstitial)
Intestinal permeability	cm/min	5.74E-4 (Fit)	-	-	Transcellular intestinal permeability
Partition coefficients	-	Diverse	Rogers and Rowland	[77, 78]	Cell to plasma partition coefficients
Cellular permeability	cm/min	6.88E-3 (Fit)	PK-Sim Standard	[79]	Permeability into the cellular space

-: not given, CL_{spec}: specific clearance, CYP: cytochrome P450, fit: optimized during parameter identification, lit: literature

6.3.2 Efavirenz-alfentanil clinical DDI studies

Table S31: Clinical studies investigating the efavirenz-alfentanil DDI

Efavirenz administration		Alfentanil administration		n	Healthy [%]	Females [%]	Age[a] [years]	Weight[a] [kg]	Height [cm]	Reference
Dose [mg]	**Route**	**Dose [mg]**	**Route**							
600	po (tab), qd (D1-D14)	3.05	po (sol), sd (D14)	12	100	50	22 (18-29)	71 (57-96)	-	Kharasch 2012 [98]
		1.06	iv, sd (D15)							

-: not given, D: day, iv: intravenous, po: oral, qd: once daily, sd: single dose, sol: solution tab: tablet

[a] mean (range)

6.3.3 Profiles

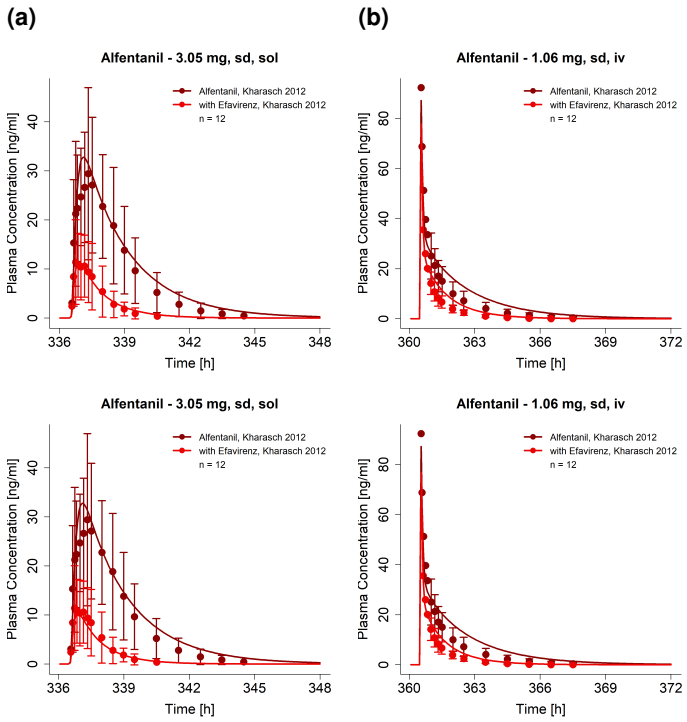

Figure S44: Predicted compared to observed alfentanil plasma concentration-time profiles (linear) before and during efavirenz co-administration, predicted with the updated efavirenz model (upper row) or the original efavirenz model (lower row). Observed data are shown as dots ± standard deviation; model predictions are shown as solid lines. Details on dosing regimens, study populations and literature references are listed in Table S31. iv: intravenous, sd: single dose, sol: solution

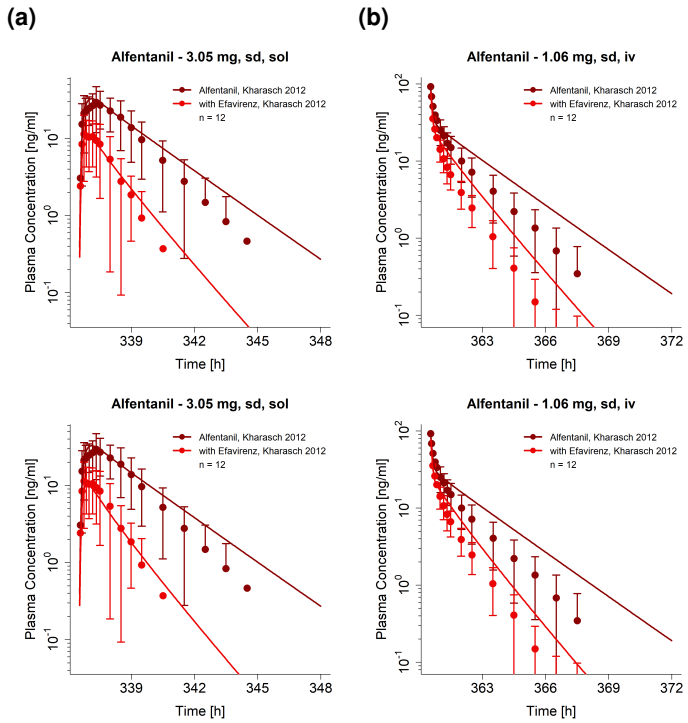

Figure S45: Predicted compared to observed alfentanil plasma concentration-time profiles (semi-logarithmic) before and during efavirenz co-administration, predicted with the updated efavirenz model (upper row) or the original efavirenz model (lower row). Observed data are shown as dots ± standard deviation; model predictions are shown as solid lines. Details on dosing regimens, study populations and literature references are listed in Table S31. iv: intravenous, sd: single dose, sol: solution

6.3.4 DDI AUC_{last} and C_{max} ratio goodness-of-fit plots

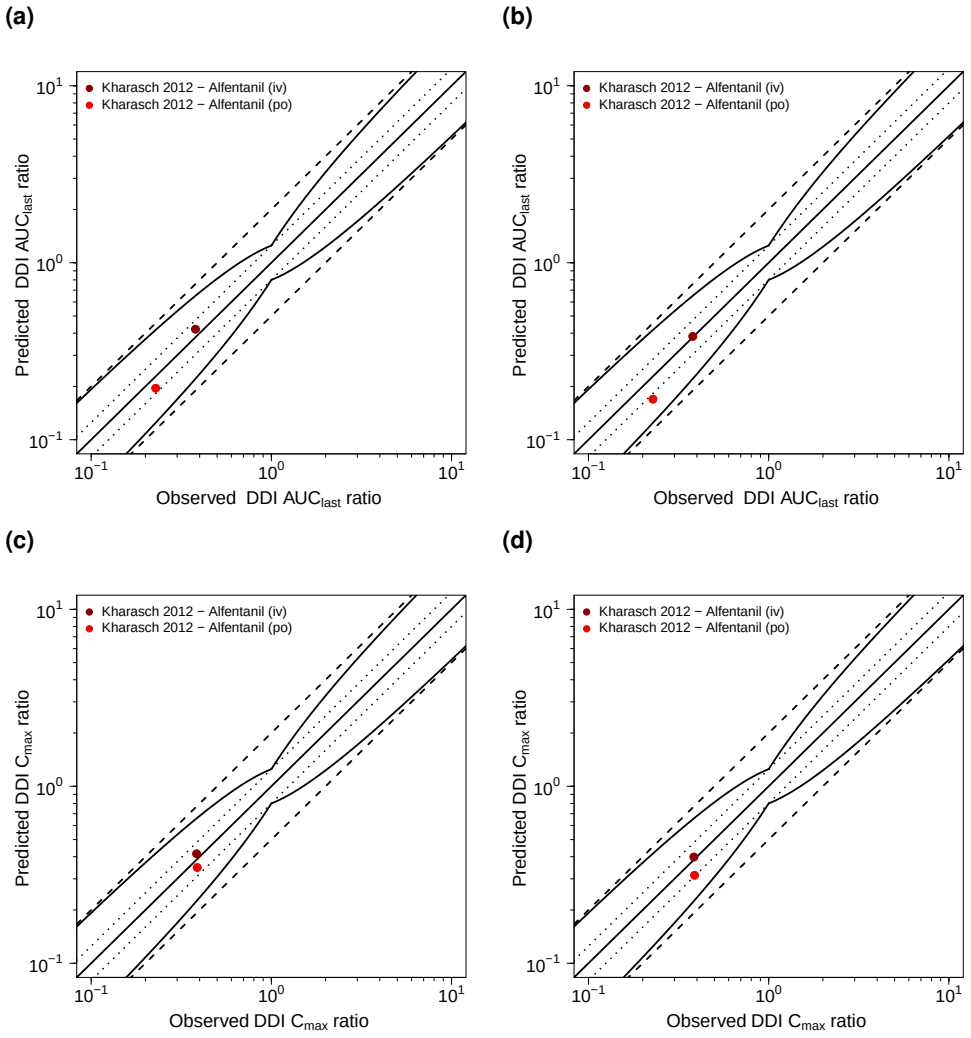

Figure S46: Predicted compared to observed efavirenz-alfentanil (a,b) DDI AUC_{last} and (c,d) DDI C_{max} ratios, predicted with the updated efavirenz PBPK model (left) or the original PBPK model (right). The straight solid line marks the line of identity, the curved solid lines show the prediction success limits proposed by Guest et al. allowing for 1.25-fold variability of the DDI ratio [109]. Dotted lines indicate 1.25-fold, dashed lines indicate 2-fold deviation. AUC_{last}: area under the plasma concentration-time curve from the time of drug administration to the last concentration measurement, C_{max}: maximum plasma concentration, DDI: drug-drug interaction, iv: intravenous, po: oral

6.3.5 Geometric mean fold error of predicted DDI AUC_{last} and C_{max} ratios

Table S32: Predicted and observed efavirenz-alfentanil DDI AUC_{last} and C_{max} ratios with geometric mean fold errors of the updated model

Perpetrator	**Victim**			**DDI AUC_{last} ratio**			**DDI C_{max} ratio**			
Efavirenz	Alfentanil	**Dose gap [h]**	**n**	**Pred**	**Obs**	**Pred/Obs**	**Pred**	**Obs**	**Pred/Obs**	**Reference**
600 mg, po, qd	3.05 mg, po, sd	-	12	0.20	0.23	0.89	0.36	0.39	0.93	Kharasch 2012 et al.[98]
600 mg, po, qd	1.06 mg, iv, sd	-	12	0.43	0.38	1.13	0.42	0.38	1.09	Kharasch 2012 et al.[98]
mean GMFE (range)						**1.13 (1.12-1.13)**			**1.09 (1.08-1.09)**	
						2/2 with GMFE ≤ 2			**2/2 with GMFE ≤ 2**	

-: not given, AUC_{last}: area under the plasma concentration-time curve from the time of drug administration to the last concentration measurement, C_{max}: maximum plasma concentration, DDI: drug-drug interaction, GMFE: geometric mean fold error, iv: intravenous, obs: observed, po: oral, pred: predicted, qd: once daily, sd: single dose

Table S33: Predicted and observed efavirenz-alfentanil DDI AUC_{last} and C_{max} ratios with geometric mean fold errors of the original model

Perpetrator	**Victim**			**DDI AUC_{last} ratio**			**DDI C_{max} ratio**			
Efavirenz	Alfentanil	**Dose gap [h]**	**n**	**Pred**	**Obs**	**Pred/Obs**	**Pred**	**Obs**	**Pred/Obs**	**Reference**
600 mg, po, qd	3.05 mg, po, sd	-	12	0.17	0.23	0.74	0.31	0.39	0.81	Kharasch 2012 [98]
600 mg, po, qd	1.06 mg, iv, sd	-	12	0.38	0.38	1.01	0.40	0.38	1.04	Kharasch 2012 [98]
mean GMFE (range)						**1.18 (1.01-1.35)**			**1.14 (1.04-1.24)**	
						2/2 with GMFE ≤ 2			**2/2 with GMFE ≤ 2**	

-: not given, AUC_{last}: area under the plasma concentration-time curve from the time of drug administration to the last concentration measurement, C_{max}: maximum plasma concentration, DDI: drug-drug interaction, GMFE: geometric mean fold error, iv: intravenous, obs: observed, po: oral, pred: predicted, qd: once daily, sd: single dose

6.4 Efavirenz-bupropion DDI

The efavirenz-bupropion DDI was modeled using a previously established whole-body PBPK model of bupropion [197]. Bupropion is a sensitive CYP2B6 substrate, with hydroxybupropion as the main metabolite. CYP2B6 metabolism is described in the model using Michaelis-Menten kinetics. The drug-dependent parameters of the bupropion model are reproduced in Table S21.

The efavirenz-bupropion DDI was modeled as induction with simultaneous competitive inhibition of bupropion CYP2B6 metabolism by efavirenz. Inhibition was described using K_i = 0.4 µmol/l from literature. The value was corrected for binding in the in vitro assay, as described in section 3.1. Induction of CYP2B6 by efavirenz was described using an EC_{50} = 0.23 µmol/l and E_{max} = 8.13. EC_{50} was taken from literature and corrected for $fu_{incubation}$, E_{max} was optimized during the efavirenz parameter identification.

Details on the modeled clinical DDI studies are given in Table S34. Model predictions of bupropion plasma concentration-time profiles before and during efavirenz co-administration, compared to observed data, are shown in Figures S47 (linear) and S48 (semi-logarithmic). The correlation of predicted to observed DDI AUC_{last} and C_{max} ratios is shown in Figure S49. Tables S35 and S36 list the corresponding predicted and observed DDI AUC_{last} ratios, DDI C_{max} ratios, as well as GMFE values for the updated and the original efavirenz PBPK model, respectively.

6.4.1 Efavirenz-bupropion clinical DDI studies

Table S34: Clinical studies investigating the efavirenz-bupropion DDI

Efavirenz administration		Bupropion administration		n	Healthy [%]	Females [%]	Age[a] [years]	Weight[a] [kg]	Height [cm]	Reference
Dose [mg]	**Route**	**Dose [mg]**	**Route**							
600	po (tab), qd (D1-D14)	150	po (tab), sd (D14)	13	100	23	39 (21-54)	86	-	Robertson 2008[b] [232]

-: not given, D: day, po: oral, qd: once daily, sd: single dose, tab: tablet

[a] mean (range)

[b] 56% intermediate metabolizers (subjects were tested for the diminished-function allele CYP2B6*6)

6.4.2 Profiles

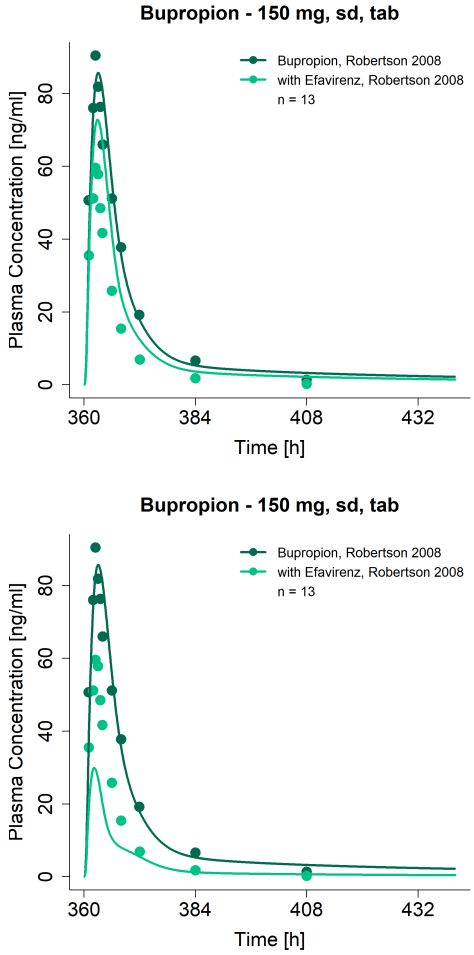

Figure S47: Predicted compared to observed bupropion plasma concentration-time profiles (linear) before and during efavirenz co-administration, predicted with the updated efavirenz model (upper row) or the original efavirenz model (lower row). Observed data are shown as dots ± standard deviation; model predictions are shown as solid lines. Details on dosing regimens, study population and literature reference are listed in Table S34. sd: single dose, tab: tablet

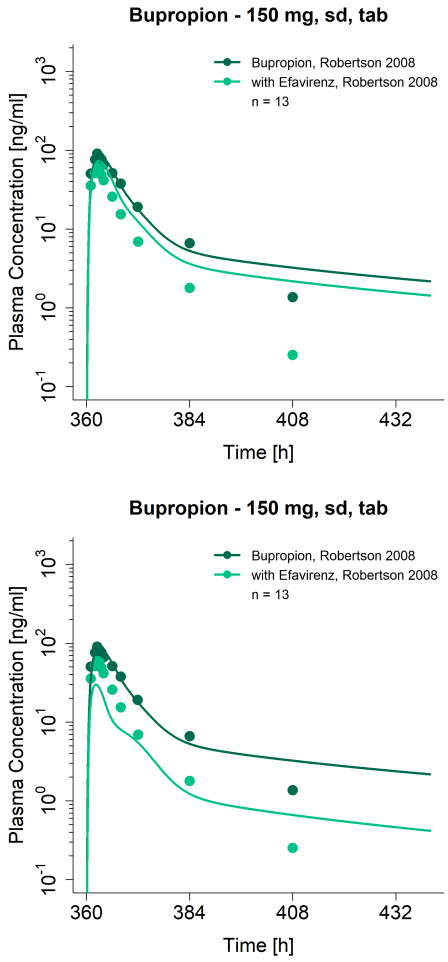

Figure S48: Predicted compared to observed bupropion plasma concentration-time profiles (semi-logarithmic) before and during efavirenz co-administration, predicted with the updated efavirenz model (upper row) or the original efavirenz model (lower row). Observed data are shown as dots ± standard deviation; model predictions are shown as solid lines. Details on dosing regimens, study population and literature reference are listed in Table S34. sd: single dose, tab: tablet

6.4.3 DDI AUC_{last} and C_{max} ratio goodness-of-fit plots

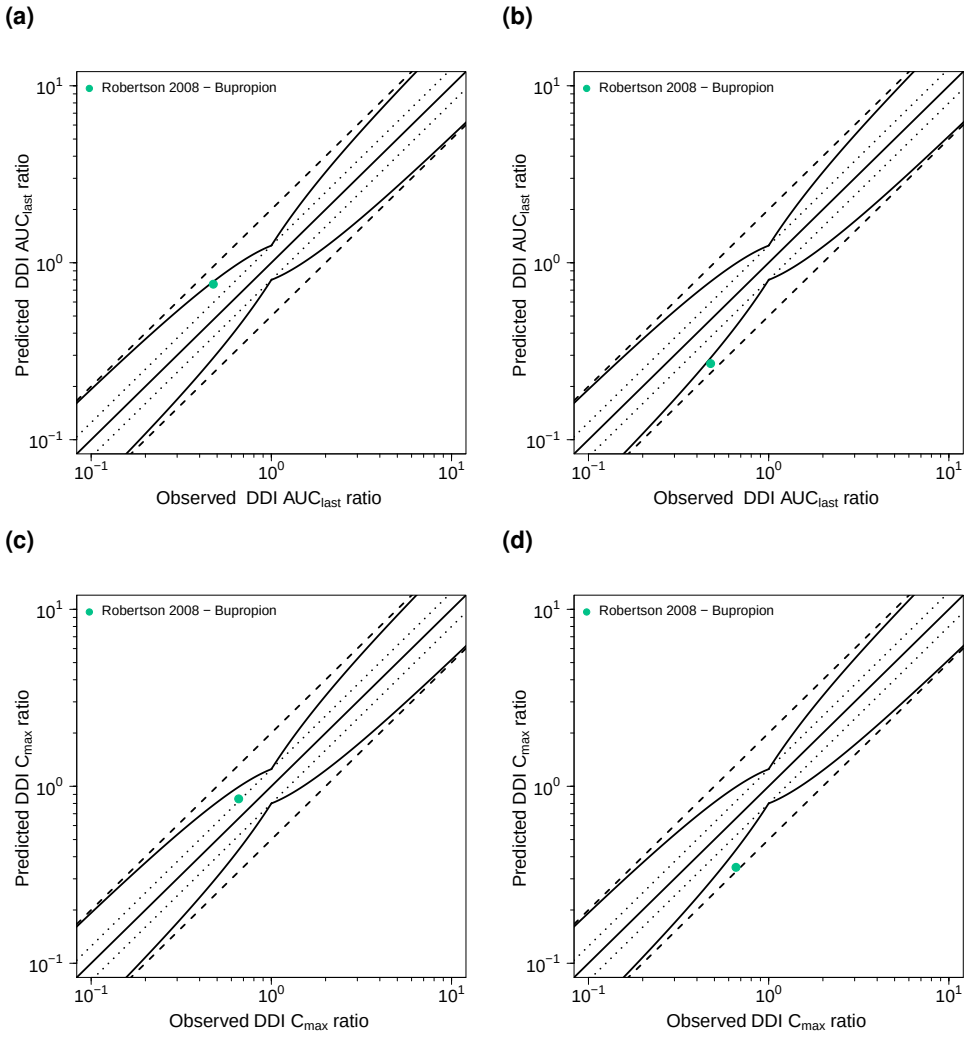

Figure S49: Predicted compared to observed efavirenz-bupropion (a,b) DDI AUC_{last} and (c,d) DDI C_{max} ratios, predicted with the updated efavirenz PBPK model (left) or the original PBPK model (right). The straight solid line marks the line of identity, the curved solid lines show the prediction success limits proposed by Guest et al. allowing for 1.25-fold variability of the DDI ratio [109]. Dotted lines indicate 1.25-fold, dashed lines indicate 2-fold deviation. AUC_{last}: area under the plasma concentration-time curve from the time of drug administration to the last concentration measurement, C_{max}: maximum plasma concentration, DDI: drug-drug interaction

6.4.4 Geometric mean fold error of predicted DDI AUC_{last} and C_{max} ratios

Table S35: Predicted and observed efavirenz-bupropion DDI AUC_{last} and C_{max} ratios with geometric mean fold errors of the updated model

Perpetrator	**Victim**			**DDI AUC_{last} ratio**			**DDI C_{max} ratio**			
Efavirenz	Bupropion	**Dose gap [h]**	**n**	**Pred**	**Obs**	**Pred/Obs**	**Pred**	**Obs**	**Pred/Obs**	**Reference**
600 mg, po, qd	150 mg, po, sd	0	13	0.76	0.48	1.59	0.85	0.66	1.29	Robertson 2008 [232]
mean GMFE						**1.59**			**1.29**	
						1/1 with GMFE ≤ 2			**1/1 with GMFE ≤ 2**	

AUC_{last}: area under the plasma concentration-time curve from the time of drug administration to the last concentration measurement, C_{max}: maximum plasma concentration, DDI: drug-drug interaction, GMFE: geometric mean fold error, obs: observed, po: oral, pred: predicted, qd: once daily, sd: single dose

Table S36: Predicted and observed efavirenz-bupropion DDI AUC_{last} and C_{max} ratios with geometric mean fold errors of the original model

Perpetrator	**Victim**			**DDI AUC_{last} ratio**			**DDI C_{max} ratio**			
Efavirenz	Bupropion	**Dose gap [h]**	**n**	**Pred**	**Obs**	**Pred/Obs**	**Pred**	**Obs**	**Pred/Obs**	**Reference**
600 mg, po, qd	150 mg, po, sd	0	13	0.27	0.48	0.57	0.35	0.66	0.53	Robertson 2008 [232]
mean GMFE						**1.77**			**1.89**	
						1/1 with GMFE ≤ 2			**1/1 with GMFE ≤ 2**	

AUC_{last}: area under the plasma concentration-time curve from the time of drug administration to the last concentration measurement, C_{max}: maximum plasma concentration, DDI: drug-drug interaction, GMFE: geometric mean fold error, obs: observed, po: oral, pred: predicted, qd: once daily, sd: single dose

6.5 Rifampin-efavirenz DDI

The rifampin-efavirenz DDI was modeled using a previously developed whole-body PBPK model of rifampin [210]. Rifampin induces the expression of CYP3A4 and CYP2B6. The drug-dependent parameters of the rifampin model are reproduced in Table S37.

The rifampin-efavirenz DDI was modeled as induction with simultaneous competitive inhibition of efavirenz CYP3A4 and CYP2B6 metabolism by rifampin. Parameters describing the CYP3A4 induction and inhibition were previously implemented and have been qualified in several different DDI predictions [210]. The K_i = 118.5 µmol/l describing the competitive CYP2B6 inhibition and E_{max} = 3.6 describing the CYP2B6 induction by rifampin were taken from literature. EC_{50} = 0.34 µmol/l was adopted from induction processes already implemented in the rifampin PBPK model (see Table S37), as induction of 3A4 and 2B6 by rifampin is both mediated via activation of the nuclear receptor PXR [210].

Details on the modeled clinical DDI studies are given in Table S38. Model predictions of efavirenz plasma concentration-time profiles before and during rifampin co-administration, compared to observed data, are shown in Figures S50 (linear) and S51 (semi-logarithmic). The correlation of predicted to observed DDI AUC_{last} and C_{max} ratios is shown in Figure S46. Tables S39 and S40 list the corresponding predicted and observed DDI AUC_{last} ratios, DDI C_{max} ratios, as well as GMFE values for the updated and the original efavirenz PBPK model, respectively.

6.5.1 Rifampin drug-dependent parameters

Table S37: Drug-dependent parameters of the rifampin PBPK model (adopted from [210])

Parameter	Unit	Model	Literature	Reference	Description
MW	g/mol	822.94 (Lit)	822.94	[233]	Molecular weight
logP	-	2.50 (Fit)	1.30, 2.70	[228, 233]	Lipophilicity
Solubility (pH)	g/l	2.8 (7.5) (Lit)	2.8 (7.5)	[234]	Solubility
fu	%	17.0 (Lit)	17.0	[235]	Fraction unbound in plasma
pKa (acid)	-	1.7 (Lit)	1.7	[236]	First acid dissociation constant
pKa (base)	-	7.9 (Lit)	7.9	[236]	Second acid dissociation constant
B/P ratio	-	0.89 (Calc)	0.90	[237]	Blood/plasma ratio
K_m (OATP1B1)	µmol/l	1.5 (Lit)	1.5	[238]	OATP1B1 Michaelis-Menten constant
k_{cat} (OATP1B1)	1/min	7.8 (Fit)	-	-	OATP1B1 transport rate constant
K_m (AADAC)	µmol/l	195.1 (Lit)	195.1	[239]	AADAC Michaelis-Menten constant
k_{cat} (AADAC)	1/min	9.87 (Fit)	-	-	AADAC catalytic rate constant
K_m (Pgp)	µmol/l	55.0 (Lit)	55.0	[240]	Pgp Michaelis-Menten constant
k_{cat} (Pgp)	1/min	0.61 (Fit)	-	-	Pgp transport rate constant
GFR fraction	-	1 (Asm)	-	-	Fraction of filtered drug in the urine
Induction EC_{50}	µmol/l	0.34 (Lit)	0.42 [a]	[66, 235]	Conc. for half-maximal induction
E_{max} (OATP1B1)	-	0.38 (Fit)	-	-	Maximum OATP1B1 induction effect
E_{max} (AADAC)	-	0.99 (Fit)	-	-	Maximum AADAC induction effect
E_{max} (Pgp)	-	2.5 (Lit)	2.5	[241]	Maximum Pgp induction effect
E_{max} (CYP3A4)	-	9.0 (Lit)	9.0	[235]	Maximum CYP3A4 induction effect
E_{max} (CYP2B6)	-	3.6 (Lit)	3.6	[242]	Maximum CYP2B6 induction effect
K_i (OATP1B1)	µmol/l	0.48 (Lit)	0.48	[243]	Concentration for half-maximal OATP1B1 inhibition
K_i (Pgp)	µmol/l	169.0 (Lit)	169.0	[244]	Concentration for half-maximal Pgp inhibition
K_i (CYP3A4)	µmol/l	18.5 (Lit)	18.5	[245]	Concentration for half-maximal CYP3A4 inhibition
K_i (CYP2B6)	µmol/l	118.5(Lit)	118.5	[246]	Concentration for half-maximal CYP2B6 inhibition
Intestinal permeability	cm/min	1.24E-5 (Fit)	3.84E-07	Calculated	Transcellular intestinal permeability
Partition coefficients	-	Diverse	Rodgers and Rowland	[77, 78]	Cell to plasma partition coefficients
Cellular permeability	cm/min	2.93E-5 (Calc)	PK-Sim Standard	[79]	Permeability into the cellular space

-: not given, AADAC: arylacetamide deacetylase, calc: calculated, CYP: cytochrome P450, GFR: glomerular filtration rate, OATP1B1: organic anion transporting polypeptide 1B1, Pgp: P-glycoprotein

[a] $fu_{incubation}$ = 0.80 was applied to in vitro literature value

6.5.2 Rifampin-efavirenz clinical DDI studies

Table S38: Clinical studies investigating the rifampin-efavirenz DDI

Rifampin administration		Efavirenz administration		n	Healthy [%]	Females [%]	Age[a] [years]	Weight[a] [kg]	Height [cm]	Reference
Dose [mg]	**Route**	**Dose [mg]**	**Route**							
600	po (tab), qd (D1-D7)	50	po (tab), sd (D7)	16	100	0	23.8 (20-35)	23.5 (20.6-27.5)[b]	-	Derungs2016[c] [89]
600	po (tab), qd (D1-D11)	600	po (-), sd (D11)	20	100	50	27.5 (19-44)	72.9 (57-88)	-	Cho 2016 [92]
600	po (-), qd (D1-D8)	600	po (-), qd (D1-D8)	11	100	55	42.6	76.9	-	Kwara 2011[d] [99]

-: not given, D: day, po: oral, qd: once daily, sd: single dose, tab: tablet

[a] mean (range)

[b] Body mass index

[c] CYP2B6 status: 9 intermediate metabolizers, 0 poor metabolizers; subjects were tested for the diminished-function allele CYP2B6*6

[d] CYP2B6 status: 2 extensive metabolizers, 6 intermediate metabolizers, 3 poor metabolizers; subjects were tested for the diminished-function allele CYP2B6*6 and CYP2B6*16

6.5.3 Profiles

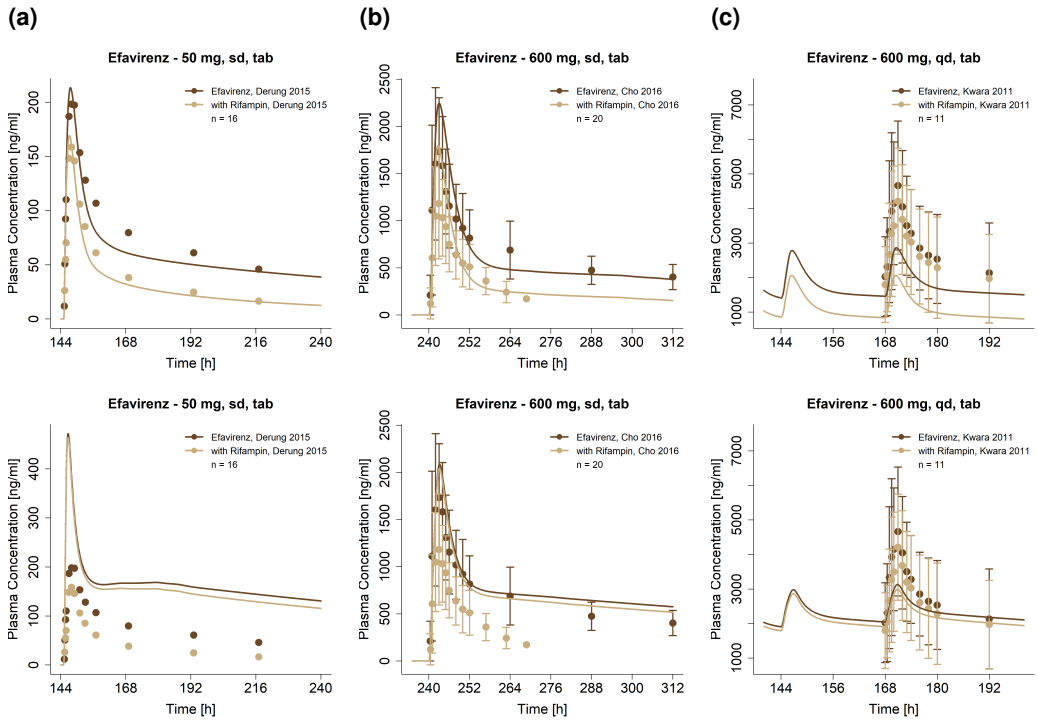

Figure S50: Predicted compared to observed efavirenz plasma concentration-time profiles (linear) before and during rifampin co-administration, predicted with the updated efavirenz model (upper row) or the original efavirenz model (lower row). Observed data are shown as dots ± standard deviation; model predictions are shown as solid lines. Details on dosing regimens, study populations and literature references are listed in Table S38. qd: once daily, sd: single dose, sol: solution, tab: tablet

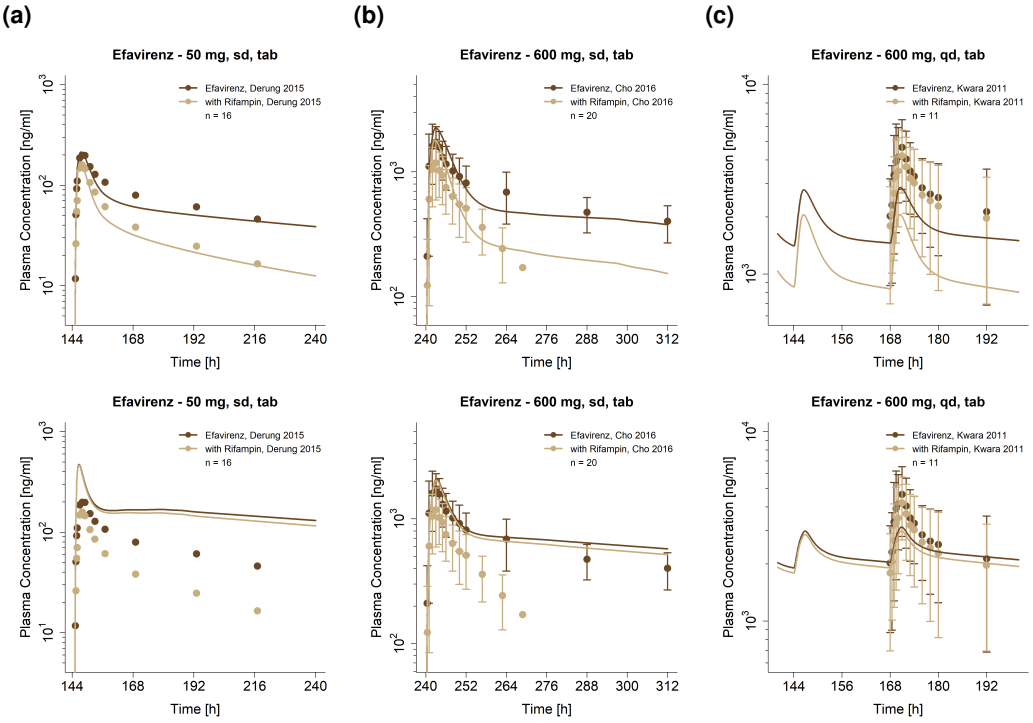

Figure S51: Predicted compared to observed efavirenz plasma concentration-time profiles (semi-logarithmic) before and during rifampin co-administration, predicted with the updated efavirenz model (upper row) or the original efavirenz model (lower row). Observed data are shown as dots ± standard deviation; model predictions are shown as solid lines. Details on dosing regimens, study populations and literature references are listed in Table S38. qd: once daily, sd: single dose, sol: solution, tab: tablet

6.5.4 DDI AUC_{last} and C_{max} ratio goodness-of-fit plots

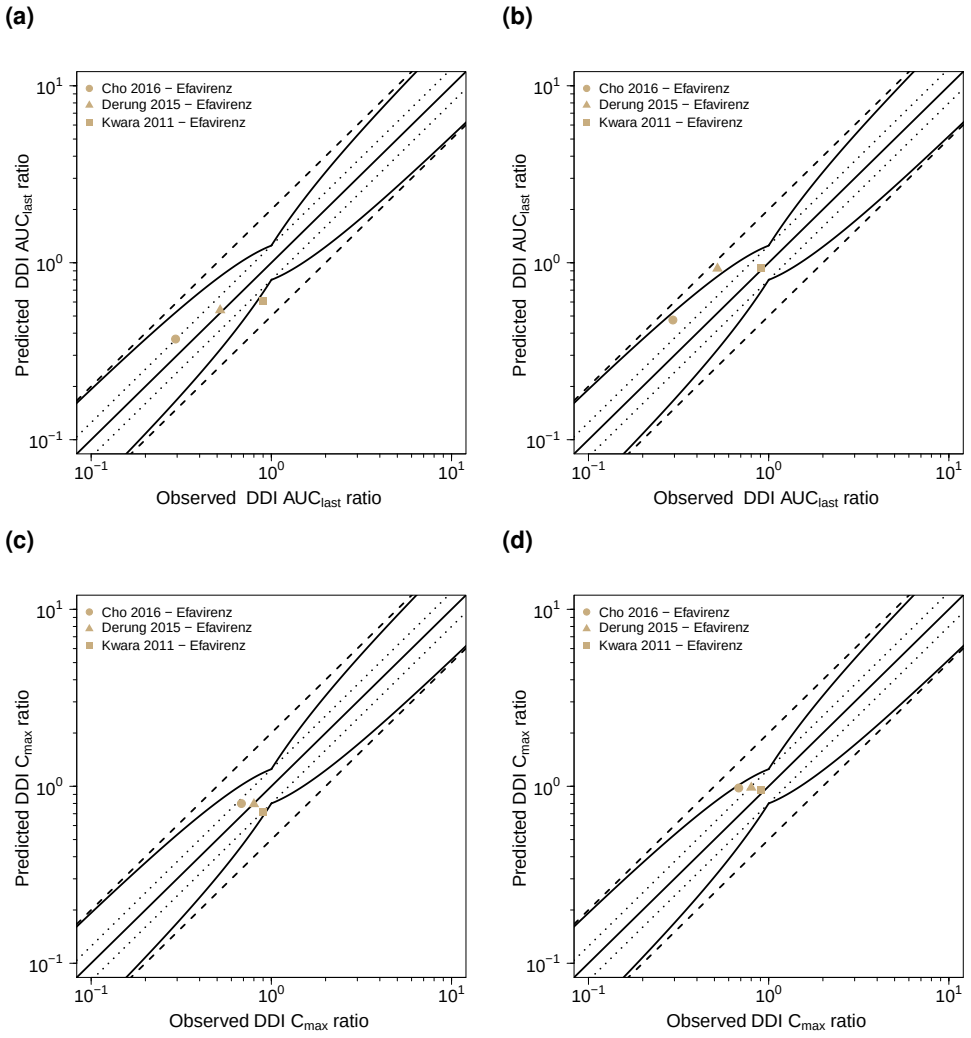

Figure S52: Predicted compared to observed rifampin-efavirenz (a,b) DDI AUC_{last} and (c,d) DDI C_{max} ratios, predicted with the updated efavirenz PBPK model (left) or the original PBPK model (right). The straight solid line marks the line of identity, the curved solid lines show the prediction success limits proposed by Guest et al. allowing for 1.25-fold variability of the DDI ratio [109]. Dotted lines indicate 1.25-fold, dashed lines indicate 2-fold deviation. AUC_{last}: area under the plasma concentration-time curve from the time of drug administration to the last concentration measurement, C_{max}: maximum plasma concentration, DDI: drug-drug interaction

6.5.5 Geometric mean fold error of predicted DDI AUC_{last} and C_{max} ratios

Table S39: Predicted and observed rifampin-efavirenz DDI AUC_{last} and C_{max} ratios with geometric mean fold errors of the updated model

Perpetrator	**Victim**			**DDI AUC_{last} ratio**			**DDI C_{max} ratio**			
Rifampin	Efavirenz	**Dose gap [h]**	**n**	**Pred**	**Obs**	**Pred/Obs**	**Pred**	**Obs**	**Pred/Obs**	**Reference**
600 mg, po, qd	50 mg, po, sd	-	16	0.54	0.52	1.04	0.79	0.80	0.99	Derungs 2015 [89]
600 mg, po, qd	600 mg, po, sd	0	20	0.37	0.29	1.26	0.80	0.68	1.17	Cho 2016 [92]
600 mg, po, qd	600 mg, po, qd	-	11	0.61	0.90	0.68	0.72	0.90	0.80	Kwara 2011 [99]
mean GMFE (range)						**1.26 (1.04-1.48)**			**1.15 (1.01-1.26)**	
						3/3 with GMFE ≤ 2			**3/3 with GMFE ≤ 2**	

-: not given, AUC_{last}: area under the plasma concentration-time curve from the time of drug administration to the last concentration measurement, C_{max}: maximum plasma concentration, DDI: drug-drug interaction, GMFE: geometric mean fold error, obs: observed, po: oral, pred: predicted, qd: once daily, sd: single dose

Table S40: Predicted and observed rifampin-efavirenz DDI AUC_{last} and C_{max} ratios with geometric mean fold errors of the original model

Perpetrator	**Victim**			**DDI AUC_{last} ratio**			**DDI C_{max} ratio**			
Rifampin	Efavirenz	**Dose gap [h]**	**n**	**Pred**	**Obs**	**Pred/Obs**	**Pred**	**Obs**	**Pred/Obs**	**Reference**
600 mg, po, qd	50 mg, po, sd	-	16	0.93	0.52	1.78	0.98	0.80	1.23	Derungs 2015 [89]
600 mg, po, qd	600 mg, po, sd	0	20	0.47	0.29	1.61	0.98	0.68	1.43	Cho 2016 [92]
600 mg, po, qd	600 mg, po, sd	-	11	0.94	0.90	1.04	0.95	0.90	1.06	Kwara 2011 [99]
mean GMFE (range)						**1.48 (1.04-1.78)**			**1.24 (1.06-1.43)**	
						3/3 with GMFE ≤ 2			**3/3 with GMFE ≤ 2**	

-: not given, AUC_{last}: area under the plasma concentration-time curve from the time of drug administration to the last concentration measurement, C_{max}: maximum plasma concentration, DDI: drug-drug interaction, GMFE: geometric mean fold error, obs: observed, po: oral, pred: predicted, qd: once daily, sd: single dose

6.6 Efavirenz-voriconazole DDI

The efavirenz-voriconazole DDI was modeled using a previously established whole-body PBPK model of voriconazole [247]. The metabolism of the CYP2C19 and CYP3A4 substrate voriconazole is described in the model using Michaelis-Menten kinetics. The drug-dependent parameters of the voriconazole model are reproduced in Table S41.

To adequately describe the voriconazole plasma concentration-time profiles, the CYP2C19 k_{cat} was adjusted (k_{cat} = 0.20 1/min) to match the control group of the modeled DDI study, assuming variability of the CYP2C19 expression in the small DDI study population.

The efavirenz-voriconazole DDI was modeled as induction with simultaneous competitive inhibition of voriconazole CYP3A4 metabolism by efavirenz and as competitive inhibition of efavirenz CYP2B6 metabolism by voriconazole. Inhibition of CYP3A4 by efavirenz was described using K_i = 9.67 µmol/l from literature, corrected for binding in the in vitro assay, as described in Section 3. The induction was described using EC_{50} = 0.23 µmol/l (taken from literature and corrected for binding in the in vitro assay). Inhibition of CYP2B6 by voriconazole was described using a K_i = 0.3 µmol/l from literature, corrected for binding in the in vitro assay.

Details on the modeled clinical DDI studies are given in Table S42. Model predictions of voriconazole and efavirenz plasma concentration-time profiles before and during co-administration, compared to observed data, are shown in Figure S53 (linear) and S54 (semi-logarithmic). The correlation of predicted to observed DDI AUC_{last} and C_{max} ratios is shown in Figure S55. Tables S43 and S44 list the corresponding predicted and observed DDI AUC_{last} ratios, DDI C_{max} ratios, as well as GMFE values for the updated and the original efavirenz PBPK model, respectively.

6.6.1 Voriconazole drug-dependent parameters

Table S41: Drug-dependent parameters of the voriconazole PBPK model (adopted from [247])

Parameter	Unit	Model	Literature	Reference	Description
MW	g/mol	349.3 (Lit)	349.3	[248]	Molecular weight
logP	log Units	1.80 (Lit)	1.65, 1.75, 1.80, 2.56	[248–252]	Lipophilicity
Solubility (pH)	mg/ml	3.2 (1.0), 2.7 (1.2), 0.1 (7.0)	3.2 (1.0), 2.7 (1.2), 0.1 (7.0)	[248, 250, 253, 254]	Solubility
fu	%	42.0 (Lit)	42.0	[250–252, 255]	Fraction unbound in plasma
pKa (base)	-	1.60 (Lit)	1.60, 1.76, 2.27	[248, 250, 251, 253, 256]	Acid dissociation constant
K_m (CYP3A4)	µmol/l	15.0 (Lit)	11.0, 15.0, 16.0, 235.0, 834.7	[250, 252, 257, 258]	CYP3A4 Michaelis-Menten constant
k_{cat} (CYP3A4)	1/min	2.12 (Fit)	0.05, 0.10, 0.14, 0.31, 32.2	[250, 252, 257, 258]	CYP3A4 catalytic rate constant
K_m (CYP2C19)	µmol/l	3.5 (Lit)	3.5, 9.3, 14.0	[250, 252, 257, 258]	CYP2C19 Michaelis-Menten constant
k_{cat} (CYP2C19)	1/min	1.19 (Lit)	0.22, 0.39, 1.19, 40.0	[250, 252, 257, 258]	CYP2C19 catalytic rate constant
GFR fraction	-	1 (Asm)	-	-	Fraction of filtered drug in the urine
K_i (CYP3A4)	µmol/l	9.33 (Lit)	9.33	[247]	Concentration for half-maximal inhibition
k_{inact} (CYP3A4)	1/min	0.015 (Fit)	0.04	[247]	Maximum inactivation rate constant
Intestinal permeability	cm/s	1.62E-2 (Fit)	1.68E-3	[252]	Transcellular intestinal permeability
Partition coefficients	-	Diverse	Poulin and Theil	[259–262]	Cell to plasma partition coefficients
Cellular permeability	cm/min	2.58E-3 (Calc)	PK-Sim Standard	[79]	Permeability into the cellular space
Tablet Weibull time	min	30.0 (Fit)	-	-	Dissolution time (50% dissolved)
Tablet Weibull shape	-	1.29 (Fit)	-	-	Dissolution profile shape

-: not given, asm: assumption, calc: calculated, CYP: cytochrome P450, fit: optimized during parameter optimization, GFR: glomerular filtration rate, lit: literature

6.6.2 Efavirenz-voriconazole clinical DDI studies

Table S42: Clinical studies investigating the efavirenz-voriconazole DDI

Efavirenz administration		Voriconazole administration		n	Healthy [%]	Females [%]	Age[a] [years]	Weight[a] [kg]	Height [cm]	Reference
Dose [mg]	**Route**	**Dose [mg]**	**Route**							
400	po (cap), qd (D1-D19)	200[b]	po (tab), bid (D11-D19)	27	100	0	34 (20-48)	79 (59-92)	-	Liu 2008 [91]

-: not given, bid: twice daily, cap: capsule, D: day, po: oral, qd: once daily, tab: tablet

[a] mean (range)

[b] Two 400 mg loading doses (bid) on day 1

6.6.3 Profiles

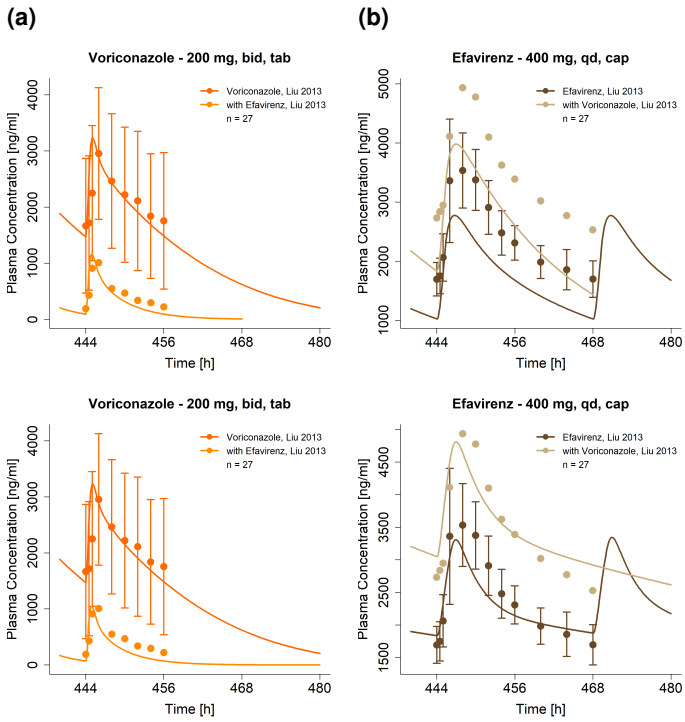

Figure S53: Predicted compared to observed voriconazole and efavirenz plasma concentration-time profiles (linear) before and during co-administration, predicted with the updated efavirenz model (upper row) or the original efavirenz model (lower row). Observed data are shown as dots ± standard deviation; model predictions are shown as solid lines. Details on dosing regimens, study population and literature reference are listed in Table S42. bid: twice daily, cap: capsule, qd: once daily, tab: tablet

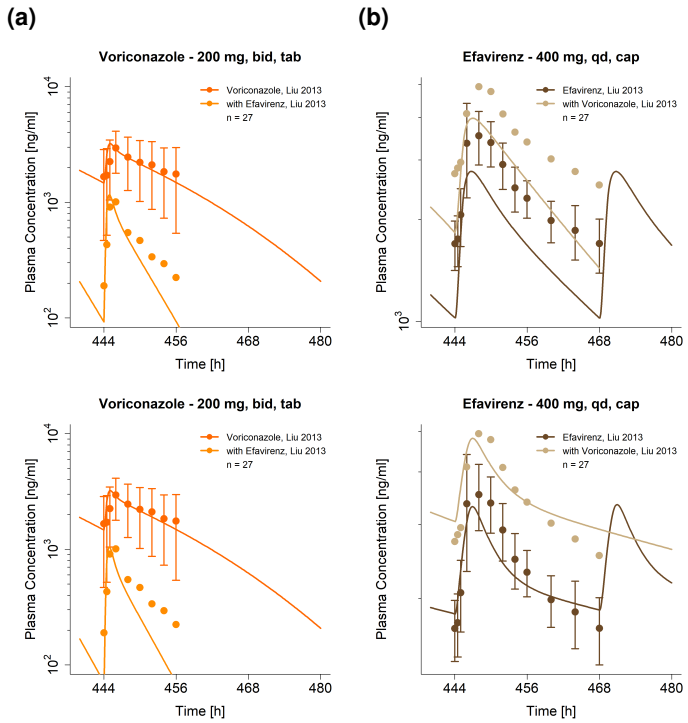

Figure S54: Predicted compared to observed efavirenz and voriconazole plasma concentration-time profiles (semi-logarithmic) before and during efavirenz and voriconazole co-administration, predicted with the updated efavirenz model (upper row) or the original efavirenz model (lower row). Observed data are shown as dots ± standard deviation; model predictions are shown as solid lines. Details on dosing regimens, study population and literature reference are listed in Table S42. bid: twice daily, cap: capsule, qd: once daily, tab: tablet

6.6.4 DDI AUC_{last} and C_{max} ratio goodness-of-fit plots

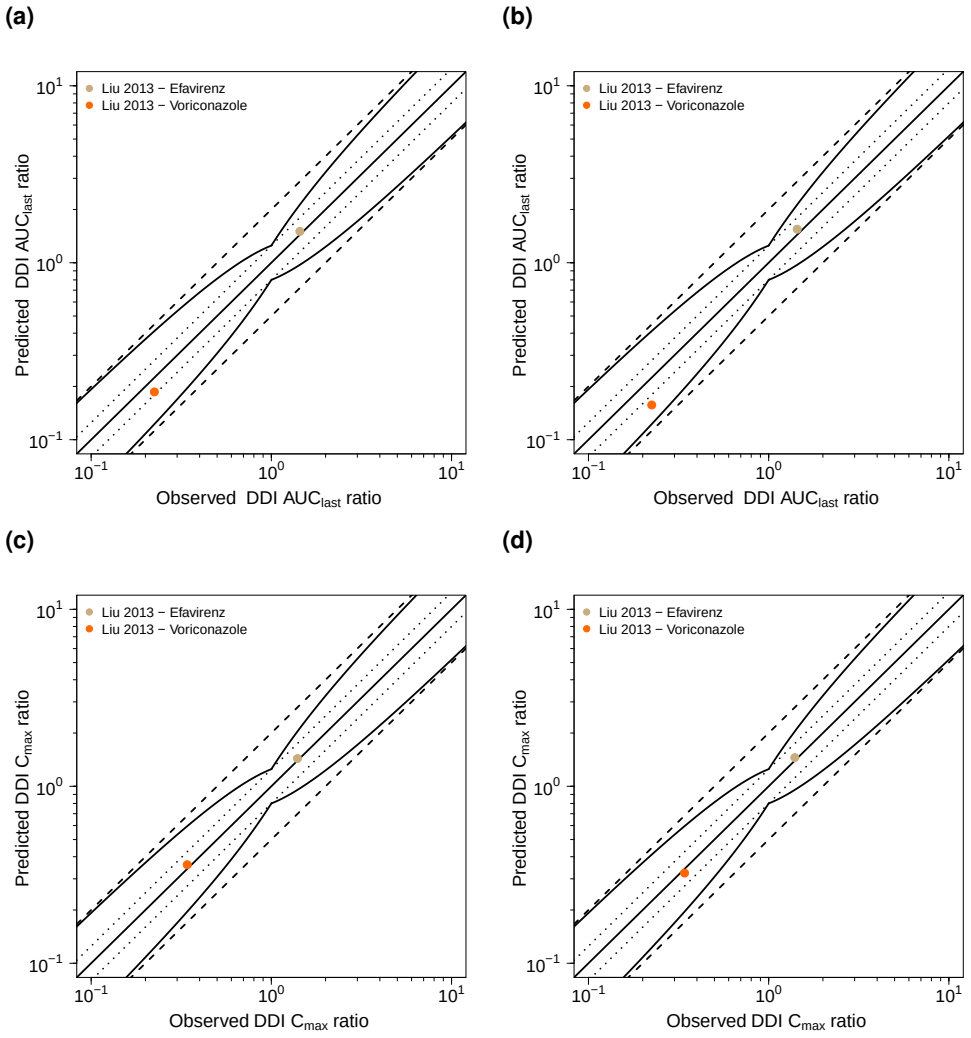

Figure S55: Predicted compared to observed efavirenz-voriconazole (a,b) DDI AUC_{last} and (c,d) DDI C_{max} ratios predicted with the updated efavirenz PBPK model (left) or the original PBPK model (right). The straight solid line marks the line of identity, the curved solid lines show the prediction success limits proposed by Guest et al. allowing for 1.25-fold variability of the DDI ratio [109]. Dotted lines indicate 1.25-fold, dashed lines indicate 2-fold deviation. AUC_{last}: area under the plasma concentration-time curve from the time of drug administration to the last concentration measurement, C_{max}: maximum plasma concentration, DDI: drug-drug interaction

6.6.5 Geometric mean fold error of predicted DDI AUC_{last} and C_{max} ratios

Table S43: Predicted and observed efavirenz-voriconazole DDI AUC_{last} and C_{max} ratios with geometric mean fold errors of the updated model

				DDI AUC_{last} ratio			DDI C_{max} ratio			
Perpetrator	**Victim**	**Dose gap [h]**	**n**	**Pred**	**Obs**	**Pred/Obs**	**Pred**	**Obs**	**Pred/Obs**	**Reference**
Voriconazole	*Efavirenz*									
200 mg, po, bid	400 mg, po, qd	0	27	1.53	1.44	1.06	1.46	1.40	1.04	Liu 2013 [91]
Efavirenz	*Voriconazole*									
200 mg, po, bid	400 mg, po, qd	0	27	0.19	0.22	0.87	0.37	0.34	1.09	Liu 2013 [91]
mean GMFE (range)						**1.11 (1.06-1.15)**			**1.06 (1.04-1.09)**	
						2/2 with GMFE ≤ 2			**2/2 with GMFE ≤ 2**	

AUC_{last}: area under the plasma concentration-time curve from the time of drug administration to the last concentration measurement, bid: twice daily, C_{max}: maximum plasma concentration, DDI: drug-drug interaction, GMFE: geometric mean fold error, obs: observed, po: oral, pred: predicted, qd: once daily

Table S44: Predicted and observed efavirenz-voriconazole DDI AUC_{last} and C_{max} ratios with geometric mean fold errors of the original model

				DDI AUC_{last} ratio			DDI C_{max} ratio			
Perpetrator	**Victim**	**Dose gap [h]**	**n**	**Pred**	**Obs**	**Pred/Obs**	**Pred**	**Obs**	**Pred/Obs**	**Reference**
Voriconazole	Efavirenz									
200 mg, po, bid	400 mg, po, qd	0	27	1.55	1.44	1.08	1.45	1.40	1.04	Liu 2013 [91]
Efavirenz	Voriconazole									
200 mg, po, bid	400 mg, po, qd	0	27	0.16	0.22	0.70	0.32	0.34	0.95	Liu 2013 [91]
mean GMFE (range)						**1.25 (1.08-1.43)**			**1.05 (1.04-1.06)**	
						2/2 with GMFE ≤ 2			**2/2 with GMFE ≤ 2**	

AUC_{last}: area under the plasma concentration-time curve from the time of drug administration to the last concentration measurement, bid: twice daily, C_{max}: maximum plasma concentration, DDI: drug-drug interaction, GMFE: geometric mean fold error, obs: observed, po: oral, pred: predicted, qd: once daily

7 System-dependent parameters

Details on the expression of metabolizing enzymes, transport proteins and protein binding partners implemented to model the pharmacokinetics of carbamazepine, carbamazepine-10,11-epoxide, efavirenz, alfentanil, alprazolam, bupropion, erythromycin, rifampin, simvastatin and voriconazole are summarized in Table S45. As enterohepatic circulation is active under physiological conditions, the parameter EHC continuous fraction was set to 1 in all individuals.

Table S45: System-dependent parameters

	Reference concentration				Half-life	
Enzyme/ Transporter Binding partner	**Mean[a] [µmol/l]**	**Relative expression[b]**	**Localization**	**Direction**	**Liver [h]**	**Intestine [h]**
11β-HSD	1.00[c] [263]	Array [265]	Intracellular	-	36	23
AADAC	1.00[c] [263]	RT-PCR [266]	Intracellular	-	36	23
CYP1A2	1.80 [267]	RT-PCR [268]	Intracellular	-	39	23
CYP2A6	2.72 [267]	RT-PCR [268]	Intracellular	-	26	23
CYP3A4	4.32 [267]	RT-PCR [268]	Intracellular	-	36 [269]	23 [139]
CYP3A5	0.04 [267]	RT-PCR [268]	Intracellular	-	36	23
CYP2B6	1.56 [267]	RT-PCR [268]	Intracellular	-	32	23
CYP2C8	2.56 [267]	RT-PCR [268]	Intracellular	-	23	23
CYP2C19	0.76 [267]	RT-PCR [268]	Intracellular	-	26	23
EPHX1	1.00[c] [263]	RT-PCR [266]	Intracellular	-	36	23
PON3	1.00[c] [263]	Array [265]	Intracellular	-	36	23
UGT1A1	1.00[c] [263]	RT-PCR [266]	Intracellular	-	36	23
UGT1A3	1.00[c] [263]	RT-PCR [266]	Intracellular	-	36	23
UGT1A4	2.32 [53]	liver only [209]	Intracellular	-	36	-
UGT2B7	2.78 [270]	EST [271]	Intracellular	-	36	23
BCRP	1.00[c] [263]	RT-PCR[d] [272]	Apical	Efflux	36	23
OATP1B1	1.00[c] [263]	RT-PCR [272]	Basolateral	Influx	36	-
Pgp	1.41 [210]	RT-PCR[e] [272]	Apical	Efflux	36	23
GABRG2	1.30 [209]	brain only [209]	Extracellular membrane	-	-	-
NAT1	1.00[c] [263]	EST [271]	Extracellular membrane	-	36	23

-: not given, 11β-HSD1: 11β-hydroxysteroid dehydrogenase 1, AADAC: arylacetamide deacetylase, array: genome expression arrays from ArrayExpress, BCRP: breast cancer resistance protein, CYP: cytochrome P450, EPHX1: epoxidehydroxylase 1, EST: expressed sequence tags expression profile, GABRG2: gamma-aminobutyric acid receptor subunit gamma 2, NAT1: norepinephrine transporter 1, OATP1B1: organic anion transporting polypeptide 1B1, Pgp: P-glycoprotein, PON3: paraoxonase 3, RT-PCR: reverse transcription-polymerase chain reaction profile, UGT: UDP-glucuronosyltransferase

[a] µmol/lol protein/l in the tissue of highest expression

[b] in the different organs (PK-Sim® expression database profile)

[c] if no information was available, the mean reference concentration was set to 1.00 µmol/l and the catalytic rate constant (kcat) was optimized [263]

[d] with the relative expression in the blood cells set to 0.3046 [264]

[e] with the relative expression in the intestinal mucosa increased by factor 3.57 [210]

List of Figures

List of Tables

Abbreviations

11β-HSD1	11β-hydroxysteroid dehydrogenase 1
AADAC	Arylacetamide deacetylase
ADME	Absorption, distribution, metabolism and excretion
AUC	Area under the concentration-time curve
AUC_{last}	AUC values calculated from the time of drug administration to the time of the last concentration measurement
asm	Assumption
BCRP	Breast cancer resistance protein
bid	Twice daily
CBZ	Carbamazepine
CBZE	Carbamazepine-10,11-epoxide
calc	Calculated
cap	Capsule
CAR	Constitutive androstane receptor
CL_{hep}	Hepatic clearance
C_{mic}	Microsomal protein concentration
CL_{spec}	Secific clearance
C_{max}	Maximum plasma concentration
CYP	Cytochrome P450
D	Day
DDI	Drug-drug interaction
DGI	Drug-gene interaction
EC50	Concentration for half maximal induction in vivo
EBUP	Erythrohydrobupropion
EHC	Enterohepatic circulation
EM	Extensive metabolizer
E_{max}	Maximal induction effect in vivo
EPHX1	Epoxide hydroxylase 1
EST	Expressed sequence tag
FaHIF	Fasted human intestinal fluid

fit	Optimized during parameter identification
fu	Fraction unbound in plasma
$fu_{incubation}$	Fraction unbound in the incubation
GABRG2	Gamma-aminobutyric acid receptor subunit gamma 2
GFR	Glomerular filtration rate
GMFE	Geometric mean fold error
IC_{50}	Half maximal inhibitory concentration
IM	Intermediate metabolizer
IR	Immediate release
iv	Intravenous
k_{cat}	Transport or catalytic rate constant
k_{deg}	Degradation rate constant
$k_{deg,\ app}$	Degradation rate constant in the presence of a mechanism based inhibitor
K_i	Dissociation constant of the inhibitor-transporter/ -enzyme complex
K_{inact}	Maximum inactivation rate
K_M	Michaelis-Menten constant
$K_{M,app}$	Michaelis-Menten constant in the presence of inhibitor
logP	Lipophilicity
lit	Literature
MRD	Mean relative deviation
MW	Molecular weight
NAT1	Norepinephrine transporter 1
OATP	Organic-anion-transporting polypeptide
obs	Observed
OSP	Open Systems Pharmacology
Pgp	P-glycoprotein
PBPK	Physiologically based pharmacokinetic
pKa	Acid dissociation constant
PM	Poor metabolizer
po	Oral
PON3	Paraoxonase 3
pred	Predicted

PXR	Pregnane X receptor
qid	Four times daily
qd	Once daily
R_{syn}	Rate of transporter or enzyme synthesis
$R_{syn,app}$	Rate of transporter or enzyme synthesis in the presence of inducer
RT-PCR	Reverse transcription-polymerase chain reaction
sd	Single dose
sol	Solution
susp	Suspension
tab	Tablet
TBUP	Threohydrobupropion
tid	Three times daily
UGT	UDP-glucuronosyltransferase
v	Reaction velocity
v_{max}	Maximum reaction velocity
XR	Extended release

Bibliography

[1] Open Systems Pharmacology Suite Community. PK-Sim® Ontogeny Database Documentation, Version 7.3, 2018. URL https://github.com/Open-Systems-Pharmacology/OSPSuite.Documentation/blob/master/PK-Sim%20Ontogeny%20Database%20Version%207.3.pdf. accessed: 14 Dec 2020.

[2] Open Systems Pharmacology Suite Community. Open Systems Pharmacology Suite Manual, 2018. URL https://docs.open-systems-pharmacology.org/. accessed: 14 Dec 2020.

[3] Novartis. Tegretol ® label, 2009. URL https://www.accessdata.fda.gov/drugsatfda_docs/label/2009/016608s101,018281s048lbl.pdf. accessed: 14 Dec 2020.

[4] M. Eichelbaum, T. Tomson, G. Tybring, and L. Bertilsson. Carbamazepine metabolism in man. Induction and pharmacogenetic aspects. *Clinical pharmacokinetics*, 10(1):80–90, 1985.

[5] T. Tomson, G. Tybring, and L. Bertilsson. Single-dose kinetics and metabolism of carbamazepine-10,11-epoxide. *Clinical Pharmacology and Therapeutics*, 33(1):58–65, jan 1983.

[6] B. M. Kerr, K. E. Thummel, C. J. Wurden, S. M. Klein, D. L. Kroetz, F. J. Gonzalez, and R. H. Levy. Human liver carbamazepine metabolism. Role of CYP3A4 and CYP2C8 in 10,11-epoxide formation. *Biochemical pharmacology*, 47(11):1969–79, jun 1994.

[7] R. E. Pearce, G. R. Vakkalagadda, and J. Steven Leeder. Pathways of carbamazepine bioactivation in vitro I. Characterization of human cytochromes P450 responsible for the formation of 2- and 3-hydroxylated metabolites. *Drug Metabolism and Disposition*, 30 (11):1170–1179, 2002.

[8] J. W. Faigle and K. F. Feldmann. *Pharmacokinetic data of carbamazepine and its major metabolites in man*. Springer Berlin Heidelberg, Berlin, Heidelberg, 1975. ISBN 978-3-642-85923-6.

[9] B. Terhaag, K. Richter, and H. Diettrich. Concentration behavior of carbamazepine in bile and plasma of man. *International journal of clinical pharmacology and biopharmacy*, 16 (12):607–9, 1978.

[10] U.S. Food and Drug Administration. Drug development and drug interactions, 2016. URL https://www.fda.gov/drugs/drug-interactions-labeling/drug-development-and-drug-interactions. accessed: 14 Dec 2020.

[11] B. M. Kerr, A. E. Rettie, A. C. Eddy, P. Loiseau, M. Guyot, A. J. Wilensky, and R. H. Levy. Inhibition of human liver microsomal epoxide hydrolase by valproate and valpromide: in vitro/in vivo correlation. *Clinical pharmacology and therapeutics*, 46(1):82–93, jul 1989.

[12] T. B. Vree, T. J. Janssen, Y. A. Hekster, E. F. Termond, A. C. van de Dries, and W. J. Wijnands. Clinical pharmacokinetics of carbamazepine and its epoxy and hydroxy metabolites in humans after an overdose. *Therapeutic drug monitoring*, 8(3):297–304, 1986.

[13] N. R. Kitteringham, C. Davis, N. Howard, M. Pirmohamed, and B. K. Park. Interindividual and interspecies variation in hepatic microsomal epoxide hydrolase activity: Studies with cis-stilbene oxide, carbamazepine 10,11- epoxide and naphthalene. *Journal of Pharmacology and Experimental Therapeutics*, 278(3):1018–1027, 1996.

[14] S. R. Faucette, T. C. Zhang, R. Moore, T. Sueyoshi, C. J. Omiecinski, E. L. LeCluyse, M. Negishi, and H. Wang. Relative activation of human pregnane X receptor versus constitutive androstane receptor defines distinct classes of CYP2B6 and CYP3A4 inducers. *Journal of Pharmacology and Experimental Therapeutics*, 320(1):72–80, 2007.

[15] R. H. Levy, W. H. Pitlick, A. S. Troupin, J. R. Green, and J. M. Neal. Pharmacokinetics of carbamazepine in normal man. *Clinical Pharmacology & Therapeutics*, 17(6):657–668, jun 1975.

[16] A. McLean, S. Browne, Y. Zhang, E. Slaughter, C. Halstenson, and R. Couch. The influence of food on the bioavailability of a twice-daily controlled release carbamazepine formulation. *Journal of Clinical Pharmacology*, 41(2):183–186, 2001.

[17] M. Sumi, N. Watari, O. Umezawa, and N. Kaneniwa. Pharmacokinetic study of carbamazepine and its epoxide metabolite in humans. *Journal of Pharmacobio-Dynamics*, 10(11):652–661, 1987.

[18] F. Pisani, M. Caputo, A. Fazio, G. Oteri, M. Russo, E. Spina, E. Perucca, and L. Bertilsson. Interaction of carbamazepine-10,11-epoxide, an active metabolite of carbamazepine, with valproate: A pharmacokinetic study. *Epilepsia*, 31(3):339–342, 1990.

[19] F. Pisani, A. Fazio, C. Artesi, G. Oteri, E. Spina, T. Tomson, and E. Perucca. Impairment of carbamazepine-10, 11-epoxide elimination by valnoctamide, a valpromide isomer, in healthy subjects. *British Journal of Clinical Pharmacology*, 34(1):85–87, 1992.

[20] A. Gérardin, J. P. Dubois, J. Moppert, and L. Geller. Absolute bioavailability of carbamazepine after oral administration of a 2% syrup. *Epilepsia*, 31(3):334–338, 1990.

[21] M. D. Rawlins, P. Collste, L. Bertilsson, and L. Palmér. Distribution and elimination kinetics of carbamazepine in man. *European journal of clinical pharmacology*, 8(2):91–6, feb 1975.

[22] J. A. Wada, A. S. Troupin, P. Friel, R. Remick, K. Leal, and J. Pearmain. Pharmacokinetic comparison of tablet and suspension dosage forms of carbamazepine. *Epilepsia*, 19(3): 251–5, 1978.

[23] A. P. Gérardin, F. V. Abadie, J. A. Campestrini, and W. Theobald. Pharmacokinetics of carbamazepine in normal humans after single and repeated oral doses. *Journal of Pharmacokinetics and Biopharmaceutics*, 4(6):521–535, 1976.

[24] S. K. Bedada, N. R. Yellu, and P. Neerati. Effect of resveratrol treatment on the pharmacokinetics of diclofenac in healthy human volunteers. *Phytotherapy Research*, 30(3): 397–401, 2016.

[25] S. K. Bedada, R. Appani, and P. K. Boga. Effect of piperine on the metabolism and pharmacokinetics of carbamazepine in healthy volunteers. *Drug research*, 67(1):46–51, jan 2017.

[26] M. Eichelbaum, K. Ekbom, L. Bertilsson, V. A. Ringberger, and A. Rane. Plasma kinetics of carbamazepine and its epoxide metabolite in man after single and multiple doses. *European Journal of Clinical Pharmacology*, 8(5):337–341, 1975.

[27] K. A. Kim, O. O. Sae, P. W. Park, and J. Y. Park. Effect of probenecid on the pharmacokinetics of carbamazepine in healthy subjects. *European Journal of Clinical Pharmacology*, 61(4):275–280, 2005.

[28] M. C. Meyer, A. B. Straughn, E. J. Jarvi, G. C. Wood, F. R. Pelsor, and V. P. Shah. The bioinequivalence of carbamazepine tablets with a history of clinical failures. *Pharmaceutical research*, 9(12):1612–6, 1992.

[29] M. C. Meyer, A. B. Straughn, R. M. Mhatre, V. P. Shah, R. L. Williams, and L. J. Lesko. The relative bioavailability and in vivo-in vitro correlations for four marketed carbamazepine tablets. *Pharmaceutical research*, 15(11):1787–91, 1998.

[30] A. Shahzadi, I. Javed, B. Aslam, F. Muhammad, M. R. Asi, M. Y. Ashraf, and Zia-Ur-Rahman. Therapeutic effects of ciprofloxacin on the pharmacokinetics of carbamazepine in healthy adult male volunteers. *Pakistan Journal of Pharmaceutical Sciences*, 24(1): 63–68, 2011.

[31] B. Saint-Salvi, D. Tremblay, A. Surjus, and M. A. Lefebvre. A study of the interaction of roxithromycin with theophylline and carbamazepine. *The Journal of antimicrobial chemotherapy*, 20 Suppl B:121–9, 1987.

[32] N. Barzaghi, G. Gatti, F. Crema, M. Monteleone, C. Amione, L. Leone, and E. Perucca. Inhibition by erythromycin of the conversion of carbamazepine to its active 10,11-epoxide metabolite. *British journal of clinical pharmacology*, 24(6):836–8, dec 1987.

[33] G. Bianchetti, P. Padovani, J. P. Thénot, J. F. Thiercelin, P. L. Morselli, J. P. Thenot, J. F. Thiercelin, and P. L. Morselli. Pharmacokinetic interactions of progabide with other antiepileptic drugs. *Epilepsia*, 28(1):68–73, 1987.

[34] I. Kovacević, J. Parojcić, I. Homsek, M. Tubić-Grozdanis, and P. Langguth. Justification of biowaiver for carbamazepine, a low soluble high permeable compound, in solid dosage forms based on IVIVC and gastrointestinal simulation. *Molecular pharmaceutics*, 6(1): 40–7, 2009.

[35] P. L. Morselli, M. Gerna, D. de Maio, G. Zanda, F. Viani, and S. Garattini. *Pharmacokinetic studies on carbamazepine in volunteers and in epileptic patients*. Springer Berlin Heidelberg, Berlin, Heidelberg, 1975. ISBN 978-3-642-85923-6. URL http://link.springer.com/10.1007/978-3-642-85921-2.

[36] S. Pynnönen. The Pharmacokinetics of Carbamazepine in Plasma and Saliva of Man. *Acta Pharmacologica et Toxicologica*, 41(5):465–471, 1977.

[37] R. E. Strandjord and S. I. Johannessen. *Clinical Pharmacology of Anti-Epileptic Drugs*. Springer Berlin Heidelberg, Berlin, Heidelberg, 1975. ISBN 978-3-642-85923-6. URL http://link.springer.com/10.1007/978-3-642-85921-2.

[38] Y. Y. Wong, T. M. Ludden, and R. D. Bell. Effect of erythromycin on carbamazepine kinetics. *Clinical pharmacology and therapeutics*, 33(4):460–4, 1983.

[39] M. J. Dalton, J. R. Powell, and J. A. Messenheimer. The influence of cimetidine on single-dose carbamazepine pharmacokinetics. *Epilepsia*, 26(2):127–130, 1985.

[40] J. Michael J. Dalton, J. Robert Powell, and John A. Messenheimer. *Drug Intelligence and Clinical Pharmacy*.

[41] L. M. Cotter, M. J. Eadie, W. D. Hooper, C. M. Lander, G. A. Smith, and J. H. Tyrer. The pharmacokinetics of carbamazepine. *European Journal of Clinical Pharmacology*, 12(6): 451–456, 1977.

[42] A. H. Burstein, R. L. Horton, T. Dunn, R. M. Alfaro, S. C. Piscitelli, and W. Theodore. Lack of effect of St John's Wort on carbamazepine pharmacokinetics in healthy volunteers. *Clinical Pharmacology and Therapeutics*, 68(6):605–612, 2000.

[43] S. E. Møller, F. Larsen, A. Z. Khan, and P. E. Rolan. Lack of effect of citalopram on the steady-state pharmacokinetics of carbamazepine in healthy male subjects. *Journal of Clinical Psychopharmacology*, 21(5):493–499, 2001.

[44] P. Ji, B. Damle, J. Xie, S. E. Unger, D. M. Grasela, and S. Kaul. Pharmacokinetic interaction between efavirenz and carbamazepine after multiple-dose administration in healthy subjects. *Journal of Clinical Pharmacology*, 48(8):948–956, 2008.

[45] M. V. Miles and M. B. Tennison. Erythromycin effects on multiple-dose carbamazepine kinetics. *Therapeutic Drug Monitoring*, 11(1):47–52, 1989.

[46] I. Bernus, R. G. Dickinson, W. D. Hooper, and M. J. Eadie. Early stage autoinduction of carbamazepine metabolism in humans. *European journal of clinical pharmacology*, 47 (4):355–60, 1994.

[47] E. Graf. *Bioäquivalenz; Qualitätsbewertung wirkstoffgleicher Fertigarzneimittel. Hsg. von H. Blume und E. Mutschler unter Mitarb. von G. Wendt, G. Stenzhorn, M. Siewert und M. Schäfer-Korting.* Govi-Verlag, 1990. URL http://doi.wiley.com/10.1002/pauz.19900190516.

[48] D. Licht, M. Zholkovsky, R. Kaplan, M. Friedman, A. Yacobi, Y. Golander, D. Moros, and B. Levitt. European patent specification. Sustained release carbamazepine formulation. EP 1044 681 B1, 2005.

[49] R. Kshirsagar, G. Shinde, and A. Kandikurwar. United States patent application publication. Extended release pharmaceutical compositions containing carbamazepine, Pub. No.: US 2014/0302138A1. URL https://patents.google.com/patent/US20140331942A1/en.

[50] R. E. Stevens, T. Limsakun, G. Evans, and D. H. Mason. Controlled, multidose, pharmacokinetic evaluation of two extended-release carbamazepine formulations (Carbatrol and Tegretol-XR). *Journal of pharmaceutical sciences*, 87(12):1531–4, dec 1998.

[51] M. Gande, R. Gondalia, M. Kothapalli, N. M. Velishala, and V. Koppuri. United States patent application publication - carbamazepine extended release dosage form, Pub. No.: US 2009/01696.19 A1. 2009.

[52] A. G. Staines, M. W. Coughtrie, and B. Burchell. N-glucuronidation of carbamazepine in human tissues is mediated by UGT2B7. *Journal of Pharmacology and Experimental Therapeutics*, 311(3):1131–1137, 2004.

[53] B. Achour, M. R. Russell, J. Barber, and A. Rostami-Hodjegan. Simultaneous quantification of the abundance of several cytochrome P450 and uridine 5-diphosphoglucuronosyltransferase enzymes in human liver microsomes using multiplexed targeted proteomics. *Drug Metabolism and Disposition*, 42(4):500–510, 2014.

[54] Drugbank. Carbamazepine, 2018. URL https://www.drugbank.ca/drugs/DB00564. accessed: 14 Dec 2020.

[55] R. P. Austin, P. Barton, S. L. Cockroft, M. C. Wenlock, and R. J. Riley. The influence of nonspecific microsomal binding on apparent intrinsic clearance, and its prediction from physicochemical properties. *Drug Metabolism and Disposition*, 30(12):1497–1503, 2002.

[56] A. Avdeef. *Absorption and Drug Development*. John Wiley & Sons, Inc., Hoboken, NJ, USA, 2012. ISBN 9781118286067.

[57] P. Annaert, J. Brouwers, A. Bijnens, F. Lammert, J. Tack, and P. Augustijns. Ex vivo permeability experiments in excised rat intestinal tissue and in vitro solubility measurements in aspirated human intestinal fluids support age-dependent oral drug absorption. *European journal of pharmaceutical sciences : official journal of the European Federation for Pharmaceutical Sciences*, 39(1-3):15–22, jan 2010.

[58] S. Clarysse, J. Brouwers, J. Tack, P. Annaert, and P. Augustijns. Intestinal drug solubility estimation based on simulated intestinal fluids: Comparison with solubility in human intestinal fluids. *European Journal of Pharmaceutical Sciences*, 43(4):260–269, 2011.

[59] T. Heikkilä, M. Karjalainen, K. Ojala, K. Partola, F. Lammert, P. Augustijns, A. Urtti, M. Yliperttula, L. Peltonen, and J. Hirvonen. Equilibrium drug solubility measurements in 96-well plates reveal similar drug solubilities in phosphate buffer pH 6.8 and human intestinal fluid. *International Journal of Pharmaceutics*, 405(1-2):132–136, 2011.

[60] E. Söderlind, E. Karlsson, A. Carlsson, R. Kong, A. Lenz, S. Lindborg, and J. J. Sheng. Simulating fasted human intestinal fluids: understanding the roles of lecithin and bile acids. *Molecular pharmaceutics*, 7(5):1498–507, oct 2010.

[61] Heumann Pharma GmbH & Co. Generica KG. Fachinformation - Carbamazepin 200/400 Heumann, 2014. URL https://www.fachinfo.de/suche/fi/006667. accessed: 11 Nov 2020.

[62] L. Bertilsson. Clinical pharmacokinetics of carbamazepine. *Clinical Pharmacokinetics*, 3:128–1473, 1978.

[63] J. Henshall, A. Galetin, A. Harrison, and J. B. Houston. Comparative analysis of CYP3A heteroactivation by steroid hormones and flavonoids in different in vitro systems and potential in vivo implications. *Drug Metabolism and Disposition*, 36(7):1332–1340, 2008.

[64] N. Cazali, A. Tran, J. M. Treluyer, E. Rey, P. Athis, J. Vincent, and G. Pons. Inhibitory effect of stiripentol on carbamazepine and saquinavir metabolism in human. *British Journal of Clinical Pharmacology*, 56(5):526, 2003.

[65] W. Huang, Y. S. Lin, D. J. McConn, J. C. Calamia, R. A. Totah, N. Isoherranen, M. Glodowski, and K. E. Thummel. Evidence of significant contribution from CYP3A5 to hepatic drug metabolism. *Drug Metabolism and Disposition*, 32(12):1434–1445, 2004.

[66] M. Shou, M. Hayashi, Y. Pan, Y. Xu, K. Morrissey, L. Xu, and G. L. Skiles. Modeling, prediction, and in vitro in vivo correlation of CYP3A4 induction. *Drug Metabolism and Disposition*, 36(11):2355–2370, 2008.

[67] D. F. McGinnity, G. Zhang, J. R. Kenny, G. A. Hamilton, S. Otmani, K. R. Stams, S. Haney, P. Brassil, D. M. Stresser, and R. J. Riley. Evaluation of multiple in vitro systems for assessment of CYP3A4 induction in drug discovery: human hepatocytes, pregnane X receptor reporter gene, and Fa2N-4 and HepaRG cells. *Drug metabolism and disposition: the biological fate of chemicals*, 37(6):1259–68, jun 2009.

[68] O. A. Fahmi, J. L. Raucy, E. Ponce, S. Hassanali, and J. M. Lasker. Utility of DPX2 cells for predicting CYP3A induction-mediated drug-drug interactions and associated structure-activity relationships. *Drug metabolism and disposition: the biological fate of chemicals*, 40(11):2204–11, nov 2012.

[69] J. G. Zhang, T. Ho, A. L. Callendrello, R. J. Clark, E. A. Santone, S. Kinsman, D. Xiao, L. G. Fox, H. J. Einolf, and D. M. Stresser. Evaluation of calibration curve-based approaches to predict clinical inducers and noninducers of CYP3A4 with plated human hepatocytes. *Drug Metabolism and Disposition*, 42(9):1379–1391, 2014.

[70] A. Moore, P. P. Chothe, H. Tsao, and N. Hariparsad. Evaluation of the interplay between uptake transport and CYP3A4 induction in micropatterned cocultured hepatocytes. *Drug Metabolism and Disposition*, 44(12):1910–1919, 2016.

[71] O. A. Fahmi, M. Kish, S. Boldt, and R. Scott Obach. Cytochrome P450 3A4 mRNA is a more reliable marker than CYP3A4 activity for detecting pregnane X receptor-activated induction of drug-metabolizing enzymes. *Drug Metabolism and Disposition*, 38(9):1605–1611, 2010.

[72] R. Zuo, F. Li, S. Parikh, L. Cao, K. L. Cooper, Y. Hong, J. Liu, R. A. Faris, D. Li, and H. Wang. Evaluation of a novel renewable hepatic cell model for prediction of clinical CYP3A4 induction using a correlation-based relative induction score approach. *Drug Metabolism and Disposition*, 45(2):198–207, 2017.

[73] J. G. Zhang, R. Patel, R. J. Clark, T. Ho, S. K. Trisdale, Y. Fang, and D. M. Stresser. Effect of Fifteen CYP3A4 in vitro Inducers on the Induction of Hepatocytes : A Trend Analysis. Poster presented at: 20th North American ISSX Meeting; 2015 18-22 Oct; Orlando Florida.

[74] O. A. Fahmi, M. Shebley, J. Palamanda, M. W. Sinz, D. Ramsden, H. J. Einolf, L. Chen, and H. Wang. Evaluation of CYP2B6 induction and prediction of clinical drug-drug interactions: Considerations from the IQ consortium induction working group - An industry perspective. *Drug Metabolism and Disposition*, 44(10):1720–1730, 2016.

[75] L. J. Dickmann and N. Isoherranen. Quantitative prediction of CYP2B6 induction by estradiol during pregnancy: Potential explanation for increased methadone clearance during pregnancy. *Drug Metabolism and Disposition*, 41(2):270–274, 2013.

[76] H. Lennernäs. Intestinal permeability and its relevance for absorption and elimination. *Xenobiotica*, 37(10-11):1015–1051, nov 2007.

[77] T. Rodgers, D. Leahy, and M. Rowland. Physiologically based pharmacokinetic modeling 1: predicting the tissue distribution of moderate-to-strong bases. *Journal of pharmaceutical sciences*, 94(6):1259–76, jun 2005.

[78] M. J. Taylor, S. Tanna, and T. Sahota. In vivo study of a polymeric glucose-sensitive insulin delivery system using a rat model. *Journal of pharmaceutical sciences*, 99(10): 4215–27, 2010.

[79] R. Kawai, M. Lemaire, J. L. Steimer, A. Bruelisauer, W. Niederberger, and M. Rowland. Physiologically based pharmacokinetic study on a cyclosporin derivative, SDZ IMM 125. *Journal of pharmacokinetics and biopharmaceutics*, 22(5):327–65, oct 1994.

[80] Drugbank. Metabolite 10,11-Epoxycarbamazepine, 2020. URL https://www.drugbank.ca/metabolites/DBMET00291. accessed: 14 Dec 2020.

[81] A. Gérardin, J. P. Dubois, J. Moppert, and L. Geller. Absolute bioavailability of carbamazepine after oral administration of a 2% syrup. *Epilepsia*, 31(3):334–8, 1990.

[82] U.S. Food and Drug Administration. SUSTIVA (efavirenz) label, 2011. URL https://www.accessdata.fda.gov/drugsatfda_docs/label/2011/020972s038lbl.pdf. accessed: 14 Dec 2020.

[83] B. A. Ward, J. C. Gorski, D. R. Jones, S. D. Hall, D. A. Flockhart, and Z. Desta. The cytochrome P450 2B6 (CYP2B6) is the main catalyst of efavirenz primary and secondary metabolism: Implication for HIV/AIDS therapy and utility of efavirenz as a substrate marker of CYP2B6 catalytic activity. *Journal of Pharmacology and Experimental Therapeutics*, 306(1):287–300, 2003.

[84] E. T. Ogburn, D. R. Jones, A. R. Masters, C. Xu, Y. Guo, and Z. Desta. Efavirenz primary and secondary metabolism in vitro and in vivo: Identification of novel metabolic pathways and cytochrome P450 2A6 as the principal catalyst of efavirenz 7-hydroxylation. *Drug Metabolism and Disposition*, 38(7):1218–1229, 2010.

[85] A. Ke, Z. Barter, K. Rowland-Yeo, and L. Almond. Towards a best practice approach in PBPK modeling: Case example of developing a unified efavirenz model accounting for induction of CYPs 3A4 and 2B6. *CPT: Pharmacometrics and Systems Pharmacology*, 5 (7):367–376, 2016.

[86] Z. Desta, R. S. Gammal, L. Gong, M. Whirl-Carrillo, A. H. Gaur, C. Sukasem, J. Hockings, A. Myers, M. Swart, R. F. Tyndale, C. Masimirembwa, O. F. Iwuchukwu, S. Chirwa, J. Lennox, A. Gaedigk, T. E. Klein, and D. W. Haas. Clinical Pharmacogenetics Implementation Consortium (CPIC) guideline for CYP2B6 and efavirenz-containing antiretroviral therapy. *Clinical Pharmacology and Therapeutics*, 106(4):726–733, 2019.

[87] S. Frechen, T. Wendel, and J. Solodenko. Building and evaluation of a PBPK model for efavirenz in healthy adults, 2020. URL https://github.com/Open-Systems-Pharmacology/OSP-PBPK-Model-Library/blob/v9.1/Efavirenz/efavirenz_evaluation_report.pdf. accessed: 13 Nov 2020.

[88] C. Xu, E. T. Ogburn, Y. Guo, and Z. Desta. Effects of the CYP2B6*6 allele on catalytic properties and inhibition of CYP2B6 in vitro: Implication for the mechanism of reduced efavirenz metabolism and other CYP2B6 substrates in vivo. *Drug Metabolism and Disposition*, 40(4):717–725, 2012.

[89] A. Derungs, M. Donzelli, B. Berger, C. Noppen, S. Krähenbühl, and M. Haschke. Effects of cytochrome P450 inhibition and induction on the phenotyping metrics of the Basel Cocktail: A randomized crossover study. *Clinical Pharmacokinetics*, 55(1):79–91, 2016.

[90] S. Mouly, K. S. Lown, D. Kornhauser, J. L. Joseph, W. D. Fiske, I. H. Benedek, and P. B. Watkins. Hepatic but not intestinal CYP3A4 displays dose-dependent induction by efavirenz in humans. *Clinical Pharmacology and Therapeutics*, 72(1):1–9, 2002.

[91] Ping Liu, G. Foster, R. R. Labadie, M. J. Gutierrez, and A. Sharma. Pharmacokinetic interaction between voriconazole and efavirenz at steady state in healthy male subjects. *Journal of Clinical Pharmacology*, 48(1):73–84, 2008.

[92] D. Y. Cho, J. H. Shen, S. M. Lemler, T. C. Skaar, L. Li, J. Blievernicht, U. M. Zanger, K. B. Kim, J. G. Shin, D. A. Flockhart, and Z. Desta. Rifampin enhances cytochrome P450 (CYP) 2B6-mediated efavirenz 8-hydroxylation in healthy volunteers. *Drug Metabolism and Pharmacokinetics*, 31(2):107–116, 2016.

[93] C. Xu, S. K. Quinney, Y. Guo, S. D. Hall, L. Li, and Z. Desta. CYP2B6 pharmacogenetics-based in vitro-in vivo extrapolation of efavirenz clearance by physiologically based pharmacokinetic modeling. *Drug Metabolism and Disposition*, 41(12):2004–2011, 2013.

[94] K. E. Dooley, J. G. Park, S. Swindells, R. Allen, D. W. Haas, Y. Cramer, F. Aweeka, I. Wiggins, A. Gupta, P. Lizak, S. Qasba, R. Van Heeswijk, and C. Flexner. Safety, tolerability, and pharmacokinetic interactions of the antituberculous agent TMC207 (Bedaquiline)

with efavirenz in healthy volunteers: AIDS clinical trials group study A5267. *Journal of Acquired Immune Deficiency Syndromes*, 59(5):455–462, 2012.

[95] B. Damle, R. LaBadie, P. Crownover, and P. Glue. Pharmacokinetic interactions of efavirenz and voriconazole in healthy volunteers. *British Journal of Clinical Pharmacology*, 65(4):523–530, 2008.

[96] V. Garg, G. Chandorkar, Y. Yang, N. Adda, L. Mcnair, K. Alves, F. Smith, and R. P. van Heeswijk. The effect of CYP3A inhibitors and inducers on the pharmacokinetics of telaprevir in healthy volunteers. *British Journal of Clinical Pharmacology*, 75(2):431–439, 2013.

[97] L. Huang, S. Parikh, P. J. Rosenthal, P. Lizak, F. Marzan, G. Dorsey, D. Havlir, and F. T. Aweeka. Concomitant efavirenz reduces pharmacokinetic exposure to the antimalarial drug artemether–lumefantrine in healthy volunteers. *JAIDS Journal of Acquired Immune Deficiency Syndromes*, 61(3):310–316, nov 2012.

[98] E. D. Kharasch, D. Whittington, D. Ensign, C. Hoffer, P. S. Bedynek, S. Campbell, K. Stubbert, A. Crafford, A. London, and T. Kim. Mechanism of efavirenz influence on methadone pharmacokinetics and pharmacodynamics. *Clinical Pharmacology and Therapeutics*, 91 (4):673–684, 2012.

[99] A. Kwara, K. T. Tashima, J. B. Dumond, P. Poethke, J. Kurpewski, A. D. Kashuba, M. H. Court, and D. J. Greenblatt. Modest but variable effect of rifampin on steady-state plasma pharmacokinetics of efavirenz in healthy African-American and Caucasian volunteers. *Antimicrobial Agents and Chemotherapy*, 55(7):3527–3533, 2011.

[100] C. D. Malvestutto, Q. Ma, G. D. Morse, J. A. Underberg, and J. A. Aberg. Lack of pharmacokinetic interactions between pitavastatin and efavirenz or darunavir/ritonavir. *Journal of Acquired Immune Deficiency Syndromes*, 67(4):390–396, 2014.

[101] G. H. Soon, P. Shen, E. L. Yong, P. Pham, C. Flexner, and L. Lee. Pharmacokinetics of darunavir at 900 milligrams and ritonavir at 100 milligrams once daily when coadministered with efavirenz at 600 milligrams once daily in healthy volunteers. *Antimicrobial Agents and Chemotherapy*, 54(7):2775–2780, 2010.

[102] Drugbank. Efavirenz, 2020. URL https://go.drugbank.com/drugs/DB00625. accessed: 14 Dec 2020.

[103] L. M. Almond, P. G. Hoggard, D. Edirisinghe, S. H. Khoo, and D. J. Back. Intracellular and plasma pharmacokinetics of efavirenz in HIV-infected individuals. *Journal of Antimicrobial Chemotherapy*, 56(4):738–744, 2005.

[104] O. Janneh, B. Chandler, R. Hartkoorn, W. S. Kwan, C. Jenkinson, S. Evans, D. J. Back, A. Owen, and S. H. Khoo. Intracellular accumulation of efavirenz and nevirapine is independent of P-glycoprotein activity in cultured CD4 T cells and primary human lymphocytes. *Journal of Antimicrobial Chemotherapy*, 64(5):1002–1007, nov 2009.

[105] R. Cristofoletti, A. Nair, B. Abrahamsson, D. Groot, S. Kopp, P. Langguth, J. E. Polli, V. P. Shah, and J. B. Dressman. Biowaiver monographs for immediate release solid oral dosage forms: Efavirenz. *Journal of Pharmaceutical Sciences*, 102(2):318–329, feb 2013.

[106] J. Gao, M. Hussain, R. Motheram, D. Gray, I. Benedek, W. Fiske, W. Doll, E. Sandefer, R. Page, and G. Digenis. Investigation of human pharmacoscintigraphic behavior of two tablets and a capsule formulation of a high dose, poorly water soluble/highly permeable drug (efavirenz). *Journal of Pharmaceutical Sciences*, 96(11):2970–2977, nov 2007.

[107] S. R. Rabel, M. B. Maurin, S. M. Rowe, and M. Hussain. Determination of the pKa and pH-solubility behavior of an ionizable cyclic carbamate, (S)-6-Chloro-4-(cyclopropylethynyl)-1,4-dihydro-4-(trifluoromethyl)-2H-3,1-benzoxazin-2-one (DMP 266). *Pharmaceutical Development and Technology*, 1(1):91–95, jan 1996.

[108] W. Schmitt. General approach for the calculation of tissue to plasma partition coefficients. *Toxicology in vitro : an international journal published in association with BIBRA*, 22(2): 457–67, mar 2008.

[109] E. J. Guest, L. Aarons, J. B. Houston, A. Rostami-Hodjegan, and A. Galetin. Critique of the two-fold measure of prediction success for ratios: application for the assessment of drug-drug interactions. *Drug metabolism and disposition: the biological fate of chemicals*, 39(2):170–3, feb 2011.

[110] S. Frechen and A. Dallmann. Building and evaluation of a PBPK model for erythromycin in healthy adults, 2020. URL https://github.com/Open-Systems-Pharmacology/OSP-PBPK-Model-Library/blob/v9.1/Erythromycin/Erythromycin_evaluation_report.pdf. accessed: 13 Nov 2020.

[111] S. Frechen. CYP3A4 DDI Qualification, 2020. URL https://github.com/Open-Systems-Pharmacology/OSP-Qualification-Reports/blob/v9.1/DDI_Qualification_CYP3A4/report.pdf. accessed: 14 Dec 2020.

[112] Drugbank. Erythromycin, 2020. URL https://go.drugbank.com/drugs/DB00199. accessed: 14 Dec 2020.

[113] E. Lien, J. Kuwahara, and R. Koda. Diffusion of drugs into prostatic fluid and milk. *Drug intelligence & Clinical Pharmacy*, 8(8):470–475, 1974.

[114] J. O. Capobianco and R. C. Goldman. Macrolide transport in Escherichia coli strains having normal and altered OmpC and/or OmpF porins. *International journal of antimicrobial agents*, 4(3):183–9, 1994.

[115] J. W. McFarland, C. M. Berger, S. A. Froshauer, S. F. Hayashi, S. J. Hecker, B. H. Jaynes, M. R. Jefson, B. J. Kamicker, C. A. Lipinski, K. M. Lundy, C. P. Reese, and C. B. Vu. Quantitative structure-activity relationships among macrolide antibacterial agents: In vitro and in vivo potency against Pasteurella multocida. *Journal of Medicinal Chemistry*, 40 (9):1340–1346, 1997.

[116] C. Hoffhine. Aqueous soluble salts of erythromycin. Issues September 4. Nr. 2,761,859, 1956. URL https://patents.google.com/patent/US2761859A/en. accessed: 14 Dec 2020.

[117] P. H. Jones, E. K. Rowley, A. L. Weiss, D. L. Bishop, and A. H. Chun. Insoluble erythromycin salts. *Journal of Pharmaceutical Sciences*, 58(3):337–339, 1969.

[118] P. K. Manna and S. K. Basu. Preparation and evaluation of erythromycin fumarate - A new derivative of erythromycin. *Drug Development and Industrial Pharmacy*, 24(9): 879–882, 1998.

[119] H. Sun, L. A. Frassetto, Y. Huang, and L. Z. Benet. Hepatic clearance, but not gut availability, of erythromycin is altered in patients with end-stage renal disease. *Clinical Pharmacology & Therapeutics*, 87(4):465–472, 2010.

[120] A. Iliopoulou, M. Aldhous, A. Johnston, and P. Turner. Pharmacokinetic interaction between theophylline and erythromycin. *British Journal of Clinical Pharmacology*, 14 (4):495–499, 1982.

[121] J. Barre, A. Mallat, J. Rosenbaum, L. Deforges, G. Houin, D. Dhumeaux, and J. Tillement. Pharmacokinetics of erythromycin in patients with severe cirrhosis. Respective influence of decreased serum binding and impaired liver metabolic capacity. *British Journal of Clinical Pharmacology*, 23(6):753–757, 1987.

[122] L. Xu, Y. Chen, Y. Pan, G. L. Skiles, and M. Shou. Prediction of human drug-drug interactions from time-dependent inactivation of CYP3A4 in primary hepatocytes using a population-based simulator. *Drug Metabolism and Disposition*, 37(12):2330–2339, 2009.

[123] R. W. Wang, D. J. Newton, T. D. Scheri, and A. Y. Lu. Human cytochrome P450 3A4-catalyzed testosterone 6 beta-hydroxylation and erythromycin N-demethylation. Competition during catalysis. *Drug metabolism and disposition: the biological fate of chemicals*, 25(4):502–7, 1997.

[124] R. J. Riley and D. Howbrook. In vitro analysis of the activity of the major human hepatic CYP enzyme (CYP3A4) using [N-methyl-14C]-erythromycin. *Journal of Pharmacological and Toxicological Methods*, 38(4):189–193, dec 1997.

[125] C. S. Lancaster, G. H. Bruun, C. J. Peer, T. S. Mikkelsen, T. J. Corydon, A. A. Gibson, S. Hu, S. J. Orwick, R. H. J. Mathijssen, W. D. Figg, S. D. Baker, and A. Sparreboom. OATP1B1 polymorphism as a determinant of erythromycin disposition. *Clinical Pharmacology & Therapeutics*, 92(5):642–650, nov 2012.

[126] T. Akiyoshi, M. Ito, S. Murase, M. Miyazaki, F. Peter Guengerich, K. Nakamura, K. Yamamoto, and H. Ohtani. Mechanism-based inhibition profiles of erythromycin and Cclarithromycin with cytochrome P450 3A4 genetic variants. *Drug Metabolism and Pharmacokinetics*, 28(5):411–415, 2013.

[127] A. Atkinson, J. R. Kenny, and K. Grime. Automated assessment of time-dependent inhibition of human cytochrome P450 enzymes using liquid chromatography-tandem mass spectrometry analysis. *Drug Metabolism and Disposition*, 33(11):1637–1647, nov 2005.

[128] S. Aueviriyavit, K. Kobayashi, and K. Chiba. Species differences in mechanism-based inactivation of CYP3A in humans, rats and mice. *Drug Metabolism and Pharmacokinetics*, 25(1):93–100, 2010.

[129] W. K. Chan and A. B. Delucchi. Resveratrol, a red wine constituent, is a mechanism-based inactivator of cytochrome P450 3A4. *Life Sciences*, 67(25):3103–3112, nov 2000.

[130] Y. Chen, L. Liu, M. Monshouwer, and A. J. Fretland. Determination of time-dependent inactivation of CYP3A4 in cryopreserved human hepatocytes and assessment of human drug-drug interactions. *Drug Metabolism and Disposition*, 39(11):2085–2092, nov 2011.

[131] Y. Ishikawa, T. Akiyoshi, A. Imaoka, and H. Ohtani. Inactivation kinetics and residual activity of CYP3A4 after treatment with erythromycin. *Biopharmaceutics & Drug Disposition*, 38(7):420–425, 2017.

[132] S. Kanamitsu, I. K, G. CE, C. Tyson, N. Shimada, and Y. Sugiyama. Prediction of in vivo interaction between triazolam and erythromycin based on in vitro studies using human liver microsomes and recombinant human CYP3A4. *Pharmaceutical Research*, 17(4): 419–426, 2000.

[133] K. Kozakai, Y. Yamada, M. Oshikata, T. Kawase, E. Suzuki, Y. Haramaki, and H. Taniguchi. Cocktail-substrate approach-based high-throughput assay for evaluation of direct and time-dependent inhibition of multiple cytochrome P450 isoforms. *Drug Metabolism and Pharmacokinetics*, 29(2):198–207, 2014.

[134] J. Mao, S. Tay, C. S. Khojasteh, Y. Chen, C. E. C. A. Hop, and J. R. Kenny. Evaluation of time dependent inhibition assays for marketed oncology drugs: Comparison of human hepatocytes and liver microsomes in the presence and absence of human plasma. *Pharmaceutical Research*, 33(5):1204–1219, 2016.

[135] D. J. McConn, Y. S. Lin, K. Allen, K. L. Kunze, and K. E. Thummel. Differences in the inhibition of cytochromes P450 3A4 and 3A5 by metabolite-inhibitor complex-forming drugs. *Drug Metabolism and Disposition*, 32(10):1083–1091, 2004.

[136] X. Zhang, D. R. Jones, and S. D. Hall. Prediction of the effect of erythromycin, diltiazem, and their metabolites, alone and in combination, on CYP3A4 inhibition. *Drug Metabolism and Disposition*, 37(1):150–160, 2009.

[137] S. Frechen and A. Dallmann. Building and evaluation of a PBPK model for alprazolam in healthy adults, 2020. URL https://github.com/Open-Systems-Pharmacology/OSP-PBPK-Model-Library/blob/v9.1/Alprazolam/Alprazolam_evaluation_report.pdf. accessed: 13 Nov 2020.

[138] Drugbank. Alprazolam, 2020. URL https://go.drugbank.com/drugs/DB00404. accessed: 14 Dec 2020.

[139] D. J. Greenblatt, L. L. Von Moltke, J. S. Harmatz, G. Chen, J. L. Weemhoff, C. Jen, C. J. Kelley, B. W. LeDuc, and M. A. Zinny. Time course of recovery of cytochrome P450 3A function after single doses of grapefruit juice. *Clinical Pharmacology and Therapeutics*, 74(2):121–29, 2003.

[140] S. G. Machatha and S. H. Yalkowsky. Estimation of the ethanol/water solubility profile from the octanol/water partition coefficient. *International Journal of Pharmaceutics*, 286 (1-2):111–115, nov 2004.

[141] T. Loftsson and D. Hreinsdôttir. Determination of aqueous solubility by heating and equilibration: A technical note. *AAPS PharmSciTech*, 7(1):E29–E32, mar 2006.

[142] F. S. Eberts, Y. Philopoulos, L. M. Reineke, and R. W. Vliek. Disposition of 14-C-alprazolam, a new anxiolytic-antidepressant, in man. *Pharmacologist*, 22(3):279, 1980.

[143] V. D. Schmith, B. Piraino, R. B. Smith, and P. D. Kroboth. Alprazolam in end-stage renal disease: I. Pharmacokinetics. *The Journal of Clinical Pharmacology*, 31(6):571–579, jun 1991.

[144] H. R. Ochs, D. J. Greenblatt, L. Labedzki, and R. B. Smith. Alprazolam kinetics in patients with renal insufficiency. *Journal of clinical psychopharmacology*, 6(5):292–294, 1986.

[145] M. Cho, T. Scahill, and J. Hester. Kinetics and equilibrium of the reversible alprazolam ring-opening reaction. *Journal of Pharmaceutical Sciences*, 72(4):356–362, apr 1983.

[146] G. G. Raymond and J. L. Born. An updated pKa listing of medicinal compounds. *Drug Intelligence & Clinical Pharmacy*, 20(9):683–686, sep 1986.

[147] K. R. Manchester, P. D. Maskell, and L. Waters. Experimental versus theoretical log D7.4, pKa and plasma protein binding values for benzodiazepines appearing as new psychoactive substances. *Drug Testing and Analysis*, 10(8):1258–1269, 2018.

[148] N. Hirota, K. Ito, T. Iwatsubo, C. E. Green, C. A. Tyson, N. Shimada, H. Suzuki, and Y. Sugiyama. In Vitro/in Vivo scaling of alprazolam metabolism by CYP3A4 and CYP3A5 in humans. *Biopharmaceutics & Drug Disposition*, 22(2):53–71, mar 2001.

[149] H. Furukori, M.D. Effect of carbamazepine on the single oral dose pharmacokinetics of alprazolam. *Neuropsychopharmacology*, 18(5):364–369, may 1998.

[150] J. Wojtyniak, H. Britz, D. Selzer, M. Schwab, and T. Lehr. Data Digitizing: Accurate and Precise Data Extraction for Quantitative Systems Pharmacology and Physiologically-Based Pharmacokinetic Modeling. *CPT: Pharmacometrics & Systems Pharmacology*, 9 (6):322–331, jun 2020.

[151] N. Tsamandouras, G. Dickinson, Y. Guo, S. Hall, A. Rostami-Hodjegan, A. Galetin, and L. Aarons. Development and application of a mechanistic pharmacokinetic model for simvastatin and its active metabolite simvastatin acid using an integrated population PBPK approach. *Pharmaceutical Research*, 32(6):1864–1883, jun 2015.

[152] H. Lennernäs and G. Fager. Pharmacodynamics and pharmacokinetics of the HMG-CoA reductase inhibitors. *Clinical Pharmacokinetics*, 32(5):403–425, may 1997.

[153] A. H. Rageh, N. N. Atia, and H. M. Abdel-Rahman. Lipophilicity estimation of statins as a decisive physicochemical parameter for their hepato-selectivity using reversed-phase thin layer chromatography. *Journal of Pharmaceutical and Biomedical Analysis*, 142: 7–14, aug 2017.

[154] Chemaxon. Chemicalize - instant cheminformatics solutions, 2020. URL https://chemicalize.com/. accessed: 14 Dec 2020.

[155] M. Rao, Y. Mandage, K. Thanki, and S. Bhise. Dissolution improvement of simvastatin by surface solid dispersion technology. *Dissolution Technologies*, 17(2):27–34, 2010.

[156] Merck Canada Inc. Product monograph: Zocor. 2006.

[157] S. Geboers, J. Stappaerts, J. Tack, P. Annaert, and P. Augustijns. In vitro and in vivo investigation of the gastrointestinal behavior of simvastatin. *International Journal of Pharmaceutics*, 510(1):296–303, aug 2016.

[158] M. Gertz, A. Harrison, J. B. Houston, and A. Galetin. Prediction of human intestinal first-pass metabolism of 25 CYP3A substrates from in vitro clearance and permeability data. *Drug Metabolism and Disposition*, 38(7):1147–1158, jul 2010.

[159] S. Vickers, C. A. Duncan, I. W. Chen, A. Rosegay, and D. E. Duggan. Metabolic disposition studies on simvastatin, a cholesterol-lowering prodrug. *Drug Metabolism and Disposition*, 18(2):138–145, 1990.

[160] T. Prueksaritanont, L. M. Gorham, B. Ma, L. Liu, X. Yu, J. J. Zhao, D. E. Slaughter, B. H. Arison, and K. P. Vyas. In vitro metabolism of simvastatin in humans [SBT] identification of metabolizing enzymes and effect of the drug on hepatic P450s. *Drug metabolism and disposition: the biological fate of chemicals*, 25(10):1191–1199, 1997.

[161] N. Le Goff, J. C. Koffel, S. Vandenschrieck, L. Jung, and G. Ubeaud. Comparison of in vitro hepatic models for the prediction of metabolic interaction between simvastatin and naringenin. *European Journal of Drug Metabolism and Pharmacokinetics*, 27(4): 233–241, dec 2002.

[162] M. Ishigam, M. Uchiyama, T. Kondo, H. Iwabuchi, S. I. Inoue, W. Takasaki, T. Ikeda, T. Komai, K. Ito, and Y. Sugiyama. Inhibition of in vitro metabolism of simvastatin by itraconazole in humans and prediction of in vivo drug-drug interactions. *Pharmaceutical Research*, 18(5):622–631, 2001.

[163] H. Lu, J. Zhu, Y. Zang, Y. Ze, and J. Qin. Cloning, high level expression of human paraoxonase-3 in Sf9 cells and pharmacological characterization of its product. *Biochemical Pharmacology*, 70(7):1019–1025, oct 2005.

[164] D. A. Taha, C. H. D. Moor, D. A. Barrett, J. B. Lee, R. D. Gandhi, C. W. Hoo, and P. Gershkovich. The role of acid-base imbalance in statin-induced myotoxicity. *Translational research: the journal of laboratory and clinical medicine,*, 174:140–160, 2016.

[165] A. Á. Lueje, C. Valenzuela, J. A. Squella, and N.-V. Joaquin Luis. Stability study of simvastatin under hydrolytic conditions assessed by liquid chromatography. *Journal of AOAC International*, 88(6):1631–1636, 2005.

[166] T. Prueksaritanont, Y. Qiu, L. Mu, K. Michel, J. Brunner, K. M. Richards, and J. H. Lin. Interconversion pharmacokinetics of simvastatin and its hydroxy acid in dogs: Effects of gemfibrozil. *Pharmaceutical Research*, 22(7):1101–1109, jul 2005.

[167] L. Huang, Y. Wang, and S. Grimm. ATP-dependent transport of rosuvastatin in membrane vesicles expressing brast cancer resistance protein. *Drug Metabolism and Disposition*, 34(5):738–742, may 2006.

[168] J. W. Deng, J.-H. Shon, H.-J. Shin, S.-J. Park, C.-W. Yeo, H.-H. Zhou, I.-S. Song, and J.-G. Shin. Effect of silymarin supplement on the pharmacokinetics of rosuvastatin. *Pharmaceutical Research*, 25(8):1807–1814, aug 2008.

[169] M. Hirano, K. Maeda, S. Matsushima, Y. Nozaki, H. Kusuhara, and Y. Sugiyama. Involvement of BCRP (ABCG2) in the biliary excretion of pitavastatin. *Molecular Pharmacology*, 68(3):800–807, sep 2005.

[170] M. Afrouzian, R. Al-Lahham, S. Patrikeeva, M. Xu, V. Fokina, W. G. Fischer, S. Z. Abdel-Rahman, M. Costantine, M. S. Ahmed, and T. Nanovskaya. Role of the efflux transporters BCRP and MRP1 in human placental bio-disposition of pravastatin. *Biochemical Pharmacology*, 156:467–478, oct 2018.

[171] S. Kitamura, K. Maeda, Y. Wang, and Y. Sugiyama. Involvement of multiple transporters in the hepatobiliary transport of rosuvastatin. *Drug Metabolism and Disposition*, 36(10): 2014–2023, oct 2008.

[172] A. Vildhede, A. Mateus, E. K. Khan, Y. Lai, M. Karlgren, P. Artursson, and M. C. Kjellsson. Mechanistic modeling of pitavastatin disposition in sandwich-cultured human hepatocytes: A proteomics-informed bottom-up approach. *Drug Metabolism and Disposition*, 44(4):505–516, feb 2016.

[173] B. M. VandenBrink, R. S. Foti, D. A. Rock, L. C. Wienkers, and J. L. Wahlstrom. Evaluation of CYP2C8 inhibition in vitro: Utility of montelukast as a selective CYP2C8 probe substrate. *Drug Metabolism and Disposition*, 39(9):1546–1554, sep 2011.

[174] R. S. Foti, D. A. Rock, L. C. Wienkers, and J. L. Wahlstrom. Selection of alternative CYP3A4 probe substrates for clinical drug interaction studies using in vitro data and in vivo simulation. *Drug Metabolism and Disposition*, 38(6):981–987, jun 2010.

[175] C. S. Cook, L. M. Berry, and E. Burton. Prediction of in vivo drug interactions with eplerenone in man from in vitro metabolic inhibition data. *Xenobiotica*, 34(3):215–228, mar 2004.

[176] M. Ishigami, T. Honda, W. Takasaki, T. Ikeda, T. Komai, K. Ito, and Y. Sugiyama. A comparison of the effects of 3-hydroxy-3-methylglutaryl-coenzyme a (HMG-CoA) reductase

inhibitors on the CYP3A4-dependent oxidation of mexazolam in vitro. *Drug metabolism and disposition: the biological fate of chemicals*, 29(3):282–8, mar 2001.

[177] H. Fujino, I. Yamada, S. Shimada, T. Nagao, and M. Yoneda. Metabolic fate of pitavastatin (NK-104), a new inhibitor of 3-hydroxy-3-methyllutaryl coenzyme A reductase. *Arzneimittelforschung*, 52(10):745–753, dec 2011.

[178] M. G. Soars, P. Barton, M. Ismair, R. Jupp, and R. J. Riley. The development, characterization, and application of an OATP1B1 inhibition assay in drug discovery. *Drug Metabolism and Disposition*, 40(8):1641–1648, aug 2012.

[179] C. Chen, R. J. Mireles, S. D. Campbell, J. Lin, J. B. Mills, J. J. Xu, and T. A. Smolarek. Differential interaction of 3-hydroxy-3-methylglutaryl-CoA reductase inhibitors with ABCB1, ABCC2 and OATP1B1. *Drug Metabolism and Disposition*, 33(4):537–546, apr 2005.

[180] E. J. Wang, C. N. Casciano, R. P. Clement, and W. W. Johnson. HMG-CoA reductase inhibitors (statins) characterized as direct inhibitors of P-glycoprotein. *Pharmaceutical Research1*, 18(6):800–806, 2001.

[181] M. Werner, B. Atil, E. Sieczkowski, P. Chiba, and M. Hohenegger. Simvastatin-induced compartmentalisation of doxorubicin sharpens up nuclear topoisomerase II inhibition in human rhabdomyosarcoma cells. *Naunyn-Schmiedeberg's Archives of Pharmacology*, 386(7):605–617, jul 2013.

[182] E.-j. Wang, C. N. Casciano, R. P. Clement, and W. W. Johnson. Active transport of fluorescent P-glycoprotein substrates: Evaluation as markers and interaction with inhibitors. *Biochemical and Biophysical Research Communications*, 289(2):580–585, nov 2001.

[183] H. Sugimoto, S.-I. Matsumoto, M. Tachibana, S.-I. Niwa, H. Hirabayashi, N. Amano, and T. Moriwaki. Establishment of in vitro P-glycoprotein inhibition assay and its exclusion criteria to assess the risk Of drug–drug interaction at the drug discovery stage. *Journal of Pharmaceutical Sciences*, 100(9):4013–4023, sep 2011.

[184] A. Poirier, A.-C. Cascais, U. Bader, R. Portmann, M.-E. Brun, I. Walter, A. Hillebrecht, M. Ullah, and C. Funk. Calibration of in vitro multidrug resistance protein 1 substrate and inhibition assays as a basis to support the prediction of clinically relevant interactions in vivo. *Drug Metabolism and Disposition*, 42(9):1411–1422, sep 2014.

[185] J. P. Keogh and J. R. Kunta. Development, validation and utility of an in vitro technique for assessment of potential clinical drug–drug interactions involving P-glycoprotein. *European Journal of Pharmaceutical Sciences*, 27(5):543–554, apr 2006.

[186] T. Sakaeda, H. Fujino, C. Komoto, M. Kakumoto, J. S. Jin, K. Iwaki, K. Nishiguchi, T. Nakamura, N. Okamura, and K. Okumura. Effects of acid and lactone forms of eight HMG-CoA reductase inhibitors on CYP-mediated metabolism and MDR1-mediated transport. *Pharmaceutical Research*, 23(3):506–512, 2006.

[187] L. M. Berezhkovskiy. Volume of distribution at steady state for a linear pharmacokinetic system with peripheral elimination. *Journal of pharmaceutical sciences*, 93(6):1628–40, jun 2004.

[188] Drugbank. Simvastatin hydroxy acid, 2020. URL https://go.drugbank.com/metabolites/DBMET00388. accessed: 14 Dec 2020.

[189] C. W. Fong. Statins in therapy: Cellular transport, side effects, drug-drug interactions and cytotoxicity -the unrecognized role of lactones. 2016.

[190] M. Yoshinari, K. Matsuzaka, S. Hashimoto, K. Ishihara, T. Inoue, Y. Oda, T. Ide, and T. Tanaka. Controlled release of simvastatin acid using cyclodextrin inclusion system. *Dental Materials Journal*, 26(3):451–456, 2007.

[191] T. Prueksaritanont, B. Ma, and N. Yu. The human hepatic metabolism of simvastatin hydroxy acid is mediated primarily by CYP3A, and not CYP2D6. *British Journal of Clinical Pharmacology*, 56(1):120–124, jul 2003.

[192] A. Tornio, M. K. Pasanen, J. Laitila, P. J. Neuvonen, and J. T. Backman. Comparison of 3-hydroxy-3-methylglutaryl Coenzyme A (HMG-CoA) reductase inhibitors (statins) as inhibitors of cytochrome P450 2C8. *Basic & Clinical Pharmacology & Toxicology*, 97(2): 104–108, aug 2005.

[193] T. Prueksaritanont, R. Subramanian, X. Fang, B. Ma, Y. Qiu, J. H. Lin, P. G. Pearson, and T. A. Baillie. Glucuronidation of statins in animals and humans: A novel mechanism of statin lactonization. *Drug Metabolism and Disposition*, 30(5):505–512, may 2002.

[194] H. Huang. *Characterization of in vitro systems for transporter studies*. Phd thesis, Uppsala University, 2010.

[195] H. Schelleman, X. Han, C. M. Brensinger, S. K. Quinney, W. B. Bilker, D. A. Flockhart, L. Li, and S. Hennessy. Pharmacoepidemiologic and in vitro evaluation of potential drug-drug interactions of sulfonylureas with fibrates and statins. *British Journal of Clinical Pharmacology*, 78(3):639–648, sep 2014.

[196] M. Ucar, M. Neuvonen, H. Luurila, R. Dahlqvist, P. J. Neuvonen, and T. Mjörndal. Carbamazepine markedly reduces serum concentrations of simvastatin and simvastatin acid. *European journal of clinical pharmacology*, 59(12):879–82, feb 2004.

[197] F. Z. Marok, L. Fuhr, N. Hanke, D. Selzer, and T. Lehr. Physiologically Based Pharmacokinetic Modeling of Bupropion and its Metabolites in a CYP2B6 Drug-Drug-Gene Interaction Network. *Pharmaceutics*, in submission, 2020.

[198] P. Muralidhar, E. Bhargav, and B. Srinath. Formulation and optimization of bupropion HCl in microspongesby 2^3 factorial design. *International Journal of Pharmaceutical Sciences and Research*, 8(3):1134–1144, 2017.

[199] M. J. Reese, R. M. Wurm, K. T. Muir, G. T. Generaux, L. St. John-Williams, and D. J. Mcconn. An in vitro mechanistic study to elucidate the desipramine/bupropion clinical drug-drug interaction. *Drug Metabolism and Disposition*, 36(7):1198–1201, jul 2008.

[200] T. Takayanagi, D. Itoh, and H. Mizugushi. Analysis of acid dissociation equilibrium of bupropion by capillary zone electrophoresis after the heat-degradation. *Chromatography*, 37(3):105–109, 2016.

[201] Y. Chen, J. Mao, and C. E. Hop. Physiologically based pharmacokinetic modeling to predict drug-drug interactions involving inhibitory metabolite: A case study of amiodarone. *Drug Metabolism and Disposition*, 43(2):182–189, 2015.

[202] X. Wang, D. R. Abdelrahman, O. L. Zharikova, S. L. Patrikeeva, G. D. Hankins, M. S. Ahmed, and T. N. Nanovskaya. Bupropion metabolism by human placenta. *Biochemical Pharmacology*, 79(11):1684–1690, jun 2010.

[203] F. I. Carroll, B. E. Blough, P. Abraham, A. C. Mills, J. A. Holleman, S. A. Wolckenhauer, A. M. Decker, A. Landavazo, K. T. McElroy, H. A. Navarro, M. B. Gatch, and M. J. Forster. Synthesis and biological evaluation of bupropion analogues as potential pharmacotherapies for cocaine addiction. *Journal of Medicinal Chemistry*, 52(21):6768–6781, 2009.

[204] PubChem Hydroxybupropion (27.11.2020). URL https://pubchem.ncbi.nlm.nih.gov/compound/446.

[205] B. T. Gufford, J. B. L. Lu, I. F. Metzger, D. R. Jones, and Z. Desta. Stereoselective glucuronidation of bupropion metabolites in vitro and in vivo. *Drug Metabolism and Disposition*, 44(4):544–553, 2016.

[206] C. Xue, X. Zhang, and W. Cai. Prediction of drug-drug interactions with bupropion and its metabolites as CYP2D6 inhibitors using a physiologically-based pharmacokinetic model. *Pharmaceutics*, 10(1):1, dec 2017.

[207] T. A. Ketter, J. B. Jenkins, D. H. Schroeder, P. J. Pazzaglia, L. B. Marangell, M. S. George, A. M. Callahan, M. L. Hinton, J. Chao, and R. M. Post. Carbamazepine but not valproate induces bupropion metabolism. *Journal of clinical psychopharmacology*, 15(5):327–33, oct 1995.

[208] G. Mikus, T. Heinrich, J. Bödigheimer, C. Röder, A. K. Matthee, J. Weiss, J. Burhenne, and W. E. Haefeli. Semisimultaneous midazolam administration to evaluate the time course of CYP3A activation by a single oral dose of efavirenz. *Journal of Clinical Pharmacology*, 57(7):899–905, 2017.

[209] S. Frechen and A. Dallmann. Building and evaluation of a PBPK model for midazolam in healthy adults, 2020. URL https://github.com/Open-Systems-Pharmacology/OSP-PBPK-Model-Library/blob/v9.1/Erythromycin/Erythromycin_evaluation_report.pdf. accessed: 14 Dec 2020.

[210] N. Hanke, S. Frechen, D. Moj, H. Britz, T. Eissing, T. Wendl, and T. Lehr. PBPK models for CYP3A4 and P-gp DDI prediction: A modeling network of rifampicin, itraconazole, clarithromycin, midazolam, alfentanil, and digoxin. *CPT: Pharmacometrics & Systems Pharmacology*, 7(10):647–659, oct 2018.

[211] Drugbank. Midazolam, 2020. URL https://go.drugbank.com/drugs/DB00683. accessed: 14 Dec 2020.

[212] Y. Wang, D. Chen, G. Hartmann, C. R. Cho, and K. Menzel. PBPK modeling strategy for predicting complex drug interactions of letermovir as a perpetrator in support of product labeling. *Clinical Pharmacology & Therapeutics*, 105(2):515–523, feb 2019.

[213] C. Dagenais, A. Avdeef, O. Tsinman, A. Dudley, and R. Beliveau. P-glycoprotein deficient mouse in situ blood–brain barrier permeability and its prediction using an in combo PAMPA model. *European Journal of Pharmaceutical Sciences*, 38(2):121–137, sep 2009.

[214] M. Bolger. Physiologically-based pharmacokinetics (PBPK) linked to pharmacodynamics: In silico and in vitro parameterization; presented at Globalization of Pharmaceutics Education Network (GPEN), 2006, Kansas.

[215] T. Rodgers and M. Rowland. Physiologically based pharmacokinetic modelling 2: predicting the tissue distribution of acids, very weak bases, neutrals and zwitterions. *Journal of pharmaceutical sciences*, 95(6):1238–57, jun 2006.

[216] A. T. Heikkinen, G. Baneyx, A. Caruso, and N. Parrott. Application of PBPK modeling to predict human intestinal metabolism of CYP3A substrates – An evaluation and case study using GastroPlus™. *European Journal of Pharmaceutical Sciences*, 47(2):375–386, sep 2012.

[217] P. F. Wang, A. Neiner, and E. D. Kharasch. Efavirenz metabolism: Influence of polymorphic CYP2B6 variants and stereochemistry. *Drug Metabolism and Disposition*, 47 (10):1195–1205, 2019.

[218] K. S. Lown, K. E. Thummel, P. E. Benedict, D. D. Shen, D. K. Turgeon, S. Berent, and P. B. Watkins. The erythromycin breath test predicts the clearance of midazolam. *Clinical Pharmacology & Therapeutics*, 57(1):16–24, jan 1995.

[219] S. Björkman, D. Wada, B. Berling, and G. Benoni. Prediction of the disposition of midazolam in surgical patients by a physiologically based pharmacokinetic model. *Journal of Pharmaceutical Sciences*, 90(9):1226–1241, sep 2001.

[220] A. Galetin, C. Brown, D. Hallifax, K. Ito, and J. B. Houston. Utility of recombinant enzyme kinetics in prediction of human clearance: Impact of variability, CYP3A5, and CYP2C19 on CYP3A4 probe substrates. *Drug Metabolism and Disposition*, 32(12):1411–1420, dec 2004.

[221] K. Ito, K. Ogihara, S.-i. Kanamitsu, and T. Itoh. Prediction of the in vivo interaction between midazolam and macrolides based on in vitro studies using human liver microsomes. *Drug Metabolism and Disposition*, 31(7):945–954, jul 2003.

[222] K. C. Patki, L. L. von Moltke, and D. J. Greenblatt. In vitro metabolism of midazolam, triazolam, nifedipine, and testosterone by human liver microsomes and recombinant cytochromes P440: Role of CYP3A4 and CYP3A5. *Drug Metabolism and Disposition*, 31(7): 938–944, jul 2003.

[223] S. Klieber, S. Hugla, R. Ngo, C. Arabeyre-Fabre, V. Meunier, F. Sadoun, O. Fedeli, M. Rival, M. Bourrie, F. Guillou, P. Maurel, and G. Fabre. Contribution of the N - glucuronidation pathway to the overall in vitro metabolic clearance of midazolam in humans. *Drug Metabolism and Disposition*, 36(5):851–862, may 2008.

[224] A. Buhr, R. Baur, and E. Sigel. Subtle changes in residue 77 of the γ subunit of $\alpha 1\beta 2\gamma 2$ GABA A receptors drastically alter the affinity for ligands of the benzodiazepine binding site. *Journal of Biological Chemistry*, 272(18):11799–11804, may 1997.

[225] S. Katzenmaier, C. Markert, and G. Mikus. Proposal of a new limited sampling strategy to predict CYP3A activity using a partial AUC of midazolam. *European Journal of Clinical Pharmacology*, 66(11):1137–1141, 2010.

[226] S. Frechen, A. Dallmann, and J. Solodenko. Building and evaluation of a PBPK model for alfentanil in healthy adults, 2020. URL https://github.com/Open-Systems-Pharmacology/OSP-PBPK-Model-Library/blob/v9.1/Erythromycin/Erythromycin_evaluation_report.pdf. accessed: 14 Dec 2020.

[227] Drugbank. Alfentanil, 2020. URL https://go.drugbank.com/drugs/DB00802. accessed: 14 Dec 2020.

[228] G. Baneyx, N. Parrott, C. Meille, A. Iliadis, and T. Lavé. Physiologically based pharmacokinetic modeling of CYP3A4 induction by rifampicin in human: influence of time between substrate and inducer administration. *European journal of pharmaceutical sciences: official journal of the European Federation for Pharmaceutical Sciences*, 56:1–15, 2014.

[229] R. Jansson, U. Bredberg, and M. Ashton. Prediction of drug tissue to plasma concentration ratios using a measured volume of distribution in combination with lipophilicity. *Journal of Pharmaceutical Sciences*, 97(6):2324–2339, jun 2008.

[230] A. N. Edginton and S. Willmann. Physiology-based simulations of a pathological condition. *Clinical Pharmacokinetics*, 47(11):743–752, 2008.

[231] L. M. Almond, S. Mukadam, I. Gardner, K. Okialda, S. Wong, O. Hatley, S. Tay, K. Rowland-Yeo, M. Jamei, A. Rostami-Hodjegan, and J. R. Kenny. Prediction of drug-drug interactions arising from CYP3A induction using a physiologically based dynamic model. *Drug metabolism and disposition: the biological fate of chemicals*, 44(6):821–32, 2016.

[232] S. M. Robertson, F. Maldarelli, V. Natarajan, E. Formentini, R. M. Alfaro, and S. R. Penzak. Efavirenz induces CYP2B6-mediated hydroxylation of bupropion in healthy subjects. *Journal of Acquired Immune Deficiency Syndromes*, 49(5):513–519, 2008.

[233] D. S. Wishart, C. Knox, A. C. Guo, S. Shrivastava, M. Hassanali, P. Stothard, Z. Chang, and J. Woolsey. DrugBank: a comprehensive resource for in silico drug discovery and exploration. *Nucleic Acids Research*, 34(Supplement 1):D668–D672, 01 2006.

[234] G. Boman and V. A. Ringberger. Binding of rifampicin by human plasma proteins. *European journal of clinical pharmacology*, 7(5):369–73, 1974.

[235] I. E. Templeton, J. B. Houston, and A. Galetin. Predictive utility of in vitro rifampin induction data generated in fresh and cryopreserved human hepatocytes, Fa2N-4, and HepaRG cells. *Drug metabolism and disposition: the biological fate of chemicals*, 39 (10):1921–9, 2011.

[236] Merck Research Laboratories. *The Merck Index 14th edition: Rifampin*. Merck & Co., Inc., Whitehouse Station, NJ, USA, 2006.

[237] U. Loos, E. Musch, J. C. Jensen, G. Mikus, H. K. Schwabe, and M. Eichelbaum. Pharmacokinetics of oral and intravenous rifampicin during chronic administration. *Klinische Wochenschrift*, 63(23):1205–11, 1985.

[238] R. G. Tirona, B. F. Leake, A. W. Wolkoff, and R. B. Kim. Human organic anion transporting polypeptide-C (SLC21A6) is a major determinant of rifampin-mediated pregnane X receptor activation. *The Journal of pharmacology and experimental therapeutics*, 304 (1):223–8, jan 2003.

[239] A. Nakajima, T. Fukami, Y. Kobayashi, A. Watanabe, M. Nakajima, and T. Yokoi. Human arylacetamide deacetylase is responsible for deacetylation of rifamycins: rifampicin, rifabutin, and rifapentine. *Biochemical pharmacology*, 82(11):1747–56, dec 2011.

[240] A. Collett, J. Tanianis-Hughes, D. Hallifax, and G. Warhurst. Predicting P-glycoprotein effects on oral absorption: correlation of transport in Caco-2 with drug pharmacokinetics in wild-type and mdr1a(-/-) mice in vivo. *Pharmaceutical research*, 21(5):819–26, may 2004.

[241] B. Greiner, M. Eichelbaum, P. Fritz, H. P. Kreichgauer, O. von Richter, J. Zundler, and H. K. Kroemer. The role of intestinal P-glycoprotein in the interaction of digoxin and rifampin. *The Journal of clinical investigation*, 104(2):147–53, 1999.

[242] A. Ramamoorthy, Y. Liu, S. Philips, Z. Desta, H. Lin, C. Goswami, A. Gaedigk, L. Li, D. A. Flockhart, and T. C. Skaar. Regulation of microRNA expression by rifampin in human hepatocytes. *Drug Metabolism and Disposition*, 41(10):1763–1768, 2013.

[243] M. Hirano, K. Maeda, Y. Shitara, and Y. Sugiyama. Drug-drug interaction between pitavastatin and various drugs via OATP1B1. *Drug metabolism and disposition: the biological fate of chemicals*, 34(7):1229–36, jul 2006.

[244] M. L. Reitman, X. Chu, X. Cai, J. Yabut, R. Venkatasubramanian, S. Zajic, J. A. Stone, Y. Ding, R. Witter, C. Gibson, K. Roupe, R. Evers, J. A. Wagner, and A. Stoch. Rifampin's acute inhibitory and chronic inductive drug interactions: experimental and model-based approaches to drug-drug interaction trial design. *Clinical pharmacology and therapeutics*, 89(2):234–42, 2011.

[245] L. I. Kajosaari, J. Laitila, P. J. Neuvonen, and J. T. Backman. Metabolism of repaglinide by CYP2C8 and CYP3A4 in vitro: effect of fibrates and rifampicin. *Basic & clinical pharmacology & toxicology*, 97(4):249–56, 2005.

[246] Y. Shimokawa, N. Yoda, S. Kondo, Y. Yamamura, Y. Takiguchi, and K. Umehara. Inhibitory Potential of Twenty Five Anti-tuberculosis Drugs on CYP Activities in Human Liver Microsomes. *Biological & Pharmaceutical Bulletin*, 38(9):1425–1429, 2015.

[247] X. Li, S. Frechen, D. Moj, T. Lehr, M. Taubert, C. hsuan Hsin, G. Mikus, P. J. Neuvonen, K. T. Olkkola, T. I. Saari, and U. Fuhr. A physiologically based pharmacokinetic model of voriconazole integrating time-dependent inhibition of CYP3A4, genetic polymorphisms of CYP2C19 and predictions of drug–drug interactions. *Clinical Pharmacokinetics*, 59(6): 781–808, 2020.

[248] Drugbank. Voriconazole, 2020. URL https://go.drugbank.com/drugs/DB00582. accessed: 14 Dec 2020.

[249] Pfizer. Voriconazole for IV infusion safety data sheet, 2018. URL https://pfe-pfizercom-prod.s3.amazonaws.com/products/material_safety_data/voriconazole_IV_infusion_22-mar-2018.pdf. accessed: 14 Dec 2020.

[250] F. Qi, L. Zhu, N. Li, T. Ge, G. Xu, and S. Liao. Influence of different proton pump inhibitors on the pharmacokinetics of voriconazole. *International Journal of Antimicrobial Agents*, 49(4):403–409, apr 2017.

[251] N. R. Zane and D. R. Thakker. A physiologically based pharmacokinetic model for voriconazole disposition predicts intestinal first-pass metabolism in children. *Clinical Pharmacokinetics*, 53(12):1171–1182, dec 2014.

[252] B. Damle, M. V. Varma, and N. Wood. Pharmacokinetics of voriconazole administered concomitantly with fluconazole and population-based simulation for sequential use. *Antimicrobial Agents and Chemotherapy*, 55(11):5172–5177, nov 2011.

[253] Pfizer Canada ULC. Product monograph VFEND voriconazole. Submission Control No: 237769, 2020. URL https://www.pfizer.ca/sites/default/files/202007/Vfend_PM_EN_237769_30June2020.pdf. accessed: 14 Dec 2020.

[254] Scientific Discussion-VFEND Procedure No. EMEA/H/ C/387/X/09. 2004.

[255] U.S. Food and Drug Administration. Pfizer Label: voriconazole for injection, tablets, oral suspension: LAB-0271-12. 2005.

[256] G. Wang, H.-P. Lei, Z. Li, Z.-R. Tan, D. Guo, L. Fan, Y. Chen, D.-L. Hu, D. Wang, and H.-H. Zhou. The CYP2C19 ultra-rapid metabolizer genotype influences the pharmacokinetics of voriconazole in healthy male volunteers. *European Journal of Clinical Pharmacology*, 65(3):281–285, mar 2009.

[257] N. Murayama, N. Imai, T. Nakane, M. Shimizu, and H. Yamazaki. Roles of CYP3A4 and CYP2C19 in methyl hydroxylated and N-oxidized metabolite formation from voriconazole, a new anti-fungal agent, in human liver microsomes. *Biochemical Pharmacology*, 73(12): 2020–2026, jun 2007.

[258] R. Hyland, B. C. Jones, and D. A. Smith. Identification of the cytochrome P450 enzymes involved in the N-oxidation of voriconazole. *Drug Metabolism and Disposition*, 31(5): 540–547, may 2003.

[259] P. Poulin, K. Schoenlein, and F. Theil. Prediction of adipose tissue: Plasma partition coefficients for structurally unrelated drugs. *Journal of Pharmaceutical Sciences*, 90(4): 436–447, apr 2001.

[260] P. Poulin and F. P. Theil. A priori prediction of tissue:plasma partition coefficients of drugs to facilitate the use of physiologically-based pharmacokinetic models in drug discovery. *Journal of pharmaceutical sciences*, 89(1):16–35, jan 2000.

[261] P. Poulin and F.-P. Theil. Prediction of pharmacokinetics prior to in vivo studies. 1. Mechanism-based prediction of volume of distribution. *Journal of pharmaceutical sciences*, 91(1):129–56, jan 2002.

[262] P. Poulin and F.-P. Theil. Prediction of pharmacokinetics prior to in vivo studies. II. Generic physiologically based pharmacokinetic models of drug disposition. *Journal of pharmaceutical sciences*, 91(5):1358–70, may 2002.

[263] M. Meyer, S. Schneckener, B. Ludewig, L. Kuepfer, and J. Lippert. Using expression data for quantification of active processes in physiologically based pharmacokinetic modeling. *Drug metabolism and disposition: the biological fate of chemicals*, 40(5):892–901, may 2012.

[264] P. Shi, M. Liao, B.-C. Chuang, R. Griffin, J. Shi, M. Hyer, J. K. Fallon, P. C. Smith, C. Li, and C. Q. Xia. Efflux transporter breast cancer resistance protein dominantly expresses on the membrane of red blood cells, hinders partitioning of its substrates into the cells, and alters drug–drug interaction profiles. *Xenobiotica*, 48(11):1173–1183, 2018.

[265] N. Kolesnikov, E. Hastings, M. Keays, O. Melnichuk, Y. A. Tang, E. Williams, M. Dylag, N. Kurbatova, M. Brandizi, T. Burdett, K. Megy, E. Pilicheva, G. Rustici, A. Tikhonov, H. Parkinson, R. Petryszak, U. Sarkans, and A. Brazma. ArrayExpress update-simplifying data submissions. *Nucleic Acids Research*, 43(D1):D1113–D1116, 2015.

[266] M. Nishimura and S. Naito. Tissue-specific mRNA expression profiles of human phase I metabolizing enzymes except for cytochrome P450 and phase II metabolizing enzymes. *Drug metabolism and pharmacokinetics*, 21(5):357–74, 2006.

[267] A. D. Rodrigues. Integrated cytochrome P450 reaction phenotyping: attempting to bridge the gap between cDNA-expressed cytochromes P450 and native human liver microsomes. *Biochemical pharmacology*, 57(5):465–80, 1999.

[268] M. Nishimura, H. Yaguti, H. Yoshitsugu, S. Naito, and T. Satoh. Tissue distribution of mRNA expression of human cytochrome P450 isoforms assessed by high-sensitivity real-time reverse transcription PCR. *Journal of the Pharmaceutical Society of Japan*, 123(5):369–75, may 2003.

[269] K. Rowland Yeo, R. L. Walsky, M. Jamei, A. Rostami-Hodjegan, and G. T. Tucker. Prediction of time-dependent CYP3A4 drug-drug interactions by physiologically based pharmacokinetic modelling: Impact of inactivation parameters and enzyme turnover. *European Journal of Pharmaceutical Sciences*, 43(3):160–73, 2011.

[270] G. Margaillan, M. Rouleau, K. Klein, J. K. Fallon, P. Caron, L. Villeneuve, P. C. Smith, U. M. Zanger, and C. Guillemette. Multiplexed targeted quantitative proteomics predicts hepatic glucuronidation potential. *Drug Metabolism and Disposition*, 43:1331–5, 2015.

[271] National Center for Biotechnology Information (NCBI). Expressed Sequence Tags (EST) from UniGene. 2019.

[272] M. Nishimura and S. Naito. Tissue-specific mRNA expression profiles of human ATP-binding cassette and solute carrier transporter superfamilies. *Drug metabolism and pharmacokinetics*, 20(6):452–77, 2005.

A.2 SUPPLEMENTARY INFORMATION - PROJECT II - PHYSIOLOGICALLY BASED PHARMACOKINETIC AND PHARMACODYNAMIC MODELING OF FELODIPINE

pharmaceutics

A physiologically-based pharmacokinetic and pharmacodynamic model of the CYP3A4 substrate felodipine for drug-drug interaction modeling

Supplementary Materials

Laura Maria Fuhr[1], Fatima Zahra Marok[1], Maximilian Mees[1], Felix Mahfoud[2,3], Dominik Selzer[1], Thorsten Lehr[1]

[1]Clinical Pharmacy, Saarland University, Saarbrücken, Germany
[2]Department of Internal Medicine III, Cardiology, Angiology, Intensive Care Medicine, Saarland University Medical Center and Saarland University Faculty of Medicine, 66421 Homburg, Germany
[3]Institute for Medical Engineering and Science, Massachusetts Institute of Technology, Cambridge, MA 02139, USA

Funding
This research was funded by the German Federal Ministry of Education and Research (BMBF), grant number 031L0161C ("OSMOSES").

Conflict of Interest
Thorsten Lehr has received research grants from the German Federal Ministry of Education and Research (grant 031L0161C). Felix Mahfoud is supported by Deutsche Gesellschaft für Kardiologie (DGK), Deutsche Forschungsgemeinschaft (SFB TRR219), and Deutsche Herzstiftung. He has received scientific support from Medronic and ReCor Medical and speaker honoraria from Astra-Zeneca, Bayer, Boehringer Ingelheim, Inari, Medtronic, Merck, and ReCor Medical. Laura Maria Fuhr, Fatima Zahra Marok, Dominik Selzer and Maximilian Mees declare no conflict of interest.

Corresponding Author
Thorsten Lehr, PhD
Clinical Pharmacy, Saarland University
Campus C2 2
66123 Saarbrücken, Germany
ORCID: 0000 0002 8372 1465
Phone: +49 681 302 70255
Email: thorsten.lehr@mx.uni-saarland.de

Contents

1 Physiologically based pharmacokinetic/pharmacodynamic (PBPK/PD) modeling

1.1 Felodipine formulations

The dissolution of oral felodipine formulations was described using the Weibull function according to Equations S1 and S2:

$$m = 1 - exp(\frac{-(t - T_{lag}^{\beta})}{\alpha}) \tag{S1}$$

$$\alpha = (T_d)^{\beta} \tag{S2}$$

where m = fraction of dissolved drug at time t, T_{lag} = lag time before the onset of dissolution, α = scale parameter, β = shape parameter, T_d = time needed to dissolve 63% of the formulation

1.2 PBPK model evaluation

As quantitative performance measures, the mean relative deviation (MRD) of predicted plasma concentrations as well as blood pressure and heart rate measurements and the geometric mean fold error (GMFE) of predicted area under the plasma concentration-time curve values calculated from the time of drug administration to the time of the last concentration measurement (AUC_{last}) and maximum plasma concentration (C_{max}) values were calculated according to Equation S3 and Equation S4, respectively. Values ≤ 2 are considered as adequate model performance metrics.

$$MRD = 10^{x}, \text{ with } x = \sqrt{\frac{1}{m}\sum_{i=1}^{m}(\log_{10} c_{pred,i} - \log_{10} c_{obs,i})^2} \tag{S3}$$

where $c_{pred,i}$ = predicted plasma concentration, $c_{obs,i}$ = corresponding observed plasma concentration and m = number of observed values.

$$GMFE = 10^{x}, \text{ with } x = \frac{1}{n}\sum_{i=1}^{n}|\log_{10}(\frac{PK_{pred,i}}{PK_{obs,i}})| \tag{S4}$$

where $PK_{pred,i}$ = predicted AUC_{last} or C_{max} value, $PK_{obs,i}$ = corresponding observed AUC_{last} or C_{max} value and n = the number of studies.

1.3 Drug-drug interaction (DDI) model evaluation

Modeled DDIs were evaluated by comparison of predicted versus observed plasma concentration-time profiles of felodipine with and without co-administration of perpetrator drugs. Furthermore, predicted DDI AUC_{last} ratios (Equation S5) and DDI C_{max} ratios (Equation S6) were calculated and compared to observed values.

$$\text{DDI } AUC_{last} \text{ ratio} = \frac{AUC_{last} \text{ victim drug during DDI}}{AUC_{last} \text{ victim drug control}} \tag{S5}$$

$$\text{DDI } C_{max} \text{ ratio} = \frac{C_{max} \text{ victim drug during DDI}}{C_{max} \text{ victim drug control}} \tag{S6}$$

Additionally, GMFE values of the predicted DDI AUC_{last} ratios and DDI C_{max} ratios were calculated according to Equation S4.

1.4 Sensitivity analysis

Sensitivity of the final models to single parameter values (local sensitivity analysis) was calculated as relative change of the area under the plasma concentration-time curve (AUC). Sensitivity analysis was carried out using a relative perturbation of 1000% (variation range 10.0, maximum number of 9 steps). Parameters were included into the analysis if they were optimized, if they are associated with optimized parameters or if they might have a strong impact due to calculation methods used in the model.

The sensitivity to a parameter value was calculated as the ratio of the relative change of the simulated AUC to the relative variation of the parameter around its value used in the final model according to Equation S7.

$$S = \frac{\Delta AUC}{AUC} \cdot \frac{p}{\Delta p} \tag{S7}$$

where S = sensitivity of the AUC to the examined model parameter, ΔAUC = change of the simulated AUC, AUC = simulated AUC with the original parameter value, Δp = change of the examined parameter value, p = original parameter value. A sensitivity of +1.0 signifies that a 10% increase of the examined parameter value causes a 10% increase of the simulated AUC.

1.5 Mathematical implementation of drug-drug interactions (DDIs)

Competitive inhibition

Competitive inhibitors reversibly bind to the active site of an enzyme or transporter and compete with the substrate for binding. The maximum reaction velocity (v_{max}) remains unaffected, while the Michaelis-Menten constant (K_m) is increased ($K_{m,app}$, Equation S8) in the presence of the inhibitor. The reaction velocity (v) during administration of a competitive inhibitor is described by Equation S9 [1]:

$$K_{m,app} = K_m \cdot \left(1 + \frac{[I]}{K_i}\right) \tag{S8}$$

$$v = \frac{v_{max} \cdot [S]}{K_{m,app} + [S]} \tag{S9}$$

where $K_{m,app}$ = Michaelis-Menten constant in the presence of the inhibitor, K_m = Michaelis-Menten constant, $[I]$ = free inhibitor concentration, K_i = dissociation constant of the inhibitor-enzyme complex, v = reaction velocity, v_{max} = maximum reaction velocity, $[S]$ = free substrate concentration.

Mechanism-based inactivation

Mechanism-based inactivation is an irreversible type of inhibition. Baseline enzyme activity will be regained after clearance of the inactivator and de novo synthesis of the enzyme (time-dependency). The enzyme degradation rate constant (k_{deg}) is increased ($k_{deg,app}$, Equation S10), while its synthesis rate (R_{syn}) remains unaffected. The enzyme turnover during administration of a mechanism-based inactivator is described by Equation S11. As mechanism-based inactivators are also competitive inhibitors, the K_m in the Michaelis-Menten reaction velocity equation is substituted by $K_{m,app}$ as shown in Equation S12 [1]:

$$k_{deg,app} = k_{deg} + \left(\frac{k_{inact} \cdot [I]}{K_I + [I]}\right) \tag{S10}$$

$$\frac{dE(t)}{dt} = R_{syn} - k_{deg,app} \cdot E(t) \tag{S11}$$

$$v = \frac{v_{max} \cdot [S]}{K_{m,app} + [S]} = \frac{k_{cat} \cdot E(t) \cdot [S]}{K_{m,app} + [S]} \tag{S12}$$

where $k_{deg,app}$ = enzyme degradation rate constant in the presence of the mechanism-based inactivator, k_{deg} = enzyme degradation rate constant, k_{inact} = maximum inactivation rate constant, $[I]$ = free inactivator concentration, K_I = concentration for half-maximal inactivation, $E(t)$ = enzyme concentration, R_{syn} = enzyme synthesis rate, v = reaction velocity, v_{max} = maximum reaction velocity, $[S]$ = free substrate concentration, $K_{m,app}$ = Michaelis-Menten constant in the presence of inactivator, k_{cat} = catalytic rate constant.

Induction

Induction of enzymes is mediated by the activation of nuclear receptors, increasing gene expression. The baseline activity of the enzyme is regained after clearance of the inducer and degradation of the enzyme (time-dependency). The enzyme synthesis rate (R_{syn}) is increased ($R_{syn,app}$, Equation S13), while its k_{deg} remains unaffected. The enzyme turnover during administration of an inducer is described by Equation S14 [1], the reaction velocity is described by Equation S15:

$$R_{syn,app} = R_{syn} \cdot \left(1 + \frac{E_{max} \cdot [Ind]}{EC_{50} + [Ind]}\right) \tag{S13}$$

$$\frac{dE(t)}{dt} = R_{syn,app} - k_{deg} \cdot E(t) \tag{S14}$$

$$v = \frac{v_{max} \cdot [S]}{K_m + [S]} = \frac{k_{cat} \cdot E(t) \cdot [S]}{K_m + [S]} \tag{S15}$$

where $R_{syn,app}$ = enzyme synthesis rate in the presence of inducer, R_{syn} = enzyme synthesis rate, E_{max} = maximal induction effect in vivo, $[Ind]$ = free inducer concentration, EC_{50} = concentration for half-maximal induction in vivo, $E(t)$ = enzyme concentration, k_{deg} = enzyme degradation rate constant, v = reaction velocity, v_{max} = maximum reaction velocity, $[S]$ = free substrate concentration, K_m = Michaelis-Menten constant, k_{cat} = catalytic rate constant.

1.6 Pharmacodynamic (PD) model building

The PBPK model of felodipine was extended by a diastolic blood pressure and heart rate PD model.

As blood pressure and heart rate undergo fluctuations throughout the day, a circadian rhythm was implemented for blood pressure and heart rate according to models by Chae et al. [2] and Lott et al. [3], respectively. Circadian variability of blood pressure is described according to Equations S16 and S17.

$$circ_{BP}(t) = amp_{24,BP} \cdot cos(\frac{2\pi}{24} \cdot (t - phase_{24,BP})) + amp_{12,BP} \cdot cos(\frac{2\pi}{12} * (t - phase_{12,BP})) \quad \text{(S16)}$$

$$BP(t) = BP_{mean} \cdot (1 + circ_{BP}(t)) \quad \text{(S17)}$$

where $circ_{BP}$ = circadian rythm of blood pressure at t, t = time, $amp_{24,BP}$ / $amp_{12,BP}$ = amplitudes, for period 24 h and 12 h, respectively, $phase_{24,BP}$ and $phase_{12,BP}$ = shift over time for period 24 h and 12 h, respectively, BP_{mean} = mean blood pressure over 24 h.

Similarly, circadian variability of heart rate is described according to Equations S18 and S19.

$$circ_{HR}(t) = amp_{HR} \cdot cos(\frac{2\pi}{24} \cdot (t - phase_{HR})) \quad \text{(S18)}$$

$$HR(t) = HR_{mean} \cdot (1 + circ_{HR}(t)) \quad \text{(S19)}$$

where $circ_{HR}$ = circadian rhythm of heart rate at t, t = time, amp_{HR} = amplitude, $phase_{HR}$ = shift over time, HR_{mean} = mean heart rate over 24h.

The effect was described using a direct maximum effect (E_{max}) model without lag time according to Equation S20.

$$E(t) = \frac{E_{max} \cdot C(t)^h}{EC_{50}^h + C(t)^h} \quad \text{(S20)}$$

where E = effect, t = time, E_{max} = maximum effect of felodipine on heart rate or blood pressure, EC_{50} = concentration necessary to achieve half of E_{max}, h = hill coefficient and C = felodipine plasma concentration.

Subsequently, blood pressure and heart rate are defined according to Equations S21 and S22, respectively.

$$BP(t) = BP_{mean} \cdot (1 + circ_{BP}(t)) - E(t) \quad \text{(S21)}$$

$$HR(t) = HR_{mean} \cdot (1 + circ_{HR}(t)) + E(t) \quad \text{(S22)}$$

The circadian rhythm of blood pressure and heart rate was optimized for each study individually. The circadian amplitudes ($amp_{24,BP}$, $amp_{12,BP}$, amp_{HR}) were adopted from Chae et al. [2] and Lott et al. [3], while circadian phases ($phase_{24,BP}$, $phase_{12,BP}$, $phase_{HR}$) and mean heart rate and blood pressure values (HR_{mean}, BP_{mean}) were optimized using the parameter identification tool implemented in MoBi. The interval between $phase_{24,BP}$ and $phase_{12,BP}$ identified by Chae et al. [2] was maintained. If clinical studies provided placebo profiles, the circadian parameters were optimized based on the placebo profiles and subsequently transferred to the

corresponding effect-time profiles measured during felodipine administration. If no placebo profiles were available, the parameters were carefully optimized based on the effect-time profiles during felodipine administration. For studies that displayed changes from baseline blood pressure instead of absolute blood pressure data in the effect-time profiles, absolute values were calculated based on the indicated baseline value before felodipine administration (BP_0). The parameters of the E_{max} model (EC_{50} and E_{max}) were optimized based on the blood pressure and heart rate training datasets, preserving the previously optimized parameters of the circadian model.

2 Felodipine

2.1 PBPK model building

All clinical studies used for model building, including information on participant demographics, the study protocol and assignment to training and test dataset, are listed in Table S1.

Felodipine has a chiral center at C4 [4], and is administered as racemic mixture. The two enantiomers are enantioselectively metabolized by cytochrome P450 (CYP) 3A4 to dehydrofelodipine, resulting in 2-fold higher maximum plasma concentrations of (S)-felodipine [4]. The stereoselective pharmacokinetics of the enantiomers could be described assuming different K_m values, without changing other drug-dependent parameters. Estimated K_m values are in accordance with literature, where approximately 2-fold higher K_m values were reported for (S)-felodipine [5]. Due to the small size of studies investigating the pharmacokinetics of (R)- and (S)-felodipine, the ability of the model to predict the stereoselective pharmacokinetics could no be thoroughly evaluated. All processes implemented in the final model are illustrated in Figure S1 and drug-dependent parameters used in the final model in comparison to parameters obtained from literature are listed in Table S2.

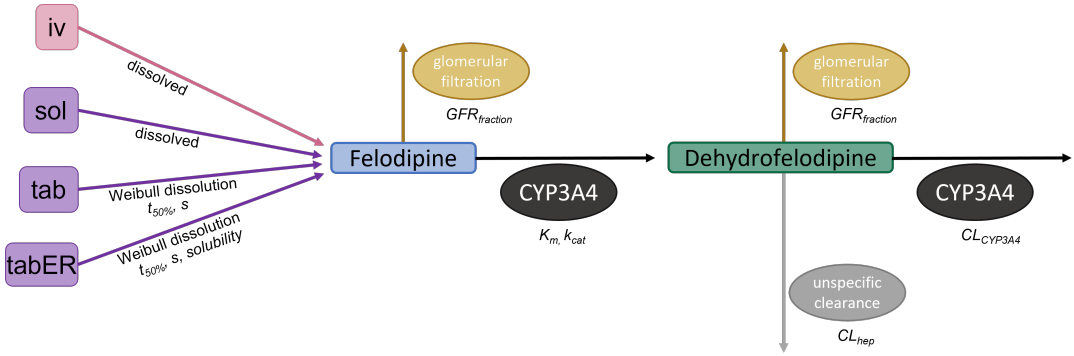

Figure S1: Implemented metabolic pathways of felodipine and dehydrofelodipine. The model describes intravenous and oral administration of felodipine. Dissolution of solid oral formulations (conventional and extended release tablets) is described using Weibull functions. Felodipine is metabolized by CYP3A4 to dehydrofelodipine and eliminated by passive glomerular filtration. Dehydrofelodipine undergoes CYP3A4 mediated clearance as well as unspecific hepatic clearance and is also eliminated by passive glomerular filtration. CL_{CYP3A4}: CYP3A4 mediated clearance, CL_{hep}: unspecific hepatic clearance, CYP3A4: cytochrome P450 3A4, $GFR_{fraction}$: Fraction of filtered drug in the urine, iv: intravenous, K_m: Michaelis-Menten constant, k_{cat}: catalytic rate constant, s: dissolution shape, sol: solution, $t_{50\%}$: dissolution time (50% dissolved), tab: tablet, tabER: extended release tablet.

Predicted compared to observed plasma concentration-time profiles of felodipine and dehydrofelodipine are displayed in Figures S2 (linear) and S3 (semi-logarithmic). Goodness-of-fit plots for plasma concentrations are presented in Figure S5, corresponding MRD values are listed in Table S3. The correlation of predicted and observed AUC_{last} and C_{max} values is presented in Figure S6. Corresponding values and overall GMFE values of all studies are listed in Table S4.

2.2 Felodipine clinical studies

Table S1: Clinical studies used for the development of the felodipine PBPK/PD model

Dose [mg]	Route	n	Women [%]	Age[a] [y]	Weight[a] [kg]	Height[a] [cm]	DHF	HR	BP	Dataset	Reference
Healthy individuals											
1	iv (20 min)	10	0	26 (22-33)	73 (67-82)		no	no	no	training	Bengtsson 1988 [6]
1	iv (20 min)	10	0	26 (22-33)	73 (66-82)	181 (171-188)	no	no	no	test	Edgar 1987 [7]
1	iv (30 min)	4	0	28 (23-36)	72 (69-73)		no	no	no	test	Sutfin 1990 [8]
1.5	iv (150 min)	10	0	32 (26-40)	73 ± 7.3	180 ± 5	no	yes	yes	test	Sluiter 1985 [9]
1.5	iv (60 min)	12	0	25 ±2	75 ±6		yes	no	no	training	Lundahl 1997 [10]
2.5	iv (30 min)	10	0	25 ± 1.3 (23-31)	74 ± 2 (66-82)		no	no	no	test	Edgar 1985 [11]
2.5	iv (30 min)	8	0	25 (22-31)	74 (69-82)		no	no	no	training	Edgar 1985a [12]
3	iv (20 min)	10	0	26 (22-33)	73 (67-82)		no	no	no	training	Bengtsson 1988 [6]
3	iv (20 min)	10	0	26 (22-33)	73 (66-82)	181 (171-188)	no	no	no	test	Edgar 1987 [7]
5	po (sol), sd	10	0	26 (22-33)	73 (67-82)		no	yes	yes	training	Bengtsson 1988 [6]
5	po (sol), sd	10	0	26 (22-33)	73 (66-82)	181 (171-188)	no	yes	yes	test	Edgar 1987 [7]
10	po (sol), sd	16	0				no	no	no	test	Abrahamsson 1994 [13]
10	po (sol), sd	9	0	28 ± 5	77 ± 4.5		no	yes	yes	test	Bengtsson 1990 [14]
10	po (sol), sd	12	0				no	no	no	test	Edgar 1987a [15]
10	po (sol), sd	16	0	24 (20-35)	72 (64-81)		no	no	no	training	Wingstrand 1990 [16]
10	po (sol), bid	18	0	(20-34)			no	no	no	test	Blychert 1990a [17]
10.35	po (sol), 0, 35 min	8	0	(22-31)			no	yes	yes	test	Johnsson 1983 [18]
15	po (sol), sd	10	0	26 (22-33)	73 (67-82)		no	yes	yes	test	Bengtsson 1988 [6]
15	po (sol), sd	10	0	26 (22-33)	73 (66-82)	181 (171-188)	no	yes	yes	test	Edgar 1987 [7]
20	po (sol), sd	12	0	25 ± 5 (20-34)	71 ± 7 (52-81)		yes	no	no	test	Soons 1993 [19]
20	po (sol), sd	4	0				yes	no	no	training	Soons 1990 [4]
27.5	po (sol), sd	10	0	25 ± 1.3 (23-31)	74 ± 2 (66-82)		no	no	no	test	Edgar 1985 [11]
27.5	po (sol), sd	8	0	25 (22-31)	75 (69-82)		no	no	no	test	Edgar 1985a [12]

assumed

[a]: mean ± standard deviation (range)

[c]: Patients were usually receiving other hypertensive medication, including beta blockers and diuretics

[d]: Doses between 0.5 - 1.5 mg were administered

[e]: 0.02 mg/min, for 105-120 min

[f]: Patients with renal impairment

°tablet brand: Plendil, * tablet brand: Hydac

- : no data available, bid: twice daily, BP: blood pressure; D: day; DHF: dehydrofelodipine, HR: heart rate, iv: intravenous, n: number of individuals, po: oral, qd: once daily, sd: single dose, sol: solution, tab: tablet, tabER: extended release tablet

Table S1: Clinical studies used for the development of the felodipine PBPK/PD model *(continued)*

Dose [mg]	Route	n	Women [%]	Age[a] [y]	Weight[a] [kg]	Height[a] [cm]	DHF	HR	BP	Dataset	Reference
40	po (sol), sd	10	0	26 (22-33)	73 (67-82)		no	yes	yes	training	Bengtsson 1988 [6]
40	po (sol), sd	10	0	26 (22-33)	73 (66-82)	181 (171-188)	no	yes	yes	test	Edgar 1987 [7]
5	po (*tab*), sd	9	0	(19-40)			yes	no	no	test	Bailey 1993 [20]
5	po (*tab*), sd	9	0	44 ± 5 (40-53)	77 ± 6.8 (66-85)		yes	no	no	training	Edgar 1992 [21]
5	po (*tab*), bid	12	0	26 (20-34)	75 (69-85)		no	no	no	test	Landahl 1988 [22]
5	po (*tab*), bid D1-D5	12	8	29 ± 8.9	72 ± 9.0		no	no	no	test	Capewell 1988 [23]
10	po (tab), sd	12	0				no	no	no	test	Edgar 1987a [15]
10	po (tab), sd	12	0	(20-27)	(51-78)	(168-183)	no	yes	yes	test	Guo 2007 [24]
10	po (tab), sd	1					no	no	no	test	Lindmark 2002 [25]
10	po (tab), sd	12	0	(22-39)	(69-92)		no	yes	yes	training	Hardy 1988 [26]
10	po (tab), bid	18	0	(20-34)			no	no	no	training	Blychert 1990a [17]
10	po (tab), qd	15	0	(18-38)			no	no	no	test	Blychert 1990a [17]
2.5, 5	po,tabER D1-D2: 2.5 mg qd; D3-8: 5 mg qd	6	67	(71-77)			no	yes	yes	test	Dresser 2000 [27]
5	po (tabER*), sd	9	44	24 (22-26)	60 (51-73)		no	yes	yes	test	Jalava 1997 [28]
5	po (tabER°), sd	30	47	26 ± 1.4	64 ± 1.2	166 ± 1.24	no	no	no	test	Aguilar-Carrasco 2015 [29]
5	po (tabER°), sd	12	58	(70-83)			no	yes	yes	training	Dresser 2000 [27]
5	po (tabER°), sd	12	0	(21-24)			no	no	no	test	Goosen 2004 [30]
5	po (tabER), sd	45	0	33 ± 2.8 (28-39)	63 ± 5.6 (50-77)		no	no	no	test	Xiang 2017 [31]
2x 2.5	po (tabER°), qd	20	0	(20-32)			no	no	no	test	Bioequivalence 1994 [32]
5	po (tabER°), qd	20	0	(20-32)			no	no	no	training	Bioequivalence 1994 [32]
10	po (tabER), sd	12	0	(18-45)			no	no	no	test	Bailey 1995 [33]
10	po (tabER), sd	12	0	29 ± 4.9	79 ± 9.0		yes	yes	yes	test	Madsen1996 [34]
10	po (tabER°), sd	12	0	(18-45)			yes	no	no	training	Bailey 1996 [35]
10	po (tabER°), sd	12	0	(18-45)			yes	no	no	test	Bailey 1998 [36]
10	po (tabER°), sd	12	17	28			no	no	no	test	Bailey 2000 [37]

assumed

[a]: mean ± standard deviation (range)

[c]: Patients were usually receiving other hypertensive medication, including beta blockers and diuretics

[d]: Doses between 0.5 - 1.5 mg were administered

[e]: 0.02 mg/min, for 105-120 min

[f]: Patients with renal impairment

° tablet brand: Plendil, * tablet brand: Hydac

- : no data available, bid: twice daily, BP: blood pressure; D: day; DHF: dehydrofelodipine, HR: heart rate, iv: intravenous, n: number of individuals, po: oral, qd: once daily, sd: single dose, sol: solution, tab: tablet, tabER: extended release tablet

Table S1: Clinical studies used for the development of the felodipine PBPK/PD model *(continued)*

Dose [mg]	Route	n	Women [%]	Age[a] [y]	Weight[a] [kg]	Height[a] [cm]	DHF	HR	BP	Dataset	Reference
10	po (tabER°), sd	6	25	(23-45)	64 (1.2)		no	no	no	test	Bailey 2003 [38]
10	po (tabER°), sd	5	40	46 (31-56)			no	no	no	test	Dresser 2017 [39]
10	po (tabER°), sd	12	0				no	no	no	test	Edgar 1987a [15]
10	po (tabER°), sd	12	0	27 (23-30)	76 (68-86)		no	yes	yes	test	Hasselgren 1990 [40]
10	po (tabER°), sd	10	0	(18-65)			no	no	no	test	Lown 1997 [41]
10	po (tabER°), sd	9	0	(23-33)	(69-86)		yes	yes	yes	test	Lundahl 1995 [42]
10	po (tabER°), sd	12	0	25 ±2	75 ±6		yes	no	no	test	Lundahl 1997 [10]
10	po (tabER°), sd	12	0	26 ±1	76 ±6		no	no	no	training	Lundahl 1998 [43]
10	po (tabER°), sd	24					no	no	no	test	Pop 2008 [44]
10	po (tabER°), sd	10	90	26 ± 5.3 (21-36)	57 ± 8.4 (52-80)	169 ± 8.8 (160-190)	yes	yes	yes	test	Gelal 2005 [45]
10	po (tabER), sd	6	50	(21-31)	(53-90)		no	no	no	test	Weitschies 2005 [46]
10	po (tabER°, fed), sd	56	0	29 ± 5.9 (18.42)	61 ± 6.7 (50-74)	168 ± 5.7 (159-182)	no	no	no	test	Patel 2011 [47]
10	po (*tab*), bid	8	0	20 (19-22)	71 (60-83)		no	no	no	test	Smith 1987 [48]
10	po (tabER), qd	15	0	(18-38)			no	no	no	test	Blychert 1990a [17]
10	po (tabER°), qd	12	0	26 ± 1	76 ± 6		no	no	no	training	Lundahl 1998 [43]
20	po (tabER°), sd	12	0	27 (23-30)	76 (68-86)		no	yes	yes	training	Hasselgren 1990 [40]
40	po (tabER°), sd	12	0	27 (23-30)	76 (68-86)		no	yes	yes	training	Hasselgren 1990 [40]
Hypertensive individuals[c]											
1[d]	iv (15 min)	7	0	45 (32-57)	75 (68-91)		no	no	no	test	Edgar 1989 [49][f]
2.25[e]	iv (105-120 min)	12	8	64 ±2	87.75		no	yes	yes	test	Blychert 1990 [50]
0.83	po (sol), sd	12	25	59 ± 2.6 (39-68)	83 ± 3.6 (62-108)		no	no	yes	test	Edgar 1985 [11]
8.3	po (sol), sd	12	25	59 ± 2.6 (39-68)	83 ± 3.6 (62-108)		no	no	yes	test	Edgar 1985 [11]
10	po (*tab*), sd	6	33	46 (38-49)	91 (54-113)		no	no	yes	test	Larsson 1990 [51]
10	po (*tab*), sd	12	17	59 (36-74)	80 (54-99)		no	no	yes	test	Larsson 1990 [51][f]
10	po (*tab*), D1: 10mg sd, D2-D6: 5mg bid, D7-D29: 10mg bid	4	20	46.75 (38-49)	99.75 (78-113)		no	no	yes	test	Larsson 1990 [51]

assumed

[a]: mean ± standard deviation (range)

[c]: Patients were usually receiving other hypertensive medication, including beta blockers and diuretics

[d]: Doses between 0.5 - 1.5 mg were administered

[e]: 0.02 mg/min, for 105-120 min

[f]: Patients with renal impairment

° tablet brand: Plendil, * tablet brand: Hydac

- : no data available, bid: twice daily, BP: blood pressure; D: day; DHF: dehydrofelodipine, HR: heart rate, iv: intravenous, n: number of individuals, po: oral, qd: once daily, sd: single dose, sol: solution, tab: tablet, tabER: extended release tablet

Table S1: Clinical studies used for the development of the felodipine PBPK/PD model *(continued)*

Dose [mg]	Route	n	Women [%]	Age[a] [y]	Weight[a] [kg]	Height[a] [cm]	DHF	HR	BP	Dataset	Reference
10	po (*tab*), D1: 10mg sd, D2-D6: 5mg bid, D7-D29: 10mg bid	12	17	58.8 (36-74)	80.25 (54-99)		no	no	yes	test	Larsson 1990 [51][f]
10	po (tab), bid	10	10	61 ±1	88 ±4	175 ±2	no	no	no	test	Hedner 1987 [52]
2.5, 5	D1-D7: po (*tab*), bid; D8-D14: po (*tab*), bid	11	73	74 (67-79)	71 (61-89)		no	no	no	test	Landahl 1988 [22]
5	po (tabER), qd	28	64	41 ± 2 (22-50)	86 ± 4		no	no	yes	test	Leenen 2010 [53]
5	po (tabER), qd	35	71	67 ± 1 (60-77)	79 ± 2		no	no	yes	test	Leenen 2010 [53]
5, 10	D1-D14: po (*tab*), bid; D15-D28: po (*tab*), bid	12	0	57 (52-63)			no	yes	yes	test	Hedner 1986 [54]
20	po (tabER), qd	9	0	64 ±3	89 ±5	176 ±3	no	no	no	test	Hedner 1987 [52]
20	po (tabER), sd	12	8	64 ±2	88		no	yes	yes	test	Blychert 1990 [50]
20	po (tabER), qd	12	8	64 ±2	88		no	yes	yes	test	Blychert 1990 [50]

assumed

[a]: mean ± standard deviation (range)

[c]: Patients were usually receiving other hypertensive medication, including beta blockers and diuretics

[d]: Doses between 0.5 - 1.5 mg were administered

[e]: 0.02 mg/min, for 105-120 min

[f]: Patients with renal impairment

°tablet brand: Plendil, * tablet brand: Hydac

- : no data available, bid: twice daily, BP: blood pressure; D: day; DHF: dehydrofelodipine, HR: heart rate, iv: intravenous, n: number of individuals, po: oral, qd: once daily, sd: single dose, sol: solution, tab: tablet, tabER: extended release tablet

2.3 Felodipine drug-dependent parameters

Table S2: Drug-dependent parameters of the final felodipine parent-metabolite PBPK model

Parameter	Unit	Value (model)	Value (literature)	Reference	Description
Felodipine					
MW	g/mol	384.25 (lit)	384.25	[55]	Molecular weight
fu	%	0.36 (lit)	0.36	[56]	Fraction unbound in plasma
Solubility (pH)	mg/l	7.15 (7) (lit)	0.5 (6.5); 1.2 (7); 7.15 (7); 14.3 (7.1); 19.7 (7)	[57–59]	Solubility
Solubility tabER (pH)	mg/l	0.89 (7.0) (opt)	-	-	Solubility (extended release tablets)
logP		4.36 (lit)	3.44; 3.80; 4.36; 4.46; 4.64	[55, 58–60]	Lipophilicity
Intestinal permeability	cm/min	2.76E-4 (opt)	4.42E-4; 3.06E-4; 2.64E-4	[59, 61]	Transcellular intestinal permeability
GFR fraction		1 (asm)	-	-	Fraction of filtered drug in the urine
K_M (CYP3A4)	µmol/l	2.81 (lit)	0.648; 0.94; 2.81; 26.4	[59, 62, 63]	CYP3A4 Michaelis-Menten constant
K_M (CYP3A4) - (R)-Felodipine	µmol/l	2.16 (opt)	6.1 (3.4 - 8.7)	[5]	CYP3A4 Michaelis-Menten constant
K_M (CYP3A4) - (S)-Felodipine	µmol/l	4.27 (opt)	12.2 (5.9 - 21.6)	[5]	CYP3A4 Michaelis-Menten constant
k_{cat} (CYP3A4)	1/min	250.44 (opt)			CYP3A4 catalytic rate constant
s (tab)		1.32(opt)	-	-	Dissolution profile shape
$t_{50\%}$ (tab)	min	54.86 (opt)	-	-	Dissolution time (50% dissolved)
s (tabER)		1.30 (opt)	-	-	Dissolution profile shape
$t_{50\%}$ (tabER)	min	173.04 (opt)	-	-	Dissolution time (50% dissolved)
Partition coefficient	-	diverse	Rodgers and Rowland	[64, 65]	Cell to plasma partition coefficients
Cellular permeability	cm/min	0.42 (calc)	PK-Sim Standard	[66]	Permeability into the cellular space
Dehydrofelodipine					
MW	g/mol	382.2 (lit)	382.2	[67]	Molecular weight
pKa (base)	-	4.06 (lit)	4.06	[67]	Acid dissociation constant
f_u	%	0.68 (lit)	-	-	Fraction unbound in plasma
Solubility (pH)	mg/l	2.93 (7) (lit)	2.93 (7)	[67]	Solubility
logP		3.32 (opt)	4.24	[67]	Lipophilicity
CL (CYP3A4)	1/min	35.74 (opt)	-	-	CYP3A4 clearance process
CL_{hep}	1/min	2.76 (opt)	-	-	Unspecific hepatic clearance process
Intestinal permeability	cm/min	1.38E-4 (calc)	-	-	Transcellular intestinal permeability
GFR fraction		1 (asm)	-	-	Fraction of filtered drug in the urine
Partition coefficient	-	diverse	Schmitt	[68]	Cell to plasma partition coefficients
Cellular permeability	cm/min	0.04 (calc)	Charge dependent Schmitt	[1]	Permeability into the cellular space

asm: assumed, calc: calculated, CYP3A4: cytochrom P450 3A4, GFR: glomerular filtration rate, lit: literature value, opt: optimized value, tab: tablet, tabER: extended release tablet

2.4 Plasma concentration-time profiles

2.4.1 Linear

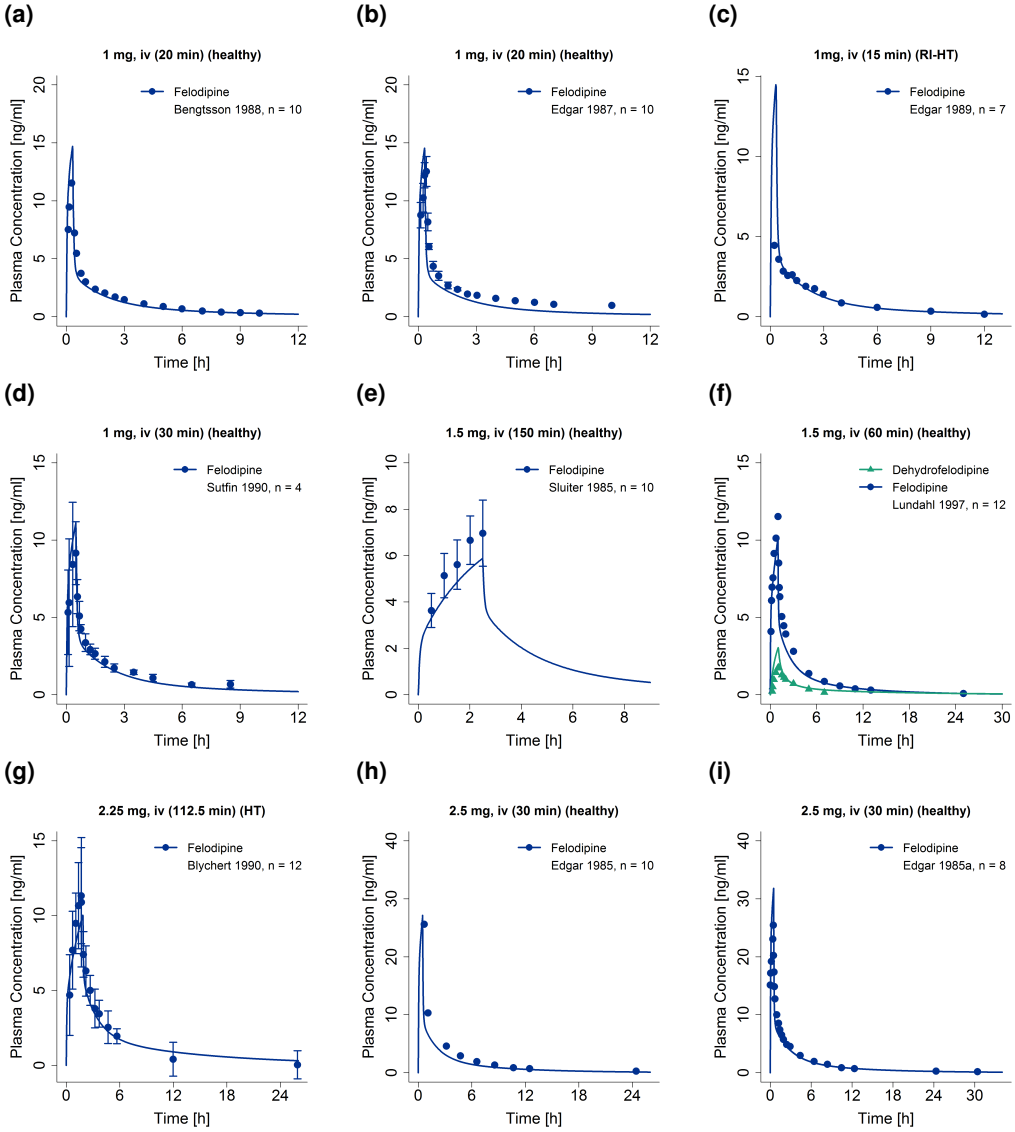

Figure S2: Predicted compared to observed felodipine and dehydrofelodipine plasma concentration-time profiles (linear) after intravenous and oral administration of felodipine. Observed data are shown as dots and triangles ± standard deviation (if available); model predictions are shown as solid lines. Details on dosing regimens, study populations and literature references are listed in Table S1. bid: twice daily, HT: hypertension, iv: intravenous, md: multiple dose, n: number of individuals, qd: once daily, RI: renal impairment, sol: solution, sd: single dose, tab: tablet, tabER: extended release tablet.

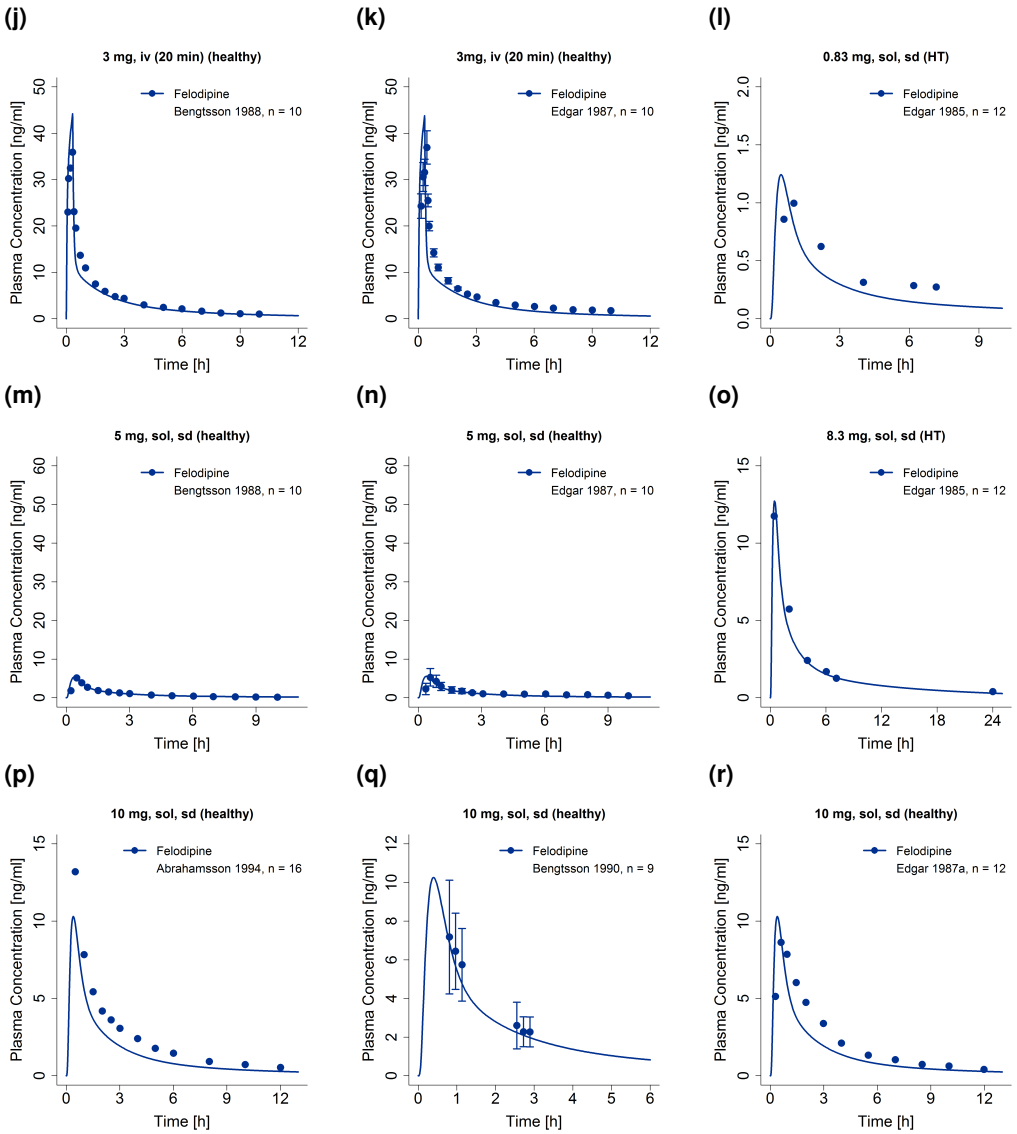

Figure S2: Predicted compared to observed felodipine and dehydrofelodipine plasma concentration-time profiles (linear) after intravenous and oral administration of felodipine. Observed data are shown as dots and triangles ± standard deviation (if available); model predictions are shown as solid lines. Details on dosing regimens, study populations and literature references are listed in Table S1. bid: twice daily, HT: hypertension, iv: intravenous, md: multiple dose, n: number of individuals, qd: once daily, RI: renal impairment, sol: solution, sd: single dose, tab: tablet, tabER: extended release tablet. *(continued)*

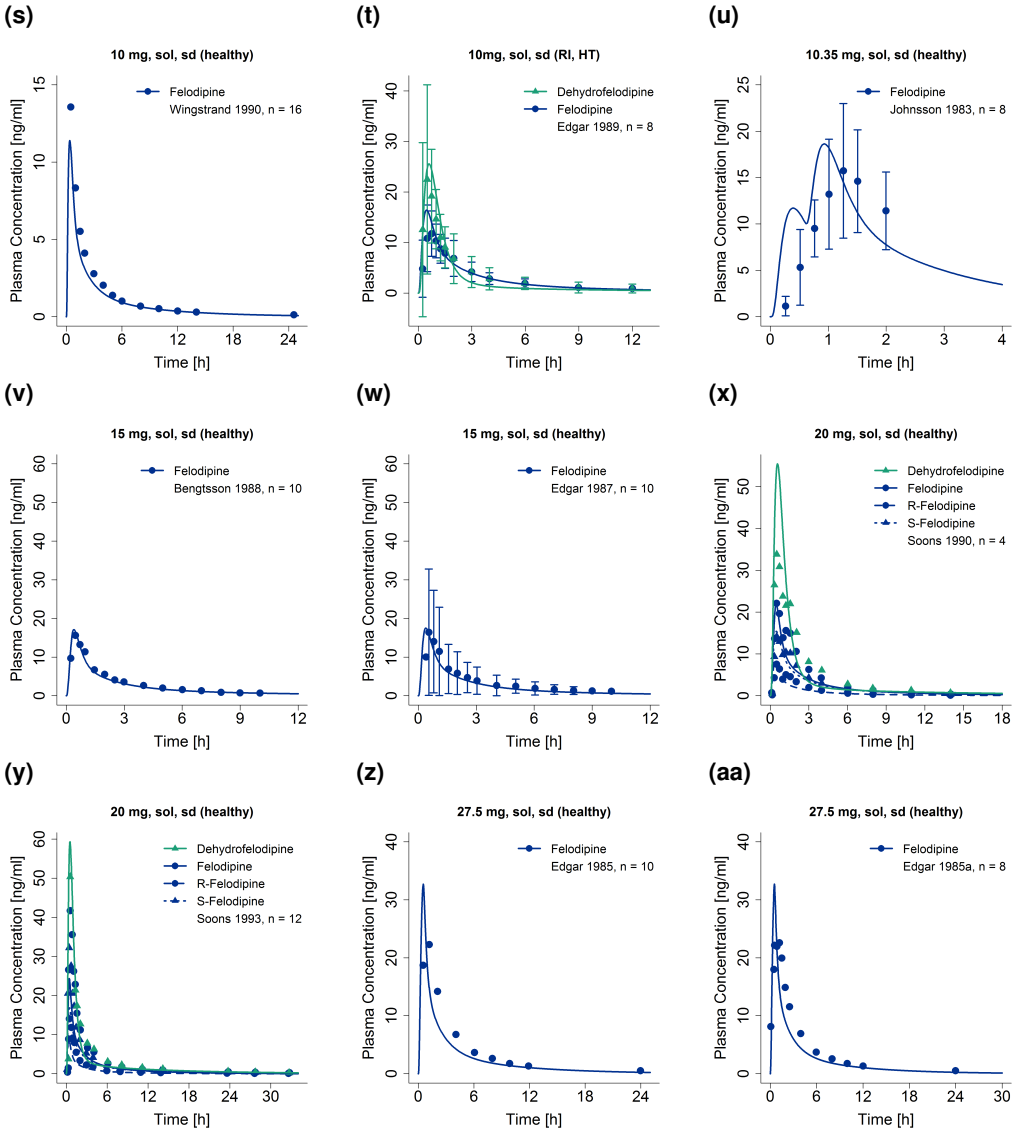

Figure S2: Predicted compared to observed felodipine and dehydrofelodipine plasma concentration-time profiles (linear) after intravenous and oral administration of felodipine. Observed data are shown as dots and triangles ± standard deviation (if available); model predictions are shown as solid lines. Details on dosing regimens, study populations and literature references are listed in Table S1. bid: twice daily, HT: hypertension, iv: intravenous, md: multiple dose, n: number of individuals, qd: once daily, RI: renal impairment, sol: solution, sd: single dose, tab: tablet, tabER: extended release tablet. *(continued)*

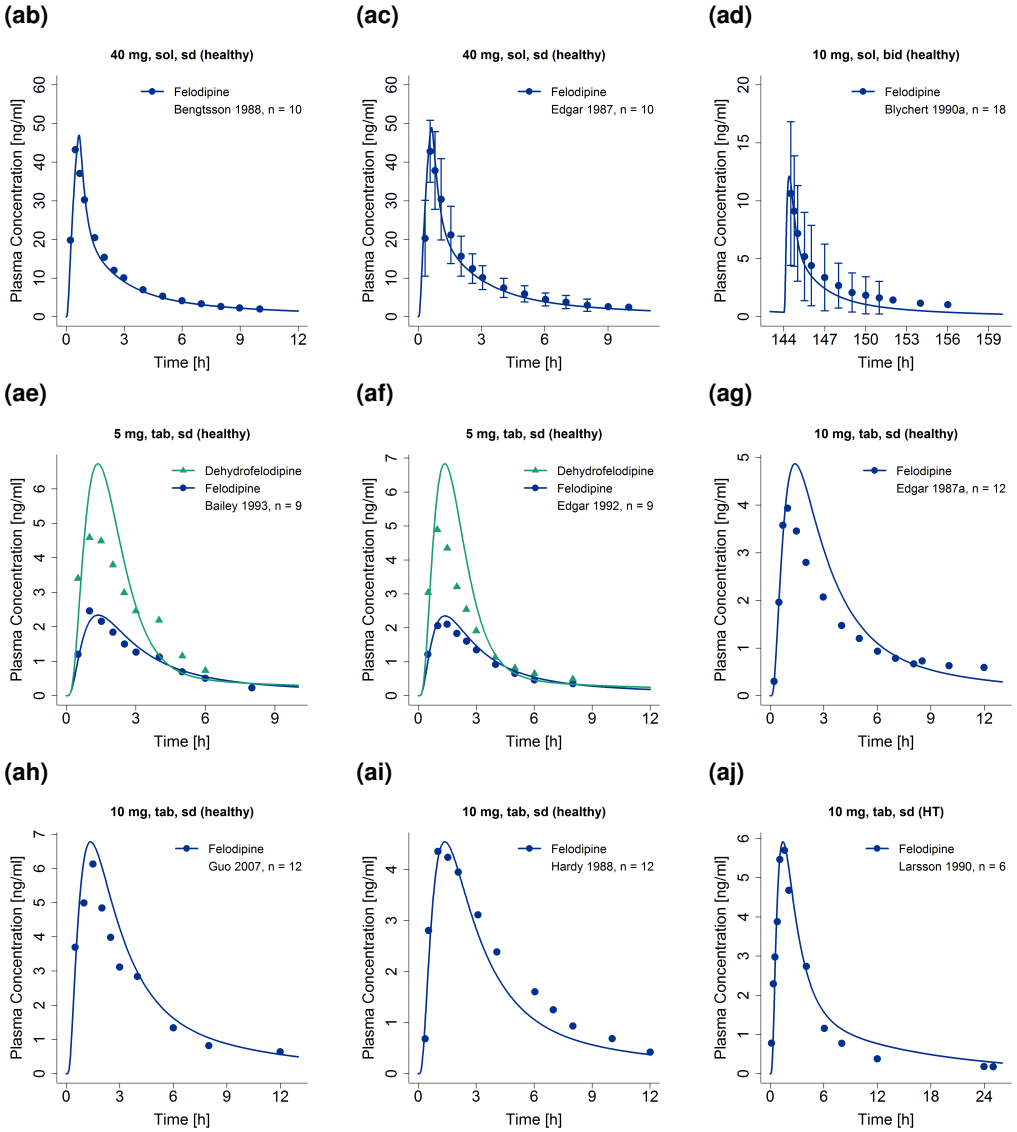

Figure S2: Predicted compared to observed felodipine and dehydrofelodipine plasma concentration-time profiles (linear) after intravenous and oral administration of felodipine. Observed data are shown as dots and triangles ± standard deviation (if available); model predictions are shown as solid lines. Details on dosing regimens, study populations and literature references are listed in Table S1. bid: twice daily, HT: hypertension, iv: intravenous, md: multiple dose, n: number of individuals, qd: once daily, RI: renal impairment, sol: solution, sd: single dose, tab: tablet, tabER: extended release tablet. *(continued)*

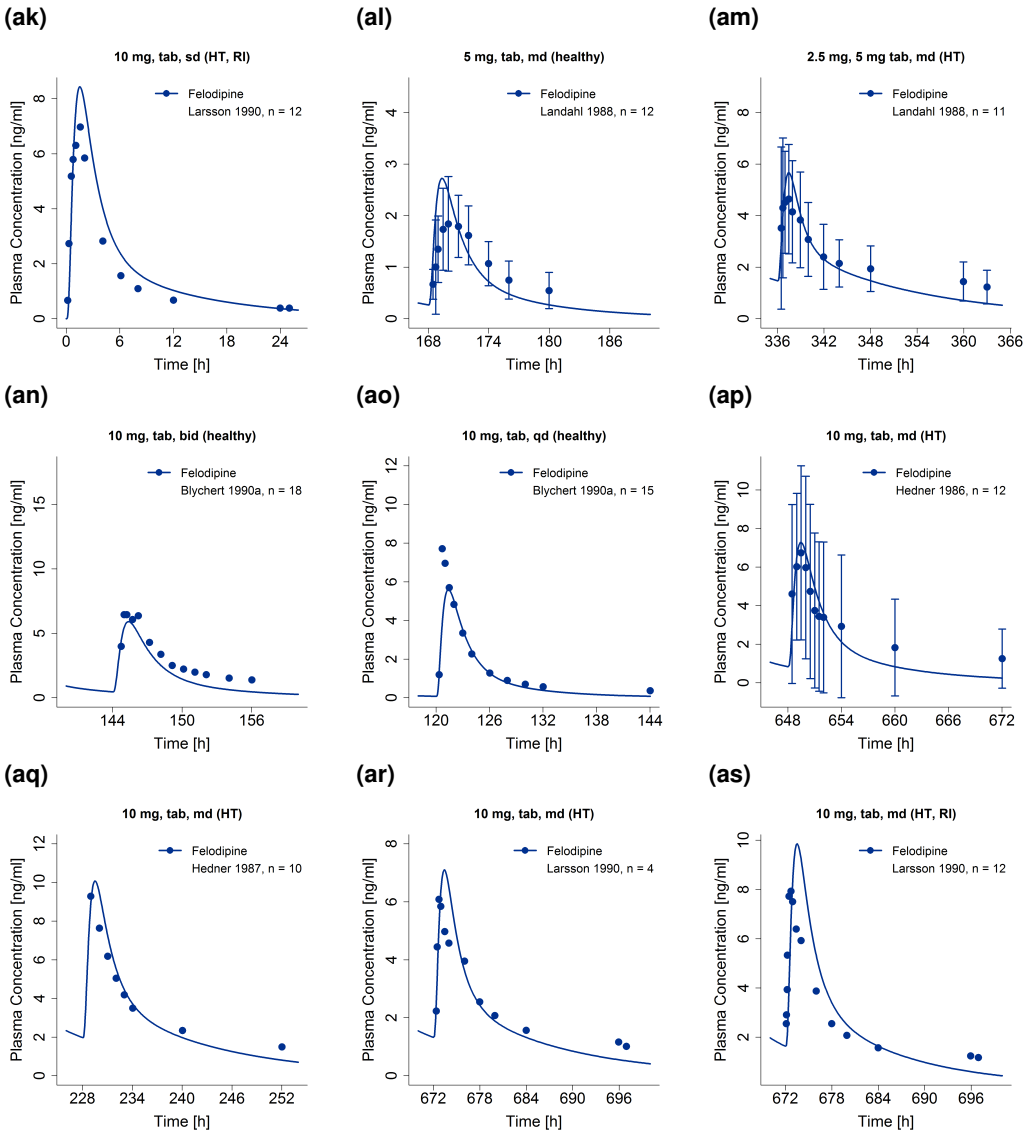

Figure S2: Predicted compared to observed felodipine and dehydrofelodipine plasma concentration-time profiles (linear) after intravenous and oral administration of felodipine. Observed data are shown as dots and triangles ± standard deviation (if available); model predictions are shown as solid lines. Details on dosing regimens, study populations and literature references are listed in Table S1. bid: twice daily, HT: hypertension, iv: intravenous, md: multiple dose, n: number of individuals, qd: once daily, RI: renal impairment, sol: solution, sd: single dose, tab: tablet, tabER: extended release tablet. *(continued)*

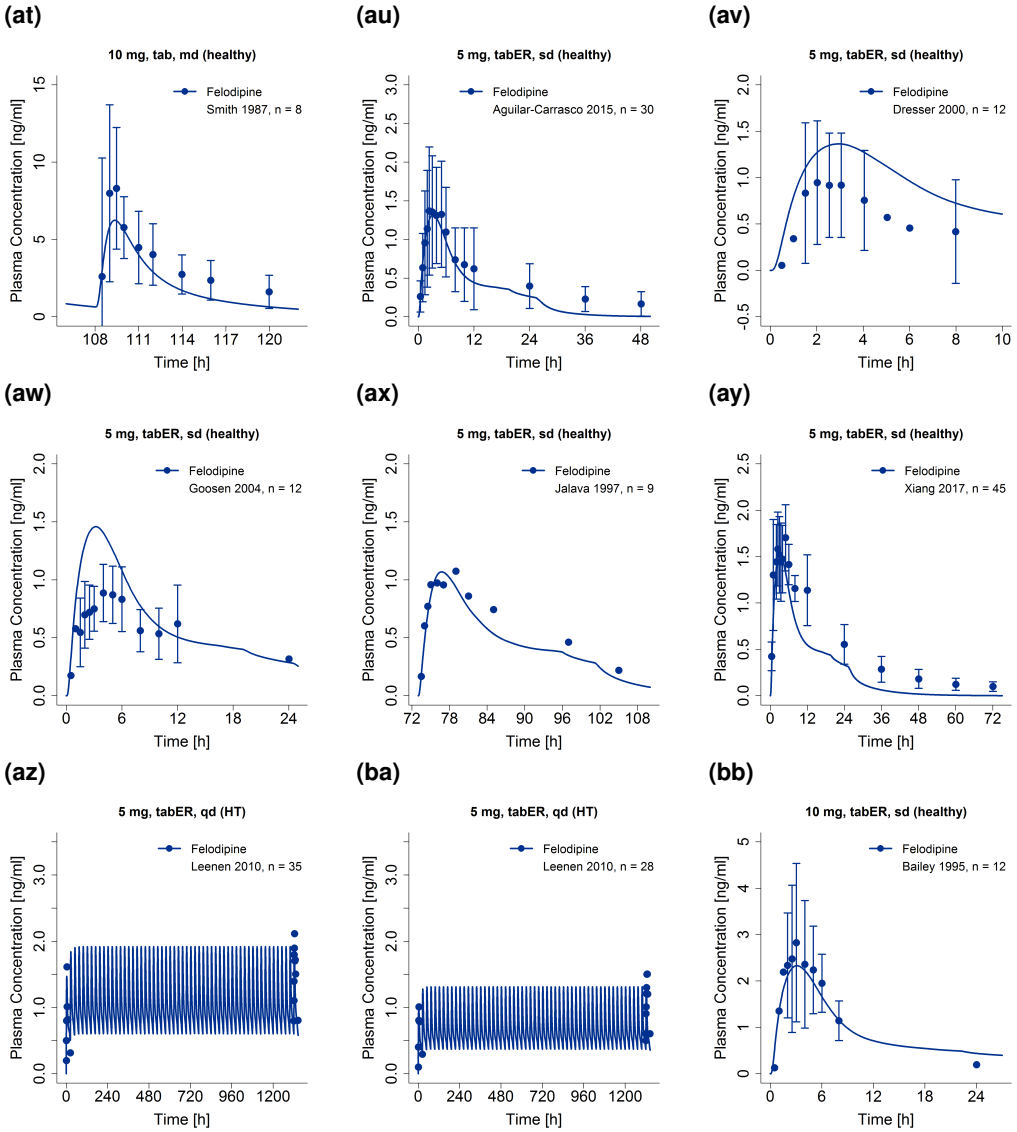

Figure S2: Predicted compared to observed felodipine and dehydrofelodipine plasma concentration-time profiles (linear) after intravenous and oral administration of felodipine. Observed data are shown as dots and triangles ± standard deviation (if available); model predictions are shown as solid lines. Details on dosing regimens, study populations and literature references are listed in Table S1. bid: twice daily, HT: hypertension, iv: intravenous, md: multiple dose, n: number of individuals, qd: once daily, RI: renal impairment, sol: solution, sd: single dose, tab: tablet, tabER: extended release tablet. *(continued)*

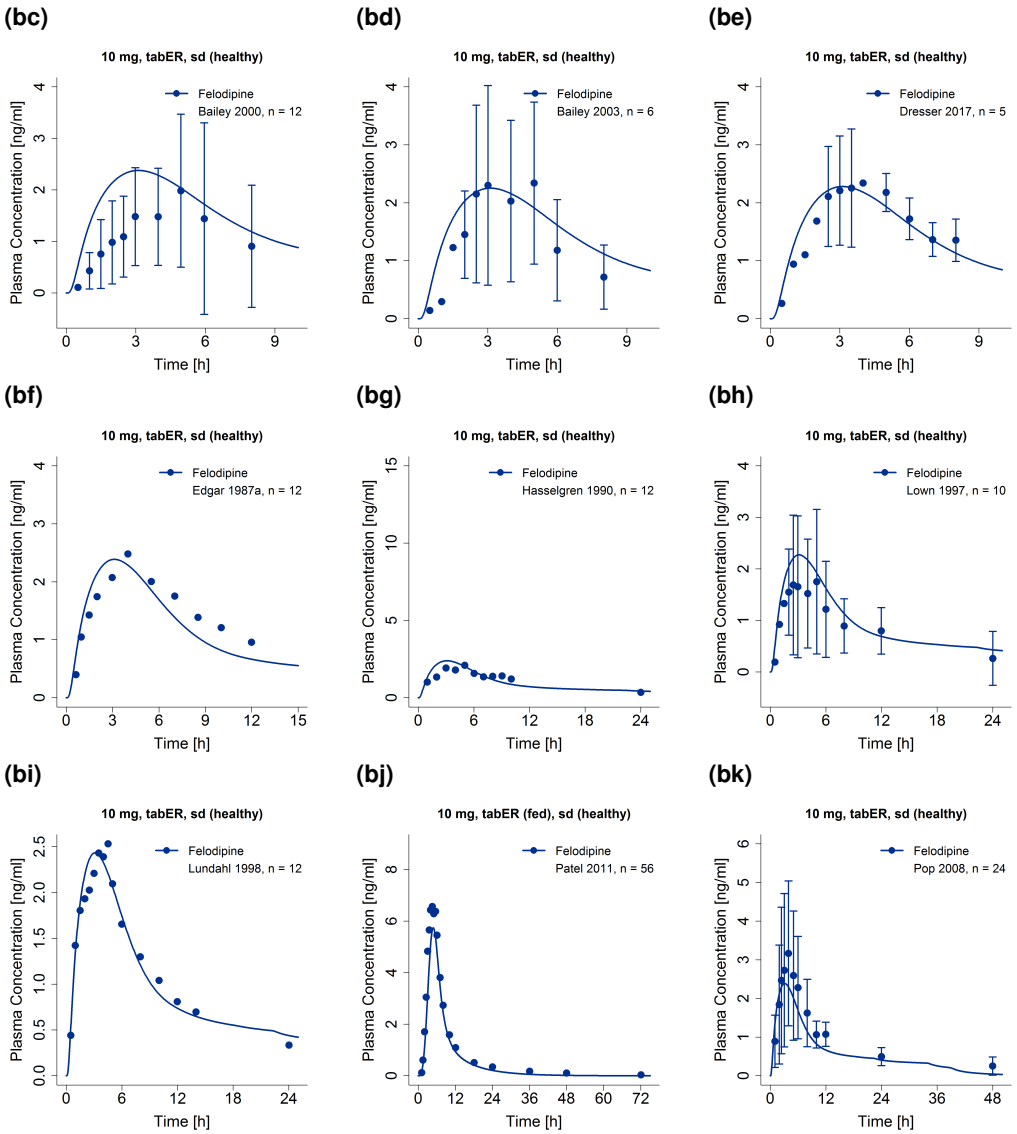

Figure S2: Predicted compared to observed felodipine and dehydrofelodipine plasma concentration-time profiles (linear) after intravenous and oral administration of felodipine. Observed data are shown as dots and triangles ± standard deviation (if available); model predictions are shown as solid lines. Details on dosing regimens, study populations and literature references are listed in Table S1. bid: twice daily, HT: hypertension, iv: intravenous, md: multiple dose, n: number of individuals, qd: once daily, RI: renal impairment, sol: solution, sd: single dose, tab: tablet, tabER: extended release tablet. *(continued)*

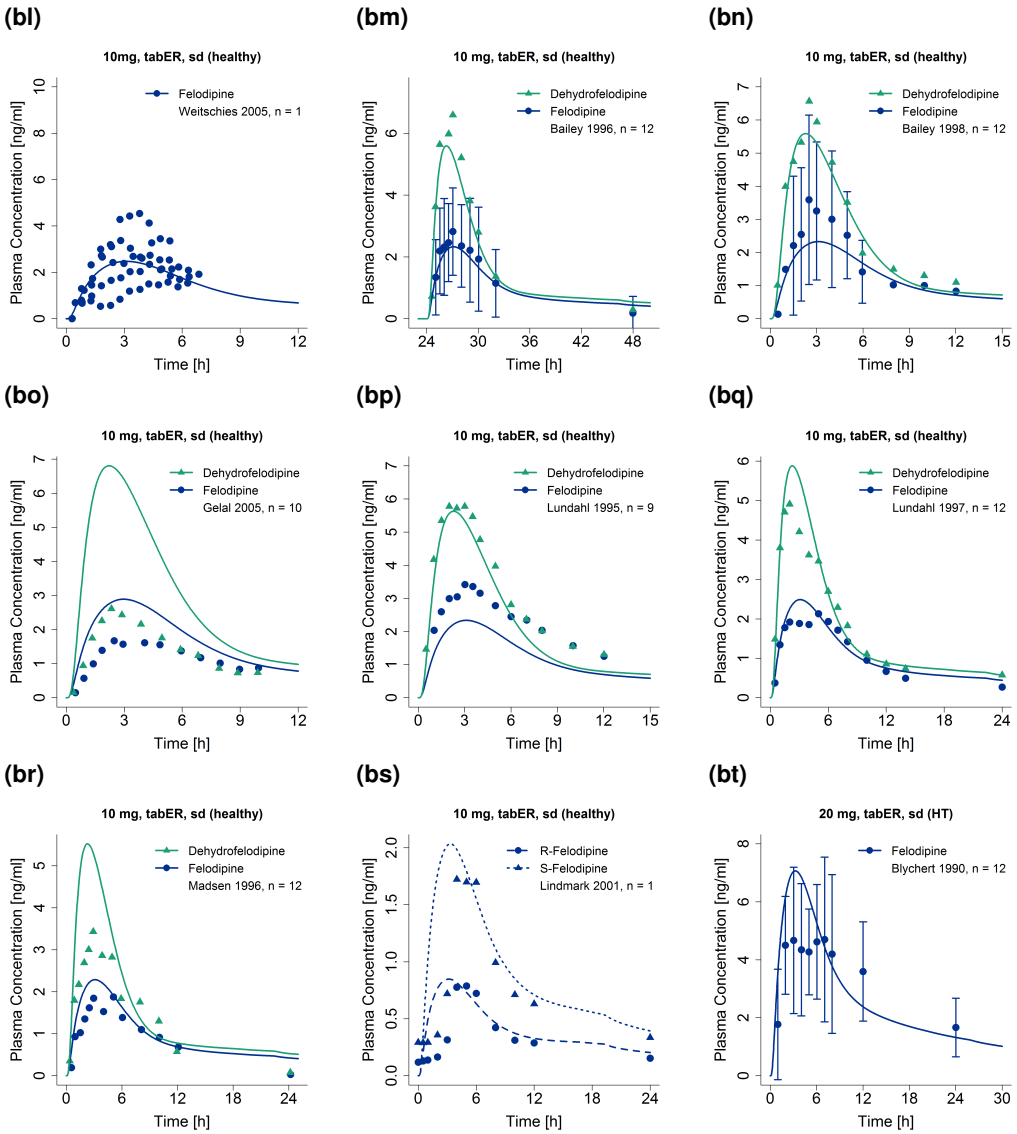

Figure S2: Predicted compared to observed felodipine and dehydrofelodipine plasma concentration-time profiles (linear) after intravenous and oral administration of felodipine. Observed data are shown as dots and triangles ± standard deviation (if available); model predictions are shown as solid lines. Details on dosing regimens, study populations and literature references are listed in Table S1. bid: twice daily, HT: hypertension, iv: intravenous, md: multiple dose, n: number of individuals, qd: once daily, RI: renal impairment, sol: solution, sd: single dose, tab: tablet, tabER: extended release tablet. *(continued)*

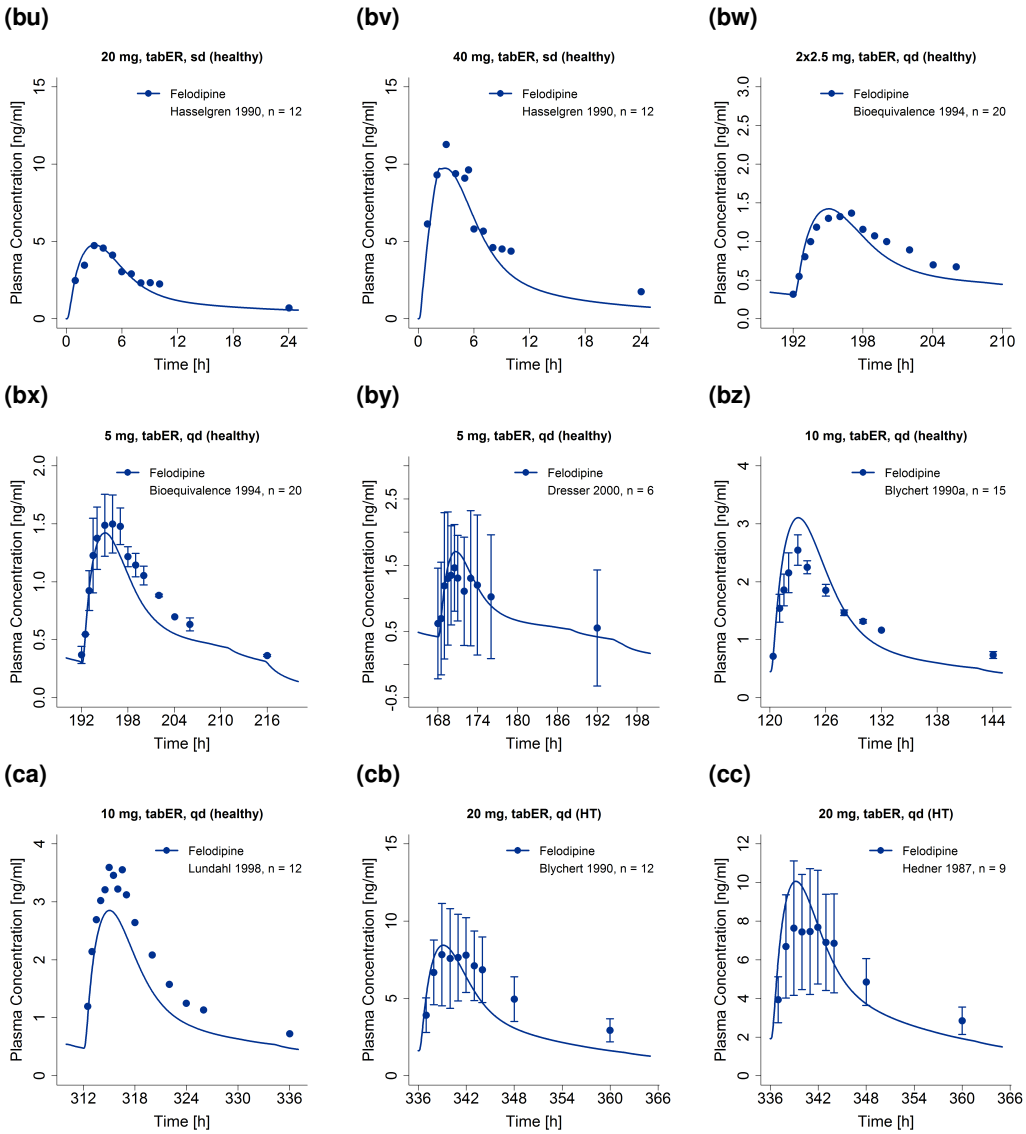

Figure S2: Predicted compared to observed felodipine and dehydrofelodipine plasma concentration-time profiles (linear) after intravenous and oral administration of felodipine. Observed data are shown as dots and triangles ± standard deviation (if available); model predictions are shown as solid lines. Details on dosing regimens, study populations and literature references are listed in Table S1. bid: twice daily, HT: hypertension, iv: intravenous, md: multiple dose, n: number of individuals, qd: once daily, RI: renal impairment, sol: solution, sd: single dose, tab: tablet, tabER: extended release tablet. *(continued)*

2.4.2 Semi-logarithmic

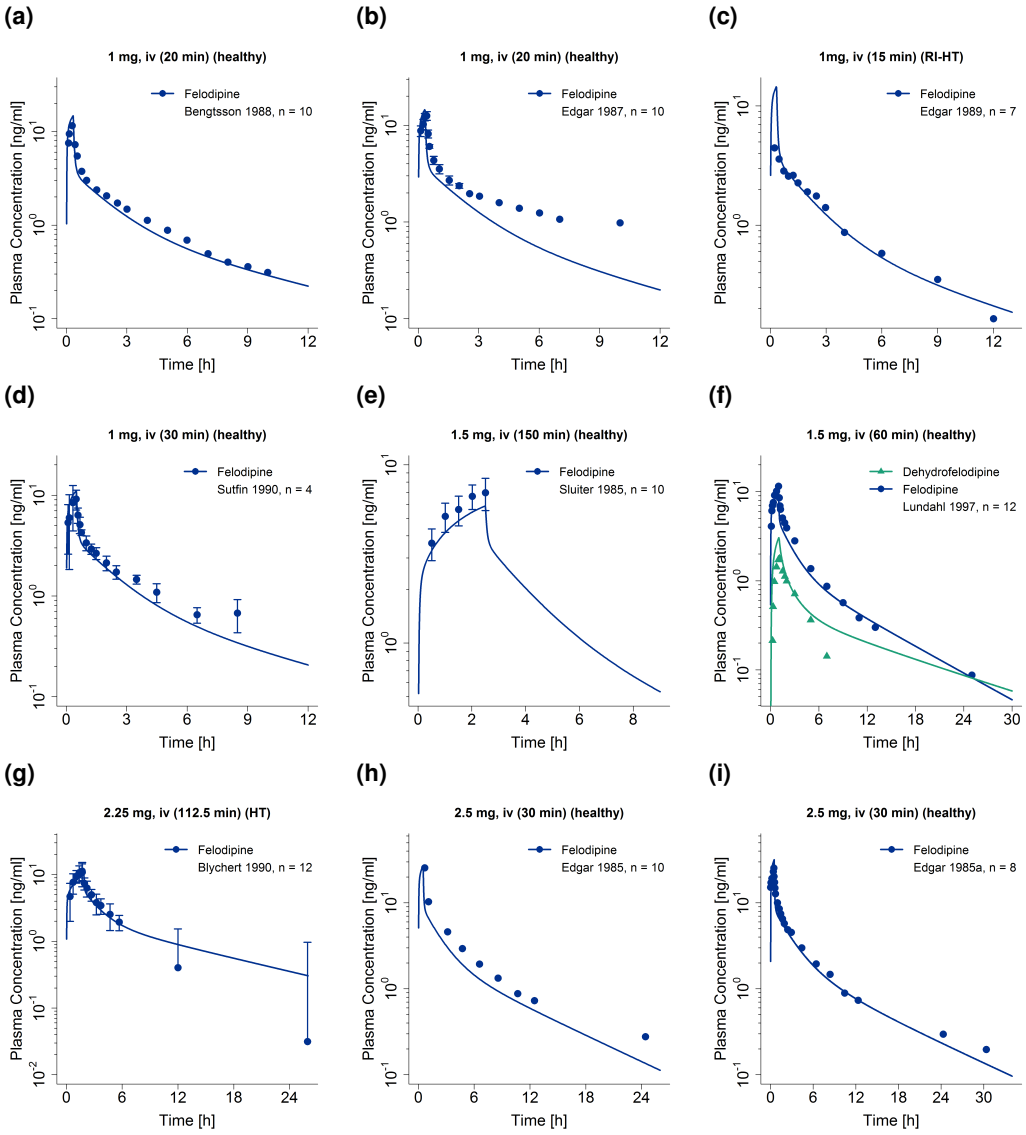

Figure S3: Predicted compared to observed felodipine and dehydrofelodipine plasma concentration-time profiles (semi-logarithmic) after intravenous and oral administration of felodipine. Observed data are shown as dots and triangles ± standard deviation; model predictions are shown as solid lines. Details on dosing regimens, study populations and literature references are listed in Table S1. bid: twice daily, HT: hypertension, iv: intravenous, md: multiple dose, n: number of individuals, qd: once daily, RI: renal impairment, sol: solution, sd: single dose, tab: tablet, tabER: extended release tablet.

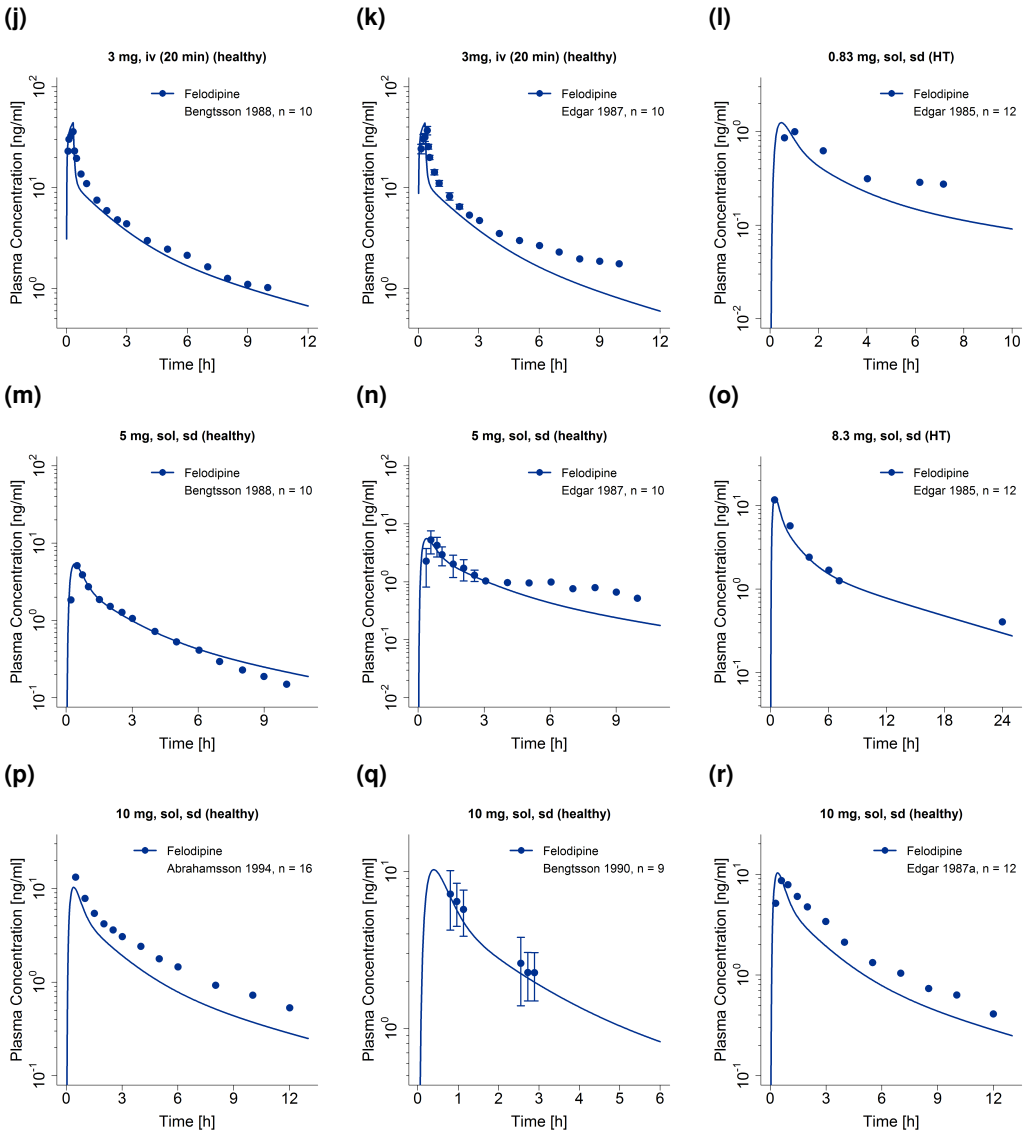

Figure S3: Predicted compared to observed felodipine and dehydrofelodipine plasma concentration-time profiles (semi-logarithmic) after intravenous and oral administration of felodipine. Observed data are shown as dots and triangles ± standard deviation; model predictions are shown as solid lines. Details on dosing regimens, study populations and literature references are listed in Table S1. bid: twice daily, HT: hypertension, iv: intravenous, md: multiple dose, n: number of individuals, qd: once daily, RI: renal impairment, sol: solution, sd: single dose, tab: tablet, tabER: extended release tablet. *(continued)*

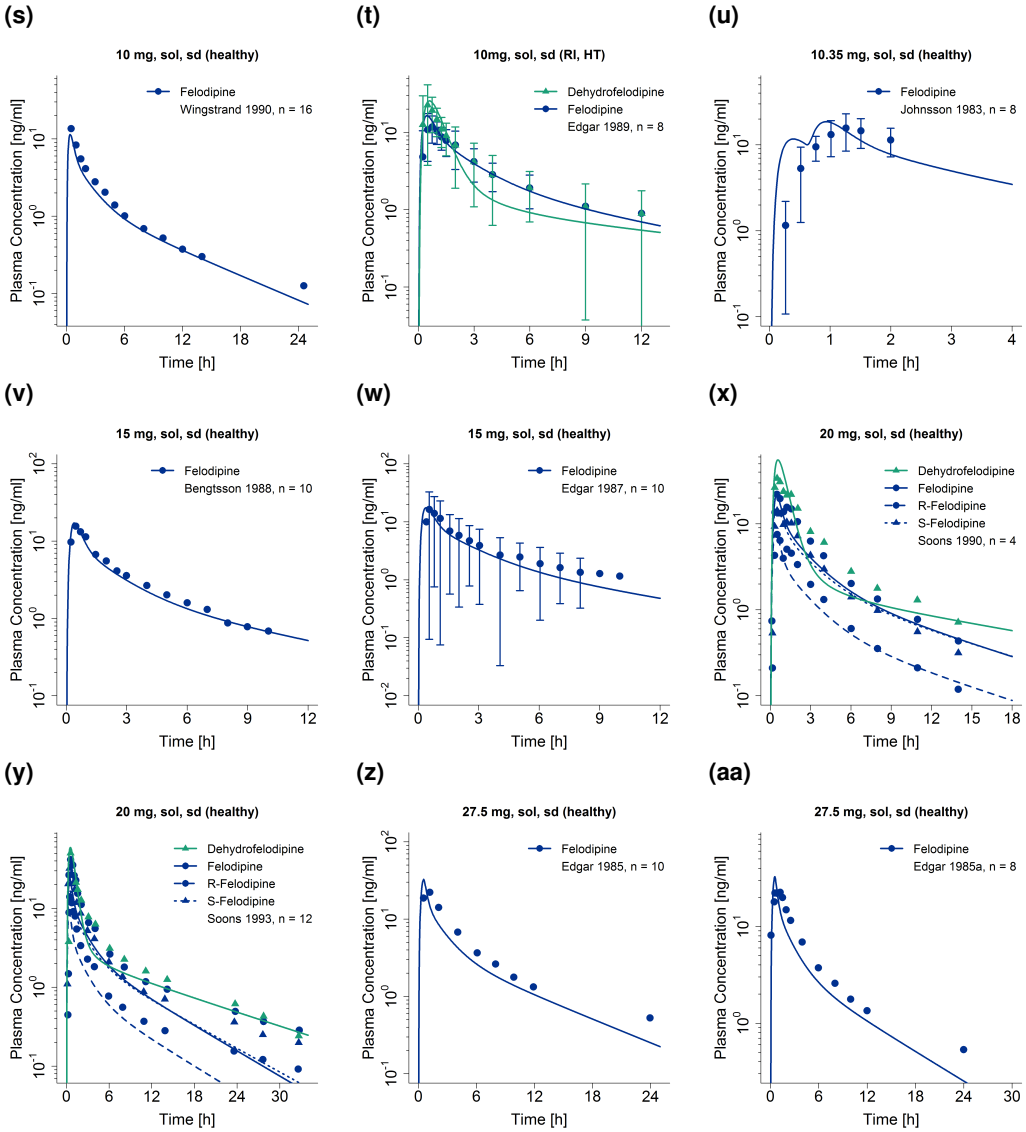

Figure S3: Predicted compared to observed felodipine and dehydrofelodipine plasma concentration-time profiles (semi-logarithmic) after intravenous and oral administration of felodipine. Observed data are shown as dots and triangles ± standard deviation; model predictions are shown as solid lines. Details on dosing regimens, study populations and literature references are listed in Table S1. bid: twice daily, HT: hypertension, iv: intravenous, md: multiple dose, n: number of individuals, qd: once daily, RI: renal impairment, sol: solution, sd: single dose, tab: tablet, tabER: extended release tablet. *(continued)*

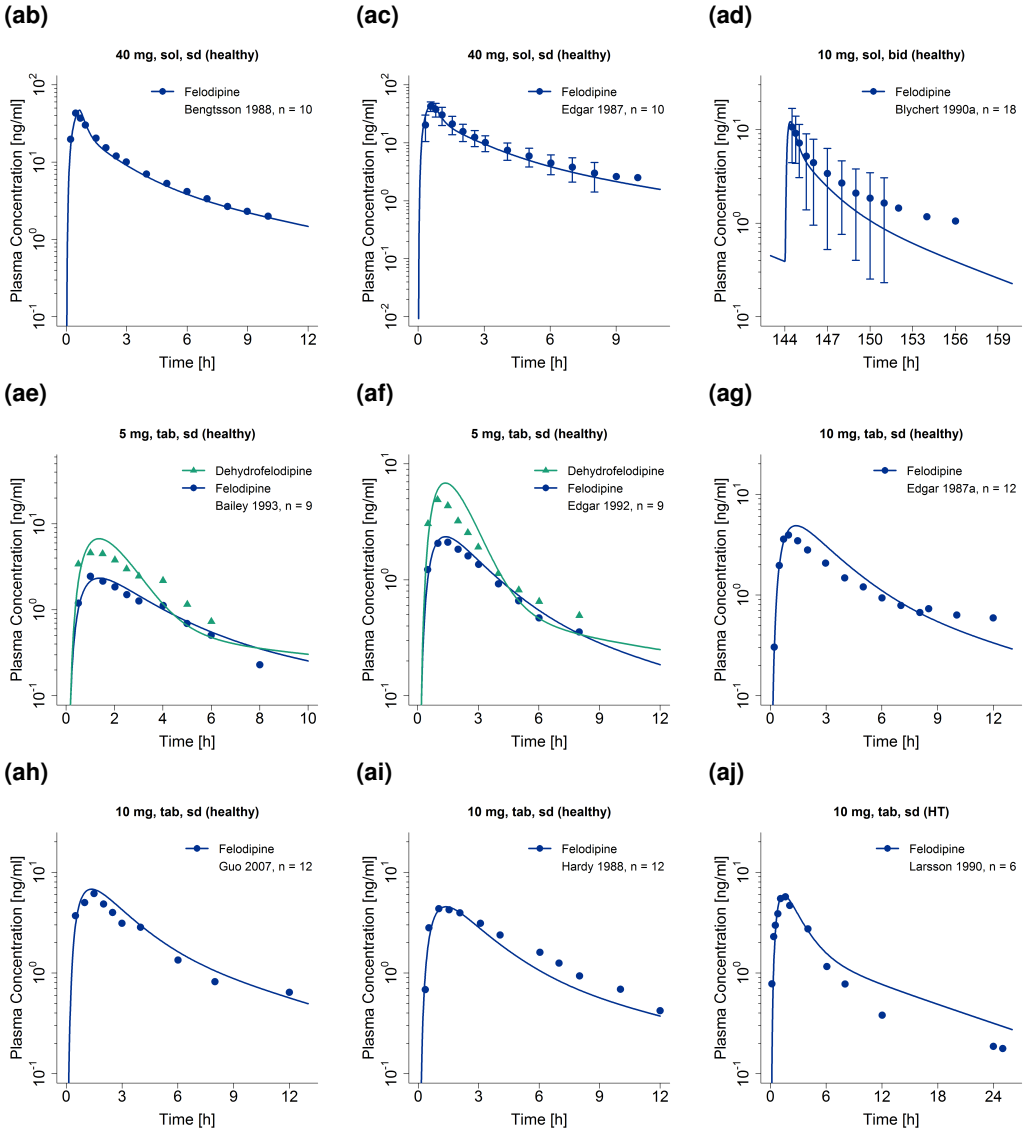

Figure S3: Predicted compared to observed felodipine and dehydrofelodipine plasma concentration-time profiles (semi-logarithmic) after intravenous and oral administration of felodipine. Observed data are shown as dots and triangles ± standard deviation; model predictions are shown as solid lines. Details on dosing regimens, study populations and literature references are listed in Table S1. bid: twice daily, HT: hypertension, iv: intravenous, md: multiple dose, n: number of individuals, qd: once daily, RI: renal impairment, sol: solution, sd: single dose, tab: tablet, tabER: extended release tablet. *(continued)*

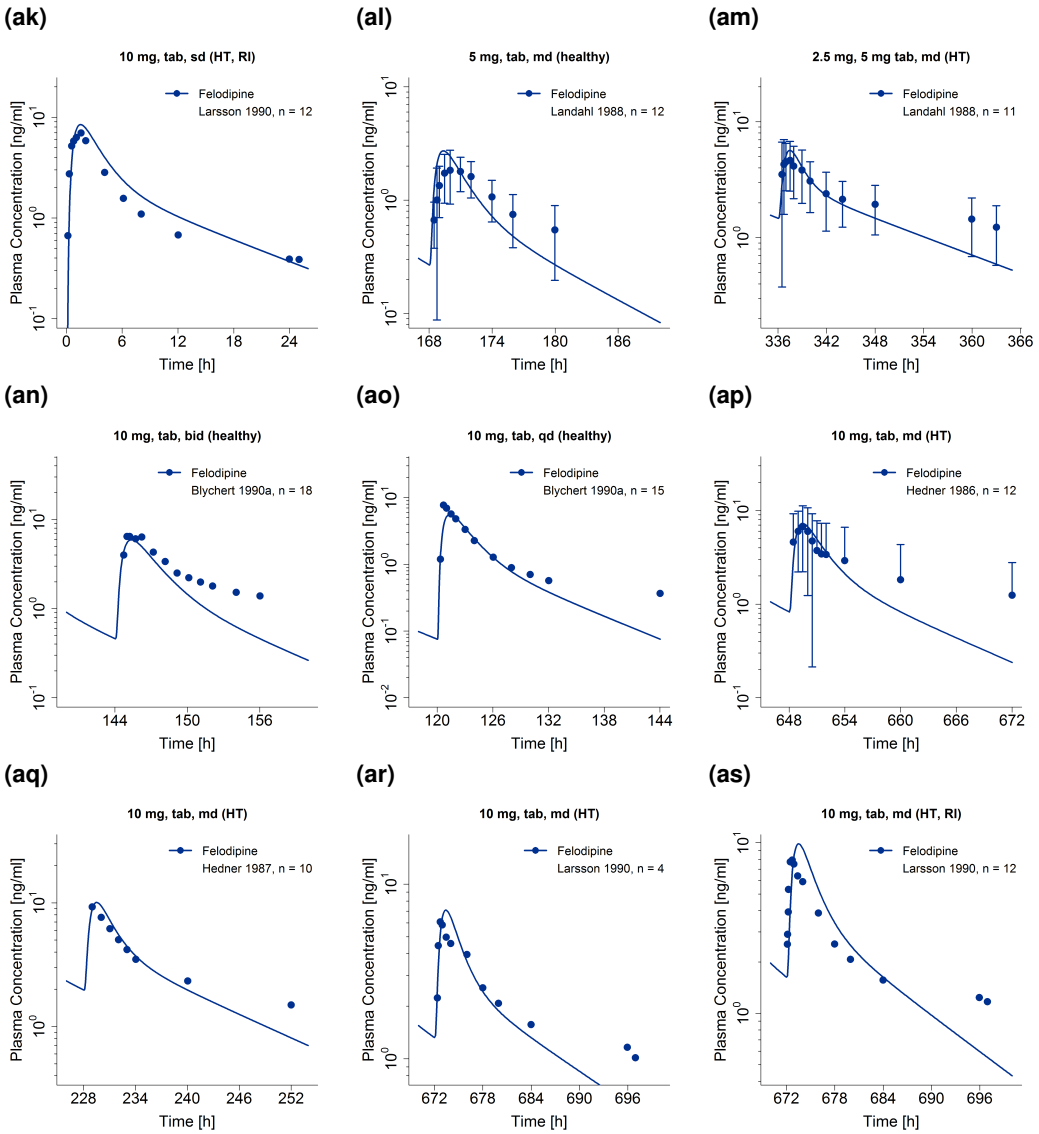

Figure S3: Predicted compared to observed felodipine and dehydrofelodipine plasma concentration-time profiles (semi-logarithmic) after intravenous and oral administration of felodipine. Observed data are shown as dots and triangles ± standard deviation; model predictions are shown as solid lines. Details on dosing regimens, study populations and literature references are listed in Table S1. bid: twice daily, HT: hypertension, iv: intravenous, md: multiple dose, n: number of individuals, qd: once daily, RI: renal impairment, sol: solution, sd: single dose, tab: tablet, tabER: extended release tablet. *(continued)*

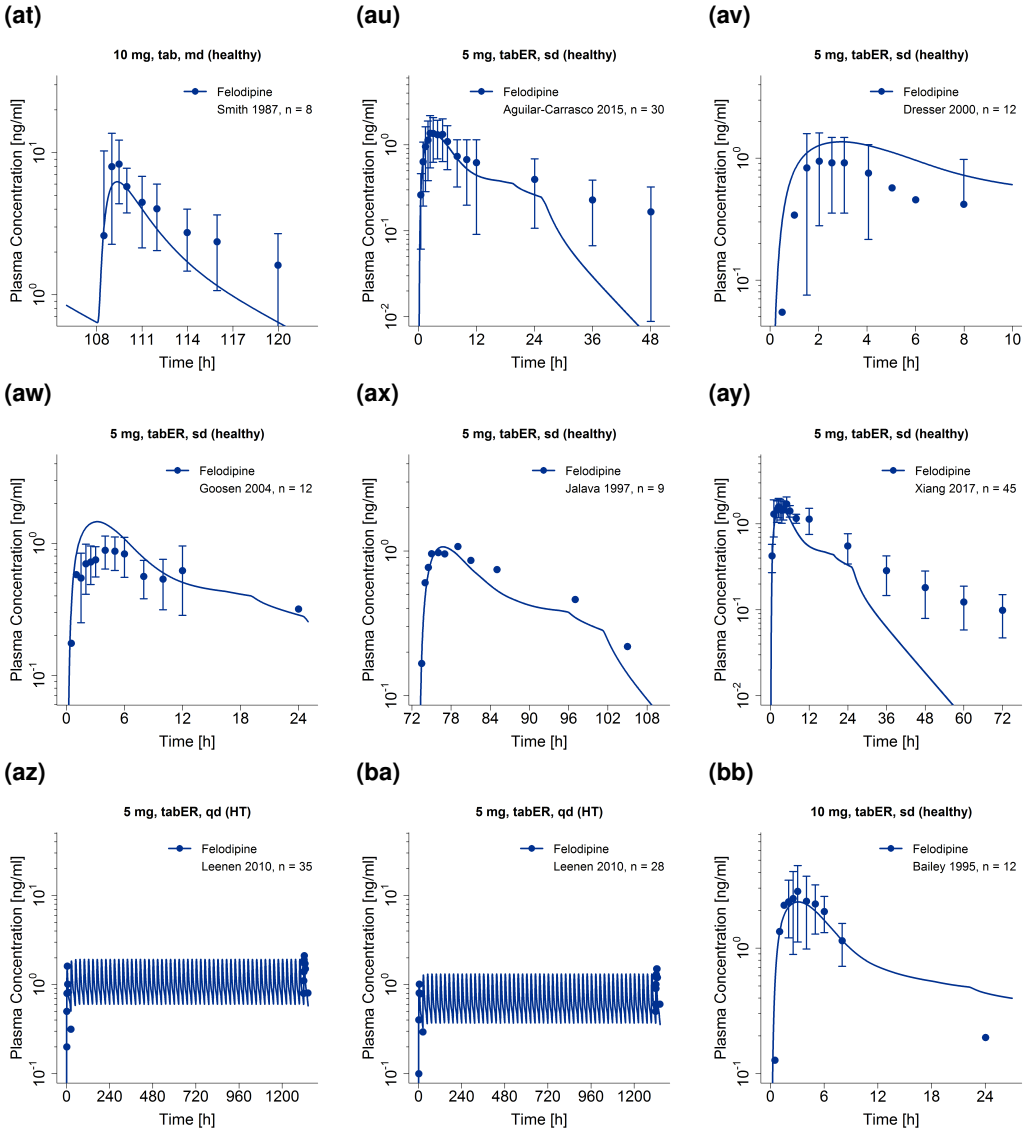

Figure S3: Predicted compared to observed felodipine and dehydrofelodipine plasma concentration-time profiles (semi-logarithmic) after intravenous and oral administration of felodipine. Observed data are shown as dots and triangles ± standard deviation; model predictions are shown as solid lines. Details on dosing regimens, study populations and literature references are listed in Table S1. bid: twice daily, HT: hypertension, iv: intravenous, md: multiple dose, n: number of individuals, qd: once daily, RI: renal impairment, sol: solution, sd: single dose, tab: tablet, tabER: extended release tablet. *(continued)*

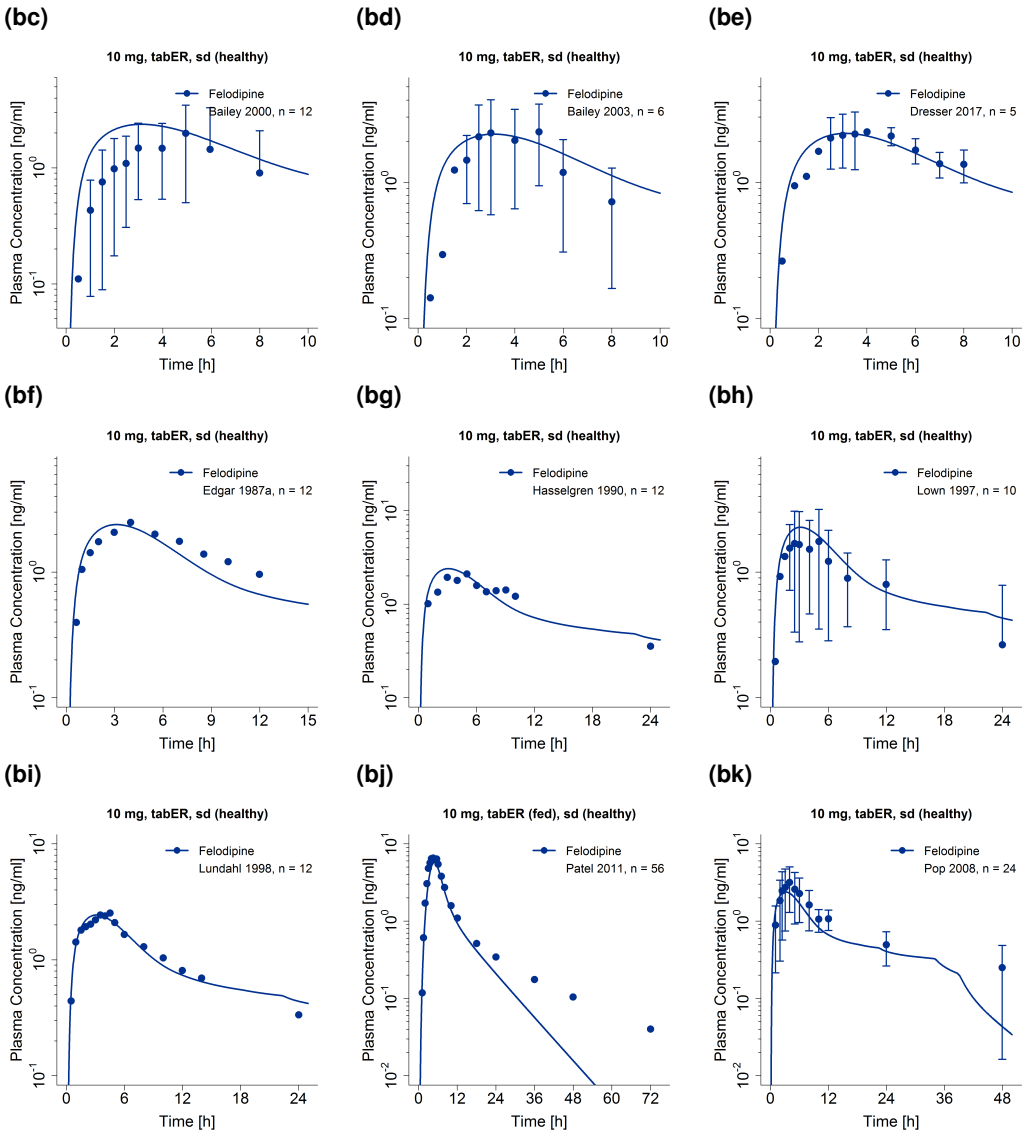

Figure S3: Predicted compared to observed felodipine and dehydrofelodipine plasma concentration-time profiles (semi-logarithmic) after intravenous and oral administration of felodipine. Observed data are shown as dots and triangles ± standard deviation; model predictions are shown as solid lines. Details on dosing regimens, study populations and literature references are listed in Table S1. bid: twice daily, HT: hypertension, iv: intravenous, md: multiple dose, n: number of individuals, qd: once daily, RI: renal impairment, sol: solution, sd: single dose, tab: tablet, tabER: extended release tablet. *(continued)*

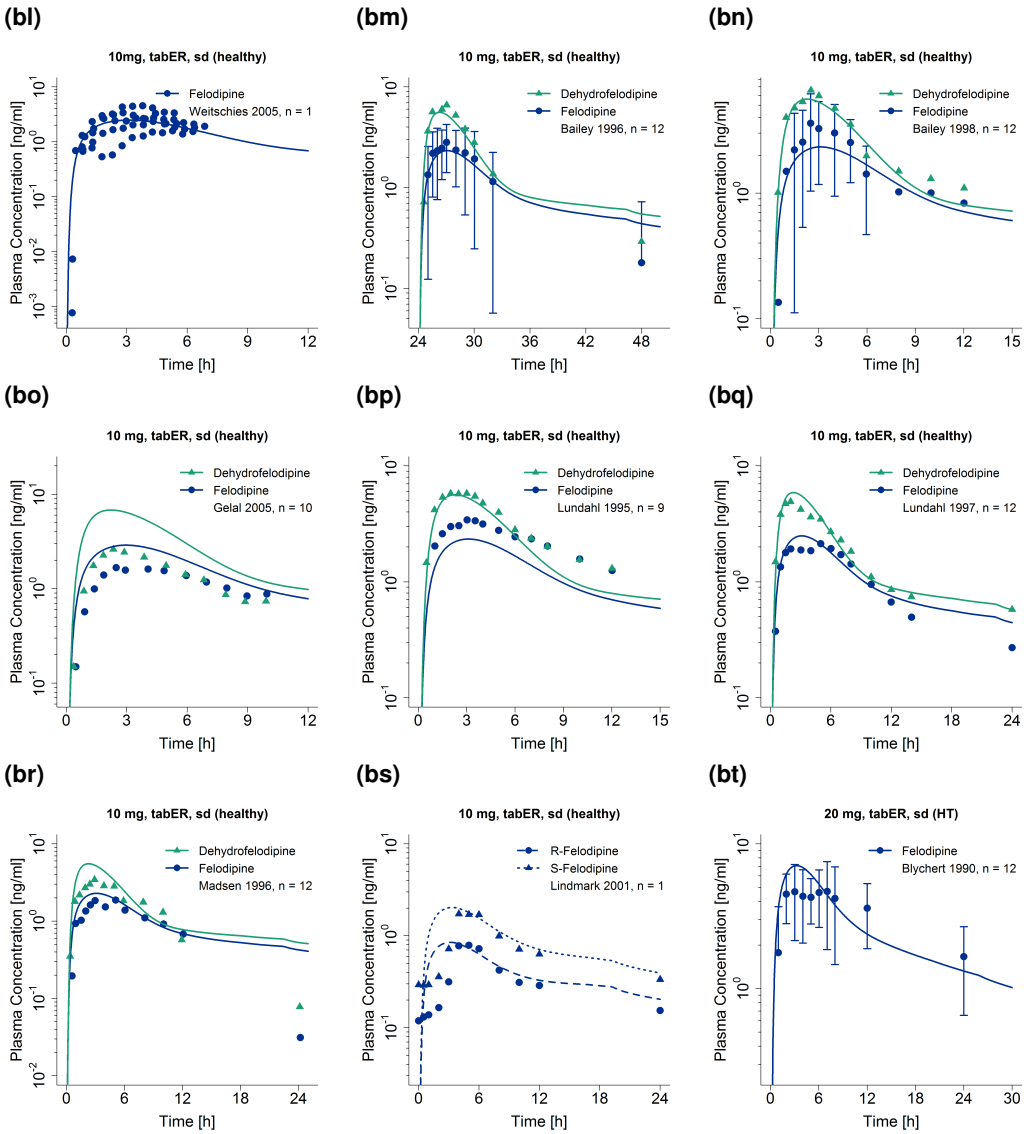

Figure S3: Predicted compared to observed felodipine and dehydrofelodipine plasma concentration-time profiles (semi-logarithmic) after intravenous and oral administration of felodipine. Observed data are shown as dots and triangles ± standard deviation; model predictions are shown as solid lines. Details on dosing regimens, study populations and literature references are listed in Table S1. bid: twice daily, HT: hypertension, iv: intravenous, md: multiple dose, n: number of individuals, qd: once daily, RI: renal impairment, sol: solution, sd: single dose, tab: tablet, tabER: extended release tablet. *(continued)*

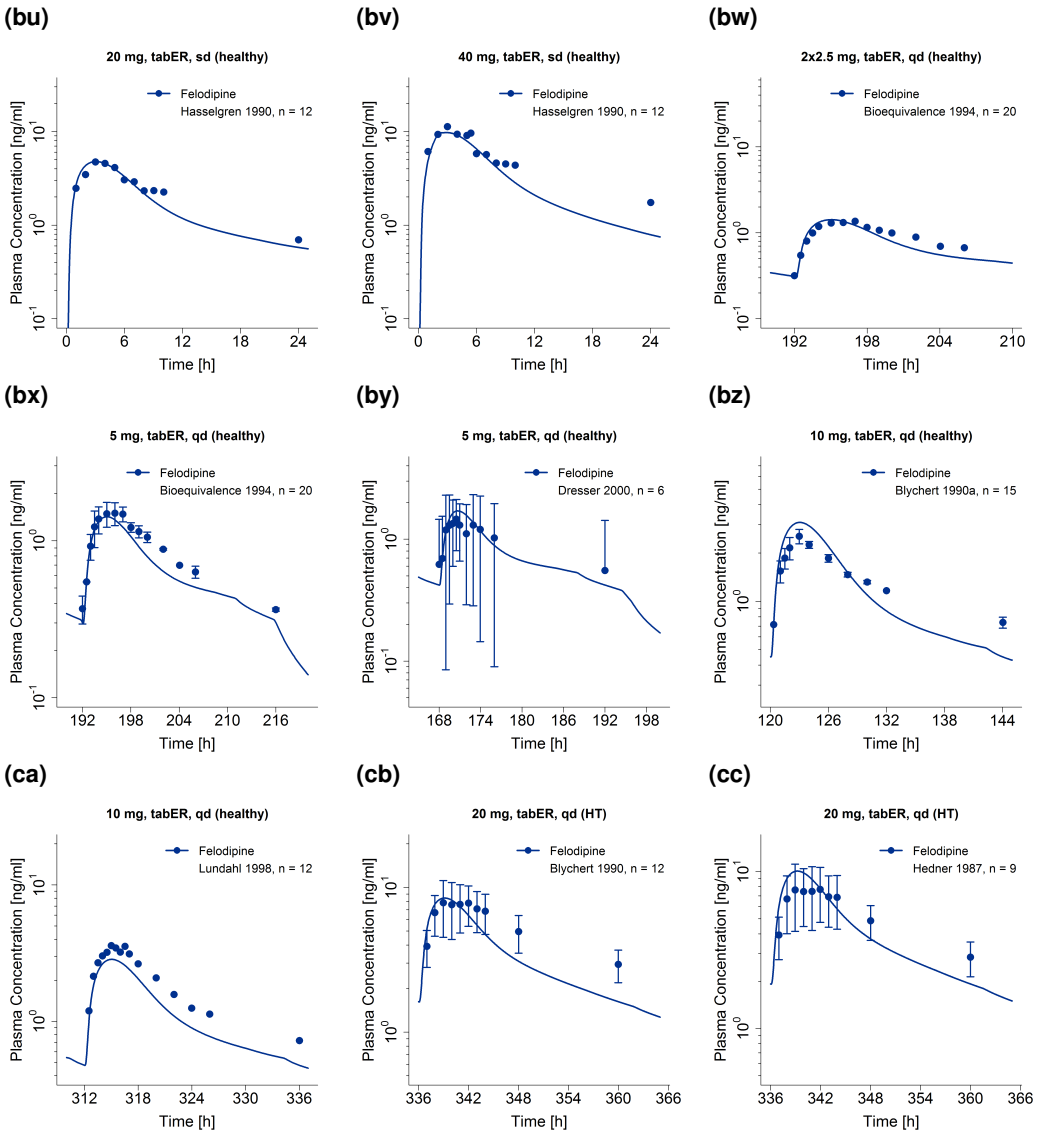

Figure S3: Predicted compared to observed felodipine and dehydrofelodipine plasma concentration-time profiles (semi-logarithmic) after intravenous and oral administration of felodipine. Observed data are shown as dots and triangles ± standard deviation; model predictions are shown as solid lines. Details on dosing regimens, study populations and literature references are listed in Table S1. bid: twice daily, HT: hypertension, iv: intravenous, md: multiple dose, n: number of individuals, qd: once daily, RI: renal impairment, sol: solution, sd: single dose, tab: tablet, tabER: extended release tablet. *(continued)*

2.4.3 Dissolution-time profile

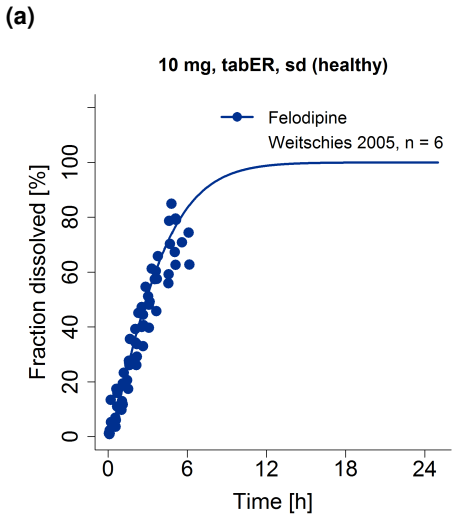

Figure S4: Predicted compared to observed dissolution-time profiles after administration of 10 mg felodipine as extended release tablet. Observed data are shown as dots; the model prediction is shown as solid line. Details on dosing regimen, study population and literature reference are listed in Table S1. n: number of individuals, sd: single dose, tabER: extended release tablet

2.5 Model evaluation

2.5.1 Plasma concentration goodness-of-fit plots

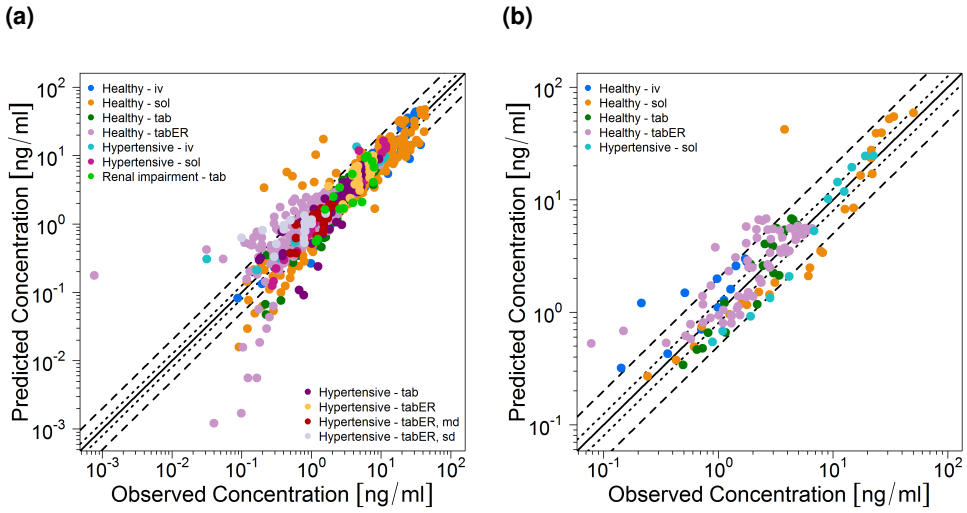

Figure S5: Predicted compared to observed plasma concentrations of (a) felodipine and (b) dehydrofelodipine. The solid line marks the line of identity. Dotted lines indicate 1.25-fold, dashed lines indicate 2-fold deviation. iv: intravenous, sol: solution, tab: tablet, tabER: extended release tablet.

2.5.2 Mean relative deviation of predicted plasma concentrations

Table S3: Mean relative deviation values of predicted plasma concentrations of felodipine and dehydrofelodipine

Compound	Felodipine route	Felodipine dose [mg]	MRD	Reference
Felodipine	iv (20 min)	1	1.23	Bengtsson 1988 [6]
Felodipine	iv (20 min)	1	1.82	Edgar 1987 [7]
Felodipine	iv (15 min)	1	1.39	Edgar 1989 [49]
Felodipine	iv (30 min)	1	1.32	Sutfin 1990 [8]
Felodipine	iv (150 min)	1.5	1.19	Sluiter 1985 [9]
Felodipine	iv (60 min)	1.5	1.26	Lundahl 1997 [10]
Dehydrofelodipine	iv (60 min)	1.5	2.06	Lundahl 1997 [10]
Felodipine	iv (105 - 120 min)	2.25	1.89	Blychert 1990 [50]
Felodipine	iv (30 min)	2.5	1.71	Edgar 1985 [11]
Felodipine	iv (30 min)	2.5	1.26	Edgar 1985a [12]
Felodipine	iv (20 min)	3	1.24	Bengtsson 1988 [6]
Felodipine	iv (20 min)	3	1.66	Edgar 1987 [7]
Felodipine	po (sol), sd	0.83	1.67	Edgar 1985 [11]
Felodipine	po (sol), sd	5	1.29	Bengtsson 1988 [6]
Felodipine	po (sol), sd	5	1.83	Edgar 1987 [7]
Felodipine	po (sol), sd	8.3	1.19	Edgar 1985 [11]
Felodipine	po (sol), sd	10	1.67	Abrahamsson 1994 [13]
Felodipine	po (sol), sd	10	1.14	Bengtsson 1990 [14]
Felodipine	po (sol), sd	10	1.57	Edgar 1987a [15]
Felodipine	po (sol), sd	10	1.28	Wingstrand 1990 [16]
Felodipine	po (sol), sd	10	1.36	Edgar 1989 [49]
Dehydrofelodipine	po (sol), sd	10	1.56	Edgar 1989 [49]
Felodipine	po (sol), sd	10.35	2.49	Johnsson 1983 [18]
Felodipine	po (sol), sd	15	1.15	Bengtsson 1988 [6]
Felodipine	po (sol), sd	15	1.42	Edgar 1987 [7]
Felodipine	po (sol), sd	20	1.72	Soons 1990 [4]
Dehydrofelodipine	po (sol), sd	20	1.74	Soons 1990 [4]
R-Felodipine	po (sol), sd	20	2.26	Soons 1990 [4]
S-Felodipine	po (sol), sd	20	1.89	Soons 1990 [4]
Felodipine	po (sol), sd	20	2.67	Soons 1993 [19]
Dehydrofelodipine	po (sol), sd	20	2.15	Soons 1993 [19]
R-Felodipine	po (sol), sd	20	2.69	Soons 1993 [19]
S-Felodipine	po (sol), sd	20	1.88	Soons 1993 [19]
Felodipine	po (sol), sd	27.5	1.57	Edgar 1985 [11]
Felodipine	po (sol), sd	27.5	1.93	Edgar 1985a [12]
Felodipine	po (sol), sd	40	1.13	Bengtsson 1988 [6]
Felodipine	po (sol), sd	40	1.20	Edgar 1987 [7]
Felodipine	po (sol), md	10	1.67	Blychert 1990a [17]
Felodipine	po (tab), sd	5	1.19	Bailey 1993 [20]
Dehydrofelodipine	po (tab), sd	5	1.51	Bailey 1993 [20]
Felodipine	po (tab), sd	5	1.12	Edgar 1992 [21]
Dehydrofelodipine	po (tab), sd	5	1.43	Edgar 1992 [21]
Felodipine	po (tab), sd	10	1.34	Edgar 1987a [15]
Felodipine	po (tab), sd	10	1.23	Guo 2007 [24]
Felodipine	po (tab), sd	10	1.31	Hardy 1988 [26]
Felodipine	po (tab), sd	10	2.03	Larsson 1990 [51]
Felodipine	po (tab), sd	10	1.90	Larsson 1990 [51]
Felodipine	po (tab), bid	5	2.07	Landahl 1988 [22]
Felodipine	po (tab), bid	5	1.39	Landahl 1988 [22]
Felodipine	po (tab), bid	10	1.67	Blychert 1990a [17]
Felodipine	po (tab), qd	10	1.70	Blychert 1990a [17]

bid: twice daily, iv: intravenous, MRD: mean relative deviation, po: oral, qd: once daily, sd: single dose, sol: solution, tab: tablet, tabER: extended release tablet

Table S3: Mean relative deviation values of predicted plasma concentrations of felodipine and dehydrofelodipine *(continued)*

Compound	Felodipine route	Felodipine dose [mg]	MRD	Reference
Felodipine	po (tab), bid	10	1.81	Hedner 1986 [54]
Felodipine	po (tab), bid	10	1.28	Hedner 1987 [52]
Felodipine	po (tab), bid	10	1.41	Larsson 1990 [51]
Felodipine	po (tab), bid	10	1.67	Larsson 1990 [51]
Felodipine	po (tab), bid	10	1.58	Smith 1987 [48]
Felodipine	po (tabER), sd	5	2.82	Aguilar-Carrasco 2015 [29]
Felodipine	po (tabER), sd	5	2.13	Dresser 2000 [27]
Felodipine	po (tabER), sd	5	1.60	Goosen 2004 [30]
Felodipine	po (tabER), sd	5	1.24	Jalava 1997 [28]
Felodipine	po (tabER), sd	5	4.39	Xiang 2017 [31]
Felodipine	po (tabER), sd	5	1.87	Leenen 2010 [53]
Felodipine	po (tabER), sd	5	2.10	Leenen 2010 [53]
Felodipine	po (tabER), sd	10	1.64	Bailey 1995 [33]
Felodipine	po (tabER), sd	10	2.20	Bailey 2000 [37]
Felodipine	po (tabER), sd	10	1.91	Bailey 2003 [38]
Felodipine	po (tabER), sd	10	1.29	Dresser 2017 [39]
Felodipine	po (tabER), sd	10	1.35	Edgar 1987a [15]
Felodipine	po (tabER), sd	10	1.29	Hasselgren 1990 [40]
Felodipine	po (tabER), sd	10	1.48	Lown 1997 [41]
Felodipine	po (tabER), sd	10	1.13	Lundahl 1998 [43]
Felodipine	po (tabER), sd	10	2.61	Patel 2011 [47]
Felodipine	po (tabER), sd	10	1.78	Pop 2008 [44]
Felodipine	po (tabER), sd	10	5.36	Weitschies 2005 [46]
Felodipine	po (tabER), sd	10	1.36	Bailey 1996 [35]
Felodipine	po (tabER), sd	10	1.57	Bailey 1998 [36]
Dehydrofelodipine	po (tabER), sd	10	1.18	Bailey 1998 [36]
Felodipine	po (tabER), sd	10	1.93	Gelal 2005 [45]
Dehydrofelodipine	po (tabER), sd	10	2.56	Gelal 2005 [45]
Felodipine	po (tabER), sd	10	1.55	Lundahl 1995 [42]
Dehydrofelodipine	po (tabER), sd	10	1.29	Lundahl1995 [42]
Felodipine	po (tabER), sd	10	1.25	Lundahl 1997 [10]
Dehydrofelodipine	po (tabER), sd	10	1.17	Lundahl 1997 [10]
Felodipine	po (tabER), sd	10	2.30	Madsen 1996 [34]

bid: twice daily, iv: intravenous, MRD: mean relative deviation, po: oral, qd: once daily, sd: single dose, sol: solution, tab: tablet, tabER: extended release tablet

Table S3: Mean relative deviation values of predicted plasma concentrations of felodipine and dehydrofelodipine *(continued)*

Compound	Felodipine route	Felodipine dose [mg]	MRD	Reference
Dehydrofelodipine	po (tabER), sd	10	2.00	Madsen 1996 [34]
R-Felodipine	po (tabER), sd	10	2.00	Lindmark 2002 [25]
S-Felodipine	po (tabER), sd	10	2.01	Lindmark 2002 [25]
Felodipine	po (tabER), sd	20	1.44	Blychert 1990 [50]
Felodipine	po (tabER), sd	20	1.19	Hasselgren 1990 [40]
Felodipine	po (tabER), sd	40	1.35	Hasselgren 1990 [40]
Felodipine	po (tabER), qd	5	1.19	Bioequivalence 1994 [32]
Felodipine	po (tabER), qd	5	1.20	Bioequivalence 1994 [32]
Felodipine	po (tabER), qd	5	1.23	Dresser 2000 [27]
Felodipine	po - tabER, md	5	1.25	Leenen 2010 [53]
Felodipine	po - tabER, md	5	1.48	Leenen 2010 [53]
Felodipine	po (tabER), qd	10	1.30	Blychert 1990a [17]
Felodipine	po (tabER), qd	10	1.31	Lundahl 1998 [43]
Felodipine	po (tabER), qd	20	1.35	Blychert 1990 [50]
Felodipine	po (tabER), qd	20	1.30	Hedner 1987 [52]
MRD (Felodipine)			**1.64 (1.12-5.36)**	
MRD (Dehydrofelodipine)			**1.70 (1.17-2.56)**	
MRD (Enantiomers)			**2.12 (1.88-2.69)**	
MRD (total)			**1.67 (1.12-5.36)**	
			79/99 with MRD < 2	

bid: twice daily, iv: intravenous, MRD: mean relative deviation, po: oral, qd: once daily, sd: single dose, sol: solution, tab: tablet, tabER: extended release tablet

2.5.3 AUC_{last} and C_{max} goodness-of-fit plots

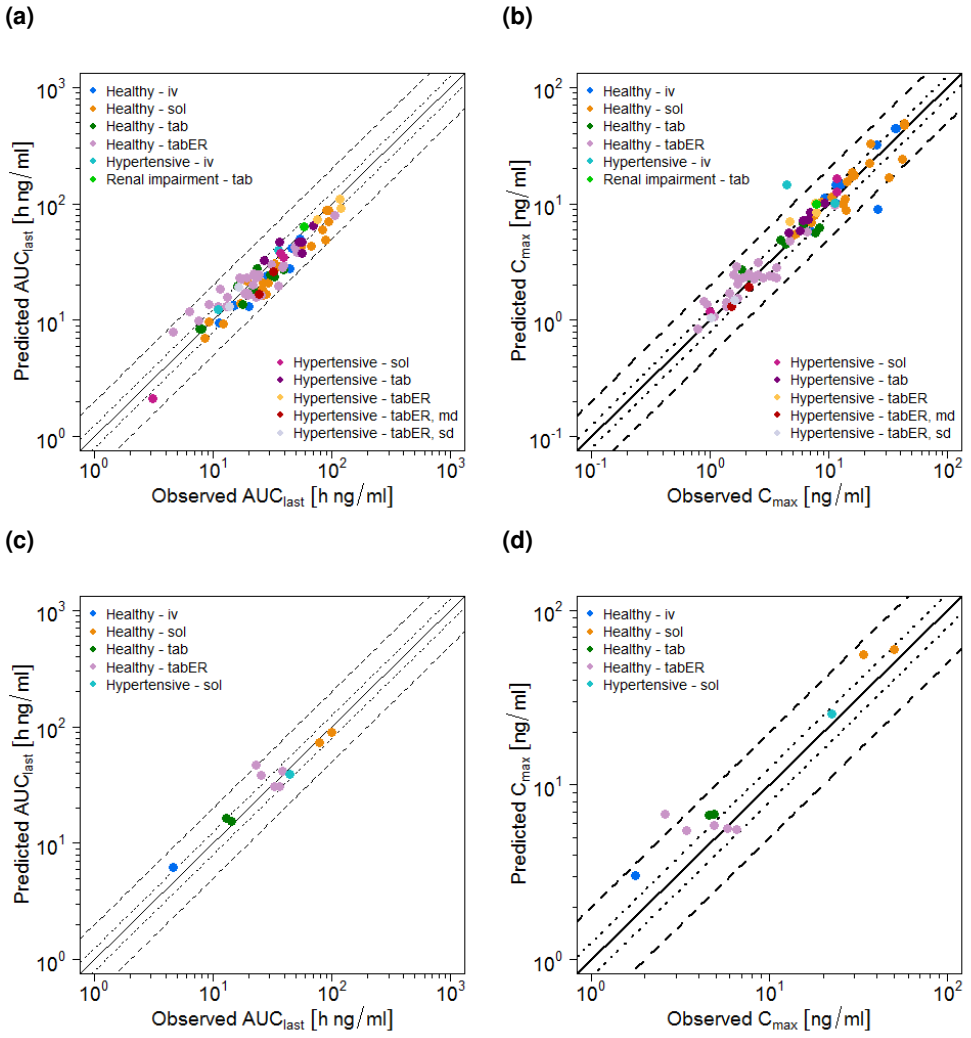

Figure S6: Predicted compared to observed AUC_{last} and C_{max} values of (a,b) felodipine and (c,d) dehydrofelodipine. The solid line marks the line of identity. Dotted lines indicate 1.25-fold, dashed lines indicate 2-fold deviation. AUC_{last}: area under the plasma concentration-time curve from the time of drug administration to the last concentration measurement, C_{max}: maximum plasma concentration, iv: intravenous, sol: solution, tab: tablet, tabER: extended release tablet.

2.5.4 Geometric mean fold error of predicted AUC_{last} and C_{max} values

Table S4: Predicted and observed AUC_{last} and C_{max} values with geometric mean fold errors of felodipine and dehydrofelodipine

			AUC_{last} $[\frac{h \cdot ng}{ml}]$			C_{max} $\frac{ng}{ml}$			
Compound	**Felodipine route**	**Felodipine dose**	**Pred**	**Obs**	**Pred/Obs**	**Pred**	**Obs**	**Pred/Obs**	**Reference**
Felodipine	iv (20 min)	1	13.51	14.68	0.92	14.69	11.53	1.27	Bengtsson 1988 [6]
Felodipine	iv (20 min)	1	13.24	20.09	0.66	14.54	12.53	1.16	Edgar 1987 [7]
Felodipine	iv (15 min)	1	12.25	11.14	1.10	14.46	4.46	3.25	Edgar 1989 [49]
Felodipine	iv (30 min)	1	13.41	15.05	0.89	11.10	9.16	1.21	Sutfin 1990 [8]
Felodipine	iv (150 min)	1.5	9.49	11.34	0.84	5.88	6.97	0.84	Sluiter 1985 [9]
Felodipine	iv (60 min)	1.5	24.01	28.34	0.85	10.12	11.52	0.88	Lundahl 1997 [10]
Dehydrofelodipine	iv (60 min)	1.5	6.17	4.57	1.35	3.04	1.77	1.72	Lundahl 1997 [10]
Felodipine	iv (105 - 120 min)	2.25	39.95	35.79	1.12	10.03	11.33	0.89	Blychert 1990 [50]
Felodipine	iv (30 min)	2.5	27.73	44.48	0.62	8.97	25.61	0.35	Edgar 1985 [11]
Felodipine	iv (30 min)	2.5	49.76	53.54	0.93	31.78	25.45	1.25	Edgar 1985a [12]
Felodipine	iv (20 min)	3	41.18	46.19	0.89	44.16	35.89	1.23	Bengtsson 1988 [6]
Felodipine	iv (20 min)	3	39.02	51.62	0.76	43.77	36.93	1.19	Edgar 1987 [7]
Felodipine	po (sol), sd	0.83	2.12	3.07	0.69	1.19	1.00	1.19	Edgar 1985 [11]
Felodipine	po (sol), sd	5	9.70	9.16	1.06	5.37	5.13	1.05	Bengtsson 1988 [6]
Felodipine	po (sol), sd	5	9.31	12.25	0.76	5.55	5.29	1.05	Edgar 1987 [7]
Felodipine	po (sol), sd	8.3	34.82	39.55	0.88	12.72	11.75	1.08	Edgar 1985 [11]
Felodipine	po (sol), sd	10	16.50	26.15	0.63	9.87	13.20	0.75	Abrahamsson 1994[13]
Felodipine	po (sol), sd	10	7.05	8.52	0.83	6.88	7.18	0.96	Bengtsson 1990 [14]
Felodipine	po (sol), sd	10	18.61	25.76	0.72	10.30	8.63	1.19	Edgar 1987a [15]
Felodipine	po (sol), sd	10	20.96	26.53	0.79	10.95	13.57	0.81	Wingstrand 1990[16]
Felodipine	po (sol), sd	10	37.62	36.65	1.03	16.41	11.75	1.40	Edgar 1989 [49]
Dehydrofelodipine	po (sol), sd	10	38.85	44.19	0.88	25.54	22.48	1.14	Edgar 1989 [49]
Felodipine	po (sol), sd	10.35	21.87	19.14	1.14	18.62	15.73	1.18	Johnsson 1983[18]
Felodipine	po (sol), sd	15	30.40	32.90	0.92	17.13	15.65	1.09	Bengtsson 1988[6]
Felodipine	po (sol), sd	15	28.63	35.30	0.81	17.50	16.43	1.07	Edgar 1987 [7]
Felodipine	po (sol), sd	20	42.08	55.35	0.76	22.07	22.11	1.00	Soons 1990 [4]
Dehydrofelodipine	po (sol), sd	20	72.60	79.22	0.92	55.48	33.80	1.64	Soons 1990 [4]
R-Felodipine	po (sol), sd	20	14.07	17.10	0.82	8.00	7.55	1.06	Soons 1990 [4]
S-Felodipine	po (sol), sd	20	35.73	37.97	0.94	15.42	14.17	1.09	Soons 1990 [4]
Felodipine	po (sol), sd	20	48.79	88.45	0.55	24.34	41.70	0.58	Soons 1993 [19]

AUC_{last}: area under the plasma concentration-time curve calculated from the time of drug administration to the time of the last concentration measurement, bid: twice daily, C_{max}: maximum plasma concentration, GMFE: geometric mean fold error, iv: intravenous, obs: observed, pred: predicted, po: oral, qd: once daily, sd: single dose, sol: solution, tab: tablet, tabER: extended release tablet

Table S4: Predicted and observed AUC_{last} and C_{max} values with geometric mean fold errors of felodipine and dehydrofelodipine *(continued)*

			AUC_{last} $[\frac{h \cdot ng}{ml}]$			C_{max} $\frac{ng}{ml}$			
Compound	**Felodipine route**	**Felodipine dose**	**Pred**	**Obs**	**Pred/Obs**	**Pred**	**Obs**	**Pred/Obs**	**Reference**
Dehydrofelodipine	po (sol), sd	20	89.59	98.76	0.91	59.32	50.36	1.18	Soons 1993 [19]
R-Felodipine	po (sol), sd	20	16.60	28.01	0.59	8.83	14.08	0.63	Soons 1993 [19]
S-Felodipine	po (sol), sd	20	43.67	67.13	0.65	16.84	32.21	0.52	Soons 1993 [19]
Felodipine	po (sol), sd	27.5	60.32	83.46	0.72	32.70	22.31	1.47	Edgar 1985 [11]
Felodipine	po (sol), sd	27.5	70.19	93.20	0.75	32.70	22.59	1.45	Edgar 1985a [12]
Felodipine	po (sol), sd	40	86.91	90.82	0.96	46.99	43.21	1.09	Bengtsson 1988 [6]
Felodipine	po (sol), sd	40	87.16	93.48	0.93	48.90	42.79	1.14	Edgar 1987 [7]
Felodipine	po (sol), md	10	20.75	29.35	0.71	11.52	10.63	1.08	Blychert 1990a [17]
Felodipine	po (tab), sd	5	8.46	7.97	1.06	2.34	2.46	0.95	Bailey 1993 [20]
Dehydrofelodipine	po (tab), sd	5	15.58	14.24	1.09	6.72	4.59	1.47	Bailey 1993 [20]
Felodipine	po (tab), sd	5	8.47	7.75	1.09	2.35	2.11	1.11	Edgar 1992 [21]
Dehydrofelodipine	po (tab), sd	5	16.54	12.95	1.28	6.83	4.89	1.40	Edgar 1992 [21]
Felodipine	po (tab), sd	10	19.67	16.14	1.22	4.87	3.94	1.24	Edgar 1987a [15]
Felodipine	po (tab), sd	10	27.77	23.67	1.17	6.78	6.13	1.11	Guo 2007 [24]
Felodipine	po (tab), sd	10	18.60	21.76	0.85	4.54	4.35	1.04	Hardy 1988 [26]
Felodipine	po (tab), sd	10	32.63	26.75	1.22	5.91	5.70	1.04	Larsson 1990 [51]
Felodipine	po (tab), sd	10	46.50	36.14	1.29	8.43	6.97	1.21	Larsson 1990 [51]
Felodipine	po (tab), bid	5	13.65	17.69	0.77	2.72	1.84	1.48	Landahl 1988 [22]
Felodipine	po (tab), bid	5	46.45	56.27	0.83	5.67	4.64	1.22	Landahl 1988 [22]
Felodipine	po (tab), bid	10	23.51	33.07	0.71	5.91	6.45	0.92	Blychert 1990a [17]
Felodipine	po (tab), qd	10	24.48	30.50	0.80	5.60	7.72	0.73	Blychert 1990a [17]
Felodipine	po (tab), bid	10	37.86	55.95	0.68	7.28	6.73	1.08	Hedner 1986 [54]
Felodipine	po (tab), bid	10	65.28	69.52	0.94	10.07	9.29	1.08	Hedner 1987 [52]
Felodipine	po (tab), bid	10	47.19	52.40	0.90	7.10	6.09	1.17	Larsson 1990 [51]
Felodipine	po (tab), bid	10	63.28	58.02	1.09	9.86	7.93	1.24	Larsson 1990 [51]
Felodipine	po (tab), bid	10	27.20	39.09	0.70	6.24	8.30	0.75	Smith 1987 [48]
Felodipine	po (tabER), sd	5	15.68	22.89	0.68	1.32	1.37	0.97	Aguilar-Carrasco 2015 [29]
Felodipine	po (tabER), sd	5	7.92	4.65	1.70	1.36	0.95	1.44	Dresser 2000 [27]
Felodipine	po (tabER), sd	5	15.79	13.10	1.21	1.46	0.89	1.65	Goosen 2004 [30]
Felodipine	po (tabER), sd	5	16.30	19.76	0.82	1.07	1.07	0.99	Jalava 1997 [28]
Felodipine	po (tabER), sd	5	19.48	35.60	0.55	1.54	1.70	0.90	Xiang 2017 [31]
Felodipine	po (tabER), md	5	19.26	16.31	1.18	1.47	1.61	0.91	Leenen 2010 [53]
Felodipine	po (tabER), md	5	13.15	13.86	0.95	1.04	1.01	1.03	Leenen 2010 [53]

AUC_{last}: area under the plasma concentration-time curve calculated from the time of drug administration to the time of the last concentration measurement, bid: twice daily, C_{max}: maximum plasma concentration, GMFE: geometric mean fold error, iv: intravenous, obs: observed, pred: predicted, po: oral, qd: once daily, sd: single dose, sol: solution, tab: tablet, tabER: extended release tablet

Table S4: Predicted and observed AUC_{last} and C_{max} values with geometric mean fold errors of felodipine and dehydrofelodipine *(continued)*

			AUC_{last} $[\frac{h \cdot ng}{ml}]$			C_{max} $\frac{ng}{ml}$			
Compound	**Felodipine route**	**Felodipine dose**	**Pred**	**Obs**	**Pred/Obs**	**Pred**	**Obs**	**Pred/Obs**	**Reference**
Felodipine	po (tabER), sd	10	23.72	23.46	1.01	2.33	2.83	0.82	Bailey 1995 [33]
Felodipine	po (tabER), sd	10	13.78	9.24	1.49	2.38	1.98	1.20	Bailey 2000 [37]
Felodipine	po (tabER), sd	10	13.05	11.06	1.18	2.25	2.34	0.96	Bailey 2003 [38]
Felodipine	po (tabER), sd	10	13.19	12.91	1.02	2.28	2.34	0.97	Dresser 2017 [39]
Felodipine	po (tabER), sd	10	17.04	18.51	0.92	2.39	2.48	0.96	Edgar 1987a [15]
Felodipine	po (tabER), sd	10	23.59	23.83	0.99	2.39	2.10	1.14	Hasselgren 1990 [40]
Felodipine	po (tabER), sd	10	22.99	19.15	1.20	2.27	1.75	1.30	Lown 1997 [41]
Felodipine	po (tabER), sd	10	24.56	24.43	1.01	2.43	2.53	0.96	Lundahl 1998 [43]
Felodipine	po (tabER), sd	10	38.26	50.33	0.76	5.74	6.57	0.87	Patel 2011 [47]
Felodipine	po (tabER), sd	10	28.43	38.21	0.74	2.39	3.17	0.75	Pop 2008 [44]
Felodipine	po (tabER), sd	10	11.90	6.33	1.88	2.48	1.58	1.57	Weitschies 2005 [46]
Felodipine	po (tabER), sd	10	23.20	22.78	1.02	2.33	2.82	0.83	Bailey 1996 [35]
Dehydrofelodipine	po (tabER), sd	10	38.76	40.97	0.95	5.59	6.59	0.85	Bailey 1996 [35]
Felodipine	po (tabER), sd	10	17.06	19.78	0.86	2.33	3.59	0.65	Bailey 1998 [36]
Dehydrofelodipine	po (tabER), sd	10	30.83	32.78	0.94	5.59	6.56	0.85	Bailey 1998 [36]
Felodipine	po (tabER), sd	10	18.64	11.59	1.61	2.89	1.67	1.73	Gelal 2005 [45]
Dehydrofelodipine	po (tabER), sd	10	47.05	22.95	2.05	6.81	2.61	2.61	Gelal 2005 [45]
Felodipine	po (tabER), sd	10	16.54	25.53	0.65	2.34	3.42	0.68	Lundahl 1995 [42]
Dehydrofelodipine	po (tabER), sd	10	30.97	36.52	0.85	5.63	5.77	0.98	Lundahl1995 [42]
Felodipine	po (tabER), sd	10	25.10	22.14	1.13	2.49	2.13	1.17	Lundahl 1997 [10]
Dehydrofelodipine	po (tabER), sd	10	41.50	38.38	1.08	5.88	4.91	1.20	Lundahl 1997 [10]
Felodipine	po (tabER), sd	10	23.19	16.72	1.39	2.29	1.88	1.22	Madsen 1996 [34]
Dehydrofelodipine	po (tabER), sd	10	38.31	25.63	1.49	5.52	3.43	1.61	Madsen 1996 [34]
R-Felodipine	po (tabER), sd	10	9.87	7.62	1.30	0.83	0.79	1.06	Lindmark 2002 [25]
S-Felodipine	po (tabER), sd	10	22.02	17.03	1.29	1.99	1.72	1.16	Lindmark 2002 [25]
Felodipine	po (tabER), sd	20	74.06	75.87	0.98	7.07	4.70	1.50	Blychert 1990 [50]
Felodipine	po (tabER), sd	20	42.22	48.54	0.87	4.78	4.73	1.01	Hasselgren 1990 [40]
Felodipine	po (tabER), sd	40	79.78	105.95	0.75	9.73	11.27	0.86	Hasselgren 1990 [40]
Felodipine	po (tabER), qd	5	16.58	18.68	0.89	1.42	1.37	1.04	Bioequivalence 1994 [32]
Felodipine	po (tabER), qd	5	16.59	19.52	0.85	1.42	1.50	0.95	Bioequivalence 1994 [32]
Felodipine	po (tabER), qd	5	19.88	21.58	0.92	1.71	1.46	1.17	Dresser 2000 [27]
Felodipine	po (tabER), md	5	25.88	32.24	0.80	1.92	2.11	0.91	Leenen 2010[53]
Felodipine	po (tabER), md	5	16.83	24.46	0.69	1.31	1.50	0.87	Leenen 2010[53]

AUC_{last}: area under the plasma concentration-time curve calculated from the time of drug administration to the time of the last concentration measurement, bid: twice daily, C_{max}: maximum plasma concentration, GMFE: geometric mean fold error, iv: intravenous, obs: observed, pred: predicted, po: oral, qd: once daily, sd: single dose, sol: solution, tab: tablet, tabER: extended release tablet

Table S4: Predicted and observed AUC_{last} and C_{max} values with geometric mean fold errors of felodipine and dehydrofelodipine *(continued)*

			AUC_{last} $[\frac{h \cdot ng}{ml}]$			C_{max} $\frac{ng}{ml}$			
Compound	**Felodipine route**	**Felodipine dose**	**Pred**	**Obs**	**Pred/Obs**	**Pred**	**Obs**	**Pred/Obs**	**Reference**
Felodipine	po (tabER), qd	10	30.28	31.24	0.97	3.11	2.55	1.22	Blychert 1990a [17]
Felodipine	po (tabER), qd	10	29.21	39.09	0.75	2.85	3.59	0.79	Lundahl 1998 [43]
Felodipine	po (tabER), qd	20	90.55	119.93	0.75	8.44	7.84	1.08	Blychert 1990 [50]
Felodipine	po (tabER), qd	20	108.61	117.57	0.92	10.06	7.69	1.31	Hedner 1987 [52]
GMFE (Felodipine)					**1.25 (1.01-1.88)**			**1.25 (1.00-3.25)**	
GMFE (Dehydrofelodipine)					**1.25 (1.06-2.05)**			**1.44 (1.03-2.61)**	
GMFE (Enantiomers)					**1.35 (1.06-1.69)**			**1.32 (1.06-1.91)**	
GMFE (total)					**1.26 (1.01-2.05)**			**1.28 (1.00-3.25)**	
					99/100 with GMFE < 2			**97/100 with GMFE < 2**	

AUC_{last}: area under the plasma concentration-time curve calculated from the time of drug administration to the time of the last concentration measurement, bid: twice daily, C_{max}: maximum plasma concentration, GMFE: geometric mean fold error, iv: intravenous, obs: observed, pred: predicted, po: oral, qd: once daily, sd: single dose, sol: solution, tab: tablet, tabER: extended release tablet

2.5.5 Sensitivity analysis

Sensitivity of the felodipine PBPK model to single parameters (local sensitivity analysis) was calculated as the relative change of the predicted felodipine and dehydrofelodipine (1) AUC from 0-24 h (AUC_{0-24}) after 1.5 mg of felodipine as intravenous infusion and (2) AUC at steady-state (AUC_{ss}) after 5 mg of felodipine once daily as extended release tablet. Parameters were included into the analysis if they were optimized (*Felodipine*: solubility tabER, intestinal permeability, k_{cat} CYP3A4, Weibull parameters [dissolution shape and dissolution time 50%]; *Dehydrofelodipine*: fraction unbound, lipophilicity, CL_{hep} and CL_{CYP3A4}), if they are associated with optimized parameters (*Felodipine*: K_m) or if they might have a strong impact due to calculation methods used in the model (*Felodipine*: fraction unbound, solubility, lipophilicity, GFR fraction; *Dehydrofelodipine*: GFR fraction). Results of the sensitivity analysis are illustrated in Figures S7 and S8. Sensitivity analyses of the felodipine parent-metabolite PBPK model revealed that the felodipine AUC_{0-24} after intravenous administration and AUC_{ss} after oral administration are mainly sensitive to felodipine lipophilicity, fraction unbound in plasma and K_m and k_{cat} of CYP3A4. Dehydrofelodipine AUC_{0-24} after intravenous administration of felodipine and AUC_{ss} after oral administration of felodipine are mainly sensitive to dehydrofelodipine fraction unbound in plasma, CYP3A4 clearance and lipophilicity.

(a)

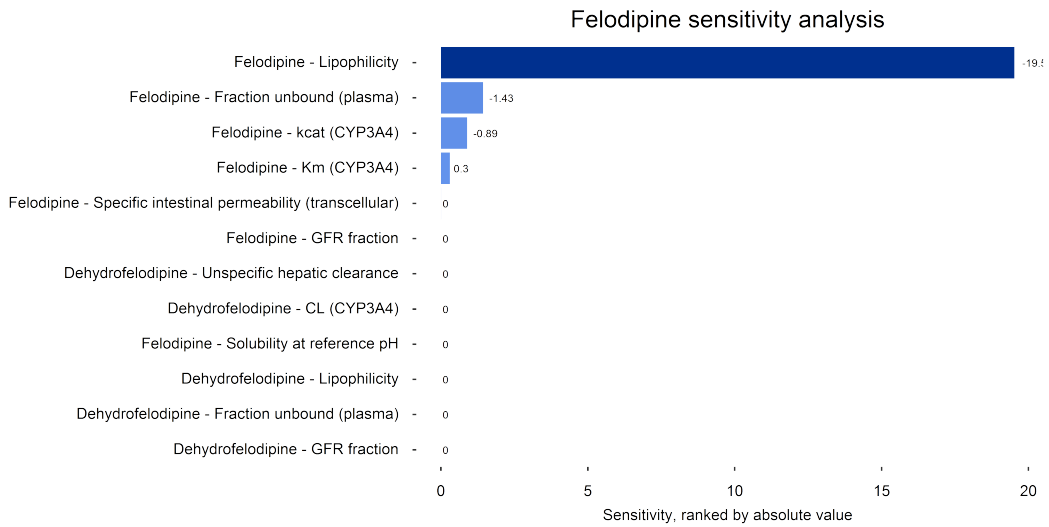

(b)

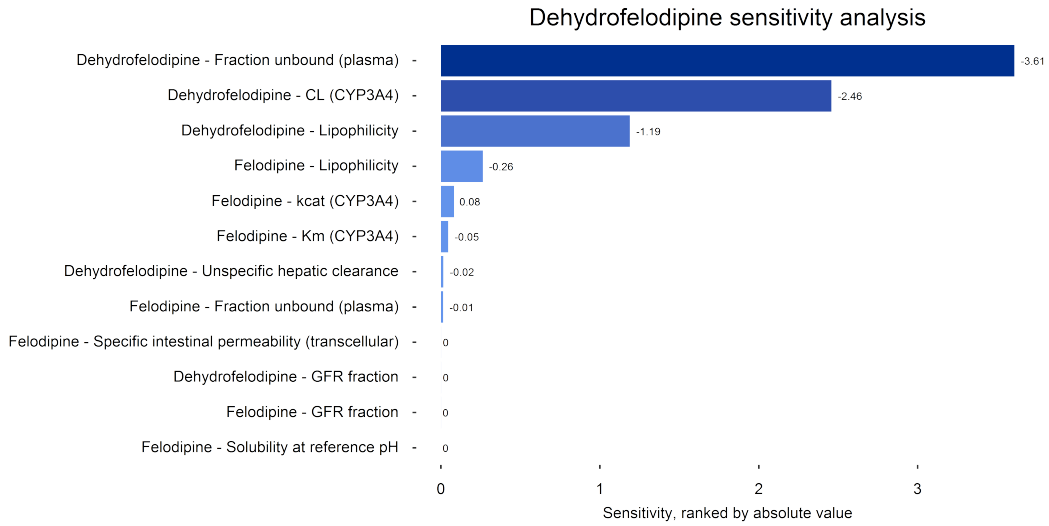

Figure S7: Felodipine parent-metabolite PBPK model sensitivity analysis for intravenous felodipine administration. Sensitivity of the felodipine PBPK model to single parameters, calculated as change of (a) the simulated felodipine $AUC_{0\text{-}24}$ and (b) the simulated dehydrofelodipine $AUC_{0\text{-}24}$ after administration of 1.5 mg felodipine as intravenous infusion. CL: clearance, CYP: cytochrome P450, GFR: glomerular filtration rate, k_{cat}: catalytic rate constant, K_m: Michaelis-Menten constant

(a)

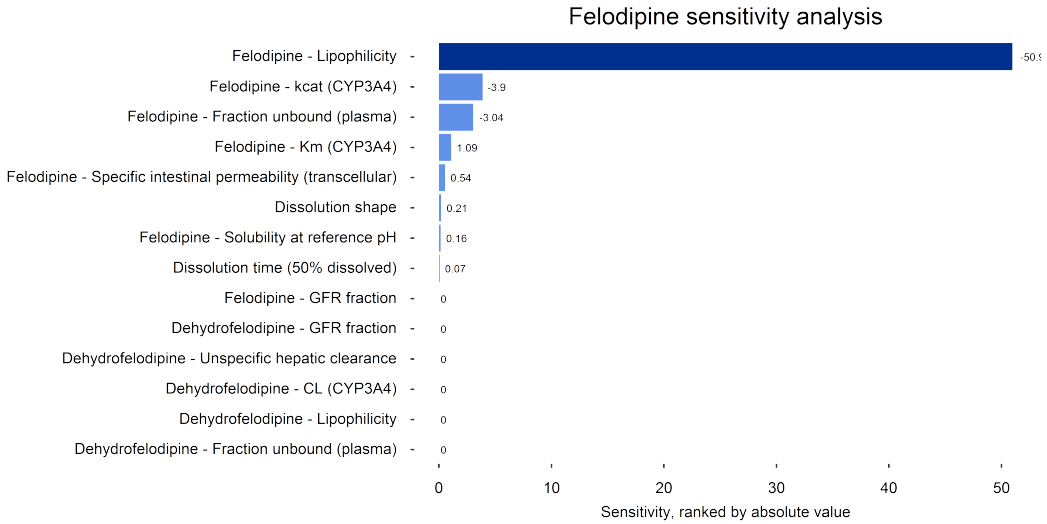

(b)

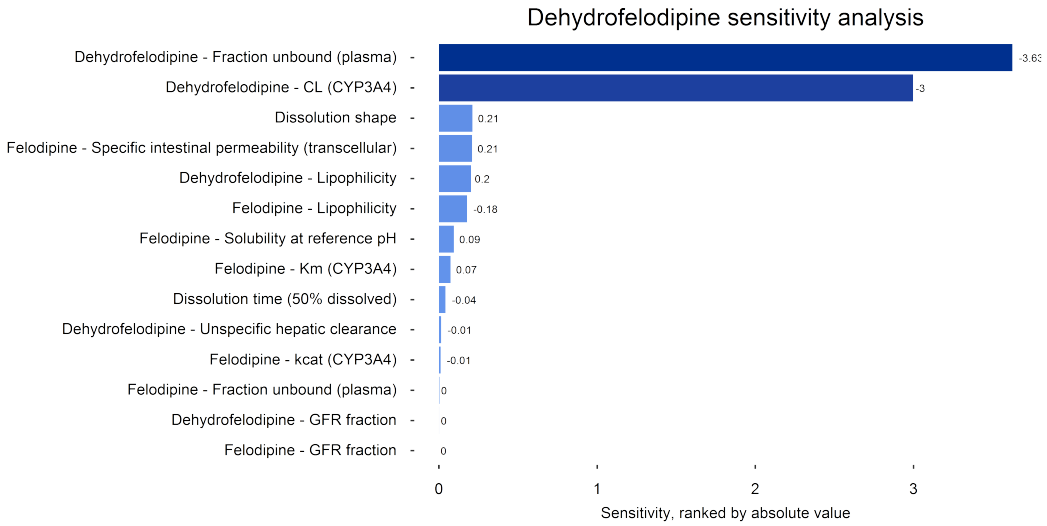

Figure S8: Felodipine parent-metabolite PBPK model sensitivity analysis for oral felodipine administration. Sensitivity of the felodipine PBPK model to single parameters, calculated as change of (a) the simulated felodipine AUC_{ss} and (b) the simulated dehydrofelodipine AUC_{ss} after administration of 5 mg of felodipine once daily as extended release tablet. CL: clearance, CYP: cytochrome P450, GFR: glomerular filtration rate, k_{cat}: catalytic rate constant, K_m: Michaelis-Menten constant

3 Felodipine - pharmacodynamic modeling

3.1 PD model building

The PD model extension describes the circadian rhythm of blood pressure and heart rate using models from Chae et al. [2] and Lott et al. [3], respectively. Circadian model parameters were optimized for each study individually, as described in Section 1. Table S5 displays optimized circadian parameters for blood pressure and heart rate for each study and indicates if placebo profiles were available. The effect of felodipine on blood pressure and heart rate was subsequently described using an E_{max} function. Parameters used in the final PD models are shown in Table S6 .

The performance of the felodipine PD model is demonstrated in linear plots of predicted compared to observed effect-time profiles in Figures S9 and S10 for blood pressure and heart rate, respectively. Goodness-of-fit plots are presented in Figure S11, corresponding MRD values are listed in Tables S7 and S8.

3.2 PD model parameters

Table S5: Optimized parameters of the circadian blood pressure and heart rate models

Dose	Route	BP_{mean}	$phase_{12,BP}$ [h]	$phase_{24,BP}$ [h]	placebo available	HR_{mean}	$phase_{HR}$	placebo available	Reference
Healthy									
1.5	iv (20min)	71.86	3.20	8.32	yes	62.18	17.31	yes	Sluiter 1985 [9]
5	po (sol), sd	68.54	0.89	6.01	yes	57.97	12.81	yes	Bengtsson 1988 [6]
5	po (sol), sd	69.57	0.95	6.07	yes	56.81	18.48	no	Edgar 1987 [7]
10	po (sol), sd	62.38	1.46	6.58	yes	56.06	12.47	yes	Bengtsson 1990 [14]
10.35	po (sol), sd	96.27	3.47	8.59	no	68.88	6.91	no	Johnsson 1983 [18]
15	po (sol), sd	68.54	0.89	6.01	yes	57.97	12.81	yes	Bengtsson 1988 [6]
15	po (sol), sd	69.57	0.95	6.07	yes	56.81	18.48	no	Edgar 1987 [7]
40	po (sol), sd	68.54	0.89	6.01	yes	57.97	12.81	yes	Bengtsson 1988 [6]
40	po (sol), sd	69.57	0.95	6.07	yes	56.81	18.48	no	Edgar 1987 [7]
10	po (tab), sd	-	-	-	-	79.03	6.68	no	Guo 2007
10	po (tab), sd	77.47	2.98	8.10	yes	77.46	8.65	yes	Hardy 1988 [26]
	po,tabER								
2.5; 5	D1-D2: 2.5 mg qd;	64.78	-0.04	5.08	no	67.11	14.54	no	Dresser 2000 [27]
	D3-8: 5 mg qd								
5	po (tabER), sd	67.42	-1.93	3.19	no	70.36	8.11	no	Jalava 1997 [28]
5	po (tabER), sd	67.42	-1.93	3.19	no	70.36	8.11	no	Jalava 1997 [28]
5	po (tabER), sd	69.5	-1.53	3.59	no	64.80	6.73	no	Dresser 2000 [27]
10	po (tabER), sd	70.81	2.18	7.3	yes	55.80	10.47	yes	Hasselgren 1990 [40]
10	po (tabER), sd	71.44	-4.42	0.70	no	62.79	0.98	no	Lundahl 1995 [42]
20	po (tabER), sd	70.81	2.18	7.3	yes	55.80	10.47	yes	Hasselgren 1990 [40]
40	po (tabER), sd	70.81	2.18	7.3	yes	55.80	10.47	yes	Hasselgren 1990 [40]
Hypertensive									
2.25	iv (15 min)	95.08	-0.71	4.41	yes	61.37	13.45	yes	Blychert 1990 [50]
0.83	po (sol), sd	77.50	-0.74	4.38	yes	-	-	-	Edgar 1985 [11]
8.3	po (sol), sd	77.50	-0.74	4.38	yes	-	-	-	Edgar 1985 [11]
10	po (tab), sd	88.63	-1.55	3.57	no	-	-	-	Larsson 1990 [51]
10	po (tab), sd	88.26	-1.59	3.53	no	-	-	-	Larsson 1990 [51]

assumed

- : no data available, bid: twice daily, BP_{mean}: mean blood pressure over 24 h, D: day, HR_{mean}: mean heart rate over 24 h, iv: intravenous, phase: circadian phase, po: oral, qd: once daily, sd: single dose, tab: tablet, tabER: extended release tablet

Table S5: Optimized parameters of the circadian blood pressure and heart rate models *(continued)*

Dose	Route	BP_{mean}	$phase_{12,BP}$ [h]	$phase_{24,BP}$ [h]	placebo available	HR_{mean}	$phase_{HR}$	placebo available	Reference
10	po (*tab*), D1: 10mg sd, D2-D6: 5mg bid, D7-D29: 10mg bid	88.63	-1.55	3.57	no	-	-	-	Larsson 1990 [51]
10	po (*tab*), D1: 10mg sd, D2-D6: 5mg bid, D7-D29: 10mg bid	88.26	-1.59	3.53	no	-	-	-	Larsson 1990 [51]
10	po (tab), bid	94.06	3.59	8.71	no	-	-	-	Hedner 1987 [52]
5; 10	D1-D14: po (*tab*), bid; D15-D28: po (*tab*), bid	87.70	-0.02	5.10	yes	66.13	13.63	yes	Hedner 1986 [54]
20	po (tabER), qd	97.16	2.60	7.72	no	-	-	-	Hedner 1987 [52]
20	po (tabER), sd	95.08	-0.71	4.41	yes	61.37	13.45	yes	Blychert 1990 [50]
20	po (tabER), qd	95.88	1.01	6.13	yes	60.92	15.24	yes	Blychert 1990 [50]

assumed

- : no data available, bid: twice daily, BP_{mean}: mean blood pressure over 24 h, D: day, HR_{mean}: mean heart rate over 24 h, iv: intravenous, phase: circadian phase, po: oral, qd: once daily, sd: single dose, tab: tablet, tabER: extended release tablet

Table S6: Drug-dependent parameter of the final felodipine diastolic blood pressure and heart rate PD model

Parameter	Unit	Value (model)	Value (literature)	Reference	Description
Pharmacokinetic model					
Diastolic blood pressure					
E_{max}	mmHg	56.18 (opt)	-	-	Maximum effect
EC_{50}	µmol/l	0.04 (opt)	-	-	Concentration for half-maximal effect
amp_{24}	%	2.14 (lit)	2.14	[2]	Amplitude for 24 h period
amp_{12}	%	5.93 (lit)	5.93	[2]	Amplitude for 12 h period
$phase_{24}$	h	individual[a]	-	-	Phase for 24 h period
$phase_{12}$	h	individual[a]	-	-	Phase for 12 h period
BP_{mean}	mmHg	individual[a]	69.5	[2]	Mean blood pressure over 24 h
Heart rate					
E_{max}	bpm	39.71 (opt)	-	-	Maximum effect
EC_{50}	µmol/l	0.05 (opt)	-	-	Concentration for half-maximal effect
h	-	1.40 (opt)	-	-	Hill coefficient
amp	%	6.3 (lit)	6.3	[3]	Amplitude
phase	h	$individual_a$	9.2	[3]	Phase
HR_{mean}	bpm	individual[a]	66.2	[3]	Mean heart rate over 24 h

lit: literature value, opt: optimized value, [a]: individual parameters for phases and BP_{mean} and HR_{mean} are listed in Table S5

3.3 Effect-time profiles

3.3.1 Diastolic blood pressure

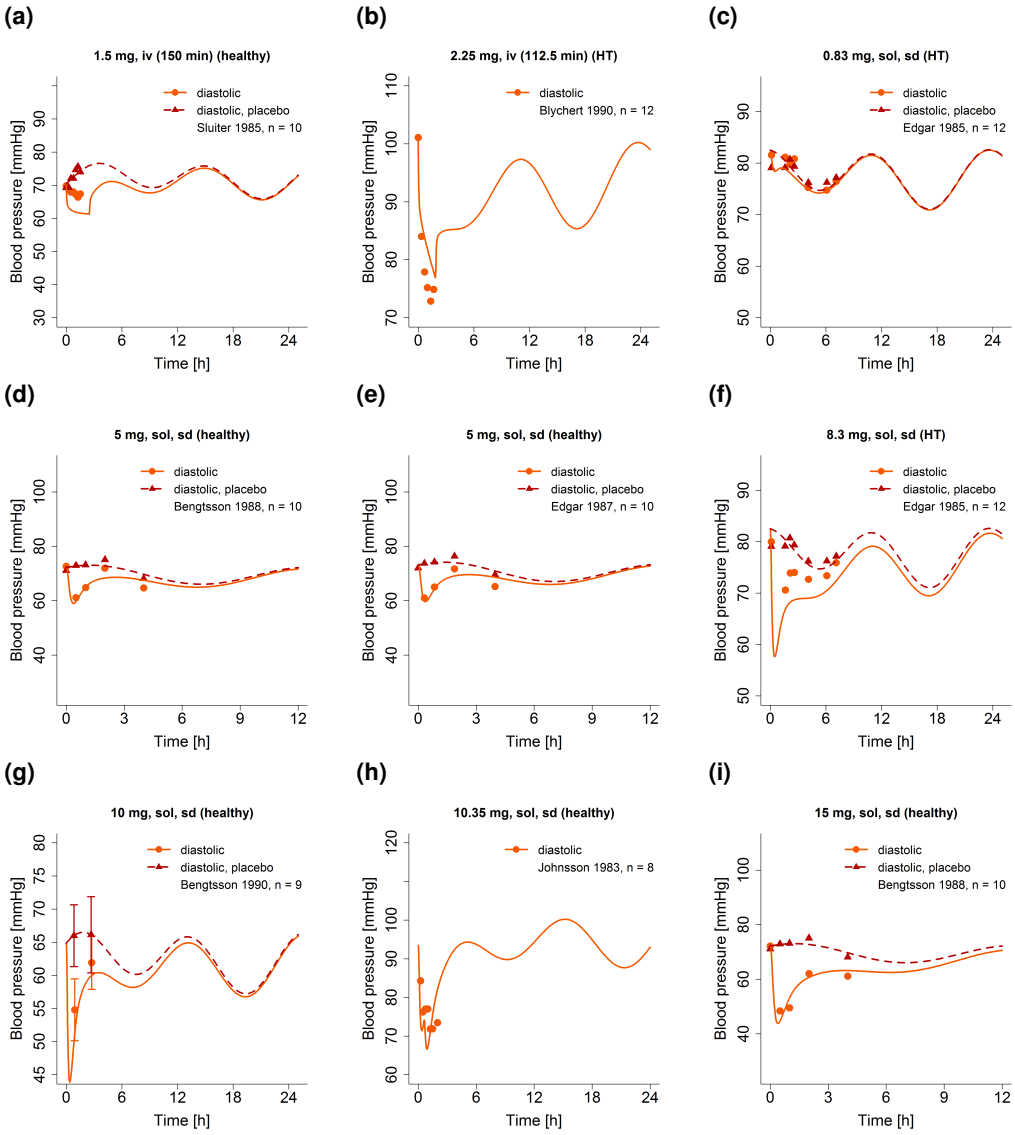

Figure S9: Predicted compared to observed effect-time profiles of diastolic blood pressure after intravenous and oral administration of felodipine. Observed data are shown as dots and triangles ± standard deviation (if available); model predictions are shown as solid lines. Details on dosing regimens, study populations and literature references are listed in Table S1. bid: twice daily, HT: hypertension, iv: intravenous, md: multiple dose, n: number of individuals, qd: once daily, RI: renal impairment, sol: solution, sd: single dose, tab: tablet, tabER: extended release tablet.

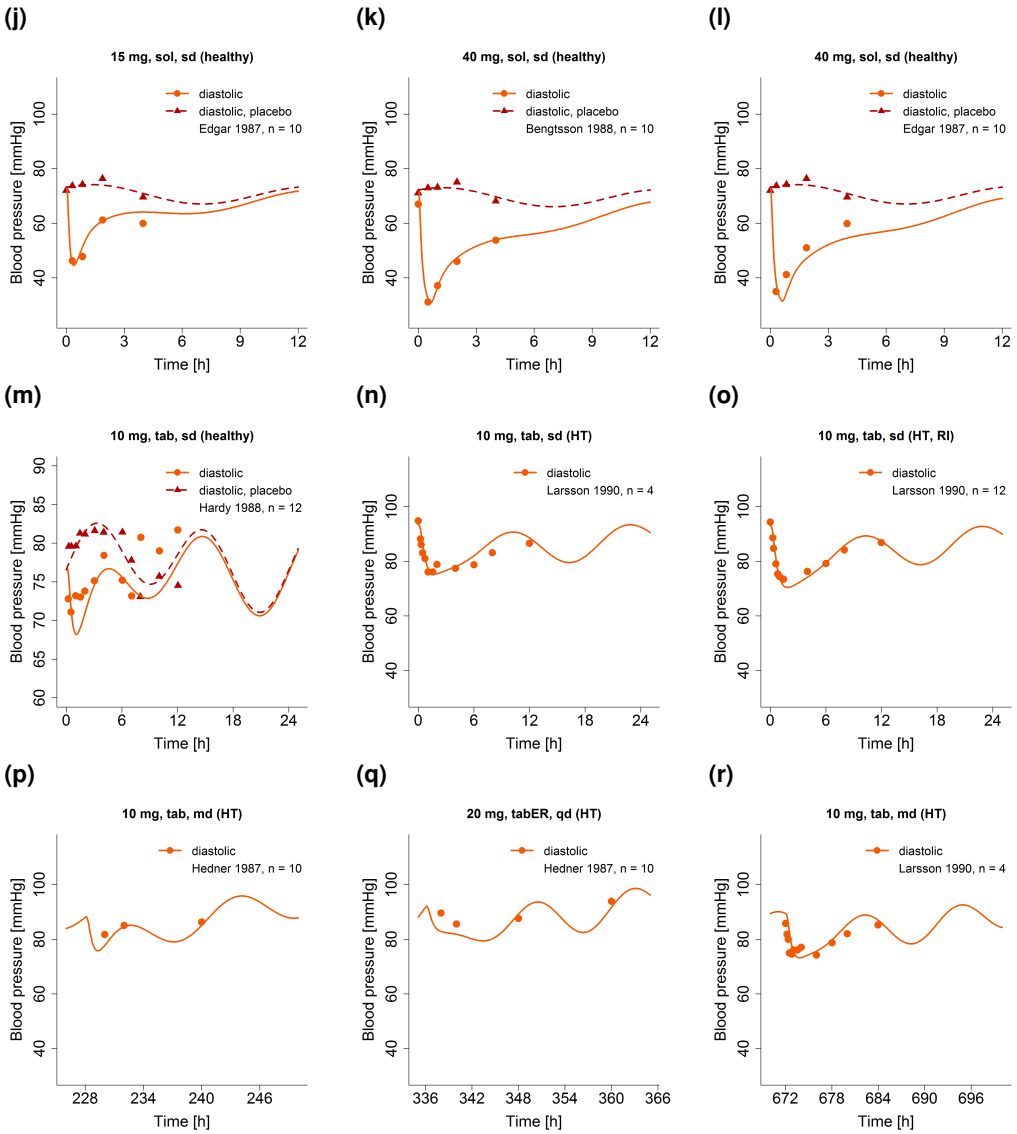

Figure S9: Predicted compared to observed effect-time profiles of diastolic blood pressure after intravenous and oral administration of felodipine. Observed data are shown as dots and triangles ± standard deviation (if available); model predictions are shown as solid lines. Details on dosing regimens, study populations and literature references are listed in Table S1. bid: twice daily, HT: hypertension, iv: intravenous, md: multiple dose, n: number of individuals, qd: once daily, RI: renal impairment, sol: solution, sd: single dose, tab: tablet, tabER: extended release tablet. *(continued)*

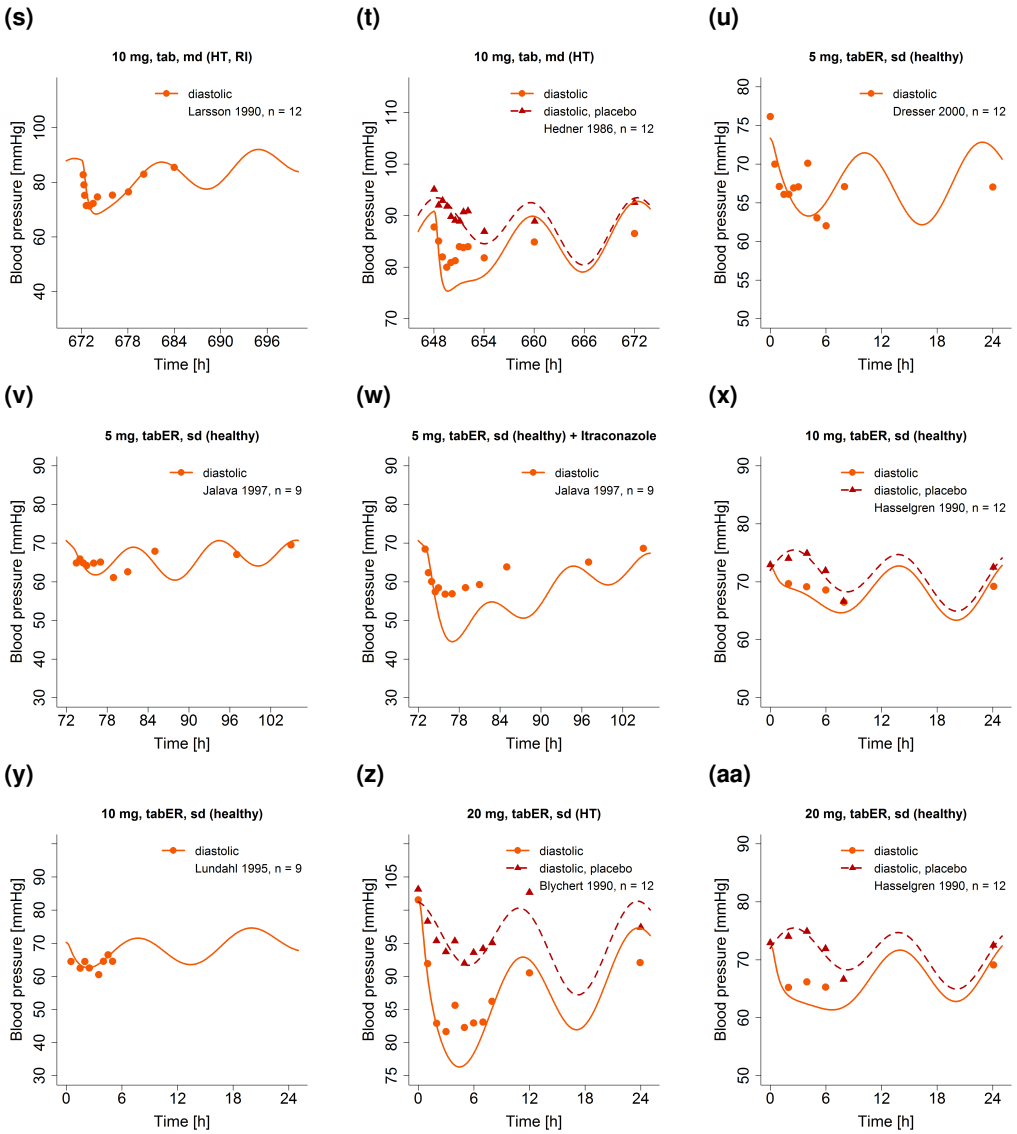

Figure S9: Predicted compared to observed effect-time profiles of diastolic blood pressure after intravenous and oral administration of felodipine. Observed data are shown as dots and triangles ± standard deviation (if available); model predictions are shown as solid lines. Details on dosing regimens, study populations and literature references are listed in Table S1. bid: twice daily, HT: hypertension, iv: intravenous, md: multiple dose, n: number of individuals, qd: once daily, RI: renal impairment, sol: solution, sd: single dose, tab: tablet, tabER: extended release tablet. *(continued)*

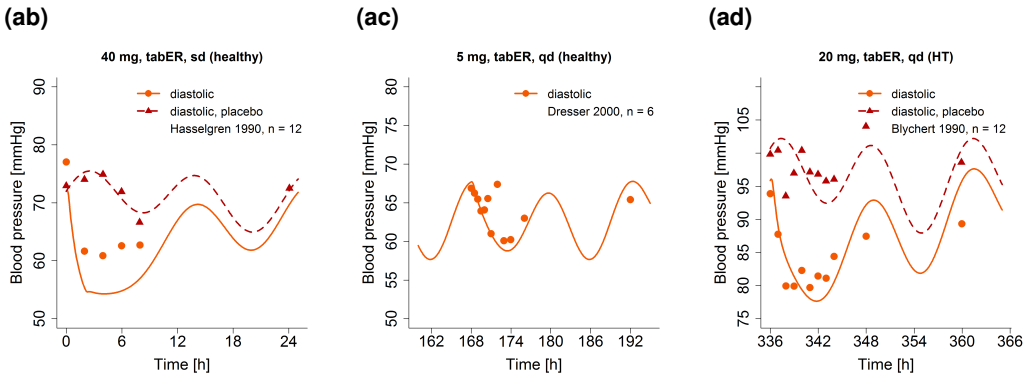

Figure S9: Predicted compared to observed effect-time profiles of diastolic blood pressure after intravenous and oral administration of felodipine. Observed data are shown as dots and triangles ± standard deviation (if available); model predictions are shown as solid lines. Details on dosing regimens, study populations and literature references are listed in Table S1. bid: twice daily, HT: hypertension, iv: intravenous, md: multiple dose, n: number of individuals, qd: once daily, RI: renal impairment, sol: solution, sd: single dose, tab: tablet, tabER: extended release tablet. *(continued)*

3.3.2 Heart rate

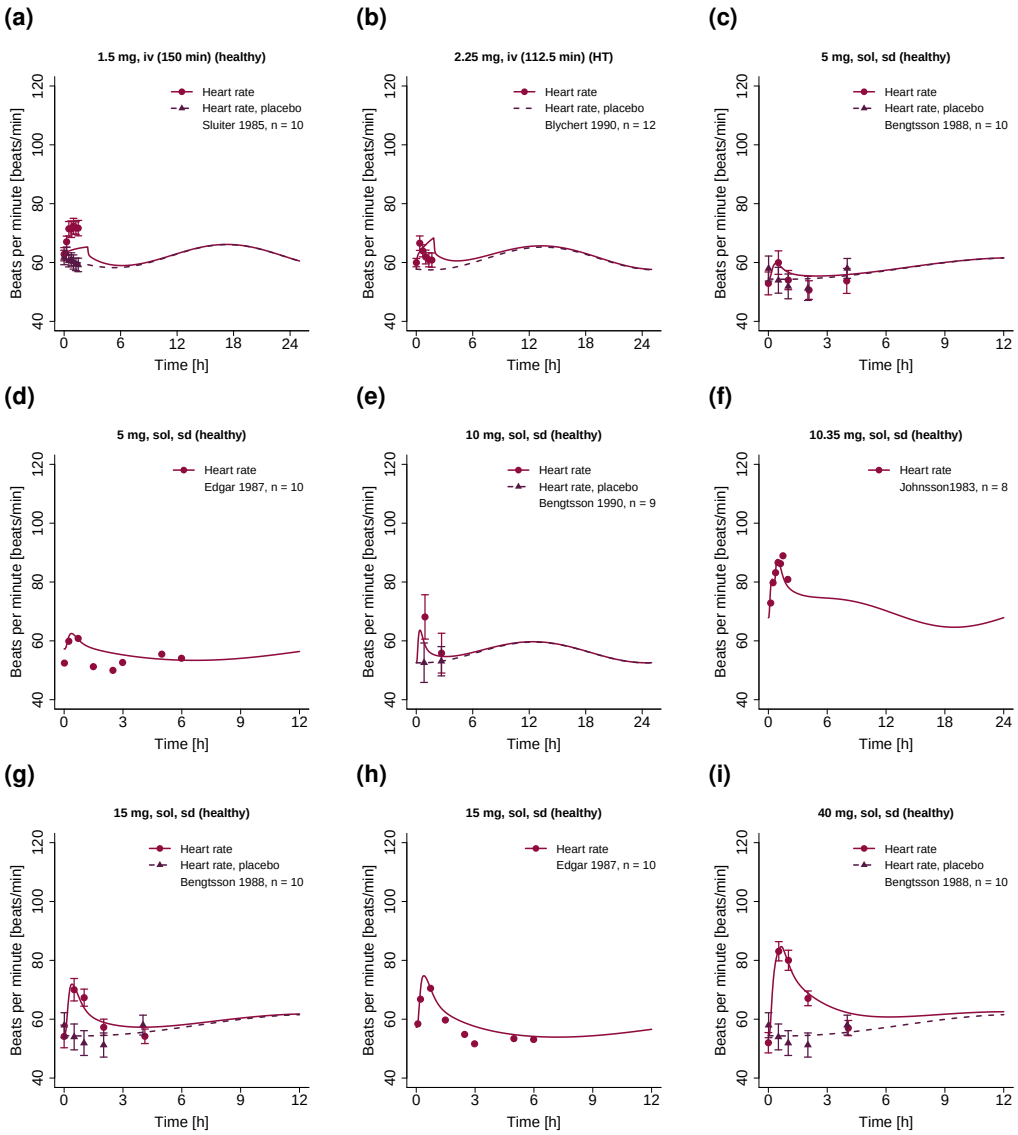

Figure S10: Predicted compared to observed effect-time profiles of heart rate after intravenous and oral administration of felodipine. Observed data are shown as dots and triangles ± standard deviation (if available); model predictions are shown as solid lines. Details on dosing regimens, study populations and literature references are listed in Table S1. bid: twice daily, HT: hypertension, iv: intravenous, md: multiple dose, n: number of individuals, qd: once daily, RI: renal impairment, sol: solution, sd: single dose, tab: tablet, tabER: extended release tablet.

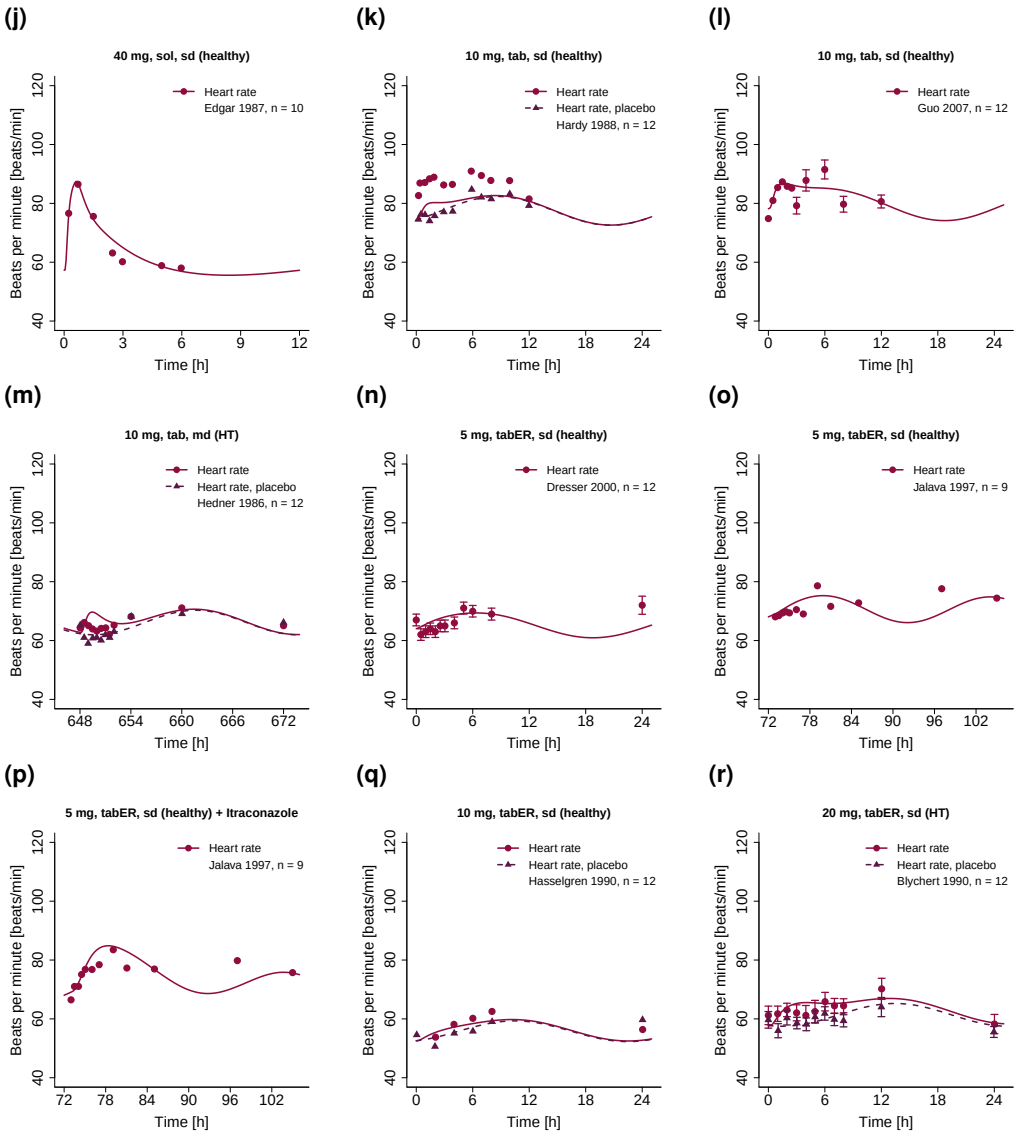

Figure S10: Predicted compared to observed effect-time profiles of heart rate after intravenous and oral administration of felodipine. Observed data are shown as dots and triangles ± standard deviation (if available); model predictions are shown as solid lines. Details on dosing regimens, study populations and literature references are listed in Table S1. bid: twice daily, HT: hypertension, iv: intravenous, md: multiple dose, n: number of individuals, qd: once daily, RI: renal impairment, sol: solution, sd: single dose, tab: tablet, tabER: extended release tablet. *(continued)*

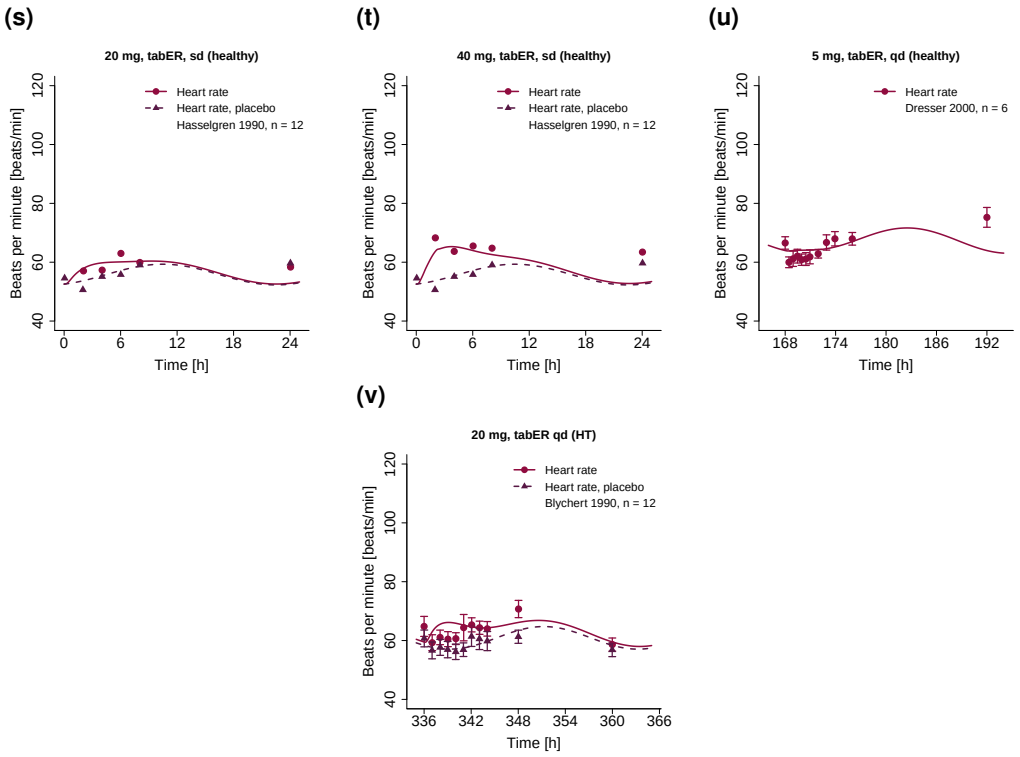

Figure S10: Predicted compared to observed effect-time profiles of heart rate after intravenous and oral administration of felodipine. Observed data are shown as dots and triangles ± standard deviation (if available); model predictions are shown as solid lines. Details on dosing regimens, study populations and literature references are listed in Table S1. bid: twice daily, HT: hypertension, iv: intravenous, md: multiple dose, n: number of individuals, qd: once daily, RI: renal impairment, sol: solution, sd: single dose, tab: tablet, tabER: extended release tablet. *(continued)*

3.4 Model evaluation

3.4.1 Goodness-of-fit plots

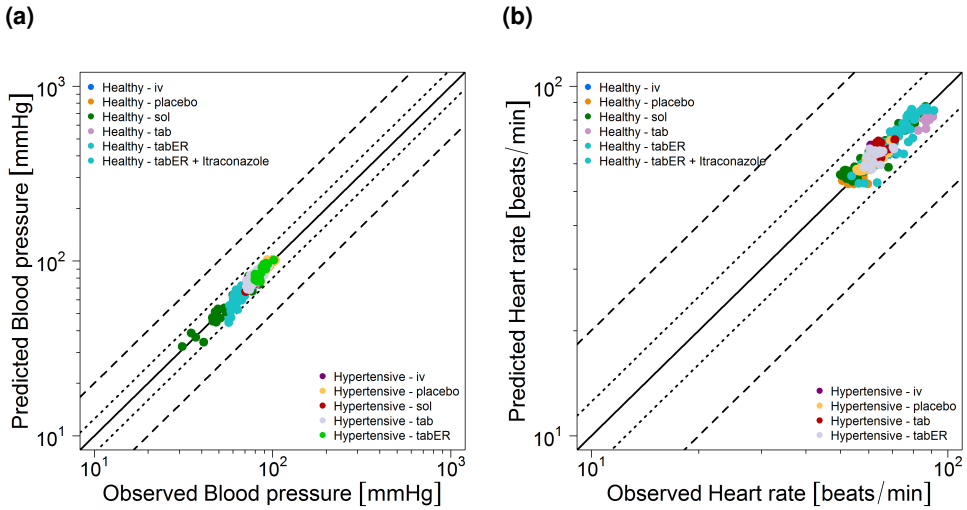

Figure S11: Predicted compared to observed (a) diastolic blood pressure and (b) heart rate measurements with and without felodipine administration. The solid line marks the line of identity. Dotted lines indicate 1.25-fold, dashed lines indicate 2-fold deviation. iv: intravenous, sol: solution, tab: tablet, tabER: extended release tablet.

3.4.2 Mean relative deviation of predicted effect measurements

Table S7: Mean relative deviation values of predicted diastolic blood pressure measurements with and without felodipine administration

Parameter	Felodipine route	Felodipine dose [mg]	MRD	Reference
Diastolic blood pressure	iv (20 min)	1.5	1.08	Sluiter 1985 [9]
Diastolic blood pressure	iv (15 min)	2.25	1.06	Blychert 1990 [50]
Diastolic blood pressure	po (sol), sd	0.83	1.02	Edgar 1985 [11]
Diastolic blood pressure	po (sol), sd	5	1.03	Bengtsson 1988 [6]
Diastolic blood pressure	po (sol), sd	5	1.03	Edgar 1987 [7]
Diastolic blood pressure	po (sol), sd	8.3	1.06	Edgar 1985 [11]
Diastolic blood pressure	po (sol), sd	10	1.06	Bengtsson 1990 [14]
Diastolic blood pressure	po (sol), sd	10.35	1.10	Johnsson 1983 [18]
Diastolic blood pressure	po (sol), sd	15	1.05	Bengtsson 1988 [6]
Diastolic blood pressure	po (sol), sd	15	1.05	Edgar 1987 [7]
Diastolic blood pressure	po (sol), sd	40	1.04	Bengtsson 1988 [6]
Diastolic blood pressure	po (sol), sd	40	1.13	Edgar 1987 [7]
Diastolic blood pressure	po (tab), sd	10	1.05	Hardy 1988 [26]
Diastolic blood pressure	po (tab), sd	10	1.03	Larsson 1990 [51]
Diastolic blood pressure	po (tab), sd	10	1.02	Larsson 1990 [51]
Diastolic blood pressure	po (tab), md	10	1.03	Hedner 1987 [52]
Diastolic blood pressure	po (tabER), qd	20	1.05	Hedner 1987 [52]
Diastolic blood pressure	po (tab), bid	10	1.05	Larsson 1990 [51]
Diastolic blood pressure	po (tab), bid	10	1.06	Larsson 1990 [51]
Diastolic blood pressure	po (tab), bid	10	1.07	Hedner 1986 [54]
Diastolic blood pressure	po (tabER), sd	5	1.05	Dresser 2000 [27]
Diastolic blood pressure	po (tabER), sd	5	1.05	Jalava 1997 [28]
Diastolic blood pressure	po (tabER), sd	5	1.14	Jalava 1997 [28]
Diastolic blood pressure	po (tabER), sd	10	1.03	Hasselgren 1990 [40]
Diastolic blood pressure	po (tabER), sd	10	1.03	Lundahl 1995 [42]
Diastolic blood pressure	po (tabER), sd	20	1.05	Blychert 1990 [50]
Diastolic blood pressure	po (tabER), sd	20	1.05	Hasselgren 1990 [40]
Diastolic blood pressure	po (tabER), sd	40	1.11	Hasselgren 1990 [40]
Diastolic blood pressure	po (tabER), qd	5	1.04	Dresser 2000 [27]
Diastolic blood pressure	po (tabER), qd	20	1.04	Blychert 1990 [50]
Diastolic blood pressure, placebo	-	-	1.02	Sluiter 1985 [9]
Diastolic blood pressure, placebo	-	-	1.00	Bengtsson 1990 [14]
Diastolic blood pressure, placebo	-	-	1.02	Bengtsson 1988 [6]
Diastolic blood pressure, placebo	-	-	1.02	Edgar 1985 [11]
Diastolic blood pressure, placebo	-	-	1.02	Hardy 1988 [26]
Diastolic blood pressure, placebo	-	-	1.02	Hedner 1986 [54]
Diastolic blood pressure, placebo	-	-	1.02	Blychert 1990 [50]
Diastolic blood pressure, placebo	-	-	1.02	Hasselgren 1990 [40]
Diastolic blood pressure, placebo	-	-	1.04	Blychert 1990 [50]
MRD (effect)			**1.06 (1.02-1.14)**	
MRD (placebo)			**1.02 (1.00-1.04)**	
MRD (total)			**1.05 (1.00-1.14)**	
			39/39 with MRD < 2	

bid: twice daily, D: day, iv: intravenous, MRD: mean relative deviation, po: oral, qd: once daily, sd: single dose, sol: solution, tab: tablet, tabER: extended release tablet

Table S8: Mean relative deviation values of predicted heart rate measurements with and without felodipine administration

Parameter	Felodipine route	Felodipine dose [mg]	MRD	Reference
Heart rate	iv (20 min)	1.5	1.10	Sluiter 1985 [9]
Heart rate	iv (15 min)	2.25	1.07	Blychert 1990 [50]
Heart rate	po (sol), sd	5	1.05	Bengtsson 1988 [6]
Heart rate	po (sol), sd	5	1.07	Edgar 1987 [7]
Heart rate	po (sol), sd	10	1.11	Bengtsson 1990 [14]
Heart rate	po (sol), sd	10.35	1.04	Johnsson1983 [18]
Heart rate	po (sol), sd	15	1.04	Bengtsson 1988 [6]
Heart rate	po (sol), sd	15	1.05	Edgar 1987 [7]
Heart rate	po (sol), sd	40	1.05	Bengtsson 1988 [6]
Heart rate	po (sol), sd	40	1.04	Edgar 1987 [7]
Heart rate	po (tab), sd	10	1.09	Hardy 1988 [26]
Heart rate	po (tab), sd	10	1.04	Guo 2007 [24]
Heart rate	po (tab), bid	10	1.05	Hedner 1986 [54]
Heart rate	po (tabER), sd	5	1.05	Dresser 2000 [27]
Heart rate	po (tabER), sd	5	1.05	Jalava 1997 [28]
Heart rate	po (tabER), sd	5	1.05	Jalava 1997 [28]
Heart rate	po (tabER), sd	10	1.04	Hasselgren 1990 [40]
Heart rate	po (tabER), sd	20	1.04	Blychert 1990 [50]
Heart rate	po (tabER), sd	20	1.05	Hasselgren 1990 [40]
Heart rate	po (tabER), sd	40	1.09	Hasselgren 1990 [40]
Heart rate	po (tabER), qd	5	1.06	Dresser 2000 [27]
Heart rate	po (tabER), qd	20	1.06	Blychert 1990 [50]
Heart rate, placebo	-	-	1.01	Sluiter 1985 [9]
Heart rate, placebo	-	-	1.00	Bengtsson 1990 [14]
Heart rate, placebo	-	-	1.05	Bengtsson 1988 [6]
Heart rate, placebo	-	-	1.02	Hardy 1988 [26]
Heart rate, placebo	-	-	1.03	Hedner 1986 [54]
Heart rate, placebo	-	-	1.03	Blychert 1990 [50]
Heart rate, placebo	-	-	1.06	Hasselgren 1990 [40]
Heart rate, placebo	-	-	1.03	Blychert 1990 [50]
MRD (effect)			**1.06 (1.04-1.11)**	
MRD (placebo)			**1.03 (1.00-1.06)**	
MRD (total)			**1.05 (1.00-1.11)**	
			30/30 with MRD < 2	

iv: intravenous, MRD: mean relative deviation, po: oral, qd: once daily, sd: single dose, sol: solution, tab: tablet, tabER: extended release tablet

4 Felodipine DDIs

4.1 DDI modeling

Three DDI studies, providing (1) three victim drug plasma concentration-time profiles of felodipine (2) one plasma concentration-time profile of dehydrofelodipine and (3) one blood pressure and heart rate effect-time profile, were utilized to evaluate the DDI performance of the felodipine PBPK model. In those studies, (1) the mechanism-based CYP3A4 inhibitor erythromycin, (2) the competitive CYP3A4 inhibitor itraconazole and (3) the CYP3A4 inducers carbamazepine and phenytoin were used as perpetrators of felodipine metabolism. The implementation of these DDIs is described in more detail in the following sections.

4.2 Erythromycin-felodipine DDI

The erythromycin-felodipine DDI was modeled using a previously developed and evaluated whole-body PBPK model of erythromycin, available in the Open Systems Pharmacology (OSP) GitHub model repository (https://github.com/Open-Systems-Pharmacology/Erythromycin-Model). [69, 70].

The implementation of the erythromycin-felodipine DDI is illustrated in Figure S12. DDI parameters were used as implemented in the erythromycin model. Drug-dependent parameters of the erythromycin PBPK model are displayed in Table S9.

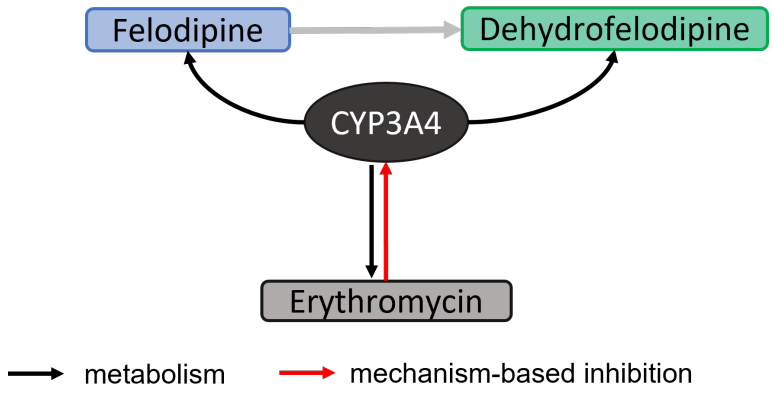

Figure S12: Implementation of the erythromycin-felodipine DDI. Erythromycin inhibits the CYP3A4 mediated metabolism of felodipine and dehydrofelodipine in a mechanism-based manner. As erythromycin is also substrate of CYP3A4, the compound also inhibits its own metabolism. CYP: cytochrome P450

Details on the modeled clinical DDI studies are given in Table S10. Predicted felodipine and dehydrofelodipine plasma concentration-time profiles with and without erythromycin co-administration, compared to observed data, are shown in Figures S13 (linear) and S14 (semi-logarithmic). The correlation of predicted to observed DDI AUC_{last} and C_{max} ratios is shown in Figure S15. Table S11 lists the corresponding predicted and observed DDI AUC_{last} ratios, DDI C_{max} ratios, as well as GMFE values.

4.2.1 Erythromycin drug-dependent parameters

Table S9: Drug-dependent parameters of the erythromycin PBPK model according to [69]

Parameter	Unit	Model	Literature	Reference	Description
MW	g/mol	733.9 (lit)	733.9	[71]	Molecular weight
logP	Log Units	2.82 (lit)	2.82 (2.48-3.06)[a]	[72–74]	Lipophilicity
Solubility (pH)	mg/ml	200.0 (7.0) (lactobionate) (lit), 0.028 (7.0) (stearate) (opt), 0.50 (7.0) (base pellets) (opt), 0.0084 (7.0) (base tablet) (opt)	200.0 (7.0) (lactobionate), 0.182 (7.0) (stearate), 2.10 (7.0) (base)	[75] [76] [77]	Solubility
fu	%	30.5 (lit)	27.0, 28.0, 30.5, 32.6	[78–81]	Fraction unbound in plasma
pKa (base)	-	8.88 (lit)	8.88	[74]	Acid dissociation constant
K_m (CYP3A4)	µmol/l	70.0 (lit)	70 (44.0-88.0)[a]	[82, 83]	CYP3A4 Michaelis-Menten constant
k_{cat} (CYP3A4)	1/min	8.50 (opt)	-	-	CYP3A4 catalytic rate constant
K_m (OATP1B1)	µmol/l	0.74 (opt)	13.2	[84]	OATP1B1 Michaelis-Menten constant
k_{cat} (OATP1B1)	1/min	2.02 (opt)	-	-	OATP1B1 transport rate constant
CL_{hep}	1/min	4.15 (opt)	-	-	Hepatic plasma clearance
GFR fraction	-	1.16 (opt)	-	-	Fraction of filtered drug in the urine
K_i (CYP3A4)	µmol/l	7.60 (opt)	18.4 (0.76-109.0)[b]	[81, 85–95]	Concentration for half-maximal inactivation
k_{inact} (CYP3A4)	1/min	0.03 (opt)	0.06 (0.01-0.30)[b]	[81, 85–95]	Maximum inactivation rate constant
Intestinal permeability	cm/min	3.87E-04 (opt)	-	-	Transcellular intestinal permeability
Partition coefficients	-	Diverse	Rogers and Rowland	[64, 65]	Cell to plasma partition coefficients
Cellular permeability	cm/min	1.22E-4 (calc)	Charge-dependent Schmitt	[1]	Permeability into the cellular space
$t_{50\%}$ (film tablet)	min	79.63 (opt)	-	-	Dissolution time (50% dissolved)
s (film tablet)	-	1.08 (opt)	-	-	Dissolution profile shape

-: not given, calc: calculated, CYP3A4: cytochrome P450 3A4, GFR: glomerular filtration rate, lit: literature, OATP1B1: organic anion transporting polypeptide 1B1, opt: optimized during parameter identification

[a] mean (range)

4.2.2 Erythromycin-felodipine clinical studies

Table S10: Clinical studies investigating the erythromycin-felodipine DDI

Erythromycin administration		Felodipine administration		Interval [h]	n	Healthy [%]	Females [%]	Age[a] [years]	Weight [kg]	Reference
Dose [mg]	Route	Dose [mg]	Route							
250	po , qid D1-D2	10	po (tabER), sd D2	0	12	100	0	(18-45)	-	Bailey et al. 1996 [35]

-: not given, D: day, po: oral, n: number of individuals, qid: four times daily, sd: single dose, tabER: extended release tablet

[a] range

4.2.3 Plasma concentration-time profiles

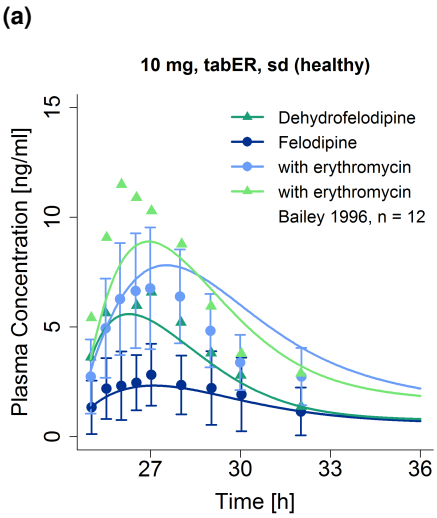

Figure S13: Predicted compared to observed felodipine and dehydrofelodipine plasma concentration-time profiles (linear) before and during erythromycin co-administration. Observed data are shown as dots and triangles ± standard deviation; model predictions are shown as solid lines. Details on dosing regimens, study population and literature reference are listed in Table S10. n: number of individuals, sd: single dose, tabER: extended release tablet.

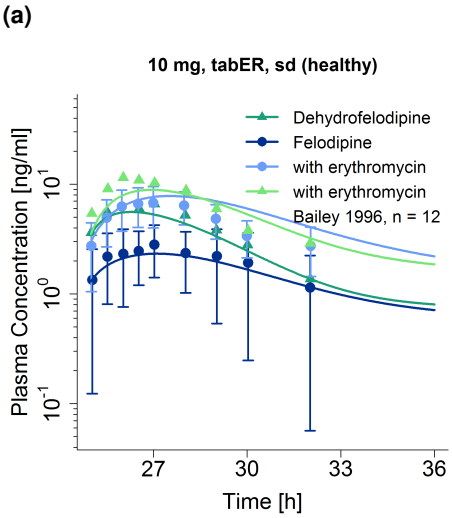

Figure S14: Predicted compared to observed felodipine and dehydrofelodipine plasma concentration-time profiles (semi-logarithmic) before and during erythromycin co-administration. Observed data are shown as dots and triangles ± standard deviation; model predictions are shown as solid lines. Details on dosing regimens, study population and literature reference are listed in Table S10. n: number of individuals, sd: single dose, tabER: extended release tablet.

4.2.4 DDI AUC_{last} and C_{max} ratio goodness-of-fit plots

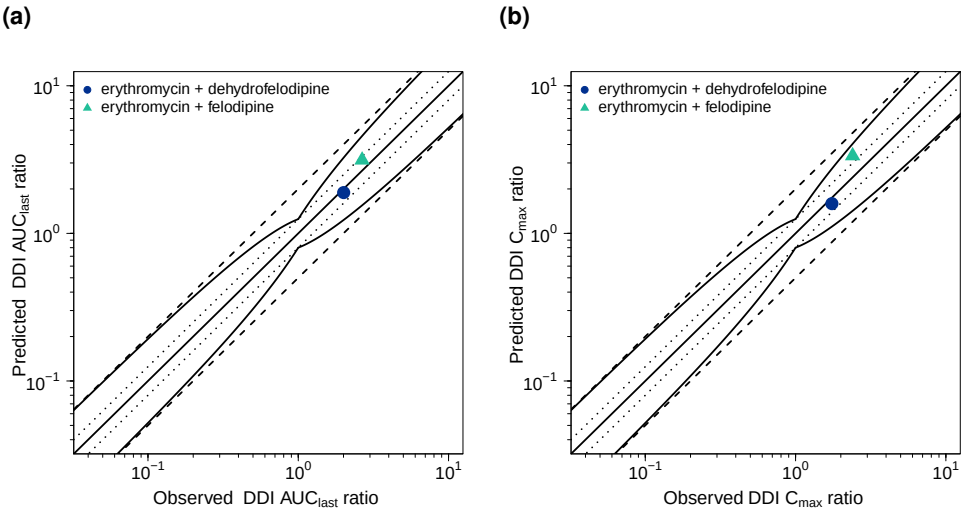

Figure S15: Predicted compared to observed erythromycin-felodipine DDI AUC_{last} and DDI C_{max} values. The straight solid line marks the line of identity, the curved solid lines show the prediction success limits proposed by Guest et al. allowing for 1.25-fold variability of the DDI ratio [96]. Dotted lines indicate 1.25-fold, dashed lines indicate 2-fold deviation. AUC_{last}: area under the plasma concentration-time curve from the time of drug administration to the last concentration measurement, C_{max}: maximum plasma concentration, DDI: drug-drug interaction

4.2.5 Geometric mean fold error of predicted DDI AUC_{last} and C_{max} ratios

Table S11: Predicted and observed erythromycin-felodipine DDI AUC_{last} ratios and DDI C_{max} ratios

Perpetrator	**Victim**	**Compound**	**Dose gap [h]**	**n**	**DDI AUC_{last} ratio**			**DDI C_{max} ratio**			
Erythromycin	Felodipine				**Pred**	**Obs**	**Pred/Obs**	**Pred**	**Obs**	**Pred/Obs**	**Reference**
250 mg, po, qid D1-D2	10 mg, po (tabER), sd D2	Felodipine	0	12	3.14	2.66	1.18	3.35	2.40	1.40	Bailey 1996 [35]
250 mg, po, qid D1-D2	10 mg, po (tabER), sd D2	Dehydrofelodipine	0	12	1.89	2.00	0.94	1.59	1.74	0.91	Bailey 1996 [35]
GMFE							**1.12 (1.06-1.18)**			**1.25 (1.10-1.40)**	
							2/2 with GMFE < 2			**2/2 with GMFE < 2**	

AUC_{last}: area under the plasma concentration-time curve calculated from the time of drug administration to the time of the last concentration measurement, C_{max}: maximum plasma concentration, D: day, DDI: drug-drug interaction, GMFE: geometric mean fold error, n: number of individuals, obs: observed, pred: predicted, po: oral, qid: four times daily, sd: single dose, tabER: extended release tablet

4.3 Itraconazole-felodipine DDI

The parent-metabolite PBPK model of itraconazole and its three metabolites was previously developed and evaluated for the prediction of CYP3A4 mediated DDIs [97]. The model can be freely downloaded from the OSP repository on GitHub (https://github.com/Open-Systems-Pharmacology/Itraconazole-Model). The implementation of the itraconazole-felodipine DDI is illustrated in Figure S16. Inhibition parameters were used as implemented in the itraconazole parent-metabolite model. Drug-dependent parameters of all compounds of the parent-metabolite PBPK model are displayed in Table S12. No information on the itraconazole formulation was provided in the itraconazole-felodipine DDI study. However, the itraconazole plasma concentration-time profile was best described assuming administration as oral solution.

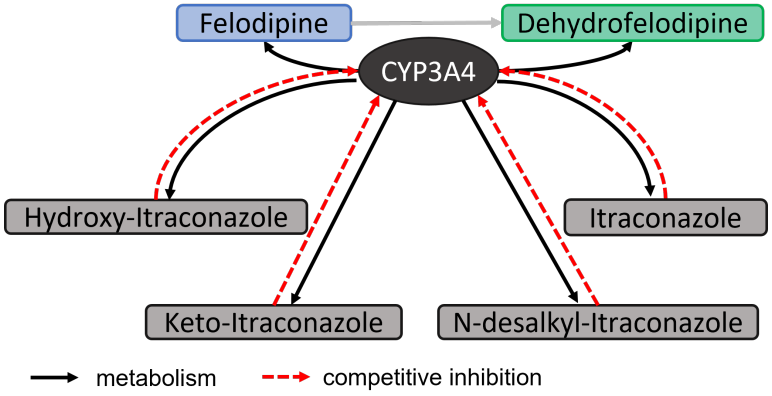

Figure S16: Implementation of the itraconazole-felodipine DDI. The CYP3A4 metabolism of felodipine and dehydrofelodipine is inhibited competitively by itraconazole and its three metabolites. Itraconazole and its metabolites are substrates of CYP3A4 as well and, therefore, inhibit each other's metabolism. CYP 3A4: cytochrome P450 3A4

Details on the modeled clinical DDI study are given in Table S13. Predicted felodipine plasma concentration-time profiles before and during itraconazole co-administration, compared to observed data, are shown in Figures S17 (linear) and S18 (semi-logarithmic). Predicted compared to observed blood pressure and heart rate effect-time profiles before and during itraconazole co-administration are shown in Figure S19. The correlation of predicted to observed DDI AUC_{last} and C_{max} ratios is shown in Figure S20. Table S14 lists the corresponding predicted and observed DDI AUC_{last} ratios, DDI C_{max} ratios, as well as GMFE values.

4.3.1 Itraconazole drug-dependent parameters

Table S12: Drug-dependent parameters of the itraconazole parent-metabolite PBPK model according to [97]

Parameter	Unit	Model	Literature	Reference	Description
Itraconazole					
MW	g/mol	705.633 (lit)	705.633		Molecular weight
pKa (basic)		3.7 (lit)	3.7	[98]	Acid dissociation constant
Solubility - solution fed	mg/l	1.58 (opt)	-	-	Solubility
logP		4.62 (opt)	5.66	[98]	Lipophilicity
fu	%	0.6 (lit)	0.2, 0.6, 1.6, 3.6	[98–101]	Fraction unbound in plasma
CYP3A4 K_m	nmol/l	2.07 (opt)	3.9	[102]	CYP3A4 Michaelis-Menten constant
CYP3A4 k_{cat}	1/min	0.04 (opt)	-	-	CYP3A4 catalytic rate constant
GFR fraction		1	-	-	Fraction of filtered drug in the urine
K_i CYP3A4	nmol/l	1.3 (lit)	1.3	[102]	Concentration for half-maximal inhibition
Cell permeabilities		calculated	PK-Sim Standard	[66]	Permeability into the cellular space
Partition coefficients		calculated	Rodgers and Rowland	[64, 65]	Cell to plasma partition coefficients
Intestinal permeability	cm/min	0.00000533	-	-	Transcellular intestinal permeability
Intestinal permeability	cm/min	0.000144 (calc)	-	-	Normalized to surface area
Hydroxyitraconazole					
MW	g/mol	721.633 (lit)	721.633		Molecular weight
pKa		3.7 (basic) (asm)	-	-	Acid dissociation constant
Solubility [pH]	mg/l	-	-	-	Solubility
logP		3.72 (opt)	4.5	[103]	Lipophilicity
fu	%	1.7 (lit)	1.7	[100]	Fraction unbound in plasma
CYP3A4 K_m	nmol/l	4.17 (opt)	27	[102]	CYP3A4 Michaelis-Menten constant
CYP3A4 k_{cat}	1/min	0.02 (opt)	-	-	CYP3A4 catalytic rate constant
GFR fraction		1 (asm)	-	-	Fraction of filtered drug in the urine
K_i CYP3A4	nmol/l	14.4 (lit)	14.4	[102]	Concentration for half-maximal inhibition
Cell permeabilities		calculated	PK-Sim Standard	[66]	Permeability into the cellular space
Partition coefficients		calculated	Rodgers and Rowland	[64, 65]	Cell to plasma partition coefficients
Intestinal permeability	cm/min	0.000000152 (calc)	-	-	Transcellular intestinal permeability
Cellular permeability	cm/min	0.0000155 (calc)	-	-	Normalized to surface area
Keto-itraconazole					
MW	g/mol	719.617 (lit)	-	-	Molecular weight

asm: assumed, CYP3A4: cytochrome P450 3A4, GFR: glomerular filtration rate, lit: literature, opt: optimized during parameter identification

Table S12: Drug-dependent parameters of the itraconazole parent-metabolite PBPK model according to [97] *(continued)*

Parameter	Unit	Model	Literature	Reference	Description
pKa		3.7 (basic) (asm)		-	Acid dissociation constant
logP		4.21 (opt)	4.5	[104]	Lipophilicity
fu	%	1 (lit)	1	[100]	Fraction unbound in plasma
CYP3A4 K_m	nmol/l	2.22 (opt)	1.4	[102]	CYP3A4 Michaelis-Menten constant
CYP3A4 k_{cat}	1/min	0.393 (opt)	-	-	CYP3A4 catalytic rate constant
GFR fraction		1 (asm)	-	-	Fraction of filtered drug in the urine
K_i CYP3A4	nmol/l	5.12[a] (lit)	5.12[a]	[102]	Concentration for half-maximal inhibition
Cell permeabilities		calculated	PK-Sim Standard	[66]	Permeability into the cellular space
Partition coefficients		calculated	Rodgers and Rowland	[64, 65]	Cell to plasma partition coefficients
Intestinal permeability	cm/min	0.000000479 (calc)	-	-	Transcellular intestinal permeability
Cellular permeability	cm/min	0.0000492 (calc)	-	-	Normalized to surface area
N-desalkyl-itraconazole					
MW	g/mol	649.527 (lit)	-	-	Molecular weight
pKa		3.7 (base) (asm)	-	-	Acid dissociation constant
logP		5.18 (opt)	4.2	[105]	Lipophilicity
fu	%	1.1 (lit)	1.1	[100]	Fraction unbound in plasma
CYP3A4 K_m	nmol/l	0.63 (opt)	-	-	CYP3A4 Michaelis-Menten constant
CYP3A4 k_{cat}	1/min	0.061 (opt)	-	-	CYP3A4 catalytic rate constant
GFR fraction		1	-	-	Fraction of filtered drug in the urine
K_i CYP3A4	nmol/l	0.32[a] (lit)	0.32	[102]	Concentration for half-maximal inhibition
Cell permeabilities		calculated	PK-Sim Standard	[66]	Permeability into the cellular space
Partition coefficients		calculated	Rodgers and Rowland	[64, 65]	Cell to plasma partition coefficients
Cellular permeability	cm/min	0.00000737 (calc)	-	-	Transcellular intestinal permeability
Intestinal permeability	cm/min	0.000891 (calc)	-	-	Normalized to surface area

asm: assumed, CYP3A4: cytochrome P450 3A4, GFR: glomerular filtration rate, lit: literature, opt: optimized during parameter identification

4.3.2 Itraconazole-felodipine clinical studies

Table S13: Clinical studies investigating the itraconazole-felodipine DDI

Itraconazole administration		Felodipine administration		Interval [h]	n	Healthy [%]	Females [%]	Age[a] [years]	Weight[a] [kg]	Reference
Dose [mg]	**Route**	**Dose [mg]**	**Route**							
200	po (*sol*), qd D1-D4	5	po (tabER), sd (D4)	1	9	100	44.4	24.44 (22-26)	59.88 (51-73)	Jalava 1997 [28]

assumed

D: day, n: number of individuals, po: oral, qd: once daily, sd: single dose, sol: solution, tabER: extended release tablet

[a] mean (range)

4.3.3 Plasma concentration-time and effect-time profiles

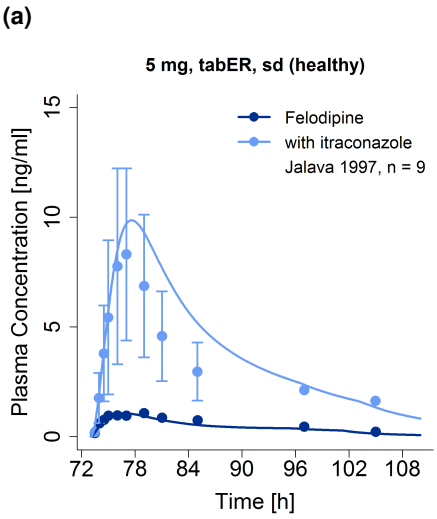

Figure S17: Predicted compared to observed felodipine plasma concentration-time profiles (linear) before and during itraconazole co-administration. Observed data are shown as dots ± standard deviation; model predictions are shown as solid lines. Details on dosing regimens, study population and literature reference are listed in Table S13. n: number of individuals, sd: single dose, tabER: extended release tablet

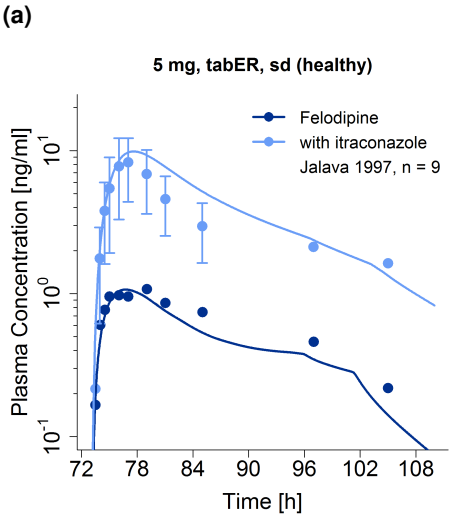

Figure S18: Predicted compared to observed felodipine plasma concentration-time profiles (semi-logarithmic) before and during itraconazole co-administration. Observed data are shown as dots ± standard deviation; model predictions are shown as solid lines. Details on dosing regimens, study population and literature reference are listed in Table S13. n: number of individuals, sd: single dose, tabER: extended release tablet.

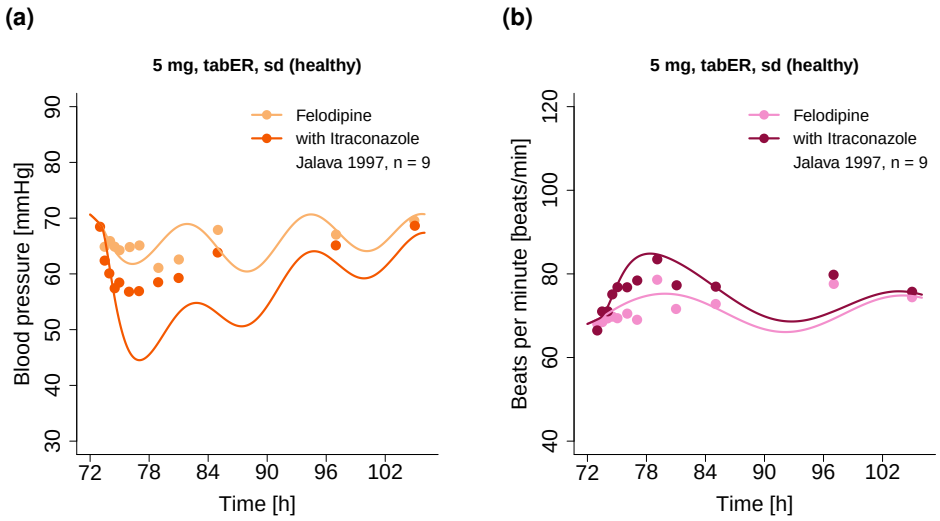

Figure S19: Predicted compared to observed (a) blood pressure and (b) heart rate effect-time profiles before and during itraconazole co-administration. Observed data are shown as dots; model predictions are shown as solid lines. Details on dosing regimens, study population and literature reference are listed in Table S13. n: number of individuals, sd: single dose, tabER: extended release tablet.

4.3.4 DDI AUC_{last} and C_{max} ratio goodness-of-fit plots

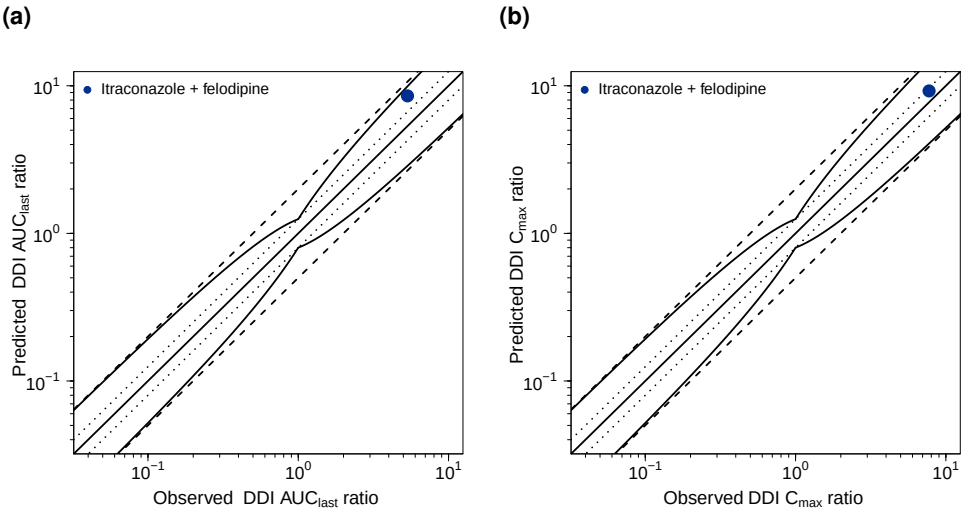

Figure S20: Predicted compared to observed itraconazole-felodipine DDI AUC_{last} and DDI C_{max} values. The straight solid line marks the line of identity, the curved solid lines show the prediction success limits proposed by Guest et al. allowing for 1.25-fold variability of the DDI ratio [96]. Dotted lines indicate 1.25-fold, dashed lines indicate 2-fold deviation. AUC_{last}: area under the plasma concentration-time curve from the time of drug administration to the last concentration measurement, C_{max}: maximum plasma concentration, DDI: drug-drug interaction

4.3.5 Geometric mean fold error of predicted DDI AUC_{last} and C_{max} ratios

Table S14: Predicted and observed itraconazole-felodipine DDI AUC_{last} ratios and DDI C_{max} ratios

Perpetrator	**Victim**	**Compound**	**Dose gap [h]**	**n**	**DDI AUC_{last} ratio**			**DDI C_{max} ratio**			
Itraconazole	Felodipine				**Pred**	**Obs**	**Pred/Obs**	**Pred**	**Obs**	**Pred/Obs**	**Reference**
200 mg po (*sol*), qd D1-D4	5, mg, po (tabER), sd D4	Felodipine	1	9	8.54	5.33	1.60	9.23	7.73	1.19	Jalava 1997 [28]
GMFE							**1.60**			**1.19**	
							1/1 with GMFE < 2			**1/1 with GMFE < 2**	

AUC_{last}: area under the plasma concentration-time curve calculated from the time of drug administration to the time of the last concentration measurement, C_{max}: maximum plasma concentration, D: day, DDI: drug-drug interaction, GMFE: geometric mean fold error, n: number of individuals, obs: observed, pred: predicted, po: oral, qd: once daily, sd: single dose, sol: solution, tabER: extended release tablet

4.4 Carbamazepine-felodipine DDI

Previously developed PBPK models of carbamazepine [106] and phenytoin (unpublished, in house) were available and already evaluated for the prediction of CYP3A4 mediated DDIs. The implementation of the carbamazepine-phenytoin-felodipine DDI is illustrated in Figure S21. Interaction parameters were used as implemented previously in the perpetrator models. Drug-dependent parameters of carbamazepine are shown in Table S15.

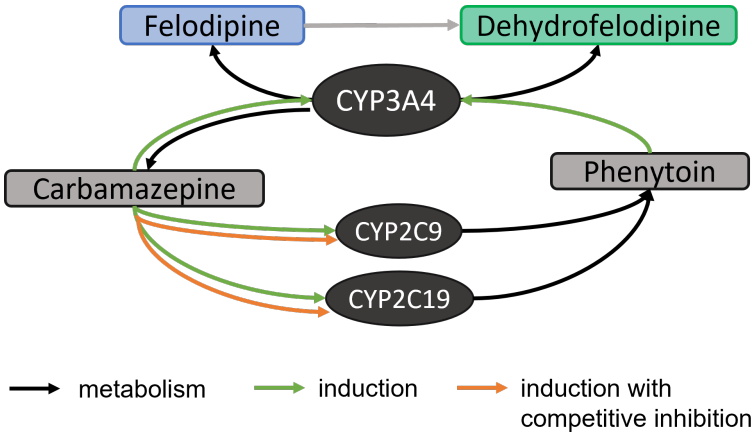

Figure S21: Implementation of the carbamazepine-phenytoin-felodipine DDI. The CYP3A4 metabolism of felodipine and dehydrofelodipine is induced by carbamazepine and phenytoin. The CYP3A4 metabolism of carbamazepine is induced by carbamazepine itself as well as phenytoin. The CYP2C9 and CYP2C19 metabolism of phenytoin is competitively inhibited and induced by carbamazepine. CYP: cytochrome P450

Details on the modeled clinical DDI study are given in Table S16. Predicted felodipine plasma concentration-time profiles with and without carbamazepine/phenytoin co-administration, compared to observed data, are shown in Figures S22 (linear) and S23 (semi-logarithmic). The correlation of predicted to observed DDI AUC_{last} and C_{max} ratios is shown in Figure S24. Table S17 lists the corresponding predicted and observed DDI AUC_{last} ratios, DDI C_{max} ratios, as well as GMFE values.

4.4.1 Carbamazepine drug-dependent parameters

Table S15: Drug-dependent parameters of the carbamazepine and carbamazepine-10,11-epoxide PBPK model according to [106]

Parameter	Unit	Model	Literature	Reference	Description
Carbamazepine					
MW	g/mol	236.27 (Lit)	236.27	[109]	Molecular weight
logP	Log Units	2.00 (Fit)	1.45, 2.10, 2.45, 2.77	[109–111]	Lipophilicity
Solubility (pH)	mg/ml	0.336 (6.2) (Lit)	0.170 (6.2), 0.283 (7.0), 0.306 (6.9), 0.336 (6.2)	[112–115]	Solubility FaHIF
fu	%	25.0 (Lit)	21.0, 24.0, 25.0	[116–119]	Fraction unbound in plasma
K_m (CYP3A4) CBZE	µmol/l	248.0 (Lit)	119.0, 248.0, 442.0, 630.0	[120–123]	CYP3A4 Michaelis-Menten constant
k_{cat} (CYP3A4) CBZE	1/min	0.75 (Fit)	1.17, 1.70, 4.87, 5.30[b]	[120–123]	CYP3A4 catalytic rate constant
K_m (CYP2C8)	µmol/l	757.0 (Lit)	757.0	[122]	CYP2C8 Michaelis-Menten constant
k_{cat} (CYP2C8)	1/min	0.67 (Lit)	0.67[b]	[122]	CYP2C8 catalytic rate constant
K_m (CYP2B6)	µmol/l	420.0 (Lit)	420.0	[124]	CYP2B6 Michaelis-Menten constant
k_{cat} (CYP2B6)	1/min	0.43 (Lit)	0.43[b]	[124]	CYP2B6 catalytic rate constant
K_m (CYP3A4)	µmol/l	282.0 (Lit)	282.0	[124]	CYP3A4 Michaelis-Menten constant
k_{cat} (CYP3A4)	1/min	0.20 (Fit)	0.16[b]	[124]	CYP3A4 catalytic rate constant
K_m (UGT2B7)	µmol/l	214.0 (Lit)	214.0	[107]	UGT2B7 Michaelis-Menten constant
k_{cat} (UGT2B7)	1/min	9.53E-3 (Lit)	9.53E-3[c]	[107]	UGT2B7 catalytic rate constant
CL_{hep}	1/min	0.02 (Fit)	-	-	Unspecified hepatic clearance
GFR fraction	-	0.03 (Fit)	-	-	Fraction of filtered drug in the urine
EC_{50} (CYP3A4)	µmol/l	20.00[a] (Lit)	4.3 - 137	[125–132]	Concentration for half-maximal induction
E_{max} (CYP3A4)	-	6.00 (Fit)	1.90 - 23.0	[125–132]	CYP3A4 maximum induction effect
EC_{50} (CYP2B6)	µmol/l	20.0[a] (Asm)	22 - 145	[132–134]	Concentration for half-maximal induction
E_{max} (CYP2B6)	-	17.0 (Fit)	3.10 - 21.50	[132–134]	CYP2B6 maximum induction effect
EC_{50} (EPHX1)	µmol/l	20.0[a] (Asm)	-	-	Concentration for half-maximal induction
E_{max} (EPHX1)	-	3.25 (Fit)	-	-	EPHX1 maximum induction effect
EC_{50} (CYP2C9)	µmol/l	20.0[a] (Asm)	-	-	Concentration for half-maximal induction
E_{max} (CYP2C9)	-	1.83 (Lit)	1.83	[132]	CYP2C9 maximum induction effect

asm: assumption, calc: calculated, CBZE: carbamazepine-10,11-epoxide, CL_{hep}: hepatic clearance, CL_{spec}: specific clearance, CYP: cytochrome P450, EPHX1: epoxide hydroxylase 1, FaHIF: fasted human intestinal fluid, IR: immediate release, fit: optimized during parameter optimization, lit: literature, UGT: UDP-glucuronosyltransferase, XR: extended release

[a] mean of literature values for EC_{50} (CYP3A4), assumed for all EC_{50} values

[b] k_{cat} values calculated within PK-Sim from V_{max}/recombinant enzyme

[c] k_{cat} value calculated within PK-Sim from V_{max} = 0.79 pmol/min/microsomal protein [107], assuming a microsomal UGT2B7 content of 82.9 pmol/mg microsomal protein [108], kcat = Vmax/ UGT2B7 content microsomes

Table S15: Drug-dependent parameters of the carbamazepine and carbamazepine-10,11-epoxide PBPK model according to [106] *(continued)*

Parameter	Unit	Model	Literature	Reference	Description
EC_{50} (CYP2C19)	µmol/l	20.0[a] (Asm)	-	-	Concentration for half-maximal induction
E_{max} (CYP2C19)	-	1.24 (Lit)	1.24	[132]	CYP2C19 maximum induction effect
K_i (CYP2C9)	µmol/l	90 (Lit)	90	[135]	Concentration for half-maximal inhibition
K_i (CYP2C19)	µmol/l	8 (Lit)	8	[135]	Concentration for half-maximal inhibition
Intestinal permeability	cm/min	2.58E-2 (Lit)	2.58E-2	[136]	Transcellular intestinal permeability
Partition coefficients	-	Diverse	Rodgers and Rowlands	[64, 65]	Cell to plasma partition coefficients
Cellular permeability	cm/min	0.02 (Calc)	PK-Sim Standard	[66]	Permeability into the cellular space
$t_{50\%}$ (IR tablet, fasted))	min	200.0	-	-	Dissolution time (50% dissolved)
s (IR tablet, fasted))	-	0.74	-	-	Dissolution profile shape
Carbamazepine-10,11-epoxide					
logP	Log Units	1.16 (Fit)	1.58, 1.97	[137]	Lipophilicity
Solubility	mg/ml	1.34 (Lit)	1.34	[137]	Solubility
fu	%	51.8 (Lit)	46.8-51.8	[138]	Fraction unbound in plasma
CL_{spec} (EPHX1)	1/min	0.01 (Fit)	0.05	-	EPHX1 first-order clearance
GFR fraction	-	0.21 (Fit)	-	-	Fraction of filtered drug in the urine
Intestinal permeability	cm/min	0.3 (Fit)	-	-	Transcellular intestinal permeability
Partition coefficients	-	Diverse	Rodgers and Rowlands	[64, 65]	Cell to plasma partition coefficients
Cellular permeability	cm/min	1.61E-3 (Calc)	PK-Sim Standard	[66]	Permeability into the cellular space

asm: assumption, calc: calculated, CBZE: carbamazepine-10,11-epoxide, CL_{hep}: hepatic clearance, CL_{spec}: specific clearance, CYP: cytochrome P450, EPHX1: epoxide hydroxylase 1, FaHIF: fasted human intestinal fluid, IR: immediate release, fit: optimized during parameter optimization, lit: literature, UGT: UDP-glucuronosyltransferase, XR: extended release

[a] mean of literature values for EC_{50} (CYP3A4), assumed for all EC_{50} values

[b] k_{cat} values calculated within PK-Sim from V_{max}/recombinant enzyme

[c] k_{cat} value calculated within PK-Sim from V_{max} = 0.79 pmol/min/microsomal protein [107], assuming a microsomal UGT2B7 content of 82.9 pmol/mg microsomal protein [108], kcat = Vmax/ UGT2B7 content microsomes

4.4.2 Carbamazepine-phenytoin-felodipine clinical studies

Table S16: Clinical studies investigating the carbamazepine-phenytoin DDI

Carbamazepine/phenytoin administration		Felodipine administration		Interval [h]	n	Healthy [%]	Females [%]	Age[a] [years]	Weight[a] [kg]	Reference
Dose [mg]	**Route**	**Dose [mg]**	**Route**							
757/325	po, md	5	po (tab), bid	-	10	0	10	28.6 ± 8.6	74 ± 15.6	Capewell 1988 [23]*
-	-	5	po (tab), bid D1-D5	-	12	100	8	28.7 ± 8.9	71.1 ± 9.0	Capewell 1988 [23]*

-: not given, bid: twice daily, D: day, md: multiple dose, n: number of individuals, po: oral, tab: tablet

[a] mean ± standard deviation

* control study (lower row) in healthy individuals, DDI study (upper row) in epileptic patients

4.4.3 Plasma concentration-time profiles

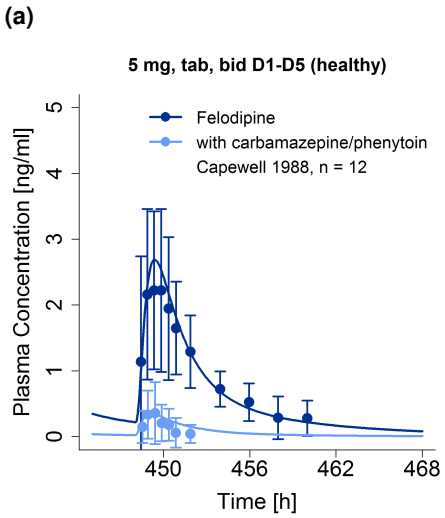

Figure S22: Predicted compared to observed felodipine plasma concentration-time profiles (linear) without and during carbamazepine and phenytoin co-administration. Observed data are shown as dots; model predictions are shown as solid lines ± standard deviation. Details on dosing regimens, study population and literature reference are listed in Table S16. bid: twice daily, D: day, n: number of individuals, tab: tablet.

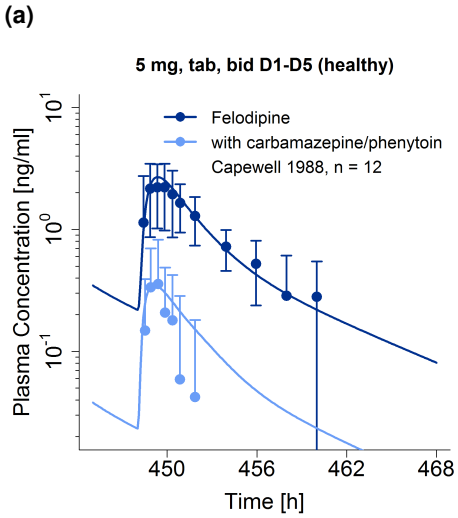

Figure S23: Predicted compared to observed felodipine plasma concentration-time profiles (semi-logarithmic) without and during carbamazepine and phenytoin co-administration. Observed data are shown as dots ± standard deviation; model predictions are shown as solid lines. Details on dosing regimens, study population and literature reference are listed in Table S16. bid: twice daily, D: day, n: number of individuals, tab: tablet.

4.4.4 DDI AUC_{last} and C_{max} ratio goodness-of-fit plots

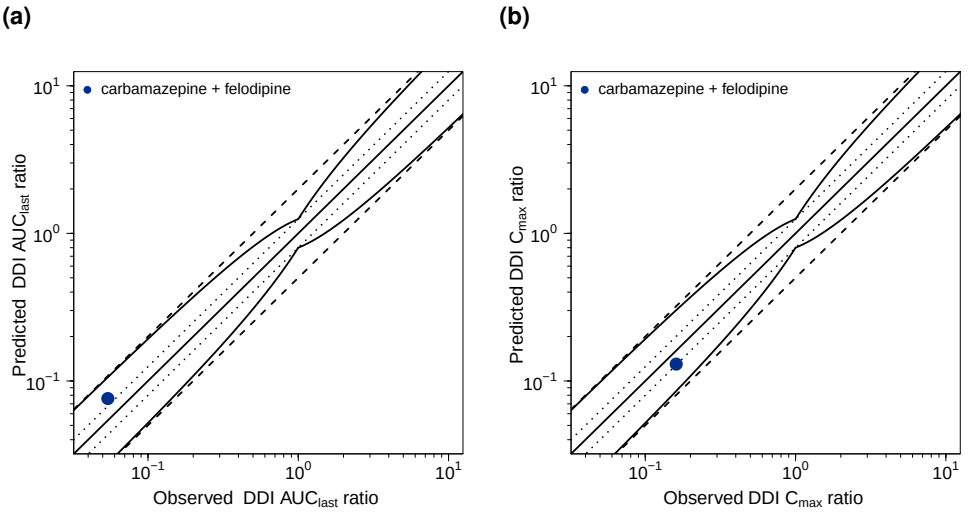

Figure S24: Predicted compared to observed carbamazepine-phenytoin-felodipine DDI AUC_{last} and DDI C_{max} values. The straight solid line marks the line of identity, the curved solid lines show the prediction success limits proposed by Guest et al. allowing for 1.25-fold variability of the DDI ratio [96]. Dotted lines indicate 1.25-fold, dashed lines indicate 2-fold deviation. AUC_{last}: area under the plasma concentration-time curve from the time of drug administration to the last concentration measurement, C_{max}: maximum plasma concentration, DDI: drug-drug interaction

4.4.5 Geometric mean fold error of predicted DDI AUC_{last} and C_{max} ratios

Table S17: Predicted and observed carbamazepine-phenytoin-felodipine DDI AUC_{last} ratios and DDI C_{max} ratios

Perpetrator	**Victim**	**Compound**	**Dose gap [h]**	**n**	**DDI AUC_{last} ratio**			**DDI C_{max} ratio**			
Carbamazepine/Phenytoin	Felodipine				**Pred**	**Obs**	**Pred/Obs**	**Pred**	**Obs**	**Pred/Obs**	**Reference**
757/325 mg, po, md	5 mg, po (tab), bid D1-D5	Felodipine	-	10	0.08	0.05	1.41	0.13	0.16	0.81	Capewell 1988 [23]
GMFE							**1.41**			**1.19**	
							1/1 with GMFE < 2			**1/1 with GMFE < 2**	

-: not given, AUC_{last}: area under the plasma concentration-time curve from the time of drug administration to the last concentration measurement, bid: twice daily, C_{max}: maximum plasma concentration, D: day, DDI: drug-drug interaction, GMFE: geometric mean fold error, md: multiple dose, n: number of individuals, obs: observed, po: oral, pred: predicted, tab: tablet

5 System-dependent parameters

Details on the expression of metabolizing enzymes and transport proteins implemented to model the pharmacokinetics of felodipine and dehydrofelodipine and of the perpetrator models erythromycin, itraconazole, carbamazepine and phenytoin are summarized in Table S18. As enterohepatic circulation is active under physiological conditions, the parameter EHC continuous fraction was set to 1 in all individuals.

Table S18: System-dependent parameters

	Reference concentration				Half-life	
Enzyme/ Transporter	**Mean[a] [µmol/l]**	**Relative expression[b]**	**Localization**	**Direction**	**Liver [h]**	**Intestine [h]**
CYP3A4	4.32 [140]	RT-PCR [141]	Intracellular	-	36 [142]	23 [143]
CYP2B6	1.56 [140]	RT-PCR [141]	Intracellular	-	32	23
CYP2C8	2.56 [140]	RT-PCR [141]	Intracellular	-	23	23
CYP2C9	3.84 [140]	RT-PCR [141]	Intracellular	-	104	23
CYP2C19	0.76 [140]	RT-PCR [141]	Intracellular	-	26	23
EPHX1	1.00[c] [139]	RT-PCR [144]	Intracellular	-	36	23
UGT2B7	2.78 [145]	EST [146]	Intracellular	-	36	23
OATP1B1	1.00[c] [139]	RT-PCR [147]	Basolateral	Influx	36	-

-: not given, CYP: cytochrome P450, EPHX1: epoxidehydroxylase 1, EST: expressed sequence tags expression profile, OATP1B1: organic anion transporting polypeptide 1B1, RT-PCR: reverse transcription-polymerase chain reaction profile, UGT: UDP-glucuronosyltransferase

[a] µmol/lol protein/l in the tissue of highest expression

[b] in the different organs (PK-Sim® expression database profile)

[c] if no information was available, the mean reference concentration was set to 1.00 µmol/l and the catalytic rate constant (kcat) was optimized [139]

List of Figures

List of Tables

Abbreviations

ADME	Absorption, distribution, metabolism and excretion
amp	Circadian amplitude
AUC	Area under the concentration-time curve
AUC_{last}	AUC values calculated from the time of drug administration to the time of the last concentration measurement
asm	Assumption
bid	Twice daily
BP	Blood pressure
calc	Calculated
CBZ	Carbamazepine
CBZE	Carbamazepine-10,11-epoxide
circ	Circadian rhythm
CL_{hep}	Hepatic clearance
CL	C clearance
C_{max}	Maximum plasma concentration
CYP	Cytochrome P450
D	Day
DDI	Drug-drug interaction
DHF	Dehydrofelodipine
EC50	Concentration for half maximal induction in vivo
EHC	Enterohepatic circulation
E_{max}	Maximum induction effect in vivo
EPHX1	Epoxide hydroxylase 1
EST	Expressed sequence tag
fu	Fraction unbound in plasma
GFR	Glomerular filtration rate
GMFE	Geometric mean fold error
HR	Heart rate
HT	Hypertension
IC_{50}	Half maximal inhibitory concentration

IR	Immediate release
iv	Intravenous
k_{cat}	Transport or catalytic rate constant
k_{deg}	Degradation rate constant
$k_{deg,\ app}$	Degradation rate constant in the presence of a mechanism based inhibitor
K_i	Dissociation constant of the inhibitor-transporter/ -enzyme complex
K_{inact}	Maximum inactivation rate
K_M	Michaelis-Menten constant
$K_{M,app}$	Michaelis-Menten constant in the presence of inhibitor
logP	Lipophilicity
lit	Literature
MRD	Mean relative deviation
md	Multiple dose
MW	Molecular weight
OATP	Organic-anion-transporting polypeptide
obs	Observed
opt	Optimized
OSP	Open Systems Pharmacology
PD	Pharmacodynamics
PBPK	Physiologically based pharmacokinetic
pKa	Acid dissociation constant
po	Oral
pred	Predicted
qid	Four times daily
qd	Once daily
RI	Renal impairment
R_{syn}	Rate of transporter or enzyme synthesis
$R_{syn,app}$	Rate of transporter or enzyme synthesis in the presence of inducer
RT-PCR	Reverse transcription-polymerase chain reaction
sd	Single dose
s	Weibull dissolution shape
sol	Solution

tab	Tablet
tabER	Extended release tablet
UGT	UDP-glucuronosyltransferase
v	Reaction velocity
$\mathbf{v_{max}}$	Maximum reaction velocity

Bibliography

[1] Open Systems Pharmacology Suite Community. Open Systems Pharmacology Suite Manual, 2018. URL https://docs.open-systems-pharmacology.org/. accessed: 14 Dec 2020.

[2] D. Chae, Y. Kim, and K. Park. Characterization of circadian blood pressure patterns using non-linear mixed effects modeling. *Translational and clinical pharmacology*, 27(1):24–32, mar 2019.

[3] D. Lott, T. Lehr, J. Dingemanse, and A. Krause. Modeling Tolerance Development for the Effect on Heart Rate of the Selective S1P1 Receptor Modulator Ponesimod. *Clinical pharmacology and therapeutics*, 103(6):1083–1092, 2018.

[4] P. A. Soons, M. C. Roosemalen, and D. D. Breimer. Enantioselective determination of felodipine and other chiral dihydropyridine calcium entry blockers in human plasma. *Journal of chromatography*, 528(2):343–56, jun 1990.

[5] U. G. Eriksson, J. Lundahl, C. Bäärnhielm, and C. G. Regårdh. Stereoselective metabolism of felodipine in liver microsomes from rat, dog, and human. *Drug metabolism and disposition*, 19(5):889–94, 1991.

[6] B. Bengtsson-Hasselgren, B. Edgar, and O. Rönn. Dose-dependent effects of felodipine on diuresis and natriuresis in healthy subjects. *Journal of cardiovascular pharmacology*, 12(2):134–9, aug 1988.

[7] B. Edgar, C. G. Regårdh, P. Lundborg, S. Romare, G. Nyberg, and O. Rönn. Pharmacokinetic and pharmacodynamic studies of felodipine in healthy subjects after various single, oral and intravenous doses. *Biopharmaceutics & drug disposition*, 8(3):235–48, 1987.

[8] T. A. Sutfin, T. Lind, M. Gabrielsson, and C. G. Regårdh. Biliary secretion of felodipine metabolites in man after intravenous [14C] felodipine. *European journal of clinical pharmacology*, 38(5):421–4, 1990.

[9] H. E. Sluiter, F. T. Huysmans, T. A. Thien, and R. A. Koene. Haemodynamic effects of intravenous felodipine in normotensive and hypertensive subjects. *Drugs*, 29(Suppl 2): 144–53, 1985.

[10] J. Lundahl, C. G. Regårdh, B. Edgar, and G. Johnsson. Effects of grapefruit juice ingestion–pharmacokinetics and haemodynamics of intravenously and orally administered felodipine in healthy men. *European journal of clinical pharmacology*, 52(2): 139–45, 1997.

[11] B. Edgar, B. Bengtsson, D. Elmfeldt, P. Lundborg, G. Nyberg, S. Raner, and O. Rönn. Acute diuretic/natriuretic properties of felodipine in man. *Drugs*, 29(Suppl 2):176–84, 1985.

[12] B. Edgar, C. G. Regårdh, G. Johnsson, L. Johansson, P. Lundborg, I. Löfberg, and O. Rönn. Felodipine kinetics in healthy men. *Clinical pharmacology and therapeutics*, 38 (2):205–11, aug 1985.

[13] B. Abrahamsson, D. Johansson, A. Torstensson, and K. Wingstrand. Evaluation of solubilizers in the drug release testing of hydrophilic matrix extended-release tablets of felodipine. *Pharmaceutical research*, 11(8):1093–7, aug 1994.

[14] B. Bengtsson-Hasselgren, O. Rönn, L. O. Blychert, B. Edgar, and S. Raner. Acute effects of felodipine and nifedipine on hepatic and forearm blood flow in healthy men. *European journal of clinical pharmacology*, 38(6):529–33, 1990.

[15] B. Edgar, P. Lundborg, and C. G. Regårdh. Clinical pharmacokinetics of felodipine. A summary. *Drugs*, 34(Suppl 3):16–27, 1987.

[16] K. Wingstrand, B. Abrahamsson, and B. Edgar. Bioavailability from felodipine extended-release tablets with different dissolution properties. *International Journal of Pharmaceutics*, 60(2):151–156, apr 1990.

[17] E. Blychert, K. Wingstrand, B. Edgar, and K. Lidman. Plasma concentration profiles and antihypertensive effect of conventional and extended-release felodipine tablets. *British journal of clinical pharmacology*, 29(1):39–45, jan 1990.

[18] G. Johnsson, G. Murray, A. Tweddel, and I. Hutton. Haemodynamic effects of a new vasodilator drug, felodipine, in healthy subjects. *European journal of clinical pharmacology*, 24(1):49–53, 1983.

[19] P. A. Soons, T. M. Mulders, E. Uchida, H. C. Schoemaker, A. F. Cohen, and D. D. Breimer. Stereoselective pharmacokinetics of oral felodipine and nitrendipine in healthy subjects: correlation with nifedipine pharmacokinetics. *European journal of clinical pharmacology*, 44(2):163–9, 1993.

[20] D. G. Bailey, J. M. Arnold, C. Munoz, and J. D. Spence. Grapefruit juice-felodipine interaction: mechanism, predictability, and effect of naringin. *Clinical pharmacology and therapeutics*, 53(6):637–42, jun 1993.

[21] B. Edgar, D. Bailey, R. Bergstrand, G. Johnsson, and C. G. Regårdh. Acute effects of drinking grapefruit juice on the pharmacokinetics and dynamics of felodipine-and its potential clinical relevance. *European journal of clinical pharmacology*, 42(3):313–7, 1992.

[22] S. Landahl, B. Edgar, M. Gabrielsson, M. Larsson, B. Lernfelt, P. Lundborg, and C. G. Regårdh. Pharmacokinetics and blood pressure effects of felodipine in elderly hypertensive patients. A comparison with young healthy subjects. *Clinical pharmacokinetics*, 14(6):374–83, jun 1988.

[23] S. Capewell, S. Freestone, J. A. Critchley, A. Pottage, and L. F. Prescott. Reduced felodipine bioavailability in patients taking anticonvulsants. *Lancet (London, England)*, 2 (8609):480–2, aug 1988.

[24] L.-Q. Guo, Q.-Y. Chen, X. Wang, Y.-X. Liu, X.-M. Chu, X.-M. Cao, J.-H. Li, and Y. Yamazoe. Different roles of pummelo furanocoumarin and cytochrome P450 3A5*3 polymorphism in the fate and action of felodipine. *Current drug metabolism*, 8(6):623–30, aug 2007.

[25] B. Lindmark, M. Ahnoff, and B.-A. Persson. Enantioselective determination of felodipine in human plasma by chiral normal-phase liquid chromatography and electrospray ionisation mass spectrometry. *Journal of pharmaceutical and biomedical analysis*, 27(3-4): 489–95, jan 2002.

[26] B. G. Hardy, W. R. Bartle, M. Myers, D. G. Bailey, and B. Edgar. Effect of indomethacin on the pharmacokinetics and pharmacodynamics of felodipine. *British journal of clinical pharmacology*, 26(5):557–62, nov 1988.

[27] G. K. Dresser, D. G. Bailey, and S. G. Carruthers. Grapefruit juice-felodipine interaction in the elderly. *Clinical pharmacology and therapeutics*, 68(1):28–34, jul 2000.

[28] K. M. Jalava, K. T. Olkkola, and P. J. Neuvonen. Itraconazole greatly increases plasma concentrations and effects of felodipine. *Clinical pharmacology and therapeutics*, 61(4): 410–5, apr 1997.

[29] J. C. A. Carrasco, M. d. C. C. Portugal, F. J. F. Murrieta, and S. C. Quinteros. Oral Pharmacokinetics of Felodipine in Mexican Healthy Volunteers: Evidence for Interethnic Differences. *International Journal of Pharmacology*, 11(4):382–386, may 2015.

[30] T. C. Goosen, D. Cillié, D. G. Bailey, C. Yu, K. He, P. F. Hollenberg, P. M. Woster, L. Cohen, J. A. Williams, M. Rheeders, and H. P. Dijkstra. Bergamottin contribution to the grapefruit juice-felodipine interaction and disposition in humans. *Clinical pharmacology and therapeutics*, 76(6):607–17, dec 2004.

[31] Q. Xiang, C. Li, X. Zhao, and Y. M. Cui. The influence of CYP3A5*3 and BCRPC421A genetic polymorphisms on the pharmacokinetics of felodipine in healthy Chinese volunteers. *Journal of clinical pharmacy and therapeutics*, 42(3):345–349, jun 2017.

[32] A comparative study on the relative bioavailability of 2.5 and 5mg ER tablets of felodipine. NDA: 19-834, 1994. URL https://www.accessdata.fda.gov/drugsatfda_docs/nda/pre96/19834-S002_PLENDILTABLETS_BIOEQR.PDF. accessed: 02 Jun 2022.

[33] D. G. Bailey, J. M. Arnold, J. R. Bend, L. T. Tran, and J. D. Spence. Grapefruit juice-felodipine interaction: reproducibility and characterization with the extended release drug formulation. *British journal of clinical pharmacology*, 40(2):135–40, aug 1995.

[34] J. K. Madsen, J. D. Jensen, L. W. Jensen, and E. B. Pedersen. Pharmacokinetic interaction between cyclosporine and the dihydropyridine calcium antagonist felodipine. *European journal of clinical pharmacology*, 50(3):203–8, 1996.

[35] D. G. Bailey, J. R. Bend, J. M. Arnold, L. T. Tran, and J. D. Spence. Erythromycin-felodipine interaction: magnitude, mechanism, and comparison with grapefruit juice. *Clinical pharmacology and therapeutics*, 60(1):25–33, jul 1996.

[36] D. G. Bailey, J. H. Kreeft, C. Munoz, D. J. Freeman, and J. R. Bend. Grapefruit juice-felodipine interaction: effect of naringin and 6',7'-dihydroxybergamottin in humans. *Clinical pharmacology and therapeutics*, 64(3):248–56, sep 1998.

[37] D. G. Bailey, G. K. Dresser, J. H. Kreeft, C. Munoz, D. J. Freeman, and J. R. Bend. Grapefruit-felodipine interaction: effect of unprocessed fruit and probable active ingredients. *Clinical pharmacology and therapeutics*, 68(5):468–77, nov 2000.

[38] D. G. Bailey, G. K. Dresser, and J. R. Bend. Bergamottin, lime juice, and red wine as inhibitors of cytochrome P450 3A4 activity: comparison with grapefruit juice. *Clinical pharmacology and therapeutics*, 73(6):529–37, jun 2003.

[39] G. K. Dresser, B. L. Urquhart, J. Proniuk, A. Tieu, D. J. Freeman, J. M. Arnold, and D. G. Bailey. Coffee inhibition of CYP3A4 in vitro was not translated to a grapefruit-like pharmacokinetic interaction clinically. *Pharmacology research & perspectives*, 5(5):1–9, 2017.

[40] B. Hasselgren, O. Rönn, B. Edgar, P. Johansson, and B. Wall. Pharmacokinetics and hemodynamic and diuretic/natriuretic effects of felodipine administered as an extended-release tablet. *Cardiovascular drugs and therapy*, 4(6):1495–500, dec 1990.

[41] K. S. Lown, D. G. Bailey, R. J. Fontana, S. K. Janardan, C. H. Adair, L. A. Fortlage, M. B. Brown, W. Guo, and P. B. Watkins. Grapefruit juice increases felodipine oral availability

in humans by decreasing intestinal CYP3A protein expression. *The Journal of clinical investigation*, 99(10):2545–53, may 1997.

[42] J. Lundahl, C. G. Regårdh, B. Edgar, and G. Johnsson. Relationship between time of intake of grapefruit juice and its effect on pharmacokinetics and pharmacodynamics of felodipine in healthy subjects. *European journal of clinical pharmacology*, 49(1-2):61–7, 1995.

[43] J. U. Lundahl, C. G. Regårdh, B. Edgar, and G. Johnsson. The interaction effect of grapefruit juice is maximal after the first glass. *European journal of clinical pharmacology*, 54(1):75–81, mar 1998.

[44] A. Pop, L. Vlase, and Leucuta. Pharmacokinetic study of felodipine after single oral dose of slow release formulations in healthy volunteers. *Farmacia*, 56(5):474–82, 2008.

[45] A. Gelal, D. Balkan, D. Ozzeybek, Y. C. Kaplan, S. Gurler, H. Guven, and N. L. Benowitz. Effect of menthol on the pharmacokinetics and pharmacodynamics of felodipine in healthy subjects. *European journal of clinical pharmacology*, 60(11):785–90, jan 2005.

[46] W. Weitschies, R.-S. Wedemeyer, O. Kosch, K. Fach, S. Nagel, E. Söderlind, L. Trahms, B. Abrahamsson, and H. Mönnikes. Impact of the intragastric location of extended release tablets on food interactions. *Journal of controlled release : official journal of the Controlled Release Society*, 108(2-3):375–85, nov 2005.

[47] S. Patel Devang, N. Shanker, K. Shah Sweety, K. Thakkar Vaishali, N. Mehta Nirali, K. Srivstava Ambrish, S. Singh, and G. Patel Chitrang. Bioequivalence Study of Two Oral Extended Release Formulations of Felodipine 10 mg Tablets in Healthy Volunteers under Fed Condition. *Pharma Science Monitor - An International Journal Of Pharmaceutical Sciences*, 2(2, Supplement 1):9–20, 2011.

[48] S. R. Smith, M. R. Wilkins, D. B. Jack, M. J. Kendall, and S. Laugher. Pharmacokinetic interactions between felodipine and metoprolol. *European journal of clinical pharmacology*, 31(5):575–8, 1987.

[49] B. Edgar, C. G. Regårdh, P. O. Attman, M. Aurell, H. Herlitz, and G. Johnsson. Pharmacokinetics of felodipine in patients with impaired renal function. *British journal of clinical pharmacology*, 27(1):67–74, jan 1989.

[50] E. Blychert, T. Hedner, C. Dahlöf, and D. Elmfeldt. Plasma concentration-effect relationships of intravenous and extended-release oral felodipine in hypertensive patients. *Journal of cardiovascular pharmacology*, 15(3):428–35, mar 1990.

[51] R. Larsson, B. E. Karlberg, A. Gelin, J. Aberg, and C. G. Regårdh. Acute and steady-state pharmacokinetics and antihypertensive effects of felodipine in patients with normal and impaired renal function. *Journal of clinical pharmacology*, 30(11):1020–30, nov 1990.

[52] T. Hedner, D. Elmfeldt, C. Dahlöf, and E. Sjögren. Comparison of antihypertensive effect and pharmacokinetics of conventional and extended release felodipine tablets in patients with arterial hypertension. *Drugs*, 34(Suppl 3):125–31, 1987.

[53] F. H. H. Leenen and E. Coletta. Pharmacokinetic and antihypertensive profile of amlodipine and felodipine-ER in younger versus older patients with hypertension. *Journal of cardiovascular pharmacology*, 56(6):669–75, dec 2010.

[54] T. Hedner, O. Samuelsson, E. Sjögren, and D. Elmfeldt. Treatment of essential hypertension with felodipine in combination with a diuretic. *European journal of clinical pharmacology*, 30(2):133–9, 1986.

[55] Human Metabolome Database. Metabocard for Felodipine (HMDB0015158). URL https://hmdb.ca/metabolites/HMDB0015158. accessed: 02 Jun 2022.

[56] C. G. Regårdh, B. Edgar, R. Olsson, M. Kendall, P. Collste, and C. Shansky. Pharmacokinetics of felodipine in patients with liver disease. *European journal of clinical pharmacology*, 36(5):473–9, 1989.

[57] K. Felle, B. Persson, and J. Vessman. Dissolution test for felodipine tablets using chemical oxidation in situ to maintain 'sink conditions'. *Journal of Pharmaceutical and Biomedical Analysis*, 2(3/4):527–536, jan 1984.

[58] DRUGBANK online - Felodipine, 2022. URL https://go.drugbank.com/drugs/DB01023. accessed: 02 Jun 2022.

[59] J. Takano, K. Maeda, M. B. Bolger, and Y. Sugiyama. The Prediction of the Relative Importance of CYP3A/P-glycoprotein to the Nonlinear Intestinal Absorption of Drugs by Advanced Compartmental Absorption and Transit Model. *Drug metabolism and disposition: the biological fate of chemicals*, 44(11):1808–1818, 2016.

[60] R. van der Lee, M. Pfaffendorf, R. P. Koopmans, J. J. van Lieshout, G. A. van Montfrans, and P. A. van Zwieten. Comparison of the time courses and potencies of the vasodilator effects of nifedipine and felodipine in the human forearm. *Blood pressure*, 10(4):217–22, 2001.

[61] P. Berben, J. Brouwers, and P. Augustijns. Assessment of Passive Intestinal Permeability Using an Artificial Membrane Insert System. *Journal of pharmaceutical sciences*, 107 (1):250–256, 2018.

[62] R. L. Walsky and R. S. Obach. Validated assays for human cytochrome P450 activities. *Drug metabolism and disposition: the biological fate of chemicals*, 32(6):647–60, jun 2004.

[63] A. Galetin, S. E. Clarke, and J. B. Houston. Quinidine and haloperidol as modifiers of CYP3A4 activity: multisite kinetic model approach. *Drug metabolism and disposition: the biological fate of chemicals*, 30(12):1512–22, dec 2002.

[64] T. Rodgers, D. Leahy, and M. Rowland. Physiologically based pharmacokinetic modeling 1: predicting the tissue distribution of moderate-to-strong bases. *Journal of pharmaceutical sciences*, 94(6):1259–76, jun 2005.

[65] M. J. Taylor, S. Tanna, and T. Sahota. In vivo study of a polymeric glucose-sensitive insulin delivery system using a rat model. *Journal of pharmaceutical sciences*, 99(10): 4215–27, 2010.

[66] R. Kawai, M. Lemaire, J. L. Steimer, A. Bruelisauer, W. Niederberger, and M. Rowland. Physiologically based pharmacokinetic study on a cyclosporin derivative, SDZ IMM 125. *Journal of pharmacokinetics and biopharmaceutics*, 22(5):327–65, oct 1994.

[67] Chemaxon. Chemicalize - Dehydrofelodipine, 2022. URL https://chemicalize.com/welcome.

[68] W. Schmitt. General approach for the calculation of tissue to plasma partition coefficients. *Toxicology in vitro : an international journal published in association with BIBRA*, 22(2): 457–67, mar 2008.

[69] S. Frechen and A. Dallmann. Building and evaluation of a PBPK model for erythromycin in healthy adults, 2020. URL https://github.com/Open-Systems-Pharmacology/OSP-PBPK-Model-Library/blob/v9.1/Erythromycin/Erythromycin_evaluation_report.pdf. accessed: 02 Jun 2022.

[70] S. Frechen. CYP3A4 DDI Qualification, 2020. URL https://github.com/Open-Systems-Pharmacology/OSP-Qualification-Reports/blob/v9.1/DDI_Qualification_CYP3A4/report.pdf. accessed: 02 Jun 2022.

[71] Drugbank. Erythromycin, 2020. URL https://go.drugbank.com/drugs/DB00199. accessed: 02 Jun 2022.

[72] E. Lien, J. Kuwahara, and R. Koda. Diffusion of drugs into prostatic fluid and milk. *Drug intelligence & Clinical Pharmacy*, 8(8):470–475, 1974.

[73] J. O. Capobianco and R. C. Goldman. Macrolide transport in Escherichia coli strains having normal and altered OmpC and/or OmpF porins. *International journal of antimicrobial agents*, 4(3):183–9, 1994.

[74] J. W. McFarland, C. M. Berger, S. A. Froshauer, S. F. Hayashi, S. J. Hecker, B. H. Jaynes, M. R. Jefson, B. J. Kamicker, C. A. Lipinski, K. M. Lundy, C. P. Reese, and C. B. Vu. Quantitative structure-activity relationships among macrolide antibacterial agents: In vitro and in vivo potency against Pasteurella multocida. *Journal of Medicinal Chemistry*, 40 (9):1340–1346, 1997.

[75] C. Hoffhine. Aqueous soluble salts of erythromycin. Issues September 4. Nr. 2,761,859, 1956. URL https://patents.google.com/patent/US2761859A/en. accessed: 02 Jun 2022.

[76] P. H. Jones, E. K. Rowley, A. L. Weiss, D. L. Bishop, and A. H. Chun. Insoluble erythromycin salts. *Journal of Pharmaceutical Sciences*, 58(3):337–339, 1969.

[77] P. K. Manna and S. K. Basu. Preparation and evaluation of erythromycin fumarate - A new derivative of erythromycin. *Drug Development and Industrial Pharmacy*, 24(9): 879–882, 1998.

[78] H. Sun, L. A. Frassetto, Y. Huang, and L. Z. Benet. Hepatic clearance, but not gut availability, of erythromycin is altered in patients with end-stage renal disease. *Clinical Pharmacology & Therapeutics*, 87(4):465–472, 2010.

[79] A. Iliopoulou, M. Aldhous, A. Johnston, and P. Turner. Pharmacokinetic interaction between theophylline and erythromycin. *British Journal of Clinical Pharmacology*, 14 (4):495–499, 1982.

[80] J. Barre, A. Mallat, J. Rosenbaum, L. Deforges, G. Houin, D. Dhumeaux, and J. Tillement. Pharmacokinetics of erythromycin in patients with severe cirrhosis. Respective influence of decreased serum binding and impaired liver metabolic capacity. *British Journal of Clinical Pharmacology*, 23(6):753–757, 1987.

[81] L. Xu, Y. Chen, Y. Pan, G. L. Skiles, and M. Shou. Prediction of human drug-drug interactions from time-dependent inactivation of CYP3A4 in primary hepatocytes using a population-based simulator. *Drug Metabolism and Disposition*, 37(12):2330–2339, 2009.

[82] R. W. Wang, D. J. Newton, T. D. Scheri, and A. Y. Lu. Human cytochrome P450 3A4-catalyzed testosterone 6 beta-hydroxylation and erythromycin N-demethylation. Competition during catalysis. *Drug metabolism and disposition: the biological fate of chemicals*, 25(4):502–7, 1997.

[83] R. J. Riley and D. Howbrook. In vitro analysis of the activity of the major human hepatic CYP enzyme (CYP3A4) using [N-methyl-14C]-erythromycin. *Journal of Pharmacological and Toxicological Methods*, 38(4):189–193, dec 1997.

[84] C. S. Lancaster, G. H. Bruun, C. J. Peer, T. S. Mikkelsen, T. J. Corydon, A. A. Gibson, S. Hu, S. J. Orwick, R. H. J. Mathijssen, W. D. Figg, S. D. Baker, and A. Sparreboom. OATP1B1 polymorphism as a determinant of erythromycin disposition. *Clinical Pharmacology & Therapeutics*, 92(5):642–650, nov 2012.

[85] T. Akiyoshi, M. Ito, S. Murase, M. Miyazaki, F. P. Guengerich, K. Nakamura, K. Yamamoto, and H. Ohtani. Mechanism-based inhibition profiles of erythromycin and clarithromycin with cytochrome P450 3A4 genetic variants. *Drug metabolism and pharmacokinetics*, 28 (5):411–5, 2013.

[86] A. Atkinson, J. R. Kenny, and K. Grime. Automated assessment of time-dependent inhibition of human cytochrome P450 enzymes using liquid chromatography-tandem mass spectrometry analysis. *Drug Metabolism and Disposition*, 33(11):1637–1647, nov 2005.

[87] S. Aueviriyavit, K. Kobayashi, and K. Chiba. Species differences in mechanism-based inactivation of CYP3A in humans, rats and mice. *Drug Metabolism and Pharmacokinetics*, 25(1):93–100, 2010.

[88] W. K. Chan and A. B. Delucchi. Resveratrol, a red wine constituent, is a mechanism-based inactivator of cytochrome P450 3A4. *Life Sciences*, 67(25):3103–3112, nov 2000.

[89] Y. Chen, L. Liu, M. Monshouwer, and A. J. Fretland. Determination of time-dependent inactivation of CYP3A4 in cryopreserved human hepatocytes and assessment of human drug-drug interactions. *Drug Metabolism and Disposition*, 39(11):2085–2092, nov 2011.

[90] Y. Ishikawa, T. Akiyoshi, A. Imaoka, and H. Ohtani. Inactivation kinetics and residual activity of CYP3A4 after treatment with erythromycin. *Biopharmaceutics & Drug Disposition*, 38(7):420–425, 2017.

[91] S. Kanamitsu, I. K, G. CE, C. Tyson, N. Shimada, and Y. Sugiyama. Prediction of in vivo interaction between triazolam and erythromycin based on in vitro studies using human liver microsomes and recombinant human CYP3A4. *Pharmaceutical Research*, 17(4): 419–426, 2000.

[92] K. Kozakai, Y. Yamada, M. Oshikata, T. Kawase, E. Suzuki, Y. Haramaki, and H. Taniguchi. Cocktail-substrate approach-based high-throughput assay for evaluation of direct and time-dependent inhibition of multiple cytochrome P450 isoforms. *Drug Metabolism and Pharmacokinetics*, 29(2):198–207, 2014.

[93] J. Mao, S. Tay, C. S. Khojasteh, Y. Chen, C. E. C. A. Hop, and J. R. Kenny. Evaluation of time dependent inhibition assays for marketed oncology drugs: Comparison of human hepatocytes and liver microsomes in the presence and absence of human plasma. *Pharmaceutical Research*, 33(5):1204–1219, 2016.

[94] D. J. McConn, Y. S. Lin, K. Allen, K. L. Kunze, and K. E. Thummel. Differences in the inhibition of cytochromes P450 3A4 and 3A5 by metabolite-inhibitor complex-forming drugs. *Drug Metabolism and Disposition*, 32(10):1083–1091, 2004.

[95] X. Zhang, D. R. Jones, and S. D. Hall. Prediction of the effect of erythromycin, diltiazem, and their metabolites, alone and in combination, on CYP3A4 inhibition. *Drug Metabolism and Disposition*, 37(1):150–160, 2009.

[96] E. J. Guest, L. Aarons, J. B. Houston, A. Rostami-Hodjegan, and A. Galetin. Critique of the two-fold measure of prediction success for ratios: application for the assessment of drug-drug interactions. *Drug metabolism and disposition: the biological fate of chemicals*, 39(2):170–3, feb 2011.

[97] N. Hanke, S. Frechen, D. Moj, H. Britz, T. Eissing, T. Wendl, and T. Lehr. PBPK Models for CYP3A4 and P-gp DDI prediction: a modeling network of rifampicin, itraconazole, clarithromycin, midazolam, alfentanil, and digoxin. *CPT: pharmacometrics & systems pharmacology*, 7(10):647–59, oct 2018.

[98] J. Heykants, A. Van Peer, V. Van de Velde, P. Van Rooy, W. Meuldermans, K. Lavrijsen, R. Woestenborghs, J. Van Cutsem, and G. Cauwenbergh. The clinical pharmacokinetics of itraconazole: an overview. *Mycoses*, 32 Suppl 1:67–87, 1989.

[99] I. E. Templeton, K. E. Thummel, E. D. Kharasch, K. L. Kunze, C. Hoffer, W. L. Nelson, and N. Isoherranen. Contribution of itraconazole metabolites to inhibition of CYP3A4 in vivo. *Clinical pharmacology and therapeutics*, 83(1):77–85, jan 2008.

[100] K. Riccardi, S. Cawley, P. D. Yates, C. Chang, C. Funk, M. Niosi, J. Lin, and L. Di. Plasma Protein Binding of Challenging Compounds. *Journal of pharmaceutical sciences*, 104(8): 2627–36, aug 2015.

[101] M. Ishigam, M. Uchiyama, T. Kondo, H. Iwabuchi, S. I. Inoue, W. Takasaki, T. Ikeda, T. Komai, K. Ito, and Y. Sugiyama. Inhibition of in vitro metabolism of simvastatin by itraconazole in humans and prediction of in vivo drug-drug interactions. *Pharmaceutical Research*, 18(5):622–631, 2001.

[102] N. Isoherranen, K. L. Kunze, K. E. Allen, W. L. Nelson, and K. E. Thummel. Role of itraconazole metabolites in CYP3A4 inhibition. *Drug metabolism and disposition: the biological fate of chemicals*, 32(10):1121–31, oct 2004.

[103] National Center for Biotechnology Information (NCBI). Hydroxy-itraconazole - PubChem Identifier: CID 108222. PubChem Database., . URL https://pubchem.ncbi.nlm.nih.gov/compound/108222. accessed: 02 Jun 2022.

[104] National Center for Biotechnology Information (NCBI). Keto-itraconazole - PubChem Identifier: CID 45039625. PubChem Database., . URL https://pubchem.ncbi.nlm.nih.gov/compound/45039625. accessed: 02 Jun 2022.

[105] National Center for Biotechnology Information (NCBI). N-Desalkyl-itraconazole - PubChem Identifier: CID 53789808. PubChem Database., . URL https://pubchem.ncbi.nlm.nih.gov/compound/53789808. accessed: 02 Jun 2022.

[106] L. M. Fuhr, F. Z. Marok, N. Hanke, D. Selzer, and T. Lehr. Pharmacokinetics of the CYP3A4 and CYP2B6 Inducer Carbamazepine and Its Drug-Drug Interaction Potential: A Physiologically Based Pharmacokinetic Modeling Approach. *Pharmaceutics*, 13(2): 1–21, feb 2021.

[107] A. G. Staines, M. W. Coughtrie, and B. Burchell. N-glucuronidation of carbamazepine in human tissues is mediated by UGT2B7. *Journal of Pharmacology and Experimental Therapeutics*, 311(3):1131–1137, 2004.

[108] B. Achour, M. R. Russell, J. Barber, and A. Rostami-Hodjegan. Simultaneous quantification of the abundance of several cytochrome P450 and uridine 5-diphosphoglucuronosyltransferase enzymes in human liver microsomes using multiplexed targeted proteomics. *Drug Metabolism and Disposition*, 42(4):500–510, 2014.

[109] Drugbank. Carbamazepine, 2018. URL https://www.drugbank.ca/drugs/DB00564. accessed: 02 Jun 2022.

[110] R. P. Austin, P. Barton, S. L. Cockroft, M. C. Wenlock, and R. J. Riley. The influence of nonspecific microsomal binding on apparent intrinsic clearance, and its prediction from physicochemical properties. *Drug Metabolism and Disposition*, 30(12):1497–1503, 2002.

[111] A. Avdeef. *Absorption and drug development - Solubility, permeability, and charge state*. 2003. ISBN 3175723993.

[112] P. Annaert, Z. Ye, B. Stieger, and P. Augustijns. Interaction of HIV protease inhibitors with OATP1B1, 1B3, and 2B1. *Xenobiotica*, 40(3):163–176, 2010.

[113] S. Clarysse, J. Brouwers, J. Tack, P. Annaert, and P. Augustijns. Intestinal drug solubility estimation based on simulated intestinal fluids: Comparison with solubility in human intestinal fluids. *European Journal of Pharmaceutical Sciences*, 43(4):260–269, 2011.

[114] T. Heikkilä, M. Karjalainen, K. Ojala, K. Partola, F. Lammert, P. Augustijns, A. Urtti, M. Yliperttula, L. Peltonen, and J. Hirvonen. Equilibrium drug solubility measurements in 96-well plates reveal similar drug solubilities in phosphate buffer pH 6.8 and human intestinal fluid. *International Journal of Pharmaceutics*, 405(1-2):132–136, 2011.

[115] E. Söderlind, E. Karlsson, A. Carlsson, R. Kong, A. Lenz, S. Lindborg, and J. J. Sheng. Simulating fasted human intestinal fluids: understanding the roles of lecithin and bile acids. *Molecular pharmaceutics*, 7(5):1498–507, oct 2010.

[116] Heumann Pharma GmbH & Co. Generica KG. Fachinformation - Carbamazepin 200/400 Heumann, 2014. URL https://www.fachinfo.de/suche/fi/006667. accessed: 11 Nov 2020.

[117] Novartis. Tegretol ® label, 2009. URL https://www.accessdata.fda.gov/drugsatfda_docs/label/2009/016608s101,018281s048lbl.pdf. accessed: 02 Jun 2022.

[118] S. Pynnönen. The Pharmacokinetics of Carbamazepine in Plasma and Saliva of Man. *Acta Pharmacologica et Toxicologica*, 41(5):465–471, 1977.

[119] L. Bertilsson. Clinical pharmacokinetics of carbamazepine. *Clinical Pharmacokinetics*, 3:128–1473, 1978.

[120] B. M. Kerr, K. E. Thummel, C. J. Wurden, S. M. Klein, D. L. Kroetz, F. J. Gonzalez, and R. H. Levy. Human liver carbamazepine metabolism. Role of CYP3A4 and CYP2C8 in 10,11-epoxide formation. *Biochemical pharmacology*, 47(11):1969–79, jun 1994.

[121] J. Henshall, A. Galetin, A. Harrison, and J. B. Houston. Comparative analysis of CYP3A heteroactivation by steroid hormones and flavonoids in different in vitro systems and potential in vivo implications. *Drug Metabolism and Disposition*, 36(7):1332–1340, 2008.

[122] N. Cazali, A. Tran, J. M. Treluyer, E. Rey, P. Athis, J. Vincent, and G. Pons. Inhibitory effect of stiripentol on carbamazepine and saquinavir metabolism in human. *British Journal of Clinical Pharmacology*, 56(5):526, 2003.

[123] W. Huang, Y. S. Lin, D. J. McConn, J. C. Calamia, R. A. Totah, N. Isoherranen, M. Glodowski, and K. E. Thummel. Evidence of significant contribution from CYP3A5 to hepatic drug metabolism. *Drug Metabolism and Disposition*, 32(12):1434–1445, 2004.

[124] R. E. Pearce, G. R. Vakkalagadda, and J. Steven Leeder. Pathways of carbamazepine bioactivation in vitro I. Characterization of human cytochromes P450 responsible for the formation of 2- and 3-hydroxylated metabolites. *Drug Metabolism and Disposition*, 30 (11):1170–1179, 2002.

[125] M. Shou, M. Hayashi, Y. Pan, Y. Xu, K. Morrissey, L. Xu, and G. L. Skiles. Modeling, prediction, and in vitro in vivo correlation of CYP3A4 induction. *Drug metabolism and disposition: the biological fate of chemicals*, 36(11):2355–70, 2008.

[126] D. F. McGinnity, G. Zhang, J. R. Kenny, G. A. Hamilton, S. Otmani, K. R. Stams, S. Haney, P. Brassil, D. M. Stresser, and R. J. Riley. Evaluation of multiple in vitro systems for assessment of CYP3A4 induction in drug discovery: human hepatocytes, pregnane X receptor reporter gene, and Fa2N-4 and HepaRG cells. *Drug metabolism and disposition: the biological fate of chemicals*, 37(6):1259–68, jun 2009.

[127] O. A. Fahmi, J. L. Raucy, E. Ponce, S. Hassanali, and J. M. Lasker. Utility of DPX2 cells for predicting CYP3A induction-mediated drug-drug interactions and associated structure-activity relationships. *Drug metabolism and disposition: the biological fate of chemicals*, 40(11):2204–11, nov 2012.

[128] J. G. Zhang, T. Ho, A. L. Callendrello, R. J. Clark, E. A. Santone, S. Kinsman, D. Xiao, L. G. Fox, H. J. Einolf, and D. M. Stresser. Evaluation of calibration curve-based approaches to predict clinical inducers and noninducers of CYP3A4 with plated human hepatocytes. *Drug Metabolism and Disposition*, 42(9):1379–1391, 2014.

[129] A. Moore, P. P. Chothe, H. Tsao, and N. Hariparsad. Evaluation of the interplay between uptake transport and CYP3A4 induction in micropatterned cocultured hepatocytes. *Drug Metabolism and Disposition*, 44(12):1910–1919, 2016.

[130] O. A. Fahmi, M. Kish, S. Boldt, and R. Scott Obach. Cytochrome P450 3A4 mRNA is a more reliable marker than CYP3A4 activity for detecting pregnane X receptor-activated induction of drug-metabolizing enzymes. *Drug Metabolism and Disposition*, 38(9):1605–1611, 2010.

[131] R. Zuo, F. Li, S. Parikh, L. Cao, K. L. Cooper, Y. Hong, J. Liu, R. A. Faris, D. Li, and H. Wang. Evaluation of a novel renewable hepatic cell model for prediction of clinical CYP3A4 induction using a correlation-based relative induction score approach. *Drug Metabolism and Disposition*, 45(2):198–207, 2017.

[132] J. G. Zhang, R. Patel, R. J. Clark, T. Ho, S. K. Trisdale, Y. Fang, and D. M. Stresser. Effect of Fifteen CYP3A4 in vitro Inducers on the Induction of Hepatocytes : A Trend Analysis. Poster presented at: 20th North American ISSX Meeting; 2015 18-22 Oct; Orlando Florida.

[133] O. A. Fahmi, M. Shebley, J. Palamanda, M. W. Sinz, D. Ramsden, H. J. Einolf, L. Chen, and H. Wang. Evaluation of CYP2B6 induction and prediction of clinical drug-drug interactions: Considerations from the IQ consortium induction working group - An industry perspective. *Drug Metabolism and Disposition*, 44(10):1720–1730, 2016.

[134] L. J. Dickmann and N. Isoherranen. Quantitative prediction of CYP2B6 induction by estradiol during pregnancy: Potential explanation for increased methadone clearance during pregnancy. *Drug Metabolism and Disposition*, 41(2):270–274, 2013.

[135] O. Pelkonen, P. Myllynen, P. Taavitsainen, A. R. Boobis, P. Watts, B. G. Lake, R. J. Price, A. B. Renwick, M. J. Gómez-Lechón, J. V. Castell, M. Ingelman-Sundberg, M. Hidestrand, A. Guillouzo, L. Corcos, P. S. Goldfarb, and D. F. Lewis. Carbamazepine: A 'blind' assessment of CYP-associated metabolism and interactions in human liver-derived in vitro systems. *Xenobiotica*, 31(6):321–343, 2001.

[136] H. Lennernäs. Intestinal permeability and its relevance for absorption and elimination. *Xenobiotica*, 37(10-11):1015–1051, nov 2007.

[137] Drugbank. Metabolite 10,11-Epoxycarbamazepine, 2020. URL https://www.drugbank.ca/metabolites/DBMET00291. accessed: 02 Jun 2022.

[138] P. L. Morselli, M. Gerna, D. de Maio, G. Zanda, F. Viani, and S. Garattini. *Pharmacokinetic studies on carbamazepine in volunteers and in epileptic patients*. Springer Berlin Heidelberg, Berlin, Heidelberg, 1975. ISBN 978-3-642-85923-6.

[139] M. Meyer, S. Schneckener, B. Ludewig, L. Kuepfer, and J. Lippert. Using expression data for quantification of active processes in physiologically based pharmacokinetic modeling. *Drug metabolism and disposition: the biological fate of chemicals*, 40(5):892–901, may 2012.

[140] A. D. Rodrigues. Integrated cytochrome P450 reaction phenotyping: attempting to bridge the gap between cDNA-expressed cytochromes P450 and native human liver microsomes. *Biochemical pharmacology*, 57(5):465–80, 1999.

[141] M. Nishimura, H. Yaguti, H. Yoshitsugu, S. Naito, and T. Satoh. Tissue distribution of mRNA expression of human cytochrome P450 isoforms assessed by high-sensitivity real-time reverse transcription PCR. *Journal of the Pharmaceutical Society of Japan*, 123(5):369–75, may 2003.

[142] K. Rowland Yeo, R. L. Walsky, M. Jamei, A. Rostami-Hodjegan, and G. T. Tucker. Prediction of time-dependent CYP3A4 drug-drug interactions by physiologically based pharmacokinetic modelling: Impact of inactivation parameters and enzyme turnover. *European Journal of Pharmaceutical Sciences*, 43(3):160–73, 2011.

[143] D. J. Greenblatt, L. L. Von Moltke, J. S. Harmatz, G. Chen, J. L. Weemhoff, C. Jen, C. J. Kelley, B. W. LeDuc, and M. A. Zinny. Time course of recovery of cytochrome P450 3A function after single doses of grapefruit juice. *Clinical Pharmacology and Therapeutics*, 74(2):121–29, 2003.

[144] M. Nishimura and S. Naito. Tissue-specific mRNA expression profiles of human phase I metabolizing enzymes except for cytochrome P450 and phase II metabolizing enzymes. *Drug metabolism and pharmacokinetics*, 21(5):357–74, 2006.

[145] G. Margaillan, M. Rouleau, K. Klein, J. K. Fallon, P. Caron, L. Villeneuve, P. C. Smith, U. M. Zanger, and C. Guillemette. Multiplexed targeted quantitative proteomics predicts hepatic glucuronidation potential. *Drug Metabolism and Disposition*, 43:1331–5, 2015.

[146] National Center for Biotechnology Information (NCBI). Expressed Sequence Tags (EST) from UniGene. 2019.

[147] M. Nishimura and S. Naito. Tissue-specific mRNA expression profiles of human ATP-binding cassette and solute carrier transporter superfamilies. *Drug metabolism and pharmacokinetics*, 20(6):452–77, 2005.

A.3 SUPPLEMENTARY INFORMATION - PROJECT III - PHYSIOLOGICALLY BASED PHARMACOKINETIC MODELING OF GRAPEFRUIT JUICE AND ITS INTERACTION POTENTIAL

Physiologically based pharmacokinetic modeling of bergamottin and 6,7-dihydroxybergamottin to describe CYP3A4 mediated grapefruit-drug interactions

Supplementary Information

Laura Maria Fuhr[1], Fatima Zahra Marok[1], Uwe Fuhr[2], Dominik Selzer[1], Thorsten Lehr[1]

[1]Clinical Pharmacy, Saarland University, Saarbrücken, Germany
[2]Department I of Pharmacology, Center for Pharmacology, Faculty of Medicine and University Hospital Cologne, University of Cologne, Cologne, Germany

Funding
This research was funded by the German Federal Ministry of Education and Research (BMBF), grant number 031L0161C ("OSMOSES").

Conflict of Interest
Thorsten Lehr has received research grants from the German Federal Ministry of Education and Research (grant 031L0161C). Laura Maria Fuhr, Fatima Zahra Marok, Uwe Fuhr and Dominik Selzer declare no conflict of interest.

Corresponding Author
Thorsten Lehr, PhD
Clinical Pharmacy, Saarland University
Campus C5 3
66123 Saarbrücken, Germany
ORCID: 0000 0002 8372 1465
Phone: +49 681 302 70255
Email: thorsten.lehr@mx.uni-saarland.de

Contents

1 Physiologically based pharmacokinetic modeling (PBPK)

1.1 PBPK model evaluation

1.1.1 Calculation of grapefruit juice-drug interaction (GFJDI) interaction ratios

Predicted GFJDI ratios of the area under the plasma concentration-time curve from the time of drug administration to the time of the last plasma concentration measurement (AUC_{last}) (Equation S1) and the maximum plasma concentrations (C_{max}) (Equation S2) of the victim drug without and with consumption of grapefruit juice were compared to their corresponding observed ratios.

$$\text{GFJDI } AUC_{last} \text{ ratio} = \frac{AUC_{last} \text{ victim drug with grapefruit juice}}{AUC_{last} \text{ victim drug alone}} \tag{S1}$$

$$\text{GFJDI } C_{max} \text{ ratio} = \frac{C_{max} \text{ victim drug with grapefruit juice}}{C_{max} \text{ victim drug alone}} \tag{S2}$$

1.1.2 Calculation of geometric mean fold errors (GMFEs)

As quantitative performance measures, the GMFE of predicted GFJDI AUC_{last} and C_{max} ratios were calculated according to Equation S3, respectively. Values ≤ 2 are considered as adequate model performance metrics.

$$GMFE = 10^{x}, \text{ with } x = \frac{1}{n}\sum_{i=1}^{n} |\log_{10}(\frac{PK_{pred,i}}{PK_{obs,i}})| \tag{S3}$$

where $PK_{pred,i}$ = predicted GFJDI AUC_{last} or C_{max} ratio, $PK_{obs,i}$ = corresponding observed GFJDI AUC_{last} or C_{max} ratio and n = the number of studies.

1.2 Mathematical implementation of drug-drug interactions (DDIs)

Mechanism-based inactivation

Mechanism-based inactivation is an irreversible type of inhibition. Baseline enzyme activity will be regained after clearance of the inactivator and de novo synthesis of the enzyme (time-dependency). The enzyme degradation rate constant (k_{deg}) is increased ($k_{deg,app}$, Equation S4), while its synthesis rate (R_{syn}) remains unaffected. The enzyme turnover during administration of a mechanism-based inactivator is described by Equation S5. As mechanism-based inactivators are also competitive inhibitors, the K_m in the Michaelis-Menten reaction velocity equation is substituted by $K_{m,app}$ as shown in Equation S6 et al. [1]:

$$k_{deg,app} = k_{deg} + \left(\frac{k_{inact} \cdot [I]}{K_I + [I]}\right) \tag{S4}$$

$$\frac{dE(t)}{dt} = R_{syn} - k_{deg,app} \cdot E(t) \tag{S5}$$

$$v = \frac{v_{max} \cdot [S]}{K_{m,app} + [S]} = \frac{k_{cat} \cdot E(t) \cdot [S]}{K_{m,app} + [S]} \tag{S6}$$

where $k_{deg,app}$ = enzyme or transporter degradation rate constant in the presence of mechanism-based inactivator, k_{deg} = enzyme or transporter degradation rate constant, k_{inact} = maximum inactivation rate constant, $[I]$ = free inactivator concentration, K_I = concentration for half-maximal inactivation, $E(t)$ = enzyme or transporter concentration, R_{syn} = enzyme or transporter synthesis rate, v = reaction velocity, v_{max} = maximum reaction velocity, $[S]$ = free substrate concentration, $K_{m,app}$ = Michaelis-Menten constant in the presence of inactivator, k_{cat} = catalytic rate constant.

The implementation of further inhibition processes or enzyme induction is described in the Open Systems Pharmacology Suite manual [1].

2 Grapefruit

2.1 Bergamottin and 6,7-dihydroxybergamottin concentrations in grapefruit juice

In total, 17 studies measuring concentrations of bergamottin an 6,7-dihydroxybergamottin in different grapefruit juice preparations were available from literature. All available measurements are listed in Table S1. Analyzing the overall content of these ingredients in the juice, the mean concentration of bergamottin was 18.49 µmol/l (range: 0.50 - 94.56 µmol/l) and the mean concentration of 6,7-dihydroxybergamottin was 28.90 µmol/l (range: 0.80 - 132.37 µmol/l). Overall, concentrations of the ingredients in the juice was highly variable, as illustrated in Figures S2. Concentrations of the ingredients vary depending on the juice preparation (frozen concentrate, commercial juice and hand squeezed juice) as well as the fruit strain (white, pink and red grapefruit).
As the fruit strain was sparsely reported, differences in concentrations between different fruit strains were not investigated in the present analysis. As hand-squeezed juice was usually not administered in the clinical studies, these measurements were excluded from the current analysis. Therefore, concentration differences were analyzed for frozen concentrate and canned juice only. When investigating bergamottin concentrations, mean concentrations in frozen concentrate and canned juice of 18.7 µmol/l (n = 20) and 16.63 µmol/l (n = 19) were calculated, while differences were not deemed to be statistically significant (t-test, p = 0.677). For 6,7-dihydroxybergamottin, mean concentrations in frozen concentrate and canned juice of 25.10 µmol/l (n = 20) and 9.92 µmol/l (n = 20) were calculated. 6,7-Dihydroxybergamottin concentrations in canned juice were observed to be statistically lower than in frozen concentrate (t-test, p = 0.00637). Furthermore, a potential correlation between bergamottin and 6,7-dihydroxybergamottin concentrations was investigated, as both result from the same pathway in the plant and 6,7-dihydroxybergamottin is a precursor of bergamottin synthesis. The correlation is illustrated in Figure S1.
Based on the administered juice volume and the ingredient concentrations indicated in the clinical studies, ingredient doses were calculated. If no concentrations were measured in the clinical studies, mean ingredient doses were calculated based on the mean concentrations of bergamottin, 6,7-dihydroxybergamottin obtained from the presented analysis. Mean calculated ingredient doses for different juice preparations and volumes are indicated in Table S2.

Table S1: Concentrations of bergamottin and 6,7-dihydroxybergamottin measured in grapefruit juice

Juice preparation	GF Type	Conc BGT [μmol/l]	Conc DHB [μmol/l]	Study
canned juice	white	28.00	42.00	Bailey et al. 2000 [2]
canned juice	red	16.50	-	Guo et al. 2007 [3]
canned juice	-	0.50	9.10	Guo et al. 2007 [3]
canned juice	-	18.80	1.00	Guo et al. 2007 [3]
canned juice	white		20.51	Bailey et al. 1998 [4]
canned juice	white	13.90	0.80	Guo et al. 2000 [5]
canned juice	pink	7.20	-	Guo et al. 2000 [5]
canned juice	white	-	28.50	Schmiedlin-Ren et al. 1997 [6]
canned juice	pink	-	12.90	Schmiedlin-Ren et al. 1997 [6]
canned juice	-	11.38	6.18	Messer et al. 2011 [7]
canned juice	-	2.72	6.20	Messer et al. 2011 [7]
canned juice	-	6.86	2.20	Messer et al. 2011 [7]
canned juice	-	11.08	2.85	Messer et al. 2011 [7]
canned juice	-	14.27	3.03	Messer et al. 2011 [7]
canned juice	-	8.81	5.72	Messer et al. 2011 [7]
canned juice	-	3.63	3.03	Messer et al. 2011 [7]
canned juice	-	8.39	4.16	Messer et al. 2011 [7]
canned juice	red	7.48	7.65	Van der Molen et al. 2013 [8]
canned juice	-	12.26	11.58	Van der Molen et al. 2013 [8]
canned juice	red	27.70	4.43	Melough et al. 2017 [9]
canned juice	-	94.56	5.37	Sakamaki et al. 2008 [10]
canned juice	-	21.87	21.21	Sakamaki et al. 2008 [10]
mean		**16.63**	**9.92**	
(range) $\pm$ SD		**(0.50–94.56) $\pm$ 20.37**	**(0.80–42) $\pm$ 10.58**	
frozen concentrate	white	26.90	43.20	Kakar et al. 2004 [11]
frozen concentrate	-	16.00	23.00	Malhotra et al. 2001 [12]
frozen concentrate	-	28.02	30.82	Paine et al. 2006 [13]
frozen concentrate	-	20.09	-	Goosen et al. 2004 [14]
frozen concentrate	white	29.00	6.70	Greenblatt et al. 2003 [15]
frozen concentrate	white	20.40	34.70	Guo et al. 2000 [5]
frozen concentrate	white	29.60	2.30	Guo et al. 2000 [5]
frozen concentrate	white	20.30	1.20	Guo et al. 2000 [5]
frozen concentrate	white	14.50	14.10	Guo et al. 2000 [5]
frozen concentrate	white	10.80	6.00	Guo et al. 2000 [5]
frozen concentrate	white	4.30	27.40	Schmiedlin-Ren et al. 1997 [6]
frozen concentrate	-	-	44.40	Schmiedlin-Ren et al. 1997 [6]
frozen concentrate	-	15.07	9.13	Sakamaki et al. 2008 [10]
frozen concentrate	-	-	9.94	Sakamaki et al. 2008 [10]
frozen concentrate	-	19.50	26.85	Sakamaki et al. 2008 [10]
frozen concentrate	-	15.07	13.69	Sakamaki et al. 2008 [10]
frozen concentrate	-	15.07	13.69	Sakamaki et al. 2008 [10]
frozen concentrate	-	21.28	-	Sakamaki et al. 2008 [10]
frozen concentrate	-	18.32	29.54	Sakamaki et al. 2008 [10]
frozen concentrate	-	13.30	-	Sakamaki et al. 2008 [10]
frozen concentrate	-	11.76	41.31	Van der Molen et al. 2013 [8]
frozen concentrate	-	24.73	89.03	Van der Molen et al. 2013 [8]
frozen concentrate	-	-	35.00	Ainslie 2014 [16]
mean		**18.7**	**25.1**	
(range) $\pm$ SD		**(4.30–29.6) $\pm$ 6.66**	**(1.20–89.03) $\pm$ 20.48**	
hand-squeezed	-	43.40	53.20	Kawaguchi-Suzuki et al. 2017 [17]
hand-squeezed	white	-	23.10	Schmiedlin-Ren et al. 1997 [6]
hand-squeezed	pink	-	16.40	Schmiedlin-Ren et al. 1997 [6]
hand-squeezed	-	-	19.60	Schmiedlin-Ren et al. 1997 [6]

BGT: bergamottin,conc: concentration, DHB: 6,7-dihydroxybergamottin, GF: grapefruit, SD: standard deviation

Table S1: Concentrations of bergamottin and 6,7-dihydroxybergamottin measured in grapefruit juice *(continued)*

Juice preparation	GF Type	Conc BGT [μmol/l]	Conc DHB [μmol/l]	Study
hand-squeezed	-	12.59	62.73	Messer et al. 2011 [7]
hand-squeezed	-	17.41	104.75	Messer et al. 2011 [7]
hand-squeezed	-	19.56	125.94	Messer et al. 2011 [7]
hand-squeezed	-	32.86	120.38	Messer et al. 2011 [7]
hand-squeezed	-	19.15	74.41	Messer et al. 2011 [7]
hand-squeezed	-	21.04	132.57	Messer et al. 2011 [7]
hand-squeezed	-	8.90	15.33	Messer et al. 2011 [7]
mean		**21.86**	**68.04**	
(range) ± SD		**(8.90–43.4) ± 11.16**	**(15.33–132.57) ± 46.59**	
unknown	-	11.76	41.31	Goosen et al. 2004 [14]
unknown	-	24.73	89.03	Goosen et al. 2004 [14]
unknown	-	7.48	7.65	Goosen et al. 2004 [14]
unknown	-	12.26	11.58	Goosen et al. 2004 [14]
unknown	-	40.22	20.25	Masuda et al. 2005 [18]
overall mean		**18.49**	**28.9**	
(range) ± SD		**(0.50–94.56) ±14.04**	**(0.80–132.57) ±33.23**	

BGT: bergamottin,conc: concentration, DHB: 6,7-dihydroxybergamottin, GF: grapefruit, SD: standard deviation

Table S2: Mean calculated doses of bergamottin and 6,7-dihydroxybergamottin ingested after consumption of different volumes of grapefruit juice based on mean concentrations indicated in Table S1

Juice volume [ml]	Dose bergamottin [mg]	Dose 6,7-dihydroxybergamottin [mg]
Frozen concentrate		
200	1.27	1.87
240	1.52	2.24
250	1.58	2.33
300	1.90	2.80
Canned juice		
200	1.13	0.74
240	1.35	0.89
250	1.41	0.92
300	1.69	1.11
Overall mean (excluding hand squeezed juice)		
200	1.20	1.30
240	1.44	1.57
250	1.50	1.63
300	1.80	1.96

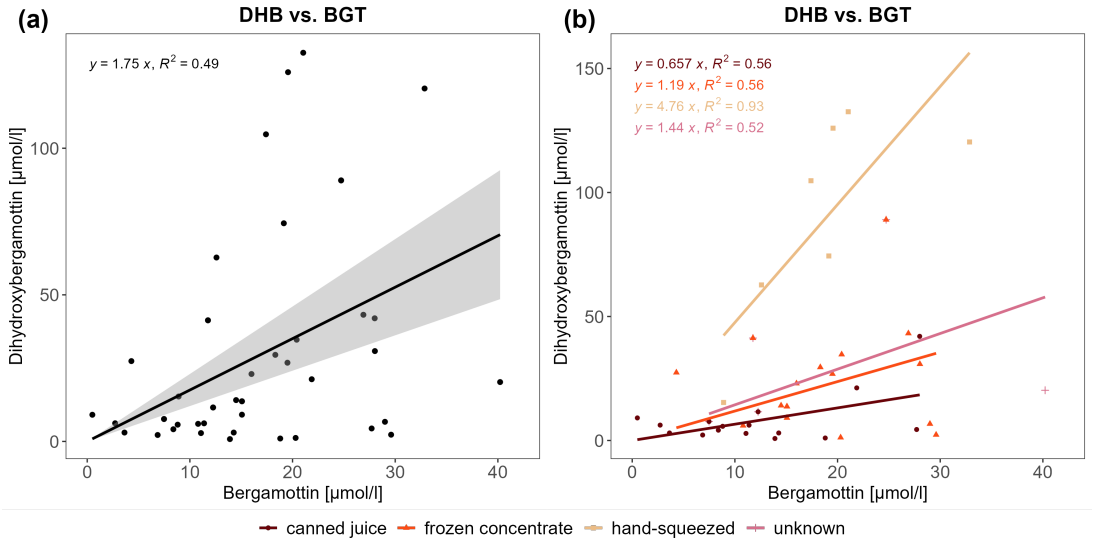

Figure S1: 6,7-dihydroxybergamottin versus corresponding bergamottin concentration measured in grapefruit juice with linear regression line for (a) all studies or (b) different grapefruit juice preparations. BGT: bergamottin, DHB: 6,7-dihydroxybergamottin

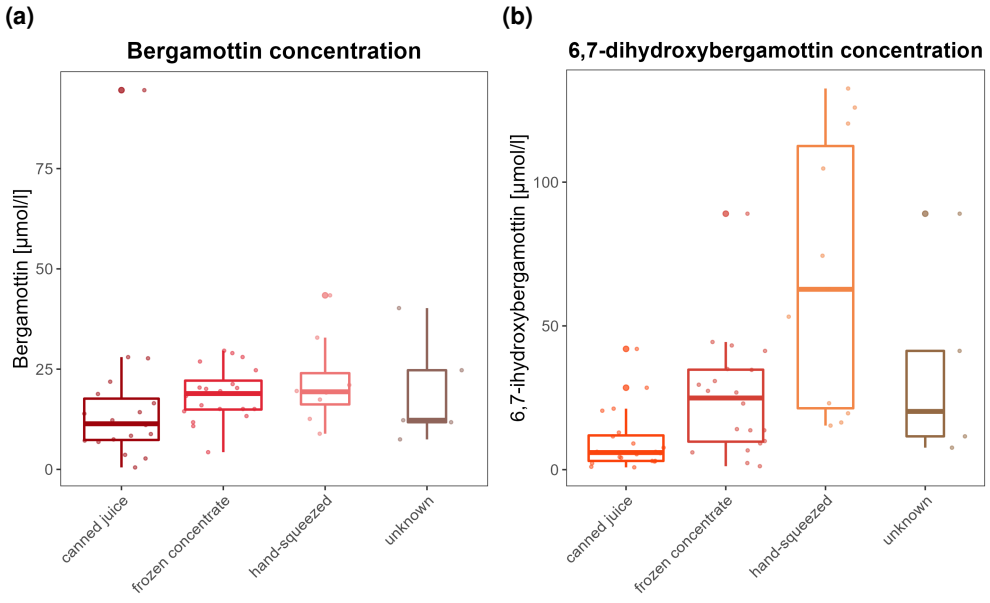

Figure S2: Measured bergamottin and 6,7-dihydroxybergamottin concentrations in different grapefruit juice preparations (frozen concentrate, hand-squeezed juice and canned juice). BGT: bergamottin, DHB: 6,7-dihydroxybergamottin

2.2 Bergamottin and 6,7-dihydroxybergamottin drug-dependent parameters

Table S3: Drug-dependent parameters of the final bergamottin and 6,7-dihydroxybergamottin PBPK models

Parameter	Unit	Bergamottin			6,7-dihydroxybergamottin			
		Model	Literature	Reference	Model	Literature	Reference	Description
MW	g/mol	338.41 (lit)	338.41	[19]	372.417 (lit)	372.417	[20]	Molecular weight
LogP		4.95 (opt)	4.81, 5.3	[19]	3.72 (opt)	2.67, 3.4	[20]	Lipophilicity
$f_{u,plasma}$	%	2.73 (lit)	2.73	[21]	7.70 (calc)	7.70	[21]	Fraction unbound in plasma
pKa		-	-	[19]	13.84 (lit)	13.84	[22]	Acid dissociation constant
Solubility (pH)	mg/l	10 (7) (lit)	10 (7)	[19]	44(7)	44 (7)	[20]	Solubility at reference pH
K_m (CYP3A4)	1/min	1.9 (asm)	-	-	1.10 (asm)	-	-	CYP3A4 Michaelis-Menten constant
k_{cat} (CYP3A4)	1/min	0.05 (opt)	-	-	2.10 (opt)	-	-	CYP3A4 catalytic rate constant
K_I (CYP3A4)	µmol/l	1.9 (lit)	1.9 – 40	[23–25]	1.10 (lit)	1.1 – 59	[6, 23, 24]	Concentration for half-maximal inactivation
K_i (CYP3A4)	µmol/l	6.10 (lit)	0.50 – 13.3	[23]	0.50 (lit)	0.40 – 0.90	[23]	Concentration for half-maximal inhibition
k_{inact} (CYP3A4)	1/min	0.7 (lit)	0.08 – 0.7	[23–25]	0.41 (lit)	0.06 – 0.52	[6, 23, 24]	Maximum inactivation rate constant
GFR fraction	-	1 (asm)	-	-	1 (asm)	-	-	Fraction of filtered drug in the urine
Intestinal permeability	cm/min	1.60 E-3 (opt)	-	-	6.41 E-5 (opt)	-	-	Transcellular instestinal permeability
Partition coefficient	-	various	R&R	[26, 27]	diverse	PK-Sim	[1]	Cell to plasma partition coefficients
Cellular permeability	cm/min	1.72 (calc)	CdS	[1]	0.06 (calc)	PK-Sim	[1]	Permeability into the cellular space

asm: assumed, calc: calculated, CdS: Charge dependent Schmitt, GFR: glomerular filtration rate, lit: literature, opt: optimized, R&R: Rodgers and Rowland

2.3 Grapefruit juice investigation studies

Table S4: Clinical studies investigating bergamottin and 6,7-dihydroxybergamottin plasma concentration-time profiles

Grapefruit juice							
Volume [ml]	**BGT [µmol/l]**	**DHB [µmol/l]**	**n**	**Female [%]**	**Age[a] [years]**	**Weight[a] [kg]**	**Reference**
474	6.5*	3.1*	2	-	(20-30)	-	Lee et al. 2016 [28]
470	27.70	4.43	9	33	(20-30)	-	Reddy et al. 2021 [29]
240	-	70	16	50	(22-59)	-	Ainslie 2014 [16]

-: not given, BGT: bergamottin, d: double-strength, D: day, DHB: 6,7-dihydroxybergamottin, iv: intravenous, po: oral, qd: once daily, s: single-strength, sd: single dose, tab: tablet, tabER: extended release tablet, tid: three times daily
*: unit [mg]

2.4 Plasma concentration-time profiles

2.4.1 Linear plasma concentration-time profiles

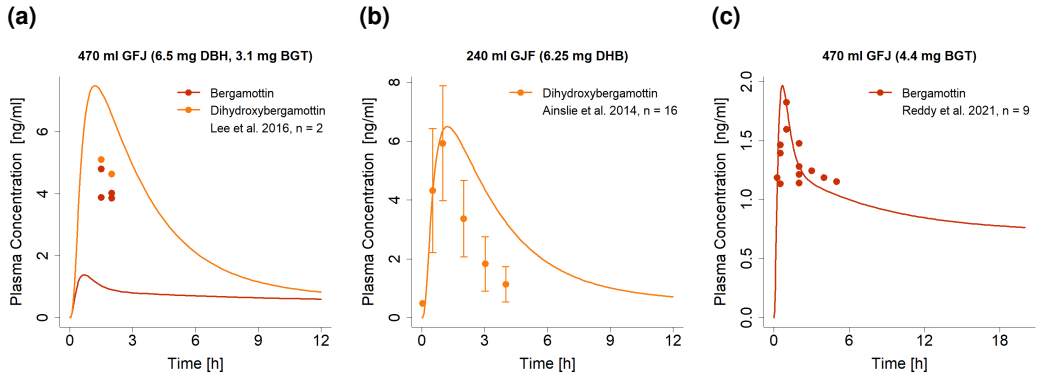

Figure S3: Predicted compared to observed bergamottin and 6,7-dihydroxybergamottin concentration-time profiles (linear) after ingestion of grapefruit juice. Observed data are shown as dots ± standard deviation; model predictions are shown as solid lines. BGT: bergamottin, DHB: 6,7-dihydroxybergamottin, n: number of individuals

2.4.2 Semi-logarithmic plasma concentration-time profiles

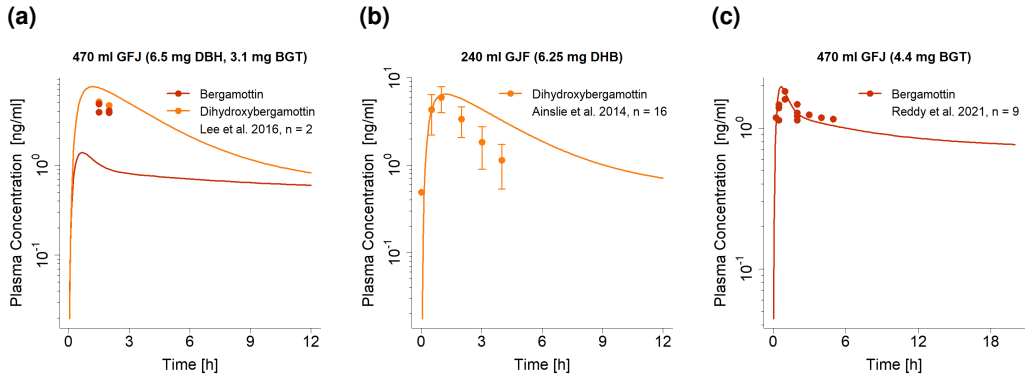

Figure S4: Predicted compared to observed bergamottin and 6,7-dihydroxybergamottin concentration-time profiles (semi-logarithmic) after ingestion of grapefruit juice. Observed data are shown as dots ± standard deviation; model predictions are shown as solid lines.

2.4.3 Model evaluation

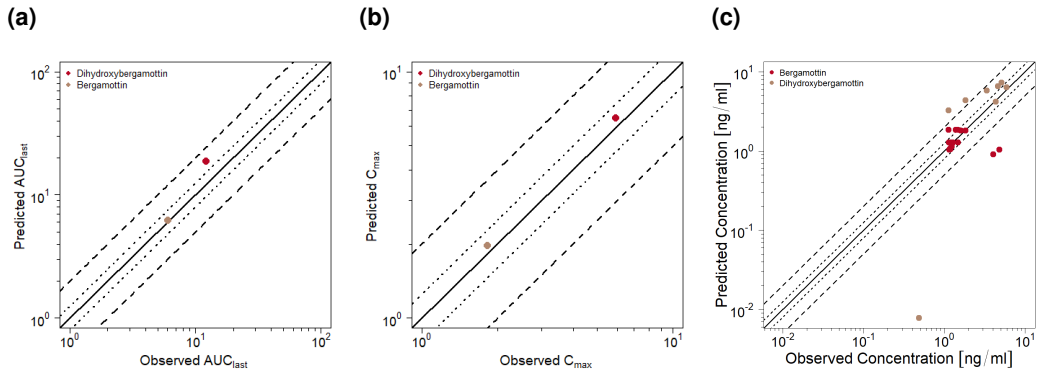

Figure S5: Predicted compared to observed bergamottin and 6,7-dihydroxybergamottin (a) AUC_{last}, (b) C_{max} values and (c) plasma concentration values after oral administration of grapefruit juice. The solid line marks the line of identity. Dotted lines indicate 1.25-fold, dashed lines indicate 2-fold deviation. AUC_{last}: area under the plasma concentration-time curve from the time of drug administration to the last concentration measurement, C_{max}: maximum plasma concentration

Table S5: Predicted and observed AUC_{last} and C_{max} values with geometric mean fold errors of bergamottin and 6,7-dihydroxybergamottin

		AUC_{last} [ng*h/ml]			C_{max} [ng/ml]			
Compound	**Dose [mg]**	**Pred**	**Obs**	**Pred/Obs**	**Pred**	**Obs**	**Pred/Obs**	**Reference**
Dihydroxybergamottin	6.25	18.69	12.21	1.53	6.50	5.93	1.10	Ainslie et al. 2014 [16]
Bergamottin	4.40	6.20	6.07	1.02	1.97	1.83	1.08	Reddy et al. 2021 [29]
GMFE				**1.28 (1.02-1.53)**			**1.09 (1.08-1.1)**	
				2/2 with GMFE < 2			**2/2 with GMFE < 2**	

AUC_{last}: area under the plasma concentration-time curve from the time of drug administration to the last concentration measurement, C_{max}: maximum plasma concentration, GMFE: geometric mean fold error, obs: observed, pred: predicted

3 Grapefruit-drug interactions

3.1 GFJDI modeling

Overall, 43 clincial GFJDI studies from literature were included in the current analysis. These studies investigated the effect of grapefruit on 10 different victim drugs, namely felodipine (metabolite: dehydrofelodipine), midazolam, aprazolam, alfentanil, carbamazepine, triazolam, itraconazole (metabolite: hydroxyitraconazole), erythromycin, simvastatin (metabolite: simvastatin acid) and (R/S)-verapamil (metabolite: (R/S)-norverapamil). The implementation of GFJDIs with all victim drugs is described in more detail in the following sections.

3.2 Grapefruit-felodipine GFJDI

The felodipine GFJDI was modeled using a previously developed and evaluated whole-body PBPK model of felodipine [30]. Drug-dependent parameters of the felodipine PBPK model are displayed in Table S6.

Details on the modeled clinical GFJDI studies are given in Table S7. Predicted felodipine and dehydrofelodipine plasma concentration-time profiles with and without grapefruit juice coadministration, compared to observed data, are shown in Figures S6 and S7 (linear) and S8 and S9 (semi-logarithmic). The correlation of predicted to observed GFJDI AUC_{last} and C_{max} ratios is shown in Figure S10. Tables S9 and S10 list the corresponding predicted and observed GFJDI AUC_{last} ratios, GFJDI C_{max} ratios as well as GMFE values of felodipine and dehydrofelodipine, respectively.

3.2.1 Felodipine drug-dependent parameters

Table S6: Drug-dependent parameters of the final felodipine parent-metabolite PBPK model according to [30]

Parameter	Unit	Value (model)	Value (literature)	Reference	Description
Felodipine					
MW	g/mol	384.25 (lit)	384.25	[31]	Molecular weight
$f_{u,plasma}$	%	0.36 (lit)	0.36	[32]	Fraction unbound in plasma
Solubility (pH)	mg/l	7.15 (7) (lit)	0.5 (6.5); 1.2 (7); 7.15 (7); 14.3 (7.1); 19.7 (7)	[33, 34, 34, 35]	Solubility
Solubility tabER (pH)	mg/l	0.89 (7.0) (opt)	-	-	Solubility extended release tablets
logP		4.36 (lit)	3.44; 3.80; 4.36; 4.46; 4.64	[31, 34, 34–36]	Lipophilicity
Intestinal permeability	cm/min	2.76E-4 (opt)	3.06E-4; 2.64E-4; 1.48E-3	[36, 37]	Transcellular intestinal permeability
GFR fraction		1 (asm)	-	-	Fraction of filtered drug in the urine
K_m (CYP3A4)	µmol/l	2.81 (lit)	0.648; 0.94; 2.81; 26.4	[35, 38, 39]	CYP3A4 Michaelis-Menten constant
k_{cat} (CYP3A4)	1/min	250.44 (opt)			CYP3A4 catalytic rate constant
s (tab)		1.32(opt)	-	-	Dissolution profile shape
$t_{50\%}$ (tab)	min	54.86 (opt)	-	-	Dissolution time (50% dissolved)
s (tabER)		1.30 (opt)	-	-	Dissolution profile shape
$t_{50\%}$ (tabER)	min	173.04 (opt)	-	-	Dissolution time (50% dissolved)
Partition coefficient	-	diverse	Rodgers and Rowland	[26, 27]	Cell to plasma partition coefficients
Cellular permeability	cm/min	(calc)	PK-Sim Standard	[40]	Permeability into the cellular space
Dehydrofelodipine					
MW	g/mol	382.2 (lit)	382.2	[41]	Molecular weight
f_u	%	0.68 (lit)	-	-	Fraction unbound in plasma
Solubility (pH)	mg/l	2.93 (7) (lit)	2.93 (7)	[41]	Solubility
logP		3.32 (opt)	4.24	[41]	Lipophilicity
CL (CYP3A4)	1/min	35.74 (opt)	-	-	CYP3A4 clearance process
CL (hepatic)	1/min	2.76 (opt)	-	-	unspecific hepatic clearance process
Intestinal permeability	cm/min	1.38E-4 (calc)	-	-	Transcellular intestinal permeability
GFR fraction		1 (asm)	-	-	Fraction of filtered drug in the urine
Partition coefficient	-	diverse	Schmitt	[42]	Cell to plasma partition coefficients
Cellular permeability	cm/min	(calc)	Charge dependent Schmitt	[1]	Permeability into the cellular space

asm: assumed, calc: calculated, CYP3A4: Cytochrom P450 3A4, GFR: glomerular filtration rate, lit: literature value, opt: optimized value, tab: tablet, tabER: extended release tablet

3.2.2 Clinical grapefruit-felodipine interaction studies

Table S7: Clinical studies investigating the grapefruit-felodipine interaction

	Felodipine		Grapefruit juice							
ID	Dose [mg]	Route	Volume [ml]	Route	BGT [µmol/l]	DHB [µmol/l]	n	Female [%]	Age[a] [years]	Weight[a] [kg]	Reference
1.1.01	5	po (*tab*), sd	200	0h	-	-	9	0	(19-40)	-	Bailey et al. 1993 [43]
1.1.02	10	po (tabER), sd	250 (s)	0h	-	-	12	0	(18-40)	-	Bailey et al. 1995 [44]
1.1.04	10	po (tabER), sd	250 (s)	0h	-	-	12	0	(18-40)	-	Bailey et al. 1996 [45]
1.1.05	10	po (tabER), sd	250	0h	-	1.91*	12	0	(18-40)	-	Bailey et al. 1998 [4]
1.1.06	10	po (tabER), sd	250	0h	28	42	12	17	(18-40)	-	Bailey et al. 2000 [2]
1.2.03	10	po (tabER), sd	250 [b]	0h	6	118	12	17	(18-40)	-	Bailey et al. 2000 [2]
1.2.02	10	po (tabER), sd	250 [c]	0h	26	11	12	17	(18-40)	-	Bailey et al. 2000 [2]
1.1.07	10	po (tabER), sd	250	0h	25	-	8	25	(23-45)	-	Bailey et al. 2003 [46]
1.2.04	10	po (tabER), sd	250	0h	25 [d]	-	8	25	(23-45)	-	Bailey et al. 2003 [46]
1.1.08	5	po (tabER), sd	250	0h	-	-	6	53	(70-83)	-	Dresser et al. 2000 [47]
1.1.09	5	po (tabER), D1-D2: 2.5 mg qd, D3-D8: 5mg qd	250	D1-D8: qd (0h)	-	-	12	66	(71-77)	-	Dresser et al. 2000 [47]
1.1.10	10	po (tabER), sd	300	-1h, 0h	-	-	5	40	46 (31-56)	-	Dresser et al. 2017 [48]
1.1.11	5	po (tab), sd	200 (s)	0h	-	-	9	0	44 (40-53) ± 5	77 (66-85) ± 7	Edgar et al. 1992 [49]
1.1.12	5	po (tab), sd	200 (d)	0h	-	-	9	0	44 (40-53) ± 5	77 (66-85) ± 7	Edgar et al. 1992 [49]
1.1.13	5	po (tabER), sd	250	0h	1.7 mg	-	12	0	(21-24)	-	Goosen et al. 2004 [14]
1.2.05	5	po (tabER), sd	BGT capsule	2mg BGT, 0h	2*	-	12	0	(21-24)	-	Goosen et al. 2004 [14]
1.2.06	5	po (tabER), sd	BGT capsule	6mg BGT, 0h	6*	-	12	0	(21-24)	-	Goosen et al. 2004 [14]
1.2.07	5	po (tabER), sd	BGT capsule	12mg BGT, 0h	12*	-	12	0	(21-24)	-	Goosen et al. 2004 [14]
1.1.14	10	po (tabER), sd	240 (s)	0h	26.9	43.2	5	60	(20-37)	(65-77)	Kakar et al. 2004 [11]

-: not given, BGT: bergamottin, d: double-strength, D: day, DHB: 6,7-dihydroxybergamottin, iv: intravenous, po: oral, qd: once daily, s: single-strength, sd: single dose, tab: tablet, tabER: extended release tablet, tid: three times daily

*: unit [mg]

[a]: mean (range) ± standard deviation

[b]: Homogenized grapefruit segments (Segments from 1 fruit ≡ 250 ml)

[c]: Ethanol extract from segment free parts of a grapefruit (diluted with water to 250 ml)

[d]: Lime juice (containing 100 µmol/l bergamottin, diluted to 1/4 strength)

[e]: Aquaeus supernatant of frozen concentrate suspended in water, containing primarily 6,7-dihydroxybergamottin

[f]: Seville orange

Table S7: Clinical studies investigating the grapefruit-felodipine interaction

	Felodipine		Grapefruit juice								
ID	Dose [mg]	Route	Volume [ml]	Route	BGT [µmol/l]	DHB [µmol/l]	n	Female [%]	Age[a] [years]	Weight[a] [kg]	Reference
1.2.08	10	po (tabER), sd	240 [e]	0h	0.2	38.2	5	60	(20-37)	(65-77)	Kakar et al. 2004 [11]
1.1.15	10	po (tabER), sd (D1, D6)	240	D1-D6: tid (0h)	-	-	10	0	(18-65)	-	Lown et al. 1997 [50]
1.1.16	10	po (tabER), sd	200 (s)	0h	-	-	9	0	(23-33)	(69-86)	Lundahl et al. 1995 [51]
1.1.17	10	po (tabER), sd	200 (s)	-1h	-	-	9	0	(23-33)	(69-86)	Lundahl et al. 1995 [51]
1.1.18	10	po (tabER), sd	200 (s)	-4h	-	-	9	0	(23-33)	(69-86)	Lundahl et al. 1995 [51]
1.1.19	10	po (tabER), sd	200 (s)	-10h	-	-	9	0	(23-33)	(69-86)	Lundahl et al. 1995 [51]
1.1.20	10	po (tabER), sd	200 (s)	-24h	-	-	9	0	(23-33)	(69-86)	Lundahl et al. 1995 [51]
1.1.21	10	po (tabER), sd	200 (s)	-0.25h	-	-	12	0	25 ± 2	75 ± 6	Lundahl et al. 1997 [52]
1.1.22	1.5	iv, sd (60min)	200 (s)	-0.25h	-	-	12	0	25 ± 2	75 ± 6	Lundahl et al. 1997 [52]
1.1.23	10	D1: po (tabER), qd	200 (s)	D1-D14: qd (0h)	-	-	12	0	26 ± 1	76 ± 6	Lundahl et al. 1998 [53]
1.1.26	10	D1-D14: po (tabER), qd	200 (s)	D1-D14: qd (0h)	-	-	12	0	26 ± 1	76 ± 6	Lundahl et al. 1998 [53]
1.1.24	10	po (tabER), sd	240 (s)	0h	16	23	10	50	(21-32)	-	Malhotra et al. 2001 [12]
1.2.09	10	po (tabER), sd	240 [f]	0h	5	36	10	50	(21-32)	-	Malhotra et al. 2001 [12]
1.1.25	10	po (tabER), sd	240	0h	9.5 ppm	11.5 ppm	18	50	34 ± 11	81 ± 23	Paine et al. 2006 [13]

-: not given, BGT: bergamottin, d: double-strength, D: day, DHB: 6,7-dihydroxybergamottin, iv: intravenous, po: oral, qd: once daily, s: single-strength, sd: single dose, tab: tablet, tabER: extended release tablet, tid: three times daily

*: unit [mg]

[a]: mean (range) ± standard deviation

[b]: Homogenized grapefruit segments (Segments from 1 fruit ≡ 250 ml)

[c]: Ethanol extract from segment free parts of a grapefruit (diluted with water to 250 ml)

[d]: Lime juice (containing 100 µmol/l bergamottin, diluted to 1/4 strength)

[e]: Aquaeus supernatant of frozen concentrate suspended in water, containing primarily 6,7-dihydroxybergamottin

[f]: Seville orange

3.2.3 Bergamottin and 6,7-dihydroxybergamottin doses

Juice preparation	BGT [mg]	DHB [mg]	Measured	ID	Reference
frozen concentrate, 200 ml	1.27	1.87	no	1.1.01	Bailey et al. 1993 [43]
frozen concentrate, 250 ml	1.58	2.33	no	1.1.02	Bailey et al. 1995 [44]
frozen concentrate, 250 ml	1.58	2.33	no	1.1.04	Bailey et al. 1996 [45]
canned juice, 250 ml	1.50	1.91	only DHB	1.1.05	Bailey et al. 1998 [4]
canned juice, 250 ml	2.36	3.91	yes	1.1.06	Bailey et al. 2000 [2]
grapefruit segements	0.508	10.99	yes	1.2.02	Bailey et al. 2000 [2]
ethanolic extract	2.2	1.02	yes	1.2.03	Bailey et al. 2000 [2]
lime juice, 250 ml	5	-	only BGT	1.2.04	Bailey et al. 2003 [46]
canned juice, 250 ml	2.12	0.92	only BGT	1.1.07	Bailey et al. 2003 [46]
frozen concentrate, 250 ml	1.58	2.33	no	1.1.08	Dresser et al. 2000 [47]
frozen concentrate, 250 ml	1.58	2.33	no	1.1.09	Dresser et al. 2000 [47]
frozen concentrate, 300 ml	1.90	2.80	no	1.1.10	Dresser et al. 2017 [48]
frozen concentrate, 200 ml	1.27	1.87	no	1.1.11	Edgar et al. 1992 [49]
frozen concentrate (double), 200 ml	2.54	3.74	no	1.1.12	Edgar et al. 1992 [49]
frozen concentrate, 250 ml	1.7	2.33	only BGT	1.1.13	Goosen et al. 2004 [14]
-	2	-	yes	1.2.05	Goosen et al. 2004 [14]
-	6	-	yes	1.2.06	Goosen et al. 2004 [14]
-	12	-	yes	1.2.07	Goosen et al. 2004 [14]
frozen concentrate, 240 ml	2.18	3.86	yes	1.1.14	Kakar et al. 2004 [11]
grapefruit serum	0.02	2.07	yes	1.2.08	Kakar et al. 2004 [11]
frozen concentrate, 240 ml	1.52	2.24	no	1.1.15	Lown et al. 1997 [50]
frozen concentrate, 240 ml	1.52	2.24	no	1.1.27	Lown et al. 1997 [50]
frozen concentrate, 200 ml	1.27	1.87	no	1.1.16	Lundahl et al. 1995 [51]
frozen concentrate, 200 ml	1.27	1.87	no	1.1.17	Lundahl et al. 1995 [51]
frozen concentrate, 200 ml	1.27	1.87	no	1.1.18	Lundahl et al. 1995 [51]
frozen concentrate, 200 ml	1.27	1.87	no	1.1.19	Lundahl et al. 1995 [51]
frozen concentrate, 200 ml	1.27	1.87	no	1.1.20	Lundahl et al. 1995 [51]
frozen concentrate, 200 ml	1.27	1.87	no	1.1.21	Lundahl et al. 1997 [52]
frozen concentrate, 200 ml	1.27	1.87	no	1.1.22	Lundahl et al. 1997 [52]
frozen concentrate, 200 ml	1.27	1.87	no	1.1.23	Lundahl et al. 1998 [53]
frozen concentrate, 200 ml	1.27	1.87	no	1.1.26	Lundahl et al. 1998 [53]
Seville orange, 240 ml	0.41	3.22	yes	1.2.09	Malhotra et al. 2001 [12]
frozen concentrate, 240 ml	1.14	2.06	yes	1.1.24	Malhotra et al. 2001 [12]
frozen concentrate, 240 ml	2.27	2.75	yes	1.1.25	Paine et al. 2006 [13]

italic: preparation assumed; BGT: bergamottin, DHB: 6,7-dihydroxybergamottin

3.2.4 Linear plasma concentration-time profiles

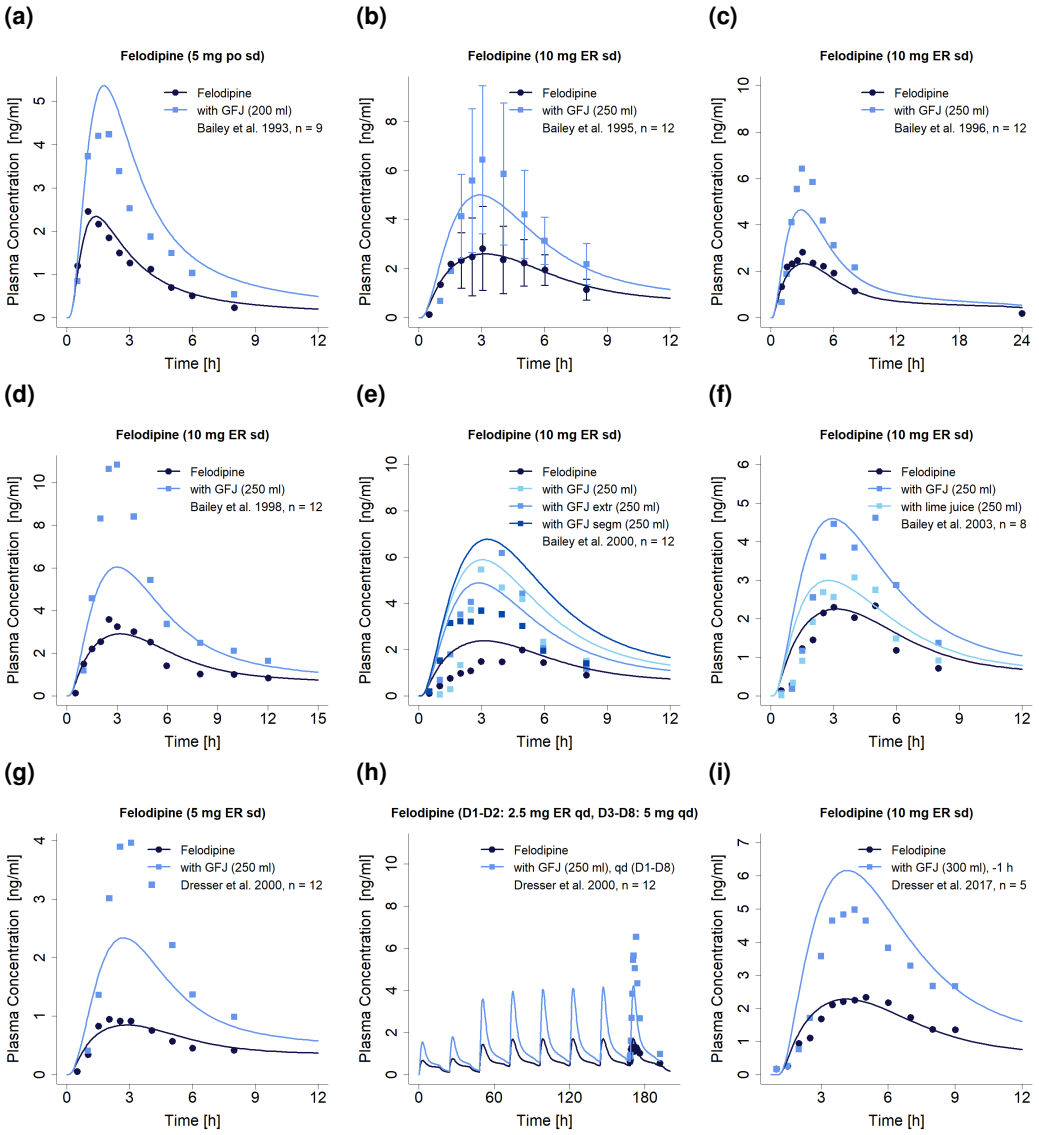

Figure S6: Predicted compared to observed felodipine plasma concentration-time profiles (linear) with and without grapefruit, Seville orange or lime juice co-administration. Observed data are shown as dots ± standard deviation (if available); model predictions are shown as solid lines. Details on dosing regimens, study population and literature reference are listed in Table S7. BGT: bergamottin, D: day, DHB: 6,7-dihydroxybergamottin, ER: extended release tablet, extr: extract, GFJ: grapefruit juice, iv: intravenous, n: number of participants, po: oral, qd: once daily, sd: single dose, segm: segments, tid: three times daily.

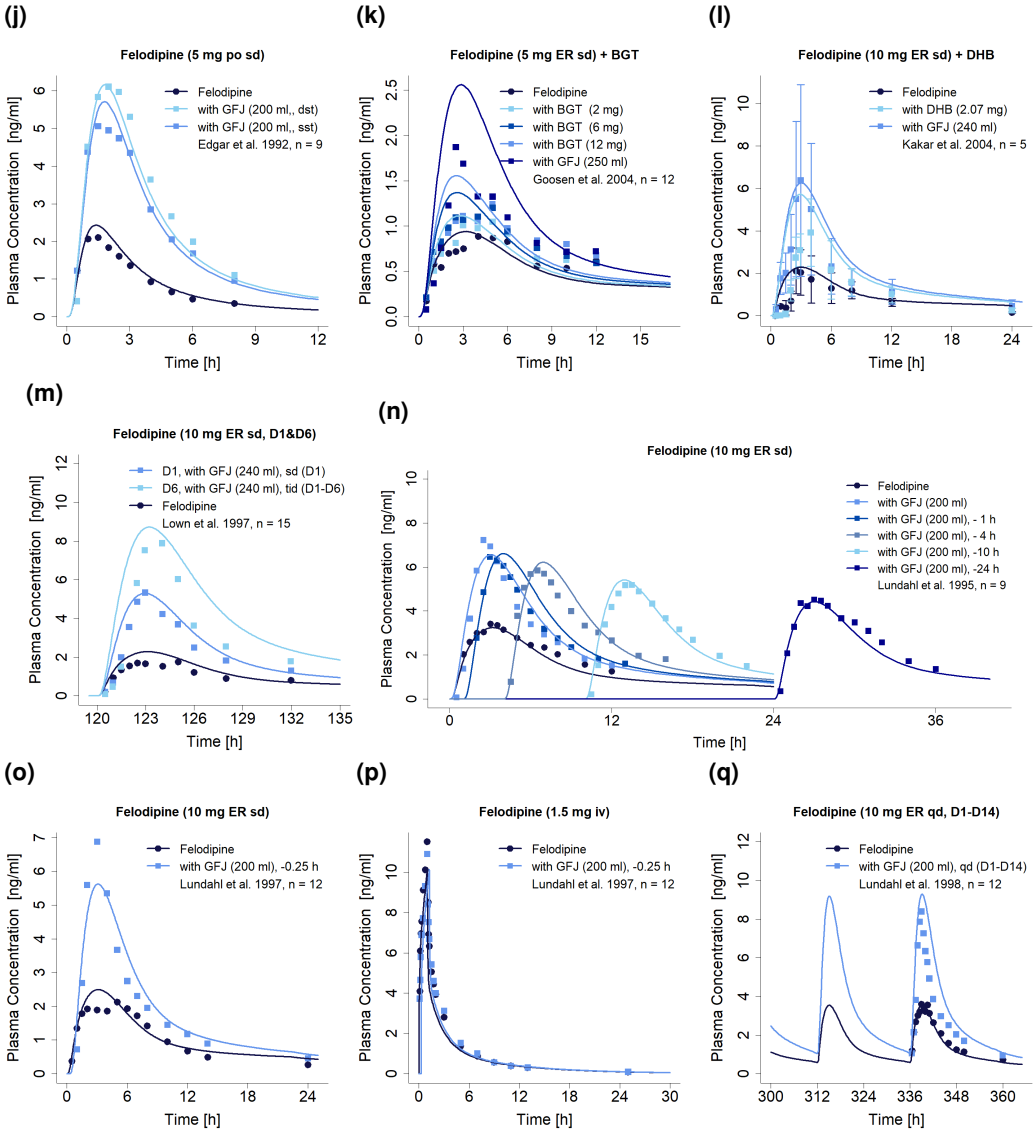

Figure S6: Predicted compared to observed felodipine plasma concentration-time profiles (linear) with and without grapefruit juice, Seville orange or lime co-administration. Observed data are shown as dots ± standard deviation (if available); model predictions are shown as solid lines. Details on dosing regimens, study population and literature reference are listed in Table S7. BGT: bergamottin, D: day, DHB: 6,7-dihydroxybergamottin, ER: extended release tablet, extr: extract, GFJ: grapefruit juice, iv: intravenous, n: number of participants, po: oral, qd: once daily, sd: single dose, segm: segments, tid: three times daily

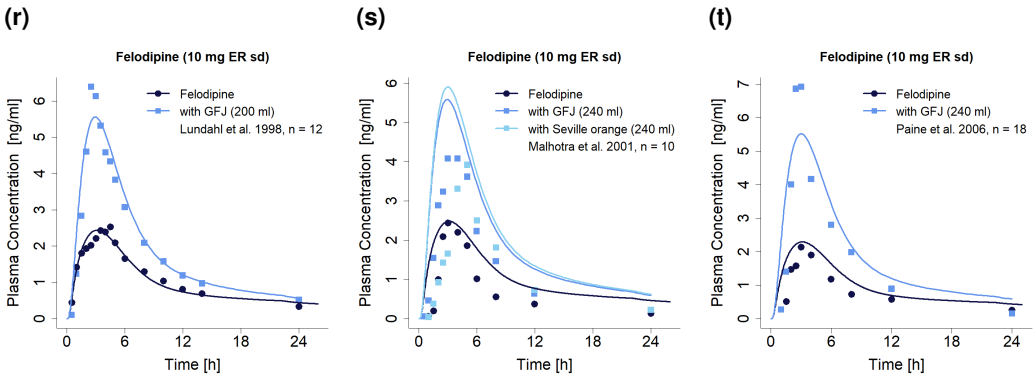

Figure S6: Predicted compared to observed felodipine plasma concentration-time profiles (linear) with and without grapefruit, Seville orange or lime juice co-administration. Observed data are shown as dots ± standard deviation (if available); model predictions are shown as solid lines. Details on dosing regimens, study population and literature reference are listed in Table S7. BGT: bergamottin, D: day, DHB: 6,7-dihydroxybergamottin, ER: extended release tablet, extr: extract, GFJ: grapefruit juice, iv: intravenous, n: number of participants, po: oral, qd: once daily, sd: single dose, segm: segments, tid: three times daily

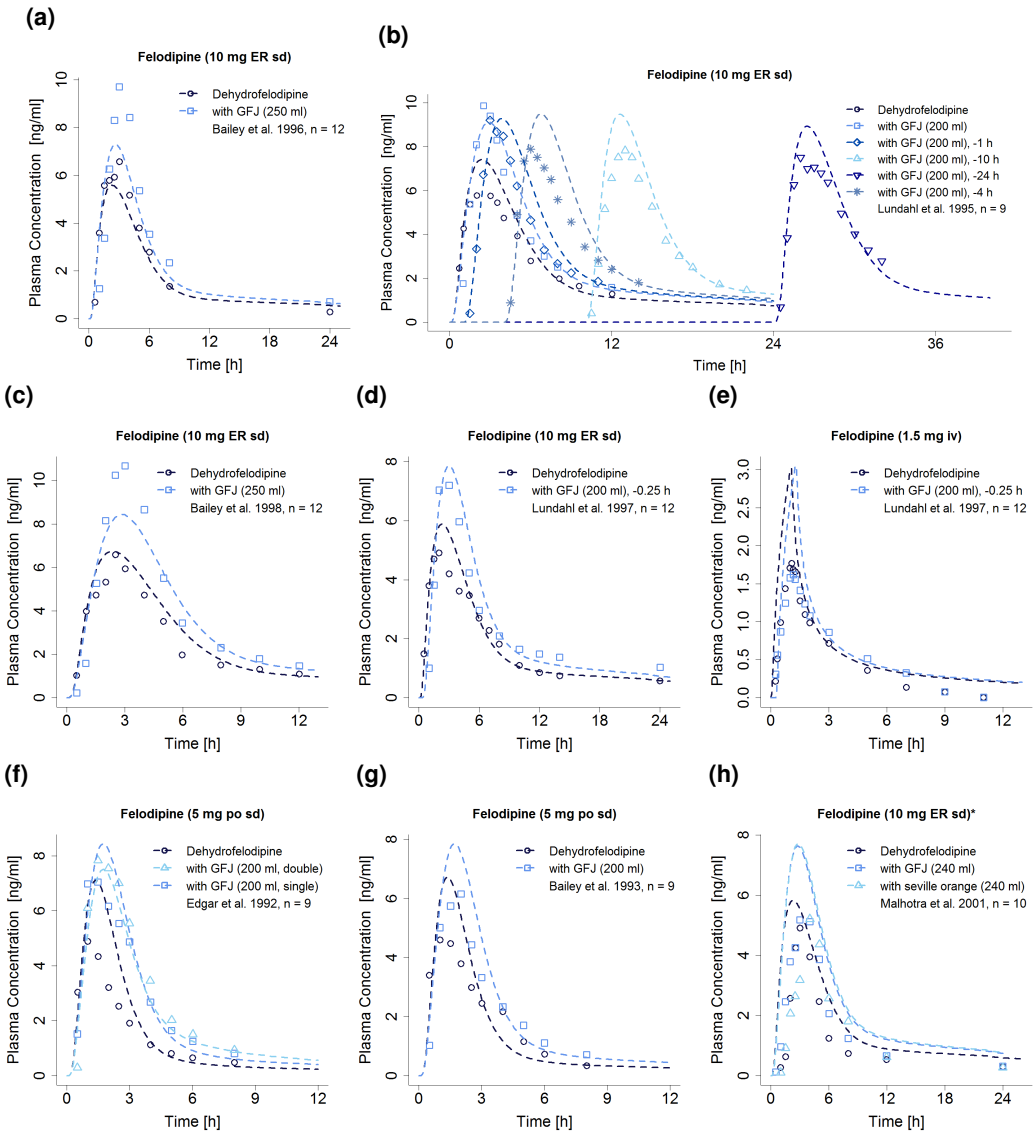

Figure S7: Predicted compared to observed dehydrofelodipine plasma concentration-time profiles (linear) with and without grapefruit, Seville orange or lime juice co-administration. Observed data are shown as dots ± standard deviation (if available); model predictions are shown as solid lines. Details on dosing regimens, study population and literature reference are listed in Table S7. BGT: bergamottin, D: day, DHB: 6,7-dihydroxybergamottin, ER: extended release tablet, extr: extract, GFJ: grapefruit juice, iv: intravenous, n: number of participants, po: oral, qd: once daily, sd: single dose, segm: segments, tid: three times daily

3.2.5 Semi-logarithmic plasma concentration-time profiles

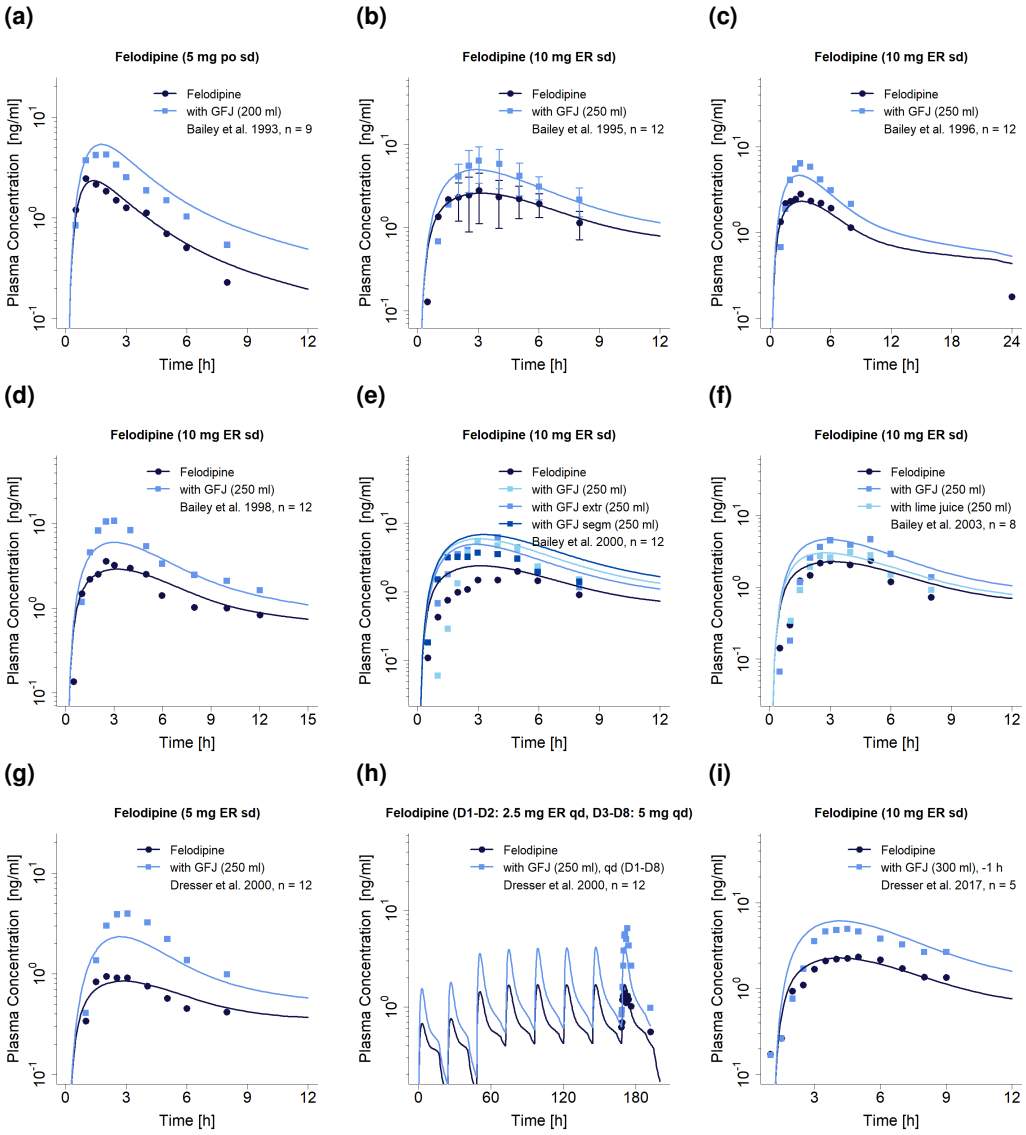

Figure S8: Predicted compared to observed felodipine plasma concentration-time profiles (semi-logarithmic) with and without grapefruit, Seville orange or lime juice co-administration. Observed data are shown as dots ± standard deviation (if available); model predictions are shown as solid lines. Details on dosing regimens, study population and literature reference are listed in Table S7. BGT: bergamottin, D: day, DHB: 6,7-dihydroxybergamottin, ER: extended release tablet, extr: extract, GFJ: grapefruit juice, iv: intravenous, n: number of participants, po: oral, qd: once daily, sd: single dose, segm: segments, tid: three times daily

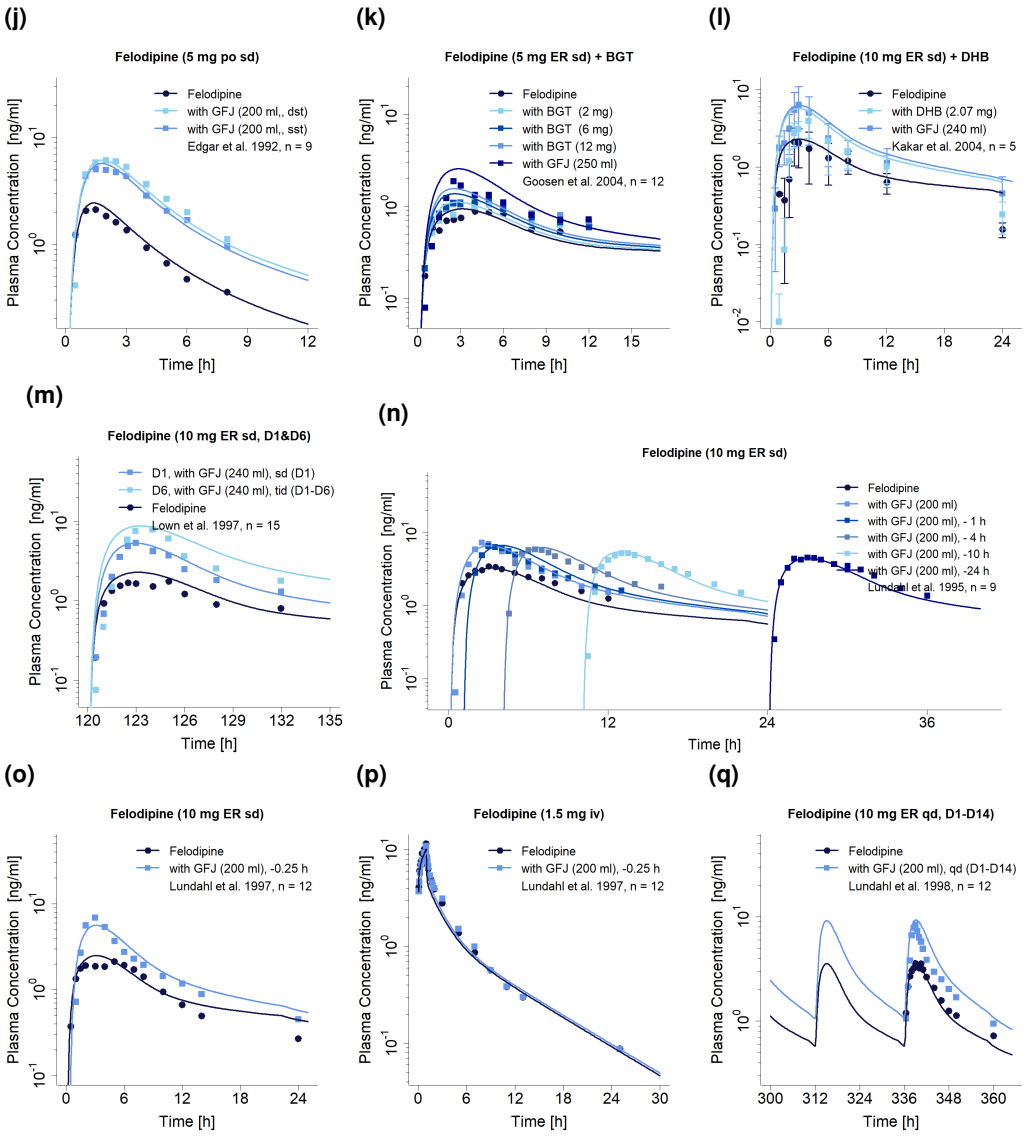

Figure S8: Predicted compared to observed felodipine plasma concentration-time profiles (semi-logarithmic) with and without grapefruit, Seville orange or lime juice co-administration. Observed data are shown as dots ± standard deviation (if available); model predictions are shown as solid lines. Details on dosing regimens, study population and literature reference are listed in Table S7. BGT: bergamottin, D: day, DHB: 6,7-dihydroxybergamottin, ER: extended release tablet, extr: extract, GFJ: grapefruit juice, iv: intravenous, n: number of participants, po: oral, qd: once daily, sd: single dose, segm: segments, tid: three times daily

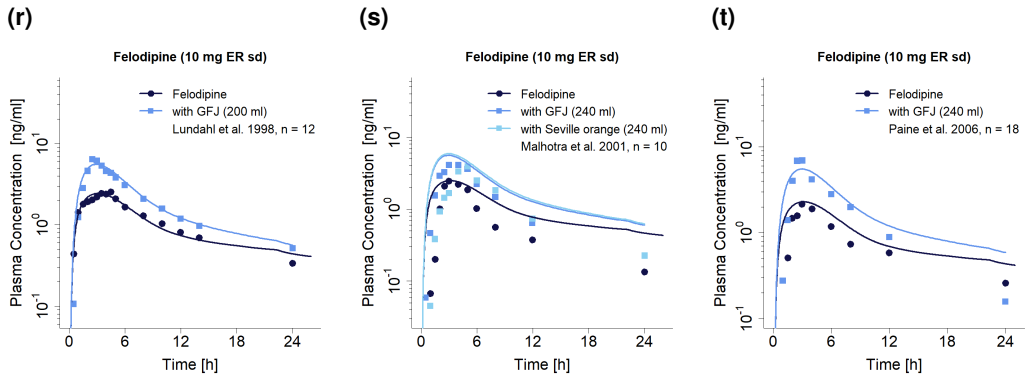

Figure S8: Predicted compared to observed felodipine plasma concentration-time profiles (semi-logarithmic) with and without grapefruit, Seville orange or lime juice co-administration. Observed data are shown as dots ± standard deviation (if available); model predictions are shown as solid lines. Details on dosing regimens, study population and literature reference are listed in Table S7. BGT: bergamottin, D: day, DHB: 6,7-dihydroxybergamottin, ER: extended release tablet, extr: extract, GFJ: grapefruit juice, iv: intravenous, n: number of participants, po: oral, qd: once daily, sd: single dose, segm: segments, tid: three times daily

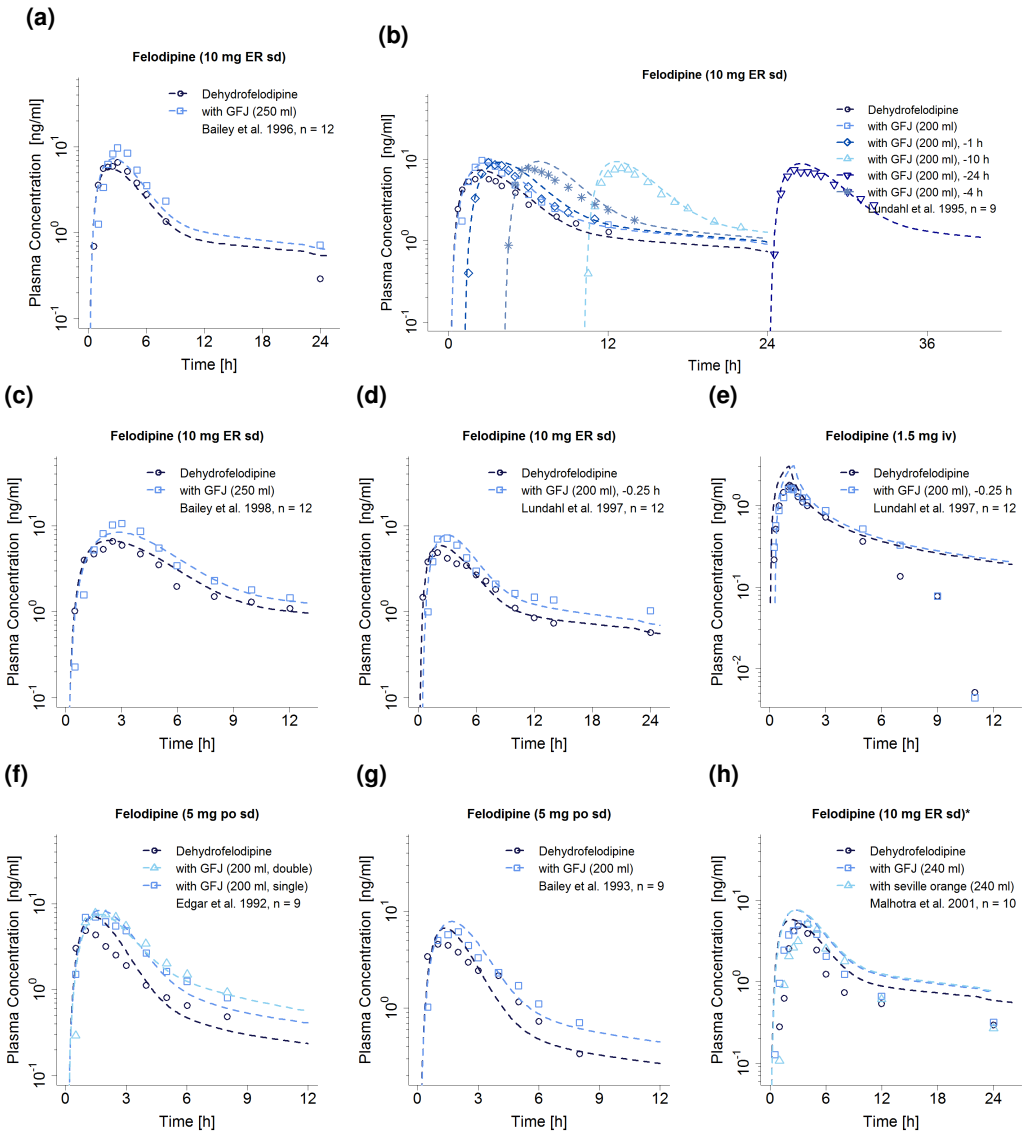

Figure S9: Predicted compared to observed dehydrofelodipine plasma concentration-time profiles (semi-logarithmic) with and without grapefruit, Seville orange or lime juice co-administration. Observed data are shown as dots ± standard deviation (if available); model predictions are shown as solid lines. Details on dosing regimens, study population and literature reference are listed in Table S7. BGT: bergamottin, D: day, DHB: 6,7-dihydroxybergamottin, ER: extended release tablet, extr: extract, GFJ: grapefruit juice, iv: intravenous, n: number of participants, po: oral, qd: once daily, sd: single dose, segm: segments, tid: three times daily

3.2.6 GFJDI AUC_{last} and C_{max} ratio goodness-of-fit plots

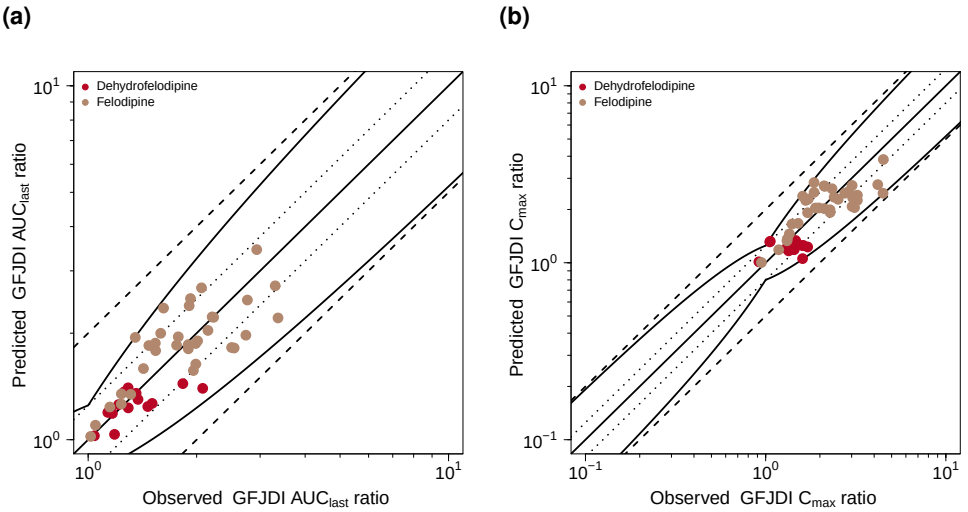

Figure S10: Predicted compared to observed GFJDI AUC_{last} and GFJDI C_{max} values. The straight solid line marks the line of identity, the curved solid lines show the prediction success limits proposed by Guest allowing for 1.25-fold variability of the GFJDI ratio [54]. Dotted lines indicate 1.25-fold, dashed lines indicate 2-fold deviation. AUC_{last}: area under the plasma concentration-time curve from the time of drug administration to the last concentration measurement, C_{max}: maximum plasma concentration, GFJDI: grapefruit juice-drug interaction

3.2.7 Geometric mean fold error of predicted GFJDI AUC_{last} and C_{max} ratios

Table S9: Predicted and observed Felodipine GFJDI AUC_{last} ratios and GFJDI C_{max} ratios.

ID			GFJDI AUC_{last} ratio			GFJDI C_{max} ratio			
	Compound	n	Pred	Obs	Pred/Obs	Pred	Obs	Pred/Obs	Reference
1.1.01	Felodipine	9	2.39	1.91	1.25	2.29	1.72	1.33	Bailey et al. 1993 [43]
1.1.02	Felodipine	12	1.57	1.96	0.80	1.92	2.28	0.84	Bailey et al. 1995 [44]
1.1.04	Felodipine	12	1.64	1.99	0.82	1.99	2.28	0.88	Bailey et al. 1996 [45]
1.1.05	Felodipine	12	1.82	2.50	0.73	2.08	3.02	0.69	Bailey et al. 1998 [4]
1.2.03	Felodipine	12	1.82	2.54	0.71	2.05	3.11	0.66	Bailey et al. 2000 [2]
1.1.06	Felodipine	12	2.22	2.21	1.01	2.47	2.75	0.90	Bailey et al. 2000 [2]
1.2.02	Felodipine	12	2.69	2.06	1.30	2.84	1.86	1.53	Bailey et al. 2000 [2]
1.1.07	Felodipine	8	1.86	1.89	0.98	2.04	1.97	1.03	Bailey et al. 2003 [46]
1.2.04	Felodipine	8	1.26	1.24	1.02	1.33	1.31	1.01	Bailey et al. 2003 [46]
1.1.09	Felodipine	12	1.97	2.74	0.72	2.47	4.48	0.55	Dresser et al. 2000 [47]
1.1.08	Felodipine	12	2.21	3.36	0.66	2.76	4.19	0.66	Dresser et al. 2000 [47]
1.1.10	Felodipine	5	2.51	1.92	1.30	2.70	2.13	1.27	Dresser et al. 2017 [48]
1.1.11	Felodipine	9	2.48	2.77	0.90	2.35	2.40	0.98	Edgar et al. 1992 [49]
1.1.12	Felodipine	9	2.72	3.30	0.82	2.53	2.89	0.87	Edgar et al. 1992 [49]
1.2.07	Felodipine	12	1.35	1.24	1.09	1.65	1.40	1.18	Goosen et al. 2004 [14]
1.2.05	Felodipine	12	1.10	1.05	1.05	1.18	1.18	1.00	Goosen et al. 2004 [14]
1.2.06	Felodipine	12	1.24	1.15	1.08	1.46	1.35	1.07	Goosen et al. 2004 [14]
1.1.13	Felodipine	12	1.95	1.35	1.44	2.72	2.11	1.29	Goosen et al. 2004 [14]
1.1.14	Felodipine	5	2.22	2.23	0.99	2.73	3.02	0.91	Kakar et al. 2004 [11]
1.2.08	Felodipine	5	2.00	1.59	1.26	2.50	1.86	1.35	Kakar et al. 2004 [11]
1.1.15	Felodipine	15	1.90	2.01	0.95	2.33	3.04	0.77	Lown et al. 1997 [50]

AUC_{last}: area under the plasma concentration-time curve from the time of drug administration to the last concentration measurement, C_{max}: maximum plasma concentration, GFJDI: grapefruit juice-drug interaction, GMFE: geometric mean fold error, n: number of individuals, obs: observed, pred: predicted

Table S9: Predicted and observed Felodipine GFJDI AUC_{last} ratios and GFJDI C_{max} ratios.

ID			GFJDI AUC_{last} ratio			GFJDI C_{max} ratio			
	Compound	**n**	**Pred**	**Obs**	**Pred/Obs**	**Pred**	**Obs**	**Pred/Obs**	**Reference**
1.1.27	Felodipine	15	3.44	2.94	1.17	3.83	4.50	0.85	Lown et al. 1997 [50]
1.1.19	Felodipine	9	1.59	1.42	1.12	1.67	1.51	1.10	Lundahl et al. 1995 [51]
1.1.17	Felodipine	9	1.85	1.47	1.25	2.04	1.89	1.08	Lundahl et al. 1995 [51]
1.1.20	Felodipine	9	1.34	1.31	1.02	1.36	1.32	1.03	Lundahl et al. 1995 [51]
1.1.16	Felodipine	9	1.87	1.54	1.22	2.02	2.11	0.96	Lundahl et al. 1995 [51]
1.1.18	Felodipine	9	1.79	1.54	1.16	1.92	1.71	1.12	Lundahl et al. 1995 [51]
1.1.22	Felodipine	12	1.02	1.02	1.01	-	-	-	Lundahl et al. 1997 [52]
1.1.21	Felodipine	12	1.81	1.90	0.95	2.25	3.23	0.70	Lundahl et al. 1997 [52]
1.1.23	Felodipine	12	2.35	1.62	1.45	2.62	2.33	1.12	Lundahl et al. 1998 [53]
1.1.26	Felodipine	12	1.85	1.76	1.05	2.28	2.52	0.90	Lundahl et al. 1998 [53]
1.1.24	Felodipine	10	1.87	1.99	0.94	2.25	1.67	1.35	Malhotra et al. 2001 [12]
1.2.09	Felodipine	10	1.95	1.78	1.10	2.38	1.60	1.48	Malhotra et al. 2001 [12]
1.1.25	Felodipine	18	2.04	2.15	0.95	2.41	3.23	0.75	Paine et al. 2006 [13]
GMFE					**1.18 (1.01-1.52)**		**1.24 (1.00-1.81)**		
					34/34 with GMFE < 2		**33/33 with GMFE < 2**		

AUC_{last}: area under the plasma concentration-time curve from the time of drug administration to the last concentration measurement, C_{max}: maximum plasma concentration, GFJDI: grapefruit juice-drug interaction, GMFE: geometric mean fold error, n: number of individuals, obs: observed, pred: predicted

Table S10: Predicted and observed Dehydrofelodipine GFJDI AUC_{last} ratios and GFJDI C_{max} ratios.

ID			GFJDI AUC_{last} ratio			GFJDI C_{max} ratio			
	Compound	**n**	**Pred**	**Obs**	**Pred/Obs**	**Pred**	**Obs**	**Pred/Obs**	**Reference**
1.1.01	Dehydrofelodipine	9	1.40	1.29	1.09	1.17	1.34	0.87	Bailey et al. 1993 [43]
1.1.04	Dehydrofelodipine	12	1.24	1.46	0.85	1.30	1.48	0.88	Bailey et al. 1996 [45]
1.1.05	Dehydrofelodipine	12	1.27	1.51	0.84	1.25	1.62	0.77	Bailey et al. 1998 [4]
1.1.11	Dehydrofelodipine	9	1.44	1.83	0.79	1.19	1.44	0.82	Edgar et al. 1992 [49]
1.1.12	Dehydrofelodipine	9	1.40	2.08	0.67	1.06	1.60	0.66	Edgar et al. 1992 [49]
1.1.16	Dehydrofelodipine	9	1.23	1.29	0.95	1.23	1.71	0.72	Lundahl et al. 1995 [51]
1.1.19	Dehydrofelodipine	9	1.26	1.21	1.03	1.28	1.36	0.94	Lundahl et al. 1995 [51]
1.1.17	Dehydrofelodipine	9	1.19	1.17	1.02	1.25	1.60	0.78	Lundahl et al. 1995 [51]
1.1.20	Dehydrofelodipine	9	1.03	1.04	0.99	1.20	1.30	0.93	Lundahl et al. 1995 [51]
1.1.18	Dehydrofelodipine	9	1.19	1.13	1.05	1.28	1.37	0.94	Lundahl et al. 1995 [51]
1.1.22	Dehydrofelodipine	12	1.04	1.18	0.87	1.01	0.92	1.10	Lundahl et al. 1997 [52]
1.1.21	Dehydrofelodipine	12	1.30	1.38	0.95	1.34	1.47	0.91	Lundahl et al. 1997 [52]
1.1.24	Dehydrofelodipine	10	1.35	1.36	1.00	1.31	1.05	1.24	Malhotra et al. 2001 [12]
1.2.09	Dehydrofelodipine	10	1.37	1.26	1.08	1.32	1.06	1.25	Malhotra et al. 2001 [12]
GMFE					**1.12 (1-1.49)**		**1.21 (1.06-1.52)**		
					14/14 with GMFE < 2		**14/14 with GMFE < 2**		

AUC_{last}: area under the plasma concentration-time curve from the time of drug administration to the last concentration measurement, C_{max}: maximum plasma concentration, GFJDI: grapefruit juice-drug interaction, GMFE: geometric mean fold error, n: number of individuals, obs: observed, pred: predicted

3.3 Grapefruit-midazolam GFJDI

The midazolam GFJDI was modeled using a previously developed and evaluated whole-body PBPK model of midazolam et al. [55]. Drug-dependent parameters of the midazolam PBPK model are displayed in Table S11.

Predicted midazolam plasma concentration-time profiles with and without grapefruit juice coadministration, compared to observed data, are shown in Figures S11 (linear) and S12 (semi-logarithmic). The correlation of predicted to observed GFJDI AUC_{last} and C_{max} ratios is shown in Figure S13. Table S14 lists the corresponding predicted and observed GFJDI AUC_{last} ratios, GFJDI C_{max} ratios as well as GMFE values.

3.3.1 Midazolam drug-dependent parameters

Table S11: Drug-dependent parameters of the midazolam PBPK model (adopted from [55])

Parameter	Unit	Model	Literature	Reference	Description
MW	g/mol	325.77 (lit)	325.77	[56]	Molecular weight
pKa (base)	-	6.15(lit)	6.15	[57]	Acid dissociation constant
Solubility (pH 6.5)	g/l	0.049 (lit)	0.049	[58]	Solubility
logP	-	3.13 (opt)	2.9, 3.9	[59, 60]	Lipophilicity
$f_{u,plasma}$	%	1.6 (lit)	1.6, 2.4	[59, 61]	Fraction unbound
CYP3A4 K_m	µmol/l	2.73 (lit)	2.73	[62]	CYP3A4 Michaelis-Menten constant
CYP3A4 k_{cat}	1/min	13.0 (opt)	-	-	CYP3A4 catalytic rate constant
GFR fraction	-	1.00 (asm)	-	-	Fraction of filtered drug in the urine
Partition coefficients	-	Diverse	Rodgers & Rowland	[26, 63]	Cell to plasma partition coefficients
Cellular permeability	cm/min	6.98E-02	PK-Sim standard	[1]	Permeability into the cellular space
Intestinal permeability	cm/min	2.00E-05 (opt)	1.88E-04	Calculated	Transcellular intestinal permeability
Tablet Weibull time	min	26.96 (opt)	-	-	Dissolution time (50% dissolved)
Tablet Weibull shape	-	0.70 (opt)	-	-	Dissolution profile shape

-: not given, asm: assumption, CYP: cytochrome P450, opt: optimized during parameter optimization, GFR: glomerular filtration rate, lit: literature

3.3.2 Clinical grapefruit-midazolam interaction studies

Table S12: Clinical studies investigating the grapefruit-midazolam interaction

	Midazolam		Grapefruit juice								
ID	Dose [mg]	Route	Volume [ml]	Route	BGT [µmol/l]	DHB [µmol/l]	n	Female [%]	Age[a] [years]	Weight[a] [kg]	Reference
						Midazolam					
2.1.01	7.5	po (tab), sd (D3)	250	D1-D3: qd (0h)	-	-	12	0	41 (35-52)	85 (66-93)	Abdlekawy et al. 2017 [64]
2.1.02	6	po, sd (D2)	240	D1: sd, D2: -1h	-	-	15	0	35 ± 9	83 ± 11	Farkas et al. 2007 [65]
2.1.03	6	po (sol), sd	300 (s)	-2h	29.0	6.7	25	16	33 (20-46)	-	Greenblatt et al. 2003 [15]
2.1.04	5	po (sol), sd (D3)	200	D1-D3: qd (0h)	43.4	53.2	12	67	30.8 ± 11.8	-	Kawaguchi-Suzuki et al. 2017 [17]
2.1.05	5	iv, sd	200 (s)	-1h, -0.25h	-	-	8	0	25 ± 1	70 ± 1	Kupferschmidt et al. 1995 [66]
2.1.06	15	po (tab), sd	200 (s)	-1h, -0.25h	-	-	8	0	25 ± 1	70 ± 1	Kupferschmidt et al. 1995 [66]
2.1.07	1	po (tab), sd (D1)	200	D-3 - D-1: tid, D1: 0h	-	-	7	0	(21-24)	-	Tanaka et al. 2013 [67]
2.1.17	1	po (tab), sd (D3)	200	D-3 - D-1: tid, D1: 0h	-	-	7	0	(21-24)	-	Tanaka et al. 2013 [67]
2.1.16	1	po (tab), sd (D7)	200	D-3 - D-1: tid, D1: 0h	-	-	7	0	(21-24)	-	Tanaka et al. 2013 [67]
2.1.13	2	po (sol), sd	240 (d)	D1-D2: tid, D3: -1.5 h, -1 h, -0.5 h	-	-	24	0	28.5 ± ´7.4	74.3 ± 9.3	Veronese et al. 2003 [68]
2.1.12	2	po (sol), sd	240 (d)	-1 h	-	-	24	0	28.5 ± 7.4	74.3 ± 9.3	Veronese et al. 2003 [68]
2.1.11	2	po (sol), sd	240 (s)	-1 h	-	-	24	0	28.5 ± 7.4	74.3 ± 9.3	Veronese et al. 2003 [68]
						Midazolam/Alfentanil					
2.1.14	1 (MDZ, 0 h) / 1.11 (ALF, 1 h)	iv, sd	240 (s) 90 (d)	-12h 0h	-	-	10	50	27 (20-39) ± 6	74 (53-96) ± 16	Kharasch et al. 2004 [69]
2.1.15	(MDZ, 0 h) / 1.70 (ALF, 1 h)	po, sd	240 (s) 90 (d)	-12h 0h	-	-	10	50	27 (20-39) ± 6	74 (53-96) ± 16	Kharasch et al. 2004 [69]

[a]: mean (range) ± standard deviation

-: not given, ALF: alfentanil, BGT: bergamottin, d: double-strength, D: day, DHB: 6,7-dihydroxybergamottin, iv: intravenous, MDZ: midazolam, po: oral, qd: once daily, s: single-strength, sd: single dose, sol: solution, tab: tablet, tid: three times daily

3.3.3 Bergamottin and 6,7-dihydroxybergamottin doses

Juice preparation	BGT [mg]	DHB [mg]	Measured	ID	Reference
canned juice, 250 ml	1.41	0.92	no	2.1.01	Abdlekawy et al. 2017 [64]
canned juice, 240 ml	1.35	0.89	no	2.1.02	Farkas et al. 2007 [65]
canned juice, 300 ml	2.94	0.747	yes	2.1.03	Greenblatt et al. 2003 [15]
hand-squeezed, 200 ml	2.9	3.86	yes	2.1.04	Kawaguchi-Suzuki et al. 2017 [17]
frozen concentrate, 200 ml	1.27	1.87	no	2.1.05	Kupferschmidt et al. 1995 [66]
frozen concentrate, 200 ml	1.27	1.87	no	2.1.06	Kupferschmidt et al. 1995 [66]
canned juice, 200 ml	1.13	0.74	no	2.1.07	Tanaka et al. 2013 [67]
canned juice, 200 ml	1.13	0.74	no	2.1.16	Tanaka et al. 2013 [67]
canned juice, 200 ml	1.13	0.74	no	2.1.17	Tanaka et al. 2013 [67]
frozen concentrate	1.58	2.33	no	2.1.11	Veronese et al. 2003 [68]
frozen concentrate	3.16	4.66	no	2.1.12	Veronese et al. 2003 [68]
frozen concentrate	3.16	4.66	no	2.1.13	Veronese et al. 2003 [68]
frozen concentrate, 90 ml (double), 240 ml (single)	1.52/1.14	2.24/1.68	no	2.1.14	Kharasch et al. 2004 [69]
frozen concentrate, 90 ml (double), 240 ml (single)	1.52/1.14	2.24/1.68	no	2.1.15	Kharasch et al. 2004 [69]

italic: preparation assumed; BGT: bergamottin, DHB: 6,7-dihydroxybergamottin

3.3.4 Linear plasma concentration-time profiles

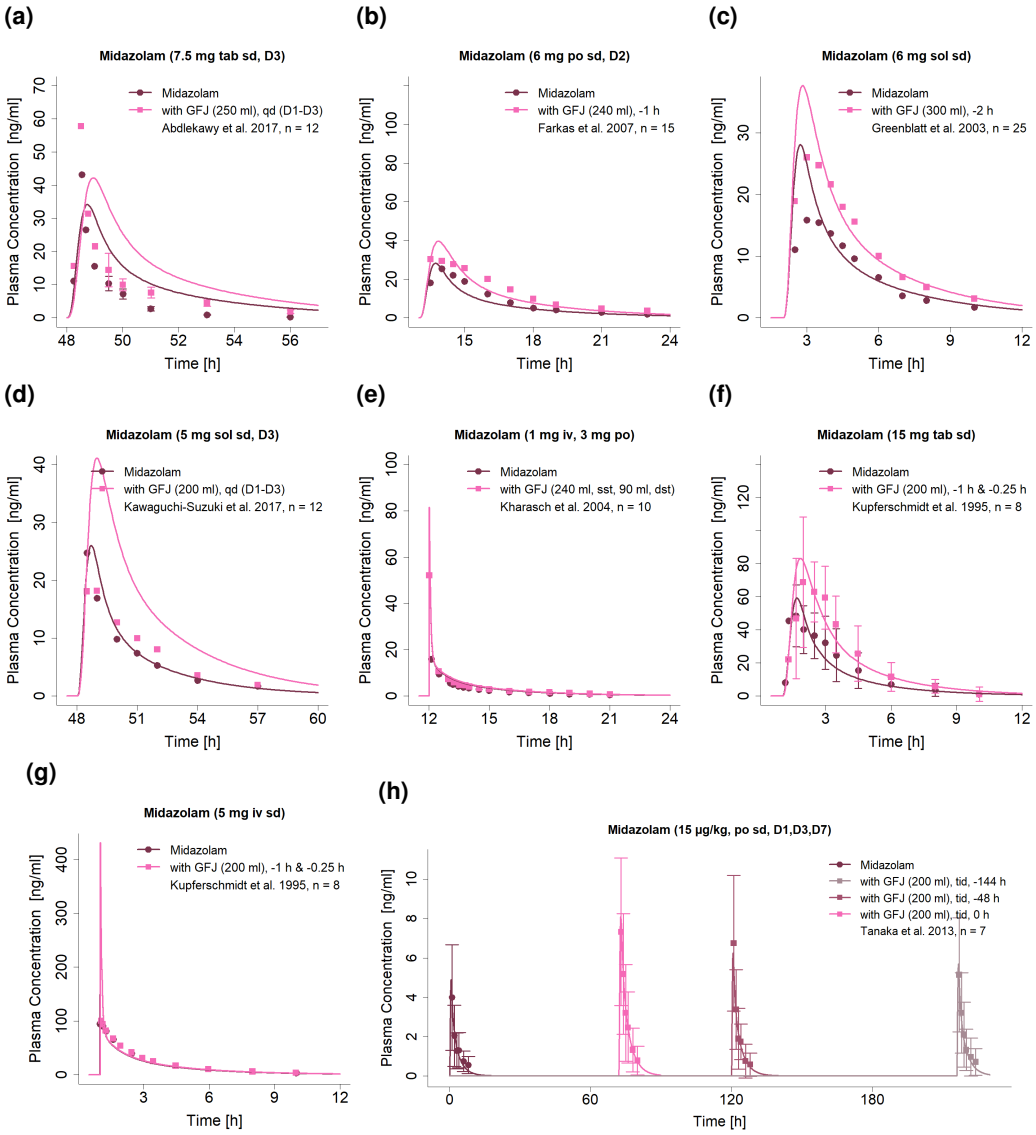

Figure S11: Predicted compared to observed midazolam plasma concentration-time profiles (linear) with and without grapefruit juice co-administration. Observed data are shown as dots ± standard deviation (if available); model predictions are shown as solid lines. Details on dosing regimens, study population and literature reference are listed in Table S12. d: double strength, D: day, dst: double strength, GFJ: grapefruit juice, iv: intravenous, n: number of participants, po: oral, qd: once daily, sst: single-strength, sd: single dose, sol: solution, tab: tablet, tid: three times daily

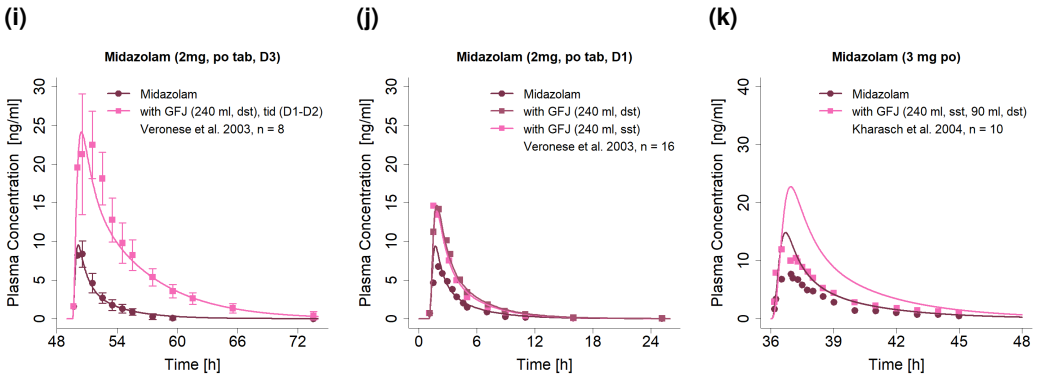

Figure S11: Predicted compared to observed midazolam plasma concentration-time profiles (linear) with and without grapefruit juice co-administration. Observed data are shown as dots ± standard deviation (if available); model predictions are shown as solid lines. Details on dosing regimens, study population and literature reference are listed in Table S12. dst: double strength, D: day, GFJ: grapefruit juice, iv: intravenous, n: number of participants, po: oral, qd: once daily, sst: single-strength, sd: single dose, sol: solution, tab: tablet, tid: three times daily

3.3.5 Semi-logarithmic plasma concentration-time profiles

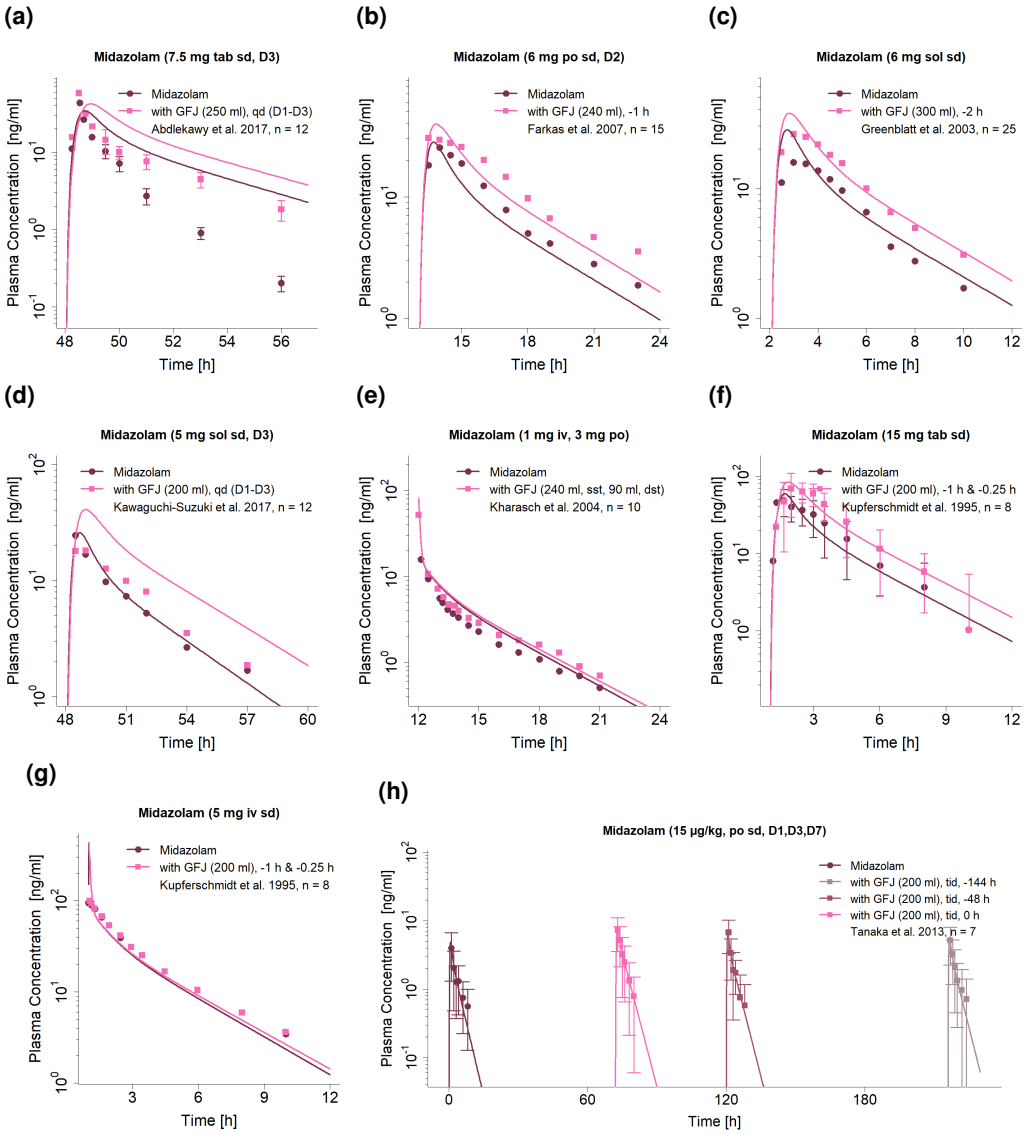

Figure S12: Predicted compared to observed midazolam plasma concentration-time profiles (semi-logarithmic) with and without grapefruit juice co-administration. Observed data are shown as dots ± standard deviation (if available); model predictions are shown as solid lines. Details on dosing regimens, study population and literature reference are listed in Table S12. dst: double strength, D: day, GFJ: grapefruit juice, iv: intravenous, n: number of participants, po: oral, qd: once daily, sst: single-strength, sd: single dose, sol: solution, tab: tablet, tid: three times daily

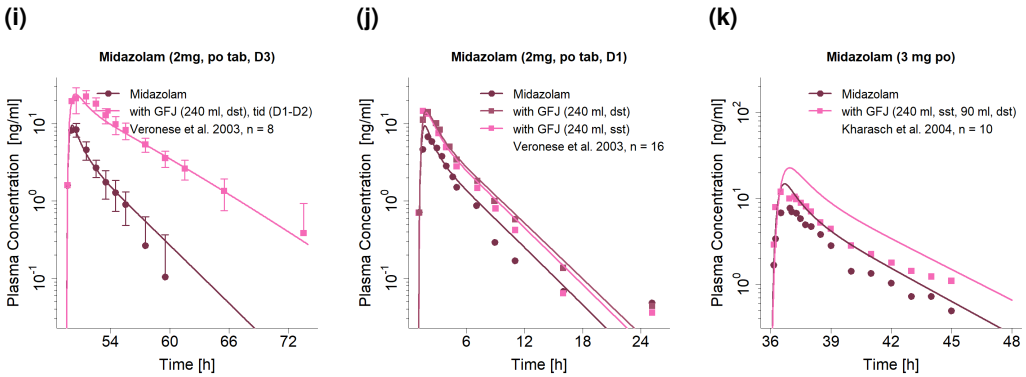

Figure S12: Predicted compared to observed midazolam plasma concentration-time profiles (semi-logarithmic) with and without grapefruit juice co-administration. Observed data are shown as dots ± standard deviation (if available); model predictions are shown as solid lines. Details on dosing regimens, study population and literature reference are listed in Table S12. dst: double strength, D: day, GFJ: grapefruit juice, iv: intravenous, n: number of participants, po: oral, qd: once daily, sst: single-strength, sd: single dose, sol: solution, tab: tablet, tid: three times daily

3.3.6 GFJDI AUC_{last} and C_{max} ratio goodness-of-fit plots

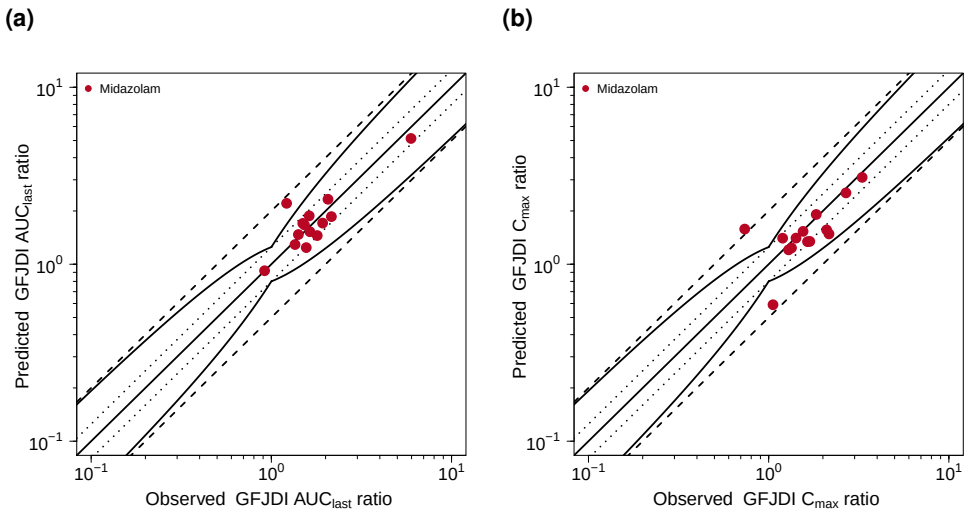

Figure S13: Predicted compared to observed GFJDI AUC_{last} and GFJDI C_{max} values. The straight solid line marks the line of identity, the curved solid lines show the prediction success limits proposed by Guest allowing for 1.25-fold variability of the GFJDI ratio [54]. Dotted lines indicate 1.25-fold, dashed lines indicate 2-fold deviation. AUC_{last}: area under the plasma concentration-time curve from the time of drug administration to the last concentration measurement, C_{max}: maximum plasma concentration, GFJDI: grapefruit juice-drug interaction

3.3.7 Geometric mean fold error of predicted GFJDI AUC_{last} and C_{max} ratios

Table S14: Predicted and observed Midazolam GFJDI AUC_{last} ratios and GFJDI C_{max} ratios.

ID			GFJDI AUC_{last} ratio			GFJDI C_{max} ratio			
	Compound	**n**	**Pred**	**Obs**	**Pred/Obs**	**Pred**	**Obs**	**Pred/Obs**	**Reference**
2.1.01	Midazolam	12	1.45	1.80	0.81	1.24	1.34	0.92	Abdlekawy et al. 2017 [64]
2.1.02	Midazolam	15	1.67	1.53	1.09	1.40	1.20	1.17	Farkas et al. 2007 [65]
2.1.03	Midazolam	25	1.53	1.64	0.93	1.34	1.64	0.82	Greenblatt et al. 2003 [15]
2.1.04	Midazolam	12	2.21	1.22	1.82	1.58	0.74	2.15	Kawaguchi-Suzuki et al. 2017 [17]
2.1.14	Midazolam	10	1.24	1.56	0.80	-	-	-	Kharasch et al. 2004 [69]
2.1.15	Midazolam	10	1.88	1.62	1.16	1.53	1.55	0.99	Kharasch et al. 2004 [69]
2.1.05	Midazolam	8	0.92	0.92	1.00	-	-	-	Kupferschmidt et al. 1995 [66]
2.1.06	Midazolam	8	1.70	1.49	1.14	1.41	1.42	0.99	Kupferschmidt et al. 1995 [66]
2.1.07	Midazolam	7	2.33	2.06	1.13	1.91	1.84	1.04	Tanaka et al. 2013 [67]
2.1.16	Midazolam	7	1.47	1.41	1.04	1.35	1.69	0.80	Tanaka et al. 2013 [67]
2.1.17	Midazolam	7	1.29	1.35	0.95	1.21	1.29	0.94	Tanaka et al. 2013 [67]
2.1.13	Midazolam	8	5.14	5.96	0.86	2.53	2.69	0.94	Veronese et al. 2003 [68]
2.1.11	Midazolam	16	1.71	1.93	0.89	1.48	2.16	0.69	Veronese et al. 2003 [68]
2.1.12	Midazolam	16	1.86	2.15	0.86	1.56	2.10	0.75	Veronese et al. 2003 [68]
GMFE					**1.17 (1-1.82)**			**1.24 (1.01-2.15)**	
					14/14 with GMFE < 2			**11/12 with GMFE < 2**	

AUC_{last}: area under the plasma concentration-time curve from the time of drug administration to the last concentration measurement, C_{max}: maximum plasma concentration, GFJDI: grapefruit juice-drug interaction, GMFE: geometric mean fold error, n: number of individuals, obs: observed, pred: predicted

3.4 Grapefruit-alprazolam GFJDI

The alprazolam GFJDI was modeled using a previously developed and evaluated whole-body PBPK model of alprazolam, available in the Open Systems Pharmacology (OSP) GitHub model repository et al. [70]. Drug-dependent parameters of the alprazolam PBPK model are displayed in Table S15.

Details on the modeled clinical GFJDI studies are given in Table S16. Predicted alprazolam and plasma concentration-time profiles with and without grapefruit juice coadministration, compared to observed data, are shown in Figures S14 (linear) and S15 (semi-logarithmic). The correlation of predicted to observed GFJDI AUC_{last} and C_{max} ratios is shown in Figure S16. Table S18 lists the corresponding predicted and observed GFJDI AUC_{last} ratios, GFJDI C_{max} ratios as well as GMFE values.

3.4.1 Alprazolam drug-dependent parameters

Table S15: Drug-dependent parameters of the alprazolam PBPK model (adopted from [70])

Parameter	Unit	Model	Literature	Reference	Description
MW	g/mol	308.77 (Lit)	308.77	[71]	Molecular weight
logP	Log Units	2.08 (Opt)	1.26 (logD)	[15]	Lipophilicity
			2.19 (logP)	[72]	
Solubility (pH)	mg/ml	0.04 (7.0) (Lit)	0.012 (1.2),	[71]	Solubility
			0.04 (7.0),	[71]	
			0.08 (7.0)	[73]	
$f_{u,plasma}$	%	23.3 (Lit)	20.0, 23.3, 31.1	[74–76]	Fraction unbound in plasma
pKa (base)	-	2.40 (Lit)	2.40, 2.48	[77–79]	Acid dissociation constant
K_m (CYP3A4) α-hydroxy	µmol/l	269.0 (Lit)	269.0	[80]	CYP3A4 Michaelis-Menten constant (α-hydroxy-alprazolam)
k_{cat} (CYP3A4) α-hydroxy	1/min	0.81 (Opt)	-	-	CYP3A4 catalytic rate constant (α-hydroxy-alprazolam)
K_m (CYP3A4) 4-hydroxy	µmol/l	704.0 (Lit)	704.0	[80]	CYP3A4 Michaelis-Menten constant (4-hydroxy-alprazolam)
k_{cat} (CYP3A4) 4-hydroxy	1/min	13.73 (Opt)	-	-	CYP3A4 catalytic rate constant (4-hydroxy-alprazolam)
GFR fraction	-	0.55 (Opt)	-	-	Fraction of filtered drug in the urine
Intestinal permeability	cm/min	7.61 (Opt)	-	-	Transcellular intestinal permeability
Partition coefficients	-	Diverse	Rogers and Rowland	[26, 27]	Cell to plasma partition coefficients
Cellular permeability	cm/min	6.22E-3 (Calc)	PK-Sim Standard	[40]	Permeability into the cellular space
Tablet (Solanax®) Weibull time	min	35.85 (Opt)	-	-	Dissolution time (50% dissolved)
Tablet (Solanax®) Weibull shape	-	0.92 (Opt)	-	-	Dissolution profile shape

-: not given, calc: calculated, CYP: cytochrome P450, GFR: glomerular filtration rate, lit: literature, opt: optimized during parameter identification

3.4.2 Clinical grapefruit-alprazolam interaction studies

Table S16: Clinical studies investigating the grapefruit-alprazolam interaction

	Alprazolam		Grapefruit juice								
ID	**Dose [mg]**	**Route**	**Volume [ml]**	**Route**	**BGT [µmol/l]**	**DHB [µmol/l]**	**n**	**Female [%]**	**Age[a] [years]**	**Weight[a] [kg]**	**Reference**
3.1.01	0.8	po (tab), sd (D8)	200 (s)	D1-D10: tid (0h)	-	-	8	0	31 ± 6.3	61.5 ± 4.7	Yasui et al. 1999 [81]

[a]: mean ± standard deviation

-: not given, BGT: bergamottin, D: day, DHB: 6,7-dihydroxybergamottin, po: oral, s: single-strength, sd: single dose, tab: tablet, tid: three times daily

3.4.3 Bergamottin and 6,7-dihydroxybergamottin doses

Juice preparation	BGT [mg]	DHB [mg]	Measured in study	ID	Reference
canned juice, 200 ml	1.13	0.74	no	3.1.01	Yasui et al. 1999 [81]

italic: preparation assumed; BGT: bergamottin, DHB: 6,7-dihydroxybergamottin

3.4.4 Linear plasma concentration-time profiles

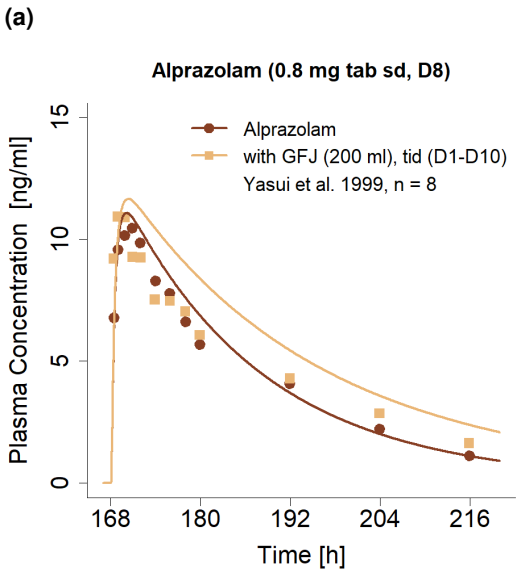

Figure S14: Predicted compared to observed alprazolam plasma concentration-time profiles (linear) with and without grapefruit juice co-administration. Observed data are shown as dots; model predictions are shown as solid lines. Details on dosing regimens, study population and literature reference are listed in Table S16. D: day, GFJ: grapefruit juice, n: number of participants, sd: single dose, tab: tablet, tid: three times daily

3.4.5 Semi-logarithmic plasma concentration-time profiles

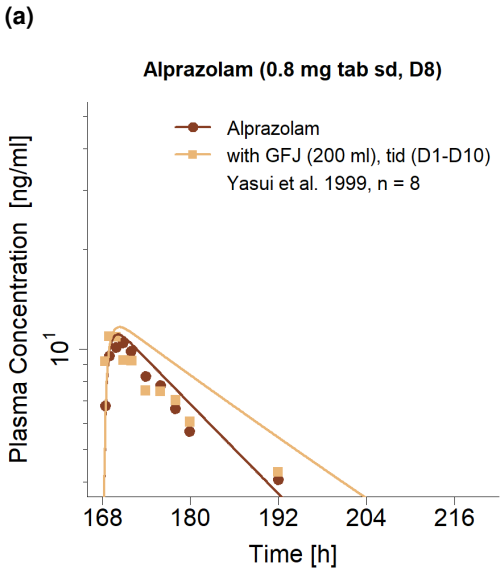

Figure S15: Predicted compared to observed alprazolam plasma concentration-time profiles (semi-logarithmic) with and without grapefruit juice co-administration. Observed data are shown as dots; model predictions are shown as solid lines. Details on dosing regimens, study population and literature reference are listed in Table S16. D: day, GFJ: grapefruit juice, n: number of participants, sd: single dose, tab: tablet, tid: three times daily

3.4.6 GFJDI AUC_{last} and C_{max} ratio goodness-of-fit plots

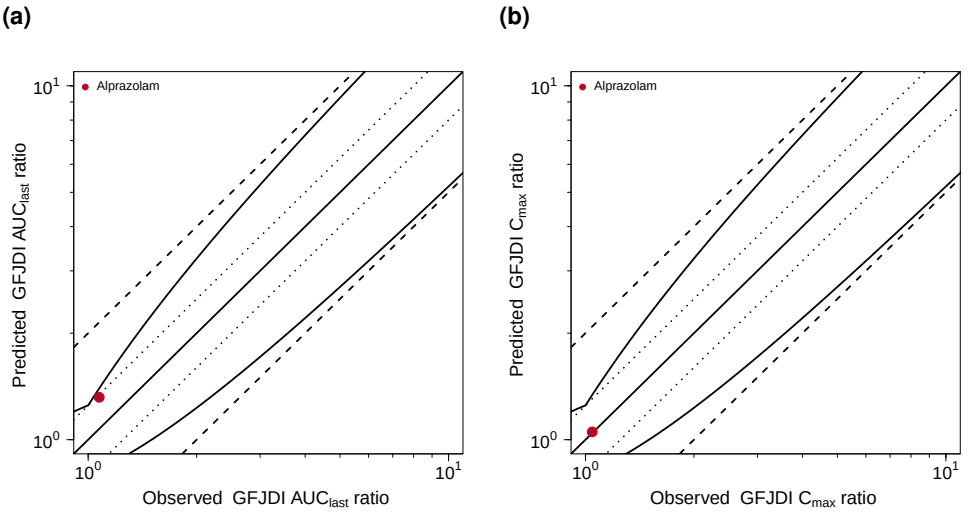

Figure S16: Predicted compared to observed GFJDI AUC_{last} and GFJDI C_{max} values. The straight solid line marks the line of identity, the curved solid lines show the prediction success limits proposed by Guest allowing for 1.25-fold variability of the GFJDI ratio [54]. Dotted lines indicate 1.25-fold, dashed lines indicate 2-fold deviation. AUC_{last}: area under the plasma concentration-time curve from the time of drug administration to the last concentration measurement, C_{max}: maximum plasma concentration, GFJDI: grapefruit juice-drug interaction

3.4.7 Geometric mean fold error of predicted GFJDI AUC_{last} and C_{max} ratios

Table S18: Predicted and observed Alprazolam GFJDI AUC_{last} ratios and GFJDI C_{max} ratios.

ID			GFJDI AUC_{last} ratio			GFJDI C_{max} ratio			
	Compound	n	Pred	Obs	Pred/Obs	Pred	Obs	Pred/Obs	Reference
3.1.01	Alprazolam	8	1.32	1.07	1.23	1.05	1.04	1.01	Yasui et al. 1999 [81]
GMFE					**1.23**		**1.01**		
					1/1 with GMFE < 2		**1/1 with GMFE < 2**		

AUC_{last}: area under the plasma concentration-time curve from the time of drug administration to the last concentration measurement, C_{max}: maximum plasma concentration, GFJDI: grapefruit juice-drug interaction, GMFE: geometric mean fold error, n: number of individuals, obs: observed, pred: predicted

3.5 Grapefruit-alfentanil GFJDI

The alfentanil GFJDI was modeled using a previously developed and evaluated whole-body PBPK model of alfentanil et al. [55]. Drug-dependent parameters of the alfentanil PBPK model are displayed in Table S15.

Details on the modeled clinical GFJDI studies are given in Table S20. Predicted alfentanil plasma concentration-time profiles with and without grapefruit juice coadministration, compared to observed data, are shown in Figures S17 (linear) and S18 (semi-logarithmic). The correlation of predicted to observed GFJDI AUC_{last} and C_{max} ratios is shown in Figure S19. Table S22 lists the corresponding predicted and observed GFJDI AUC_{last} ratios, GFJDI C_{max} ratios as well as GMFE values.

3.5.1 Alfentanil drug-dependent parameters

Table S19: Drug-dependent parameters of alfentanil (adopted from [55])

Parameter	Unit	Model	Literature	Reference	Description
MW	g/mol	416.52 (Lit)	416.52	[82]	Molecular weight
logP	Log Units	1.75 (Opt)	2.10, 2.20 (logD)	[83, 84]	Lipophilicity
Solubility (pH)	mg/ml	0.992 (6.5) (Lit)	0.992 (6.5)	[83]	Solubility
$f_{u,plasma}$	%	10.0 (Lit)	8.6, 10.0, 12.0	[83, 85, 86]	Fraction unbound in plasma
pKa (base)	-	6.50 (Lit)	6.50	[84]	Acid dissociation constant
CL_{spec} (CYP3A4)	l/min	0.32 (Opt)	-	-	CYP3A4 clearance
GFR fraction	-	0.06 (Opt)	-	-	Fraction of filtered drug in the urine
Intestinal permeability	cm/min	3.48E-6 (Opt)	-	-	Transcellular intestinal permeability
Partition coefficients	-	Diverse	Rogers and Rowland	[26, 27]	Cell to plasma partition coefficients
Cellular permeability	cm/min	6.88E-3 (Opt)	PK-Sim Standard	[40]	Permeability into the cellular space

-: not given, CL_{spec}: specific clearance, CYP: cytochrome P450, GFR: glomerular filtration rate, lit: literature, opt: optimized during parameter identification

3.5.2 Clinical grapefruit-alfentanil interaction studies

Table S20: Clinical studies investigating the grapefruit-alfentanil interaction

	Alfentanil		Grapefruit juice								
ID	Dose [mg]	Route	Volume [ml]	Route	BGT [µmol/l]	DHB [µmol/l]	n	Female [%]	Age[a] [years]	Weight[a] [kg]	Reference
						Midazolam/Alfentanil					
4.1.01	1 (MDZ, 0 h) 1.11 (ALF, 1 h)	iv, sd	240 (s) 90 (d)	-12h 0h	-	-	10	50	27 (20-39) ± 6	74 (53-96) ± 16	Kharasch et al. 2004 [69]
4.1.03	3 (MDZ, 0 h) 1.70 (ALF, 1 h)	po, sd	240 (s) 90 (d)	-12h 0h	-	-	10	50	27 (20-39) ± 6	74 (53-96) ± 16	Kharasch et al. 2004 [69]
						Alfentanil					
4.1.02	1 4 1 ; 4	12h: iv, sd 15h: po, sd 37h: iv, sd + po, sd	240 90 240 90	0h 14h 24h 36h	-	-	6	50	28 (21-33) ± 6	79 (63-106) ± 17	Kharasch et al. 2011 [87]

[a]: mean (range) ± standard deviation

-: not given, ALF: alfentanil, BGT: bergamottin, d: double-strength, DHB: 6,7-dihydroxybergamottin, iv: intravenous, MDZ: midazolam, po: oral, s: single-strength, sd: single dose

3.5.3 Bergamottin and 6,7-dihydroxybergamottin doses

Juice preparation	BGT [mg]	DHB [mg]	Measured	ID	Reference
frozen concentrate, 90 ml (double), 240 ml (single)	1.52/1.14	2.24/1.68	no	4.1.01	Kharasch et al. 2004 [69]
frozen concentrate, 90 ml (double), 240 ml (single)	1.52/1.14	2.24/1.68	no	4.1.03	Kharasch et al. 2004 [69]
frozen concentrate, 90 ml (double), 240 ml (single)	1.52/1.14	2.24/1.68	no	4.1.02	Kharasch et al. 2011 [87]

italic: preparation assumed; BGT: bergamottin, DHB: 6,7-dihydroxybergamottin

3.5.4 Linear plasma concentration-time profiles

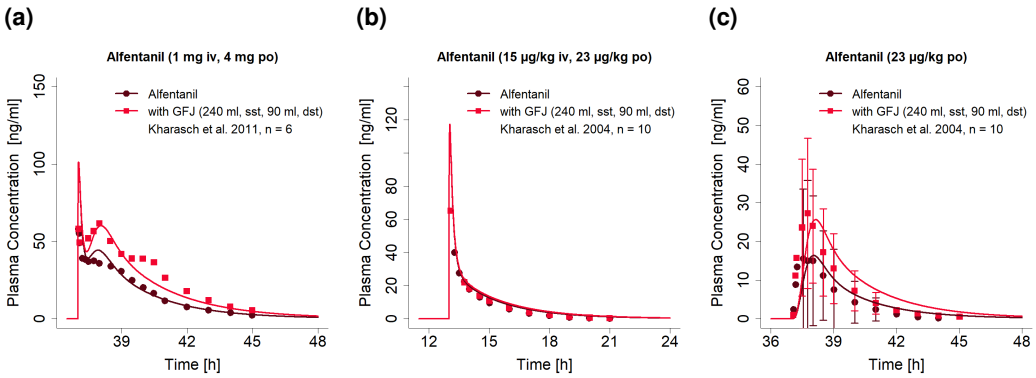

Figure S17: Predicted compared to observed alfentanil plasma concentration-time profiles (linear) with and without grapefruit juice co-administration. Observed data are shown as dots ± standard deviation (if available); model predictions are shown as solid lines. Details on dosing regimens, study population and literature reference are listed in Table S20. dst: double-strengh, GFJ: grapefruit juice, iv: intravenous, n: number of participants, po: oral, sst: single-strength

3.5.5 Semi-logarithmic plasma concentration-time profiles

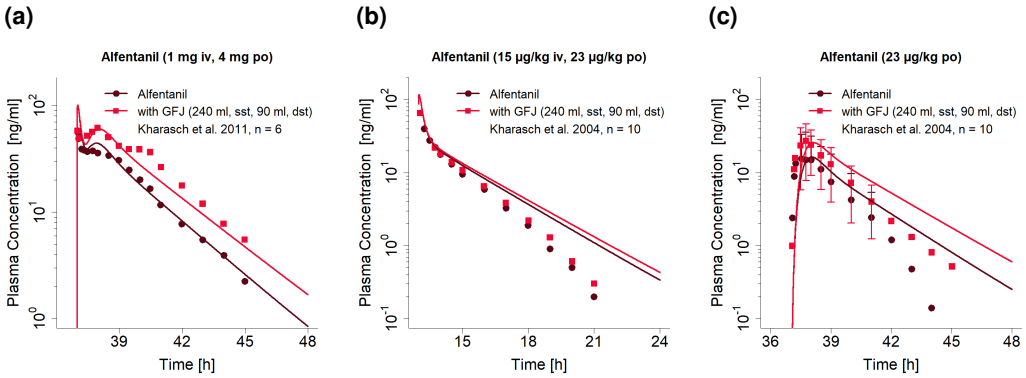

Figure S18: Predicted compared to observed alfentanil plasma concentration-time profiles (semi-logarithmic) with and without grapefruit juice co-administration. Observed data are shown as dots ± standard deviation (if available); model predictions are shown as solid lines. Details on dosing regimens, study population and literature reference are listed in Table S20. dst: double-strengh, GFJ: grapefruit juice, iv: intravenous, n: number of participants, po: oral, sst: single-strength

3.5.6 GFJDI AUC_{last} and C_{max} ratio goodness-of-fit plots

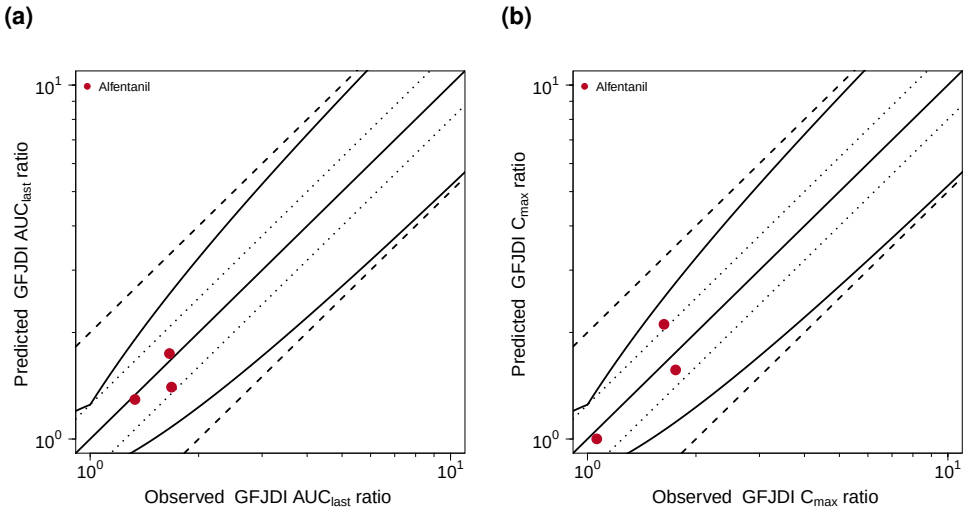

Figure S19: Predicted compared to observed GFJDI AUC_{last} and GFJDI C_{max} values. The straight solid line marks the line of identity, the curved solid lines show the prediction success limits proposed by Guest allowing for 1.25-fold variability of the GFJDI ratio [54]. Dotted lines indicate 1.25-fold, dashed lines indicate 2-fold deviation. AUC_{last}: area under the plasma concentration-time curve from the time of drug administration to the last concentration measurement, C_{max}: maximum plasma concentration, GFJDI: grapefruit juice-drug interaction

3.5.7 Geometric mean fold error of predicted GFJDI AUC_{last} and C_{max} ratios

Table S22: Predicted and observed Alfentanil GFJDI AUC_{last} ratios and GFJDI C_{max} ratios.

ID			GFJDI AUC_{last} ratio			GFJDI C_{max} ratio			
	Compound	**n**	**Pred**	**Obs**	**Pred/Obs**	**Pred**	**Obs**	**Pred/Obs**	**Reference**
4.1.01	Alfentanil	10	1.29	1.33	0.97	-	-	-	Kharasch et al. 2004 [69]
4.1.03	Alfentanil	10	1.74	1.66	1.05	1.57	1.76	0.89	Kharasch et al. 2004 [69]
4.1.02	Alfentanil	6	1.40	1.68	0.83	-	-	-	Kharasch et al. 2011 [87]
GMFE					**1.09 (1.03-1.2)**		**1.09**		
					3/3 with GMFE < 2		**1/1 with GMFE < 2**		

AUC_{last}: area under the plasma concentration-time curve from the time of drug administration to the last concentration measurement, C_{max}: maximum plasma concentration, GFJDI: grapefruit juice-drug interaction, GMFE: geometric mean fold error, n: number of individuals, obs: observed, pred: predicted

3.6 Grapefruit-triazolam GFJDI

The triazolam GFJDI was modeled using a previously developed and evaluated whole-body PBPK model of triazolam, available in the Open Systems Pharmacology (OSP) GitHub model repository et al. [88]. Drug-dependent parameters of the triazolam PBPK model are displayed in Table S23.

Details on the modeled clinical GFJDI studies are given in Table S24. Predicted triazolam plasma concentration-time profiles with and without grapefruit juice coadministration, compared to observed data, are shown in Figures S20 (linear) and S21 (semi-logarithmic). The correlation of predicted to observed GFJDI AUC_{last} and C_{max} ratios is shown in Figure S22. Table S26 lists the corresponding predicted and observed GFJDI AUC_{last} ratios, GFJDI C_{max} ratios as well as GMFE values.

3.6.1 Triazolam drug-dependent parameters

Table S23: Drug-dependent parameters of the triazolam PBPK model (adopted from [88])

Parameter	Unit	Model	Literature	Reference	Description
MW	g/mol	343.21 (Lit)	343.21	[89]	Molecular weight
logP	Log Units	1.90 (Opt)	2.42 (logP) 1.63 logD	[89] [90]	Lipophilicity
Solubility (pH)	mg/l	4.53 (7.0) (Lit)	4.53 (7.0)	[89]	Solubility
$f_{u,plasma}$	%	17 (Lit)	9.9; 11; 17.4; 18.8; 21.3; 22.9	[91–95]	Fraction unbound in plasma
pKa (base)	-	1.52 (Lit)	1.52	[96]	Acid dissociation constant
K_m (CYP3A4) α-hydroxy	µmol/l	74.20 (Lit)	74.20	[97]	CYP3A4 Michaelis-Menten constant (α-hydroxy-triazolam)
k_{cat} (CYP3A4) α-hydroxy	1/min	4.03 (Opt)	-	-	CYP3A4 catalytic rate constant (α-hydroxy-triazolam)
K_m (CYP3A4) 4-hydroxy	µmol/l	305.0 (Lit)	305.0	[97]	CYP3A4 Michaelis-Menten constant (4-hydroxy-triazolam)
k_{cat} (CYP3A4) 4-hydroxy	1/min	17.54 (Opt)	-	-	CYP3A4 catalytic rate constant (4-hydroxy-triazolam)
Intestinal permeability	cm/min	7.02E-5 (Opt)	-	-	Transcellular intestinal permeability
Partition coefficients	-	Diverse	Rogers and Rowland	[26, 27]	Cell to plasma partition coefficients
Cellular permeability	cm/min	3.16E-3 (Calc)	PK-Sim Standard	[40]	Permeability into the cellular space
Tablet (Halicon®) Weibull time	min	1.80 (Opt)	-	-	Dissolution time (50% dissolved)
Tablet (Halicon®) Weibull shape	-	2.52 (Opt)	-	-	Dissolution profile shape

-: not given, calc: calculated, CYP: cytochrome P450, GFR: glomerular filtration rate, lit: literature, opt: optimized during parameter identification

3.6.2 Clinical grapefruit-triazolam interaction studies

Table S24: Clinical studies investigating the grapefruit-triazolam interaction

	Triazolam		Grapefruit juice								
ID	Dose [mg]	Route	Volume [ml]	Route	BGT [µmol/l]	DHB [µmol/l]	n	Female [%]	Age[a] [years]	Weight[a] [kg]	Reference
5.1.01	0.1875	po, sd (D1,3)	300	D2-D11: qd (-0.5h)	-	-	7	14	29 ± 7	73 ± 7	Culm-Merdek et al. 2006 [98]
5.1.07	0.1875	po, sd (D11)	300	D2-D11: qd (-0.5h)	-	-	7	14	29 ± 7	73 ± 7	Culm-Merdek et al. 2006 [98]
5.1.08	0.1875	po, sd (D15)	300	D2-D11: qd (-0.5h)	-	-	7	14	29 ± 7	73 ± 7	Culm-Merdek et al. 2006 [98]
5.1.02	0.25	po (tab), sd	250	0h	-	-	10	40	(22-29)	(49-107)	Hukkinen et al. 1995 [99]
5.1.03	0.25	po (tab), sd	200 (s)	0h	-	-	12	50	(19-28)	(53-97)	Lilja et al. 2000 [100]
5.1.04	0.25	po (tab), sd	200 (d)	0h	-	-	12	50	(19-28)	(53-97)	Lilja et al. 2000 [100]
5.1.05	0.25	po (tab), sd (D3)	200 (d)	D1-D2: tid, D3: 0h, 0.5h, 1.5h	-	-	12	50	(19-28)	(53-97)	Lilja et al. 2000 [100]
5.1.06	0.25	po (tab), sd (D4)	250 (s)	D1-D4:tid (0h)	-	-	9	0	(23-44)	(56-80)	Sugimoto et al. 2006 [101]

-

[a]: mean (range) ± standard deviation

-: not given, BGT: bergamottin, d: double-strength, D: day, po: oral, DHB: 6,7-dihydroxybergamottin qd: once daily, s: single-strength, sd: single dose, tab: tablet, tid: three times daily

3.6.3 Bergamottin and 6,7-dihydroxybergamottin doses

Juice preparation	BGT [mg]	DHB [mg]	Measured	ID	Reference
canned juice, 300 ml	1.69	1.11	no	5.1.01	Culm-Merdek et al. 2006 [98]
frozen concentrate, 250 ml	1.58	2.33	no	5.1.02	Hukkinen et al. 1995 [99]
frozen concentrate, 200 ml	1.27	1.87	no	5.1.03	Lilja et al. 2000 [100]
frozen concentrate (double), 200 ml	2.54	3.74	no	5.1.04	Lilja et al. 2000 [100]
frozen concentrate (double), 200 ml	2.54	3.74	no	5.1.05	Lilja et al. 2000 [100]
canned juice, 250 ml	1.41	0.92	no	5.1.06	Sugimoto et al. 2006 [101]

italic: preparation assumed; BGT: bergamottin, DHB: 6,7-dihydroxybergamottin

3.6.4 Linear plasma concentration-time profiles

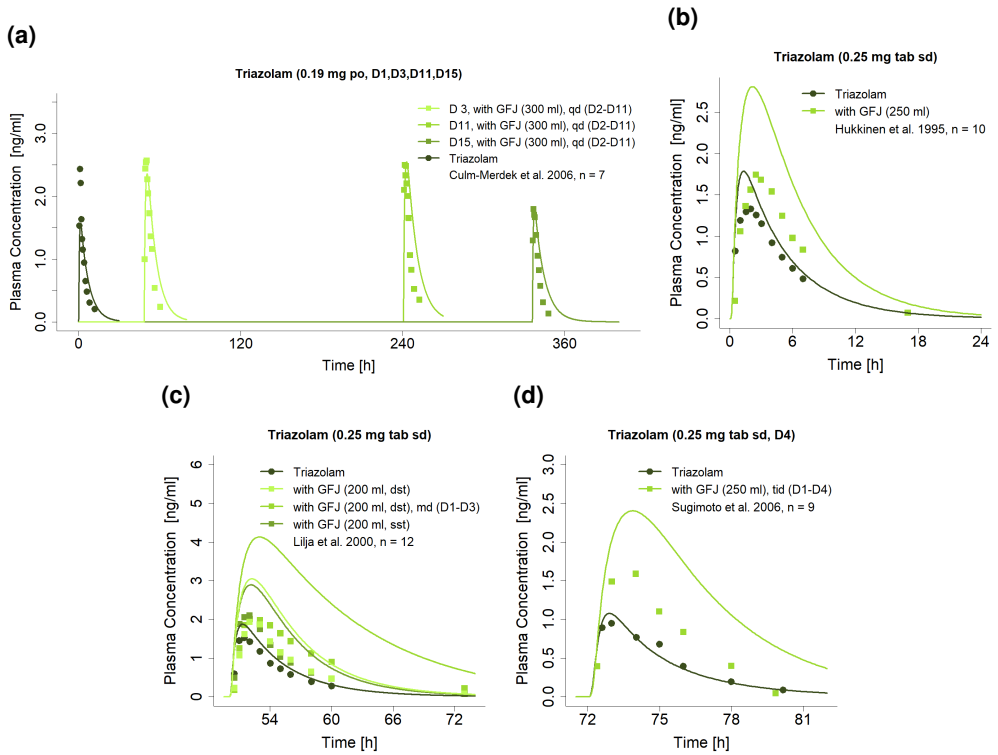

Figure S20: Predicted compared to observed triazolam plasma concentration-time profiles (linear) with and without grapefruit juice co-administration. Observed data are shown as dots; model predictions are shown as solid lines. Details on dosing regimens, study population and literature reference are listed in Table S24. D: day, dst: double strength, GFJ: grapefruit juice, md: multiple dose, n: number of participants, po: oral, sd: single dose, sst: single strength, tab: tablet, tid: three times daily

3.6.5 Semi-logarithmic plasma concentration-time profiles

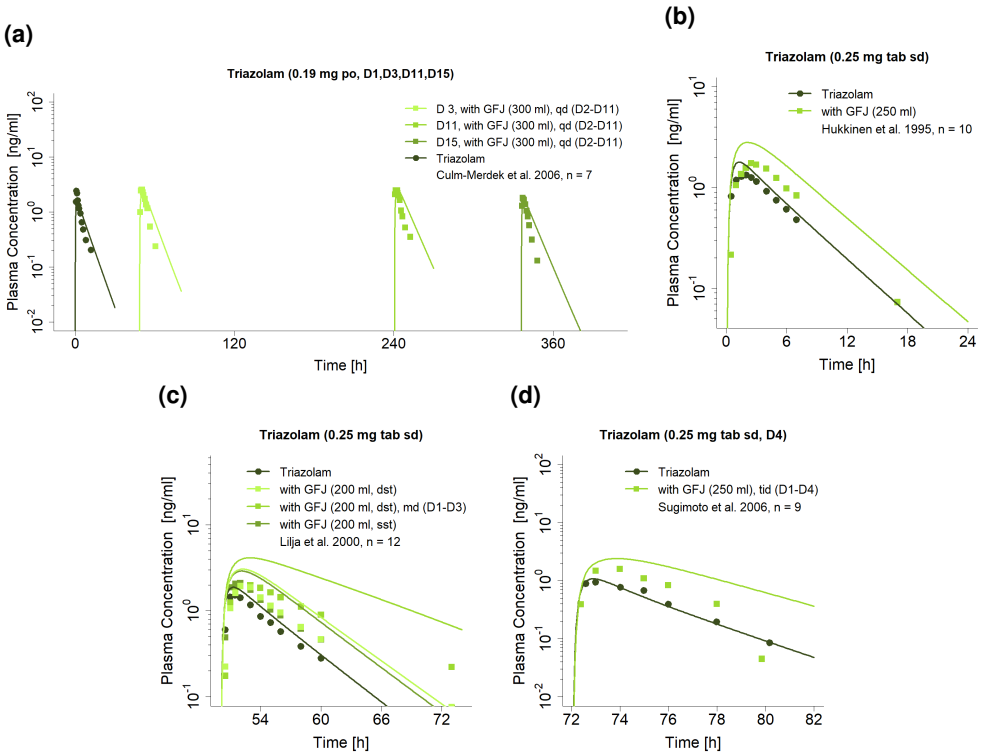

Figure S21: Predicted compared to observed triazolam plasma concentration-time profiles (semi-logarithmic) with and without grapefruit juice co-administration. Observed data are shown as dots; model predictions are shown as solid lines. Details on dosing regimens, study population and literature reference are listed in Table S24. D: day, dst: double strength, GFJ: grapefruit juice, md: multiple dose, n: number of participants, po: oral, sd: single dose, sst: single strength, tab: tablet, tid: three times daily

3.6.6 GFJDI AUC_{last} and C_{max} ratio goodness-of-fit plots

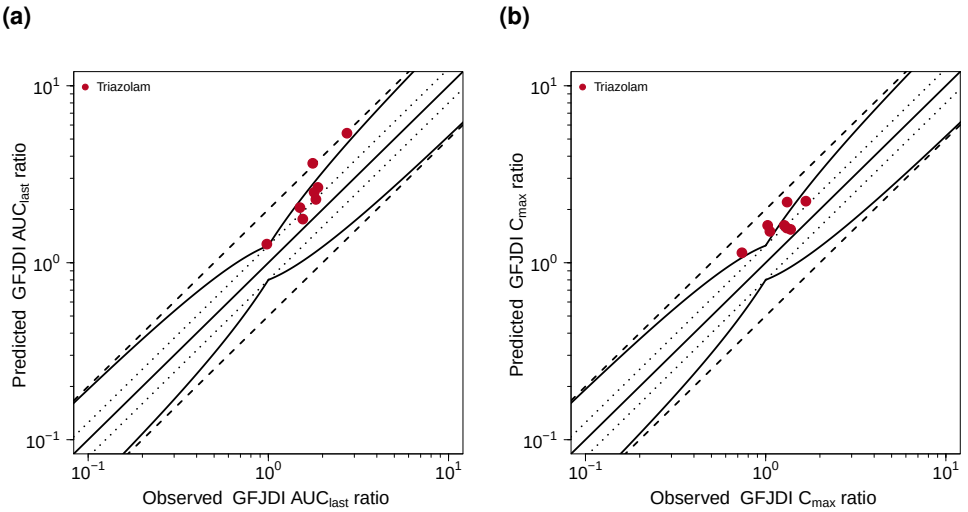

Figure S22: Predicted compared to observed GFJDI AUC_{last} and GFJDI C_{max} values. The straight solid line marks the line of identity, the curved solid lines show the prediction success limits proposed by Guest allowing for 1.25-fold variability of the GFJDI ratio [54]. Dotted lines indicate 1.25-fold, dashed lines indicate 2-fold deviation. AUC_{last}: area under the plasma concentration-time curve from the time of drug administration to the last concentration measurement, C_{max}: maximum plasma concentration, GFJDI: grapefruit juice-drug interaction

3.6.7 Geometric mean fold error of predicted GFJDI AUC_{last} and C_{max} ratios

Table S26: Predicted and observed Triazolam GFJDI AUC_{last} ratios and GFJDI C_{max} ratios.

ID			GFJDI AUC_{last} ratio			GFJDI C_{max} ratio			
	Compound	**n**	**Pred**	**Obs**	**Pred/Obs**	**Pred**	**Obs**	**Pred/Obs**	**Reference**
5.1.07	Triazolam	7	2.05	1.50	1.37	1.63	1.03	1.59	Culm-Merdek et al. 2006 [98]
5.1.08	Triazolam	7	1.27	0.98	1.30	1.14	0.74	1.54	Culm-Merdek et al. 2006 [98]
5.1.01	Triazolam	7	1.76	1.55	1.14	1.50	1.06	1.43	Culm-Merdek et al. 2006 [98]
5.1.02	Triazolam	10	2.66	1.88	1.41	1.57	1.31	1.20	Hukkinen et al. 1995 [99]
5.1.05	Triazolam	12	5.40	2.73	1.98	2.20	1.32	1.67	Lilja et al. 2000 [100]
5.1.03	Triazolam	12	2.28	1.84	1.24	1.54	1.38	1.12	Lilja et al. 2000 [100]
5.1.04	Triazolam	12	2.50	1.80	1.39	1.63	1.27	1.28	Lilja et al. 2000 [100]
5.1.06	Triazolam	9	3.65	1.76	2.07	2.23	1.67	1.33	Sugimoto et al. 2006 [101]
GMFE					**1.49 (1.14-2.07)**		**1.4 (1.12-1.67)**		
					7/8 with GMFE < 2		**8/8 with GMFE < 2**		

AUC_{last}: area under the plasma concentration-time curve from the time of drug administration to the last concentration measurement, C_{max}: maximum plasma concentration, GFJDI: grapefruit juice-drug interaction, GMFE: geometric mean fold error, n: number of individuals, obs: observed, pred: predicted

3.7 Grapefruit-itraconazole GFJDI

The itraconazole GFJDI was modeled using a previously developed and evaluated whole-body PBPK model of itraconazole et al. [55]. Drug-dependent parameters of the itraconazole PBPK model are displayed in Table S27.

Details on the modeled clinical GFJDI studies are given in Table S28. Predicted itraconazole and hydroxyitraconazole plasma concentration-time profiles with and without grapefruit juice coadministration, compared to observed data, are shown in Figures S23 and S24 (linear) and S25 and S26 (semi-logarithmic). The correlation of predicted to observed GFJDI AUC_{last} and C_{max} ratios is shown in Figure S27. Tables S30 and S31 list the corresponding predicted and observed GFJDI AUC_{last} ratios, GFJDI C_{max} ratios as well as GMFE values of itraconazole and hydroxyitraconazole, respectively.

3.7.1 Itraconazole drug-dependent parameters

Table S27: Drug-dependent parameters of the itraconazole parent-metabolite PBPK model according to [102]

Parameter	Unit	Model	Literature	Reference	Description
Itraconazole					
MW	g/mol	705.633	705.633		Molecular weight
pKa (basic)		3.7	3.7	[103]	Acid dissociation constant
Solubility - solution fed	mg/l	1.58 (opt)	-	-	Solubility
Solubility - caps fed	mg/l	0.70 (opt)	-	-	Solubility
logP		4.62	5.66	[103]	Lipophilicity
$f_{u,plasma}$	%	0.6	0.2, 1.6, 3.6	[103–106]	Fraction unbound in plasma
CYP3A4 K_m	nmol/l	2.07	3.9	[107]	CYP3A4 Michaelis-Menten constant
CYP3A4 k_{cat}	1/min	0.04	-	-	CYP3A4 catalytic rate constant
GFR fraction		1	-	-	Fraction of filtered drug in the urine
K_i CYP3A4	nmol/l	1.3	1.3	[107]	Concentration for half-maximal inhibition
s (caps, fed)		0.82 (opt)	-	-	Dissolution profile shape
$t_{50\%}$ (caps, fed)	min	139 (opt)	-	-	Dissolution time (50% dissolved)
Cell permeabilities		calculated	PK-Sim Standard	[40]	Permeability into the cellular space
Partition coefficients		calculated	Rodgers and Rowland	[26, 27]	Cell to plasma partition coefficients
Intestinal permeability	cm/min	5.33E-6	-		Transcellular intestinal permeability
Hydroxyitraconazole					
MW	g/mol	721.633			Molecular weight
pKa		3.7 (basic)	assumed		Acid dissociation constant
Solubility [pH]	mg/l	-	-	-	Solubility
logP		3.72	4.5	[108]	Lipophilicity
$f_{u,plasma}$	%	1.7	1.7	[105]	Fraction unbound in plasma
CYP3A4 K_m	nmol/l	4.17	27	[107]	CYP3A4 Michaelis-Menten constant
CYP3A4 k_{cat}	1/min	0.02	-	-	CYP3A4 catalytic rate constant
GFR fraction		1	-	-	Fraction of filtered drug in the urine
K_i CYP3A4	nmol/l	14.4	14.4	[107]	Concentration for half-maximal inhibition
Cell permeabilities		calculated	PK-Sim Standard	[40]	Permeability into the cellular space
Partition coefficients		calculated	Rodgers and Rowland	[26, 27]	Cell to plasma partition coefficients
Intestinal permeability	cm/min	1.52E-5	calculated		Transcellular intestinal permeability

caps: capsule, CYP3A4: cytochrome P450 3A4, GFR: glomerular filtration rate, lit: literature, opt: optimized during parameter identification

Table S27: Drug-dependent parameters of the itraconazole parent-metabolite PBPK model according to [102] *(continued)*

Parameter	Unit	Model	Literature	Reference	Description
Keto-itraconazole					
MW	g/mol	719.617	-	-	Molecular weight
pKa		3.7 (basic)	assumed	-	Acid dissociation constant
logP		4.21	4.5	[109]	Lipophilicity
$f_{u,plasma}$	%	1	1	[105]	Fraction unbound in plasma
CYP3A4 K_m	nmol/l	2.22	1.4	[107]	CYP3A4 Michaelis-Menten constant
CYP3A4 k_{cat}	1/min	0.393	-	-	CYP3A4 catalytic rate constant
GFR fraction		1	-	-	Fraction of filtered drug in the urine
K_i CYP3A4	nmol/l	5.12[a]	5.12 [a]	[107]	Concentration for half-maximal inhibition
Cell permeabilities		calculated	PK-Sim Standard	[40]	Permeability into the cellular space
Partition coefficients		calculated	Rodgers and Rowland	[26, 27]	Cell to plasma partition coefficients
Intestinal permeability	cm/min	4.79E-5	calculated	-	Transcellular intestinal permeability
N-desalkyl-itraconazole					
MW	g/mol	649.527	-	-	Molecular weight
pKa		3.7 (base)	assumed	-	Acid dissociation constant
logP		5.18	4.2	[110]	Lipophilicity
$f_{u,plasma}$	%	1.1	1.1	[105]	Fraction unbound in plasma
CYP3A4 K_m	nmol/l	0.63	-	-	CYP3A4 Michaelis-Menten constant
CYP3A4 k_{cat}	1/min	0.061	-	-	CYP3A4 catalytic rate constant
GFR fraction		1	-	-	Fraction of filtered drug in the urine
K_i CYP3A4	nmol/l	0.32[a]	0.32	[107]	Concentration for half-maximal inhibition
Cell permeabilities		calculated	PK-Sim Standard	[40]	Permeability into the cellular space
Partition coefficients		calculated	Rodgers and Rowland	[26, 27]	Cell to plasma partition coefficients
Intestinal permeability	cm/min	7.37E-4	calculated		Transcellular intestinal permeability

caps: capsule, CYP3A4: cytochrome P450 3A4, GFR: glomerular filtration rate, lit: literature, opt: optimized during parameter identification

3.7.2 Clinical grapefruit-itraconazole interaction studies

Table S28: Clinical studies investigating the grapefruit-itraconazole interaction

	Itraconazole		Grapefruit juice								
ID	Dose [mg]	Route	Volume [ml]	Route	BGT [µmol/l]	DHB [µmol/l]	n	Female [%]	Age[a] [years]	Weight[a] [kg]	Reference
6.1.02	200	D3: po (sol, fed), sd	240 (s)	D1-D2: tid, D3: 0h, 2h	-	-	20	50	25.9 (22-39) ± 4.5	74.7 (51.3 - 105.2) ± 18.5	Gubbins et al. 2004 [111]
6.1.01	2x100	po (caps, fed), sd	240 (d)	0h, 2h	-	-	11	50	28 (23-38) ± 4.9	-	Penzak et al. 1999 [112]

[a]: mean (range) ± standard deviation

-: not given, BGT: bergamottin, caps: capsule, d: double-strength, D: day, DHB: dihydroxybergamottin, po: oral, s: single-strength, sd: single dose, sol: solution, tid: three times daily

3.7.3 Bergamottin and 6,7-dihydroxybergamottin doses

Juice preparation	BGT [mg]	DHB [mg]	Measured	ID	Reference
frozen concentrate (double), 240 ml	3.04	4.48	no	6.1.01	Penzak et al. 1999 [112]
frozen concentrate, 240 ml	1.52	2.24	no	6.1.02	Gubbins et al. 2004 [111]

italic: preparation assumed; BGT: bergamottin, DHB: 6,7-dihydroxybergamottin

3.7.4 Linear plasma concentration-time profiles

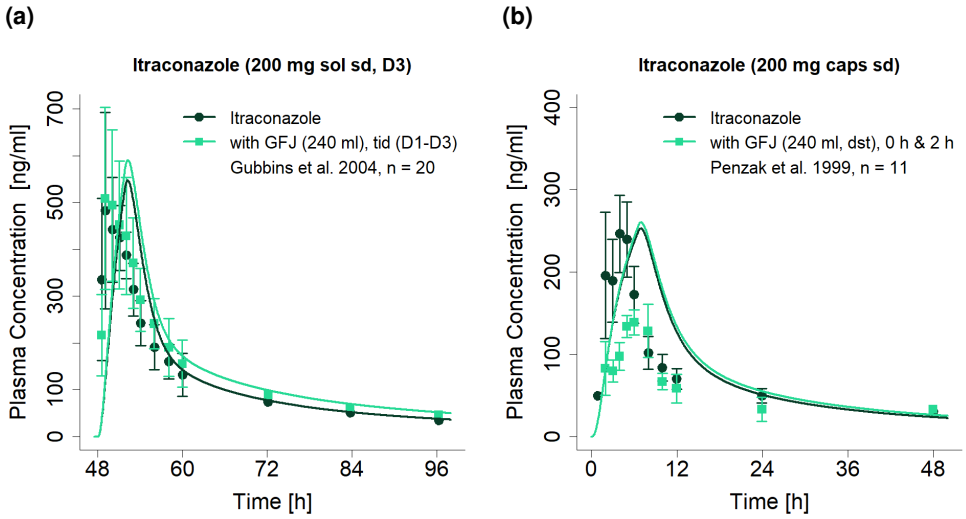

Figure S23: Predicted compared to observed itraconazole plasma concentration-time profiles (linear) with and without grapefruit juice co-administration. Observed data are shown as dots ± standard deviation (if available); model predictions are shown as solid lines. Details on dosing regimens, study population and literature reference are listed in Table S28. caps: capsule, D: day, dst: double strength, GFJ: grapefruit juice, n: number of participants, sol: solution, sd: single dose, tid: three times daily

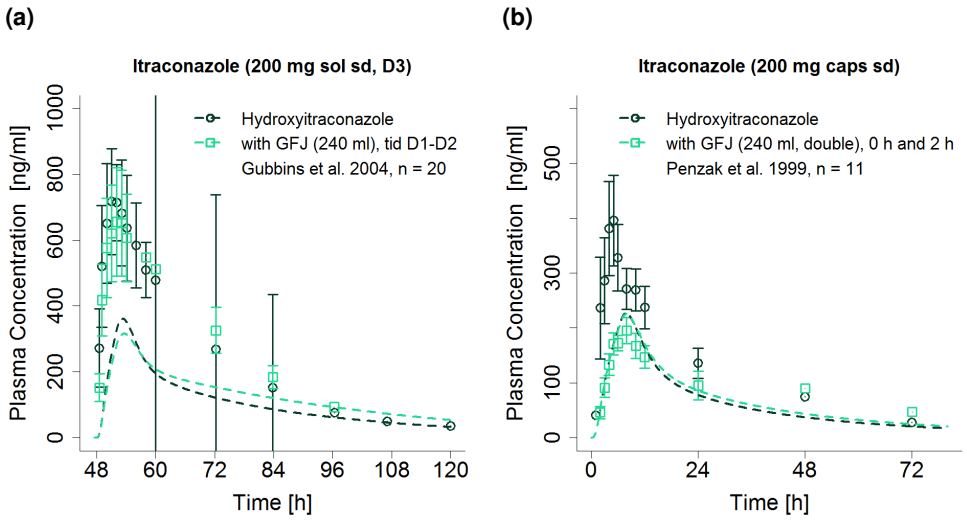

Figure S24: Predicted compared to observed hydroxyitraconazole plasma concentration-time profiles (linear) with and without grapefruit juice co-administration. Observed data are shown as dots ± standard deviation (if available); model predictions are shown as solid lines. Details on dosing regimens, study population and literature reference are listed in Table S28. caps: capsule, D: day, dst: double-strength, GFJ: grapefruit juice, n: number of participants, sol: solution, sd: single dose, tid: three times daily

3.7.5 Semi-logarithmic plasma concentration-time profiles

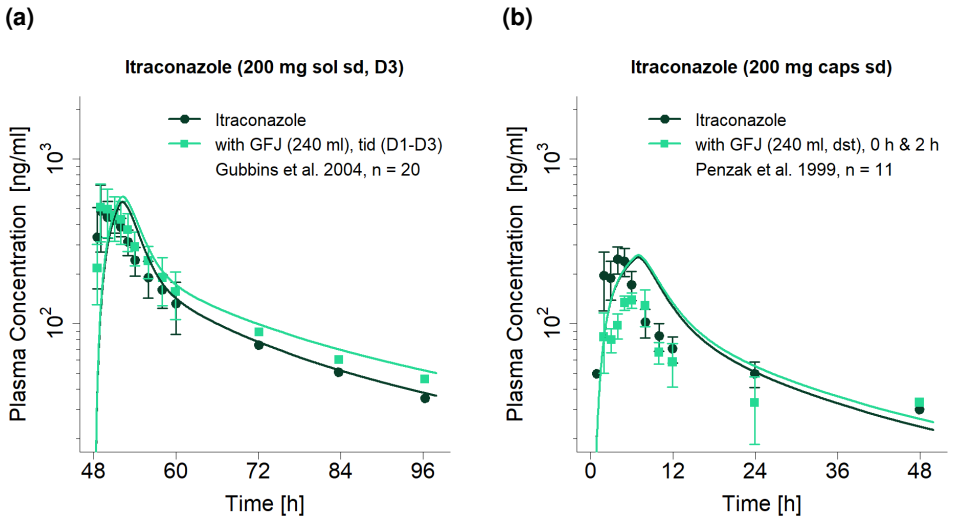

Figure S25: Predicted compared to observed itraconazole plasma concentration-time profiles (semi-logarithmic) with and without grapefruit juice co-administration. Observed data are shown as dots ± standard deviation (if available); model predictions are shown as solid lines. Details on dosing regimens, study population and literature reference are listed in Table S28. caps: capsule, D: day, dst: double strength, GFJ: grapefruit juice, n: number of participants, sol: solution, sd: single dose, tid: three times daily

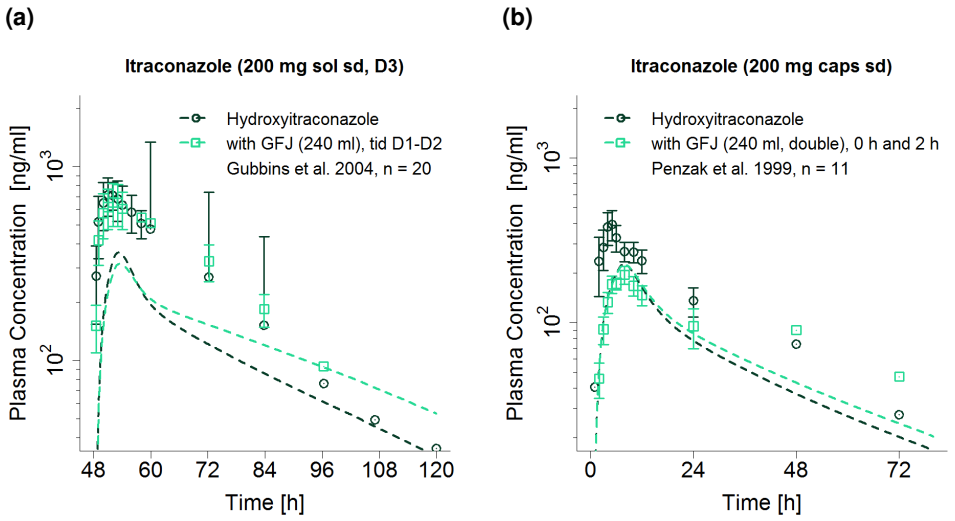

Figure S26: Predicted compared to observed hydroxyitraconazole plasma concentration-time profiles (semi-logarithmic) with and without grapefruit juice co-administration. Observed data are shown as dots ± standard deviation (if available); model predictions are shown as solid lines. Details on dosing regimens, study population and literature reference are listed in Table S28. caps: capsule, D: day, dst: double strength, GFJ: grapefruit juice, n: number of participants, sol: solution, sd: single dose, tid: three times daily

3.7.6 GFJDI AUC_{last} and C_{max} ratio goodness-of-fit plots

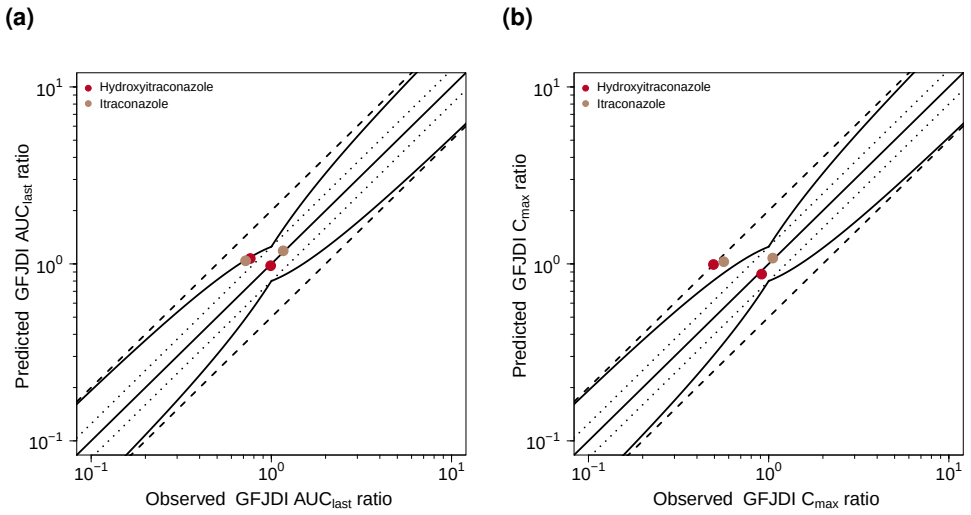

Figure S27: Predicted compared to observed GFJDI AUC_{last} and GFJDI C_{max} values. The straight solid line marks the line of identity, the curved solid lines show the prediction success limits proposed by Guest allowing for 1.25-fold variability of the GFJDI ratio [54]. Dotted lines indicate 1.25-fold, dashed lines indicate 2-fold deviation. AUC_{last}: area under the plasma concentration-time curve from the time of drug administration to the last concentration measurement, C_{max}: maximum plasma concentration, GFJDI: grapefruit juice-drug interaction

3.7.7 Geometric mean fold error of predicted GFJDI AUC_{last} and C_{max} ratios

Table S30: Predicted and observed Itraconazole GFJDI AUC_{last} ratios and GFJDI C_{max} ratios.

ID			GFJDI AUC_{last} ratio			GFJDI C_{max} ratio			
	Compound	**n**	**Pred**	**Obs**	**Pred/Obs**	**Pred**	**Obs**	**Pred/Obs**	**Reference**
6.1.02	Itraconazole	20	1.19	1.16	1.02	1.08	1.05	1.02	Gubbins et al. 2004 [111]
6.1.01	Itraconazole	11	1.04	0.72	1.45	1.03	0.56	1.83	Penzak et al. 1999 [112]
GMFE					**1.23 (1.02-1.45)**		**1.43 (1.02-1.83)**		
					2/2 with GMFE < 2		**2/2 with GMFE < 2**		

AUC_{last}: area under the plasma concentration-time curve from the time of drug administration to the last concentration measurement, C_{max}: maximum plasma concentration, GFJDI: grapefruit juice-drug interaction, GMFE: geometric mean fold error, n: number of individuals, obs: observed, pred: predicted

Table S31: Predicted and observed Hydroxyitraconazole GFJDI AUC_{last} ratios and GFJDI C_{max} ratios.

ID			GFJDI AUC_{last} ratio			GFJDI C_{max} ratio			
	Compound	**n**	**Pred**	**Obs**	**Pred/Obs**	**Pred**	**Obs**	**Pred/Obs**	**Reference**
6.1.02	Hydroxyitraconazole	20	0.98	0.99	0.99	0.88	0.91	0.96	Gubbins et al. 2004 [111]
6.1.01	Hydroxyitraconazole	11	1.07	0.76	1.40	0.99	0.49	2.01	Penzak et al. 1999 [112]
GMFE					**1.21 (1.01-1.4)**		**1.53 (1.04-2.01)**		
					2/2 with GMFE < 2		**1/2 with GMFE < 2**		

AUC_{last}: area under the plasma concentration-time curve from the time of drug administration to the last concentration measurement, C_{max}: maximum plasma concentration, GFJDI: grapefruit juice-drug interaction, GMFE: geometric mean fold error, n: number of individuals, obs: observed, pred: predicted

3.8 Grapefruit-erythromycin GFJDI

The erythromycin GFJDI was modeled using a previously developed and evaluated whole-body PBPK model of erythromycin, available in the Open Systems Pharmacology (OSP) GitHub model repository et al. [113]. Drug-dependent parameters of the erythromycin PBPK model are displayed in Table S32.

Details on the modeled clinical GFJDI studies are given in Table S33. Predicted erythromycinplasma concentration-time profiles with and without grapefruit juice coadministration, compared to observed data, are shown in Figures S28 (linear) and S29 (semi-logarithmic). The correlation of predicted to observed GFJDI AUC_{last} and C_{max} ratios is shown in Figure S30. Table S35 lists the corresponding predicted and observed GFJDI AUC_{last} ratios, GFJDI C_{max} ratios as well as GMFE values.

3.8.1 Erythromycin drug-dependent parameters

Table S32: Drug-dependent parameters of the erythromycin PBPK model (adopted from [113])

Parameter	Unit	Model	Literature	Reference	Description
MW	g/mol	733.9 (lit)	733.9	[114]	Molecular weight
logP	Log Units	2.82 (asm)	2.82 (2.48-3.06)[a]	[115–117]	Lipophilicity
Solubility (pH)	mg/ml	200.0 (7.0) (lactobionate) (opt), 0.028 (7.0) (stearate) (opt), 0.50 (7.0) (base pellets) (opt), 0.0084 (7.0) (base tablet) (opt)	200.0 (7.0) (lactobionate), 0.182 (7.0) (stearate), 2.10 (7.0) (base)	[118] [119] [120]	Solubility
$f_{u,plasma}$	%	30.5 (lit)	27.0, 28.0, 30.5, 32.6	[121–124]	Fraction unbound in plasma
pKa (base)	-	8.88 (lit)	8.88	[117]	Acid dissociation constant
K_m (CYP3A4)	µmol/l	70.0 (lit)	70 (44.0-88.0)[a]	[125, 126]	CYP3A4 Michaelis-Menten constant
k_{cat} (CYP3A4)	1/min	8.50 (opt)	-	-	CYP3A4 catalytic rate constant
K_m (OATP1B1)	µmol/l	0.74 (opt)	13.2	[127]	OATP1B1 Michaelis-Menten constant
k_{cat} (OATP1B1)	1/min	2.02 (opt)	-	-	OATP1B1 transport rate constant
CL_{hep}	1/min	4.15 (opt)	-	-	Hepatic plasma clearance
GFR fraction	-	1.16 (opt)	-	-	Fraction of filtered drug in the urine
K_i (CYP3A4)	µmol/l	7.60 (opt)	18.4 (0.76-109.0)[b]	[124, 128–138]	Concentration for half-maximal inactivation
k_{inact} (CYP3A4)	1/min	0.03 (opt)	0.06 (0.01-0.30)[b]	[124, 128–138]	Maximum inactivation rate constant
Intestinal permeability	cm/min	3.87E-04 (opt)	-	-	Transcellular intestinal permeability
Partition coefficients	-	Diverse	Rogers and Rowland	[26, 27]	Cell to plasma partition coefficients
Cellular permeability	cm/min	1.22E-4 (calc)	Charge-dependent Schmitt	[1]	Permeability into the cellular space
Coated pellets Weibull time	min	1.75 (opt)	-	-	Dissolution time (50% dissolved)
Coated pellets Weibull lag time	min	54.35 (opt)	-	-	Dissolution lag time
Coated pellets Weibull shape	-	1.06 (opt)	-	-	Dissolution profile shape
Coated tablet Weibull time	min	79.63 (opt)	-	-	Dissolution time (50% dissolved)
Coated tablet Weibull lag time	min	78.79 (opt)	-	-	Dissolution lag time

Coated tablet Weibull shape	-	1.08 (opt)	-	-	Dissolution profile shape
Film tablet Weibull time	min	1.70 (opt)	-	-	Dissolution time (50% dissolved)
Film tablet Weibull shape	-	1.10 (opt)	-	-	Dissolution profile shape

-: not given, asm: assumed, calc: calculated, CYP3A4: cytochrome P450 3A4, GFR: glomerular filtration rate, lit: literature, OATP1B1: organic anion transporting polypeptide 1B1, opt: optimized during parameter identification

[a] mean (range)

3.8.2 Clinical grapefruit-erythromycin interaction studies

Table S33: Clinical studies investigating the grapefruit-erythromycin interaction

	Erythromycin		Grapefruit juice								
ID	**Dose [mg]**	**Route**	**Volume [ml]**	**Route**	**BGT [µmol/l]**	**DHB [µmol/l]**	**n**	**Female [%]**	**Age[a] [years]**	**Weight[a] [kg]**	**Reference**
7.1.01	400	po (ECtab), sd	300 (d)	-0.5h	-	-	6	0	33.5 ± 9.7	62.3 ± 5.2	Kanazawa et al. 2001 [139]

[a]: mean (range) ± standard deviation

-: not given, d: double-strength, ECtab: enteric coated tablet, po: oral, sd: single dose

3.8.3 Bergamottin and 6,7-dihydroxybergamottin doses

Juice preparation	BGT [mg]	DHB [mg]	Measured	ID	Reference
frozen concentrate (double), 300 ml	3.8	5.6	no	7.1.01	Kanazawa et al. 2001 [139]

italic: preparation assumed; BGT: bergamottin, DHB: 6,7-dihydroxybergamottin

3.8.4 Linear plasma concentration-time profiles

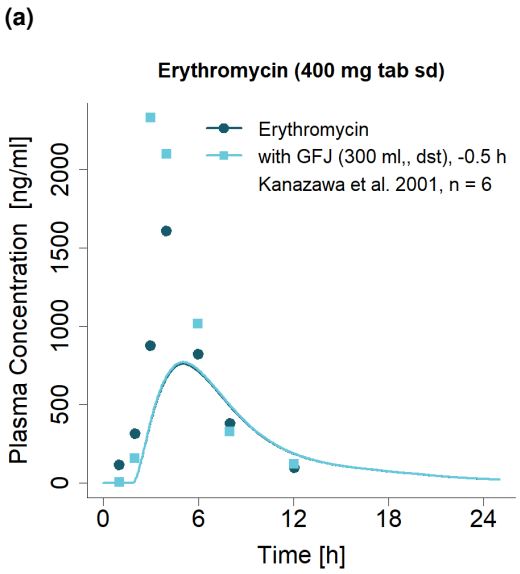

Figure S28: Predicted compared to observed erythromycin plasma concentration-time profiles (linear) with and without grapefruit juice co-administration. Observed data are shown as dots; model predictions are shown as solid lines. Details on dosing regimens, study population and literature reference are listed in Table S33. dst: double strength, GFJ: grapefruit juice, n: number of participants, sd: single dose, tab: tablet

3.8.5 Semi-logarithmic plasma concentration-time profiles

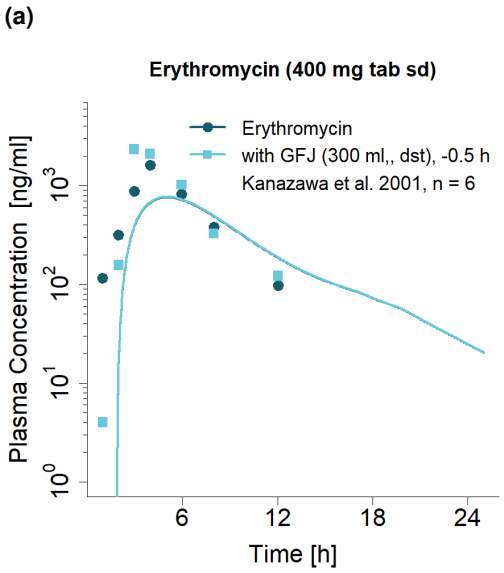

Figure S29: Predicted compared to observed erythromycin plasma concentration-time profiles (semi-logarithmic) with and without grapefruit juice co-administration. Observed data are shown as dots; model predictions are shown as solid lines. Details on dosing regimens, study population and literature reference are listed in Table S33. dst: double strength, GFJ: grapefruit juice, n: number of participants, sd: single dose, tab: tablet

3.8.6 GFJDI AUC_{last} and C_{max} ratio goodness-of-fit plots

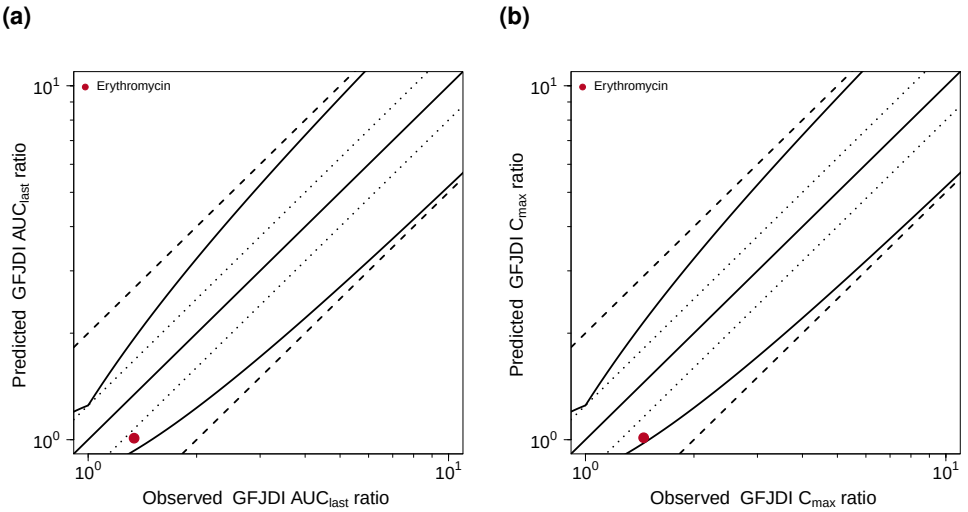

Figure S30: Predicted compared to observed GFJDI AUC_{last} and GFJDI C_{max} values. The straight solid line marks the line of identity, the curved solid lines show the prediction success limits proposed by Guest allowing for 1.25-fold variability of the GFJDI ratio [54]. Dotted lines indicate 1.25-fold, dashed lines indicate 2-fold deviation. AUC_{last}: area under the plasma concentration-time curve from the time of drug administration to the last concentration measurement, C_{max}: maximum plasma concentration, GFJDI: grapefruit juice-drug interaction

3.8.7 Geometric mean fold error of predicted GFJDI AUC_{last} and C_{max} ratios

Table S35: Predicted and observed Erythromycin GFJDI AUC_{last} ratios and GFJDI C_{max} ratios.

ID			GFJDI AUC_{last} ratio			GFJDI C_{max} ratio			
	Compound	**n**	**Pred**	**Obs**	**Pred/Obs**	**Pred**	**Obs**	**Pred/Obs**	**Reference**
7.1.01	Erythromycin	6	1.01	1.34	0.75	1.01	1.45	0.70	Kanazawa et al. 2001 [139]
GMFE					**1.33**		**1.43**		
					1/1 with GMFE < 2		**1/1 with GMFE < 2**		

AUC_{last}: area under the plasma concentration-time curve from the time of drug administration to the last concentration measurement, C_{max}: maximum plasma concentration, GFJDI: grapefruit juice-drug interaction, GMFE: geometric mean fold error, n: number of individuals, obs: observed, pred: predicted

3.9 Grapefruit-carbamazepine GDI

The carbamazepine GDI was modeled using a previously developed and evaluated whole-body PBPK model of carbamazepine, available in the Open Systems Pharmacology (OSP) GitHub model repository. Drug-dependent parameters of the carbamazepine PBPK model are displayed in Table S36.

Details on the modeled clinical GDI study are given in Table S37. Predicted carbamazepine plasma concentration-time profiles with and without grapefruit juice coadministration, compared to observed data, are shown in Figures S31 (linear) and S32 (semi-logarithmic). The correlation of predicted to observed GDI AUC_{last} and C_{max} ratios is shown in Figure S33. Table S39 lists the corresponding predicted and observed GDI AUC_{last} ratios, GDI C_{max} ratios as well as GMFE values.

3.9.1 Carbamazepine drug-dependent parameters

Table S36: Drug-dependent parameters of the carbamazepine and carbamazepine-10,11-epoxide PBPK model according to [140]

Parameter	Unit	Model	Literature	Reference	Description
Carbamazepine					
MW	g/mol	236.27 (Lit)	236.27	[143]	Molecular weight
logP	Log Units	2.00 (Fit)	1.45, 2.10, 2.45, 2.77	[143–145]	Lipophilicity
Solubility (pH)	mg/ml	0.336 (6.2) (Lit)	0.170 (6.2), 0.283 (7.0), 0.306 (6.9), 0.336 (6.2)	[146–149]	Solubility FaHIF
fu	%	25.0 (Lit)	21.0, 24.0, 25.0	[150–153]	Fraction unbound in plasma
K_m (CYP3A4) CBZE	µmol/l	248.0 (Lit)	119.0, 248.0, 442.0, 630.0	[154–157]	CYP3A4 Michaelis-Menten constant
k_{cat} (CYP3A4) CBZE	1/min	0.75 (Fit)	1.17, 1.70, 4.87, 5.30[b]	[154–157]	CYP3A4 catalytic rate constant
K_m (CYP2C8)	µmol/l	757.0 (Lit)	757.0	[156]	CYP2C8 Michaelis-Menten constant
k_{cat} (CYP2C8)	1/min	0.67 (Lit)	0.67[b]	[156]	CYP2C8 catalytic rate constant
K_m (CYP2B6)	µmol/l	420.0 (Lit)	420.0	[158]	CYP2B6 Michaelis-Menten constant
k_{cat} (CYP2B6)	1/min	0.43 (Lit)	0.43[b]	[158]	CYP2B6 catalytic rate constant
K_m (CYP3A4)	µmol/l	282.0 (Lit)	282.0	[158]	CYP3A4 Michaelis-Menten constant
k_{cat} (CYP3A4)	1/min	0.20 (Fit)	0.16[b]	[158]	CYP3A4 catalytic rate constant
K_m (UGT2B7)	µmol/l	214.0 (Lit)	214.0	[141]	UGT2B7 Michaelis-Menten constant
k_{cat} (UGT2B7)	1/min	9.53E-3 (Lit)	9.53E-3[c]	[141]	UGT2B7 catalytic rate constant
CL_{hep}	1/min	0.02 (Fit)	-	-	Unspecified hepatic clearance
GFR fraction	-	0.03 (Fit)	-	-	Fraction of filtered drug in the urine
EC_{50} (CYP3A4)	µmol/l	20.00[a] (Lit)	4.3 - 137	[159–166]	Concentration for half-maximal induction
E_{max} (CYP3A4)	-	6.00 (Fit)	1.90 - 23.0	[159–166]	CYP3A4 maximum induction effect
EC_{50} (CYP2B6)	µmol/l	20.0[a] (Asm)	22 - 145	[166–168]	Concentration for half-maximal induction
E_{max} (CYP2B6)	-	17.0 (Fit)	3.10 - 21.50	[166–168]	CYP2B6 maximum induction effect
EC_{50} (EPHX1)	µmol/l	20.0[a] (Asm)	-	-	Concentration for half-maximal induction
E_{max} (EPHX1)	-	3.25 (Fit)	-	-	EPHX1 maximum induction effect
Intestinal permeability	cm/min	2.58E-2 (Lit)	2.58E-2	[169]	Transcellular intestinal permeability
Partition coefficients	-	Diverse	Rodgers and Rowlands	[26, 27]	Cell to plasma partition coefficients

asm: assumption, calc: calculated, CBZE: carbamazepine-10,11-epoxide, CL_{hep}: hepatic clearance, CL_{spec}: specific clearance, CYP: cytochrome P450, EPHX1: epoxide hydroxylase 1, FaHIF: fasted human intestinal fluid, IR: immediate release, fit: optimized during parameter optimization, lit: literature, UGT: UDP-glucuronosyltransferase, XR: extended release

[a] mean of literature values for EC_{50} (CYP3A4), assumed for all EC_{50} values

[b] k_{cat} values calculated within PK-Sim from V_{max}/recombinant enzyme

[c] k_{cat} value calculated within PK-Sim from V_{max} = 0.79 pmol/min/microsomal protein [141], assuming a microsomal UGT2B7 content of 82.9 pmol/mg microsomal protein [142], kcat = Vmax/ UGT2B7 content microsomes

Table S36: Drug-dependent parameters of the carbamazepine and carbamazepine-10,11-epoxide PBPK model according to [140] *(continued)*

Parameter	Unit	Model	Literature	Reference	Description
Cellular permeability	cm/min	0.02 (Calc)	PK-Sim Standard	[40]	Permeability into the cellular space
IR tablet (fasted) Weibull time	min	200.0	-	-	Dissolution time (50% dissolved)
IR tablet (fasted) Weibull shape	-	0.74	-	-	Dissolution profile shape
Carbamazepine-10,11-epoxide					
logP	Log Units	1.00 (Fit)	1.58, 1.97	[170]	Lipophilicity
Solubility	mg/ml	1.34 (Lit)	1.34	[170]	Solubility
fu	%	51.8 (Lit)	46.8-51.8	[171]	Fraction unbound in plasma
CL_{spec} (EPHX1)	1/min	0.01 (Fit)	0.05	-	EPHX1 first-order clearance
GFR fraction	-	0.21 (Fit)	-	-	Fraction of filtered drug in the urine
Intestinal permeability	cm/min	0.3 (Fit)	-	-	Transcellular intestinal permeability
Partition coefficients	-	Diverse	Rodgers and Rowlands	[26, 27]	Cell to plasma partition coefficients
Cellular permeability	cm/min	1.61E-3 (Calc)	PK-Sim Standard	[40]	Permeability into the cellular space

asm: assumption, calc: calculated, CBZE: carbamazepine-10,11-epoxide, CL_{hep}: hepatic clearance, CL_{spec}: specific clearance, CYP: cytochrome P450, EPHX1: epoxide hydroxylase 1, FaHIF: fasted human intestinal fluid, IR: immediate release, fit: optimized during parameter optimization, lit: literature, UGT: UDP-glucuronosyltransferase, XR: extended release

[a] mean of literature values for EC_{50} (CYP3A4), assumed for all EC_{50} values

[b] k_{cat} values calculated within PK-Sim from V_{max}/recombinant enzyme

[c] k_{cat} value calculated within PK-Sim from V_{max} = 0.79 pmol/min/microsomal protein [141], assuming a microsomal UGT2B7 content of 82.9 pmol/mg microsomal protein [142], kcat = Vmax/ UGT2B7 content microsomes

3.9.2 Clinical grapefruit-carbamazepine interaction studies

Table S37: Clinical studies investigating the grapefruit-carbamazepine interaction

	Victim drug		Grapefruit juice								
ID	Dose [mg]	Route	Volume [ml]	Route	BGT [µmol/l]	DHB [µmol/l]	n	Females [%]	Age [years]	Weight [kg]	Reference
10.1.01	200	po (tab), tid	300	0h	-	-	10	30	28 (19-51) ± 10	59 (52-78) ± 9	Garg et al. 1998 [172]

[a] mean (range) ± standard deviation

-: not given, po: oral, tab: tablet, tid: three times daily

3.9.3 Bergamottin and 6,7-dihydroxybergamottin doses

Juice preparation	BGT [mg]	DHB [mg]	Measured in study	ID	Reference
hand-squeezed, 300 ml	2.22	7.60	no	10.1.01	Garg et al 1998 [172]

italic: preparation assumed; BGT: bergamottin, DHB: 6,7-dihydroxybergamottin

3.9.4 Linear plasma concentration-time profiles

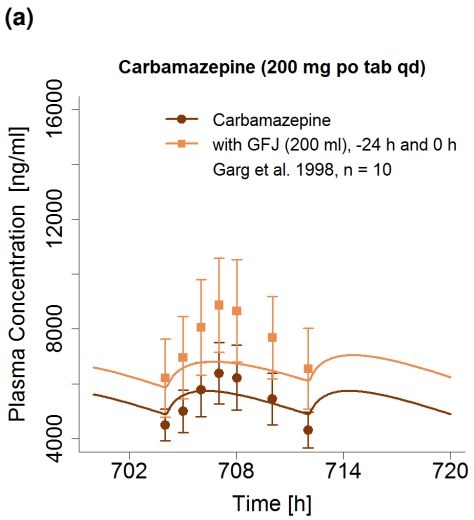

Figure S31: Predicted compared to observed carbamazepine plasma concentration-time profiles (linear) before and during grapefruit co-administration. Observed data are shown as dots; model predictions are shown as solid lines. Details on dosing regimens, study population and literature reference are listed in Table S37. GFJ: grapefruit juice, n: number of individuals, po: oral, qd: once daily, tab: tablet

3.9.5 Semi-logarithmic plasma concentration-time profiles

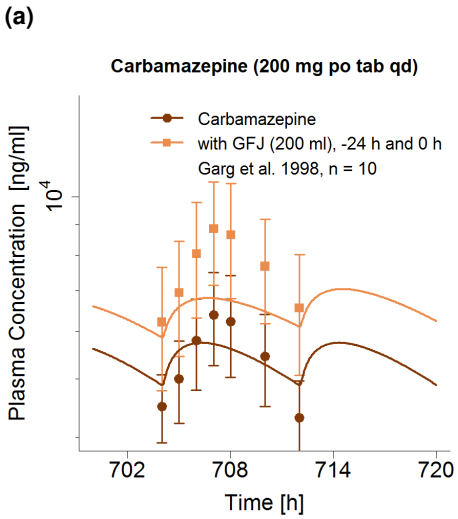

Figure S32: Predicted compared to observed carbamazepine plasma concentration-time profiles (semi-logarithmic) before and during grapefruit co-administration. Observed data are shown as dots; model predictions are shown as solid lines. Details on dosing regimens, study population and literature reference are listed in Table S37. GFJ: grapefruit juice, n: number of individuals, po: oral, qd: once daily, tab: tablet

3.9.6 DDI AUClast and Cmax ratio goodness-of-fit plots

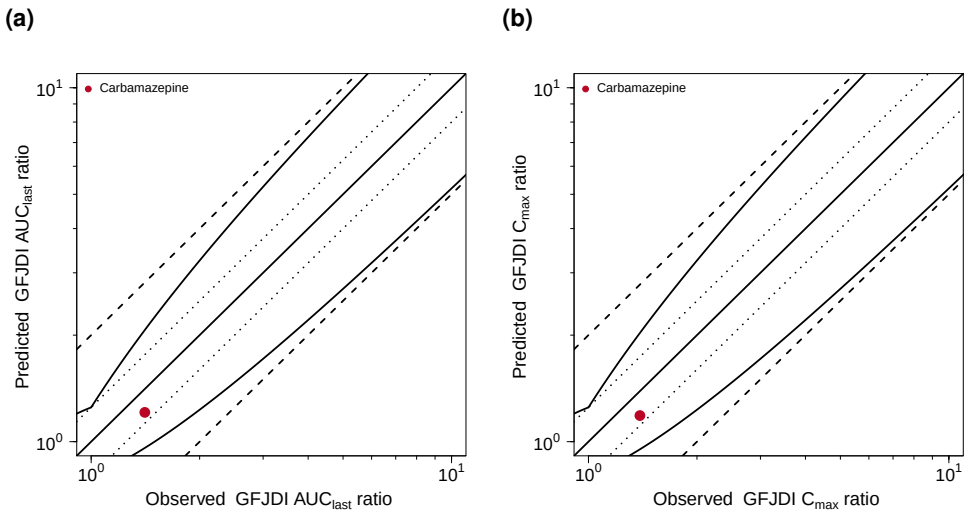

Figure S33: Predicted compared to observed GDI AUC_{last} and GDI C_{max} values. The straight solid line marks the line of identity, the curved solid lines show the prediction success limits proposed by Guest et al. allowing for 1.25-fold variability of the DDI ratio [54]. Dotted lines indicate 1.25-fold, dashed lines indicate 2-fold deviation.AUC_{last}: area under the plasma concentration-time curve from the time of drug administration to the last concentration measurement, C_{max}: maximum plasma concentration, DDI: drug-drug interaction

3.9.7 Geometric mean fold error of predicted DDI AUClast and Cmax ratios

Table S39: Predicted and observed Carbamazepine GFJDI AUC_{last} ratios and GFJDI C_{max} ratios.

ID			GFJDI AUC_{last} ratio			GFJDI C_{max} ratio			
	Compound	**n**	**Pred**	**Obs**	**Pred/Obs**	**Pred**	**Obs**	**Pred/Obs**	**Reference**
10.1.01	Carbamazepine	10	1.21	1.41	0.86	1-.19	1.39	0.85	Garg et al. 1998 [172]
GMFE					**1.16**		**1.17**		
					1/1 with GMFE < 2		**1/1 with GMFE < 2**		

AUC_{last}: area under the plasma concentration-time curve from the time of drug administration to the last concentration measurement, C_{max}: maximum plasma concentration, GFJDI: grapefruit juice-drug interaction, GMFE: geometric mean fold error, n: number of individuals, obs: observed, pred: predicted

3.10 Grapefruit-simvastatin GFJDI

The simvastatin GFJDI was modeled using a previously developed and evaluated whole-body PBPK model of simvastatin et al. [173]. Drug-dependent parameters of the simvastatin PBPK model are displayed in Table S40.

Details on the modeled clinical GFJDI studies are given in Table S41. Predicted simvastatin and simvastatin acid plasma concentration-time profiles with and without grapefruit juice coadministration, compared to observed data, are shown in Figures S34 and S35 (linear) and S36 and S37 (semi-logarithmic). The correlation of predicted to observed GFJDI AUC_{last} and C_{max} ratios is shown in Figure S38. Tables S43 and S44 list the corresponding predicted and observed GFJDI AUC_{last} ratios, GFJDI C_{max} ratios as well as GMFE values of simvastatin and simvastatin acid, respectively.

3.10.1 Simvastatin drug-dependent parameters

Table S40: Drug-dependent parameters of the simvastatin PBPK model (adopted from [173])

Parameter	Unit	Model	Literature[a]	Reference	Description
Simvastatin					
MW	g/mol	418.57 (Lit)	418.57	[174]	Molecular weight
logP	Log Units	4.68 (Lit)	4.60 (2.06-5.19)	[175, 176]	Lipophilicity
Solubility (pH)	mg/ml	0.016 (5.0) (Lit)	0.016 (1.40E-3-0.061) (5.0)	[22, 174, 175, 177–179]	Solubility
$f_{u,plasma}$	%	1.34 (Lit)	2.37 (1.09-6.00)	[175, 180, 181]	Fraction unbound in plasma
K_m (CYP3A4)	µmol/l	21.0 (Lit)	2.55 (0.46-30.0)	[106, 182, 183]	CYP3A4 Michaelis-Menten constant
k_{cat} (CYP3A4)	1/min	5194.04 (Opt)	-	-	CYP3A4 catalytic rate constant
K_m (CYP3A5)	µmol/l	39.1 (Opt)	88.0 (62.0-91.0)	[182]	CYP3A5 Michaelis-Menten constant
k_{cat} (CYP3A5)	1/min	162281.57 (Opt)	-	-	CYP3A5 catalytic rate constant
K_m (PON3)	µmol/l	840.0 (Lit)	840.0	[184]	PON3 Michaelis-Menten constant
k_{cat} (PON3)	1/min	4952.08 (Opt)	-	-	PON3 catalytic rate constant
Chemical hydrolysis rate	l/µmol/min	9.80E-4 (Lit)	8.21E-4 (1.67E-06-1.96E-2)	[174, 185, 186]	Chemical hydrolysis rate (ubiquitous)
Plasma hydrolysis rate	l/µmol/min	6.03E-2 (Lit)	6.03E-2	[187]	Plasma hydrolysis rate
K_m (BCRP)	µmol/l	5.00[b] (Asm)	(1.20-10.8)	[188–193]	BCRP Michaelis-Menten constant
k_{cat} (BCRP)	1/min	32.61 (Opt)	-	-	BCRP catalytic rate constant
GFR fraction	-	1 (Asm)	-	-	Fraction of filtered drug in the urine
K_i (CYP2C8)	µmol/l	1.10 (Lit)	5.7 (1.10-12.3)	[194]	Concentration for half-maximal inhibition
K_i (CYP3A4)	µmol/l	0.16 (Lit)	2.1 (0.16-35.0)	[182, 195–198]	Concentration for half-maximal inhibition
K_i (OATP1B1)	µmol/l	5.00 (Lit)	7.85 (5.00-12.5)	[199, 200]	Concentration for half-maximal inhibition
K_i (Pgp)	µmol/l	4.60 (Lit)	37.7 (4.60-209.0)	[201, 201–207]	Concentration for half-maximal inhibition
Intestinal permeability	cm/min	1.08E-3 (Opt)	0.258	[174]	Transcellular intestinal permeability
Partition coefficients	-	Diverse	Berezhkovskiy	[208]	Cell to plasma partition coefficients

-: not given, asm: assumption, BCRP: breast cancer resistance protein, calc: calculated, CYP: cytochrome P450, opt: optimized during parameter identification, GFR: glomerular filtration rate, lit: literature, OATP: organic anion transporting polypeptide, opt: optimized during parameter identification, Pgp: P-glycoprotein, PON3: paraoxonase 3, UGT: UDP-glucuronosyltransferase

[a] median (range)

[b] assumed from other statins

[c] calculated from V_{max}

[d] calculated from liver S9

Table S40: Drug-dependent parameters of the simvastatin PBPK model (adopted from [173]) *(continued)*

Parameter	Unit	Model	Literature[a]	Reference	Description
Cellular permeability	cm/min	0.26 (Calc)	PK-Sim Standard	[40]	Permeability into the cellular space
Tablet Weibull time	min	86.38 (Opt)	-	-	Dissolution time (50% dissolved)
Tablet Weibull shape	-	1.30 (Opt)	-	-	Dissolution profile shape
Simvastatin acid					
MW	g/mol	436.58 (Lit)	436.58	[209]	Molecular weight
logP	Log Units	1.45 (Lit)	3.82 (1.45-4.70)	[22, 174, 175, 209, 210]	Lipophilicity
Solubility (pH)	mg/ml	13.09 (6.8) (Lit)	45.1 (0.13-51.5) (6.8)	[22, 179, 209]	Solubility
$f_{u,plasma}$	%	5.68 (Lit)	6.26 (5.48-9.61)	[181]	Fraction unbound in plasma
pKa (acidic)	-	4.21 (Lit)	4.20 (4.18-5.5)	[175, 209–211]	Acid dissociation constant
K_m (CYP3A4)	µmol/l	26.0 (Lit)	26.0 (21.0-29.0)	[212]	CYP3A4 Michaelis-Menten constant
k_{cat} (CYP3A4)	1/min	31.0[c] (Lit)	-	-	CYP3A4 catalytic rate constant
K_m (CYP2C8)	µmol/l	38.6 (Lit)	38.6 (16.0-88.0)	[212, 213]	CYP2C8 Michaelis-Menten constant
k_{cat} (CYP2C8)	1/min	52.3[c] (Lit)	-	-	CYP2C8 catalytic rate constant
K_m (UGT1A1)	µmol/l	349.0 (Lit)	349.0	[214]	UGT1A1 Michaelis-Menten constant
k_{cat} (UGT1A1)	1/min	6.5[c] (Lit)	-	-	UGT1A1 catalytic rate constant
K_m (UGT1A3)	µmol/l	349.0 (Lit)	349.0	[214]	UGT1A3 Michaelis-Menten constant
k_{cat} (UGT1A3)	1/min	6.5[c] (Lit)	-	-	UGT1A3 catalytic rate constant
Liver lactonization rate	l/µmol/min	2.43E-3 (Lit)	2.43E-3[d]	[174]	Liver lactonization rate
K_m (Pgp)	µmol/l	10.0 (Asm)	-	-	Pgp Michaelis-Menten constant
k_{cat} (Pgp)	1/min	50.0 (Opt)	-	-	Pgp transport rate constant
K_m (OATP1B1)	µmol/l	2.00 (Lit)	1.99 (1.17-2.53)	[215]	OATP1B1 Michaelis-Menten constant
k_{cat} (OATP1B1)	1/min	10.25 (Opt)	-	-	OATP1B1 transport rate constant
K_m (OATP1B3)	µmol/l	2.0 (Asm)	-	-	OATP1B3 Michaelis-Menten constant
k_{cat} (OATP1B3)	1/min	2.15 (Opt)	-	-	OATP1B3 transport rate constant
GFR fraction	-	1 (Asm)	-	-	Fraction of filtered drug in the urine

-: not given, asm: assumption, BCRP: breast cancer resistance protein, calc: calculated, CYP: cytochrome P450, opt: optimized during parameter identification, GFR: glomerular filtration rate, lit: literature, OATP: organic anion transporting polypeptide, opt: optimized during parameter identification, Pgp: P-glycoprotein, PON3: paraoxonase 3, UGT: UDP-glucuronosyltransferase

[a] median (range)

[b] assumed from other statins

[c] calculated from V_{max}

[d] calculated from liver S9

Table S40: Drug-dependent parameters of the simvastatin PBPK model (adopted from [173]) *(continued)*

Parameter	Unit	Model	Literature[a]	Reference	Description
K_i (CYP2C8)	µmol/l	41.1 (Lit)	41.1	[213]	Concentration for half-maximal inhibition
K_i (CYP3A4)	µmol/l	69.6 (Lit)	56.1 (42.6-69.6)	[197, 216]	Concentration for half-maximal inhibition
K_i (BCRP)	µmol/l	18 (Lit)	18	[190]	Concentration for half-maximal inhibition
K_i (OATP1B1)	µmol/l	3.6 (Lit)	3.6	[200]	Concentration for half-maximal inhibition
Intestinal permeability	cm/min	5.92E-07 (Calc)	-	-	Transcellular intestinal permeability
Partition coefficients	-	Diverse	Schmitt	[42]	Cell to plasma partition coefficients
Cellular permeability	cm/min	1.17E-4 (Calc)	Charge-dependent Schmitt normalized to PK-Sim	[1]	Permeability into the cellular space

-: not given, asm: assumption, BCRP: breast cancer resistance protein, calc: calculated, CYP: cytochrome P450, opt: optimized during parameter identification, GFR: glomerular filtration rate, lit: literature, OATP: organic anion transporting polypeptide, opt: optimized during parameter identification, Pgp: P-glycoprotein, PON3: paraoxonase 3, UGT: UDP-glucuronosyltransferase

[a] median (range)

[b] assumed from other statins

[c] calculated from V_{max}

[d] calculated from liver S9

3.10.2 Clinical grapefruit-simvastatin interaction studies

Table S41: Clinical studies investigating the simvastatin-grapefruit interaction

	Simvastatin		Grapefruit juice								
ID	Dose [mg]	Route	Volume [ml]	Route	BGT [µmol/l]	DHB [µmol/l]	n	Female [%]	Age[a] [years]	Weight[a] [kg]	Reference
8.1.01	60	po (tab), sd (D3)	200 (d)	D1-D2: tid, D3: 0h, 0.5h, 15h	-	-	10	50	22 (19-30)	68 (55-101)	Lilja et al. 1998 [217]
8.1.03	40	po (tab), sd (D3)	200 (s)	D1-D2: qd, D3: 0h	-	-	10	0	(20-24)	(63-80)	Lilja et al. 2004 [218]
8.1.02	40	po (tab), sd (D3)	200 (d)	D1-D2: tid, D3: 0h, 0.5h, 15h	-	-	10	10	(20-24)	(58-79)	Lilja et al. 2000 [219]
8.1.04	40	po (tab), sd (D4)	200 (d)	D1-D3: tid	-	-	10	10	(20-24)	(58-79)	Lilja et al. 2000 [219]
8.1.05	40	po (tab), sd (D6)	200 (d)	D1-D2: tid, D3: 0h, 0.5h, 15h	-	-	10	10	(20-24)	(58-79)	Lilja et al. 2000 [219]
8.1.06	40	po (tab), sd (D11)	200 (d)	D1-D3: tid	-	-	10	10	(20-24)	(58-79)	Lilja et al. 2000 [219]

[a] mean (range)

-: not given, BGT: bergamottin, d: double-strength, DHB: dihydroxybergamottin, D: day, po: oral, qd: once daily, s: single-strength, sd: single dose, tab: tablet, tid: three times daily

3.10.3 Bergamottin and 6,7-dihydroxybergamottin doses

Juice preparation	BGT [mg]	DHB [mg]	Measured	ID	Reference
frozen concentrate (double), 200 ml	2.54	3.74	no	8.1.01	Lilja et al. 1998 [217]
frozen concentrate (double), 200 ml	2.54	3.74	no	8.1.02	Lilja et al. 2000 [219]
frozen concentrate (double), 200 ml	2.54	3.74	no	8.1.04	Lilja et al. 2000 [219]
frozen concentrate (double), 200 ml	2.54	3.74	no	8.1.05	Lilja et al. 2000 [219]
frozen concentrate (double), 200 ml	2.54	3.74	no	8.1.06	Lilja et al. 2000 [219]
frozen concentrate, 200 ml	1.27	1.87	no	8.1.03	Lilja et al. 2004 [218]

italic: preparation assumed; BGT: bergamottin, DHB: 6,7-dihydroxybergamottin

3.10.4 Linear plasma concentration-time profiles

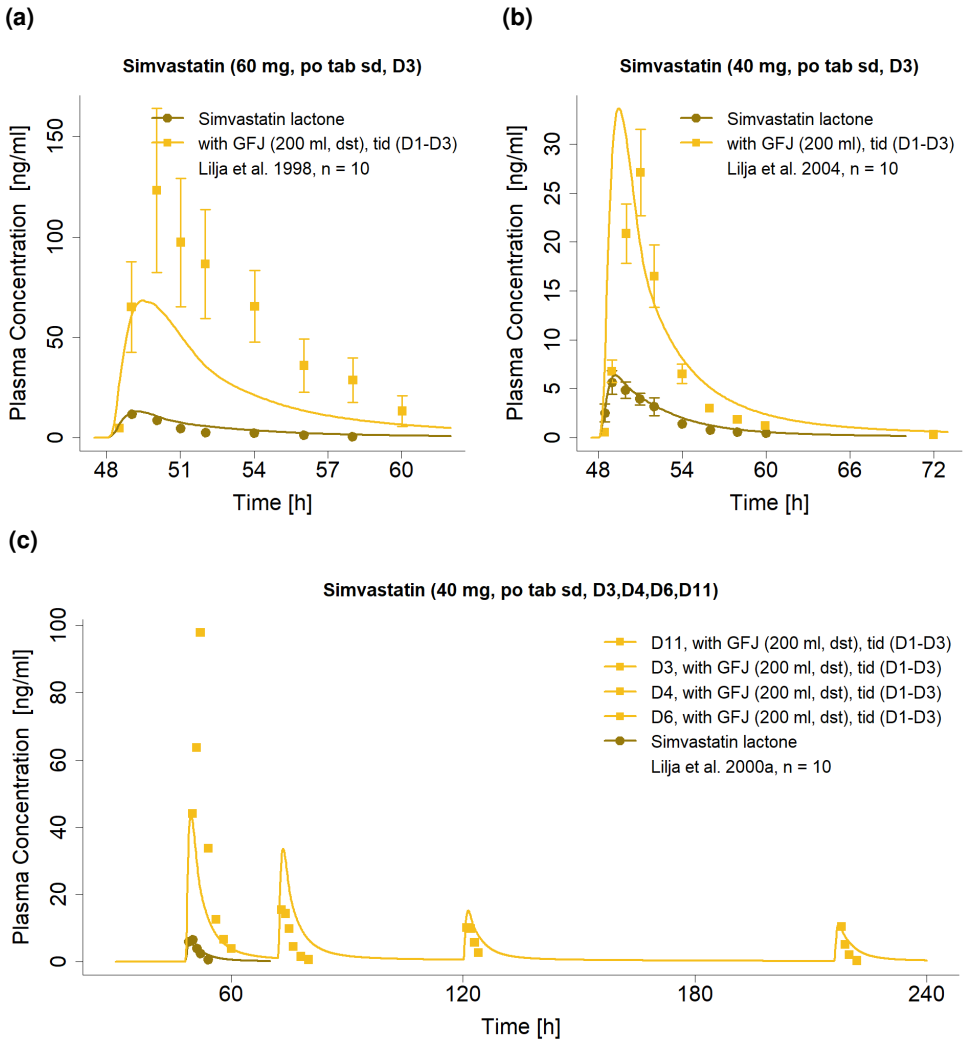

Figure S34: Predicted compared to observed simvastatin plasma concentration-time profiles (linear) with and without grapefruit juice co-administration. Observed data are shown as dots ± standard deviation (if available); model predictions are shown as solid lines. Details on dosing regimens, study population and literature reference are listed in Table S41. D: day, dst: double-strength, GFJ: grapefruit juice, sd: single dose, tab: tablet, tid: three times daily

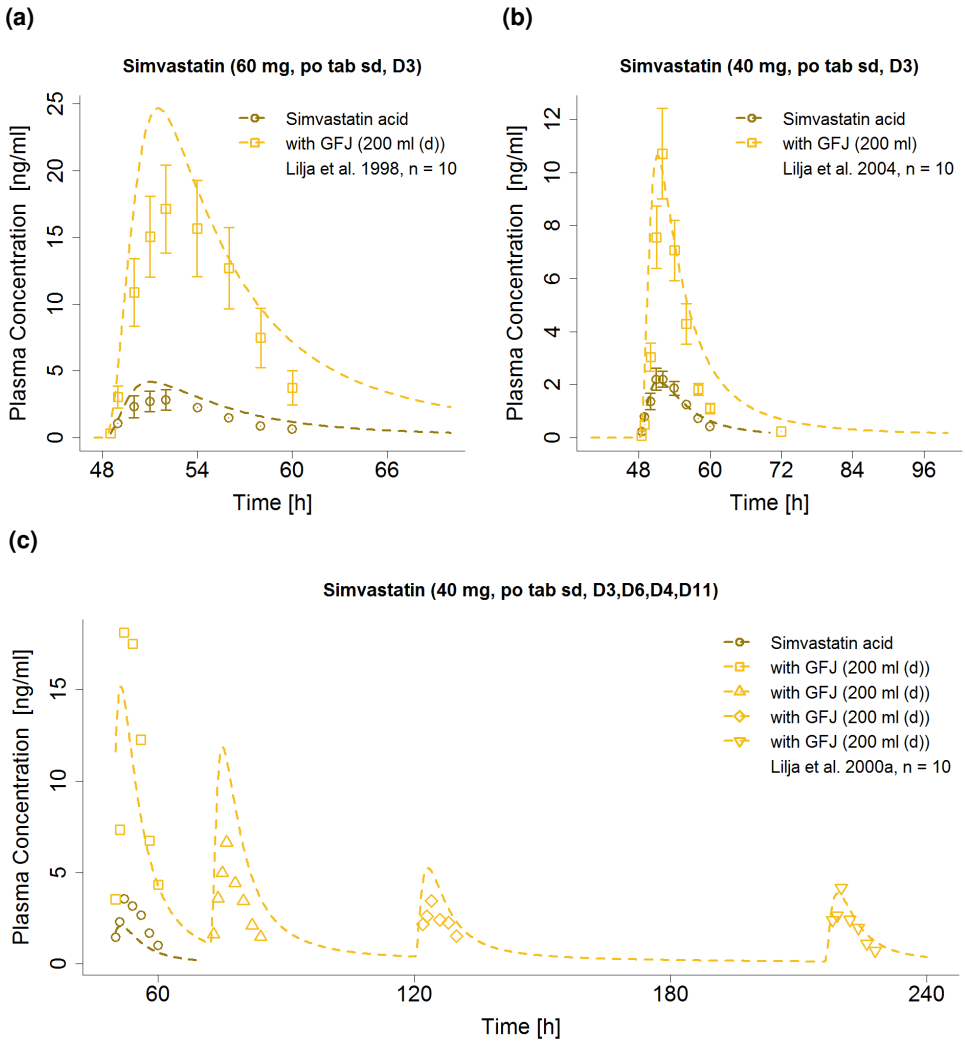

Figure S35: Predicted compared to observed simvastatin acid plasma concentration-time profiles (linear) with and without grapefruit juice co-administration. Observed data are shown as dots ± standard deviation (if available); model predictions are shown as solid lines. Details on dosing regimens, study population and literature reference are listed in Table S41. D: day, dst: double-strength, GFJ: grapefruit juice, sd: single dose, tab: tablet, tid: three times daily

3.10.5 Semi-logarithmic plasma concentration-time profiles

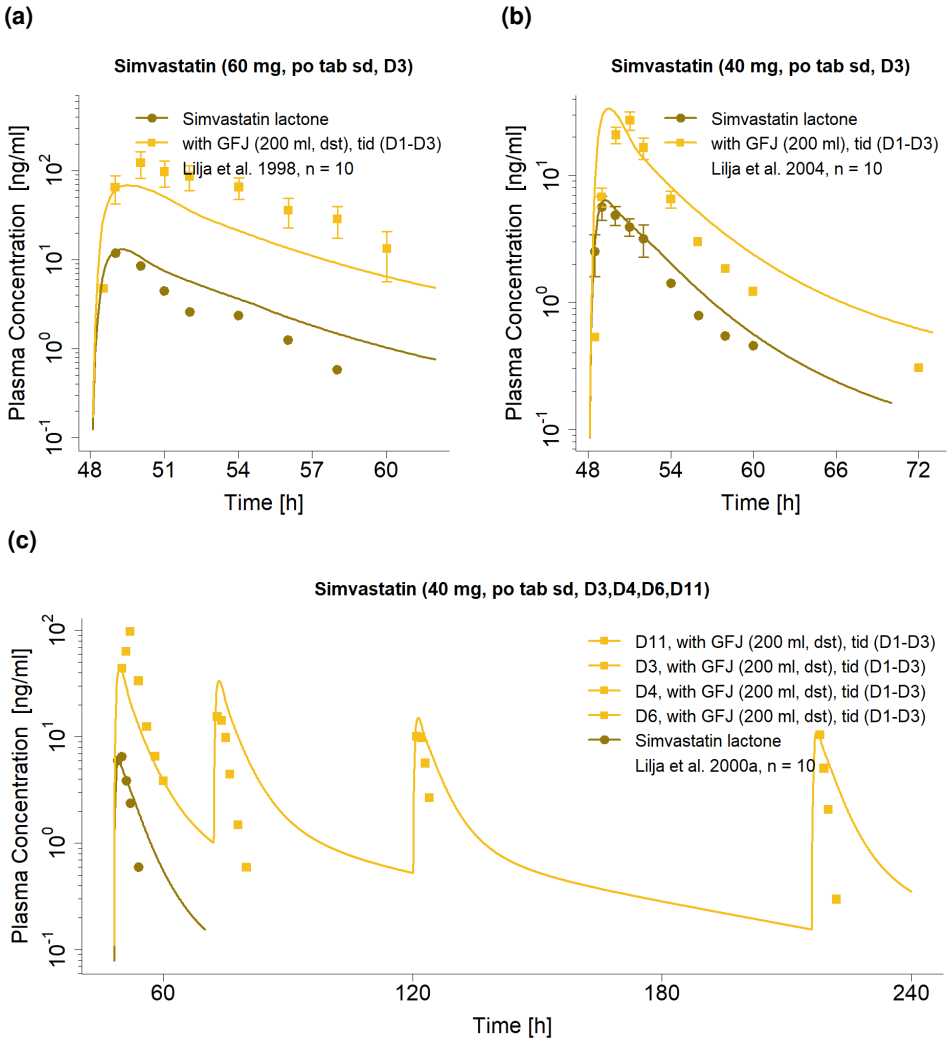

Figure S36: Predicted compared to observed simvastatin plasma concentration-time profiles (semi-logarithmic) with and without grapefruit juice co-administration. Observed data are shown as dots ± standard deviation (if available); model predictions are shown as solid lines. Details on dosing regimens, study population and literature reference are listed in Table S41. D: day, dst: double-strength, GFJ: grapefruit juice, sd: single dose, tab: tablet, tid: three times daily

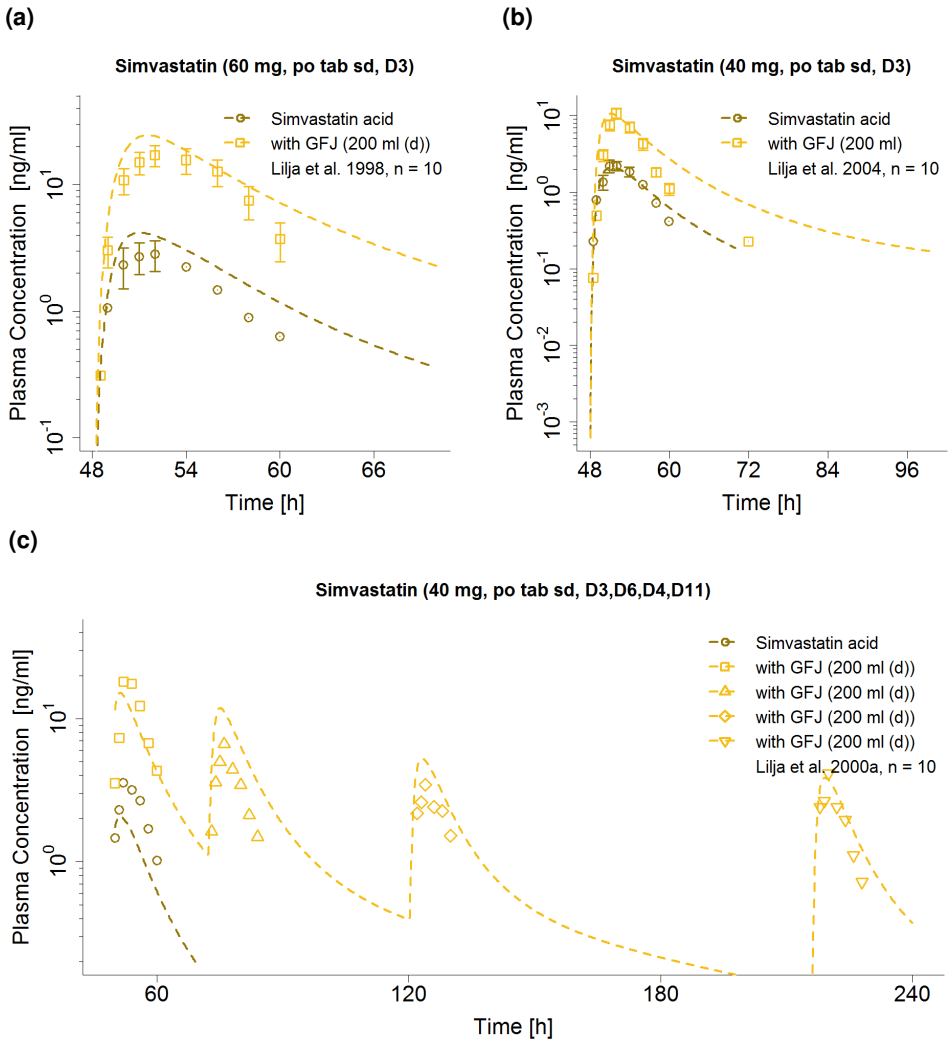

Figure S37: Predicted compared to observed simvastatin acid plasma concentration-time profiles (semi-logarithmic) with and without grapefruit juice co-administration. Observed data are shown as dots ± standard deviation (if available); model predictions are shown as solid lines. Details on dosing regimens, study population and literature reference are listed in Table S41. D: day, dst: double-strength, GFJ: grapefruit juice, sd: single dose, tab: tablet, tid: three times daily

3.10.6 GFJDI AUC_{last} and C_{max} ratio goodness-of-fit plots

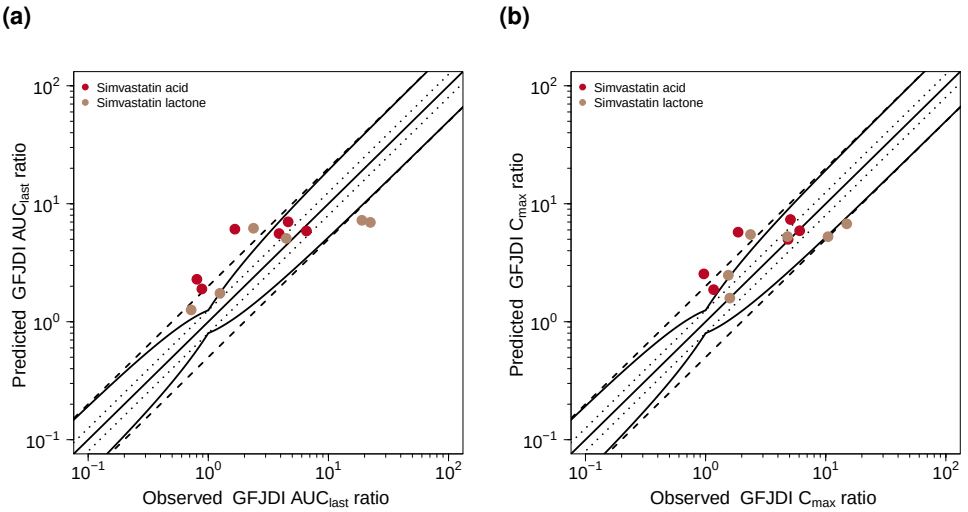

Figure S38: Predicted compared to observed GFJDI AUC_{last} and GFJDI C_{max} values. The straight solid line marks the line of identity, the curved solid lines show the prediction success limits proposed by Guest allowing for 1.25-fold variability of the GFJDI ratio [54]. Dotted lines indicate 1.25-fold, dashed lines indicate 2-fold deviation. AUC_{last}: area under the plasma concentration-time curve from the time of drug administration to the last concentration measurement, C_{max}: maximum plasma concentration, GFJDI: grapefruit juice-drug interaction

3.10.7 Geometric mean fold error of predicted GFJDI AUC_{last} and C_{max} ratios

Table S43: Predicted and observed Simvastatin lactone GFJDI AUC_{last} ratios and GFJDI C_{max} ratios.

ID			GFJDI AUC_{last} ratio			GFJDI C_{max} ratio			
	Compound	n	Pred	Obs	Pred/Obs	Pred	Obs	Pred/Obs	Reference
8.1.01	Simvastatin lactone	10	6.95	22.35	0.31	5.26	10.44	0.50	Lilja et al. 1998 [217]
8.1.02	Simvastatin lactone	10	7.24	18.98	0.38	6.77	14.95	0.45	Lilja et al. 2000a [219]
8.1.06	Simvastatin lactone	10	1.26	0.72	1.75	1.59	1.59	1.00	Lilja et al. 2000a [219]
8.1.04	Simvastatin lactone	10	6.20	2.38	2.61	5.49	2.36	2.32	Lilja et al. 2000a [219]
8.1.05	Simvastatin lactone	10	1.74	1.25	1.39	2.48	1.55	1.60	Lilja et al. 2000a [219]
8.1.03	Simvastatin lactone	10	5.09	4.46	1.14	5.27	4.81	1.09	Lilja et al. 2004 [218]
GMFE					**2.12 (1.14-3.21)**			**1.7 (1-2.32)**	
					3/6 with GMFE < 2			**4/6 with GMFE < 2**	

AUC_{last}: area under the plasma concentration-time curve from the time of drug administration to the last concentration measurement, C_{max}: maximum plasma concentration, GFJDI: grapefruit juice-drug interaction, GMFE: geometric mean fold error, n: number of individuals, obs: observed, pred: predicted

Table S44: Predicted and observed Simvastatin acid GFJDI AUC_{last} ratios and GFJDI C_{max} ratios.

ID			GFJDI AUC_{last} ratio			GFJDI C_{max} ratio			
	Compound	n	Pred	Obs	Pred/Obs	Pred	Obs	Pred/Obs	Reference
8.1.01	Simvastatin acid	10	5.88	6.57	0.90	5.91	6.07	0.97	Lilja et al. 1998 [217]

AUC_{last}: area under the plasma concentration-time curve from the time of drug administration to the last concentration measurement, C_{max}: maximum plasma concentration, GFJDI: grapefruit juice-drug interaction, GMFE: geometric mean fold error, n: number of individuals, obs: observed, pred: predicted

Table S44: Predicted and observed Simvastatin acid GFJDI AUC_{last} ratios and GFJDI C_{max} ratios.

ID			GFJDI AUC_{last} ratio			GFJDI C_{max} ratio			
	Compound	**n**	**Pred**	**Obs**	**Pred/Obs**	**Pred**	**Obs**	**Pred/Obs**	**Reference**
8.1.02	Simvastatin acid	10	7.03	4.62	1.52	7.35	5.09	1.45	Lilja et al. 2000a [219]
8.1.06	Simvastatin acid	10	1.90	0.88	2.15	1.87	1.17	1.60	Lilja et al. 2000a [219]
8.1.04	Simvastatin acid	10	6.09	1.66	3.66	5.75	1.86	3.08	Lilja et al. 2000a [219]
8.1.05	Simvastatin acid	10	2.29	0.80	2.85	2.54	0.97	2.63	Lilja et al. 2000a [219]
8.1.03	Simvastatin acid	10	5.59	3.89	1.44	5.00	4.86	1.03	Lilja et al. 2004 [218]
GMFE					**2.12 (1.12-3.66)**			**1.8 (1.03-3.08)**	
					3/6 with GMFE < 2			**4/6 with GMFE < 2**	

AUC_{last}: area under the plasma concentration-time curve from the time of drug administration to the last concentration measurement, C_{max}: maximum plasma concentration, GFJDI: grapefruit juice-drug interaction, GMFE: geometric mean fold error, n: number of individuals, obs: observed, pred: predicted

3.11 Grapefruit-verapamil GFJDI

The verapamil GFJDI was modeled using a previously developed and evaluated whole-body PBPK model of verapamil et al. [220]. Drug-dependent parameters of the verapamil PBPK model are displayed in Table S45.

Details on the modeled clinical GFJDI studies are given in Table S46. Predicted verapamil and norverapamil plasma concentration-time profiles with and without grapefruit juice coadministration, compared to observed data, are shown in Figures S39 and S40 (linear) and S41 and S42 (semi-logarithmic). The correlation of predicted to observed GFJDI AUC_{last} and C_{max} ratios is shown in Figure S43. Tables S48/S49 and S50/S51 list the corresponding predicted and observed GFJDI AUC_{last} ratios, GFJDI C_{max} ratios as well as GMFE values of verapamil and norverapamil, respectively.

3.11.1 Verapamil drug-dependent parameters

Table S45: Drug-dependent parameters of the verapamil PBPK model (adopted from [220])

Parameter	Value	Unit	Source	Literature	Reference	Value	Unit	Source	Literature	Reference	Description
	R-Verapamil					**S-Verapamil**					
MW	454.611	g/mol	Literature	454.611	[56]	454.611	g/mol	Literature	454.611	[56]	Molecular weight
pKa (base)	8.75	-	Literature	8.75	[221]	8.75	-	Literature	8.75	[221]	Acid dissociation constant
Solubility (pH 6.54)	46.0	g/l	Literature	46.0	[222]	46.0	g/l	Literature	46.0	[222]	Solubility
logP	2.84 *	-	Optimized	3.79	[223]	2.84 *	-	Optimized	3.79	[223]	Lipophilicity
$f_{u,plasma}$	5.1	%	Literature	5.1	[224]	11.0	%	Literature	11.0	[224]	Fraction unbound
CYP3A4 K_m -> Norvera	19.59	µmol/l	Literature	31.1*0.63 ‡	[225]	9.72	µmol/l	Literature	16.2*0.60 ‡	[225]	CYP3A4 Michaelis-Menten constant
CYP3A4 k_{cat} -> Norvera	34.94	1/min	Optimized	-	-	26.17	1/min	Optimized	-	-	CYP3A4 catalytic rate constant
CYP3A4 K_m -> D617	35.34	µmol/l	Literature	56.1*0.63 ‡	[225]	23.64	µmol/l	Literature	39.4*0.60 ‡	[225]	CYP3A4 Michaelis-Menten constant
CYP3A4 k_{cat} -> D617	43.98	1/min	Optimized	-	-	56.42	1/min	Optimized	-	-	CYP3A4 catalytic rate constant
Pgp K_m	1.01	µmol/l	Literature	1.01	[226]	1.01	µmol/l	Literature	1.01	[226]	Pgp Michaelis-Menten constant
Pgp k_{cat}	12.60 °	1/min	Optimized	-	-	12.60 °	1/min	Optimized	-	-	Pgp transport rate constant
GFR fraction	1.00	-	Assumed	-	-	1.00	-	Assumed	-	-	Fraction of filtered drug in the urine
EHC continuous fraction	1.00	-	Assumed	-	-	1.00	-	Assumed	-	-	Fraction of bile continually released
CYP3A4 MBI K_I	27.63	µmol/l	Literature	32.5*0.85 ‡	[225]	3.85	µmol/l	Literature	4.94*0.78 ‡	[225]	Conc. for half-maximal inactivation
CYP3A4 MBI k_{inact}	0.038	1/min	Literature	0.038	[225]	0.034	1/min	Literature	0.034	[225]	Maximum inactivation rate
Pgp non-competitive K_i	0.038 *	µmol/l	Optimized	0.31	[227]	0.038 *	µmol/l	Optimized	0.31	[227]	Conc. for half-maximal inhibition
Partition coefficients	Diverse	-	Calculated	R&R	[26, 63]	Diverse	-	Calculated	R&R	[26, 63]	Cell to plasma partition coefficients
Cellular permeability	9.94E-02 *	cm/min	Optimized	PK-Sim	[1]	9.94E-02 *	cm/min	Optimized	PK-Sim	[1]	Permeability into the cellular space
Intestinal permeability	3.54E-06 *	cm/min	Optimized	1.21E-05	Calculated	3.54E-06 *	cm/min	Optimized	1.21E-05	Calculated	Transcellular intestinal permeability
SR tablet Weibull time	155.24	min	Optimized	-	[228]	155.24	min	Optimized	-	[228]	Dissolution time (50% dissolved)
SR tablet Weibull shape	2.37	-	Optimized	-	[228]	2.37	-	Optimized	-	[228]	Dissolution profile shape

* assumed to be the same for all four compounds, ° assumed to be the same for enantiomers, ‡ in vitro value corrected for binding in the assay, [a] assumed to be the same for R-verapamil/R-norverapamil, [b] assumed to be the same for S-verapamil/S-norverapamil, [c] IC_{50} at very low substrate concentration, conc: concentration, CYP3A4: cytochrome P450 3A4, D617: verapamil metabolite, D620: norverapamil metabolite, EHC: enterohepatic circulation,GFR: glomerular filtration rate, MBI: mechanism-based inactivation, Norvera: norverapamil, Pgp: P-glycoprotein, PK-Sim: PK-Sim standard calculation method, R&R: Rodgers and Rowland calculation method, SR: sustained release formulation

Table S45: R- and S- verapamil drug-dependent parameters *(continued)*

Parameter	Value	Unit	Source	Literature	Reference	Value	Unit	Source	Literature	Reference	Description
	R-Norverapamil					**S-Norverapamil**					
MW	440.584	g/mol	Literature	440.584	[56]	440.584	g/mol	Literature	440.584	[56]	Molecular weight
pKa (base)	8.75	-	Literature	8.6 - 8.9	[229]	8.75	-	Literature	8.6 - 8.9	[229]	Acid dissociation constant
logP	2.84 *	-	Optimized	-	-	2.84 *	-	Optimized	-	-	Lipophilicity
$f_{u,plasma}$	5.1 [a]	%	Assumed	-	-	11.0 [b]	%	Assumed	-	-	Fraction unbound
CYP3A4 K_m -> D620	144.0	µmol/l	Literature	144.0	[230]	36.0	µmol/l	Literature	36.0	[230]	CYP3A4 Michaelis-Menten constant
CYP3A4 k_{cat} -> D620	145.64	1/min	Optimized	-	-	41.10	1/min	Optimized	-	-	CYP3A4 catalytic rate constant
Pgp K_m	1.01 *	µmol/l	Assumed	-	-	1.01 *	µmol/l	Assumed	-	-	Pgp Michaelis-Menten constant
Pgp k_{cat}	3.39 °	1/min	Optimized	-	-	3.39 °	1/min	Optimized	-	-	Pgp transport rate constant
GFR fraction	1.00	-	Assumed	-	-	1.00	-	Assumed	-	-	Fraction of filtered drug in the urine
EHC continuous fraction	1.00	-	Assumed	-	-	1.00	-	Assumed	-	-	Fraction of bile continually released
CYP3A4 MBI K_I	6.10	µmol/l	Literature	10.7*0.57 ‡	[225]	2.90	µmol/l	Literature	4.92*0.59 ‡	[225]	Conc. for half-maximal inactivation
CYP3A4 MBI k_{inact}	0.048	1/min	Literature	0.048	[225]	0.080	1/min	Literature	0.080	[225]	Maximum inactivation rate
Pgp non-competitive K_i	0.038 *	µmol/l	Optimized	0.30 [c]	[231]	0.038 *	µmol/l	Optimized	0.30 [c]	[231]	Conc. for half-maximal inhibition
Partition coefficients	Diverse	-	Calculated	R&R	[26, 63]	Diverse	-	Calculated	R&R	[26, 63]	Cell to plasma partition coefficients
Cellular permeability	9.94E-02 *	cm/min	Optimized	PK-Sim	[1]	9.94E-02 *	cm/min	Optimized	PK-Sim	[1]	Permeability into the cellular space
Intestinal permeability	3.54E-06 *	cm/min	Optimized	1.40E-05	Calculated	3.54E-06 *	cm/min	Optimized	1.40E-05	Calculated	Transcellular intestinal permeability

* assumed to be the same for all four compounds, ° assumed to be the same for enantiomers, ‡ in vitro value corrected for binding in the assay, [a] assumed to be the same for R-verapamil/R-norverapamil, [b] assumed to be the same for S-verapamil/S-norverapamil, [c] IC_{50} at very low substrate concentration, conc: concentration, CYP3A4: cytochrome P450 3A4, D617: verapamil metabolite, D620: norverapamil metabolite, EHC: enterohepatic circulation,GFR: glomerular filtration rate, MBI: mechanism-based inactivation, Norvera: norverapamil, Pgp: P-glycoprotein, PK-Sim: PK-Sim standard calculation method, R&R: Rodgers and Rowland calculation method, SR: sustained release formulation

3.11.2 Clinical grapefruit-verapamil interaction studies

Table S46: Clinical studies investigating the simvastatin-grapefruit interaction

	Verapamil		Grapefruit juice								
ID	Dose [mg]	Route	Volume [ml]	Route	BGT [µmol/l]	DHB [µmol/l]	n	Female [%]	Age[a] [years]	Weight[a] [kg]	Reference
9.1.01	120	po (tabER), bid (D1-D7)	250	D5-D7: 0h, 3h, 8h, 12h	-	-	24	50	27 ± 4	70 ± 11	Fuhr et al. 2002 [232]
9.1.02	120	po (tabER), bid (D3-D6)	200	D1-D6: bid (0h)	-	-	9	0	26 (19-40) ± 7	72 (62-80) ± 6	Ho et al. 2000 [233]*

[a] mean (range) ± standard deviation

-: not given, *:control with orange juice, bid: twice daily, BGT: bergamottin, D: day, DHB: dihydroxybergamottin, po: oral, tabER: extended release tablet

3.11.3 Bergamottin and 6,7-dihydroxybergamottin doses

Juice preparation	BGT [mg]	DHB [mg]	Measured	ID	Reference
canned juice, 250 ml	1.41	0.92	no	9.1.01	Fuhr et al. 2002 [232]
canned juice, 200 ml	1.13	0.74	no	9.1.02	Ho et al. 2000 [233]

italic: preparation assumed; BGT: bergamottin, DHB: 6,7-dihydroxybergamottin

3.11.4 Linear plasma concentration-time profiles

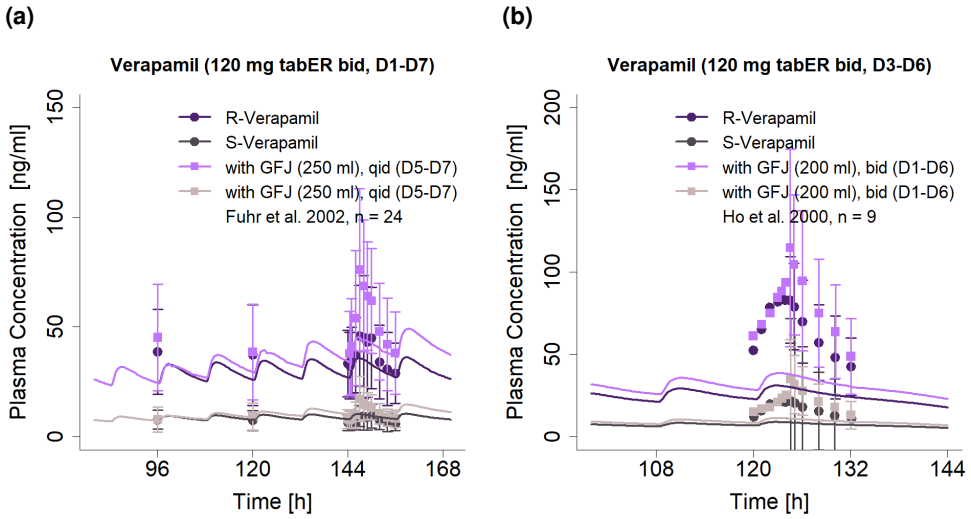

Figure S39: Predicted compared to observed verapamil plasma concentration-time profiles (linear) with and without grapefruit juice co-administration. Observed data are shown as dots ± standard deviation; model predictions are shown as solid lines. Details on dosing regimens, study population and literature reference are listed in Table S46. bid: twice daily, D: day, GFJ: grapefruit juice, n: number of participants, qid: four times daily, tabER: extended release tablet

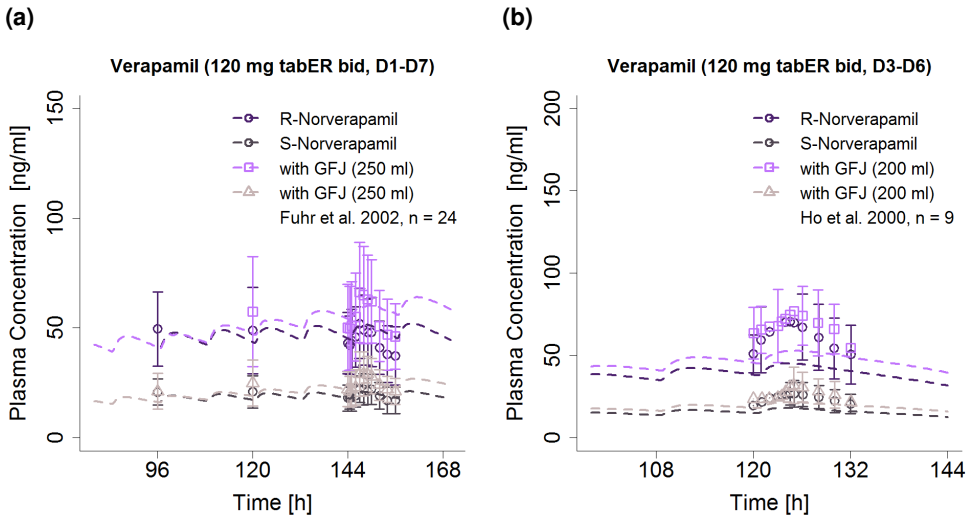

Figure S40: Predicted compared to observed norverapamil plasma concentration-time profiles (linear) with and without grapefruit juice co-administration. Observed data are shown as dots ± standard deviation; model predictions are shown as solid lines. Details on dosing regimens, study population and literature reference are listed in Table S46. bid: twice daily, D: day, GFJ: grapefruit juice, n: number of participants, qid: four times daily, tabER: extended release tablet

3.11.5 Semi-logarithmic plasma concentration-time profiles

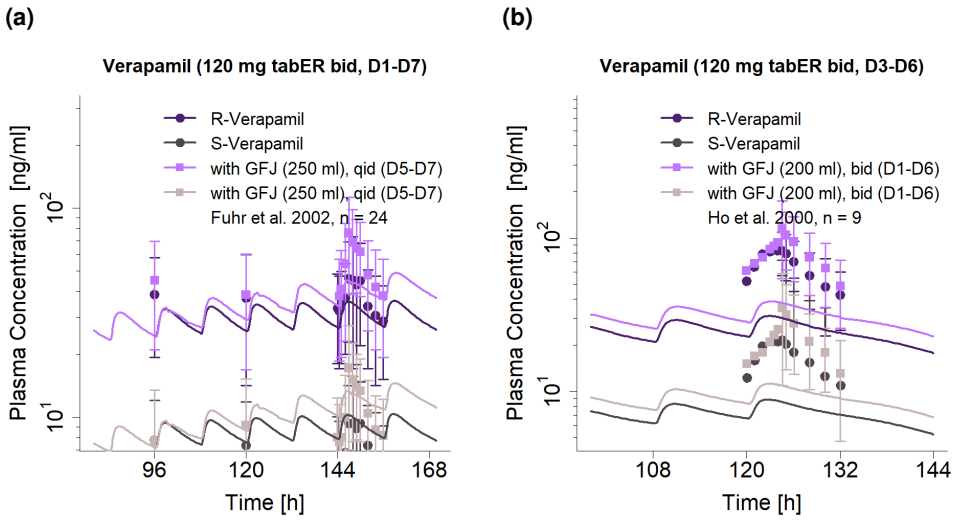

Figure S41: Predicted compared to observed verapamil plasma concentration-time profiles (semi-logarithmic) with and without grapefruit juice co-administration. Observed data are shown as dots ± standard deviation; model predictions are shown as solid lines. Details on dosing regimens, study population and literature reference are listed in Table S46. bid: twice daily, D: day, GFJ: grapefruit juice, n: number of participants, qid: four times daily, tabER: extended release tablet

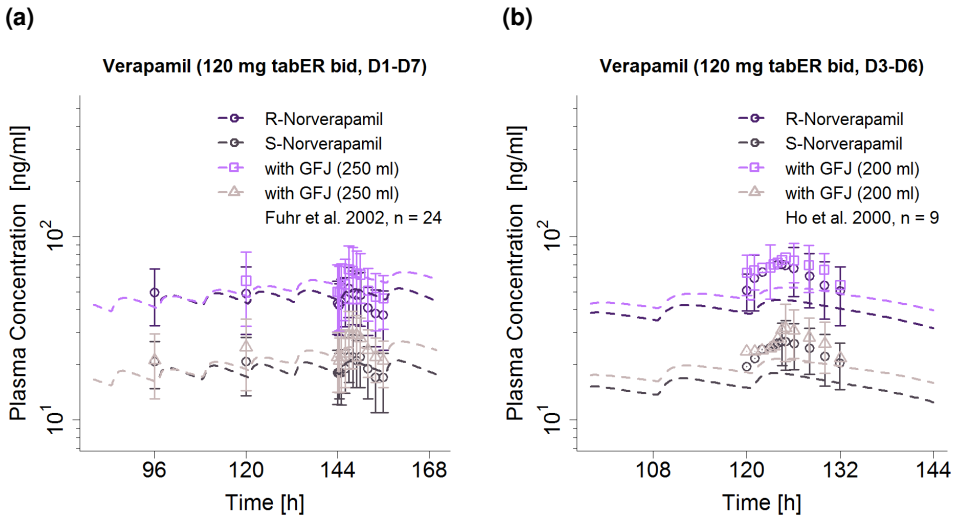

Figure S42: Predicted compared to observed norverapamil plasma concentration-time profiles (semi-logarithmic) with and without grapefruit juice co-administration. Observed data are shown as dots ± standard deviation; model predictions are shown as solid lines. Details on dosing regimens, study population and literature reference are listed in Table S46. bid: twice daily, D: day, GFJ: grapefruit juice, n: number of participants, qid: four times daily, tabER: extended release tablet

3.11.6 GFJDI AUC_{last} and C_{max} ratio goodness-of-fit plots

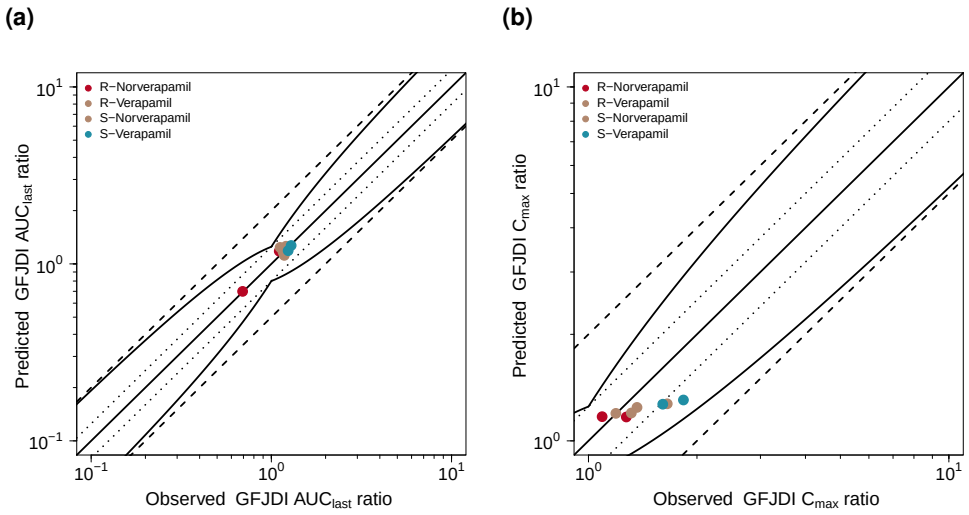

Figure S43: Predicted compared to observed GFJDI AUC_{last} and GFJDI C_{max} values. The straight solid line marks the line of identity, the curved solid lines show the prediction success limits proposed by Guest allowing for 1.25-fold variability of the GFJDI ratio [54]. Dotted lines indicate 1.25-fold, dashed lines indicate 2-fold deviation. AUC_{last}: area under the plasma concentration-time curve from the time of drug administration to the last concentration measurement, C_{max}: maximum plasma concentration, GFJDI: grapefruit juice-drug interaction

3.11.7 Geometric mean fold error of predicted GFJDI AUC_{last} and C_{max} ratios

Table S48: Predicted and observed R-Verapamil GFJDI AUC_{last} ratios and GFJDI C_{max} ratios.

ID			GFJDI AUC_{last} ratio			GFJDI C_{max} ratio			
	Compound	n	Pred	Obs	Pred/Obs	Pred	Obs	Pred/Obs	Reference
9.1.01	R-Verapamil	24	1.17	1.16	1.01	1.27	1.65	0.77	Fuhr et al. 2002 [232]
9.1.02	R-Verapamil	9	1.26	1.21	1.04	1.24	1.36	0.91	Ho et al. 2000 [233]
GMFE					**1.02 (1.01-1.04)**		**1.2 (1.1-1.3)**		
					2/2 with GMFE < 2		**2/2 with GMFE < 2**		

AUC_{last}: area under the plasma concentration-time curve from the time of drug administration to the last concentration measurement, C_{max}: maximum plasma concentration, GFJDI: grapefruit juice-drug interaction, GMFE: geometric mean fold error, n: number of individuals, obs: observed, pred: predicted

Table S49: Predicted and observed S-Verapamil GFJDI AUC_{last} ratios and GFJDI C_{max} ratios.

ID			GFJDI AUC_{last} ratio			GFJDI C_{max} ratio			
	Compound	n	Pred	Obs	Pred/Obs	Pred	Obs	Pred/Obs	Reference
9.1.01	S-Verapamil	24	1.19	1.24	0.96	1.30	1.83	0.71	Fuhr et al. 2002 [232]
9.1.02	S-Verapamil	9	1.27	1.29	0.99	1.27	1.61	0.79	Ho et al. 2000 [233]
GMFE					**1.03 (1.01-1.04)**		**1.34 (1.27-1.41)**		
					2/2 with GMFE < 2		**2/2 with GMFE < 2**		

AUC_{last}: area under the plasma concentration-time curve from the time of drug administration to the last concentration measurement, C_{max}: maximum plasma concentration, GFJDI: grapefruit juice-drug interaction, GMFE: geometric mean fold error, n: number of individuals, obs: observed, pred: predicted

Table S50: Predicted and observed R-Norverapamil GFJDI AUC_{last} ratios and GFJDI C_{max} ratios.

ID			GFJDI AUC_{last} ratio			GFJDI C_{max} ratio			
	Compound	n	Pred	Obs	Pred/Obs	Pred	Obs	Pred/Obs	Reference
9.1.01	R-Norverapamil	24	0.70	0.69	1.01	1.17	1.27	0.92	Fuhr et al. 2002 [232]
9.1.02	R-Norverapamil	9	1.18	1.11	1.07	1.17	1.09	1.07	Ho et al. 2000 [233]
GMFE					**1.04 (1.01-1.07)**		**1.08 (1.07-1.09)**		
					2/2 with GMFE < 2		**2/2 with GMFE < 2**		

AUC_{last}: area under the plasma concentration-time curve from the time of drug administration to the last concentration measurement, C_{max}: maximum plasma concentration, GFJDI: grapefruit juice-drug interaction, GMFE: geometric mean fold error, n: number of individuals, obs: observed, pred: predicted

Table S51: Predicted and observed S-Norverapamil GFJDI AUC_{last} ratios and GFJDI C_{max} ratios.

ID			GFJDI AUC_{last} ratio			GFJDI C_{max} ratio			
	Compound	n	Pred	Obs	Pred/Obs	Pred	Obs	Pred/Obs	Reference
9.1.01	S-Norverapamil	24	1.12	1.18	0.95	1.20	1.31	0.91	Fuhr et al. 2002 [232]
9.1.02	S-Norverapamil	9	1.24	1.12	1.11	1.20	1.19	1.00	Ho et al. 2000 [233]
GMFE					**1.08 (1.06-1.11)**		**1.05 (1-1.1)**		
					2/2 with GMFE < 2		**2/2 with GMFE < 2**		

AUC_{last}: area under the plasma concentration-time curve from the time of drug administration to the last concentration measurement, C_{max}: maximum plasma concentration, GFJDI: grapefruit juice-drug interaction, GMFE: geometric mean fold error, n: number of individuals, obs: observed, pred: predicted

4 System-dependent parameters

Details on the expression of metabolizing enzymes and transport proteins implemented to model the pharmacokinetics of felodipine and dehydrofelodipine as well as the perpetrator models erythromycin, itraconazole, carbamazepine and phenytoin are summarized in Table S52. As enterohepatic circulation is active under physiological conditions, the parameter EHC continuous fraction was set to 1 in all individuals.

Table S52: System-dependent parameters

	Reference concentration				Half-life	
Enzyme/ Transporter	**Mean[a] [µmol/l]**	**Relative expression[b]**	**Localization**	**Direction**	**Liver [h]**	**Intestine [h]**
CYP3A4	4.32 [235]	RT-PCR [236]	Intracellular	-	36 [237]	23 [15]
CYP2B6	1.56 [235]	RT-PCR [236]	Intracellular	-	32	23
CYP2C8	2.56 [235]	RT-PCR [236]	Intracellular	-	23	23
EPHX1	1.00[c] [234]	RT-PCR [238]	Intracellular	-	36	23
UGT2B7	2.78 [239]	EST [240]	Intracellular	-	36	23
PON3	1.00[c] [234]	Array [241]	Intracellular	-	36	23
UGT1A1	1.00[c] [234]	RT-PCR [238]	Intracellular	-	36	23
UGT1A3	1.00[c] [234]	RT-PCR [238]	Intracellular	-	36	23
OATP1B1	1.00[c] [234]	RT-PCR [242]	Basolateral	Influx	36	-
BCRP	1.00[c] [234]	RT-PCR[d] [242]	Apical	Efflux	36	23
Pgp	1.41 [55]	RT-PCR[d] [242]	Apical	Efflux	36	23

-: not given, BCRP: breast cancer resistance protein, CYP: cytochrome P450, EST: expressed sequence tags expression profile, OATP1B1: organic anion transporting polypeptide 1B1, Pgp: P-glycoprotein, PON3: paraoxonase 3, RT-PCR: reverse transcription-polymerase chain reaction profile, UGT: UDP-glucuronosyltransferase

[a] µmol/lol protein/l in the tissue of highest expression

[b] in the different organs (PK-Sim® expression database profile)

[c] if no information was available, the mean reference concentration was set to 1.00 µmol/l and the catalytic rate constant (kcat) was optimized [234]

[d] with the relative expression in the intestinal mucosa increased by factor 3.57 [55]

List of Figures

List of Tables

Bibliography

[1] Open Systems Pharmacology Suite Community. Open Systems Pharmacology Suite Manual, 2018. URL https://docs.open-systems-pharmacology.org/. accessed: 14 Dec 2020.

[2] D. G. Bailey, G. K. Dresser, J. H. Kreeft, C. Munoz, D. J. Freeman, and J. R. Bend. Grapefruit-felodipine interaction: effect of unprocessed fruit and probable active ingredients. *Clinical pharmacology and therapeutics*, 68(5):468–77, nov 2000.

[3] L.-Q. Guo, Q.-Y. Chen, X. Wang, Y.-X. Liu, X.-M. Chu, X.-M. Cao, J.-H. Li, and Y. Yamazoe. Different roles of pummelo furanocoumarin and cytochrome P450 3A5*3 polymorphism in the fate and action of felodipine. *Current drug metabolism*, 8(6):623–30, aug 2007.

[4] D. G. Bailey, J. H. Kreeft, C. Munoz, D. J. Freeman, and J. R. Bend. Grapefruit juice-felodipine interaction: effect of naringin and 6',7'-dihydroxybergamottin in humans. *Clinical pharmacology and therapeutics*, 64(3):248–56, sep 1998.

[5] L. Q. Guo, K. Fukuda, T. Ohta, and Y. Yamazoe. Role of furanocoumarin derivatives on grapefruit juice-mediated inhibition of human CYP3A activity. *Drug metabolism and disposition: the biological fate of chemicals*, 28(7):766–71, jul 2000.

[6] P. Schmiedlin-Ren, D. J. Edwards, M. E. Fitzsimmons, K. He, K. S. Lown, P. M. Woster, A. Rahman, K. E. Thummel, J. M. Fisher, P. F. Hollenberg, and P. B. Watkins. Mechanisms of enhanced oral availability of CYP3A4 substrates by grapefruit constituents: Decreased enterocyte CYP3A4 concentration and mechanism-based inactivation by furanocoumarins. *Drug Metabolism and Disposition*, 25(11):1228–1233, 1997.

[7] A. Messer, A. Nieborowski, C. Strasser, C. Lohr, and D. Schrenk. Major furocoumarins in grapefruit juice I: Levels and urinary metabolite(s). *Food and Chemical Toxicology*, 49 (12):3224–3231, 2011.

[8] K. M. Vandermolen, N. B. Cech, M. F. Paine, and N. H. Oberlies. Rapid Quantitation of Furanocoumarins and Flavonoids in Grapefruit Juice using Ultra-Performance Liquid Chromatography. *Phytochemical analysis : PCA*, 24(6):654–60, nov 2013.

[9] M. M. Melough, T. M. Vance, S. G. Lee, A. A. Provatas, C. Perkins, A. Qureshi, E. Cho, and O. K. Chun. Furocoumarin Kinetics in Plasma and Urine of Healthy Adults following Consumption of Grapefruit (Citrus paradisi Macf.) and Grapefruit Juice. *Journal of Agricultural and Food Chemistry*, 65(14):3006–3012, 2017.

[10] N. Sakamaki, M. Nakazato, H. Matsumoto, K. Hagino, K. Hirata, and H. Ushiyama. Contents of furanocoumarins in grapefruit juice and health foods. *Journal of the Food Hygienic Society of Japan*, 49(4):326–331, 2008.

[11] S. M. Kakar, M. F. Paine, P. W. Stewart, and P. B. Watkins. 6'7'-Dihydroxybergamottin contributes to the grapefruit juice effect. *Clinical pharmacology and therapeutics*, 75(6): 569–79, jun 2004.

[12] S. Malhotra, D. G. Bailey, M. F. Paine, and P. B. Watkins. Seville orange juice-felodipine interaction: comparison with dilute grapefruit juice and involvement of furocoumarins. *Clinical pharmacology and therapeutics*, 69(1):14–23, jan 2001.

[13] M. F. Paine, W. W. Widmer, H. L. Hart, S. N. Pusek, K. L. Beavers, A. B. Criss, S. S. Brown, B. F. Thomas, and P. B. Watkins. A furanocoumarin-free grapefruit juice establishes furanocoumarins as the mediators of the grapefruit juice-felodipine interaction. *The American journal of clinical nutrition*, 83(5):1097–105, may 2006.

[14] T. C. Goosen, D. Cillié, D. G. Bailey, C. Yu, K. He, P. F. Hollenberg, P. M. Woster, L. Cohen, J. A. Williams, M. Rheeders, and H. P. Dijkstra. Bergamottin contribution to the grapefruit juice-felodipine interaction and disposition in humans. *Clinical pharmacology and therapeutics*, 76(6):607–17, dec 2004.

[15] D. J. Greenblatt, L. L. Von Moltke, J. S. Harmatz, G. Chen, J. L. Weemhoff, C. Jen, C. J. Kelley, B. W. LeDuc, and M. A. Zinny. Time course of recovery of cytochrome P450 3A function after single doses of grapefruit juice. *Clinical Pharmacology and Therapeutics*, 74(2):121–29, 2003.

[16] G. R. Ainslie. *A TRANSLATIONAL APPROACH TO ASSESS THE RISK OF DIETARY SUBSTANCE-DRUG INTERACTIONS*. PhD thesis, 2014. URL http://journal.stainkudus.ac.id/index.php/equilibrium/article/view/1268/1127.

[17] M. Kawaguchi-Suzuki, N. Nasiri-Kenari, J. Shuster, F. G. Gmitter, P. Cancalon, F. de Oliveria, J. Kight, E. M. Handberg, C. J. Pepine, R. F. Frye, and R. M. Cooper-DeHoff. Effect of Low-Furanocoumarin Hybrid Grapefruit Juice Consumption on Midazolam Pharmacokinetics. *Journal of clinical pharmacology*, 57(3):305–311, 2017.

[18] S. Masuda, T. Terada, A. Yonezawa, Y. Tanihara, K. Kishimoto, T. Katsura, O. Ogawa, and K.-i. Inui. Identification and functional characterization of a new human kidney-specific H+/organic cation antiporter, kidney-specific multidrug and toxin extrusion 2. *Journal of the American Society of Nephrology : JASN*, 17(8):2127–35, aug 2006.

[19] Human Metabolome Database. Metabocard for bergamottin (HMDB0033782)., 2022. URL https://hmdb.ca/metabolites/HMDB0033782.

[20] Human Metabolome Database. Metabocard for 6,7-dihydroxybergamottin (HMDB0039066)., 2022. URL https://hmdb.ca/metabolites/HMDB0039066.

[21] R. Watanabe, T. Esaki, H. Kawashima, Y. Natsume-Kitatani, C. Nagao, R. Ohashi, and K. Mizuguchi. Predicting Fraction Unbound in Human Plasma from Chemical Structure: Improved Accuracy in the Low Value Ranges. *Molecular pharmaceutics*, 15(11):5302–5311, nov 2018.

[22] Chemaxon. Chemicalize - instant cheminformatics solutions, 2020. URL https://chemicalize.com/. accessed: 14 Dec 2020.

[23] M. F. Paine, A. B. Criss, and P. B. Watkins. Two major grapefruit juice components differ in intestinal CYP3A4 inhibition kinetic and binding properties. *Drug Metabolism and Disposition*, 32(10):1146–1153, 2004.

[24] W. Tassaneeyakul, L. Q. Guo, K. Fukuda, T. Ohta, and Y. Yamazoe. Inhibition selectivity of grapefruit juice components on human cytochromes P450. *Archives of Biochemistry and Biophysics*, 378(2):356–363, 2000.

[25] K. He, K. R. Iyer, R. N. Hayes, M. W. Sinz, T. F. Woolf, and P. F. Hollenberg. Inactivation of cytochrome P450 3A4 by bergamottin, a component of grapefruit juice. *Chemical Research in Toxicology*, 11(4):252–259, 1998.

[26] T. Rodgers, D. Leahy, and M. Rowland. Physiologically based pharmacokinetic modeling 1: predicting the tissue distribution of moderate-to-strong bases. *Journal of pharmaceutical sciences*, 94(6):1259–76, jun 2005.

[27] M. J. Taylor, S. Tanna, and T. Sahota. In vivo study of a polymeric glucose-sensitive insulin delivery system using a rat model. *Journal of pharmaceutical sciences*, 99(10): 4215–27, 2010.

[28] S. G. Lee, K. Kim, T. M. Vance, C. Perkins, A. Provatas, S. Wu, A. Qureshi, E. Cho, and O. K. Chun. Development of a comprehensive analytical method for furanocoumarins in grapefruit and their metabolites in plasma and urine using UPLC-MS/MS: a preliminary study. *International journal of food sciences and nutrition*, 67(8):881–7, dec 2016.

[29] V. Pilla Reddy, H. Jo, and S. Neuhoff. Food constituent– and herb–drug interactions in oncology: Influence of quantitative modelling on Drug labelling. *British Journal of Clinical Pharmacology*, 87(10):3988–4000, oct 2021.

[30] L. M. Fuhr, F. Z. Marok, M. Mees, F. Mahfoud, D. Selzer, and T. Lehr. A Physiologically Based Pharmacokinetic and Pharmacodynamic Model of the CYP3A4 Substrate Felodipine for Drug–Drug Interaction Modeling. *Pharmaceutics*, 14(7):1474, jul 2022.

[31] Human Metabolome Database. Metabocard for Felodipine (HMDB0015158). URL https://hmdb.ca/metabolites/HMDB0015158.

[32] C. G. Regårdh, B. Edgar, R. Olsson, M. Kendall, P. Collste, and C. Shansky. Pharmacokinetics of felodipine in patients with liver disease. *European journal of clinical pharmacology*, 36(5):473–9, 1989.

[33] K. Felle, B. Persson, and J. Vessman. Dissolution test for felodipine tablets using chemical oxidation in situ to maintain 'sink conditions'. *Journal of Pharmaceutical and Biomedical Analysis*, 2(3/4):527–536, jan 1984.

[34] DRUGBANK online - Felodipine, 2022. URL https://go.drugbank.com/drugs/DB01023.

[35] J. Takano, K. Maeda, M. B. Bolger, and Y. Sugiyama. The Prediction of the Relative Importance of CYP3A/P-glycoprotein to the Nonlinear Intestinal Absorption of Drugs by Advanced Compartmental Absorption and Transit Model. *Drug metabolism and disposition: the biological fate of chemicals*, 44(11):1808–1818, 2016.

[36] R. van der Lee, M. Pfaffendorf, R. P. Koopmans, J. J. van Lieshout, G. A. van Montfrans, and P. A. van Zwieten. Comparison of the time courses and potencies of the vasodilator effects of nifedipine and felodipine in the human forearm. *Blood pressure*, 10(4):217–22, 2001.

[37] P. Berben, J. Brouwers, and P. Augustijns. Assessment of Passive Intestinal Permeability Using an Artificial Membrane Insert System. *Journal of pharmaceutical sciences*, 107 (1):250–256, 2018.

[38] R. L. Walsky and R. S. Obach. Validated assays for human cytochrome P450 activities. *Drug metabolism and disposition: the biological fate of chemicals*, 32(6):647–60, jun 2004.

[39] A. Galetin, S. E. Clarke, and J. B. Houston. Quinidine and haloperidol as modifiers of CYP3A4 activity: multisite kinetic model approach. *Drug metabolism and disposition: the biological fate of chemicals*, 30(12):1512–22, dec 2002.

[40] R. Kawai, M. Lemaire, J. L. Steimer, A. Bruelisauer, W. Niederberger, and M. Rowland. Physiologically based pharmacokinetic study on a cyclosporin derivative, SDZ IMM 125. *Journal of pharmacokinetics and biopharmaceutics*, 22(5):327–65, oct 1994.

[41] Chemaxon. Chemicalize - Dehydrofelodipine, 2022. URL https://chemicalize.com/welcome.

[42] W. Schmitt. General approach for the calculation of tissue to plasma partition coefficients. *Toxicology in vitro : an international journal published in association with BIBRA*, 22(2): 457–67, mar 2008.

[43] D. G. Bailey, J. M. Arnold, C. Munoz, and J. D. Spence. Grapefruit juice-felodipine interaction: mechanism, predictability, and effect of naringin. *Clinical pharmacology and therapeutics*, 53(6):637–42, jun 1993.

[44] D. G. Bailey, J. M. Arnold, J. R. Bend, L. T. Tran, and J. D. Spence. Grapefruit juice-felodipine interaction: reproducibility and characterization with the extended release drug formulation. *British journal of clinical pharmacology*, 40(2):135–40, aug 1995.

[45] D. G. Bailey, J. R. Bend, J. M. Arnold, L. T. Tran, and J. D. Spence. Erythromycin-felodipine interaction: magnitude, mechanism, and comparison with grapefruit juice. *Clinical pharmacology and therapeutics*, 60(1):25–33, jul 1996.

[46] D. G. Bailey, G. K. Dresser, and J. R. Bend. Bergamottin, lime juice, and red wine as inhibitors of cytochrome P450 3A4 activity: comparison with grapefruit juice. *Clinical pharmacology and therapeutics*, 73(6):529–37, jun 2003.

[47] G. K. Dresser, D. G. Bailey, and S. G. Carruthers. Grapefruit juice-felodipine interaction in the elderly. *Clinical pharmacology and therapeutics*, 68(1):28–34, jul 2000.

[48] G. K. Dresser, B. L. Urquhart, J. Proniuk, A. Tieu, D. J. Freeman, J. M. Arnold, and D. G. Bailey. Coffee inhibition of CYP3A4 in vitro was not translated to a grapefruit-like pharmacokinetic interaction clinically. *Pharmacology research & perspectives*, 5(5):1–9, 2017.

[49] B. Edgar, D. Bailey, R. Bergstrand, G. Johnsson, and C. G. Regårdh. Acute effects of drinking grapefruit juice on the pharmacokinetics and dynamics of felodipine-and its potential clinical relevance. *European journal of clinical pharmacology*, 42(3):313–7, 1992.

[50] K. S. Lown, D. G. Bailey, R. J. Fontana, S. K. Janardan, C. H. Adair, L. A. Fortlage, M. B. Brown, W. Guo, and P. B. Watkins. Grapefruit juice increases felodipine oral availability in humans by decreasing intestinal CYP3A protein expression. *The Journal of clinical investigation*, 99(10):2545–53, may 1997.

[51] J. Lundahl, C. G. Regårdh, B. Edgar, and G. Johnsson. Relationship between time of intake of grapefruit juice and its effect on pharmacokinetics and pharmacodynamics of felodipine in healthy subjects. *European journal of clinical pharmacology*, 49(1-2):61–7, 1995.

[52] J. Lundahl, C. G. Regårdh, B. Edgar, and G. Johnsson. Effects of grapefruit juice ingestion–pharmacokinetics and haemodynamics of intravenously and orally administered felodipine in healthy men. *European journal of clinical pharmacology*, 52(2): 139–45, 1997.

[53] J. U. Lundahl, C. G. Regårdh, B. Edgar, and G. Johnsson. The interaction effect of grapefruit juice is maximal after the first glass. *European journal of clinical pharmacology*, 54(1):75–81, mar 1998.

[54] E. J. Guest, L. Aarons, J. B. Houston, A. Rostami-Hodjegan, and A. Galetin. Critique of the two-fold measure of prediction success for ratios: application for the assessment of drug-drug interactions. *Drug metabolism and disposition: the biological fate of chemicals*, 39(2):170–3, feb 2011.

[55] N. Hanke, S. Frechen, D. Moj, H. Britz, T. Eissing, T. Wendl, and T. Lehr. PBPK models for CYP3A4 and P-gp DDI prediction: A modeling network of rifampicin, itraconazole, clarithromycin, midazolam, alfentanil, and digoxin. *CPT: Pharmacometrics & Systems Pharmacology*, 7(10):647–659, oct 2018.

[56] D. S. Wishart, C. Knox, A. C. Guo, S. Shrivastava, M. Hassanali, P. Stothard, Z. Chang, and J. Woolsey. DrugBank: a comprehensive resource for in silico drug discovery and exploration. *Nucleic Acids Research*, 34(Supplement 1):D668–D672, 01 2006.

[57] A. Walser, L. E. Benjamin, T. Flynn, C. Mason, R. Schwartz, and R. I. Fryer. Quinazolines and 1,4-benzodiazepines. 84. Synthesis and reactions of imidazo[1,5-a][1,4]benzodiazepines. *The Journal of Organic Chemistry*, 43(5):936–944, mar 1978.

[58] A. T. Heikkinen, G. Baneyx, A. Caruso, and N. Parrott. Application of PBPK modeling to predict human intestinal metabolism of CYP3A substrates – an evaluation and case study using GastroPlus® . *European Journal of Pharmaceutical Sciences*, 47(2):375–386, 2012.

[59] M. Vossen, M. Sevestre, C. Niederalt, I.-J. Jang, S. Willmann, and A. N. Edginton. Dynamically simulating the interaction of midazolam and the CYP3A4 inhibitor itraconazole using individual coupled whole-body physiologically-based pharmacokinetic (WB-PBPK) models. *Theoretical Biology and Medical Modelling*, 4(1):13, 2007.

[60] F. Lemaitre, N. Hasni, P. Leprince, E. Corvol, G. Belhabib, P. Fillâtre, C.-E. Luyt, C. Leven, R. Farinotti, C. Fernandez, and A. Combes. Propofol, midazolam, vancomycin and cyclosporine therapeutic drug monitoring in extracorporeal membrane oxygenation circuits primed with whole human blood. *Critical Care*, 19(1):40, 2015.

[61] S. Björkman, D. Wada, B. Berling, and G. Benoni. Prediction of the disposition of midazolam in surgical patients by a physiologically based pharmacokinetic model. *Journal of Pharmaceutical Sciences*, 90(9):1226–1241, sep 2001.

[62] K. C. Patki, L. L. von Moltke, and D. J. Greenblatt. In vitro metabolism of midazolam, triazolam, nifedipine, and testosterone by human liver microsomes and recombinant cytochromes P450: role of CYP3A4 and CYP3A5. *Drug Metabolism and Disposition*, 31(7): 938–944, 2003.

[63] T. Rodgers and M. Rowland. Physiologically based pharmacokinetic modelling 2: predicting the tissue distribution of acids, very weak bases, neutrals and zwitterions. *Journal of pharmaceutical sciences*, 95(6):1238–57, jun 2006.

[64] K. S. Abdlekawy, A. M. Donia, and F. Elbarbry. Effects of Grapefruit and Pomegranate Juices on the Pharmacokinetic Properties of Dapoxetine and Midazolam in Healthy Subjects. *European journal of drug metabolism and pharmacokinetics*, 42(3):397–405, jun 2017.

[65] D. Farkas, L. E. Oleson, Y. Zhao, J. S. Harmatz, M. A. Zinny, M. H. Court, and D. J. Greenblatt. Pomegranate juice does not impair clearance of oral or intravenous midazolam, a probe for cytochrome P450-3A activity: comparison with grapefruit juice. *Journal of clinical pharmacology*, 47(3):286–94, mar 2007.

[66] H. H. Kupferschmidt, H. R. Ha, W. H. Ziegler, P. J. Meier, and S. Krähenbühl. Interaction between grapefruit juice and midazolam in humans. *Clinical pharmacology and therapeutics*, 58(1):20–8, jul 1995.

[67] S. Tanaka, S. Uchida, S. Miyakawa, N. Inui, K. Takeuchi, H. Watanabe, and N. Namiki. Comparison of inhibitory duration of grapefruit juice on organic anion-transporting polypeptide and cytochrome P450 3A4. *Biological & pharmaceutical bulletin*, 36(12):1936–41, 2013.

[68] M. L. Veronese, L. P. Gillen, J. P. Burke, E. P. Dorval, W. W. Hauck, E. Pequignot, S. A. Waldman, and H. E. Greenberg. Exposure-dependent inhibition of intestinal and hepatic CYP3A4 in vivo by grapefruit juice. *Journal of clinical pharmacology*, 43(8):831–9, aug 2003.

[69] E. D. Kharasch, A. Walker, C. Hoffer, and P. Sheffels. Intravenous and oral alfentanil as in vivo probes for hepatic and first-pass cytochrome P450 3A activity: noninvasive assessment by use of pupillary miosis. *Clinical pharmacology and therapeutics*, 76(5): 452–66, nov 2004.

[70] S. Frechen and A. Dallmann. Building and evaluation of a PBPK model for alprazolam in healthy adults, 2020. URL https://github.com/Open-Systems-Pharmacology/OSP-PBPK-Model-Library/blob/v11.0/Alprazolam/Alprazolam_evaluation_report.pdf. accessed: 13 Nov 2022.

[71] Drugbank. Alprazolam, 2020. URL https://go.drugbank.com/drugs/DB00404. accessed: 14 Dec 2020.

[72] S. G. Machatha and S. H. Yalkowsky. Estimation of the ethanol/water solubility profile from the octanol/water partition coefficient. *International Journal of Pharmaceutics*, 286 (1-2):111–115, nov 2004.

[73] T. Loftsson and D. Hreinsdôttir. Determination of aqueous solubility by heating and equilibration: A technical note. *AAPS PharmSciTech*, 7(1):E29–E32, mar 2006.

[74] F. S. Eberts, Y. Philopoulos, L. M. Reineke, and R. W. Vliek. Disposition of 14-C-alprazolam, a new anxiolytic-antidepressant, in man. *Pharmacologist*, 22(3):279, 1980.

[75] V. D. Schmith, B. Piraino, R. B. Smith, and P. D. Kroboth. Alprazolam in end-stage renal disease: I. Pharmacokinetics. *The Journal of Clinical Pharmacology*, 31(6):571–579, jun 1991.

[76] H. R. Ochs, D. J. Greenblatt, L. Labedzki, and R. B. Smith. Alprazolam kinetics in patients with renal insufficiency. *Journal of clinical psychopharmacology*, 6(5):292–294, 1986.

[77] M. Cho, T. Scahill, and J. Hester. Kinetics and equilibrium of the reversible alprazolam ring-opening reaction. *Journal of Pharmaceutical Sciences*, 72(4):356–362, apr 1983.

[78] G. G. Raymond and J. L. Born. An updated pKa listing of medicinal compounds. *Drug Intelligence & Clinical Pharmacy*, 20(9):683–686, sep 1986.

[79] K. R. Manchester, P. D. Maskell, and L. Waters. Experimental versus theoretical log D7.4, pKa and plasma protein binding values for benzodiazepines appearing as new psychoactive substances. *Drug Testing and Analysis*, 10(8):1258–1269, 2018.

[80] N. Hirota, K. Ito, T. Iwatsubo, C. E. Green, C. A. Tyson, N. Shimada, H. Suzuki, and Y. Sugiyama. In Vitro/in Vivo scaling of alprazolam metabolism by CYP3A4 and CYP3A5 in humans. *Biopharmaceutics & Drug Disposition*, 22(2):53–71, mar 2001.

[81] N. Yasui, T. Kondo, H. Furukori, S. Kaneko, T. Ohkubo, T. Uno, T. Osanai, K. Sugawara, and K. Otani. Effects of repeated ingestion of grapefruit juice on the single and multiple oral-dose pharmacokinetics and pharmacodynamics of alprazolam. *Psychopharmacology*, 150(2):185–90, jun 2000.

[82] Drugbank. Alfentanil, 2020. URL https://go.drugbank.com/drugs/DB00802. accessed: 14 Dec 2020.

[83] G. Baneyx, N. Parrott, C. Meille, A. Iliadis, and T. Lavé. Physiologically based pharmacokinetic modeling of CYP3A4 induction by rifampicin in human: influence of time between substrate and inducer administration. *European journal of pharmaceutical sciences: official journal of the European Federation for Pharmaceutical Sciences*, 56:1–15, 2014.

[84] R. Jansson, U. Bredberg, and M. Ashton. Prediction of drug tissue to plasma concentration ratios using a measured volume of distribution in combination with lipophilicity. *Journal of Pharmaceutical Sciences*, 97(6):2324–2339, jun 2008.

[85] A. N. Edginton and S. Willmann. Physiology-based simulations of a pathological condition. *Clinical Pharmacokinetics*, 47(11):743–752, 2008.

[86] L. M. Almond, S. Mukadam, I. Gardner, K. Okialda, S. Wong, O. Hatley, S. Tay, K. Rowland-Yeo, M. Jamei, A. Rostami-Hodjegan, and J. R. Kenny. Prediction of drug-drug interactions arising from CYP3A induction using a physiologically based dynamic model. *Drug metabolism and disposition: the biological fate of chemicals*, 44(6):821–32, 2016.

[87] E. D. Kharasch, S. Vangveravong, N. Buck, A. London, T. Kim, J. Blood, and R. H. Mach. Concurrent assessment of hepatic and intestinal cytochrome P450 3A activities using deuterated alfentanil. *Clinical pharmacology and therapeutics*, 89(4):562–70, apr 2011.

[88] S. Frechen, A. Dallmann, and J. Solodenko. Building and evaluation of a PBPK model for triazolam in healthy adults, 2020. URL https://github.com/Open-Systems-Pharmacology/OSP-PBPK-Model-Library/blob/master/Triazolam/Triazolam_evaluation_report.pdf. accessed: 01 Dec 2022.

[89] DRUGBANK online - Triazolam., 2022. URL https://go.drugbank.com/drugs/DB00897.

[90] D. J. Greenblatt, R. M. Arendt, D. R. Abernethy, H. G. Giles, E. M. Sellers, and R. I. Shader. *British journal of anaesthesia*, (10), oct .

[91] R. Jochemsen, J. G. Wesselman, C. J. van Boxtel, J. Hermans, and D. D. Breimer. Comparative pharmacokinetics of brotizolam and triazolam in healthy subjects. *British journal of clinical pharmacology*, 16 Suppl 2(Suppl 2):291S–297S, 1983.

[92] F. S. Eberts, Y. Philopoulos, L. M. Reineke, and R. W. Vliek. Triazolam disposition. *Clinical pharmacology and therapeutics*, 29(1):81–93, jan 1981.

[93] H. Friedman, D. J. Greenblatt, E. S. Burstein, J. M. Scavone, J. S. Harmatz, and R. I. Shader. Triazolam kinetics: interaction with cimetidine, propranolol, and the combination. *Journal of clinical pharmacology*, 28(3):228–33, mar 1988.

[94] H. R. Ochs, D. J. Greenblatt, and E. S. Burstein. Lack of influence of cigarette smoking on triazolam pharmacokinetics. *British journal of clinical pharmacology*, 23(6):759–63, jun 1987.

[95] D. J. Greenblatt, M. Divoll, D. R. Abernethy, L. J. Moschitto, R. B. Smith, and R. I. Shader. Reduced clearance of triazolam in old age: relation to antipyrine oxidizing capacity. *British journal of clinical pharmacology*, 15(3):303–9, mar 1983.

[96] M. Konishi, K. Hirai, and Y. Mori. Kinetics and mechanism of the equilibrium reaction of triazolam in aqueous solution. *Journal of pharmaceutical sciences*, 71(12):1328–34, dec 1982.

[97] L. L. von Moltke, D. J. Greenblatt, J. S. Harmatz, S. X. Duan, L. M. Harrel, M. M. Cotreau-Bibbo, G. A. Pritchard, C. E. Wright, and R. I. Shader. Triazolam biotransformation by human liver microsomes in vitro: effects of metabolic inhibitors and clinical confirmation of a predicted interaction with ketoconazole. *The Journal of pharmacology and experimental therapeutics*, 276(2):370–9, feb 1996.

[98] K. E. Culm-Merdek, L. L. von Moltke, L. Gan, K. A. Horan, R. Reynolds, J. S. Harmatz, M. H. Court, and D. J. Greenblatt. Effect of extended exposure to grapefruit juice on cytochrome P450 3A activity in humans: comparison with ritonavir. *Clinical pharmacology and therapeutics*, 79(3):243–54, mar 2006.

[99] S. K. Hukkinen, A. Varhe, K. T. Olkkola, and P. J. Neuvonen. Plasma concentrations of triazolam are increased by concomitant ingestion of grapefruit juice. *Clinical pharmacology and therapeutics*, 58(2):127–31, aug 1995.

[100] J. J. Lilja, K. T. Kivistö, J. T. Backman, and P. J. Neuvonen. Effect of grapefruit juice dose on grapefruit juice-triazolam interaction: repeated consumption prolongs triazolam half-life. *European journal of clinical pharmacology*, 56(5):411–5, aug 2000.

[101] K.-i. Sugimoto, N. Araki, M. Ohmori, K.-i. Harada, Y. Cui, S. Tsuruoka, A. Kawaguchi, and A. Fujimura. Interaction between grapefruit juice and hypnotic drugs: comparison of triazolam and quazepam. *European journal of clinical pharmacology*, 62(3):209–15, mar 2006.

[102] N. Hanke, S. Frechen, D. Moj, H. Britz, T. Eissing, T. Wendl, and T. Lehr. PBPK models for CYP3A4 and P-gp DDI prediction: a modeling network of rifampicin, itraconazole, clarithromycin, midazolam, alfentanil and digoxin. *CPT: pharmacometrics & systems pharmacology*, page Supplementary document, aug 2018.

[103] J. Heykants, A. Van Peer, V. Van de Velde, P. Van Rooy, W. Meuldermans, K. Lavrijsen, R. Woestenborghs, J. Van Cutsem, and G. Cauwenbergh. The clinical pharmacokinetics of itraconazole: an overview. *Mycoses*, 32 Suppl 1:67–87, 1989.

[104] I. E. Templeton, K. E. Thummel, E. D. Kharasch, K. L. Kunze, C. Hoffer, W. L. Nelson, and N. Isoherranen. Contribution of itraconazole metabolites to inhibition of CYP3A4 in vivo. *Clinical pharmacology and therapeutics*, 83(1):77–85, jan 2008.

[105] K. Riccardi, S. Cawley, P. D. Yates, C. Chang, C. Funk, M. Niosi, J. Lin, and L. Di. Plasma Protein Binding of Challenging Compounds. *Journal of pharmaceutical sciences*, 104(8): 2627–36, aug 2015.

[106] M. Ishigam, M. Uchiyama, T. Kondo, H. Iwabuchi, S. I. Inoue, W. Takasaki, T. Ikeda, T. Komai, K. Ito, and Y. Sugiyama. Inhibition of in vitro metabolism of simvastatin by itraconazole in humans and prediction of in vivo drug-drug interactions. *Pharmaceutical Research*, 18(5):622–631, 2001.

[107] N. Isoherranen, K. L. Kunze, K. E. Allen, W. L. Nelson, and K. E. Thummel. Role of itraconazole metabolites in CYP3A4 inhibition. *Drug metabolism and disposition: the biological fate of chemicals*, 32(10):1121–31, oct 2004.

[108] National Center for Biotechnology Information (NCBI). Hydroxy-itraconazole - PubChem Identifier: CID 108222. PubChem Database., . URL https://pubchem.ncbi.nlm.nih.gov/compound/108222.

[109] National Center for Biotechnology Information (NCBI). Keto-itraconazole - PubChem Identifier: CID 45039625. PubChem Database., . URL https://pubchem.ncbi.nlm.nih.gov/compound/45039625.

[110] N. C. f. B. I. (NCBI). N-Desalkyl-itraconazole - PubChem Identifier: CID 53789808. PubChem Database. URL https://pubchem.ncbi.nlm.nih.gov/compound/53789808.

[111] P. O. Gubbins, S. A. McConnell, B. J. Gurley, T. K. Fincher, A. M. Franks, D. K. Williams, S. R. Penzak, and M. Saccente. Influence of grapefruit juice on the systemic availability of itraconazole oral solution in healthy adult volunteers. *Pharmacotherapy*, 24(4):460–7, apr 2004.

[112] S. R. Penzak, P. O. Gubbins, B. J. Gurley, P. L. Wang, and M. Saccente. Grapefruit juice decreases the systemic availability of itraconazole capsules in healthy volunteers. *Therapeutic drug monitoring*, 21(3):304–9, jun 1999.

[113] S. Frechen and A. Dallmann. Building and evaluation of a PBPK model for erythromycin in healthy adults, 2020. URL https://github.com/Open-Systems-Pharmacology/OSP-PBPK-Model-Library/blob/866528e2443c3f535f9d09628c78ff2ecdcbd4b5/Erythromycin/Erythromycin_evaluation_report.md. accessed: 13 Nov 2022.

[114] Drugbank. Erythromycin, 2020. URL https://go.drugbank.com/drugs/DB00199. accessed: 14 Dec 2020.

[115] E. Lien, J. Kuwahara, and R. Koda. Diffusion of drugs into prostatic fluid and milk. *Drug intelligence & Clinical Pharmacy*, 8(8):470–475, 1974.

[116] J. O. Capobianco and R. C. Goldman. Macrolide transport in Escherichia coli strains having normal and altered OmpC and/or OmpF porins. *International journal of antimicrobial agents*, 4(3):183–9, 1994.

[117] J. W. McFarland, C. M. Berger, S. A. Froshauer, S. F. Hayashi, S. J. Hecker, B. H. Jaynes, M. R. Jefson, B. J. Kamicker, C. A. Lipinski, K. M. Lundy, C. P. Reese, and C. B. Vu. Quantitative structure-activity relationships among macrolide antibacterial agents: In vitro and in vivo potency against Pasteurella multocida. *Journal of Medicinal Chemistry*, 40 (9):1340–1346, 1997.

[118] C. Hoffhine. Aqueous soluble salts of erythromycin. Issues September 4. Nr. 2,761,859, 1956. URL https://patents.google.com/patent/US2761859A/en. accessed: 14 Dec 2020.

[119] P. H. Jones, E. K. Rowley, A. L. Weiss, D. L. Bishop, and A. H. Chun. Insoluble erythromycin salts. *Journal of Pharmaceutical Sciences*, 58(3):337–339, 1969.

[120] P. K. Manna and S. K. Basu. Preparation and evaluation of erythromycin fumarate - A new derivative of erythromycin. *Drug Development and Industrial Pharmacy*, 24(9): 879–882, 1998.

[121] H. Sun, L. A. Frassetto, Y. Huang, and L. Z. Benet. Hepatic clearance, but not gut availability, of erythromycin is altered in patients with end-stage renal disease. *Clinical Pharmacology & Therapeutics*, 87(4):465–472, 2010.

[122] A. Iliopoulou, M. Aldhous, A. Johnston, and P. Turner. Pharmacokinetic interaction between theophylline and erythromycin. *British Journal of Clinical Pharmacology*, 14 (4):495–499, 1982.

[123] J. Barre, A. Mallat, J. Rosenbaum, L. Deforges, G. Houin, D. Dhumeaux, and J. Tillement. Pharmacokinetics of erythromycin in patients with severe cirrhosis. Respective influence of decreased serum binding and impaired liver metabolic capacity. *British Journal of Clinical Pharmacology*, 23(6):753–757, 1987.

[124] L. Xu, Y. Chen, Y. Pan, G. L. Skiles, and M. Shou. Prediction of human drug-drug interactions from time-dependent inactivation of CYP3A4 in primary hepatocytes using a population-based simulator. *Drug Metabolism and Disposition*, 37(12):2330–2339, 2009.

[125] R. W. Wang, D. J. Newton, T. D. Scheri, and A. Y. Lu. Human cytochrome P450 3A4-catalyzed testosterone 6 beta-hydroxylation and erythromycin N-demethylation. Competition during catalysis. *Drug metabolism and disposition: the biological fate of chemicals*, 25(4):502–7, 1997.

[126] R. J. Riley and D. Howbrook. In vitro analysis of the activity of the major human hepatic CYP enzyme (CYP3A4) using [N-methyl-14C]-erythromycin. *Journal of Pharmacological and Toxicological Methods*, 38(4):189–193, dec 1997.

[127] C. S. Lancaster, G. H. Bruun, C. J. Peer, T. S. Mikkelsen, T. J. Corydon, A. A. Gibson, S. Hu, S. J. Orwick, R. H. J. Mathijssen, W. D. Figg, S. D. Baker, and A. Sparreboom. OATP1B1 polymorphism as a determinant of erythromycin disposition. *Clinical Pharmacology & Therapeutics*, 92(5):642–650, nov 2012.

[128] T. Akiyoshi, M. Ito, S. Murase, M. Miyazaki, F. P. Guengerich, K. Nakamura, K. Yamamoto, and H. Ohtani. Mechanism-based inhibition profiles of erythromycin and clarithromycin with cytochrome P450 3A4 genetic variants. *Drug metabolism and pharmacokinetics*, 28 (5):411–5, 2013.

[129] A. Atkinson, J. R. Kenny, and K. Grime. Automated assessment of time-dependent inhibition of human cytochrome P450 enzymes using liquid chromatography-tandem mass spectrometry analysis. *Drug Metabolism and Disposition*, 33(11):1637–1647, nov 2005.

[130] S. Aueviriyavit, K. Kobayashi, and K. Chiba. Species differences in mechanism-based inactivation of CYP3A in humans, rats and mice. *Drug Metabolism and Pharmacokinetics*, 25(1):93–100, 2010.

[131] W. K. Chan and A. B. Delucchi. Resveratrol, a red wine constituent, is a mechanism-based inactivator of cytochrome P450 3A4. *Life Sciences*, 67(25):3103–3112, nov 2000.

[132] Y. Chen, L. Liu, M. Monshouwer, and A. J. Fretland. Determination of time-dependent inactivation of CYP3A4 in cryopreserved human hepatocytes and assessment of human drug-drug interactions. *Drug Metabolism and Disposition*, 39(11):2085–2092, nov 2011.

[133] Y. Ishikawa, T. Akiyoshi, A. Imaoka, and H. Ohtani. Inactivation kinetics and residual activity of CYP3A4 after treatment with erythromycin. *Biopharmaceutics & Drug Disposition*, 38(7):420–425, 2017.

[134] S. Kanamitsu, I. K, G. CE, C. Tyson, N. Shimada, and Y. Sugiyama. Prediction of in vivo interaction between triazolam and erythromycin based on in vitro studies using human liver microsomes and recombinant human CYP3A4. *Pharmaceutical Research*, 17(4): 419–426, 2000.

[135] K. Kozakai, Y. Yamada, M. Oshikata, T. Kawase, E. Suzuki, Y. Haramaki, and H. Taniguchi. Cocktail-substrate approach-based high-throughput assay for evaluation of direct and time-dependent inhibition of multiple cytochrome P450 isoforms. *Drug Metabolism and Pharmacokinetics*, 29(2):198–207, 2014.

[136] J. Mao, S. Tay, C. S. Khojasteh, Y. Chen, C. E. C. A. Hop, and J. R. Kenny. Evaluation of time dependent inhibition assays for marketed oncology drugs: Comparison of human hepatocytes and liver microsomes in the presence and absence of human plasma. *Pharmaceutical Research*, 33(5):1204–1219, 2016.

[137] D. J. McConn, Y. S. Lin, K. Allen, K. L. Kunze, and K. E. Thummel. Differences in the inhibition of cytochromes P450 3A4 and 3A5 by metabolite-inhibitor complex-forming drugs. *Drug Metabolism and Disposition*, 32(10):1083–1091, 2004.

[138] X. Zhang, D. R. Jones, and S. D. Hall. Prediction of the effect of erythromycin, diltiazem, and their metabolites, alone and in combination, on CYP3A4 inhibition. *Drug Metabolism and Disposition*, 37(1):150–160, 2009.

[139] S. Kanazawa, T. Ohkubo, and K. Sugawara. The effects of grapefruit juice on the pharmacokinetics of erythromycin. *European journal of clinical pharmacology*, 56(11):799–803, 2001.

[140] L. M. Fuhr, F. Z. Marok, N. Hanke, D. Selzer, and T. Lehr. Pharmacokinetics of the CYP3A4 and CYP2B6 Inducer Carbamazepine and Its Drug-Drug Interaction Potential: A Physiologically Based Pharmacokinetic Modeling Approach. *Pharmaceutics*, 13(2): 1–21, feb 2021.

[141] A. G. Staines, M. W. Coughtrie, and B. Burchell. N-glucuronidation of carbamazepine in human tissues is mediated by UGT2B7. *Journal of Pharmacology and Experimental Therapeutics*, 311(3):1131–1137, 2004.

[142] B. Achour, M. R. Russell, J. Barber, and A. Rostami-Hodjegan. Simultaneous quantification of the abundance of several cytochrome P450 and uridine 5-diphosphoglucuronosyltransferase enzymes in human liver microsomes using multiplexed targeted proteomics. *Drug Metabolism and Disposition*, 42(4):500–510, 2014.

[143] Drugbank. Carbamazepine, 2018. URL https://www.drugbank.ca/drugs/DB00564. accessed: 14 Dec 2020.

[144] R. P. Austin, P. Barton, S. L. Cockroft, M. C. Wenlock, and R. J. Riley. The influence of nonspecific microsomal binding on apparent intrinsic clearance, and its prediction from physicochemical properties. *Drug Metabolism and Disposition*, 30(12):1497–1503, 2002.

[145] A. Avdeef. *Absorption and drug development - Solubility, permeability, and charge state*. 2003. ISBN 3175723993.

[146] P. Annaert, Z. Ye, B. Stieger, and P. Augustijns. Interaction of HIV protease inhibitors with OATP1B1, 1B3, and 2B1. *Xenobiotica*, 40(3):163–176, 2010.

[147] S. Clarysse, J. Brouwers, J. Tack, P. Annaert, and P. Augustijns. Intestinal drug solubility estimation based on simulated intestinal fluids: Comparison with solubility in human intestinal fluids. *European Journal of Pharmaceutical Sciences*, 43(4):260–269, 2011.

[148] T. Heikkilä, M. Karjalainen, K. Ojala, K. Partola, F. Lammert, P. Augustijns, A. Urtti, M. Yliperttula, L. Peltonen, and J. Hirvonen. Equilibrium drug solubility measurements in 96-well plates reveal similar drug solubilities in phosphate buffer pH 6.8 and human intestinal fluid. *International Journal of Pharmaceutics*, 405(1-2):132–136, 2011.

[149] E. Söderlind, E. Karlsson, A. Carlsson, R. Kong, A. Lenz, S. Lindborg, and J. J. Sheng. Simulating fasted human intestinal fluids: understanding the roles of lecithin and bile acids. *Molecular pharmaceutics*, 7(5):1498–507, oct 2010.

[150] Heumann Pharma GmbH & Co. Generica KG. Fachinformation - Carbamazepin 200/400 Heumann, 2014. URL https://www.fachinfo.de/suche/fi/006667. accessed: 11 Nov 2020.

[151] Novartis. Tegretol ® label, 2009. URL https://www.accessdata.fda.gov/drugsatfda_docs/label/2009/016608s101,018281s048lbl.pdf. accessed: 14 Dec 2020.

[152] S. Pynnönen. The Pharmacokinetics of Carbamazepine in Plasma and Saliva of Man. *Acta Pharmacologica et Toxicologica*, 41(5):465–471, 1977.

[153] L. Bertilsson. Clinical pharmacokinetics of carbamazepine. *Clinical Pharmacokinetics*, 3:128–1473, 1978.

[154] B. M. Kerr, K. E. Thummel, C. J. Wurden, S. M. Klein, D. L. Kroetz, F. J. Gonzalez, and R. H. Levy. Human liver carbamazepine metabolism. Role of CYP3A4 and CYP2C8 in 10,11-epoxide formation. *Biochemical pharmacology*, 47(11):1969–79, jun 1994.

[155] J. Henshall, A. Galetin, A. Harrison, and J. B. Houston. Comparative analysis of CYP3A heteroactivation by steroid hormones and flavonoids in different in vitro systems and potential in vivo implications. *Drug Metabolism and Disposition*, 36(7):1332–1340, 2008.

[156] N. Cazali, A. Tran, J. M. Treluyer, E. Rey, P. Athis, J. Vincent, and G. Pons. Inhibitory effect of stiripentol on carbamazepine and saquinavir metabolism in human. *British Journal of Clinical Pharmacology*, 56(5):526, 2003.

[157] W. Huang, Y. S. Lin, D. J. McConn, J. C. Calamia, R. A. Totah, N. Isoherranen, M. Glodowski, and K. E. Thummel. Evidence of significant contribution from CYP3A5 to hepatic drug metabolism. *Drug Metabolism and Disposition*, 32(12):1434–1445, 2004.

[158] R. E. Pearce, G. R. Vakkalagadda, and J. Steven Leeder. Pathways of carbamazepine bioactivation in vitro I. Characterization of human cytochromes P450 responsible for the formation of 2- and 3-hydroxylated metabolites. *Drug Metabolism and Disposition*, 30 (11):1170–1179, 2002.

[159] M. Shou, M. Hayashi, Y. Pan, Y. Xu, K. Morrissey, L. Xu, and G. L. Skiles. Modeling, prediction, and in vitro in vivo correlation of CYP3A4 induction. *Drug metabolism and disposition: the biological fate of chemicals*, 36(11):2355–70, 2008.

[160] D. F. McGinnity, G. Zhang, J. R. Kenny, G. A. Hamilton, S. Otmani, K. R. Stams, S. Haney, P. Brassil, D. M. Stresser, and R. J. Riley. Evaluation of multiple in vitro systems for assessment of CYP3A4 induction in drug discovery: human hepatocytes, pregnane X receptor reporter gene, and Fa2N-4 and HepaRG cells. *Drug metabolism and disposition: the biological fate of chemicals*, 37(6):1259–68, jun 2009.

[161] O. A. Fahmi, J. L. Raucy, E. Ponce, S. Hassanali, and J. M. Lasker. Utility of DPX2 cells for predicting CYP3A induction-mediated drug-drug interactions and associated structure-activity relationships. *Drug metabolism and disposition: the biological fate of chemicals*, 40(11):2204–11, nov 2012.

[162] J. G. Zhang, T. Ho, A. L. Callendrello, R. J. Clark, E. A. Santone, S. Kinsman, D. Xiao, L. G. Fox, H. J. Einolf, and D. M. Stresser. Evaluation of calibration curve-based approaches to predict clinical inducers and noninducers of CYP3A4 with plated human hepatocytes. *Drug Metabolism and Disposition*, 42(9):1379–1391, 2014.

[163] A. Moore, P. P. Chothe, H. Tsao, and N. Hariparsad. Evaluation of the interplay between uptake transport and CYP3A4 induction in micropatterned cocultured hepatocytes. *Drug Metabolism and Disposition*, 44(12):1910–1919, 2016.

[164] O. A. Fahmi, M. Kish, S. Boldt, and R. Scott Obach. Cytochrome P450 3A4 mRNA is a more reliable marker than CYP3A4 activity for detecting pregnane X receptor-activated induction of drug-metabolizing enzymes. *Drug Metabolism and Disposition*, 38(9):1605–1611, 2010.

[165] R. Zuo, F. Li, S. Parikh, L. Cao, K. L. Cooper, Y. Hong, J. Liu, R. A. Faris, D. Li, and H. Wang. Evaluation of a novel renewable hepatic cell model for prediction of clinical CYP3A4 induction using a correlation-based relative induction score approach. *Drug Metabolism and Disposition*, 45(2):198–207, 2017.

[166] J. G. Zhang, R. Patel, R. J. Clark, T. Ho, S. K. Trisdale, Y. Fang, and D. M. Stresser. Effect of Fifteen CYP3A4 in vitro Inducers on the Induction of Hepatocytes : A Trend Analysis. Poster presented at: 20th North American ISSX Meeting; 2015 18-22 Oct; Orlando Florida.

[167] O. A. Fahmi, M. Shebley, J. Palamanda, M. W. Sinz, D. Ramsden, H. J. Einolf, L. Chen, and H. Wang. Evaluation of CYP2B6 induction and prediction of clinical drug-drug interactions: Considerations from the IQ consortium induction working group - An industry perspective. *Drug Metabolism and Disposition*, 44(10):1720–1730, 2016.

[168] L. J. Dickmann and N. Isoherranen. Quantitative prediction of CYP2B6 induction by estradiol during pregnancy: Potential explanation for increased methadone clearance during pregnancy. *Drug Metabolism and Disposition*, 41(2):270–274, 2013.

[169] H. Lennernäs. Intestinal permeability and its relevance for absorption and elimination. *Xenobiotica*, 37(10-11):1015–1051, nov 2007.

[170] Drugbank. Metabolite 10,11-Epoxycarbamazepine, 2020. URL https://www.drugbank.ca/metabolites/DBMET00291. accessed: 14 Dec 2020.

[171] P. L. Morselli, M. Gerna, D. de Maio, G. Zanda, F. Viani, and S. Garattini. *Pharmacokinetic studies on carbamazepine in volunteers and in epileptic patients*. Springer Berlin Heidelberg, Berlin, Heidelberg, 1975. ISBN 978-3-642-85923-6. URL http://link.springer.com/10.1007/978-3-642-85921-2.

[172] S. K. Garg, N. Kumar, V. K. Bhargava, and S. K. Prabhakar. Effect of grapefruit juice on carbamazepine bioavailability in patients with epilepsy. *Clinical Pharmacology and Therapeutics*, 64(3):286–288, 1998.

[173] J. Wojtyniak, H. Britz, D. Selzer, M. Schwab, and T. Lehr. Data Digitizing: Accurate and Precise Data Extraction for Quantitative Systems Pharmacology and Physiologically-Based Pharmacokinetic Modeling. *CPT: Pharmacometrics & Systems Pharmacology*, 9 (6):322–331, jun 2020.

[174] N. Tsamandouras, G. Dickinson, Y. Guo, S. Hall, A. Rostami-Hodjegan, A. Galetin, and L. Aarons. Development and application of a mechanistic pharmacokinetic model for simvastatin and its active metabolite simvastatin acid using an integrated population PBPK approach. *Pharmaceutical Research*, 32(6):1864–1883, jun 2015.

[175] H. Lennernäs and G. Fager. Pharmacodynamics and pharmacokinetics of the HMG-CoA reductase inhibitors. *Clinical Pharmacokinetics*, 32(5):403–425, may 1997.

[176] A. H. Rageh, N. N. Atia, and H. M. Abdel-Rahman. Lipophilicity estimation of statins as a decisive physicochemical parameter for their hepato-selectivity using reversed-phase thin layer chromatography. *Journal of Pharmaceutical and Biomedical Analysis*, 142: 7–14, aug 2017.

[177] M. Rao, Y. Mandage, K. Thanki, and S. Bhise. Dissolution improvement of simvastatin by surface solid dispersion technology. *Dissolution Technologies*, 17(2):27–34, 2010.

[178] Merck Canada Inc. Product monograph: Zocor. 2006.

[179] S. Geboers, J. Stappaerts, J. Tack, P. Annaert, and P. Augustijns. In vitro and in vivo investigation of the gastrointestinal behavior of simvastatin. *International Journal of Pharmaceutics*, 510(1):296–303, aug 2016.

[180] M. Gertz, A. Harrison, J. B. Houston, and A. Galetin. Prediction of human intestinal first-pass metabolism of 25 CYP3A substrates from in vitro clearance and permeability data. *Drug Metabolism and Disposition*, 38(7):1147–1158, jul 2010.

[181] S. Vickers, C. A. Duncan, I. W. Chen, A. Rosegay, and D. E. Duggan. Metabolic disposition studies on simvastatin, a cholesterol-lowering prodrug. *Drug Metabolism and Disposition*, 18(2):138–145, 1990.

[182] T. Prueksaritanont, L. M. Gorham, B. Ma, L. Liu, X. Yu, J. J. Zhao, D. E. Slaughter, B. H. Arison, and K. P. Vyas. In vitro metabolism of simvastatin in humans [SBT] identification of metabolizing enzymes and effect of the drug on hepatic P450s. *Drug metabolism and disposition: the biological fate of chemicals*, 25(10):1191–1199, 1997.

[183] N. Le Goff, J. C. Koffel, S. Vandenschrieck, L. Jung, and G. Ubeaud. Comparison of in vitro hepatic models for the prediction of metabolic interaction between simvastatin and naringenin. *European Journal of Drug Metabolism and Pharmacokinetics*, 27(4): 233–241, dec 2002.

[184] H. Lu, J. Zhu, Y. Zang, Y. Ze, and J. Qin. Cloning, high level expression of human paraoxonase-3 in Sf9 cells and pharmacological characterization of its product. *Biochemical Pharmacology*, 70(7):1019–1025, oct 2005.

[185] D. A. Taha, C. H. D. Moor, D. A. Barrett, J. B. Lee, R. D. Gandhi, C. W. Hoo, and P. Gershkovich. The role of acid-base imbalance in statin-induced myotoxicity. *Translational research: the journal of laboratory and clinical medicine,*, 174:140–160, 2016.

[186] A. Á. Lueje, C. Valenzuela, J. A. Squella, and N.-V. Joaquin Luis. Stability study of simvastatin under hydrolytic conditions assessed by liquid chromatography. *Journal of AOAC International*, 88(6):1631–1636, 2005.

[187] T. Prueksaritanont, Y. Qiu, L. Mu, K. Michel, J. Brunner, K. M. Richards, and J. H. Lin. Interconversion pharmacokinetics of simvastatin and its hydroxy acid in dogs: Effects of gemfibrozil. *Pharmaceutical Research*, 22(7):1101–1109, jul 2005.

[188] L. Huang, Y. Wang, and S. Grimm. ATP-dependent transport of rosuvastatin in membrane vesicles expressing brast cancer resistance protein. *Drug Metabolism and Disposition*, 34(5):738–742, may 2006.

[189] J. W. Deng, J.-H. Shon, H.-J. Shin, S.-J. Park, C.-W. Yeo, H.-H. Zhou, I.-S. Song, and J.-G. Shin. Effect of silymarin supplement on the pharmacokinetics of rosuvastatin. *Pharmaceutical Research*, 25(8):1807–1814, aug 2008.

[190] M. Hirano, K. Maeda, S. Matsushima, Y. Nozaki, H. Kusuhara, and Y. Sugiyama. Involvement of BCRP (ABCG2) in the biliary excretion of pitavastatin. *Molecular Pharmacology*, 68(3):800–807, sep 2005.

[191] M. Afrouzian, R. Al-Lahham, S. Patrikeeva, M. Xu, V. Fokina, W. G. Fischer, S. Z. Abdel-Rahman, M. Costantine, M. S. Ahmed, and T. Nanovskaya. Role of the efflux transporters BCRP and MRP1 in human placental bio-disposition of pravastatin. *Biochemical Pharmacology*, 156:467–478, oct 2018.

[192] S. Kitamura, K. Maeda, Y. Wang, and Y. Sugiyama. Involvement of multiple transporters in the hepatobiliary transport of rosuvastatin. *Drug Metabolism and Disposition*, 36(10): 2014–2023, oct 2008.

[193] A. Vildhede, A. Mateus, E. K. Khan, Y. Lai, M. Karlgren, P. Artursson, and M. C. Kjellsson. Mechanistic modeling of pitavastatin disposition in sandwich-cultured human hepatocytes: A proteomics-informed bottom-up approach. *Drug Metabolism and Disposition*, 44(4):505–516, feb 2016.

[194] B. M. VandenBrink, R. S. Foti, D. A. Rock, L. C. Wienkers, and J. L. Wahlstrom. Evaluation of CYP2C8 inhibition in vitro: Utility of montelukast as a selective CYP2C8 probe substrate. *Drug Metabolism and Disposition*, 39(9):1546–1554, sep 2011.

[195] R. S. Foti, D. A. Rock, L. C. Wienkers, and J. L. Wahlstrom. Selection of alternative CYP3A4 probe substrates for clinical drug interaction studies using in vitro data and in vivo simulation. *Drug metabolism and disposition*, 38(6):981–7, jun 2010.

[196] C. S. Cook, L. M. Berry, and E. Burton. Prediction of in vivo drug interactions with eplerenone in man from in vitro metabolic inhibition data. *Xenobiotica*, 34(3):215–228, mar 2004.

[197] M. Ishigami, T. Honda, W. Takasaki, T. Ikeda, T. Komai, K. Ito, and Y. Sugiyama. A comparison of the effects of 3-hydroxy-3-methylglutaryl-coenzyme a (HMG-CoA) reductase inhibitors on the CYP3A4-dependent oxidation of mexazolam in vitro. *Drug metabolism and disposition: the biological fate of chemicals*, 29(3):282–8, mar 2001.

[198] H. Fujino, I. Yamada, S. Shimada, T. Nagao, and M. Yoneda. Metabolic fate of pitavastatin (NK-104), a new inhibitor of 3-hydroxy-3-methyllutaryl coenzyme A reductase. *Arzneimittelforschung*, 52(10):745–753, dec 2011.

[199] M. G. Soars, P. Barton, M. Ismair, R. Jupp, and R. J. Riley. The development, characterization, and application of an OATP1B1 inhibition assay in drug discovery. *Drug Metabolism and Disposition*, 40(8):1641–1648, aug 2012.

[200] C. Chen, R. J. Mireles, S. D. Campbell, J. Lin, J. B. Mills, J. J. Xu, and T. A. Smolarek. Differential interaction of 3-hydroxy-3-methylglutaryl-CoA reductase inhibitors with ABCB1, ABCC2 and OATP1B1. *Drug Metabolism and Disposition*, 33(4):537–546, apr 2005.

[201] E. J. Wang, C. N. Casciano, R. P. Clement, and W. W. Johnson. HMG-CoA reductase inhibitors (statins) characterized as direct inhibitors of P-glycoprotein. *Pharmaceutical Research1*, 18(6):800–806, 2001.

[202] M. Werner, B. Atil, E. Sieczkowski, P. Chiba, and M. Hohenegger. Simvastatin-induced compartmentalisation of doxorubicin sharpens up nuclear topoisomerase II inhibition in human rhabdomyosarcoma cells. *Naunyn-Schmiedeberg's Archives of Pharmacology*, 386(7):605–617, jul 2013.

[203] E.-j. Wang, C. N. Casciano, R. P. Clement, and W. W. Johnson. Active transport of fluorescent P-glycoprotein substrates: Evaluation as markers and interaction with inhibitors. *Biochemical and Biophysical Research Communications*, 289(2):580–585, nov 2001.

[204] H. Sugimoto, S.-I. Matsumoto, M. Tachibana, S.-I. Niwa, H. Hirabayashi, N. Amano, and T. Moriwaki. Establishment of in vitro P-glycoprotein inhibition assay and its exclusion criteria to assess the risk Of drug–drug interaction at the drug discovery stage. *Journal of Pharmaceutical Sciences*, 100(9):4013–4023, sep 2011.

[205] A. Poirier, A.-C. Cascais, U. Bader, R. Portmann, M.-E. Brun, I. Walter, A. Hillebrecht, M. Ullah, and C. Funk. Calibration of in vitro multidrug resistance protein 1 substrate and inhibition assays as a basis to support the prediction of clinically relevant interactions in vivo. *Drug Metabolism and Disposition*, 42(9):1411–1422, sep 2014.

[206] J. P. Keogh and J. R. Kunta. Development, validation and utility of an in vitro technique for assessment of potential clinical drug–drug interactions involving P-glycoprotein. *European Journal of Pharmaceutical Sciences*, 27(5):543–554, apr 2006.

[207] T. Sakaeda, H. Fujino, C. Komoto, M. Kakumoto, J. S. Jin, K. Iwaki, K. Nishiguchi, T. Nakamura, N. Okamura, and K. Okumura. Effects of acid and lactone forms of eight HMG-CoA reductase inhibitors on CYP-mediated metabolism and MDR1-mediated transport. *Pharmaceutical Research*, 23(3):506–512, 2006.

[208] L. M. Berezhkovskiy. Volume of distribution at steady state for a linear pharmacokinetic system with peripheral elimination. *Journal of pharmaceutical sciences*, 93(6):1628–40, jun 2004.

[209] Drugbank. Simvastatin hydroxy acid, 2020. URL https://go.drugbank.com/metabolites/DBMET00388. accessed: 14 Dec 2020.

[210] C. W. Fong. Statins in therapy: Cellular transport, side effects, drug-drug interactions and cytotoxicity -the unrecognized role of lactones. 2016.

[211] M. Yoshinari, K. Matsuzaka, S. Hashimoto, K. Ishihara, T. Inoue, Y. Oda, T. Ide, and T. Tanaka. Controlled release of simvastatin acid using cyclodextrin inclusion system. *Dental Materials Journal*, 26(3):451–456, 2007.

[212] T. Prueksaritanont, B. Ma, and N. Yu. The human hepatic metabolism of simvastatin hydroxy acid is mediated primarily by CYP3A, and not CYP2D6. *British Journal of Clinical Pharmacology*, 56(1):120–124, jul 2003.

[213] A. Tornio, M. K. Pasanen, J. Laitila, P. J. Neuvonen, and J. T. Backman. Comparison of 3-hydroxy-3-methylglutaryl Coenzyme A (HMG-CoA) reductase inhibitors (statins) as inhibitors of cytochrome P450 2C8. *Basic & Clinical Pharmacology & Toxicology*, 97(2):104–108, aug 2005.

[214] T. Prueksaritanont, R. Subramanian, X. Fang, B. Ma, Y. Qiu, J. H. Lin, P. G. Pearson, and T. A. Baillie. Glucuronidation of statins in animals and humans: A novel mechanism of statin lactonization. *Drug Metabolism and Disposition*, 30(5):505–512, may 2002.

[215] H. Huang. *Characterization of in vitro systems for transporter studies*. Phd thesis, Uppsala University, 2010.

[216] H. Schelleman, X. Han, C. M. Brensinger, S. K. Quinney, W. B. Bilker, D. A. Flockhart, L. Li, and S. Hennessy. Pharmacoepidemiologic and in vitro evaluation of potential drug-drug interactions of sulfonylureas with fibrates and statins. *British Journal of Clinical Pharmacology*, 78(3):639–648, sep 2014.

[217] J. J. Lilja, K. T. Kivistö, and P. J. Neuvonen. Grapefruit juice-simvastatin interaction: effect on serum concentrations of simvastatin, simvastatin acid, and HMG-CoA reductase inhibitors. *Clinical pharmacology and therapeutics*, 64(5):477–83, nov 1998.

[218] J. J. Lilja, M. Neuvonen, and P. J. Neuvonen. Effects of regular consumption of grapefruit juice on the pharmacokinetics of simvastatin. *British journal of clinical pharmacology*, 58 (1):56–60, jul 2004.

[219] J. J. Lilja, K. T. Kivistö, and P. J. Neuvonen. Duration of effect of grapefruit juice on the pharmacokinetics of the CYP3A4 substrate simvastatin. *Clinical pharmacology and therapeutics*, 68(4):384–90, oct 2000.

[220] N. Hanke, D. Türk, D. Selzer, S. Wiebe, É. Fernandez, P. Stopfer, V. Nock, and T. Lehr. A Mechanistic, Enantioselective, Physiologically Based Pharmacokinetic Model of Verapamil and Norverapamil, Built and Evaluated for Drug–Drug Interaction Studies. *Pharmaceutics*, 12(6):556, jun 2020.

[221] J. Hasegawa, T. Fujita, Y. Hayashi, K. Iwamoto, and J. Watanabe. pKa determination of verapamil by liquid-liquid partition. *Journal of pharmaceutical sciences*, 73(4):442–5, apr 1984.

[222] H. Vogelpoel, J. Welink, G. L. Amidon, H. E. Junginger, K. K. Midha, H. Möller, M. Olling, V. P. Shah, and D. M. Barends. Biowaiver monographs for immediate release solid oral dosage forms based on biopharmaceutics classification system (BCS) literature data: verapamil hydrochloride, propranolol hydrochloride, and atenolol. *Journal of pharmaceutical sciences*, 93(8):1945–56, aug 2004.

[223] C. Hansch, A. Leo, and D. Hoekman. *Exploring QSAR: hydrophobic, electronic, steric constants*. 1995.

[224] F. Sanaee, J. D. Clements, A. W. G. Waugh, R. N. Fedorak, R. Lewanczuk, and F. Jamali. Drug-disease interaction: Crohn's disease elevates verapamil plasma concentrations but reduces response to the drug proportional to disease activity. *British journal of clinical pharmacology*, 72(5):787–97, nov 2011.

[225] J. Wang, S. Xia, W. Xue, D. Wang, Y. Sai, L. Liu, and X. Liu. A semi-physiologically-based pharmacokinetic model characterizing mechanism-based auto-inhibition to predict stereoselective pharmacokinetics of verapamil and its metabolite norverapamil in human. *European journal of pharmaceutical sciences : official journal of the European Federation for Pharmaceutical Sciences*, 50(3-4):290–302, nov 2013.

[226] Y. Shirasaka, T. Sakane, and S. Yamashita. Effect of P-glycoprotein expression levels on the concentration-dependent permeability of drugs to the cell membrane. *Journal of pharmaceutical sciences*, 97(1):553–65, jan 2008.

[227] S. Döppenschmitt, P. Langguth, C. G. Regårdh, T. B. Andersson, C. Hilgendorf, and H. Spahn-Langguth. Characterization of binding properties to human P-glycoprotein: Development of a [3H]verapamil radioligand-binding assay. *Journal of Pharmacology and Experimental Therapeutics*, 1999.

[228] H. Blume and E. Mutschler. *Bioäquivalenz: Qualitätsbewertung wirkstoffgleicher Fertigarzneimittel: Anleitung, Methoden, Materialien*. Govi-Verlag, 1989.

[229] Sigma-Aldrich Inc. A Case Study in SPE Method Development - Understanding the Dual Interaction Properties of Discovery DSC-SCX SPE Using Verapamil (and Metabolite) from Serum as a Test Example. https://www.sigmaaldrich.com/technical-documents/articles/reporter-eu/a-case-study-in-spe.html, 2013. Accessed: 2020-02-25.

[230] T. S. Tracy, K. R. Korzekwa, F. J. Gonzalez, and I. W. Wainer. Cytochrome P450 isoforms involved in metabolism of the enantiomers of verapamil and norverapamil. *British journal of clinical pharmacology*, 47(5):545–52, may 1999.

[231] C. Pauli-Magnus, O. von Richter, O. Burk, A. Ziegler, T. Mettang, M. Eichelbaum, and M. F. Fromm. Characterization of the major metabolites of verapamil as substrates and inhibitors of P-glycoprotein. *The Journal of pharmacology and experimental therapeutics*, 293(2):376–82, may 2000.

[232] U. Fuhr, H. Müller-Peltzer, R. Kern, P. Lopez-Rojas, M. Jünemann, S. Harder, and A. H. Staib. Effects of grapefruit juice and smoking on verapamil concentrations in steady state. *European journal of clinical pharmacology*, 58(1):45–53, apr 2002.

[233] P. C. Ho, K. Ghose, D. Saville, and S. Wanwimolruk. Effect of grapefruit juice on pharmacokinetics and pharmacodynamics of verapamil enantiomers in healthy volunteers. *European journal of clinical pharmacology*, 56(9-10):693–8, dec 2000.

[234] M. Meyer, S. Schneckener, B. Ludewig, L. Kuepfer, and J. Lippert. Using expression data for quantification of active processes in physiologically based pharmacokinetic modeling. *Drug metabolism and disposition: the biological fate of chemicals*, 40(5):892–901, may 2012.

[235] A. D. Rodrigues. Integrated cytochrome P450 reaction phenotyping: attempting to bridge the gap between cDNA-expressed cytochromes P450 and native human liver microsomes. *Biochemical pharmacology*, 57(5):465–80, 1999.

[236] M. Nishimura, H. Yaguti, H. Yoshitsugu, S. Naito, and T. Satoh. Tissue distribution of mRNA expression of human cytochrome P450 isoforms assessed by high-sensitivity real-time reverse transcription PCR. *Journal of the Pharmaceutical Society of Japan*, 123(5):369–75, may 2003.

[237] K. Rowland Yeo, R. L. Walsky, M. Jamei, A. Rostami-Hodjegan, and G. T. Tucker. Prediction of time-dependent CYP3A4 drug-drug interactions by physiologically based pharmacokinetic modelling: Impact of inactivation parameters and enzyme turnover. *European Journal of Pharmaceutical Sciences*, 43(3):160–73, 2011.

[238] M. Nishimura and S. Naito. Tissue-specific mRNA expression profiles of human phase I metabolizing enzymes except for cytochrome P450 and phase II metabolizing enzymes. *Drug metabolism and pharmacokinetics*, 21(5):357–74, 2006.

[239] G. Margaillan, M. Rouleau, K. Klein, J. K. Fallon, P. Caron, L. Villeneuve, P. C. Smith, U. M. Zanger, and C. Guillemette. Multiplexed targeted quantitative proteomics predicts hepatic glucuronidation potential. *Drug Metabolism and Disposition*, 43:1331–5, 2015.

[240] National Center for Biotechnology Information (NCBI). Expressed Sequence Tags (EST) from UniGene. 2019.

[241] N. Kolesnikov, E. Hastings, M. Keays, O. Melnichuk, Y. A. Tang, E. Williams, M. Dylag, N. Kurbatova, M. Brandizi, T. Burdett, K. Megy, E. Pilicheva, G. Rustici, A. Tikhonov, H. Parkinson, R. Petryszak, U. Sarkans, and A. Brazma. ArrayExpress update-simplifying data submissions. *Nucleic Acids Research*, 43(D1):D1113–D1116, 2015.

[242] M. Nishimura and S. Naito. Tissue-specific mRNA expression profiles of human ATP-binding cassette and solute carrier transporter superfamilies. *Drug metabolism and pharmacokinetics*, 20(6):452–77, 2005.

B

PUBLICATIONS

B.1 ORIGINAL ARTICLES

I Fuhr, L.M.; Marok, F.Z.; Fuhr, U.; Selzer, D.; Lehr, T. Physiologically based pharmacokinetic modeling of bergamottin and 6,7-dihydroxybergamottin to describe CYP3A4 mediated grapefruit-drug interactions. Clinical Pharmacology & Therapeutics. 2023. 114(2): 470-482. doi: 10.1002/cpt.2968.

II Marok, F.Z.; Wojtyniak, J.-G.; Fuhr, L.M.; Selzer, D.; Schwab, M.; Weiss, J.; Haefeli, W.E.; Lehr, T. A physiologically based pharmacokinetic model of ketoconazole and its metabolites as drug–drug interaction perpetrators. Pharmaceutics. 2023. 15(2): 679. doi: 10.3390/pharmaceutics15020679.

III Fuhr, L.M.; Marok, F.Z.; Mees, M.; Mahfoud, F.; Selzer, D.; Lehr, T. A physiologically based pharmacokinetic and pharmacodynamic model of the CYP3A4 substrate felodipine for drug-drug interaction modeling. Pharmaceutics. 2022. 14(7): 1474. doi: 10.3390/pharmaceutics14071474

IV Marok, F.Z.; Fuhr, L.M.; Hanke, N.; Selzer, D.; Lehr, T. Physiologically based pharmacokinetic modeling of bupropion and its metabolites in a CYP2B6 drug-drug-gene interaction network. Pharmaceutics. 2021. 13(3): 331. doi: 10.3390/pharmaceutics13030331.

V Fuhr, L.M.; Marok, F.Z.; Hanke, N.; Selzer, D.; Lehr, T. Pharmacokinetics of the CYP3A4 and CYP2B6 Inducer Carbamazepine and Its Drug-Drug Interaction Potential: A Physiologically Based Pharmacokinetic Modeling Approach. Pharmaceutics. 2021. 13(2): 270. doi: 10.3390/pharmaceutics13020270.

VI Fuhr, L.M.; Hanke, N.; Meibohm, B.; Lehr, T. Effective removal of dabigatran by idarucizumab or hemodialysis: a physiologically based pharmacokinetic modeling analysis. Clinical Pharmacokinetics. 2020. 59(6): 809-825. doi: 10.1007/s40262-019-00857-y.

B.2 REVIEW ARTICLES

I Türk, D.; Fuhr, L.M.; Marok, F.Z.; Rüdesheim, S.; Kühn, A.; Selzer, D.; Schwab, M.; Lehr T. Novel models for the prediction of drug-gene interactions. Expert Opinion on Drug Metabolism & Toxicology. 2021. 17(11): 1293-1310. doi: 10.1080/17425255.2021.1998455.

B.3 CONFERENCE ABSTRACTS

I Fuhr, L.M.; Marok, F.Z.; Lehr, T. Peeling the grapefruit – investigating the drug interaction potential of grapefruit juice as CYP3A4 inhibitor using physiologically-based pharmacokinetic modeling – Abstr. 10147. In: PAGE Meeting. Ljubljana, Slovenia (June 2022)

II Marok, F.Z.; Wojtyniak, J.-G.; Fuhr, L.M.; Schwab, M.; Weiss, J.; Haefeli, W.E.; Lehr, T. Physiologically-based pharmacokinetic modeling of drug-drug interactions with ketoconazole and its metabolite deacetylketoconazole – Abstr. 9986. In: PAGE Meeting. Ljubljana, Slovenia (June 2022)

III Fuhr, L.; Hanke, N.; Lehr, T. Physiologically based pharmacokinetic modeling of the dabigatran antidote idarucizumab – Abstr 8905. In: PAGE Meeting. Stockholm, Sweden (June 2019)

IV Wojtyniak, J.-G.; Britz, H.; Marok, F.Z.; Türk, D.; Fuhr, L.; Kovar, L.; Hanke, H., Schwab, M., Lehr, T. Physiologically-based pharmaokinetic (PBPK) modelling of a CYP3A4/P-gp ddi network with ketoconazole, midazolam, alfentanil, repaglinide and digoxin. In: DPhG Doktorandentagung (2019)